
# JMRI

Journal of Magnetic Resonance Imaging

*Published by the Society for Magnetic Resonance Imaging*

## 1992 SMRI Annual Meeting Printed Program

**Guest Editors**

**S. E. Harms, M.D.**
**W. Kucharczyk, M.D.**
**K. R. Maravilla, M.D.**
**F. W. Wehrli, Ph.D.**
**M. L. Wood, Ph.D.**

*A Supplement to JMRI March/April 1992 Issue, Volume 2 (P)*

SIEMENS

There's only one
MRI system
that does it all in 40 m².
MAGNETOM Impact.

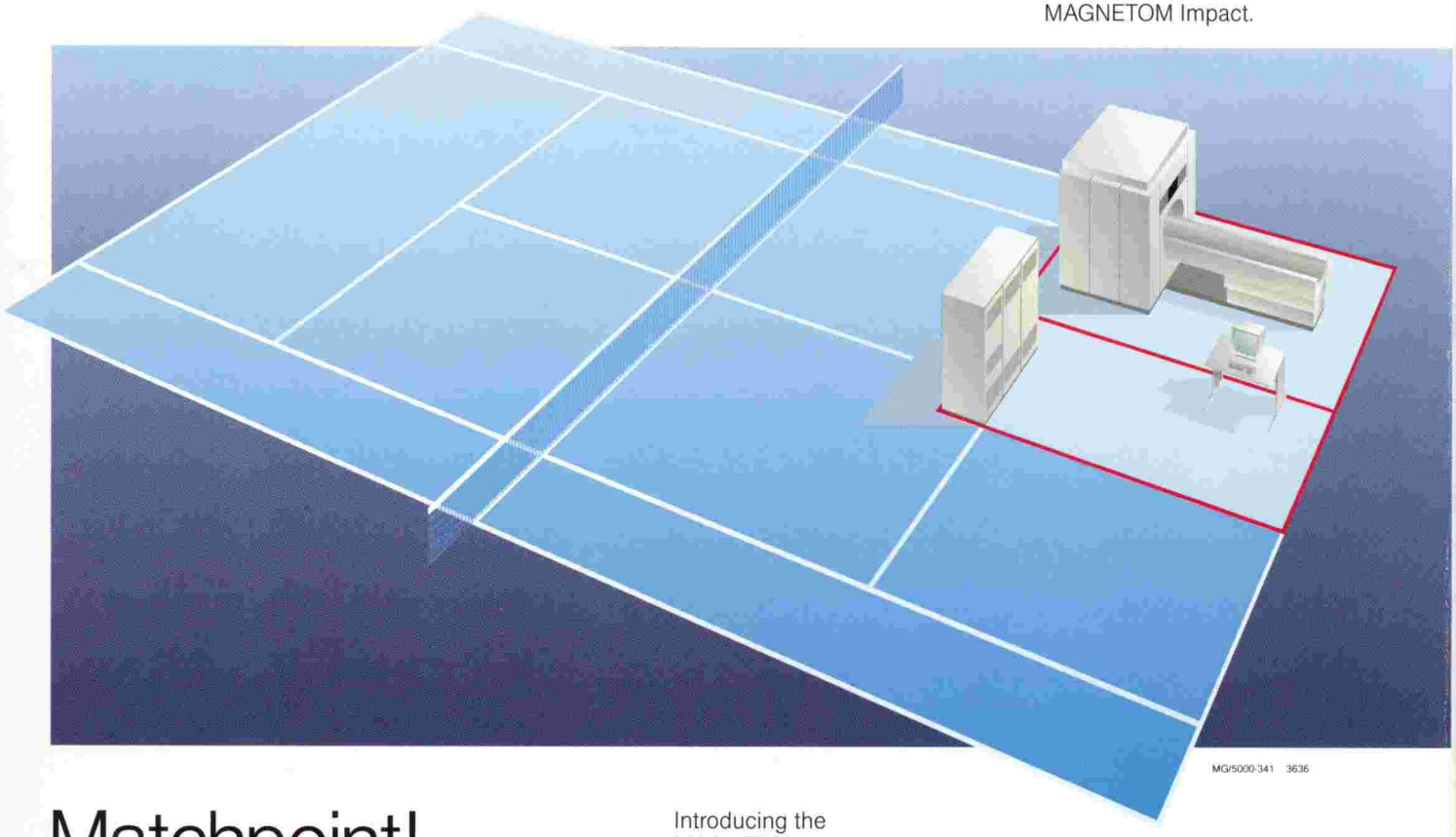

MG/5000-341 3636

# Matchpoint!

# 1 Tesla impact in 40 m²

Introducing the MAGNETOM Impact 1.0 T MRI system: Advancing the clinical Routine.

To stay in the game in today's MR market, a system must have it all: convenient siting, low installation and operating costs, high throughput, and advanced applications.

## Advantage

The whole system fits neatly into 40 m²: less space than 0.5 T systems require. Place it in your old CT suite, at twice the S/N of other MR solutions!

## Ace

With an installation time of only three weeks, the MAGNETOM Impact is quick off the mark. And once you get going, you won't slow down: only three cryogen refills are needed per year.

It's as easy to learn as it is to install. Clinically optimized protocols, a simplified user interface, and integrated filming assure high throughput... from day one.

The MAGNETOM Impact sets the pace for the new clinical routine: three minutes MRA exams of the head, liver studies in seconds, subsecond cardiac studies.

## Matchpoint

True to the MAGNETOM® tradition, 3D capabilities are fully integrated. You won't need to buy a separate workstation for 3D post-processing MIP vessel displays in seconds, and real-time multi-planar reconstructions.

Siemens Medical Systems, Inc.
186 Wood Avenue South
Iselin, NJ 08830
(908) 321-4500

JMRI Journal of Magnetic Resonance Imaging

*Owned and published by the Society for Magnetic Resonance Imaging, and produced with the assistance of the Radiological Society of North America.*

JMRI Journal of Magnetic Resonance Imaging



## EDITORIALS



## SMRI '92 PROGRAM ABSTRACTS

### PLENARY SYMPOSIA

#### Sunday Morning



#### Sunday Afternoon



#### Monday Morning



#### Monday Afternoon



#### Tuesday Morning



#### Tuesday Afternoon



#### Wednesday Morning



#### Wednesday Afternoon



### PROFFERED PAPER ABSTRACTS

#### Monday Morning



#### Monday Afternoon



*Continued*

# SMRI at Work

## SMRI Officers

E. Mark Haacke, PhD, *President*
Robert B. Lufkin, MD, *Past President*
Steven E. Harms, MD, *President-Elect*
David D. Stark, MD, *Treasurer*
Stephen R. Thomas, PhD, *Secretary*

## Board of Directors

Scott W. Atlas, MD
William G. Bradley, Jr, MD, PhD *(ex officio)*
Thomas J. Brady, MD
Michael N. Brant-Zawadzki, MD
Michael J. Bronskill, PhD
John V. Crues, III, MD
W. Thomas Dixon, PhD
Richard L. Ehman, MD
Jens Frahm, PhD
Gary D. Fullerton, PhD *(Editor)*
R. Edward Hendrick, PhD *(ex officio)*
J. Bruce Kneeland, MD
James R. MacFall, PhD
Kenneth R. Maravilla, MD
Ronald R. Price, PhD
Stephen J. Riederer, PhD
Frank G. Shellock, PhD
Perry Sprawls, PhD
Jeffrey C. Weinreb, MD
Ian Young, PhD
Stuart W. Young, MD

## Past Presidents

Robert B. Lufkin, MD, 1990-1991
R. Edward Hendrick, PhD, 1989–1990
William G. Bradley, Jr, MD, PhD, 1988–1989
Gary D. Fullerton, PhD, 1986–1988
Luis E. Todd, MD, 1984–1986
William S. Moore, PhD, 1984
Sharad R. Amtey, PhD, 1983–1984
Francis W. Smith, PhD, 1983–1984

## Committee Chairmen

### Councils

- **Basic Science Council:** Stephen R. Thomas, PhD
  - **Instrumentation Committee:** James R. MacFall, PhD
  - **Relaxometry and Biophysics Committee:** Robert V. Mulkern, PhD
  - **Imaging Committee:** Stephen J. Riederer, PhD
  - **Clinical Applications Committee:** Richard Ehman, MD
  - **Spectroscopy Committee:** Michael W. Weiner, MD
  - **Scientist Education and Training Committee:** James Sorenson, PhD
- **Corporate Council:** William G. Bradley, Jr, MD, PhD
  - **Reimbursement Committee:** Stuart W. Young, MD
  - **Industrial Committee:** William T. C. Yuh, MD, MSEE
  - **Government Liaison Committee:** A. Everette James, Jr, MD
  - **Technical Exhibits Committee:** Robert R. Edelman, MD
- **Medical Science Council:** Steven E. Harms, MD
  - **Body Imaging Committee:** Richard D. White, MD
  - **MR Safety Committee:** Emanuel Kanal, MD, and Frank G. Shellock, PhD
  - **Continuing Physician Education Committee:** Perry Sprawls, PhD
  - **Neuro Imaging Committee:** Scott W. Atlas, MD
  - **Resident Training Committee:** Donald G. Mitchell, MD

### Standing Committees

**Annual Meeting Organizing Committee:** Felix W. Wehrli, PhD, and Kenneth R. Maravilla, MD
**Executive Committee:** E. Mark Haacke, PhD
**Finance Committee:** David D. Stark, MD
**Membership Committee:** Lawrence R. Muroff, MD
**Nominating Committee:** Robert B. Lufkin, MD
**Publications Committee:** R. Edward Hendrick, PhD
**Rules Committee:** Jeffrey C. Weinreb, MD
**Society Liaison Committee:** E. Mark Haacke, PhD

### Ad Hoc Committees

**Awards Committee:** Francis W. Smith, MD
**10th Anniversary Committee:** Francis W. Smith, MD
**Electronics Committee:** Robert B. Lufkin, MD
**Joint Technologist Committee:** E. Mark Haacke, PhD
**Joint Workshop Committee:** R. Mark Henkelman, PhD

## Future Annual Meetings

1992: New York, April 25–29
1993: San Francisco, March 27–31
1994: Dallas, March 5–9

## Central Office

Society for Magnetic Resonance Imaging
213 West Institute Place, Suite 501
Chicago, Illinois 60610
Tel: (312) 751-2590
FAX: (312) 951-6474

# SMRI

## Letter from the President

The SMRI invites you to attend the 1992 Annual Meeting in New York City. This 10th anniversary Meeting features several new programs in addition to the traditionally superior scientific and clinical presentations. The 1992 Meeting introduces an all-invited lecture program during Sunday's MR Angiography topical symposia; the inaugural Annual Meeting of the SMRT, a combined technologist section of the SMRI and SMRM; a special plenary session on the history of SMRI, MRI and spectroscopy by Drs. Frank Smith, Paul Lauterbur and Jens Frahm; and a 10th anniversary retrospective exhibit of SMRI and MR. The Meeting again delivers an important close to the Educational Program with Monday's Economic Symposia as well as presenting the premier, U.S. exhibition of clinical MR equipment and accessories with an expanded Technical Exhibits Program.

The 1992 Annual Meeting offers the excitement of New York City as well as an interesting SMRI Social Program. The SMRI will host a number of receptions during the Meeting. All attendees are invited to join the Society at the **Technical Exhibits Opening Reception** on Saturday, April 25 (5:00 pm - 7:00 pm); **Poster Exhibit Reception** on Sunday, April 26 (7:00 pm - 9:00 pm); and the SMRI **Gala Reception** on Monday, April 27 (7:30 pm - 10:30 pm). As usual, these receptions will provide you with the opportunity to visit with colleagues and share your enthusiasm with MR, your present research and future directions.

This year, I would like to encourage you to submit your technical and clinical papers to the Society's journal, the **Journal of Magnetic Resonance Imaging (JMRI)**. **JMRI** will occupy booth #1517 in Americas Hall I of the Technical Exhibits Area and manuscripts may be submitted for consideration there. Launched in 1991, **JMRI** has quickly risen to occupy a strategic place for the clinical MR practitioner and scientific researcher and your manuscript, if accepted, will be widely read by the nearly 2,000 member, non-member and institutional subscribers.

Without further ado, the SMRI looks forward to meeting with you at this very important gathering of MR professionals.

See you in the Big Apple!

Sincerely,

E. Mark Haacke

**E. Mark Haacke, Ph.D.**
SMRI *President*

# SMRI

## Society History

1992 marks the 10th anniversary of the Society for Magnetic Resonance Imaging (SMRI). The Society was chartered in November, 1982 to:

**provide** an equal opportunity to clinical and basic scientists to contribute to the development of **MRI**.

**offer** an international multidisciplinary forum for the advancement of magnetic resonance imaging.

**promote** the applications of magnetic resonance techniques to medicine and biology, with specific emphasis on imaging.

**prepare** and disseminate technical and product information related to research techniques, equipment and clinical applications of magnetic resonance.

**develop** educational and training material and methods for the application of magnetic resonance to medicine and biology.

Since its inception, the SMRI has grown to an international association of 2,000 clinical and basic scientists dedicated to research and the application of MR as a diagnostic technique in medicine. The professionalism and experience of its members has guided the Society to its current position as the major resource for the clinical MRI practitioner.

## Journal of Magnetic Resonance Imaging (JMRI)

1991 marked an important milestone for the Society. In January, SMRI launched publication of its official journal, the **Journal of Magnetic Resonance Imaging (JMRI)**. Owned and self-published by the SMRI, **JMRI** is produced in collaboration with the Radiological Society of North America, publisher of **Radiology** and other radiology-related journals.

**JMRI**, under the direction of Gary D. Fullerton, Ph.D., Professor and Chief of Radiological Sciences at the University of Texas Health Science Center, San Antonio, presents a balance of technical and clinical articles on MR imaging and spectroscopy research. **JMRI** bi-monthly publishes 120 pages of peer-reviewed original research, works in progress, review articles, educational articles, SMRI reports and other special features, with more than 90 manuscripts published annually.

## Past Meetings

Organizational Meeting (1982)
*Houston, Texas*

First Annual Meeting (1983)
*Broadmoor Hotel*
*Denver, Colorado*

Second Annual Meeting (1984)
*Greenlefe Hotel*
*Orlando, Florida*

Third Annual Meeting (1985)
*Town and Country Hotel*
*San Diego, California*

Fourth Annual Meeting (1986)
*Wyndham Franklin Plaza*
*Philadelphia, Pennsylvania*

Fifth Annual Meeting (1987)
*Palacio del Rio*
*San Antonio, Texas*

Sixth Annual Meeting (1988)
*Westin Copley Place*
*Boston, Massachusetts*

Seventh Annual Meeting (1989)
*Century Plaza Hotel*
*Los Angeles, California*

Eighth Annual Meeting (1990)
*Washington Hilton and Towers*
*Washington, D.C.*

Ninth Annual Meeting (1991)
*Hyatt Regency Hotel*
*Chicago, Illinois*

Tenth Annual Meeting (1992)
*New York Hilton and Towers*
*New York, New York*

## Future Meetings

Eleventh Annual Meeting (1993)
*San Francisco Hilton*
*San Francisco, California*
*March 27-31*

Twelfth Annual Meeting (1994)
*Loews Anatole Hotel*
*Dallas, Texas*
*March 5-9*

Thirteenth Annual Meeting (1995)
*Washington Hilton and Towers*
*Washington, D.C.*
*March 25-29*

## Annual Business Meeting

The Annual Business Meeting of the SMRI is scheduled in the East Ballroom on Monday, April 27, 9:30 a.m. - 10:00 a.m. All members are invited and encouraged to attend this very important meeting of the Society.

## 1991-92 Officers

E. Mark Haacke, Ph.D.
*President*

Steven E. Harms, M.D.
*President-Elect*

Robert B. Lufkin, M.D.
*Past President*

David D. Stark, M.D.
*Treasurer*

Stephen R. Thomas, Ph.D.
*Secretary*

## Organizing Committee

**Organizing Committee Chairmen**
Kenneth R. Maravilla, M.D.
Felix W. Wehrli, Ph.D.

**Scientific Program Chairmen**
Steven E. Harms, M.D.
Walter Kucharczyk, M.D.
Michael L. Wood, Ph.D.

**Educational Program Chairmen**
Laurence P. Clarke, Ph.D.
Jeffrey S. Ross, M.D.
David Thickman, M.D.

**Economics Symposium Chairmen**
Gerald L. Wolf, M.D., Ph.D.
Stuart W. Young, M.D.

**Poster Program Chairmen**
Scott W. Atlas, M.D.
Stephen J. Riederer, Ph.D.

**Evening Tutorial Program Chairmen**
Paul J. Keller, Ph.D.
William Sattin, Ph.D.
William T.C. Yuh, M.D., M.S.E.E.

**Technologist Program Chairmen**
Rodney Bell, R. T.
John V. Crues, III, M.D.
William H. Faulkner, B.S.R.T.
Lori B. Irilli, R.T., Chairman
Carolyn Kaut-Watson, R.T., Chairman

SMRI

SOCIETY FOR MAGNETIC RESONANCE IMAGING

SMRI

## About the Award...

Honorary membership in the Society for Magnetic Resonance Imaging is conferred on an individual who has rendered unusual service to the science of Magnetic Resonance Imaging. It is the highest honor the Society can bestow upon an individual.

## Past Honorary Member Award Recipients

**1990:**
Francis W. Smith, M.D.

**1989:**
Paul C. Lauterbur, Ph.D.

# 1992 SMRI HONORARY MEMBER AWARD RECIPIENT

## Graeme E. Bydder, M.D.

After obtaining his medical degree from the University of Otago, Graeme served as a resident and registrar in New Zealand before moving to London, England in 1978 to work at Northwick Park Hospital with the then new Wholebody CT scanner. In 1989, he moved to the Royal Postgraduate Medical School at the Hammersmith Hospital in London to work with Ian Young on MRI. During the past twelve years his scientific work, in all aspects of MRI, has been prolific and his scientific contributions to our understanding and application of MRI to clinical medicine have been outstanding. Graeme's quiet, unassuming personality belies his ability as both an outstanding teacher and scientist. His ability to make the most difficult concept appear simple has put him in great demand as a lecturer worldwide. He is Professor of Radiology at the Hammersmith Hospital and a Fellow of the Royal College of Radiologists. Graeme's contribution to the Society has been great, having served as a Board Member from 1988-91. In 1987, he received the Gold Medal of the Society of Magnetic Resonance in Medicine, in 1989, served as President of SMRM and in 1991, was honored with the Fellow of the Society Award by the SMRI. Graeme is one of the earliest pioneers of clinical MRI and continues to work in the field, demonstrating new ways of using NMR to improve clinical diagnosis.

# 1992 FELLOW OF THE SOCIETY AWARD RECIPIENTS

## E. Mark Haacke, Ph.D.

Mark retires as President of the SMRI during the 10th Annual Meeting, following a highly successful year in office. His work on behalf of the Society is well known and includes three years service on the Board of Directors as well as service on the Annual Meeting Organizing Committee (1989-1991), the final year of which he served as Co-chairman. After a distinguished academic career at the University of Toronto where he obtained his Bsc. MSc. and Ph.D. in physics, he spent some time as a Research Geophysicist with Gulf Oil in Pittsburgh before moving to Cleveland as a Senior Research Scientist with Picker International. During his time with Picker he developed his interest in FAST imaging. He has refined this interest since moving to his present position as Associate Professor in Physics and BioMedical Engineering at Case Western Reserve University.

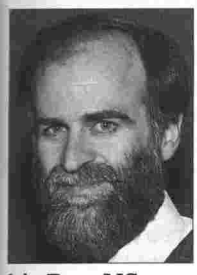

## Kenneth R. Maravilla, M.D.

After obtaining his BS in Chemistry from St. John's University, Ken studied Medicine at the Downstate Medical Center of the State University of New York. This followed with an internship at Baylor, residency at Parkland Memorial Hospital in Dallas and a fellowship at the University of Pittsburgh. He is presently Professor of Radiology and Neurological Surgery and Director of Neuroradiology at the University of Washington Medical Center in Seattle. His major research interest is in the application and clinical correlation of new imaging techniques, including contrast agents, for the evaluation of CNS pathology. Ken has made significant contributions in the application of CT, DSA and MRI to neuroradiologic practice. This year he is Co-chairman of the Annual Meeting Organizing Committee, having served as Co-chairman of the Scientific Program in 1991, Educational Program in 1990 and the Evening Tutorial Program in 1989.

## Jeffrey C. Weinreb, M.D.

Jeff is an Associate Professor of Radiology and Director of MRI at the New York University School of Medicine. He was educated at MIT and the Mt. Sinai School of Medicine in New York City prior to holding positions at HUP, University of Texas Health Science Center in Houston, Southwestern Medical School and Columbia University. He is a prolific researcher in MRI applications to the body, with over sixty scientific papers, ten chapters and two books to his name. A past Secretary of the Society, he has served on the Executive, Publications, Safety and Technologists Committees as well as acting as Co-chairmen of the Educational Program in 1990 and the Evening Tutorial Program in 1989. He is currently serving a three year term, 1991-94, on the SMRI Board of Directors.

## Michael L. Wood, Ph.D.

After obtaining his Ph.D. from the University of Toronto in 1986, Michael worked as Assistant Professor of Physics at Tufts University School of Medicine, before returning to Toronto as a physicist at St. Michael's Hospital. His main interest is in finding methods for removing artifacts from MR images. Mike's contribution to the Society are extensive, serving as the 1988 Local Arrangements Committee Chairman, 1988-91 Board Member, 1990 Evening Tutorial Co-chairman, 1991 Educational Program Co-chairman, and currently, 1992 Scientific Program Co-chairman.

SMRI

## About the Award...

Fellow of the Society for Magnetic Resonance Imaging Awards are conferred on those individuals who have made both a significant contribution to the science of MRI and rendered outstanding service to the Society.

## Past Fellow of the Society Award Recipients

### 1991:

Graeme Bydder, M.D.
R. Mark Henkelman, Ph.D.
Robert B. Lufkin, M.D.
Felix W. Wehrli, Ph.D.

### 1990:

C. Leon Partain, M.D., Ph.D.
Val M. Runge, M.D.
David D. Stark, M.D.

### 1989:

Sharad R. Amtey, Ph.D.
Paul A. Bottomley, Ph.D.
William G. Bradley, Jr., M.D., Ph.D.
Gary D. Fullerton, Ph.D.
John C. Gore, Ph.D.
Carlton T. Hazlewood, Ph.D.
R. Edward Hendrick, Ph.D.
Andre Luiten, Ph.D.
William J. MacIntyre, Ph.D.
Ray L. Nunnally, Ph.D.
Francis W. Smith, M.D.
Luis E. Todd, M.D.

# GENERAL INFORMATION

## Presenters of Papers

- Last minute concerns about a presentation, call the SMRI Central Office at (312)751-2590 before April 22. After this date, call the New York Hilton/SMRI Registration area at 212/586-7000.
- Contact authors of abstracts printed in the Program by writing to the SMRI Central Office at 213 West Institute Place, Suite 501, Chicago, Illinois 60610. Requests will be forwarded to the author.
- The Slide Preview Room is located in the Gibson Suite, second floor. The hours are as follows:

Sat. April 25 - Tue. April 28:
*7:00 am - 6:00 pm*
Wed. April 29: *7:00 am - 4:30 pm*

## Registration

All meeting registration will take place on the Second Floor Promenade of the New York Hilton and Towers according to the following hours:

Saturday, April 25
*7:00 am - 5:00 pm*

Sunday, April 26
*7:00 am - 6:00 pm*

Monday, April 27
*7:00 am - 6:30 pm*

Tuesday. April 28
*7:00 am - 6:00 pm*

Wednesday, April 29
*7:00 am - 3:00 pm*

## Registration Entitlements

In completing the Registration Form, please use the following guide in selecting a Program to attend:

**Educational Program**
Entitled to attendance at Educational (including the Economics Symposia) or Technologist Programs (including the MR Manufacturers Workshop). Those who wish to attend only the Economics Symposia or MR Manufacturers Workshop may register on-site.

**Scientific Program**
Entitled to attendance at Scientific Program (including the MR Angiography Topical Conference).

**Scientific/Educational Program**
Entitled to attendance at both Educational and Scientific Programs.

## Schedule of Events

For alumni groups and other SMRI-affiliated committees and organizations that have made meeting arrangements through the SMRI Central Office, a schedule of events is available for review at the Registration Desk, Second Floor Promenade of the New York Hilton and Towers.

## Scientific Poster Exhibit Hours

Scientific Poster Exhibits are located in Americas Hall II accessible from the second floor of the New York Hilton and Towers. Exhibit hours are Sunday-Tuesday 8:00 am - 8:00 pm and Wednesday 8:00 am - 1:00 pm.

## SMRI Membership Services

Membership applications will be available at the Registration Desk, Second Floor Promenade, for all non-member attendees wishing to join the Society. Due to the review process required, membership applications may not be approved on-site. However, you will be notified of your acceptance within six weeks following the Annual Meeting. Membership inquiries by current members may also be addressed at the Registration Desk.

## SMRI Business Meeting

All SMRI members are encouraged to attend the Annual Business Meeting of the Society to be held Monday, April 27, 9:30 am - 10:00 am in the East Grand Ballroom.

## SMRI Publications

For subscription or manuscript information regarding the **Journal of Magnetic Resonance Imaging (JMRI)**, visit booth #1517 in the Technical Exhibits Area. Manuscripts for submission to **JMRI** may be submitted to the booth.

## SMRT Business Meeting

All SMRT members are encouraged to attend the Annual Business Meeting of the Combined Section to be held Sunday, April 26, 3:45 pm - 5:00 pm in the Trianon Ballroom.

## Social Program

The SMRI cordially invites all attendees (single day registrants must visit the Social Program Desk to purchase tickets) to join in an evening of fellowship at the following receptions:

**Technical Exhibits Opening Reception**
Technical Exhibits Area
Saturday, April 25
*5:00 pm - 7:00 pm*

**Poster Exhibit Reception**
Poster Exhibit Area
Sunday, April 26
*7:00 pm - 9:00 pm*

**SMRI Gala Reception**
Trianon Ballroom Complex
Monday, April 27
*7:30 pm - 10:30 pm*

A Social Program Desk will be staffed in the Registration Area for participants wishing to purchase tickets for accompanying guests.

## Technical Exhibits

The SMRI Technical Exhibits Program will display the latest in MR equipment, supplies, and services in Americas' Hall I and II, beginning with a reception Saturday, April 25 from 5:00 pm - 7:00 pm. Thereafter, the exhibits will be on display Sunday, April 26, 9:30 am - 6:00 pm, Monday, April 27 through Tuesday, April 28, 9:30 am - 4:00 pm and Wednesday, April 29, 9:30 am - 1:00 pm.

### Who's Who—Official Badges

Badges are color-coded as follows:

**Blue:** Member SMRI/SMRT
**Red:** Non-member
**Green:** Accompanying Family Members
**Brown:** Technical Exhibitors

## Accreditation for Category I

The Society for Magnetic Resonance Imaging Annual Meeting is accredited by the American College of Radiology as providing continuing medical education for physicians. The Society designates that Educational and Scientific Programs meet the criteria for category 1 credit for the American Medical Association. Credit hours are earned on an hour-for-hour basis. A maximum of 33 credit hours can be accrued by participation in the SMRI Annual Meeting.

## Announcement Board

An area is set aside in the Registration Area, Second Floor Promenade, for posting announcements of future meetings and seminars and for publicizing events during the SMRI Meeting. Announcements may not be larger than 8½ x 11 inches.

## Annual Meeting Printed Program: A How To Guide

This Program contains a complete listing, with abstracts, of all scientific courses, sessions, and exhibits. Material is organized by category (Plenary Symposia, Proffered Papers, Scientific Poster Exhibits, Etc.) and ordered chronologically within each category. The Sections and Symbols throughout these pages are guides to information you wish to locate. Beginning with Plenary Symposia and continuing with Indices and Information, each section is preceded by a divider page. Please review the text on each divider page for important information and announcements relating to that particular section.

**EP** designates an Educational Session. Educational Program material will be distributed on-site to Educational Program attendees. The Educational Program will be presented in the West Grand Ballroom.

**PS** designates a Plenary Symposium. Plenary Symposia will be presented in the East Ballroom.

**ET** designates an Evening Tutorial presentation. Evening Tutorial sessions will be presented in the rooms detailed later in this section.

**P** designates a Poster Scientific Paper. Poster Papers will be presented in the Poster Exhibit Area, located in Americas Hall II of the Technical Exhibit Area. Posters will be on display Sunday-Wednesday.

**T** designates a Technologist Scientific Paper. Technologist papers will be presented in the Trianon Ballroom.

## Attendance Record

A CME Certificate of Attendance may be found at the rear of this Printed Program. It is the responsibility of all individuals to correct their record in accordance with the honor system observed in reporting continuing medical education credits. This record of attendance is available only to the individual and will not be submitted to accrediting agencies and other organizations. All individuals should maintain their records of attendance; no cumulative records are maintained by the SMRI. To have your CME Certificate of Attendance signed by the certifying official, please stop by the Registration Area, Second Floor Promenade.

Technologists wishing to record ECE credits should sign in at the Technologist Program upon entering the meeting room. A record of these attendance sheets will be forwarded to the ASRT for accreditation.

## Bank

To exchange foreign currency or to cash U.S.-denominated travelers checks, visit the Credit Desk located in the hotel lobby (first floor).

## Business Center

The hotel Business Centers, located on the 2nd Floor (Hotel Guest Extension 5408) and 4th Floor (Hotel Guest Extension 5575), offer the following services: photocopying, FAX transmissions, UPS, Federal Express (priority and economy), word processing and typing.

## Coat Check

A coat check service is provided by the New York Hilton and Towers for a nominal fee and is located in the hotel lobby, first floor. A second coat check area will be located in the Registration Area; its hours will be posted during the Annual Meeting.

## Emergency Information

In case of an emergency, please contact the hotel Assistant Manager on any house telephone at extension 5746.

## Food Service

Pre-session coffee service is available in the Registration Area, 7:00 am-8:00 am, daily. In addition, coffee breaks and luncheon service is provided. Saturday's morning coffee service and afternoon soda breaks will be provided in the Rendezvous Trianon, third floor, while luncheon service will be provided in the Sutton Complex, second floor. Thereafter, all breaks will be in the Technical Exhibit Area. Please refer to the following "Walk Through SMRI '92" for specific service schedules.

## Job Bulletin

Technologist job listings may be posted in SMRT booth #1316, the booth of the Combined Section of Magnetic Resonance Technologists (SMRT). All other job listings may be posted on the Job Bulletin Board set aside in the Registration Area, Second Floor Promenade. Posted materials regarding positions available and positions sought may not exceed 8½ x 11 inches.

## Lost and Found

Lost and Found articles may be picked up at the Hotel Security Office, located in the Hotel lobby, 1st floor. Please contact the Security Office on any house telephone at extension 5742.

## Message Center

A Message Center Board is set aside in the Registration Area, Second Floor Promenade, for posting messages during the SMRI Annual Meeting. Notepads and pencils will be available for message deposit and retrieval.

## Post Office

Should attendees require postal services, please contact Hotel Guest Service on any house telephone at extension 5321.

## Saturday, April 25

**7:00 am - 5:00 pm**
General Registration

### Educational Program

**8:00 am - 10:00 am**
- ☐ Physics/MR Acronyms
- ☐ Brain Imaging Optimization
- ☐ Brain Tumors
- ☐ Congenital Brain

**10:00 am - 10:30 am**
*Break*

**10:30 am - 12:00 pm**
- ☐ White Matter/ Hydrocephalus
- ☐ Fast Scanning
- ☐ Cerebrovascular Disease: Anatomy, Pathophysiology and MRI

**12:00 pm - 1:30 pm**
*Luncheon*

**1:30 pm - 3:00 pm**
- ☐ Head and Neck
- ☐ MR Angiography
- ☐ Spine Anatomy: MRI and Cryotome Sections

**3:00 pm - 3:30 pm**
*Break*

**3:00 pm - 5:00 pm**
- ☐ Degenerative Disk Disease
- ☐ MR Intradural Spine
- ☐ Congenital Spine

### Technologist Program

**8:00 am - 10:00 am**
- ☐ Opening Remarks
- ☐ Basic NMR Physics
- ☐ Intro to NMR Spectroscopy
- ☐ Proffered Papers T001-T002

**10:00 am - 10:30 am**
*Break*

**10:30 am - 12:15 pm**
- ☐ Cardiac Gating
- ☐ SNR and CNR
- ☐ Proffered Papers T003-T004

**12:15 pm - 1:15 pm**
*Luncheon*

**1:15 pm - 2:45 pm**
- ☐ MR of the Shoulder
- ☐ Artifacts
- ☐ Proffered Papers T005-T006

**2:45 pm - 3:00 pm**
*Break*

**3:00 pm - 5:00 pm**
- ☐ MR Manufacturer's Workshop: General Electric Medical Systems, Philips Medical Systems, Picker International, Resonex, Toshiba America Medical Systems

### Educational Program

**8:00 am - 10:00 am**
- ☐ Liver: Hepatic MRI
- ☐ Abdomen: MRI of Kidney, Adrenal and Retroperitoneum
- ☐ Pelvis
- ☐ MRI of the Pediatric Abdomen

**10:00 am - 10:30 am**
*Break*

**10:30 am - 12:00 pm**
- ☐ Body Technique Optimization
- ☐ Practical Aspects of Vascular MR Imaging
- ☐ Cardiac

**12:00 pm-1:30 pm**
*Luncheon*
Scientific Poster Discussion Period: Neuro, Head & Neck, Spine, Pediatrics

**1:30 pm - 3:00 pm**
- ☐ Musculoskeletal Optimization
- ☐ MR Imaging of the Knee
- ☐ MR Imaging of the Shoulder

**3:00 pm - 3:30 pm**
*Break*

**3:30 pm - 5:00 pm**
- ☐ MR Imaging of the Foot and Ankle
- ☐ MR Imaging of the Hand, Wrist and Elbow
- ☐ MR Imaging of Bone Tumor and Other Marrow Disorders

**TECHNICAL EXHIBITS RECEPTION**
**5:00 pm - 7:00 pm**

## Sunday, April 26

**7:00 am - 6:00 pm**
General Registration
**9:30 am - 6:00 pm**
Technical Exhibits
**8:00 am - 8:00 pm**
Poster Sessions

### Technologist Program

**8:00 am - 10:00 am**
- ☐ Principles of Flow
- ☐ Applications of MRA
- ☐ Proffered Papers T007-T008

**10:00 am - 10:15 am**
*Break*

**10:15 am - 12:00 pm**
- ☐ Effects of Contrast Media in MR
- ☐ FAST Scanning
- ☐ Proffered Papers T009-T010

**12:00 pm - 1:00 pm**
*Luncheon*
Scientific Poster Discussion Period: Neuro, Head & Neck, Spine, Pediatrics

**1:00 pm - 2:45 pm**
- ☐ MR Computer Tutorial
- ☐ MR in Obstetrics and Gynecology
- ☐ Proffered Papers T011-T012

**2:45 pm - 3:00 pm**
*Break*

**3:00 pm - 3:45 pm**
- ☐ Proffered Papers T013-T015

**3:45 pm - 5:00 pm**
SMRT Business Meeting

### Topical Conference

**8:00 am - 10:00 am**
HEAD AND NECK MRA
- ☐ Overview of MRA Techniques
- ☐ Current Status
- ☐ Neuroradiologic Applications
- ☐ Clinical Experience
- ☐ Panel Discussion

**10:00 am - 10:30 am**
*Break*

**10:30 am - 12:15 pm**
CHALLENGES FOR MRA
- ☐ Vascular System
- ☐ Pulse Sequences
- ☐ Visualization
- ☐ Panel Discussion

**12:15 pm - 1:30 pm**
*Luncheon*
Scientific Poster Discussion Period: Neuro, Head & Neck, Spine, Pediatrics

**1:30 pm - 3:00 pm**
TECHNIQUES FOR MRA
- ☐ Extremities
- ☐ Body
- ☐ Coronary and Cardiac Vessels
- ☐ Panel Discussion

**3:00 pm - 3:30 pm**
*Break*

**3:30 pm - 5:15 pm**
NEW HORIZONS FOR MRA
- ☐ Velocity Quantification
- ☐ Economics
- ☐ Future Directions
- ☐ Panel Discussion

**Evening Tutorial Program**
**5:30 pm - 7:30 pm**
- ☐ Musculoskeletal
- ☐ Introduction to Physics

**POSTER RECEPTION**
**7:00 pm - 9:00 pm**

## PERSONAL ITINERARY:

**SAT**

**SUN**

# SMRI '92 ANNUAL MEETING

## Monday, April 27

**7:00 am - 6:30 pm**
General Registration
**9:30 am - 4:00 pm**
Technical Exhibits
**8:00 am - 8:00 pm**
Poster Sessions

### Scientific Program

**8:00 am - 9:30 am**
THE FIRST DECADE OF MRI
- ☐ Award Presentations
- ☐ History of the SMRI
- ☐ Advances in MR Imaging
- ☐ Advances in MR Spectroscopy
- ☐ Rabi Award Paper Presentation

**9:30 am - 10:00 am**
SMRI Business Meeting

**10:00 am - 10:30 am**
*Break*

**10:30 am - 12:15 pm**
- ☐ Proffered Papers

**12:15 pm - 1:30 pm**
*Luncheon*
Scientific Poster
Discussion Period:
Body, Musculoskeletal

**1:30 pm - 3:00 pm**
RAPID IMAGING
- ☐ Strategies for Covering K-Space
- ☐ Fast Spin Echo Imaging
- ☐ Magnetization Preparation

**3:00 pm - 3:45 pm**
*Break*

**3:45 pm - 5:30 pm**
- ☐ Proffered Papers

### MRI Economics Symposium

**8:00 am - 10:15 am**
- ☐ Opening Comments
- ☐ Field Strengths & Site Planning
- ☐ Operational Impact of Vendor Selections
- ☐ MRI Scanner Competition

**10:15 am - 10:45 am**
*Break*

**10:45 am - 12:30 pm**
- ☐ Imagers and Imaging Facilities: Anti Trust Implications
- ☐ Contrast Media Reimbursement

**12:30 pm - 1:30 pm**
*Luncheon*
Scientific Poster
Discussion Period:
Body, Musculoskeletal

**1:30 pm - 3:00 pm**
- ☐ Self Referral and Imaging Services
- ☐ Optimizing Throughput Without Sacrificing Quality
- ☐ Architectural Planning

**3:00 pm - 3:45 pm**
*Break*

**3:45 pm - 5:30 pm**
- ☐ Marketing of MRI
- ☐ Competitive Strategies in MRI

### Evening Tutorial Program

**5:30 pm - 7:30 pm**
- ☐ Body
- ☐ Brain

**GALA RECEPTION**
**7:30 pm - 10:30 pm**

## Tuesday, April 28

**7:00 am - 6:00 pm**
General Registration
**9:30 am - 4:00 pm**
Technical Exhibits
**8:00 am - 8:00 pm**
Poster Sessions

### Scientific Program

**8:00 am - 9:30 am**
ADVANCES IN NEUROLOGICAL MRI
- ☐ Diffusion, Perfusion and Function
- ☐ Spine MRI - Faster and Better
- ☐ Role of Contrast Agents

**9:30 am - 10:30 am**
*Break*

**10:30 am - 12:15 pm**
- ☐ Proffered Papers

**12:15 pm - 1:30 pm**
*Luncheon*
Scientific Poster
Discussion Period:
Imaging Techniques

**1:30 pm - 3:00 pm**
NEW CLINICAL APPLICATIONS
- ☐ Chest MRI
- ☐ Breast MRI
- ☐ Interventional MRI

**3:00 pm - 3:45 pm**
*Break*

**3:45 pm - 5:30 pm**
- ☐ Proffered Papers

### Evening Tutorial Program

**5:30 pm - 7:30 pm**
- ☐ Spine
- ☐ Application of Physics

## Wednesday, April 29

**7:00 am - 3:30 pm**
General Registration
**9:30 am - 1:00 pm**
Technical Exhibits
**8:00 am - 1:00 pm**
Poster Sessions

### Scientific Program

**8:00 am - 9:30 am**
CHALLENGES FOR SHOULDER IMAGING
- ☐ Intro to the Shoulder
- ☐ Cuff: Intra-articular Contrast
- ☐ Cuff: Without Contrast Agents
- ☐ Instability: Intra-articular Contrast
- ☐ Instability: Without Contrast Agents

**9:30 am - 10:30 am**
*Break*

**10:30 am - 12:15 pm**
- ☐ Proffered Papers

**12:15 pm - 1:00 pm**
*Luncheon*
Scientific Poster
Discussion Period:
Spectroscopy, Instrumentation, Image Processing, and Miscellaneous

**1:00 pm - 2:30 pm**
FRONTIERS IN BODY IMAGING
- ☐ Manganese Contrast Agents
- ☐ Particulate Contrast Agents
- ☐ Rapid Imaging

**2:30 pm - 2:45 pm**
*Break*

**2:45 pm - 4:30 pm**
- ☐ Proffered Papers




## PERSONAL ITINERARY:

| MON | TUE | WED |
|---|---|---|
| | | |
| | | |
| | | |
| | | |
| | | |

# Technologist Program

Trianon Ballroom

***Moderators:** L. B. Irilli, R.T., R. Bell, B.S.R.T.*

## Saturday, April 25

**8:00 am - 10:00 am**
Basic NMR Physics ..... *P. L. Davis, M.D.*
Introduction to NMR Spectroscopy ..... *R. E. Lee, R. T.*
Proffered Papers T001-T002

**10:00 am - 10:30 am**
*Coffee Break* ..... Rendezvous Trianon

**10:30 am - 12:15 am**
Cardiac Gating ..... *L. Culbreth, M.Ed.*
SNR and CNR ..... *C. Kaut-Watson, R.T.*
Proffered Papers T003-T004

**12:15 pm - 1:15 pm**
*Luncheon* ..... Sutton Complex

**1:15 pm - 2:45 pm**
MR of the Shoulder ..... *D. L. Burk, M.D.*
Artifacts ..... *B. Keene, B.S.R.T.*
Proffered Papers T005-T006

**2:45 pm - 3:00 pm**
*Coffee Break* ..... Rendezvous Trianon

**3:00 pm - 5:00 pm**
MR Manufacturer's Workshop ..... General Electric, Philips Medical Systems, Picker International, Resonex, and Toshiba America Medical Systems

## Sunday, April 26

**8:00 am - 10:00 am**
Principles of Flow ..... *K. K. King, R.T.*
Applications of MRA ..... *C. L. Harris, R.T.*
Proffered Papers T007-T008

**10:00 am - 10:15 am**
*Coffee Break* ..... Americas Hall I and II

**10:15 am - 12:00 pm**
Fast Scanning ..... *W. H. Faulkner, B.S.R.T.*
Effects of Contrast Media in MR ..... *J. C. Gore, Ph.D.*
Proffered Papers T009-T010

**12:00 pm - 1:00 pm**
*Luncheon* ..... Americas Hall I and II

**1:00 pm - 2:45 pm**
MR Computer Tutorial ..... *E. Kanal, M.D.*
MR in Obstetrics and Gynecology .... *S. M. McCarthy, M.D., Ph.D.*
Proffered Papers T011-T012

**2:45 pm - 3:00 pm**
*Coffee Break* ..... Americas Hall I and II

**3:00 pm - 3:45 pm**
Proffered Papers T013-T015

**3:45 pm - 5:00 pm**
SMRT Business Meeting

# Educational Program

West Ballroom

## Saturday, April 25

**8:00 am - 10:00 am**
***Moderator:*** *A. S. Smith, M.D.*

Physics/MR Acronyms ..... *R. E. Hendrick, Ph.D.*
Brain Imaging Optimization ..... *M. N. Brant-Zawadzki, M.D.*
Brain Tumors ..... *A. S. Smith, M.D.*
Congenital Brain ..... *W. S. Ball, Jr., M.D.*

**10:00 am - 10:30 am**
*Coffee Break* ..... Rendezvous Trianon

**10:30 am - 12:00 pm**
***Moderator:*** *W. G. Bradley, Jr., M.D., Ph.D.*

White Matter/
Hydrocephalus ..... *W. G. Bradley, Jr., M.D., Ph.D.*
Fast Scanning ..... *S. W. Atlas, M.D.*
Cerebrovascular Disease: Anatomy,
Pathophysiology and MRI ..... *E. K. Fram, M.D.*

**12:00 pm - 1:30 pm**
*Luncheon* ..... Sutton Complex, Second Floor

**1:30 pm - 3:00 pm**
***Moderator:*** *T. J. Masaryk, M.D.*

Head and Neck ..... *W. R. K. Smoker, M.D.*
MR Angiography ..... *T. J. Masaryk, M.D.*
Spine Anatomy: MRI and Cryotome Sections . *V. M. Haughton, M.D.*

**3:00 pm - 3:30 pm**
*Coffee Break* ..... Rendezvous Trianon

**3:30 pm - 5:00 pm**
***Moderator:*** *G. K. Sze, M.D.*

Degenerative Disk Disease ..... *E. J. Russell, M.D.*
MR of Intradural Spine ..... *G. K. Sze, M.D.*
Congenital Spine ..... *T. P. Naidich, M.D.*

## Sunday, April 26

**8:00 am - 10:00 am**
***Moderator:*** *P. L. Choyke, M.D.*

Liver: Hepatic MRI ..... *D. G. Mitchell, M.D.*
Abdomen: MRI of Kidney, Adrenal and
Retroperitoneum ..... *P. L. Choyke, M.D.*
Pelvis ..... *H. Y. Kressel, M.D.*
MRI of the Pediatric Abdomen ..... *G. S. Bissett, M.D.*

**10:00 am - 10:30 am**
*Coffee Break* ..... Americas Hall I and II

**10:30 am - 12:00 pm**
***Moderator:*** *C. E. Spritzer, M.D.*

Body Technique Optimization ..... *R. L. Ehman, M.D.*
Practical Aspects of Vascular MR Imaging .... *C. E. Spritzer, M.D.*
Cardiac ..... *R. D. White, M.D.*

**12:00 pm - 1:30 pm**
*Luncheon* ..... Americas Hall I and II

**1:30 pm - 3:00 pm**
***Moderator:*** *L. L. Seeger, M .D.*

Musculoskeletal Optimization ..... *T. H. Berquist, M.D.*
MR Imaging of the Knee ..... *J. V. Crues, III, M.D.*
MR Imaging of the Shoulder ..... *L. L. Seeger, M.D.*

**3:00 pm - 3:30 pm**
*Coffee Break* ..... Americas Hall I and II

**3:30 pm - 5:00 pm**
***Moderator:*** *J. B. Kneeland, M.D.*

MR Imaging of the Foot and Ankle ..... *Z. S. Rosenberg, M.D.*
MR Imaging of the Hand, Wrist and Elbow ... *J. B. Kneeland, M.D.*
MR Imaging of Bone Tumor and
Other Marrow Disorders ..... *J. Beltran, M.D.*

## Monday, April 27 MRI Economics Symposium

***Moderators:***
*G. L. Wolf, M.D., Ph.D.*
*S. W. Young, M.D.*

**8:00 am - 10:15 am**
Field Strengths and Site Planning ..... *M. J. Bronskill, Ph.D.*
Vendor Selection: Implications for Operational Economics ..... *A. J. Lazos, Ph.D.*
Competition in the Diffusion of MRI Scanners ..... *B. R. Hillman, M.D.*

**10:15 am - 10:45 am**
*Coffee Break* ..... Americas Hall I and II

**10:45 am - 12:30 pm**
Competition Among Imagers and Imaging Facilities: Anti Trust Implications ..... *H. S. Allen, Jr., J.D.*
Contrast Media Research: Implications for MRI Reimbursement ..... *G. L. Wolf, M.D., Ph.D.*

**12:30 pm - 1:30 pm**
*Luncheon* ..... Americas Hall I and II

**1:30 pm - 3:00 pm**
A Strategy for Dealing with Self Referral for Imaging Services ..... *M. N. Brant-Zawadzki, M.D.*
Optimizing Throughput Without Sacrificing Quality ..... *K. C. Johnson, M.S.*
Architectural Planning: Implications for Patient Throughput ..... *K. C. Johnson, M.S.*

**3:00 pm - 3:45 pm**
*Coffee Break* ..... Americas Hall I and II

**3:45 pm - 5:30 pm**
Marketing of MRI ..... *M. A. Solomon, M.D.*
Strategic Planning, Reimbursement and Competitive Strategies in MRI ..... *S. W. Young, M.D.*

# Scientific Program

**East Ballroom**

## Sunday, April 26 Topical Conference MR Angiography

**8:00 am - 10:00 am : Head and Neck MRA**
***Moderator:*** *T. M. Grist, M.D.*

Overview of MRA Techniques ..... *P. J. Keller, Ph.D.*
Clinical Experience at Cleveland Clinic ..... *T. J. Masaryk, M.D.*
Neuroradiologic Applications of MRA ..... *E. K. Fram, M.D.*
Clinical Experience at Emory University ..... *S. B. Peterman, M.D.*

**10:00 am - 10:30 am**
*Coffee Break* ..... Americas Hall I and II

**10:30 am - 12:15 am : Challenges for MRA**
***Moderator:*** *W. G. Bradley, Jr., M.D., Ph.D.*

MRA of the Vascular System: A Surgeon's Perspective ..... *T. S. Riles, M.D.*
Pulse Sequences for MRA ..... *D. L. Parker, Ph.D.*
Post Processing and Display Technology ..... *H. E. Cline, Ph.D.*

**12:15 pm - 1:30 pm**
*Luncheon* ..... Americas Hall I and II

**1:30 pm - 3:00 pm : Techniques for MRA**
***Moderator:*** *C. Dumoulin, Ph.D.*

Techniques for MRA of the Extremities ..... *D. P. Flamig, Ph.D.*
Techniques for MRA of the Body ..... *R. R. Edelman, M.D.*
MR Angiography of Coronary and Cardiac Vessels ..... *D. G. Nishimura, Ph.D.*

**3:00 pm - 3:30 pm**
*Coffee Break* ..... Americas Hall I and II

**3:30 pm - 5:15 pm : New Horizons for MRA**
***Moderator:*** *R. R. Edelman, M.D.*

Flow Velocity Quantification ..... *D. N. Firmin, Ph.D.*
Current Status of MRA Economics ..... *S. W. Young, M.D.*
Future Directions for MRA ..... *E. M. Haacke, Ph.D.*

## Monday, April 27

**8:00 am - 9:30 am : The First Decade of MRI**
***Moderator:*** *E. M. Haacke, Ph.D.*

Award Presentations ..... *E. M. Haacke, Ph.D.*
History of SMRI ..... *F. W. Smith, M.D.*
Advances in MRI ..... *P. C. Lauterbur, Ph.D.*
Advances in Magnetic Resonance Spectroscopy ..... *J. Frahm, Ph.D.*
Rabi Award Paper Presentation: Spectroscopic Imaging in Epilepsy ..... *J. W. Hugg, Ph.D.*

**9:30 am - 10:00 am**
SMRI Business Meeting

**10:00 am - 10:45 am**
*Coffee Break* ..... Americas Hall I and II

**10:45 am - 12:30 pm**
Proffered Papers ..... Second Floor Meeting Rooms

**12:30 pm - 1:30 pm**
*Luncheon* ..... Americas Hall I and II

**1:30 pm - 3:00 pm : Rapid Imaging**
***Moderator:*** *M. L. Wood, Ph.D.*

Strategies for Covering K-Space ..... *F. W. Wehrli, Ph.D.*
Fast Spin Echo Imaging ..... *F. A. Jolesz, M. D.*
Magnetization Preparation Sequences: A More Versatile Control of Image Contrast ..... *J. P. Mugler, III, Ph.D.*

**3:00 pm - 3:45 pm**
*Coffee Break* ..... Americas Hall I and II

**3:45 pm - 5:30 pm**
Proffered Papers ..... Second Floor Meeting Rooms

## Tuesday, April 28

**8:00 am - 9:30 am : Advances in Neurological MRI**
***Moderator:*** *W. Kucharczyk, M.D.*

Diffusion/Perfusion and Functional MRI ..... *M. E. Moseley, Ph.D.*
MR Imaging in the Spine: Faster and Better ..... *G. K. Sze, M.D.*
Contrast Agents for Neurological MRI ..... *M. N. Brant-Zawadzki, M.D.*

**9:30 am - 10:30 am**
*Coffee Break* ..... Americas Hall I and II

**10:30 am - 12:15 pm**
Proffered Papers ..... Second Floor Meeting Rooms

**12:15 pm - 1:30 pm**
*Luncheon* ..... Americas Hall I and II

**1:30 pm - 3:00 pm : New Clinical Applications**
***Moderator:*** *M. J. Bronskill, Ph.D.*

MRI of the Chest ..... *R. J. Herfkens, M.D.*
Fat Suppressed MRI of the Breast ..... *S. E. Harms, M.D.*
Interventional MRI ..... *R. B. Lufkin, M.D.*

**3:00 pm - 3:45 pm**
*Coffee Break* ..... Americas Hall I and II

**3:45 pm - 5:30 pm**
Proffered Papers ..... Second Floor Meeting Rooms

## Wednesday, April 29

**8:00 am - 9:30 am : Challenges for Shoulder Imaging**
***Moderator:*** *J. V. Crues, III, M.D.*

Intro. to Challenges for Shoulder Imaging ..... *J. V. Crues, III, M.D.*
Evaluation of Rotator Cuff Tears: Conventional MRI vs. MR Arthrography ..... *B. D. Flannigan Sprague, M.D.*
Diagnosis of Rotator Cuff Tears without Gd DTPA ..... *M. Rafii, M.D.*
Diagnosis of Shoulder Instability with Gd DTPA ..... *J. J. Busch, M.D.*
Diagnosis of Shoulder Instability without Gd DTPA ..... *M. B. Zlatkin, M.D.*

**9:30 am - 10:30 am**
*Coffee Break* ..... Americas Hall I and II

**10:30 am - 12:15 pm**
*Proffered Papers* ..... Second Floor Meeting Rooms

**12:15 pm - 1:00 pm**
*Luncheon* ..... Americas Hall I and II

**1:00 pm - 2:30 pm**
**Frontiers in Body Imaging**
***Moderator:*** *J. C. Weinreb, M.D.*

Manganese Contrast Agents for the Liver ..... *M. E. Bernardino, M.D.*
Contrast Agents for MRI ..... *D. D. Stark, M.D.*
Rapid Scan MR Imaging of the Abdomen ..... *S. J. Riederer, Ph.D.*

**2:30 pm - 2:45 pm**
*Coffee Break* ..... Americas Hall I and II

**2:45 pm - 4:30 pm**
Proffered Papers ..... Second Floor Meeting Rooms

# Scientific Program Proffered Papers
## MONDAY, APRIL 26

## 10:45 am - 12:30 pm

**Papers 001-008**
**Ultrafast Imaging**
Beekman Parlor

***Moderators:***
*A. P. Crawley, Ph.D.*
*S. J. Riederer, Ph.D.*

001 **10:45 am**
002 **10:57 am**
003 **11:09 am**
004 **11:21 am**
005 **11:33 am**
006 **11:45 am**
007 **11:57 am**
008 **12:09 pm**

**Papers 009-016**
**Soft Tissue/Marrow**
Sutton Parlor North

***Moderators:***
*J. Beltran, M.D.*
*P. T. Weatherall, M.D.*

009 **10:45 am**
010 **10:57 am**
011 **11:09 am**
012 **11:21 am**
013 **11:33 am**
014 **11:45 am**
015 **11:57 am**
016 **12:09 pm**

**Papers 017-023**
**Proton MRS of Human Brain**
Sutton Parlor Center

***Moderators:***
*J. Frahm, Ph.D.*
*R. J. Ordidge, Ph.D.*

017 **10:45 am**
018 **10:57 am**
019 **11:09 am**
020 **11:21 am**
021 **11:33 am**
022 **11:45 am**
023 **11:57 am**

**Papers 024-031**
**MRA Techniques**
Sutton Parlor South

***Moderators:***
*R. L. Ehman, M.D.*
*D. G. Nishimura, Ph.D.*

024 **10:45 am**
025 **10:57 am**
026 **11:09 am**
027 **11:21 am**
028 **11:33 am**
029 **11:45 am**
030 **11:57 am**
031 **12:09 pm**

**Papers 032-039**
**Contrast Agents: Experimental**
Regent Parlor

***Moderators:***
*T. J. Brady, M.D.*
*P. A. Rinck, M.D.*

032 **10:45 am**
033 **10:57 am**
034 **11:09 am**
035 **11:21 am**
036 **11:33 am**
037 **11:45 am**
038 **11:57 am**
039 **12:09 pm**

## 3:45 pm - 5:30 pm

**Papers 040-047**
**RARE**
Beekman Parlor

***Moderators:***
*D. B. Plewes, Ph.D.*
*H. E. Simon, Ph.D.*

040 **3:45 pm**
041 **3:57 pm**
042 **4:09 pm**
043 **4:21 pm**
044 **4:33 pm**
045 **4:45 pm**
046 **4:57 pm**
047 **5:09 pm**

**Papers 048-055**
**Flow Quantification**
Sutton Parlor North

***Moderators:***
*P. J. Keller, Ph.D.*
*F. W. Wehrli, Ph.D.*

048 **3:45 pm**
049 **3:57 pm**
050 **4:09 pm**
051 **4:21 pm**
052 **4:33 pm**
053 **4:45 pm**
054 **4:57 pm**
055 **5:09 pm**

**Papers 056-062**
**MRS of Cerebral Metabolism**
Sutton Parlor Center

***Moderators:***
*T. R. Brown, Ph.D.*
*R. K. Gupta, Ph.D.*

056 **3:45 pm**
057 **3:57 pm**
058 **4:09 pm**
059 **4:21 pm**
060 **4:33 pm**
061 **4:45 pm**
062 **4:57 pm**

**Papers 063-070**
**MRA: Brain and Neck**
Sutton Parlor South

***Moderators:***
*S. W. Atlas, M.D.*
*A. W. Litt, M.D.*

063 **3:45 pm**
064 **3:57 pm**
065 **4:09 pm**
066 **4:21 pm**
067 **4:33 pm**
068 **4:45 pm**
069 **4:57 pm**
070 **5:09 pm**

**Papers 071-079**
**Contrast Agents: Hepatobiliary and GI**
Regent Parlor

***Moderators:***
*D. G. Mitchell, M.D.*
*D. D. Stark, M.D.*

071 **3:45 pm**
072 **3:57 pm**
073 **4:09 pm**
074 **4:21 pm**
075 **4:33 pm**
076 **4:45 pm**
077 **4:57 pm**
078 **5:09 pm**
079 **5:21 pm**

**PERSONAL ITINERARY:**

**Morning**

**Afternoon**

# Scientific Program Proffered Papers
## TUESDAY, APRIL 27

## 10:30 am - 12:15 pm

**Papers 101-108**
**Rapid Imaging: Clinical Applications**
Beekman Parlor

***Moderators:***
*C. E. Spritzer, M.D.*
*D. A. Vallet, Ph.D.*

101 **10:30 am**
102 **10:42 am**
103 **10:54 am**
104 **11:06 am**
105 **11:18 am**
106 **11:30 am**
107 **11:42 am**
108 **11:54 am**

**Papers 109-116**
**Brain**
Sutton Parlor North

***Moderators:***
*M. N. Brant-Zawadzki, M.D.*
*G. Bydder, M.D.*

109 **10:30 am**
110 **10:42 am**
111 **10:54 am**
112 **11:06 am**
113 **11:18 am**
114 **11:30 am**
115 **11:42 am**
116 **11:54 am**

**Papers 117-123**
**Multinuclear MRS**
Sutton Parlor Center

***Moderators:***
*R. G. Gonzalez, Ph.D.*
*R. E. Lenkinzki, Ph.D.*

117 **10:30 am**
118 **10:42 am**
119 **10:54 am**
120 **11:06 am**
121 **11:18 am**
122 **11:30 am**
123 **11:42 am**

**Papers 124-131**
**MRA: Heart, Kidneys and Peripheral Vessels**
Sutton Parlor South

***Moderators:***
*D. E. Bohning, Ph.D.*
*S. W. Young, M.D.*

124 **10:30 am**
125 **10:42 am**
126 **10:54 am**
127 **11:06 am**
128 **11:18 am**
129 **11:30 am**
130 **11:42 am**
131 **11:54 am**

**Papers 132-139**
**Perfusion, Diffusion and Functional Imaging**
Regent Parlor

***Moderators:***
*M. S. Cohen, Ph.D.*
*J. R. MacFall, Ph.D.*

132 **10:30 am**
133 **10:42 am**
134 **10:54 am**
135 **11:06 am**
136 **11:18 am**
137 **11:30 am**
138 **11:42 am**
139 **11:54 am**

## 3:45 pm - 5:30 pm

**Papers 140-147**
**Rapid Imaging: Interventional and 3-D**
Beekman Parlor

***Moderators:***
*R. Kikinis, M.D.*
*R. B. Lufkin, M.D.*

140 **3:45 pm**
141 **3:57 pm**
142 **4:09 pm**
143 **4:21 pm**
144 **4:33 pm**
145 **4:45 pm**
146 **4:57 pm**
147 **5:09 pm**

**Papers 148-155**
**Muscle/Joints**
Sutton Parlor North

***Moderators:***
*R. Kier, M.D.*
*J. B. Kneeland, M.D.*

148 **3:45 pm**
149 **3:57 pm**
150 **4:09 pm**
151 **4:21 pm**
152 **4:33 pm**
153 **4:45 pm**
154 **4:57 pm**
155 **5:09 pm**

**Papers 156-163**
**Cardiac Imaging**
Sutton Parlor Center

***Moderators:***
*L. Eastwood, Ph.D.*
*C. B. Higgins, M.D.*

156 **3:45 pm**
157 **3:57 pm**
158 **4:09 pm**
159 **4:21 pm**
160 **4:33 pm**
161 **4:45 pm**
162 **4:57 pm**
163 **5:09 pm**

**Papers 164-172**
**MRA and Perfusion Techniques**
Sutton Parlor South

***Moderators:***
*W. T. Dixon, Ph.D.*
*O. Nalcioglu, Ph.D.*

164 **3:45 pm**
165 **3:57 pm**
166 **4:09 pm**
167 **4:21 pm**
168 **4:33 pm**
169 **4:45 pm**
170 **4:57 pm**
171 **5:09 pm**
172 **5:21 pm**

**Papers 173-180**
**Contrast Agents: Chest, Breast and Bone**
Regent Parlor

***Moderators:***
*V. M. Runge, M.D.*
*D. Thickman, M.D.*

173 **3:45 pm**
174 **3:57 pm**
175 **4:09 pm**
176 **4:21 pm**
177 **4:33 pm**
178 **4:45 pm**
179 **4:57 pm**
180 **5:09 pm**

**Papers 181-189**
**Artifacts and Safety**
Nassau Suite

***Moderators:***
*R. R. Price, Ph.D.*
*S. R. Thomas, Ph.D.*

181 **3:45 pm**
182 **3:57 pm**
183 **4:09 pm**
184 **4:21 pm**
185 **4:33 pm**
186 **4:45 pm**
187 **4:57 pm**
188 **5:09 pm**
189 **5:21 pm**

## PERSONAL ITINERARY:

**Morning**

**Afternoon**

# Scientific Program Proffered Papers
## WEDNESDAY, APRIL 28

## 10:30 am - 12:15 pm

**Papers 201-208**
**Knee/Shoulder**
Sutton Parlor North

***Moderators:***
*J. J. Busch, M.D.*
*F. G. Shellock, Ph.D.*

201 **10:30 am**
202 **10:42 am**
203 **10:54 am**
204 **11:06 am**
205 **11:18 am**
206 **11:30 am**
207 **11:42 am**
208 **11:54 am**

**Papers 209-216**
**Spine/Head and Neck**
Sutton Parlor Center

***Moderators:***
*K. R. Maravilla, M.D.*
*J. S. Ross, M.D.*

209 **10:30 am**
210 **10:42 am**
211 **10:54 am**
212 **11:06 am**
213 **11:18 am**
214 **11:30 am**
215 **11:42 am**
216 **11:54 am**

**Papers 217-224**
**Abdomen**
Sutton Parlor South

***Moderators:***
*P. L. Davis, M.D.*
*P. Y. Poon, M.D.*

217 **10:30 am**
218 **10:42 am**
219 **10:54 am**
220 **11:06 am**
221 **11:18 am**
222 **11:30 am**
223 **11:42 am**
224 **11:54 am**

**Papers 225-232**
**Image Processing**
Regent Parlor

***Moderators:***
*L. P. Clarke, Ph.D.*
*J. L. Duerk, Ph.D.*

225 **10:30 am**
226 **10:42 am**
227 **10:54 am**
228 **11:06 am**
229 **11:18 am**
230 **11:30 am**
231 **11:42 am**
232 **11:54 am**

**Papers 233-240**
**Relaxometry and Experimental Contrast Agents**
Murray Hill Suite

***Moderators:***
*P. A. Hardy, Ph.D.*
*R. L. Nunnally, Ph.D.*

233 **10:30 am**
234 **10:42 am**
235 **10:54 am**
236 **11:06 am**
237 **11:18 am**
238 **11:30 am**
239 **11:42 am**
240 **11:54 am**

## 2:45 pm - 4:30 pm

**Papers 241-248**
**Rapid Imaging**
Sutton Parlor North

***Moderators:***
*D. P. Flamig, Ph.D.*
*J. Listerud, Ph.D., M.D.*

241 **2:45 pm**
242 **2:57 pm**
243 **3:09 pm**
244 **3:21 pm**
245 **3:33 pm**
246 **3:45 pm**
247 **3:57 pm**
248 **4:09 pm**

**Papers 249-256**
**Brain/Orbit**
Sutton Parlor Center

***Moderators:***
*B. D. Pressman, M.D.*
*W. T. C. Yuh, M.D., M.S.E.E.*

249 **2:45 pm**
250 **2:57 pm**
251 **3:09 pm**
252 **3:21 pm**
253 **3:33 pm**
254 **3:45 pm**
255 **3:57 pm**
256 **4:09 pm**

**Papers 257-264**
**Chest/Pelvis**
Sutton Parlor South

***Moderators:***
*M. J. Fulmer, M.D.*
*D. H. Sostman, M.D.*

257 **2:45 pm**
258 **2:57 pm**
259 **3:09 pm**
260 **3:21 pm**
261 **3:33 pm**
262 **3:45 pm**
263 **3:57 pm**
264 **4:09 pm**

**Papers 265-272**
**Pulse Sequences**
Regent Parlor

***Moderators:***
*L. Axel, M.D.*
*B. K. Rutt, Ph.D.*

265 **2:45 pm**
266 **2:57 pm**
267 **3:09 pm**
268 **3:21 pm**
269 **3:33 pm**
270 **3:45 pm**
271 **3:57 pm**
272 **4:09 pm**

**Papers 273-280**
**Contrast Agents: Hepatobiliary and GI**
Murray Hill Suite

***Moderators:***
*M. E. Bernardino, M.D.*
*G. D. Fullerton, Ph.D.*

273 **2:45 pm**
274 **2:57 pm**
275 **3:09 pm**
276 **3:21 pm**
277 **3:33 pm**
278 **3:45 pm**
279 **3:57 pm**
280 **4:09 pm**

## PERSONAL ITINERARY:

**Morning**

**Afternoon**

# Evening Tutorial Program

## Sunday, April 26

**5:30 pm - 7:30 pm**

Musculoskeletal ..... *J. V. Crues, III, M.D.*
Beekman Parlor *L. L. Seeger, M.D.*
*J. B. Kneeland, M.D.*

Introduction to Physics ..... *P. L. Davis, M.D.*
Sutton Parlor North *J. Listerud, Ph.D., M.D.*
*P. J. Keller, Ph.D.*

## Monday, April 27

**5:30 pm - 7:30 pm**

Body ..... *R. J. Herfkens, M.D.*
Beekman Parlor *M. E. Bernardino, M.D.*
*P. G. Fritzsche, M.D.*

Brain ..... *E. K. Fram, M.D.*
Sutton Parlor North *J. H. Simon, M.D., Ph.D.*
*V. M. Runge, M.D.*

## Tuesday, April 28

**5:30 pm - 7:30 pm**

Spine ..... *G. K. Sze, M.D.*
Beekman Parlor *J. S. Ross, M.D.*
*J. R. Jinkins, M.D.*

Application of Physics ..... *K. M. Link, M.D.*
Sutton Parlor North *J. B. Murdoch, Ph.D.*
*W. Sattin, Ph.D.*

# The New York Hilton

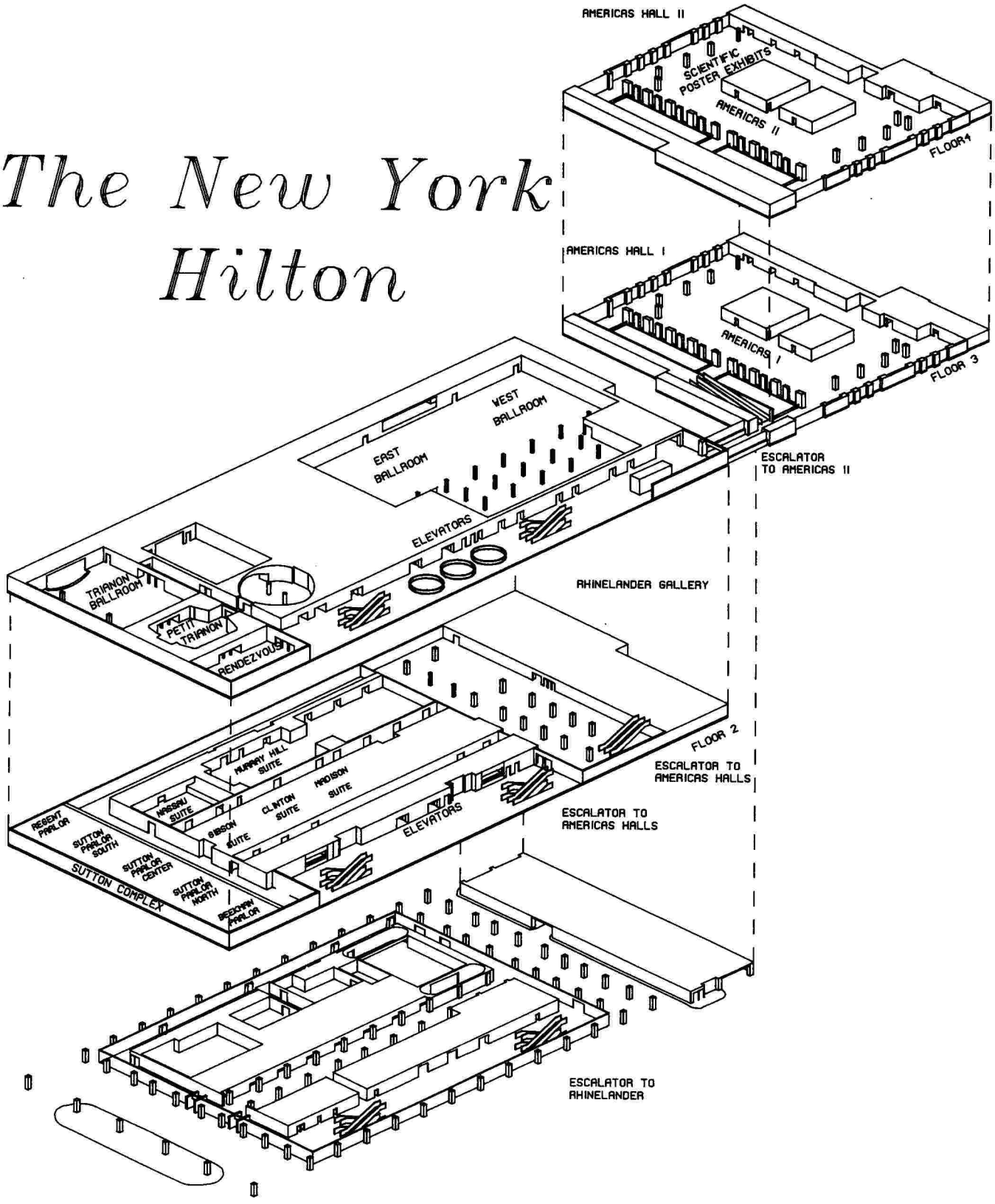

**Editorial**

# SMRI 1992: Annual Meeting Overview

THIS YEAR MARKS THE 10th anniversary of the Annual Meeting of the Society for Magnetic Resonance Imaging (SMRI). The 1992 meeting, to be held in New York City, promises to be one of the most memorable in the history of the Society. The SMRI had its tentative beginnings after an organizational meeting held in Houston in 1982. The first scientific meeting of the SMRI was held at the Broadmoor Hotel in Denver in 1983, and since that small gathering, the Society has grown steadily in size and diversity, gaining wide recognition for carrying out its chosen mandate of promoting educational, scientific, and technical information dissemination to a multidisciplinary group of clinical and basic scientists involved in magnetic resonance (MR) imaging. In this year's program, the Society continues its successful tradition of fostering communication among the medical users of the modality, basic scientists, engineers, and support personnel. While the submissions of papers for the meeting last year indicated some stagnation, we are delighted to report substantial growth in scientific paper submissions, from 419 last year to 506 (+21%). This figure includes scientific papers (403), scientific paper/posters (10), posters (78), and submissions for the Technologist Program (15).

The current program is probably the richest to date as far as the diversity and depth of the program components are concerned. Two concurrent teaching programs will be held on Saturday and Sunday, April 25–26, one designed for physicians/scientists and one for technologists. This will be complemented by an Evening Tutorial program, with sessions on Sunday, Monday, and Tuesday.

As it was last year, the Scientific Program will open on Sunday with a one-day Topical Symposium, which this year is devoted to the rapidly evolving field of MR angiography. The remainder of the Scientific Program will be divided into six sessions, with 18 plenary talks. The scientific papers have been organized into 68 sessions that encompass the entire spectrum of the ever-expanding field of MR. To accommodate the increase in oral papers, it was necessary to add an additional parallel session, bringing the number of concurrent paper presentations to seven, and thus posting a particular challenge for subdividing these into appropriate topical categories.

The success last year of the MR imaging economic symposium clearly called for a repeat of this event. This one-day symposium will be held concurrently with the Scientific Program and is likely to attract substantial attendance by people involved in managerial aspects of MR imaging.

The program would not have become reality without the dedication of all those who took on responsibility for its development and execution. We therefore express our sincere thanks to the chairmen of the individual program components. First and foremost, our thanks go to the Co-chairmen of the Scientific Program, Steven Harms, MD, Walter Kucharczyk, MD, and Michael Wood, PhD, who were responsible for designing the Scientific Program, the paper review process, and the organization of the very large number of proffered paper sessions. We further gratefully acknowledge the leadership and dedication of the following individuals: Scott Atlas, MD, and Stephen J. Riederer, PhD, (Poster Program); Jeffrey C. Weinreb, MD (local arrangements), David Thickman, MD, Jeffrey S. Ross, MD, and Laurence P. Clarke, PhD (Educational Program), Paul J. Keller, PhD, William Sattin, PhD, and William T.C. Yuh, MD (Evening Tutorial), John V. Crues III, MD, Lori B. Irilli, RT, Connie Gibbs, RT, and William Faulkner, RT (Technologist Program). Last but not least, we are indebted to our able and dedicated staff at the Society's Business Office, Kristen Coe, Karen Bacidore, and Patty Sweet.

Mark April 25–29, 1992, as priority dates on your calendar. We are confident that this year's meeting will be a valuable educational and lasting scientific experience for all attendees. We look forward to seeing you in New York at the Tenth Annual Meeting of the SMRI.

FELIX W. WEHRLI, PhD
KENNETH R. MARAVILLA, MD
*Co-Chairmen, Annual Meeting Coordination Committee, and Guest Editors*

**Index terms:** Editorials • Radiology and radiologists, education • Society for Magnetic Resonance Imaging • Society for Magnetic Resonance Imaging, annual meeting

**JMRI 1992;** 2(P):19

# SMRI 1992 ON SITE REGISTRATION FORM

**1. NAME:** (first)_____

(middle)_____

(last)_____ (degree)_____

**2. ADDRESS:**

(Inst., Dept.)_____

(Street)_____

(City/State)_____

(Zip/Country)_____

(Telephone) (_____)_____

**List Guest /Spouse for Registration:**_____

☐ **Exclude my name from exhibitor mailing list.**

**3. PROFESSIONAL AFFILIATIONS:**

| | | | |
|---|---|---|---|
| (a) AAN | (d) ARRS | (g) ESMRMB | (j) SMRM |
| (b) AAPM | (e) ASRN | (h) JMRM | (k)SMRT |
| (c) ACR | (f) ASRT | (i) RSNA | (l) SNM |

**4. CLASSIFICATION CODE:**

Enter number/letter code which best describes your professional classification:_____

**1. Clinical Scientist**
**2. Basic Scientist**
**3. Educational Faculty**
**4. Resident Trainee**
**5. Radiology Support Personnel and Hospital Staff:**

(a) technologist
(b) engineer
(c) radiology business manager
(d) radiology administrator
(e) nurse
(f) hospital administrator
(g) radiology educator
(h) hospital purchasing agent

**6. Qualified Non-Health Sciences Personnel:**

(a) architect
(b) computer analyst

**7. Non-Hospital-Based Medical Care Provider:**

(a) purchasing consultant
(b) equipment consultant
(c) imaging center entreprenuer

**5. PROGRAM SELECTION:**

**Please select appropriate box:**

| | Educational (Incl. Econ. Symp.) | Scientific (Incl. MRA Prog.,) | Both (All) |
|---|---|---|---|
| **MEMBER** | | | |
| ☐ General | ☐ $300 | ☐ $250 | ☐ $45 |
| ☐ Technologist | ☐ $200 | ☐ $175 | ☐ $30 |
| ☐ Student | ☐ $200 | ☐ $175 | ☐ $30 |
| **NON-MEMBER** | | | |
| ☐ General | ☐ $350 | ☐ $350 | ☐ $50 |
| ☐ Technologist | ☐ $225 | ☐ $225 | ☐ $35 |
| ☐ Student | ☐ $225 | ☐ $225 | ☐ $35 |

**SPECIAL**

☐ **One Day (MR Manufacturer's Workshop) $100**
☐ **One Day (MRA Topical Program) $100**
☐ **One Day (MR Economics Symposium) $100**
☐ **Spouse $40**

**6. REGISTRATION FEE:**

**Total Payment (U.S. Funds Only) $**_____

**Editorial**

# SMRI 1992: Scientific Program

THIS IS THE TENTH ANNUAL MEETING of the Society for Magnetic Resonance Imaging (SMRI), and, as such, it has special significance. During this past decade, the SMRI has expanded in step with magnetic resonance (MR) imaging itself. This year's Scientific Program testifies to this growth. One need only peruse the abstracts included in this Printed Program to see just how much the Annual Meeting has grown in size and quality.

A record number of abstracts were submitted for this year's Scientific Program. From about 500 abstracts submitted, the Scientific Program Committee was able to accept about 300 for oral presentation in the regular Scientific Program and Works-in-Progress Program. As anticipated, rapid imaging, MR angiography, and contrast agents were the focus of many abstracts, so the Scientific Program includes parallel sessions on these subjects almost every morning and afternoon.

The overall design of the Scientific Program follows that of previous years. This format has evolved gradually, thanks to the experience of previous Scientific Program committees and the SMRI Central Office. In fact, Kristen Coe, Karen Bacidore, and Patty Sweet at the Central Office have become indispensable in organizing the Annual Meeting. This year's Scientific Program was organized by a larger committee than usual. We are grateful to Truman R. Brown, PhD, Robert E. Lenkinski, PhD, Peter A. Rinck, PhD, and Ronald R. Price, PhD, for their contribution to the Scientific Program Committee. More than 40 people donated their time to review the abstracts. These abstract reviewers are listed in the Printed Program, and we greatly appreciate their contribution. We also thank the people who agreed to serve as moderators. We could not have assembled the Scientific Program without help from all the people mentioned above.

The tradition of beginning the Scientific Program with a full-day Topical Symposium on the opening Sunday continues. This Topical Symposium allows the Program Committee to emphasize one particular subspecialty of MR imaging, without compromising the many other branches. The subject of this year's Topical Symposium is MR angiography. The Topical Symposium on MR angiography is designed for a broad audience, because MR angiography has attracted specialists from diverse branches of medicine. Moreover, MR angiography is accessible to most users of MR imaging, regardless of equipment. This symposium consists entirely of invited presentations summarizing important principles of MR angiography and surveying its applications to all anatomic sites.

The head and neck is perhaps the site most widely examined with MR angiography. Accordingly, one of the primary goals of the Topical Symposium is to derive a consensus for the clinical use of MR angiography in the head and neck. Three experts with several years of experience using equipment from different vendors will outline the role of head and neck MR angiography at their institutions. The ensuing panel discussion is intended to clarify precisely what can be done clinically with MR angiography right now.

MR angiography faces many challenges in its quest for a place in medicine. What clinical decisions can MR angiography help make? This question needs to be discussed with the clinicians who use the information provided by MR angiography. For example, when does a surgeon feel confident in making a clinical decision based on the findings from MR angiography? Exactly how must MR angiographic techniques improve? We have invited speakers to discuss problems with pulse sequences and image display. The presentations delineating the challenges for MR angiography will show researchers what clinicians need from MR angiography and also help clinicians appreciate the technical obstacles facing this modality.

Techniques for MR angiography of the extremities and the body will be discussed, in the hope that these techniques might be used more productively. Methods for measuring flow velocities will be explored. Accurate and precise velocity measurements would expand the scope of MR imaging to an extent that stretches the imagination. Then there are the coronary arteries, which have long evaded MR imaging; however, recent efforts to produce MR images of the coronary arteries show promise. The Topical Symposium concludes with a look toward the future and a chance for the audience and speakers to contemplate the present and future of MR angiography. Similarly to previous meetings, the schedule for Monday, Tuesday, and Wednesday is divided into six half-days. Each half-day begins with plenary lectures, followed by five parallel sessions and one Works-in-Progress session. The plenary lectures review certain subjects considered of general interest to the MR community. These lectures provide a foundation for the new advances to be reported in the parallel sessions.

In recognition that this meeting marks the tenth anni-

**Index terms:** Editorials • Radiology and radiologists, education • Society for Magnetic Resonance Imaging • Society for Magnetic Resonance Imaging, annual meeting

**JMRI 1992;** 2(P):21–22

versary of the SMRI, a special plenary symposium has been organized for Monday morning. This First Decade of MRI Symposium begins with a brief history of the SMRI and is followed by a review of the progress in MR imaging and MR spectroscopy. We are fortunate to have several luminary figures participating in this symposium. As they review the many milestones from the past decade, perhaps we will better appreciate how far MR imaging has come and perhaps also catch a hint of what might lie ahead. Rapid imaging has long captivated the attention of the MR imaging community. It has been the subject of topical symposia at two previous SMRI annual meetings. There are now so many rapid MR imaging techniques, that it would be useful to consolidate them. Technical features shared by many rapid imaging techniques constitute the subject for the Rapid Imaging Symposium on Monday afternoon. A distinguishing characteristic of many rapid imaging techniques is the order in which data are collected or, more technically, the k-space trajectory. The symposium includes a presentation on a technique known as RARE (rapid acquisition with relaxation enhancement), fast spin echo, or turbo spin echo, depending on the vendor. This technique elicits multiple echoes after each radio-frequency (RF) pulse, designating these echoes as distinct phase-encoding steps. This saves time by reducing the total number of separate RF excitations. The symposium includes a third topic, magnetization preparation, which is used in ultrafast imaging techniques such as TurboFLASH (fast low-angle shot) and MP-RAGE (magnetization-prepared rapid gradient echo). Given the advances in ultrafast MR imaging presented at last year's meeting, we need to appreciate the concept of first preparing the magnetization, letting the magnetization evolve for a designated period, and then acquiring the data rapidly.

Although a great deal of attention in neurologic MR imaging has focused on the developments and clinical applications of MR angiography, other innovations are equally exciting. Three of these have been chosen for the plenary lectures on Tuesday morning. "Diffusion and Perfusion and Functional MR Imaging" will cover the fascinating research demonstrating the capability of MR imaging to examine the effects of various stimuli and pharmacologic manipulations on cerebral function. "MR Imaging of the Spine: Faster and Better" will emphasize the enhanced capabilities provided by new hardware and software, such as multiplexed phased-array coils, fast spin-echo pulse sequences, and 512-pixel resolution. Better images covering more anatomy are being acquired with ever increasing speed. The third lecture, "Advances in Neurologic MR Imaging: Contrast Agents," concerns the clinical use of contrast agents. Paramagnetic contrast agents have been used longer for neurologic diagnosis than in any other anatomic area. Despite these many years of use, there exists a wide variety of clinical indications and frequency of administration. New agents are now entering clinical practices, and different pulse sequences are being used for postcontrast imaging. This lecture will provide an overview of important indications for contrast agent use, analyze the similarities and differences among agents, and discuss the advantages of various postcontrast imaging methods.

Several developments could open entirely new applications for MR imaging. New techniques for imaging the breast might possibly extend the diagnostic capability of MR imaging beyond that of conventional mammography. The development of extremely short TE MR imaging techniques is interesting for imaging of the chest, because these techniques enable evaluation of lung parenchyma. The concept of using MR imaging to guide various therapies is being explored for applications such as laser surgery and hyperthermia. These exciting new uses for MR imaging are the subject of the New Clinical Applications Symposium on Tuesday afternoon.

The Challenges for Shoulder Imaging Symposium on Wednesday morning addresses an important clinical issue for the many radiologists who practice shoulder imaging. This symposium brings together five experts to discuss two approaches for diagnosing rotator cuff disease and shoulder instability. The question they try to answer is, should these shoulder examinations be done with gadopentetate dimeglumine (Gd-DTPA) or without any contrast agents? A panel discussion after the brief presentations will evaluate the pros and cons of the two approaches for examining the shoulder.

Innovative strategies for body imaging are emerging. Manganese-based contrast agents will be discussed in detail, with predictions as to the future role for these agents and for MR imaging diagnosis in the body. Particulate agents have been proposed for imaging the bowel, liver, bone marrow, and lymph nodes. These agents will be described along with potential clinical applications. Rapid imaging methods, including MR fluoroscopy, are now emerging for clinical use. These new methods will be reviewed along with early clinical examples.

Throughout the past decade, the friendly atmosphere at SMRI meetings has encouraged clinicians, clinical scientists, and basic scientists to discuss problems and share ideas. We hope that this Scientific Program will continue that admirable tradition, providing a forum for basic scientists and clinical scientists to present their research and learn about the progress of others. With this as our goal, it has been both a privilege and pleasure to assemble the Scientific Program.

STEVEN E. HARMS, MD
WALTER KUCHARCZYK, MD
MICHAEL L. WOOD, PhD
*Co-Chairmen of the Scientific Program and Guest Editors*

**Editorial**

# A 10-Year History of the SMRI

ALTHOUGH NUCLEAR MAGNETIC RESONANCE (MR) had been demonstrated in 1946 and had grown into a major analytic instrument in chemistry and physics over the subsequent decades, it was not until 1973 that Dr Paul Lauterbur demonstrated its imaging capabilities. Two years earlier, in 1971, Dr Ray Damadian published his work in *Science* that described relaxation differences between cancerous and normal cells. A natural question was whether the two discoveries would merge. Sharad Amtey, PhD, a medical physicist and innocent bystander to these events, was in Europe a short time later and had the opportunity to discuss these developments with Drs Mallard, Hutchison, and the Aberdeen group and Dr Peter Mansfield and his colleagues in Nottingham, who convinced him of the promise of this new imaging modality. Because he witnessed and participated in the birth, growth, and evolution of nuclear medicine, Dr Amtey's interest was piqued.

On his return to Houston, Dr Amtey realized that for the exciting new modality to be brought not only into the marketplace but also into clinical application a concerted cooperative effort between basic scientists and physicians would be required. Specifically, he believed that a massive developmental effort and sharing of information beyond that which normally occurs in the university setting was required to demonstrate the utility of MR imaging to physicians. In an attempt to begin this mutual cooperation, the "First Annual Workshop on Nuclear Magnetic Resonance Imaging" was planned for Houston, in early 1981.

At the Royal Society Meeting (March 14–15, 1979) in London, Drs Andrew, Lauterbur, Damadian, Mansfield, Moore, Mallard, Locher, and Hoult and Dr Ian Young and the EMI group (and many others not in imaging) presented many interesting MR results, including discussions of three-dimensional and T1 imaging. A short time later, on October 26–27, 1980, what many consider to be the first organized MR imaging symposium in the United States occurred in Nashville, under the auspices of Drs Everette James and Leon Partain at Vanderbilt. An impressive faculty attended, with growing interest among the attendees in formalizing a unified organizing body.

To help organize Dr Amtey's First Workshop, Steve Thomas, PhD, another medical physicist and member of the American Association of Physicists in Medicine (AAPM), was contacted after some initial discussions. Drs Thomas and Amtey approached the AAPM's Continuing Education Committee, chaired by Gary Fullerton, PhD, to determine if the AAPM would cosponsor the gathering. At the time, the AAPM had no MR committee (they did, however, have the MR Task Group of the General Medical Physics Committee) and, ironically, questioned whether they should help sponsor the meeting because there were "no AAPM members involved in medical NMR." Fortunately, the potential of the new modality, and opportunities for physicists in the future, persuaded the AAPM to cosponsor the event. In 1982, the AAPM formally established a stand-alone MR committee.

The First Annual Workshop on Nuclear Magnetic Resonance Imaging was held on February 19–20, 1981, in Houston, under the directorship of Dr Amtey. The meeting was a notable success, drawing such people to the faculty as Drs Lauterbur, Damadian Tom Budinger, Paul Bottomley, Lawrence Crooks, Carlton Hazlewood, Bill Edelstein, and many others. The belief that a society was warranted began to surface.

After the success of the first meeting, a second workshop on MR imaging was held eight months later, on October 1–3, 1981, at the Bowman Gray School of Medicine in Winston-Salem, NC. The meeting had essentially the same faculty, with the participation of Drs Graeme Bydder, Frank Smith, Brian Worthington, and Ian Young from Great Britain, and was organized by Drs Partain, Crooks, James, Lauterbur, Nolan Karstaedt, C. Douglas Maynard, William Moore, and Richard Witcofski. It is interesting to note that up until that time, there was considerably less MR imaging activity in the United States than in Europe. Dr John Gore remembers that "most conferences in the United States relied heavily on the Aberdeen group, the Hammersmith-EMI group, Dr Mansfield, and Dr Bill Moore. Of course, some images from the States were being obtained by Leon Kaufman on his small-bore animal instrument as well."

The Bowman Gray meeting represents the point at which considerable serious discussion and organizational meetings about the formation of an MR society emerged. Dr Amtey began circulating information and applications for such a society. It was to include basic scientists and physicians. Unfortunately, many thought that it was presumptuous of someone with interest but no training in MR to be the founder of the society. Similarly, others thought that it was inappropriate to have physicians (users) as equal members with basic scientists (developers). Two separate groups emerged: one

**Index terms:** Editorials • Society for Magnetic Resonance Imaging • Society for Magnetic Resonance Imaging, annual meeting

**JMRI 1992;** 2(P):23–26

**History of the SMRI**

| Year | Annual Meeting | President |
|---|---|---|
| 1980 | October—First U.S. meeting on MR imaging, Nashville | Organized by Vanderbilt University group |
| 1981 | February—First Workshop on MR imaging, Houston | Organized by Sharad R. Amtey, PhD |
| | October—Bowman Gray workshop on MR imaging, Winston-Salem, NC | |
| 1982 | March—Second Annual Workshop on MR imaging, Houston | SMRI chartered after meeting |
| 1983–1984 | March 1983—First Annual Meeting of SMRI, Colorado Springs | Francis W. Smith, MD, followed by Sharad R. Amtey, PhD |
| 1984–1985 | March 1984—Second Annual Meeting, Orlando | William S. Moore, PhD (died), followed by Luis E. Todd, MD |
| 1985–1986 | 1985—Third Annual Meeting, San Diego | Luis E. Todd, MD |
| 1986–1987 | 1986—Fourth Annual Meeting, Philadelphia | Gary D. Fullerton, PhD |
| 1987–1988 | 1987—Fifth Annual Meeting, San Antonio | Gary D. Fullerton, PhD |
| 1988–1989 | 1988—Sixth Annual Meeting, Boston | William G. Bradley, Jr, MD, PhD |
| 1989–1990 | 1989—Seventh Annual Meeting, Los Angeles | R. Edward Hendrick, PhD |
| 1990–1991 | 1990—Eighth Annual Meeting, Washington, DC | Robert B. Lufkin, MD |
| 1991–1992 | 1991—Ninth Annual Meeting, Chicago | E. Mark Haacke, PhD |

composed of those with classical training and experience in MR spectroscopy and another consisting of individuals with interest but less formal MR and/or clinical training. Dr Hazlewood described it thusly: "There was a division between those with 'pedigree' [ie, classical MR training] and the mavericks with a broader 'bootstrap' education."

After several attempts to resolve the differences between the two groups, it became apparent that a unified society was not going to evolve. As Dr Bottomley reflected: "The Meeting [which was a final attempt to develop into one, unsegregated society] was called off. The cliques went to their corners, and two societies emerged." Thus, it can be argued that the seeds for the Society for Magnetic Resonance Imaging (SMRI) and the Society of Magnetic Resonance in Medicine (SMRM) were both planted in the MR workshops organized by Dr Amtey, with a mitosis occurring at the Bowman Gray meeting in October 1981.

Despite the disappointment of the split between the two future societies and pressure to form a clinicians-only society to counter the primarily basic science orientation of the SMRM, Dr Amtey and others believed that the basic goals of cooperation between scientists and clinicians necessitated an equal-access membership perspective. The concept of clinicians and scientists as equal members in a society was adopted by the SMRI, and membership increased, several members holding membership in the SMRM as well. Some basic tenets of the SMRI that survive today, such as rotating the presidency between scientists and clinicians, were adopted at this time, in late 1981 and early 1982.

As the development of the precursor to the SMRI continued, it was important to establish a communication forum for research by members. Dr Amtey contacted Pergamon Press to inquire about the establishment of a new journal, since they had experience in publishing both scientific and clinical material. He visited their office in New York and was met with an enthusiastic welcome by people who understood the role of a new modality and the role of a journal. The journal, *Magnetic Resonance Imaging*, was created, and Dr Amtey was appointed its editor. Pergamon also recommended to Dr Amtey the Society Association Services Corporation (SASC) to oversee the day-to-day activities of the future society. This relationship with the SASC later proved to be one of the darker points in the evolution of the SMRI.

After Dr Amtey's Second Annual Workshop on NMR Imaging, March 3–6, 1982, at the Stouffers Plaza Hotel in Houston, the SMRI was officially chartered, with a constitution and bylaws and the completion of other necessary procedures. Frank Smith, MD (author of the SMRI constitution and bylaws), was elected by the Board of Directors to be the first president. (Dr Smith later stepped down, and the remainder of his term was served out by Dr Amtey.) The First Annual Meeting of the SMRI took place at the Broadmoor Hotel in Colorado Springs in March 1983. By the time of the first meeting, the journal was already a year old. At about this time, Dr Amtey began planning for a large-scale, concentrated MR group in his home state of Texas, which necessitated allocating his time among editorial duties for the journal, organizational activities for the Society, and his plans for the future. It is the impression of many that Dr Amtey was spread too thin and that the SMRI sustained a loss of momentum as a result of poor organization. In MR imaging at the time, the debate between the middle-field- and high-field-strength camps was beginning to build.

The diagnostic uses of MR imaging continued to expand, and greater engineering and imaging results were presented at both the SMRM and SMRI meetings, scheduled only six months apart. Clearly, the demarcation between the societies was no longer quite as distinct as at their inception. Many individuals were members of both societies, with some serving roles within the organizational structures of both. It was natural to question whether two societies were required for the future. On at least two occasions, the SMRI contacted the SMRM about merging the journals and the societies. No response was obtained, and the course of separate societies was cast.

The Second Annual Meeting of the SMRI was held at the Greenlefe Resort outside Orlando in March 1984. When asked about the unusual location away from the vast recreational facilities in the Orlando area, Dr Amtey responded: "My plan for the annual meetings was to provide an atmosphere where people would naturally interact and have fun. I felt we should make the meetings different, [primarily] providing education, papers, recognition, awards, and [then] time for pleasure. The idea wasn't to make money."

Most members characterized the meeting as a disaster, marked by poor attendance (somewhere between 150 and 250) and worse organization. As Dr Gore said: "It went so far as having people's names appear on the program without them receiving prior notification. It was a real low point in the history of SMRI." Dr Hazlewood described it as "light on organization but strong on commitment." With great promise for the future, William Moore, PhD, was elected President of the Society by the Board. Unfortunately, Dr Moore died shortly after taking office, adding to the complexity and confusion facing the early Society. President-Elect Luis Todd, MD, a strong supporter of Dr Damadian and Fonar, took office for both the remaining term of Dr Moore and his own Board-appointed term.

Although it was officially chartered, the Society still had not adopted the constitution and bylaws that had been drawn up, or moved to establish procedures, committees, and the like. The areas of greatest concern after the Florida meeting were the financial obligations and procedures of the Society under Dr Amtey. Heated debate surrounded points of contention such as airfare and honoraria for invited speakers and the financial commitments to the SASC. It was reported that at the Florida Board meeting, the SASC asked for a five-year contract and talked of suing the Society. A non–open bid contract for the services of the SASC was extended, some say directly by Dr Amtey, without the approval of the Board. The lack of cooperation with the SASC continued for three more years. It has been stated that accurate financial records, membership roles, minutes of meetings, and the like were not maintained during this period, severely affecting the fledgling Society's ability to gain momentum.

As 1984 progressed, tensions between the SMRI Board and Dr Amtey increased, and it was agreed that his services as editor of the journal would no longer be required. Disenchanted by his lack of success, various misunderstandings, and the burden on his family to relocate, Dr Amtey left the field and has not been active in MR imaging since. Pergamon and the Society discussed ceasing publication of the journal. To increase credibility and broaden support for the journal, both Dr Hazlewood and the team of Drs Gore and Smith were proposed by the Society Board as potential future editors. Drs Gore and Smith assumed the duties, rather than terminate publication, and provided *Magnetic Resonance Imaging* with a visible clinical/scientific editorial perspective and international appeal. Dr Ian Pykett indicated later that the change in editorship "marked a point of increased quality for the SMRI and the journal in particular."

By 1985, the Society had begun to right itself and become organized. As Dr Gore, director of the Educational Program put it: "We were able to have our first half-organized meeting in San Diego. Our success, however, was still overshadowed by the fact that we had 300 attendees while the SMRM had something approaching 2,000." Dr Fullerton, director of the Scientific Program, recruited several well-known clinicians, including Drs Robert Lufkin and William Bradley, both of whom were to become presidents of the SMRI. At this point, the Society consisted of approximately 70% basic scientists and 30% clinicians.

Later in 1985, the membership held its first election and elected Dr Fullerton as President. Previously, Drs Todd, Moore, Amtey, and Smith had been appointed by the Board, as opposed to being elected by the Society membership. Dr Fullerton assumed his duties as President soon after, completing the final portion of Dr Todd's term. The SMRI Board believed that it was better to have Dr Fullerton assume his duties immediately, since he represented the choice of the membership.

Some consider this period the turning point for the Society. During his tenure, Dr Fullerton implemented the committee structure of the Society that we are familiar with today. Dr Fullerton later said: "We pulled together the committee structure so that SMRI could begin to solve problems and provide answers related to the clinical and basic science issues associated with diagnostic applications of NMR. We felt that the actions that needed to be taken as a society could be done through grassroots changes in the field."

Problems and disenchantment with the SASC continued through the 1986 meeting in Philadelphia. Although no specific events have been described, a general concern with regard to finances and persistent difficulties with membership rolls (and subsequent journal delivery) continued. Alternative organizations for running the business activities of the Society were investigated. Dr Fullerton continued as President of the Society and began recruiting, as he called them, "future grandfathers in the field" for key Board positions. Specifically, people such as Drs Axel, Runge, Harms, Stark, Partain, Wood, Wehrli, Haacke, Henkelman, and others were recruited into the Society. Ed Hendrick, PhD, became Treasurer and came to realize the extent of the Society's financial difficulties, primarily the result of the Orlando and San Diego meetings. As he put it later, "The Philadelphia meeting was to have a profound positive impact on the Society in the future."

San Antonio was the site of the Fifth Annual Meeting of the SMRI, in 1987. Virtually everyone recognizes that this meeting was the first one at which organization was cohesive, scientific quality was high, and exhibitor support was strong. Things were looking up for the Society. The success of the meeting drew other individuals active in MR imaging into the Society. At this time, the Scientific Committee decided to adopt the suggestion of Dr Mark Haacke to extend the Scientific Program by one day and host a topical session on Sunday. This workshoplike atmosphere was designed to draw people together for a single, relaxed session before the three days of limited talks and parallel sessions.

Immediately after the meeting, the contract with the SASC was not renewed and the relationship with the Radiological Society of North America (RSNA) for obtaining organizational support was established. Although not directly involved in managing the activities of the Society, the RSNA agreed to educate personnel in the operations of an SMRI central office. In April 1987, a two-year agreement with the RSNA was signed, and in June, George Schuyler of the RSNA hired Kristen Q. Coe on the Society's behalf. All activities were then placed under the control of the SMRI, and organizational growth within the Society emerged. Mr Schuyler's help in getting the SMRI effectively organized was critical.

Consecutive financially successful meetings, increased membership, sound business records and procedures, and increased quality of publications and meetings over the next few years ensured the future of the SMRI. Three specific points have been identified as reasons that the SMRI was able to continue gaining momentum: (*a*) increased credibility of the second editorial staff of the journal, (*b*) changing from an outside to an inside business office arrangement, and (*c*) leadership and recruit-

ment during 1985–1987. Many have suggested that during the 1985–1987 years, the Society Board began to function as such, discussing options, evaluating pros and cons, and strategically plotting a future for the Society as opposed to acting on ulterior motives. This Board consisted of many new members, as well as a core of the founding members. Those showing interest in both the growth of the Society and MR imaging were able to move into positions of leadership. Ed Hendrick, Past President of the Society, notes: "SMRI has been open to new leadership. I believe that we're a very egalitarian Society."

Since 1987, the Society has continued its rapid growth, providing a forum wherein scientist and clinician can meet and share their knowledge and expertise in MR imaging. Today, the Society boasts more than 1,700 members, holds its Annual Scientific Meeting that attracts a similar number of attendees and more than 500 scientific papers, and publishes the *Journal of Magnetic Resonance Imaging* (*JMRI*).

Coordinated by its efficient business office in Chicago, the SMRI of 1992 certainly fulfills the aims laid out by its founding members and looks forward to the next decade with confidence.

JEFFREY L. DUERK, PhD, *Pulse Editor*
FRANCIS W. SMITH, MD, *Associate Editor*

SMRI

## PLENARY SESSIONS

From the MRA Topical Symposia on Sunday through the Frontiers in Body Imaging session on Wednesday, the Plenary Sessions, spaced throughout the week, highlight the Annual Meeting's educational programming. The plenary sessions also provide the opportunity to recognize Award recipients and to honor individuals who have made important contributions to MRI.

**SUNDAY, APRIL 26**
8:00 am - 10:00 am
Current Status of Head & Neck MRA

10:30 am - 12:15 am
Challenges for MRA

1:30 pm - 3:00 pm
Techniques for MRA

3:30 pm - 5:15 pm
New Horizons for MRA

**MONDAY, APRIL 27**
8:00 am - 9:30 am
Award Presentations
The First Decade of MRI

1:30 pm - 3:00 pm
Rapid Imaging

**TUESDAY, APRIL 28**
8:00 am - 9:30 am
Advances in Neurological MRI

1:30 pm - 3:00 pm
New Clinical Applications

**WEDNESDAY, APRIL 29**
8:00 am - 9:30 am
Challenges for Shoulder Imaging

1:00 pm - 2:30 pm
Frontiers in Body Imaging

SOCIETY FOR MAGNETIC RESONANCE IMAGING

# ISIDOR I. RABI

# *Award*

This award is named in memory of Isidor Isaac Rabi, physicist, statesman, and pioneer of modern science. During the 1930's Rabi and his co-workers at Columbia University developed and used nuclear magnetic resonance methods to measure, with extreme accuracy, the magnetic properties of nuclei. This work earned Rabi the 1944 Nobel prize in physics and directly stimulated research on collective nuclear magnetic resonance in solids and liquids, which has led to magnetic resonance spectroscopy and imaging. I.I. Rabi died in 1988 at the age of 89.

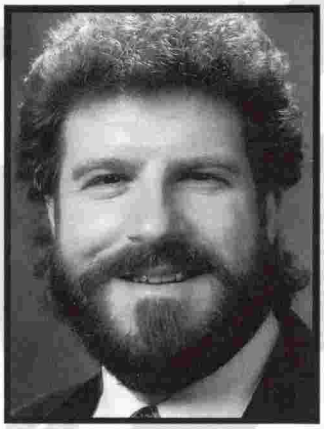

**James W. Hugg, Ph.D.**

James is a NIH Postdoctoral Research Fellow at the Cardiovascular Research Institute, University of California, San Francisco, working on the development of RF coils and pulse-programmed 3D for $^{31}P$ MR Spectroscopic Imaging (MRSI). He holds both Bachelors (with honors) and Masters degrees in Physics from the California Institute of Technology, Pasadena, and Masters and Doctoral degrees in Physics and Nuclear Physics from Stanford University. Prior to entering the field of medical imaging, Dr. Hugg spent ten years in the oil industry working on the processing and interpretation of geophysical data.

SMRI

# SMRI '92 Tenth Annual Meeting
# Plenary Symposia

## Sunday Morning • East Ballroom
## Plenary Symposia 001–007

### CURRENT STATUS OF HEAD AND NECK MRA

MODERATOR: TM Grist, MD

PS 001 • 8:00 AM

**Current Status of Head and Neck MR Angiography: Overview of MR Angiographic Techniques**

PJ Keller, PhD
*Barrow Neurological Institute, St. Joseph's Hospital, Phoenix*

Over the past couple of years, MR angiography has rapidly moved from academia to the routine clinical scene. While perhaps as many as two dozen different acquisition methods have been proposed, at the time of this writing, a rather limited subset of these have gained clinical acceptance. It is customary to divide MR angiographic acquisition methods in two divisions denoted as phase-contrast methods and time-of-flight techniques. Division within time-of-flight MR angiography is according to the acquisition mode. Three of these modes are currently prominent: the original 3D (volumetric) acquisition, sequential-section 2D acquisition, and a recent compromise between these in which thin contiguous or overlapping 3D slabs are sequentially acquired. The relative merits of these modes will be discussed with respect to flow phase and flow amplitude effects. Phase-contrast methods are uniquely sensitive to preset flow directions and ranges of velocities. The properties of these methods yield very high flow/stationary tissue contrast, but require some degree of foreknowledge of the flow velocities to be imaged. Progress has also been made in the use of variants of phase-contrast methods for the quantitation of flow velocities as a function of cardiac phase. Finally, numerous alternatives to the standard maximum-intensity pixel projection have been proposed; their potential application in the head and neck will be discussed.

PS 002 • 8:30 AM

**MR Angiography in the Head and Neck: Clinical Experience**

TJ Masaryk, MD
*The Cleveland Clinic Foundation, Cleveland*

The purpose of this report is to briefly review the underlying physics concepts of various MR angiographic techniques, followed by a detailed description of their application to neurovascular disease. Special emphasis will be placed on the diagnostic pitfalls of each method. Recent technical advances that may improve image quality or circumvent artifacts will be highlighted. MR has the capacity to create anatomic images through the use of radio-frequency (RF) excitation and refocusing pulses as well as spatial localizing magnetic field gradients. Motion (blood flow) in the presence of the RF pulse sequence creates so-called time-of-flight (TOF) effects, while motion during the application, and direction, of the magnetic field gradients produces spin phase phenomena. Each of these effects can be manipulated relatively independently to create vascular contrast and thus angiographic images. TOF techniques create vascular contrast via the inflow of blood protons into a region of interest previously prepared by an RF excitation, inversion, or saturation pulse. The most popular techniques consist of relatively simple 2D and 3D gradient-echo pulse sequences whereby the inflow of spins produces high signal within the vessels on the basis of the TOF effect, known as flow-related enhancement. Angiographic images are then derived from such data sets through the use of computer postprocessing techniques. Disadvantages of these techniques include suboptimal background (stationary tissue) suppression, sensitivity to signal loss secondary to turbulence, and saturation of spins resulting in low vascular contrast with the 3D method. Phase-contrast (PC) angiography is an angiographic technique based on changes in signal phase due to the motion of spins along imaging gradients. In this way flow direction, velocity, and hemodynamic effects are included into the vascular image. PC angiographic bipolar gradients are used to encode a range of velocities in a specific gradient (x,y,z) direction. The fastest PC methods image a projection slab; so-called 2D PC angiography. The 2D PC angiograms can also be acquired as a cardiac-gated, time-resolved acquisition similar to a cardiac cine technique. The most versatile PC angiographic method for neurovascular imaging is to acquire the data as a 3D volume acquisition (where there is additional phase encoding in the section-select direction). This method generates a 3D volume data set with all of the features of 2D PC but the added advantage of very small voxels. The vascular data in the 3D volume set may also be segmented, and the selective vascular information can be projected into any desired plane by using maximum-intensity pixel ray-tracing techniques, much like the TOF techniques. Disadvantages of the PC techniques include long imaging and postprocessing times, sensitivity to signal loss from turbulence, and aliasing of signal outside the range prescribed by the flow-encoding gradients. Future improvements include shorter acquisition times, shorter echo times, improved and innovative postprocessing algorithms, as well as prospective clinical trials to ensure clinical acceptance.

PS 003 • 9:00 AM

**Neuroradiologic Applications of MR Angiography**

EK Fram, MD
*Barrow Neurological Institute, St Joseph's Hospital, Phoenix*

Although MR angiographic images resemble those obtained with conventional angiography, they differ significantly in the way they are obtained and often in the infor-

mation they contain. In conventional angiography, the vessel lumen is opacified with iodinated contrast material, producing an image of the anatomy. In MR angiography, no contrast agent is injected. Instead, blood movement is detected, producing an image that depends on both anatomy and physiology. Therefore blood movement itself is the contrast agent. When blood flow within a vessel is simple, the MR angiogram will usually depict the anatomy accurately. However, when blood movement is turbulent or slow, as within and distal to stenoses, signal loss occurs and artifacts result. Thus MR angiography depends on both anatomy and physiology. MR angiographic techniques available include 2D and 3D time-of-flight (TOF) MR angiography, 2D and 3D phase-contrast MR angiography, and MOTSA (multiple overlapping thin slab acquisition), which combines many of the advantages of 2D and 3D TOF MR angiography (developed by Dennis Parker). There is no universal pulse sequence that is optimal for all applications. Each has strengths and weaknesses. There are often several good ways of solving a particular clinical problem and at other times different techniques will complement one another. For evaluation of extracranial carotid and vertebral disease, the author uses 2D TOF MR angiography (developed by Paul Keller). For evaluation of vertebrobasilar insufficiency, the author adds MOTSA MR angiography to image the distal vertebral arteries and basilar artery. For evaluation of intracerebral atherosclerotic disease and aneurysms, the author uses 3D TOF MR angiography. For intracranial venous occlusive disease, the author uses 2D TOF MR angiography in the coronal plane. For measurement of flow and determination of flow direction, phase-contrast techniques are used.

PS 004 • 9:30 AM

### Clinical Experience with MR Angiography

SB Peterman, MD

*Department of Radiology, Emory University School of Medicine, Atlanta*

Techniques for MR angiography have undergone rapid evolution. Good-quality images can now be reliably obtained, and their clinical applications are being explored. The author's MR angiographic experience is with a 1.5-T Phillips ACS system. A 2D time-of-flight (TOF) technique is used for examining the carotid artery bifurcations. Image degradation secondary to patient motion has been less than with 3D TOF techniques; stenosis exaggeration secondary to turbulence has not been a problem clinically. Three-dimensional TOF techniques are used at the skull base and the circle of Willis. The smaller voxel size allows better definition, and patient motion is less of a problem at this location. Two-dimensional TOF with or without intravenous gadolinium is used for evaluation of dural sinus patency. Current clinical applications of MR angiography include the noninvasive follow-up of neurovascular lesions such as arterial pseudoaneurysms, dissections, or aneurysms that are being treated conservatively. A second clinical application is the evaluation of dural venous sinus patency in patients with clinical problems such as parasagittal meningiomas or pseudotumor cerebri. Early clinical studies show promise for MR angiography as a screen for extracranial and intracranial cerebrovascular atherosclerosis. Phase-contrast MR angiography may be useful in evaluating dural venous sinus patency and the velocity changes associated with atherosclerotic narrowing. Neurovascular MR angiography is an exciting field under continuing development that has become a useful noninvasive method that complements intraarterial angiography in evaluating the neurovascular system.

## CHALLENGES FOR MRA

MODERATOR: WG Bradley, Jr, MD, PhD

PS 005 • 10:30 AM

### Challenges for MR Angiography: MR Angiography of the Vascular System from a Surgeon's Perspective

TS Riles, MD

*New York University Medical Center, New York, NY*

From its conceptual and theoretical beginnings, MR angiography is finally approaching its ultimate goal of becoming an important tool in the management of patients with vascular disease. Wide clinical acceptance of MR angiography will come only after the new technology has been critically compared with the current technologies of digital and conventional angiography and US. Among the questions that will be asked is whether MR angiography provides new information not previously available. There will be obvious questions of cost and convenience. Most important will be questions of accuracy, safety, and contraindications. Currently, the major focus of MR angiography has been in the diagnosis of cerebrovascular disease. The need for new technology in this area is great, since conventional cerebral angiography (CCA) remains one of the most feared diagnostic tests by patients and clinicians. Assuming that MR angiography can be performed without risk, the next question is if the information from MR angiography is sufficiently reliable (*a*) to advise patients to undergo an operation that may be associated with a 1%–4% risk of stroke or death, or (*b*) to counsel a patient not to have surgery knowing that for some categories of carotid disease, the yearly stroke rate is 15% if treated nonoperatively. To accept MR angiography as a replacement for conventional angiography, it will be important to demonstrate that the risk of poor outcome from a positive or false-negative test is less than the risk of CCA. As we embark on these early clinical trials, it is important that our observations are carefully recorded and that this information be shared with the MR manufacturers, the programmers, the radiologists performing and reading the tests and the clinicians making patient management decisions. Close cooperation of the various groups will facilitate the development and application of MR angiography for clinical use. There is a great challenge for all of us to harness the enormous potential of MR angiography so that it can be an aid to the patients with vascular disease.

PS 006 • 11:00 AM

### Pulse Sequences for MR Angiography

DL Parker, PhD

*University of Utah School of Medicine, Salt Lake City*

Although MR angiography has achieved clinical utility in many applications, it is evident that significant improvement in vessel detail must occur before MR angiography procedures can replace conventional angiography. Such improvements will be made by developing optimum imaging techniques in accordance with the fundamental physical processes. Recent research in MR angiography image quality indicates that there is a complex interrelationship among image quality, the various related imaging parameters and vessel dimensions, orientation, and the nature and magnitude of flow. There is some evidence that the "best" imaging technique is highly task dependent. In this paper, the current state of some common pulse sequences used in MR angiography is reviewed. The complex interrelationship among muscle/blood contrast, the nature and magnitude of flow, vessel dimensions and orientation, and imaging technique is discussed. Imaging technique parameters include voxel dimensions, section and slab di-

mensions, echo time, repetition time, flip angles, the order of gradient moment nulling, and the nature of signal conditioning between echoes (spoiling, rephasing, etc). Given the great variety in pulse sequences and the significant variability in technique factors, it is observed that any variation that (*a*) increases the net magnetization within a voxel, (*b*) increases the voxel dimensions, and/or (*c*) decreases the phase dispersion of the signal within the voxel may increase the signal obtained from the voxel. These three properties are usually not independent; it is not only possible but highly likely that a change in one of the parameters (eg, voxel dimension) will cause a corresponding change in another parameter (eg, phase dispersion), resulting sometimes in an "anomalous" or apparently contradictory change in signal intensity. Finally, the extent to which pulse sequences can be modified to maximize vessel detail is constrained by physical limitations on MR imaging gradient systems. The optimization of vessel detail in the presence of technical limitations is one of the greatest challenges facing the development of clinically useful MR angiography techniques.

PS 007 • 11:30 AM

### Challenges for MR Angiography: Postprocessing and Display Technology

HE Cline, PhD, WE Lorensen, MS
*GE Corporate Research and Development Center, Schenectady, NY*

Interactive retrospective display of the blood vessels from MR time-of-flight or phase-contrast angiography involves oblique maximum-intensity projections through a stack of images. An efficient algorithm projects each point in the data onto a raster display retaining the maximum value at each pixel location, followed by 2D scaling. Blood vessels are extracted with connectivity to suppress the noise background. In phase-contrast angiography, both flow magnitude and stationary-tissue images are reconstructed from a single 3D acquisition. The two 3D data sets are combined with a multispectral analysis to segment both brain matter and blood and blood vessels. A 3D model of the brain surface and vasculature is generated with the "dividing cubes algorithm" to plan stereotactic surgery. A velocity vector field is reconstructed with three sets of 3D phase-contrast angiography data flow encoded along each axis. Integration of the time-averaged flow velocity vector from selected points within the blood vessels provides streamlines characteristic of the fluid flow. The steady-state vorticity is displayed by twisted ribbons and the speed is shown with color. Computed flow visualization from MR angiography is in agreement with experimental flow patterns in phantoms. A bolus injection is simulated by computing the evolution of a tagged region with time. A future challenge is the visualization of pulsatile cardiac blood flow.

## Sunday Afternoon • East Ballroom
## Plenary Symposia 008–013

## TECHNIQUES FOR MRA

MODERATOR: C Dumoulin, PhD

PS 008 • 1:30 PM

### Techniques for MR Angiography of the Extremities

DP Flamig
*Baylor University Medical Center, Dallas*

MR angiography of the extremities presents several challenges. The flow is often slow, and the vessel size is small. Time-of-flight (TOF) methods, especially 2D TOF, can be used to obtain MR angiograms with the method of maximum-intensity projection. However, the examination times can be long, as a large volume of anatomy must be explored (eg, the whole length of the lower leg), and for the best results, the sections must be thin. The 3D TOF methods are usually less than ideal because of the slow flow, and the T1 saturation effects will dominate. The TOF methods must use the primary acquisition plane to maximize the inflow of fresh spins. Another class of 3D methods, such as 3D FATS, can give good results by virtue of being both fat suppressed and somewhat density weighted. The fat-suppressed images can be processed by means of maximum-intensity projection, and the density weighting gives less T1 saturation effects. However, the T1 saturation effects will still determine the success or failure of the method. Of course, the 3D methods will have higher resolution for examination of smaller vessels. The phase-contrast methods, both 2D and 3D, can be used but usually require several acquisitions when searching for the optimum flow-encoding gradient strength for the vessels of interest. It is often tempting to use contrast agents such as Gd-DTPA in conjunction with any of the above methods; however, all vessels will show some signal intensity, and usually there will be too much information unless postprocessing methods to select structures of interest are used. In the routine clinical environment, several imaging methods are used in each patient, and usually one of the above methods will give diagnostic results.

PS 009 • 2:00 PM

### Techniques for MR Angiography of the Body

RR Edelman, MD
*Department of Radiology, Beth Israel Hospital, Boston*

The goal of MR angiography is to noninvasively depict the vascular system. MR angiography already has proved to be an accurate means for grading stenoses of the extracranial carotid bifurcations and detecting intracranial aneurysms. Efforts to apply MR angiography to areas of the body outside the head and neck have been deterred due to several technical problems including respiratory motion, cardiac pulsation, and lack of optimum local coils. Nonetheless, promising clinical results have been obtained for evaluation of the systemic veins and portal venous system, aorta (including plaque, dissection, and atherosclerotic aneurysm), and renal arteries (stenosis and occlusion). Two-dimensional and 3D time-of-flight and phase imaging techniques each have relative advantages in specific clinical applications. Technical refinements, including fat saturation, magnetization transfer pulses, selective presaturation and preinversion, k-space segmentation, phase-encode reordering, and ultrafast acquisitions with turboFLASH or echo-planar imaging may further improve study quality by reducing motion artifacts or enhancing flow contrast. Flow quantification is feasible with use of bolus tracking or phase imaging methods. Most recently, considerable progress has been made in depicting the pulmonary and coronary arteries. For instance, it is now routinely possible to show the proximal (and often distal) coronary arteries with segmented turboFLASH or spiral imaging techniques.

PS 010 • 2:30 PM

### MR Angiography of Coronary and Cardiac Vessels

DG Nishimura, PhD
*Magnetic Resonance Systems Research Laboratory, Stanford University, Stanford, Calif*

Noninvasive coronary angiography, though actively pursued, has long been difficult to achieve. Efforts at coronary artery imaging must contend with a formidable set of

challenges—cardiac motion, respiratory motion, neighboring heart chambers and vessels, and small vessel size. With MR, several approaches to coronary angiography have been investigated, including both "black blood" and "white blood" imaging with 2D projective or 3D acquisitions. The author has developed a selective-tagging method and a thin-section blood-imaging method for coronary artery imaging. Both methods use breath-hold imaging (with either a fast 2DFT or spiral-image sequence), which significantly improves vessel visualization by minimizing respiratory artifacts. Proximal portions of the major arteries can now be imaged on a consistent basis. Given the unprecedented flexibility of MR, further improvements in tackling the challenges should be forthcoming. Overall, the author's experiences, along with recent advances by several other research groups, instill considerable optimism about the feasibility of MR coronary angiography.

## NEW HORIZONS FOR MRA

MODERATOR: RR Edelman, MD

PS 011 • 3:30 PM

### New Horizons for MR Angiography: Flow Velocity Quantification

DN Firmin, PhD

*Royal Brompton National Heart and Lung Hospital, London*

The study of the effects of flow and motion on the MR signal has a history almost as long as the experimental studies of MR itself. Only 2 years after the first experimental evidence of MR, Bloembergen et al studied the effect of molecular motion on the signal linewidth. A survey of the literature on MR flow reveals that the early research worker merely set out to analyze the flow effects without detailing a particular application. Hahn, for example, was the first to note the effect of diffusion, while the first to study the effect of coherent flow was Suryan. Applications were soon developed, however, utilizing Suryan's original finding that flow effects effectively reduced T1. There were two main areas of interest: to increase the signal-to-noise ratio in high-resolution MR spectroscopy and to help accurately measure the value of T1 for various liquids. Although a number of the studies on MR effects, including Suryan's, clearly indicated that flow measurement would be possible, it was not until 1959 that groups presented techniques actually designed for this purpose. It is interesting to note that, in fact, a number of these early studies were actually developed with the measurement of blood flow in mind, as opposed to industrial or other possible applications. In the following years, a wide variety of methods of flow measurement were developed, all of which used one of three different effects: time-of-flight, wash-in/washout, or phase shift. After the introduction of MR imaging techniques, numerous methods were described for obtaining flow data in the form of an image. Again the above effects were used, and many of these methods have now been applied and validated both in vitro and in vivo. Clinical applications are now widespread, with techniques being used to study the physiology of flow, as well as for improving diagnosis in various forms of cardiovascular disease. More recently, rapid flow imaging techniques been developed that allow sudden changes in blood flow to be monitored. The methods also allow 3D flow velocity data to be acquired in 3D space, all in a relatively short imaging time ( ~ 20 min). The rapid progress in the development of these techniques suggests that, in the not to distant future, reliable flow measurements in the small, tortuous, and moving coronary vessels should be possible.

PS 012 • 4:00 PM

### Current Status of MR Angiographic Economics

SW Young, MD

*Department of Radiology, Stanford University School of Medicine, Stanford, Calif*

Eight manufacturers of MR imaging units currently offer MR angiography packages, and there are several other manufacturers with MR angiography software add-ons nearing commerical availability. Depending on the level of the current software package operating at a given site, MR angiography upgrades can cost between $40,000 and $100,000. Depending on the body part being examined, MR angiography requires from 1 to 45 minutes to acquire the image. Most centers are billing between $200 and $500 for the procedure, depending on whether it is added on to an existing sequence or being performed as a stand-alone procedure. Most manufacturers have obtained FDA marketing clearance, and selected commercial insurers are already reimbursing for both add-on and stand-alone MR angiography sequences. CPT codes have not been assigned as of the 1991 AMA CPT code book. One approach that works is to bill the MR angiography procedure with CPT codes for angiography to the body site and for MR imaging to the body site. This combination of CPT codes results in a payment schedule comparable to the payer's reimbursement schedule for MR imaging procedures by body site. Some centers are currently trying to avoid the confusion about the status of MR angiography by billing them as if they were reformatting procedures or other (not MR angiography) procedures. Some MR angiography is being billed as CPT Code 76449, which is a catchall for unlisted diagnostic procedures. Physicians using this approach must describe the nature of and indications for the procedure to be reimbursed. However, MR angiography should properly be billed as an additional sequence. Some prominent commercial insurance firms (eg, Travellers, among others) are recognizing MR angiography as both an additional sequence and a stand-alone procedure. California, which is a bellwether state for reimbursement policy, along with Florida and Texas, has temporarily adopted a policy for the part B Medicare plan such that MR angiography, if it is performed as part of a two-sequence MR imaging procedure, is reimbursed at 100% of the conventional payment rate established for MR imaging. However, for more than two sequences, the payment is 120% or 140% of the two-sequence rate for the third and fourth sequences, respectively. However, case and payer mix, regional Medicare administrative policy, and the prevalence of prepaid health care plans, all significantly affect the decision for any given institution providing MR angiography services. At this point, there is little standardized policy available to guide MR angiography providers.

PS 013 • 4:30 PM

### New Horizons: Future Directions For MR Angiography

EM Haacke, PhD

*Department of Radiology, University Hospitals of Cleveland, Cleveland*

The goals of MR angiography are to give both morphologic and physiologic information about vascular systems in the body. In the former case, it will be necessary to have sufficient resolution to address the issue at hand and to be able to accomplish MR angiography in a reasonable time. The method used may be time-of-flight or phase contrast. Within either of these, one sequence may serve better for one region of interest than another. Within a given se-

quence type, either a 1D, 2D, or 3D approach may give the best image. In the latter case, very rapid 2D cine images may be required to resolve velocities during the cardiac cycle and evaluate flow rates to different body parts. Phase imaging can accomplish this at the macrocirculatory level, while perfusion methods may be required to determine local regions of tissue blood supply. Progress is being made to improve overall methodology, sequence performance, and available contrast material. This includes better RF and gradient hardware for improved performance. Future sequence development and MR angiography evaluation will include shorter echo times, modified image reconstruction, more rapid data acquisition, higher resolution, improved contrast, and new postprocessing techniques. As the dust settles and the broad scope of MR angiography capabilities becomes apparent, specific protocols for a given body region and disease type will develop.

## Monday Morning • East Ballroom
## Plenary Symposia 014–016

### THE FIRST DECADE OF MRI

MODERATOR: EM Haacke, PhD

PS 014 • 8:20 AM

**History of the SMRI**

FW Smith, MD

*Aberdeen Royal Infirmary, Foresterhill, Aberdeen, Scotland*

The Society for Magnetic Resonance Imaging (SMRI) was founded in 1982 by a small group of young clinicians and physicists with the aim of promoting research into the clinical applications of MR imaging and teaching those interested in this new medical imaging technique. After a slow start and many tribulations, the Society has grown into a large and successful organization that promotes its aims through its Annual Scientific Meeting and the Journal. The early years of the Society were often difficult. At its Second Annual Meeting, the registrants were outnumbered by the invited speakers and the commercial exhibitors and the meeting of the Board of Directors was longer than the time allowed for proffered papers. The success of the Society is undoubtedly due to the enthusiasm of a number of young physical and clinical scientists who have worked hard to create the SMRI that we know today and to the continuing, unstinting support of our commercial exhibitors.

PS 015 • 8:30 AM

**Advances in MR Imaging**

PC Lauterbur, PhD

*Biomedical Magnetic Resonance Laboratory, University of Illinois, Urbana, Ill*

MR imaging continues to develop in many directions. In addition to those of immediate clinical usefulness, there are a number of areas of considerable scientific interest that may be harbingers of applications to come. These include microscopy, which has reached about 10 μm 3D resolution in vitro and which now faces questions of motion sensitivity in vivo, as well as various forms of functional imaging. Such studies include measurements of tissue perfusion and of tissue composition, as measured by spectroscopic localization and chemical shift imaging. In both of these areas, new techniques are developing rapidly.

PS 016 • 8:45 AM

**Advances in MR Spectroscopy**

J Frahm, PhD

*MPI für Biophysikalische Chemie, Göttingen, Germany*

The past decade has seen revolutionary development of in vivo MR spectroscopy. A large variety of new methods and applications opened insights into the human body hitherto believed to be impossible. Advances from classical MR imaging to clinical MR spectroscopy are further rapidly progressing with considerable impact on both natural sciences and clinical practice. From a historical perspective, the metamorphosis from MR imaging to MR spectroscopy has been accompanied by preconceptions and skepticism, in particular in the field of human applications. However, major steps in the replacement of test tubes with living subjects were based on our ability to go from invasive to noninvasive strategies and, thus, to complement classical analytic studies with modalities that offer a new quality of questions to be addressed in vivo. MR imaging/spectroscopy emerges as a unique tool that expands our approaches from morphology to metabolism in providing noninvasive access to structural, functional, and physiologic/biochemical insights into the intact living organism. Future expansions are likely, and some aspects are foreseeable: a technologic feedback to classical NMR, applications in clinical chemistry (body fluids) and histopathology, and animal studies in areas of applied (neuro-) biology (pharmaceutical research). At least two human applications that will become routine clinical examinations are phosphorus MR spectroscopy studies of muscle bioenergetics and proton MR spectroscopy studies of cerebral metabolism. Since there is little doubt that the integrated MR imaging/spectroscopy examination of brain pathologies on state-of-the-art high-field MR systems fulfills "the dream of an imaging system that can do both routine clinical imaging and routine clinical spectroscopy" (DA Ortendahl, Radiology, December 1988), the status of MR imaging/spectroscopy scientists and clinicians in the year 2000 may be quite different from now: moving from radiology to ?

PS 017 • 9:00 AM

**Lateralization of Human Focal Epilepsy with P-31 and H-1 MR Spectroscopic Imaging**

JW Hugg, PhD, KD Laxer, MD, GB Matson, PhD, MW Weiner, MD

*Department of Veterans Affairs Medical Center and University of California, San Francisco*

The goal of this study was to determine how well a blinded investigator using phosphorus-31 and hydrogen-1 magnetic resonance spectroscopic imaging (MRSI) could interictally lateralize the epileptogenic focus (seven temporal lobe foci and one frontal lobe focus) in medically refractory unilateral complex partial seizures. Three-dimensional P-31 and two-dimensional H-1 MRSI studies (45 minutes each) with spin echoes and gradient phase encoding were performed on a 2-T Phillips Gyroscan. Single effective voxel spectra (25 $cm^3$ P-31, 4 $cm^3$ H-1) were extracted and fit from the hippocampal (or mesial frontal) regions with custom MRSI display and analysis software. Eight healthy control subjects showed bilateral symmetry in all phosphorus and proton metabolites. The seizure focus was more alkaline (pH = 7.17 ± 0.03 vs 7.06 ± 0.02) in all eight cases, phosphomonoesters (PME) were reduced (68% ± 9%) in seven cases, inorganic phosphate was increased (240% ± 52%) in seven cases, and N-acetyl aspartate (NAA) was reduced (78% ± 2%) in all casescompared with the contralateral side. No other phosphorus or proton metabolites were significantly altered, and no lactate was observed. By comparison, MR imaging correctly

lateralized four cases, SPECT two cases, and combined P-31 and H-1 MRSI all eight cases. Reduced NAA without change in total phosphorus is consistent with selective neuronal loss and gliosis. Alkalosis is associated with increased neuronal excitability and may be a factor in causing seizures. In conclusion, combined P-31 and H-1 MRSI is a useful tool for the clinical assessment of focal epilepsy and can accurately lateralize the epileptogenic focus.

## Monday Afternoon • East Ballroom
## Plenary Symposia 018–020

## RAPID IMAGING

MODERATOR: ML Wood, PhD

PS 018 • 1:30 PM

### Rapid Imaging: Strategies for Covering K Space

FW Wehrli, PhD

*Department of Radiology, University of Pennsylvania Medical Center, Philadelphia*

This lecture addresses the concept of k space, the spatial frequency domain, and its relationship to the image. The dependence of the major imaging parameters such as field of view, spatial resolution, and S/N on sampling interval and k-space size are discussed, and it will be shown how k space is traversed in typical data acquisition sequences. Salient properties such as conjugate symmetry and its implications on partial Fourier imaging are also briefly reviewed. Typically, the order in which k space is sampled has no implications on image contrast, and the phase-encoding gradient is usually stepped monotonically. This is true, as long as the magnetization builds up in a recurrent fashion between successive excitations (ie, for pulse sequences operating in a steady-state mode) and only one data line is sampled during the pulse sequence interval. However, in multiline sampling techniques such as RARE and its derivatives or in magnetization-prepared high-speed gradient-echo imaging, in which multiple lines are collected during the evolution of the transverse or longitudinal magnetization, respectively, the order in which the individual views are collected has substantial contrast implications. Since the low spatial frequencies contribute more to overall S/N, contrast can be controlled by judiciously assigning the low-frequency views to a particular time point during magnetization evolution. The consequences of discontinuous sampling will be discussed and illustrated with images for some of the more recent pulse sequences. Finally, view ordering is also a means to minimize modulation artifacts from periodic motion.

PS 019 • 2:00 PM

### Fast Spin-Echo Imaging

FA Jolesz, MD

*Department of Radiology, Harvard Medical School and Brigham and Women's Hospital, Boston*

Various rapid imaging techniques achieve shorter acquisition times by sacrificing image quality and/or diagnostic efficacy. This explains why conventional SE imaging remained the standard of diagnosis, and rapid imaging methods are mostly complementary. Fast SE is a direct extension of the original RARE sequence developed by Hennig with reduced acquisition time and SE-like contrast. Improvements over RARE are the following: superior image quality of fast SE due to hardware features of the MR imaging system; availability of the full contrast range (T1, proton density, T2 weighting) of SE; a double-echo version; three types of contrast (T1, proton density, T2) from the same acquisition; and T2-weighted, multislab 3D imaging. Because of these characteristics, fast SE has the potential to replace SE and some of the gradient-echo techniques in clinical practice. Reduced acquisition time (up to 16 in the author's department) can be used not only for shorter imaging time and thus throughput but also to improve overall image quality, primarily by increasing signal-to-noise ratios with multiple excitations. The most important application of this method is high-spatial-resolution imaging with small FOVs, when images are obtained with up to 16 NEX. Long TR, heavily T2-weighted images provide a myelographic appearance without artifacts characteristic of gradient-echo images. While fast SE imaging has unique features (brightness of fat on T2-weighted images) and artifacts, it will provide a convenient replacement for conventional SE. Most important, fast SE improves image quality, spatial resolution, and T2 weighting, and therefore improves the diagnostic potential of MR imaging.

PS 020 • 2:30 PM

### Magnetization Preparation Sequences: A More Versatile Control of Image Contrast

JP Mugler III

*Departments of Radiology and Biomedical Engineering, University of Virginia, Charlottesville, Va*

With recent advances in MR imager hardware and software capabilities, ultrarapid image acquisition techniques are becoming increasingly available. A common feature of these sequences is that a large number of phase-encoding steps ($\geq 64$) can be acquired in a short time ($< 1$ second). The image data can be generated by using repeated gradient echoes (EPI and variants), SEs (RARE and variants), or stimulated echoes (TurboSTEAM) after a single excitation pulse, ultrashort TR low-flip-angle gradient-echo acquisitions (snapshot FLASH or GRASS, TurboFLASH, MP-RAGE), or a hybrid of these methods. In these ultrarapid sequences, short acquisition periods have been traded for the flexibility to achieve a wide range of contrast behaviors. However, by preceding data acquisition with a prescribed series of RF pulses, gradient pulses, and/or time delays to prepare the magnetization, the range of image contrast that can be attained with ultrarapid acquisitions is greatly enhanced. For example, a 180° RF pulse followed by a delay (inversion-recovery magnetization preparation) has been successfully employed with EPI, RARE, and ultrashort TR gradient-echo acquisition techniques to produce heavily T1-weighted "snapshot" images. Other commonly used preparations include chemical shift selective pulses and 90°-180°-90° pulse sets for encoding T2, flow, or diffusion contrast. Recently, much research effort has been devoted to refining further the magnetization preparation sequences that use an ultrashort TR gradient echo for data acquisition. By optimization of the acquisition parameters (eg, phase-encoding order, flip angle, number of acquisition segments), T1- and T2-weighted images of diagnostic quality have been acquired with use of commercial whole-body imagers in acquisition times ranging from a few seconds to less than 1 second. Magnetization preparation sequences show promise for clinical applications in abdominal, cardiac and rapid 3D imaging, dynamic contrast enhancement and diffusion/perfusion studies, and joint kinematics, among other areas.

## Tuesday Morning • East Ballroom
## Plenary Symposia 021–023

### ADVANCES IN NEUROLOGIC MRI

MODERATOR: W Kucharczyk, MD

PS 021 • 8:00 AM

**Advances in Neurologic MR Imaging: Diffusion and Perfusion and Functional MR Imaging**

ME Moseley, PhD
*Department of Radiology, University of California, San Francisco*

Promising advances in neurologic MR imaging with diffusion and perfusion MR imaging have continued to evolve. Water proton directional "apparent diffusion" processes can be imaged in a rapid and accurate manner at high speed. The use of anisotropic proton apparent diffusion (differing diffusional rates along one or more of the three magnet axes), best observed in vivo in motor and somatosensory nerve fibers in cerebral and spinal white matter and in peripheral nerves shows promise in depiction of demyelinating processes. Apparent water proton diffusion, which is significantly slowed in cerebral gray matter within the first minutes following ischemia, has led to further insights and understanding of the ischemic process in brain. Also, "perfusion" in and through the microcirculation, which can be followed by the time-resolved passage of an MR contrast agent, complements rapid diffusion MR imaging to identify cerebral regions at vascular risk from those at metabolic risk within minutes. Within the last year, studies have demonstrated the ability to map regional changes in blood volume from contrast-transit images. Further studies have shown that such regional changes can be mapped in volunteers subjected to visual stimulation. The ability to dynamically follow blood volume changes with MR imaging signifies the advent of functional MR imaging. Today, functional MR imaging encompasses such topics as black blood perfusion and tissue oxygenation mapping. Functional mapping with high-speed techniques may one day complete the concept of a comprehensive, "one-stop" MR examination.

PS 022 • 8:30 AM

**MR Imaging in the Spine: Faster and Better**

G Sze, MD
*Department of Radiology, Yale University School of Medicine, New Haven, Conn*

Although spinal MR imaging has reached a point in which high-quality images have become the rule, not the exception, it can still be hampered by long acquisition times and motion artifact, circumstances that have been more successfully dealt with in brain imaging. However, a number of recent advances promise to permit the acquisition of even better images in shorter acquisitions times. Fast SE imaging, both 2DFT and 3DFT, potentially may replace conventional sequences in many circumstances. New parameters, such as echo train length and echo spacing, control image contrast in addition to TR and TE. Comparisons of fast SE with conventional sequences suggests that fast SE imaging is comparable in the sagittal plane, although further improvements are needed in the axial plane. Phased-array coils, consisting of four or six coils arranged in a linear array, promise to provide better signal to noise over a larger field of view. Images of up to 48-cm field of view can be acquired, allowing imaging of much of the bony spine and all of the cord in a single acquisition. When combined with fast SE techniques, images of the entire cord with the contrast of long TR SE imaging can be obtained in a few minutes. Other developments in MR imaging of the spine include applications in the pediatric population, down to 1 day of age, and improved methods of image display. The clinical applications of all these advances will be discussed.

PS 023 • 9:00 AM

**Advances in Neurologic MR Imaging: Contrast Agents**

MN Brant-Zawadzki, MD, FACR
*Hoag Memorial Hospital, Newport Beach, Calif*

The use of paramagnetic contrast agents in MR imaging of the central nervous system has grown rapidly. Clear-cut indications include screening for metastatic disease, follow up of patients treated for brain tumor, characterization of lesions, and screening for leptomeningeal disease. More recently, applications in acute cerebral infarction have been suggested. These include depiction of involved vessel enhancement, enhancement of the meninges at the site of ischemia, and enhancement of transient ischemic change. New, nonionic paramagnetic contrast agents have undergone clinical trials. These offer the theoretical advantage of a greater safety index, particularly in studies that might require higher concentrations of the agent. Preliminary data suggest that greater sensitivity can be obtained with a higher concentration (0.3 mmol/kg). The role of paramagnetic contrast agents, a review of their safety and efficacy, and some of the emerging applications will be the focus of this session.

## Tuesday Afternoon • East Ballroom
## Plenary Symposia 024–026

### NEW CLINICAL APPLICATIONS

MODERATOR: MJ Bronskill, PhD

PS 024 • 1:30 PM

**MR Imaging of the Chest**

RJ Herfkens, MD
*Department of Radiology, Stanford University, Stanford, Calif*

Imaging of the chest offers significant challenges and ultimately significant advantages for MR imaging. The intrinsic sensitivity of MR imaging to motion has made imaging of the chest somewhat difficult due to the complex cardiac, blood, and respiratory motions present. The classic solutions to these, including gating and respiratory compensation, have afforded excellent images of cardiac and major vascular structures. Routine gated, respiratory-compensated SE images have proved useful in evaluation of mediastinal neoplasms and in complex congenital heart disease, as well as in major vascular disease such as aortic dissections. The lung parenchyma has continued to provide significant challenges to MR imaging secondary to the tremendous susceptibility provided by the multiple air-water interfaces in the lung parenchyma. More recent advances including phase-contrast imaging have afforded MR imaging with unique capabilities to characterize flow and improve the sensitivity and specificity of MR imaging techniques for the definition of major vascular abnormalities including congenital heart disease and dissection. Recent advances in rapid imaging techniques have presented opportunities to image lungs in a single breath hold with relatively short echo times, thus eliminating any respiratory motion problems and providing the potential for pulmonary angiography to be performed in a noninvasive setting with a single breath hold. These techniques coupled with maximum-intensity pixel projection methods can provide excellent pulmonary angiograms in those patients

capable of breath holds for moderate periods of time. Recent advances in imaging sequences that are capable of mapping the susceptibility changes in the lungs or minimizing these changes have provided information regarding pulmonary water content and pulmonary blood content. The progression of MR imaging techniques from routine SE imaging to breath-hold ultrafast imaging has created a series of examinations for evaluation of chest pathology, from tumor staging to imaging of major vessel abnormalities and now pulmonary, arterial, and parenchymal pathologies. These rapid changes in technology have opened new areas of investigation that only a few years ago would have been thought virtually impossible.

PS 025 • 2:00 PM

### Fat-suppressed MR Imaging of the Breast

SE Harms, DP Flamig
*Department of Radiology, Baylor University Medical Center, Dallas*

The use of 3D fat-suppressed acquisition provides improved diagnosis of breast masses. Image contrast is provided by a new pulse sequence, RODEO (rotating delivery of excitation off-resonance), for robust fat suppression with T1 weighting. RODEO 18/3.6, when combined with a nearly isotropic 3D (128 × 256 × 256) acquisition, delivers the efficiency (imaging time = 4 minutes) and resolution (1.6 × 0.8 × 0.8 mm) needed for high-quality breast imaging. Images are obtained prior to and after gadolinium administration (0.1 mmol/kg). Precontrast images are obtained without RF spoiling, while postcontrast images are acquired with RF spoiling. A series of 57 mastectomy candidates were evaluated with this new method. One hundred percent (42 of 42) of cancers were detected with MR imaging; 33% of mammograms were false-negative; 62% of the lesions missed with mammography were cancers. Fat-suppressed MR imaging of the breast has a number of potential clinical roles: (*a*) evaluation of lumpectomy candidates who have presumed solitary nodules for the multifocal disease, (*b*) evaluation of patients with a high clinical suspicion of breast cancer but with negative or equivocal mammographic findings, (*c*) evaluation of patients with silicone implants/injections or scar formation that may limit the diagnostic capability of conventional mammography.

PS 026 • 2:30 PM

### Interventional MR Imaging

RB Lufkin, MD
*UCLA School of Medicine, Los Angeles*

Many of the advantages of MR that make it such a powerful clinical imaging tool are also valuable during interventional procedures. The lack of ionizing radiation and oblique and multiplanar imaging capabilities are particularly useful during invasive procedures. Perhaps the greatest advantage of MR is the high soft-tissue contrast resolution, which allows the early and sensitive detection of tissue changes during interventional procedures. One of the first applications of MR imaging–guided procedures has been in aspiration cytology. While this technique has long been used under US and CT guidance, MR applications are increasing. Several approaches are also currently under evaluation for the treatment of pathology with MR guidance. Interstitial laser phototherapy offers the advantage of transmitting energy directly into the deep tissue through a fiberoptic guide and producing frank tissue coagulation with thermal energy deposition. Interstitial RF ablation also deposits energy in a well-defined fashion, with minimal damage to adjacent structures. This technique has been used for lesions in brain, gasserian ganglia, liver, or the conductive pathway in the heart. Other investigators have already demonstrated the possibility of MR-guided catheter placement for intratumoral alcohol and chemotherapy injections. Interventional MR imaging is clearly in the early stages of development. While the value of MR-guided aspiration cytology and MR evaluation of deep electrode implantation in the brain has already been confirmed with human clinical studies, the future of MR-guided interstitial therapy remains to be defined.

## Wednesday Morning • East Ballroom
## Plenary Symposia 027–031

### CHALLENGES FOR SHOULDER IMAGING

MODERATOR: JV Crues, III, MD

PS 027 • 8:00 AM

### Introduction to Challenges for Shoulder Imaging

JV Crues, III, MD
*Cottage Community Magnetic Resonance Center, Santa Barbara, Calif*

MR imaging has become a primary noninvasive imaging technique for the clinical evaluation of a wide spectrum of musculoskeletal disease processes. One region of the body in which the use of MR imaging has recently rapidly expanded in the setting of widely differing claims of efficacy is the shoulder. The present plenary session will address two common disease processes in the shoulder: rotator cuff disease and instability. It will emphasize potential advantages and disadvantages of intraarticular contrast material in the MR examination of the shoulder. The author will briefly review a theory of the etiology of rotator cuff injury and tears and some of the controversies surrounding instability of the glenohumeral joint. Drs Rafii, Sprague, Zlatkin, and Busch will discuss the MR imaging evaluation of these disease process without and with intrarticular contrast material. Rotator cuff tears are almost always the end-stage result of a lengthy, progressive degeneration of the tendon. Microscopic tears of collagen fibers continually occur with normal activity. Healing occurs but is imperfect, leading to degeneration and progressive loss of mechanical integrity. Diseases that accelerate this process can be detected with MR imaging and potentially treated early in the course of the disease. Because of the extreme mobility required of this joint for normal activity, the shoulder is intrinsically the most unstable joint in the body. The capsule and capsular ligaments are extremely important for stability, and injury and redundancy of these structures can be surgically corrected.

PS 028 • 8:18 AM

### Evaluation of Rotator Cuff Tears: Comparison of Conventional MR Imaging with MR Arthrography of the Shoulder

BF Sprague, MD, G Applegate, MD, F Snyder, MD, R Karzel, MD, L Reyes, MD
*Southern California Orthopedic Institute, Santa Monica, Calif*

Although the diagnosis of a complete rotator cuff tear can be obvious with conventional MR imaging, partial tears of the undersurface of the cuff can be more difficult to diagnose. This is particularly true when the patient lacks enough native joint fluid to clearly outline the undersurface of the cuff on a coronal oblique T2-weighted image. This study was undertaken to determine if the authors could improve the sensitivity and specificity of MR imag-

ing in the evaluation of rotator cuff tears, both partial and complete, by introducing intraarticular contrast material and obtaining postcontrast T1-weighted images. Coronal oblique images were obtained for evaluation of the rotator cuff. In addition, axial images were obtained for evaluation of the labrum. Over 400 patients with shoulder pain were studied over 3 years. Each patient underwent conventional MR imaging of the shoulder and postinjection imaging. The injection was performed in a manner comparable with that of shoulder arthrography. Approximately 15–20 mL of a Gd-DTPA/saline mixture was injected into each patient's shoulder joint. The joint was then exercised, and postinjection, T1-weighted, coronal and axial images were obtained. The total examination time, including the injection images, the injection, and the postinjection images, was 90 minutes per patient. Of these 400 patients, 180 underwent subsequent surgery for a variety of diagnoses, including rotator cuff tears, labral tears, and acromioclavicular joint disease. The precontrast and postinjection images of these patients were reviewed retrospectively by two experienced, blinded MR radiologists for evaluation of the rotator cuff and labrum. Results were correlated with surgical findings in all cases. Preliminary data suggest that the use of MR arthrography improved both sensitivity and specificity for the diagnosis of a partial tear of the undersurface of the rotator cuff tendon. In addition, MR arthrography allowed better delineation of complete tears by clearly defining the location and size of the tear and the condition of the tendon ends. Evaluation of the labrum was also improved.

**PS 029 • 8:36 AM**

### Challenges for Shoulder Imaging: Diagnosis of Rotator Cuff Tears without Gd-DTPA

M Rafii, MD
*NYU Medical Center, New York, NY*

Shoulder pain related to disorders of the rotator cuff and its underlying etiology and associated pathologic changes have been a matter of investigation for decades. Impingement of the cuff between the humeral head and the acromion process (due to abnormal slope of the acromion, hypertrophic changes of the acromion and the acromioclavicular joint, and instability of the glenohumeral joint) or overuse of the shoulder (in work-related or athletic endeavors) are important etiologic factors. Pathologic changes range from tendinitis to degeneration and eventual tearing of the cuff. MR imaging is the single imaging modality capable of evaluating the rotator cuff and the associated or underlying pathologic processes of the coracoacromial arch and the glenohumeral joint in a noninvasive manner. The author's surgically verified data as well as those of others have documented the high accuracy of unenhanced MR imaging in detection of cuff tears, including partial intratendinous and bursal surface tears. The most specific criterion for the diagnosis of cuff tears, based on combined morphologic and signal abnormality of the cuff tendons, consists of a contour abnormality or a defect of the signal void tendon characterized by intense or markedly increased signal intensity on T2-weighted images. Infrequently, full-thickness or partial cuff tears, particularly when small, may not demonstrate this pathognomonic finding. The diagnosis in these cases mainly depends on morphologic changes of the tendon and is assisted by secondary findings (ie, fluid in the subacromial subdeltoid bursa and retraction of the musculotendinous junction). Nevertheless, conventional MR imaging fails to enable detection or accurate differentiation of a small number of full-thickness and partial tears. This slight shortcoming, however, has little or no effect on choosing the appropriate treatment plan because the primary repair of small or partial tears is no longer universally advocated in favor of a conventional or an arthroscopic acromioplasty and decompression of the subacromial space.

**PS 030 • 8:54 AM**

### Diagnosis of Shoulder Instability with Gd-DTPA

JJ Busch, MD, J Nelson, MD, G Huntzinger, MD
*Hutcheson Medical Center, Fort Oglethorpe, Ga*

Recent advances in arthroscopic surgery and the new reconstructive techniques in the treatment of shoulder instability now require imaging techniques precisely detailing the anatomy of the glenohumeral and capsular mechanisms. MR shoulder arthrography facilitates this goal. Intraarticular contrast material (gadolinium-saline mixture) with rapid T1-weighted imaging in multiple planes provides excellent contrast and separation of the variable anatomy of the glenohumeral mechanism, secondary to T1 shortening. In addition, joint distention easily separates individual ligaments, allowing a more detailed description of normals, normal variants, and pathologic relationships of the anterior capsular mechanism, particularly at critical sites along the labrum. Variability of size and number of glenohumeral ligaments, subscapularis, and long head of the biceps tendon are consistently demonstrated. Likewise, posterior capsular variations are separated from the infraspinatus and posterior labral variations. All of the above advantages of MR arthrography with SE T1-weighted imaging are further enhanced with 3D FISP imaging and on-line multiplanar reconstruction. Very thin sections (0.7–0.8 mm) allow complete evaluation of small structures (labrum) and small structural defects. Additional orthogonal planes can enhance the diagnosis in difficult cases. Three-dimensional FISP arthrography makes a difficult job easier.

**PS 031 • 9:12 AM**

### Diagnosis of Shoulder Instability without Gd-DTPA

MB Zlatkin, MD
*Memorial Hospital, Hollywood, Fla*

Evaluating patients with shoulder instability is the second most common indication for shoulder MR imaging. These are patients with recurrent subluxations and dislocations, or clicking or locking of the shoulder (functional instability). MR imaging can document the bone lesions, including Hill-Sachs defects of the humeral head, with excellent accuracy. Fractures of the glenoid margin ("Bony Bankart") may also be detected, with more difficulty. Soft-tissue lesions include injuries to the glenoid labrum and/or capsule. Proper interpretation of soft-tissue lesions requires detailed knowledge of the normal and variable anatomy of the shoulder capsular mechanism. In addition, high-resolution images are needed with smaller fields of view (14–16 cm) and thin sections (at minimum, 3–4 mm). The combination of SE (intermediate and long TR/TE sequences) and gradient-echo sequences are the most sensitive and specific. A dedicated shoulder coil is necessary. Pathology is more easily detected in patients with recurrent subluxations and dislocations (who usually have a number of pathologic lesions and a joint effusion) than in patients with functional instability (who generally have isolated labral tears). The diagnostic performance of MR imaging without Gd-DTPA for labral pathology is good. The results indicate a sensitivity of 88% and a specificity of 93%. Others have had similar results. Capsular anatomy and pathology can be well outlined even in the absence of an effusion. In conclusion, with knowledge of anatomy, reader experience, and attention to proper technique, the abnormalities that occur with shoulder instabil-

ity can be appreciated in nearly all patients, without the use of Gd-DTPA.

## Wednesday Afternoon • East Ballroom
## Plenary Symposia 032–034

### FRONTIERS IN BODY IMAGING

MODERATOR: JC Weinreb, MD

PS 032 • 1:00 PM

#### Manganese Contrast Agents for the Liver

ME Bernardino, MD

*Department of Radiology, Emory University School of Medicine, Atlanta*

The purpose is to demonstrate the use of Mn-DPDP in hepatic MR imaging. The results of phase II studies here and abroad will be presented. Patients selected for phase II were patients with known hepatic disease. Adverse side effects were strictly monitored, as were serum blood chemistries. The results demonstrated an increased sensitivity for hepatic focal lesion detection. This increased sensitivity was primarily due to heightened contrast between the normal hepatic parenchyma and focal liver lesions. Also noted was increased sensitivity to detecting smaller focal masses, as well as the possibility of missing lesions with gaps between sections. The contrast agent appears to be safe in all dose ranges. However, at the higher concentrations, flushing is noted in over 50% of the patients. This flushing is momentary and of no consequence. The contrast agent was also administered as a bolus in the U.S. series. There was very little difference between efficacy or contrast agent reactions in the bolus versus the infusion group. The window of opportunity to use the contrast agent may be as long as 6 hours. Thus, it has significant advantages over contrast agents such as Gd-DTPA. Also, the pancreas and kidneys are enhanced. Mn-DPDP is a highly effective, safe, and promising hepatic MR contrast agent that warrants further study.

PS 033 • 1:30 PM

#### Contrast Agents for MR Imaging

DD Stark, MD

*Department of Radiology, Harvard Medical School, Boston*

Contrast agents are pharmaceuticals that increase the information on diagnostic images. MR contrast agents incorporate diamagnetic, paramagnetic, superparmagnetic, ferrimagnetic, or ferromagnetic materials. After establishing the physical basis for relaxation enhancement, the chemistry and biology of magnetopharmaceuticals will be explored. Various routes of administration, pharmacokinetics, and distribution are used to achieve maximal concentration of the pharmaceutical in the normal or diseased tissue, but not both. Selective distribution of the contrast agent produces selective relaxation enhancement, which serves to increase the signal difference between two tissues on the diagnostic image. Once the imaging process is complete, the ideal contrast agent would vanish or be metabolized without physiologic effects. Many contrast agents must be redistributed and excreted by an organ such as the kidney, which may receive no benefit from the examination (as in imaging of the brain). Therefore, toxicity to nontarget organs must be considered. Mechanisms of acute, subacute, and chronic toxicity are commonly studied in vitro, in laboratory animals, and finally in clinical trials. The advantages and limitations of various models in predicting adverse drug reactions in humans will be discussed. Potential mechanisms for chemotoxicity, immunoreactivity, neurotoxicity, cardiac toxicity, and other complex interactions such as carcinogenicity and teratogenicity will be considered. Current commercial developments in contrast media for the central nervous system and the body include second-generation extracellular contrast agents offering potential advantages over Gd-DTPA. Nonionic contrast media and the issue of osmolality will be discussed. New contrast media targeted to cell-specific physiologic processes such as phagocytosis or receptor-mediated endocytosis are currently undergoing clinical trials. Superparamagnetic iron oxides targeted to the reticuloendothelial system and paramagnetic, low-molecular-weight complexes targeted to the hepatocyte anionic receptor have shown promising results in phase I and II clinical trials. Efficacy will be reviewed, and potential interactions and toxicity will be discussed.

PS 034 • 2:00 PM

#### Rapid MR Imaging of the Abdomen

SJ Riederer, PhD

*MR Laboratory, Mayo Clinic, Rochester, Minn*

MR imaging of the abdomen has historically been difficult because of several factors. Perhaps the most important of these is motion, primarily respiratory, cardiovascular, and peristaltic. The purpose of this presentation is to describe how advances in fast MR imaging have circumvented much of the motion problem by using reduced acquisition times while maintaining good contrast-to-noise ratio. "Fast" for this work is defined as a time within a comfortable breath hold for a patient, typically in the 5–15-second, range. Traditional SE methods have recently been accelerated with several means, including fast SE techniques, use of 100–200 msec TR times, and use of excitation pulses different from 90°. Gradient-echo techniques have incorporated short ( < 10-msec) TR times into the acquisition and, in conjunction with magnetization preparation, have provided effective T1-weighted results. Finally, echo-planar techniques have been applied either in single shot ( ~ 50-msec acquisition) or multishot mode (several individual shots with intervening recovery periods). Results from all of these acquisition techniques will be compared with the more traditional SE methods. Variations of these fast imaging techniques can also be used for vascular abdominal imaging.

# Notes

# Notes

# SMRI

## PROFFERED PAPERS

The Scientific Program Committee has assembled a fine selection of scientific paper presentations from the more than 500 abstracts submitted this year. The final program offers a total of 248 papers in 31 parallel sessions during the week.

Seating for the scientific sessions is on a space-available basis. You are invited and encouraged to move from one meeting room to another during a time block to hear different presentations. Please, however, be sensitive to the presenter and other attendees while implementing your itinerary.

# 1992 Scientific Abstract Reviewers

**Scott W. Atlas, M.D.**
*Hospital of the University of Pennsylvania*

**Javier Beltran, M.D.**
*Hospital for Joint Disease*

**Thomas J. Brady, M.D.**
*Massachusetts General Hospital-NMR Center*

**Michael N. Brant-Zawadzki, M.D.**
*Hoag Hospital/Newport Harbor Radiology*

**Mark Cohen, Ph.D.**
*Massachusetts General Hospital-NMR Center*

**John V. Crues, III, M.D.**
*Santa Barbara Cottage Hospital*

**Peter L. Davis, M.D.**
*Pittsburgh NMR Institute*

**William P. Dillon, M.D.**
*University of California/ San Francisco*

**W. Thomas Dixon, Ph.D.**
*Emory University School of Medicine*

**Jeffrey L. Duerk, Ph.D.**
*MetroHealth Science Center*

**Charles Dumoulin, Ph.D.**
*General Electric*

**Linda Eastwood, Ph.D.**
*Picker International, Inc.*

**Robert R. Edelman, M.D.**
*Beth Israel Hospital*

**Richard L. Ehman, M.D.**
*Mayo Clinic*

**Duane P. Flamig, Ph.D.**
*Baylor University Medical Center*

SMRI

**Jens Frahm, Ph.D.**
*Max-Planck Institut fur Biophysikalische Chemie*

**Mark J. Fulmer, M.D.**
*Baylor University Medical Center*

**Anton N. Hasso, M.D.**
*Loma Linda University*

**R. Mark Henkelman, Ph.D.**
*Sunnybrook Medical Center*

**G. Allan Johnson, Ph.D.**
*Duke University Medical Center*

**Ruben Kier, M.D.**
*Yale University School of Medicine*

**Donald H. Lee, M.D.**
*University Hospital*

**John Listerud, M.D., Ph.D.**
*Hospital of the University of Pennsylvania*

**James R. MacFall, Ph.D.**
*Duke University Medical Center*

**Donald G. Mitchell, M.D.**
*Thomas Jefferson University Hospital*

**Michael T. Modic, M.D.**
*Cleveland Clinic Foundation*

**Orhan Nalcioglu, Ph.D.**
*University of California at Irvine*

**Ponnada A. Narayana, Ph.D.**
*University of Texas Medical School at Houston*

**Dwight G. Nishimura, Ph.D.**
*Stanford University*

**Ray L. Nunnally, Ph.D.**
*Otsuka Electronics*

**Norbert Pelc, Ph.D.**
*Stanford University*

**Peter Y. Poon, M.D.**
*St. Michael's Hospital*

**Barry D. Pressman, M.D.**
*Cedars Sinai Medical Center*

**Ronald R. Price, Ph.D.**
*Vanderbilt University Medical School*

**Peter A. Rinck, Ph.D.**
*University of Trondheim*

**Val M. Runge, M.D.**
*University of Kentucky Medical Center*

**Frank G. Shellock, Ph.D.**
*Cedars Sinai Medical Center*

**Dirk H. Sostman, M.D.**
*Duke University Medical Center*

**Charles E. Spritzer, M.D.**
*Duke University Medical Center*

**David D. Stark, M.D.**
*Massachusetts General Hospital*

**Gordon Sze, M.D.**
*Yale Medical School*

**Stephen R. Thomas, Ph.D.**
*University of Cinncinati*

**Jean A. Tkach, Ph.D.**
*Cleveland Clinic Foundation*

**Patrick A. Turski, M.D.**
*University of Wisconsin*

**Dale A. Vellet, M.D.**
*University Hospital*

**Jeffrey C. Weinreb, M.D.**
*New York University Medical Center*

**Stuart W. Young, M.D.**
*Stanford University Medical Center*

# SMRI '92 Tenth Annual Meeting
# Scientific Paper Abstracts

## Monday Morning • Beekman Parlor
## Papers 001–008

### ULTRAFAST IMAGING
MODERATORS: AP Crawley, PhD • SJ Riederer, PhD

001 • 10:45 AM
**Scrolling through K Space to Optimize Contrast and Acquisition Time of Snapshot IR Techniques**

DG Mitchell, T Foo*, A Sawyer*, TA Tasciyan
*Department of Radiology, Jefferson Medical College of Thomas Jefferson University, Philadelphia, and *GE Medical Systems, Milwaukee*

Snapshot inversion recovery images are obtained by preceding a rapid gradient echo (GRE) sequence with a single inversion pulse. Tissue contrast in these images is determined primarily by the interval between the inversion pulse and the central views of k space, the effective TI ($TI_{ef}$). If the central views of k space are acquired first (centric order), $TI_{ef}$ approximates TI, the interval between the inversion pulse and the onset of the GRE sequence. Unfortunately, time is wasted during the "dead space" of the TI, restricting the number of images that can be acquired during a single suspended respiration. This problem can be solved by "scrolling through k space," whereby the timing of the central views of k space can be chosen in a flexible manner. Centric view order can be modified so that an operator-designated number of views can be acquired prior to the central views. Thus, TI can be decreased to the minimum allowed by the system (84 msec when bandwidth = ±16 KHz). $TI_{ef}$ can be adjusted by choosing the number of views by which the central views are offset from the initiation of the GRE sequence. Five subjects were imaged with a 1.5-T GE Signa unit (TR/TE/$\alpha$ = 9.1/2.6/30°). Images acquired with a TI of 500 msec and conventional centric order were compared with images acquired with a TI of 84 msec with a variable offset of view order. With the parameters specified above, images obtained at TI = 84 msec and with view offsets ranging from 20 to 26 had tissue contrast (absent signal from spleen) comparable with that of images obtained at TI = 500 msec. Edges were slightly less sharp, but acquisition time for eight images was 28 seconds at TI = 500 msec but only 20 seconds at TI = 84 msec. Acquisition time for snapshot IR images can be reduced by minimizing TI. Tissue contrast can be controlled by selecting $TI_{ef}$ by means of scrolling through k space. Improvements in edge sharpness are anticipated as hardware improvements allow further reduction of TR.

002 • 10:57 AM
**Gadolinium Bolus Tracking with Reformatted Echo-Planar Images of the Head Acquired with a Commercial 1.5-T MR System**

C von Weymarn*, MS Elmandjra†, W Wichmann†
*Department of Medical Radiology and †Section of Neuroradiology, University Hospital Zürich, Zürich, Switzerland; †General Electric–CGR Medical Systems, Buc, France*

Echo-planar MR imaging is the ideal technique for acquiring images in a short time and therefore measuring fast dynamic processes in a whole volume. In this study a pulse sequence based on the known spin-echo echo-planar imaging sequence was used. The pulse sequence was implemented on a commercial 1.5-T MR system (GE Signa Advantage) equipped with an additional z-gradient head coil and a fast receiver allowing sampling frequencies of up to 500 kHz (1). Forty-six sections (64 × 128 pixels) were acquired in 5 seconds, giving an almost isotropic resolution of 3.5 mm. Images were postprocessed and reformatted to any desired plane. By reducing the number of sections to nine, covering a volume of interest of 35 × 220 × 440 mm, the total acquisition time could be reduced to 1 second, allowing a time resolution of 1 second for the tracking of a gadolinium bolus in the head. The desired T1 weighting could be selected by choosing different numbers for interleaved imaging of k space. The technique could successfully be applied in patients with aneurysm or other pathologies of the head, showing a well-resolved time course for the gadolinium bolus. With a single-section technique, it was even possible to resolve the time course in 200-msec intervals. Echo-planar MR imaging is fast enough to measure whole volumes in the head in the 1-second range with a spatial resolution of 3–4 mm.

1. von Weymarn C. In: Book of abstracts: SMRM 1991; 1234.

003 • 11:09 AM
**Segmented K-Space Echo-Planar Imaging at 1 T**

M Stehling, M Fang, R Ladebeck, F Schmitt
*Siemens Medical Systems, Erlangen, Germany*

Standard EPI sequences provide 128 × 128 data matrices (1). An EPI prototype imager can achieve up to 1.5 × 1.5 $mm^2$ resolution in the head and 1.7 × 2.5 $mm^2$ in the body. Higher resolution can be achieved with segmented k-space techniques such as MESH and MOSAIC (2). A technique has been developed whereby single-shot raw data are interleaved in the raw data matrix. The method has been tested for up to four segments and can be extended to combine more segments. Typically the imaging is repeated with a TR of a few seconds. High-resolution imaging can therefore be performed in a single breath hold. Because the readout module takes only 107 or 76 msec, the time between measurements can be utilized for multisection imaging and allows volumetric imaging in 5–10 seconds. It is also possible to perform the method in

a single shot. A 45°-acquisition-90°-acquisition sequence (3) can be used to measure a double-segmented data set. Because this technique is highly susceptible to periodic image ghosting, the data have to be corrected for phase and amplitude incongruities. The proposed technique was performed in patients with cerebral and abdominal pathology, and diagnostic images with resolution in the submillimeter range were obtained.

1. Stehling MK, et al. Echo-planar imaging: magnetic resonance imaging in a fraction of a second. Science 1991 (October). 2. Rzedzian RR. U.S. patent 4,767,991. 3. Mansfield P, Morris PG. In: NMR imaging in biomedicine. Academic Press.

004 • 11:21 AM

## Increased Time Resolution in Dynamic Imaging

JJ van Vaals*, HH Tuithof*, WT Dixon†

*Philips Medical Systems, Best, The Netherlands, and †Emory University, Atlanta*

In MR imaging there is an increasing interest in perfusion studies that monitor the wash-in/wash-out of a contrast agent such as Gd-DTPA. A method to increase the time resolution of such dynamic studies is presented herein. Before the contrast agent is administered, an image with high spatial resolution is acquired. Then, the inflow of a contrast agent is monitored by rapidly acquiring only the middle 20–40 phase-encoding profiles for each dynamic image. These central phase-encoding profiles, which contain the contrast information, are substituted in the precontrast high-resolution data set. This procedure provides increased temporal resolution in dynamic studies by combining the high spatial resolution of a precontrast image (eg, 256 × 256 matrix size) with the contrast changes observed in a low-resolution dynamic mode. Simulations indicated that acquiring approximately 40 low-order phase-encoding profiles and using the substitution procedure is sufficient to obtain dynamic images with only minor spatial blurring. This was verified in clinical tests monitoring the inflow of Gd-DTPA in abdominal organs (eg, kidneys). The gadolinium-enhanced regions were well delineated. Comparison of standard protocols with the substitution procedure showed that the faster new procedure can be applied without significant reduction in diagnostic image quality. The substitution procedure substantially reduces the imaging time per dynamic image, typically by a factor of three to five. This procedure can be used either to increase the temporal resolution of the dynamic study or to increase the number of sections measured per dynamic phase.

005 • 11:33 AM

## Development of a Method of Tracking the Left Ventricular Base-Apex Axis throughout the Cardiac Cycle

JD Pearlman, G Aaronson, H Frank

*Massachusetts General Hospital and Harvard Medical School, Boston*

When cardiac images are obtained as a time series, the usual MR methods show the contents of a fixed plane that does not move with the heart. The heart exhibits complex motions including shortening, twist, and axial tilt. Thus it is difficult to evaluate changes throughout the cardiac cycle at a particular location moving with the heart. One potential solution is 3D imaging with interpolation required to correct for changes in orientation. Alternatively, direct observation of changes at a specific short-axis level at optimal resolution may be achieved by modifying the prescription at each point in the cardiac cycle, which in turn requires tracking the motion of the base-apex axis in three dimensions. Both approaches have been implemented with the Signa Instascan. The latter approach was implemented by applying rules of linear algebra that simplify the task to add-multiply conversion of the coordinates of the center of the basal section [CB(t)] and the apex [A(t)] at each time point $t$. Given a two-chamber projection [TC(t)] and a four-chamber, perpendicular projection [FC(t)] one gets CB(t) = [TBx[t] + FBx[t] − Cx, TBy[t] + FBy[t] − Cy, [TBz(t) + FBz(t)]/2]. In normals, CB moves approximately 2 cm, A < 0.2 cm. For accurate prescription, CB must be identified from images of different contrast mechanisms. A comparison of GRASS imaging with spin-echo imaging showed the clear superiority of Instascan spin echo for this purpose.

006 • 11:45 AM

## Regional Cerebral Tissue Oxygenation Studied with EPI at Clinical Field Strengths

K Kwong, B Hoppel, R Weisskoff, S Kiihne, B Barrere, J Moore, B Poncelet, B Rosen, K Thulborn

*Massachusetts General Hospital NMR Center, Charlestown, Mass*

The magnetic field inhomogeneities induced by the differences in magnetic susceptibility ($\Delta\chi$) between paramagnetic deoxygenated blood and surrounding diamagnetic tissue within a voxel result in a frequency dispersion that can be measured as increased water resonance linewidth (LW) and shortening of T2 and T2*. Linewidth is related to T2′ via LW = $1/(\pi \times T2')$. An echo-planar implementation (Advanced NMR, Instascan) of gradient-echo (GRE), spin-echo (SE), and Dixon offset spin-echo (OSE) imaging has been used in rabbits and humans brain to observe signal changes under the perturbation of breath hold of 45–60 seconds. Under breath-hold conditions, $\Delta\chi$ is increased as blood becomes more deoxygenated (with blood gas confirmation). Figures 1 and 2 show that during breath hold for one rabbit, peak signal drops for the SE demonstrated a change in $\Delta R2$ of 1.3 $sec^{-1}$, and GREs showed a $\Delta R2^*$ of 3.7 $sec^{-1}$. The OSE data for linewidth calculation (Fig 3) show a $\Delta R2'$ change of 1.9 $s^{-1}$. As expected, $\Delta R2' + \Delta R2 \sim \Delta R2^*$. Data from human subjects showed changes similar to those seen in the rabbit (Fig 4).

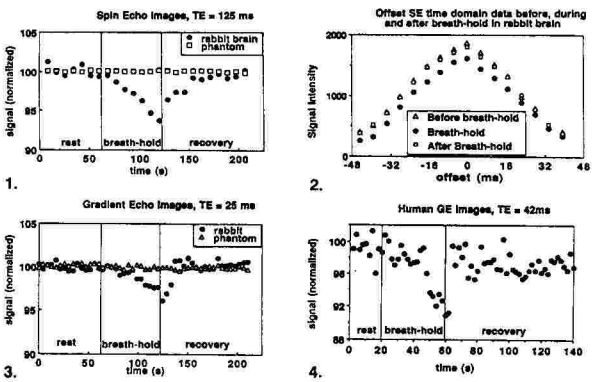


007 • 11:57 AM

## Kinematic MR Imaging of the Knee with Biplanar Acquisition.

SM Brown*, DJ Atkinson†, MA Nissenbaum*, SJ Song*, BE Widoff*, K Yan*, PR Kurzweil*, D Jackson*, WG Bradley*

*Long Beach Memorial Medical Center, Long Beach, Calif and †Siemens Medical Systems, Iselin, NJ*

Accurate diagnosis of patellar malalignment can be difficult to make with clinical examination alone. Biplanar kinematic MR imaging of the knee visualizes the orientation of the patella in relation to the femoral trochlear

groove. With the patient actively flexing and extending the knee, an ultrafast technique (TurboFLASH) accurately tracks this motion. Twenty-five patients with patellofemoral symptoms and clinically suspected tracking problems were studied with real-time patellar tracking prior to and, in some cases, after a lateral release or other realignment procedure was performed. MR imaging was performed at 1.5 T with a standard MR imager (Siemens 63SP) and surface coil. The TurboFLASH pulse sequence was used (TR, 6.5 msec; TE, 3 msec; flip angle, 10°; section thickness, 10 mm; field of view, 250 mm; matrix, 100 × 128). Biplanar acquisition was accomplished by interleaving sections acquired in the axial and sagittal planes. Each knee was imaged separately as the patient actively flexed and extended the knee while lying prone in the magnet. For 40 cine frames (20 each of axial and sagittal sections, interleaved), average acquisition time was 26 seconds per knee. Cine loop display of both biplanar images made it possible to determine the degree of flexion at which patellar malalignment occurs without using any special positioning device. In addition, improvement or worsening of patellofemoral incongruency with different degrees of flexion could be determined. While other imaging techniques examine the relationship of the patella to the trochlea under static conditions, ultrafast kinematic MR imaging with biplane acquisition allows visualization of the patellofemoral joint while all muscle forces are acting, thereby accurately delineating patellofemoral malalignment.

008 • 12:09 PM

### Metastatic Lesion Detection in the Liver: Increased Sensitivity of Dynamic Ultrafast Imaging

MA Nissenbaum, DJ Atkinson, SJ Song, SM Brown, K Yan, BE Widoff, J Blitzer, WG Bradley
*Long Beach Memorial Medical Center, Long Beach, Calif*

The purpose of this study was to assess ultrafast T1-weighted sequences in the detection of hepatic lesions in patients with suspected metastatic disease. Fifteen patients with known or suspected metastatic disease were examined with conventional T1- and T2-weighted spin-echo and TurboFLASH sequences optimized to include asymmetric k-space sampling and k-space segmentation (9/4/15, 96 × 256, 1 NEX, 350 FOV). Images were acquired at a rate of less than 1 second per section, enabling complete imaging of the liver within a single breath hold (< 10 seconds), as well as during quiet breathing. Twelve complete multisection liver studies were dynamically acquired within 2 minutes of gadolinium injection. Each image was assessed for conspicuity ([S(lesion) − S(liver)]/noise), as were the spin-echo images and the nonenhanced TurboFLASH images. When available, CT and US studies were compared. Lesion conspicuity was highest on the dynamic TurboFLASH images acquired 40 to 80 seconds after gadolinium injection; subcentimeter metastases were identified. Nonenhanced TurboFLASH images displayed greater sensitivity than did spin-echo, CT, or US images. Lesions detected with TurboFLASH imaging during breath hold did not appear significantly different from those detected during quiet breathing. Unenhanced and dynamic optimized T1-weighted TurboFLASH imaging revealed subcentimeter lesions undetected with optimized T1 and T2 spin-echo sequences. T1 TurboFLASH imaging, in conjunction with T2-weighted spin-echo sequences, promises to be useful in the assessment of disease metastatic to the liver.

## Monday Morning • Sutton Parlor North
## Papers 009–016

## SOFT TISSUE/MARROW

MODERATORS: J Beltran, MD • PT Weatherall, MD

009 • 10:45 AM

### Fat-suppressed Imaging of Musculoskeletal Neoplasms with T2-weighted Selective Partial Inversion Recovery

MR Terk, H deVerdier, JR Gober, PM Colletti
*Department of Radiology, University of Southern California School of Medicine, LAC and University of Southern California Imaging Science Center, Los Angeles*

Selective partial inversion recovery (SPIR) is a useful technique for fat suppression in MR imaging and is characterized by the use of a chemically selective inversion pulse at the resonant frequency of fat-bound protons. The technique has typically been implemented as a T1-weighted sequence; by combining selective partial inversion with reduced angle spin-echo imaging, however, T2-weighted SPIR images could be obtained. Forty-two patients with known or suspected musculoskeletal neoplasms were studied with this technique as well as T1- and T2-weighted spin-echo techniques. Comparison was made among the imaging techniques used. The results of these examinations indicate that T2-weighted fat-suppressed images are superior to those obtained with the other imaging techniques in several ways: (*a*) The signal intensity relative to normal tissue was substantially higher in all cases. (*b*) Marrow evolvement was demonstrated more sensitively. (*c*) The bone cortex, as well as pathologic involvement, were more clearly visible. (*d*) Superficial extension into fat-containing subcutaneous tissues was far better demonstrated and more easily characterized. This study showed T2-weighted SPIR imaging to be an important MR technique in the imaging of musculoskeletal neoplasms, providing clearer depiction of tumor margins in relation to bone cortex, bone marrow, and superficial fat-containing tissues.

010 • 10:57 AM

### Automated Pixel-Mapping of Osteosarcoma Response to Preoperative Chemotherapy

SL Hanna, WE Reddick, DM Parham, SA Gronemeyer, JS Taylor, BD Fletcher
*Department of Diagnostic Imaging, St. Jude Children's Research Hospital, Memphis*

To improve the accuracy of dynamic Gd-DTPA–enhanced MR imaging in evaluating the response of osteosarcoma to chemotherapy, an automated technique for pixel-by-pixel mapping of tumor necrosis and viability was developed. Six patients with osteosarcoma underwent MR imaging at diagnosis and before resection following preoperative chemotherapy. At each evaluation, FLASH images (TR/TE/no. of excitations, 30/10/2; flip angle, 40°) were obtained at 15-second intervals starting before and continuing for 3+ minutes after Gd-DTPA injection in a single representative, reproducible coronal plane. Interactively selected tumor areas, displayed on a 256° matrix, ranged from 1,003 to 9,996 pixels (mean, 2,901). Slopes representing percent increase in tumor signal intensity per minute over baseline were calculated for each pixel with an automated postprocessing algorithm. Changes in median of distribution (MOD) for pixel slopes were then compared with quantitative histologic grading of response of the resected tumors. Four tumors met histologic criteria for response and two were nonresponders. Postchemotherapy MOD values of tumor slopes correctly predicted histologic re-

sults, with slopes ranging from 42%/min to 58%/min (mean, 51.7%/min) for the four responders and from 72%/min to 96%/min (mean, 84%/min) for the two nonresponders. Region-by-region comparison of the processed dynamic FLASH maps with the matching histologic maps of viable and necrotic tumor showed a high degree of correlation, with minimal false-positive indications of tumor viability due to vascular fibroblastic proliferation. This automated rapid postprocessing technique is a promising method for achieving more accurate evaluation of tumor activity and prediction of osteosarcoma response to preoperative chemotherapy.

011 • 11:09 AM

### Increased Confidence in Diagnosis of Ewing Sarcoma with T2-weighted MR Images

SL Hanna, SC Kaste, BD Fletcher, DL Fairclough, DM Parham

*Department of Diagnostic Imaging, St. Jude Children's Research Hospital, Memphis*

Ewing sarcoma (ES) is the most common lytic malignant bone tumor of childhood, but other solitary benign and malignant lesions often have a similar appearance on radiographs. To assess whether MR imaging could assist in the diagnosis of Ewing sarcoma, T1-, T2-weighted, STIR, and dynamic and static Gd-DTPA–enhanced MR images of 32 consecutive bone lesions were retrospectively analyzed, including histologically proved ES ($n$ = 18), telangiectatic osteosarcoma (TO) ($n$ = 2), chondrosarcoma ($n$ = 1), eosinophilic granuloma (EG) ($n$ = 3), aneurysmal bone cyst (ABC) ($n$ = 5), and osteomyelitis ($n$ = 3). The T2-weighted marrow signal intensities of the lesions were independently scored by two readers as follows: 5 = water, 3 = fat and 1 = muscle. No signal intensity differences among the various lesions were noted on T1-weighted or STIR images. Sixteen of 18 ES showed a predominantly homogeneous, T2-weighted intramedullary signal, isointense to fat, which correlated with marked tumor cellularity. Two TO showed considerable signal heterogeneity; the remaining 12 lesions were brighter than fat on T2-weighted images. The median maximum transverse dimension of the soft-tissue components was 4.5 cm for ES, 10.5 cm for TO, and 0.0 cm for EG, ABC, chondrosarcoma, and osteomyelitis. The slopes of Gd-DTPA uptake derived from dynamic FLASH imaging were not significantly different for ES (median, 54.5%/min) as compared with those for other lesions (median, 72%/min). In conclusion, most cases of ES were characterized by a homogeneous intramedullary signal on T2-weighted images, which was isointense to fat. This finding, along with an associated soft-tissue mass, helps differentiate ES from other lytic lesions ($P < .01$).

012 • 11:21 AM

### Posttreatment MR Imaging Features of Soft-Tissue Sarcomas

EE Kim, K Alekhteyar, HI Libshitz, A Porter

*Department of Diagnostic Radiology, University of Texas M.D. Anderson Cancer Center, Houston, and Department of Radiation Oncology, Wayne State University, Detroit*

The differential diagnosis of recurrent or residual tumor from posttreatment changes in patients with musculoskeletal tumors has been a diagnostic challenge. To thoroughly evaluate posttreatment changes on MR images, serial MR studies in 55 adult patients with soft-tissue sarcomas were retrospectively reviewed after surgery, radiotherapy, chemotherapy, or combinations thereof. MR images were generally obtained prior to therapy and every 3–6 months after therapy up to 3 years. Imaging was performed with a 1.5-T superconducting magnet (GE Signa), and multisection multiplanar imaging was performed with T1- or T2-weighted spin-echo or gradient-echo techniques. In selected cases a postgadolinium T1-weighted image was obtained to evaluate a vascularity change. MR findings were confirmed with histologic diagnosis or a clinical follow-up of at least 3 years. Focal nodular lesions with high signal intensity on T2-weighted images were either tumors or seromas, with seromas showing a gradual decrease in size over a period of up to 1 year. Wide local excision produced a compartmental, slightly increased signal intensity with a feathery appearance on T2-weighted images. These images also showed minimal enhancement diffusely, suggesting hyperemia rather than interstitial edema. Additional radiation therapy resulted in diffuse changes. Marginal excision showed only a surgical defect or scar in the subcutaneous tissue. No therapy resulted in diffuse bone marrow abnormalities in extremities. Intraarterial chemotherapy resulted in a focal infarct in bone marrow. In conclusion, certain MR imaging patterns showing posttreatment changes can be useful in making a differential diagnosis and depend on the type of treatment as well as the time sequence.

013 • 11:33 AM

### MR Imaging of Skin Tumors

A Zemtsov*, L Dixon†, J Reed*

*Departments of *Dermatology and †Radiology, Texas Tech School of Medicine, Lubbock*

Good resolution and clinically useful MR images of basal and squamous cell carcinomas, malignant melanoma, verrucous carcinoma, cutaneous B-cell lymphoma, and a variety of other benign and malignant skin neoplasms can be obtained by using standard, commercially available surface coils and spin-echo techniques with a 1.5-T Siemens or GE superconducting system. Skin tumor depth as measured with MR imaging correlates well with postoperative histologic tumor depth, indicating that MR imaging is a useful modality for preoperative evaluation of the depth and extent of primary and recurrent cutaneous neoplasms. Furthermore, malignant melanocytic and nonmelanocytic skin tumors can usually be differentiated from benign cutaneous lesions. MR imaging should become the imaging technique of choice for plastic and dermatologic surgeons in assessing the depth and extent of skin tumors located in anatomically important areas. In addition, MR imaging is potentially useful to dermatologists and other physicians dealing with cutaneous disease in helping to differentiate between benign and malignant melanocytic skin lesions.

014 • 11:45 AM

### Bone Marrow Repopulation after Total Body Irradiation and Autologous Blood Stem Cell Transplantation; Quantification with Chemical Shift Imaging

H-U Kauczor*, B Dietl†, G Brix*, P Schraube†, W Semmler*, M Wannenmacher†, G van Kaick*

**German Cancer Research Center, Heidelberg, and †Radiotherapy Department, University of Heidelberg*

The purpose of this study was to evaluate the repopulation of bone marrow in patients with hemoblastosis who had previously undergone bone marrow ablation with total body irradiation (14.4 Gy) and chemotherapy followed by autologous blood stem cell transplantation. MR imaging of the lumbar spine, pelvis, and femur was performed in 12 patients 1–7 years after autologous blood stem cell transplantation. All were in complete remission and had normal blood cell counts. Twelve age-matched volunteers served as a reference. Spin-echo imaging (SE 600/20, 4 NEX, 500-mm FOV, 5-mm section thickness) was performed in the coronal and sagittal planes. *H-1 chemical

shift imaging (CSI) (SE 1200/22, 1 NEX, 500-mm FOV, 5-mm section thickness) was performed in a single section, according to the Dixon method, in the coronal plane with modified postprocessing. Spin-echo images were classified visually, and CSI marrow data were analyzed with ROI technique, leading to the relative fat fraction (RFF). The patients' bone marrow exhibited a homogeneous hypointense or spotty pattern. No significant difference in the bone marrow of the age-matched volunteers was observed. A hyperintense pattern, commonly seen after high-dose irradiation, was not observed in any case. CSI revealed an increase of the RFF in most patients (10 of 12) as compared with volunteers: 15% in the lumbar spine, 10% in the pelvis, and 5% in the femur. No dependence on the patient's age or the time interval after autologous blood stem cell transplantation was observed. Only CSI could depict the long-term, clinically inapparent changes in the bone marrow after myeloablation with total body irradiation and chemotherapy, as well as autologous blood stem cell transplantation. The increase of the RFF correlated well with decreased cellularity and fatty replacement in the marrow.

015 • 11:57 AM

### Relative Conspicuity of Bone Marrow Lesions on MR Images: Comparison of Conventional and Fat-suppressed SE and IR Pulse Sequences

SA Mirowitz, WR Reinus

*Jewish Hospital, Washington University School of Medicine, St. Louis*

The purpose of this study was to determine which pulse sequence offers the greatest degree of conspicuity for detection of bone marrow lesions at MR imaging. Twenty patients with marrow lesions, including primary and metastatic neoplasms, avascular necrosis, and osteomyelitis, were evaluated at 1.5 T with conventional T1-weighted (TR/TE = 600/15), fat-suppressed SD/T2-weighted (TR/TE = 2500/20–70), and STIR (TR/TE/TI = 2500/20/160) pulse sequences. The conspicuity of marrow lesions was evaluated subjectively, as well as quantitatively with percent contrast measurements. A high degree of conspicuity was present at all pulse sequences. Qualitative results indicated no significant differences in lesion conspicuity among various sequences. Quantitative measures of lesion conspicuity indicated that the relative conspicuity in descending order was fat-suppressed T2-weighted, STIR, fat-suppressed SD-weighted, and conventional T1-weighted sequences, with mean percent contrast measurements of 59, 56, 37, and 32, respectively. In conclusion, T1-weighted, fat-suppressed SD/T2-weighted, and STIR pulse sequences all provide a high degree of conspicuity for marrow lesions. Quantitative results indicate that among these pulse sequences, fat-suppressed T2-weighted and STIR images are superior.

016 • 12:09 PM

### Fatty Replacement of Bone Marrow after Radiation Therapy in Hodgkin Disease: Quantification with Chemical Shift Imaging

H-U Kauczor*, B Dietl†, G Brix*, K Jarosch*, W Semmler*, M Wannenmacher†, G van Kaick*

**German Cancer Research Center, Heidelberg, and †Radiotherapy Department, University of Heidelberg*

The purpose of this study was to quantify the fat content of irradiated and nonirradiated bone marrow in patients with Hodgkin disease (HD) and to evaluate its relationship to time, age, and dosage. Twenty patients (mean age, 34 years) in complete remission who had been irradiated for HD according to the protocol of the German Hodgkin Study Group, which uses mediastinal and/or paraaortal fields (mean dose, 34 Gy [25–40 Gy]; mean postradiation interval, 47 months [15–126 months]), and 20 age-matched volunteers were examined. Spin-echo imaging (SE 600/20; 4 NEX, FOV, 500 mm; section thickness, 3–5 mm) was performed in the coronal and/or sagittal plane in the lumbar or thoracic spine. CSI was performed in a single section according to the Dixon method (SE 1200/22, 1 NEX; FOV 500 mm; section thickness, 5 mm) in the coronal or sagittal plane with modified postprocessing. Spin-echo images were classified visually, and CSI marrow data were analyzed with ROI technique, leading to the relative fat fraction (RFF). Irradiated marrow always exhibited a mostly homogeneous hyperintense pattern rather than the normal hypointense or spotty pattern, and the margins of the fields were well delineated. The RFF in irradiated marrow increased by 30% in the thoracic and lumbar spine and by 10% in the pelvis, compared with healthy, age-matched volunteers. The degree of fatty replacement was not dependent on the dose applied, the patient's age, or the interval after radiation therapy. In HD patients the RFF in the nonirradiated marrow decreased slightly (5% in the pelvis and 10% in the femur) and exhibited a spotty pattern. In all HD patients radiation therapy caused long-term fatty replacement of the bone marrow in the irradiated field. A discrete indication of compensatory mechanisms (eg, decreased relative fat fraction) was seen in the nonirradiated marrow.

## Monday Morning
## Sutton Parlor Center
## Papers 017–023

## PROTON SPECTROSCOPY OF HUMAN BRAIN

MODERATORS: J Frahm, PhD • RJ Ordidge, PhD

017 • 10:45 AM

### C-13 MR Detection of Pathology in Cartilage

LA Jelicks*, PK Paul†, EM O'Byrne†, RK Gupta*†

*Departments of *Physiology and Biophysics and †Biochemistry, Albert Einstein College of Medicine, New York, NY and †Ciba-Geigy Corporation*

Cartilage degradation is initiated by a loss of proteoglycan. Investigation has already been made of the application of Na-23 MR spectroscopy in the development of noninvasive clinical detection of early cartilage degradation (such as

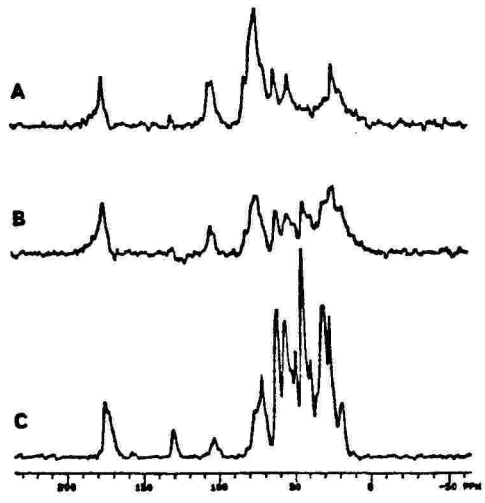

would occur, for example, in osteoarthritis). Studies have recently been undertaken to ascertain the applicability of C-13 MR spectroscopy as an even more sensitive test for cartilage pathology. In the late 1970s natural abundance C-13 MR spectra of intact bovine nasal cartilage (BNC) and isolated proteoglycan fragments were reported. The C-13 MR spectra of intact BNC were dramatically altered on papain digestion (44 hours at 37°C and 12 hours at 50°C). In order to test the sensitivity of C-13 MR for the detection of cartilage pathology, studies were performed with a much milder treatment protocol. The C-13 MR spectrum of a sample of intact BNC incubated in Dulbecco's modified Eagle's medium supplemented with 10% bovine serum albumin is shown in the Figure (*A*). Spectrum *B* is of the C-13 MR spectrum of a sample from the same BNC after 1 hour of treatment with trypsin, and spectrum *C* is of a similar sample after 12 hours of treatment with trypsin. Spectra result from signal averaging 13,500 transients acquired at 37°C and 50.3 MHz with broad-band proton decoupling and a 0.51-second recycle time. A line broadening of 50 Hz was applied. It is clear from these spectra that large alterations in the C-13 MR spectrum appear at 30–45 ppm, 70–80 ppm, and 100–110 ppm even after only 1 hour of treatment. These results suggest that C-13 MR has the potential to be sensitive to early changes in the proteoglycan matrix of cartilage. Further investigation will be required to assign the C-13 MR resonances affected by degradation and to better define the sensitivity of the technique for detecting pathologic changes.

018 • 10:57 AM

## Assessment of Changes in Tumor Oxygenation Due to Nicotinamide with F-19 MR Relaxometry

PS Hees* and CH Sotak*†

**Department of Biomedical Engineering, Worcester Polytechnic Institute, and †Department of Radiology, University of Massachusetts Medical School, Worcester, Mass*

The hypoxic environment frequently found in solid tumors is generally thought to reduce the F-19 effectiveness of many radiotherapeutic and chemotherapeutic treatment regimens. The authors are currently measuring F-19 MR spin-lattice relaxation rates (R1 = 1/T1) of F-44E, a perfluorocarbon emulsion, sequestered in solid tumors and using the dependence of R1 on oxygen tension to assess tumor oxygenation. These techniques allow the evaluation of agents that modify tumor oxygenation and thus enhance the efficacy of conventional therapies. The authors have evaluated the in vivo time series response of the R1 values of F-44E to nicotinamide, a radiosensitizer that is believed to increase tumor oxygenation. In RIF-1 murine tumors, a statistically significant improvement in tumor $Po_2$ for a nicotinamide-treated group was found, with $\Delta Po_2 = 6.5 \pm 3$ torr (mean ± SEM) at 60 min ($P < .05$) and $\Delta Po_2 = 7.5 \pm 3$ torr at 70 min ($P < .05$) after intraperitoneal injection, compared with saline-treated controls. Each group consisted of cohorts of five animals, and the statistics were based on the Student one-tailed group *t* test. Furthermore, in the nicotinamide group, there was a statistically significant increase in tumor oxygenation at 60 and 70 min after injection compared with the baseline preinjection values ($P < .05$, based on the paired Student *t* test). The postinjection time needed to achieve the maximal treatment effect (60–70 min) is consistent with results obtained by others using radiobiologic methods and supports the contention that radiosensitization by nicotinamide occurs through enhanced tumor oxygenation.

019 • 11:09 AM

## Double-Quantum Filtered Na-23 MR Spectroscopy of Perfused Rat Heart

LA Jelicks* and RK Gupta†

**Departments of Physiology and Biophysics and †Biochemistry, Albert Einstein College of Medicine of Yeshiva University, New York, NY*

It has been suggested in the literature that more than 90% of the double-quantum filtered (DQF) Na-23 signal in perfused liver arises from intracellular $Na^+$ and that addition of shift reagent (SR) to liver perfused with phosphate ($P_i$)-containing media results in a large, shifted DQF signal of unknown origin. To further investigate this phenomenon, examination was made of DQF Na-23 spectra of rat hearts perfused with several different HEPES-based solutions ($P_i$-free, $P_i$-free with SR, $P_i$-containing, and $P_i$-containing with SR). DQF Na-23 spectra were acquired with a $90°–\tau/2–180°–\tau/2–90°–\delta–90°–t$ (acquisition) pulse sequence and 256-step phase table. Preparation time $\tau$ was set at 4, 8, or 16 msec, $\delta$ was fixed at 20 μsec, and 4,096 transients were averaged. HEPES-based buffer alone did not give rise to a DQF Na-23 signal at any of the $\tau$ values studied, and the addition of $P_i$ or SR did not alter the spectra. Thus, any DQF Na-23 signal observed in the perfused heart must arise from intracellular $Na^+$ or extracellular $Na^+$ interacting with membrane surfaces. Comparison of DQF Na-23 spectra of the heart before and after perfusion with SR-containing media demonstrated a considerable contribution from extracellular $Na^+$ to the observed DQF signal. The Figure shows DQF Na-23 MR spectra of a rat heart before (upper trace) and during perfusion with $P_i$ and SR (middle trace) and $P_i$-free and SR-containing (lower trace) media; $\tau$ was set at 8 msec. The presence of SR did not induce an increase in the total DQF signal, nor did the presence of $P_i$ in the perfusing solution significantly alter the DQF spectra, demonstrating that $P_i$ has no measurable influence on the extracellular contribution to the DQF Na-23 spectrum of the perfused heart. It is possible that the effect of $P_i$ observed in perfused liver results from interactions with a microprecipitate that forms when SR is added to bicarbonate-based buffers.

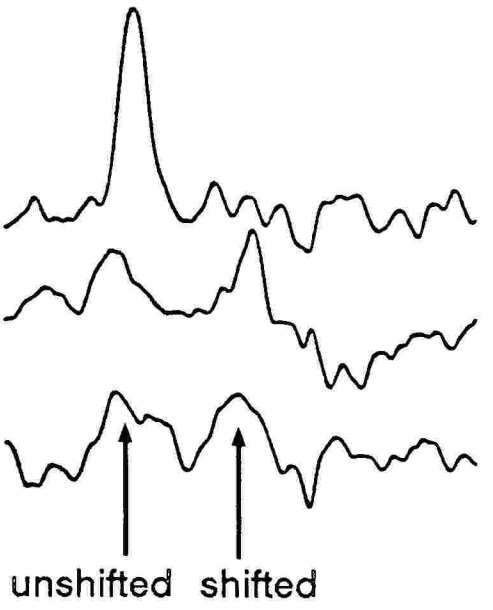

020 • 11:21 AM

## Simultaneous and Interleaved H-1 and P-31 MR Spectroscopy in the Brain

O Gonen, R Srinivasan, J Murphy-Boesch, TR Brown
*Department of NMR, Fox Chase Cancer Center, Philadelphia*

In vivo localized spectroscopy is a diagnostic tool correlating the anatomy from the MR image with underlying physiology and metabolism. Spectroscopy examinations take longer than does imaging, however, especially if more than one nucleus is desired. In such a case the examination must be performed serially, one nucleus at a time. A method is herein presented to perform chemical shift spectroscopy (CSS) simultaneously on several heteronuclei (eg, H-1, P-31). The difficulty is that different $\gamma$ nuclei will differ in amount of phase encoding for a given gradient. This difficulty was overcome by exciting each higher $\gamma$ nucleus, successively, at later times, during the same phase-encoding gradient waveform. The timing of the RF excitation within the gradient waveform was adjusted to give an identical field of view for all nuclei. Since CSS inherently employs only broad-band, short-duration RF pulses, it is possible to halt the waveforms of the gradient(s) briefly for the RF pulse and resume them immediately. Additionally, protons have a shorter T1 and order-of- magnitude higher sensitivity than the rest of in vivo observed nuclei. Thus it is possible to interleave additional "H-1–only" acquisitions between the simultaneous observations for a higher-spatial-resolution proton CSS image. Preliminary results of the experiments, performed separately for each nucleus, show that the technique works and can be used for multinuclear spectroscopy data collection without lengthening the procedure.

021 • 11:33 AM

## Phosphorus Heart Spectroscopy with Double Resonance Techniques

H Kolem, R Sauter, K Wicklow, M Schneider, M Friedrich
*Siemens, Medical Engineering Group and the University of Erlangen, Germany*

Evaluation was made of the use of double resonance techniques for phosphorus heart spectroscopy in combination with the 4D chemical shift–resolved spectroscopic imaging (CSI) localization technique. Measurements were performed in volunteers with a whole-body MR system operating at 1.5 T and equipped with an experimental second RF transmitter. A concentric pair of surface coils was used (diameter H-1, 17 cm; diameter P-31, 11 cm). Decoupling was applied in order to resolve the Pi peak from the resonances of DPG of blood. The nuclear Overhauser effect was used to increase the signal-to-noise ratio. An electrocardiograph-triggered 3D CSI technique was implemented with $8 \times 8 \times 8$ phase-encoding steps. Voxel size was typically $2 \times 2 \times 5$ cm, and the long axis of the voxels was oriented double oblique in order to align with the long axis of the heart. Total acquisition time for P-31 spectroscopy was typically 20 minutes. Results were quantitated by using spectra from chest muscle as an internal reference. The signal-to-noise ratio of PCr in the heart could be increased by 60% with nuclear Overhauser enhancement. Spectra from the anterior wall and, in some cases, from the septum showed a reasonable signal-to-noise ratio for quantitation. This volunteer study provides reference data for a clinical study of patients with coronary artery disease. The results give consistent data on the PCr/ATP ratio for a healthy heart muscle. Although the Pi peak could be detected by decoupling, quantitation was made difficult by overlapping peak areas.

022 • 11:45 AM

## Proton-decoupled P-31 3D CSI of the Brain for Spatial Resolutions from 43 to 6 $cm^3$

J Murphy-Boesch, R Srinivasan, R Stoyanova, T Willard, TR Brown
*Fox Chase Cancer Center, Philadelphia*

Chemical shift imaging (CSI) has been used to obtain high-sensitivity P-31 spectra from well-localized voxels in the brain. A dual-tuned quadrature head coil was constructed recently, making it possible to acquire H-1 images and proton-decoupled, NOE-enhanced P-31 spectra. With improvements in both spectral resolution and signal-to-noise ratio under conditions of bilevel decoupling, it now becomes important to determine the ultimate resolution of P-31 CSI spectra in the brain under these new conditions. For this purpose, a series of five studies were conducted in a single volunteer, with resolutions ranging from 43 $cm^3$ ($3.5 \times 3.5 \times 3.5$ cm) to 6 $cm^3$ ($1.8 \times 1.8 \times 1.8$ cm). All spectra were acquired with a Siemens 1.5 T Magnetom with a second RF channel added for proton decoupling. Data sets with voxel sizes of 43, 18, 12, 9, and 6 $cm^3$ were acquired with four acquisitions per phase-encode step (TR = 1 second), yielding total examination times of 35, 35, 51, 115, and 115 minutes, respectively. The 43-$cm^3$ and 18-$cm^3$ examinations were performed with an $8 \times 8 \times 8$ sample or phase-encoding sets, the 12-$cm^3$ examination with $12 \times 8 \times 8$ samples, and the 9-$cm^3$ and 6-$cm^3$ examinations with $12 \times 12 \times 12$ samples. All spectra had excellent spectral resolution, as evidenced by well-resolved phosphocreatine peaks and the $\gamma$-ATP doublet. The metabolic images constructed from the higher-resolution data sets showed excellent agreement with the variations in phosphorylated metabolite levels in the brain. In addition, as the voxel size was reduced to 12, 9, and 6 $cm^3$, metabolic images constructed from the PCr peak areas apparently began to resolve gray/white matter regions of the brain. These studies demonstrate that metabolite images from proton-decoupled P-31 CSI spectra from the entire brain can be obtained at 2-cm resolution. Adequate signal-to-noise is available at slightly higher resolutions for the construction of both pH and $[Mg^{2+}]$ maps.

023 • 11:57 AM

## Multiple-Volume ISIS for in Vivo P-31 Spectroscopy of Cerebral Metabolism at 3 T

RJ Ordidge*, RA Knight*, JA Helpern*†
**Department of Neurology, Henry Ford Hospital and Health Science Center, and †Physics Department, Oakland University, Rochester, Mich*

The purpose of this study was to simultaneously investigate multiple selected tissue volumes in human brain with in vivo P-31 spectroscopy, thereby minimizing experimental duration when MR spectroscopic measurements of different brain regions are required (eg, for control spectra). The ISIS localization method was modified to allow simul-

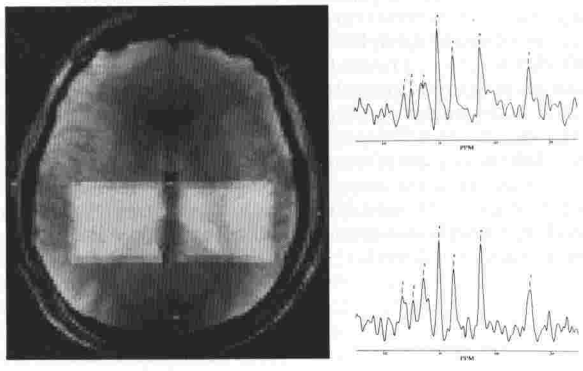

taneous investigation of two or more cubic volumes of tissue that could be independently located within the brain. The increased number of spin-inversion preparation experiments required by the modified ISIS sequence was easily accommodated within the time frame required for in vivo P-31 measurements, with no resultant reduction in the S/N ratio obtained in the final spectrum compared with those obtained in a single-cube ISIS spectrum. Experiments were performed with a 3-T magnet (Magnex Scientific, Abingdon, UK) equipped with actively shielded gradients. The Figure shows the transverse FLASH image used to select the location of two ISIS volumes (highlighted) in the human head and investigated with P-31 in vivo spectroscopy (512 views, TR = 2 seconds, total imaging time = 17 minutes). The P-31 spectra were simultaneously measured from each volume (64 mL) and are shown at right. Peak assignments are (left to right) PME, Pi, PDE, PCr, γ-ATP, α-ATP, and β-ATP.

# Monday Morning • Sutton Parlor South Papers 024–031

## MRA TECHNIQUES

MODERATORS: PJ Keller, PhD
DG Nishimura, PhD

024 • 10:45 AM

### Technique Optimization for Renal Artery MR Angiography

JF Debatin, HD Sostman, C Beam, TM Grist, C Senft, CE Spritzer
*Department of Radiology, Duke University Medical Center, Durham, NC*

MR angiography has been shown to depict proximal renal artery stenosis accurately, but visualization of distal renal artery segments has been hampered by low signal and pulsatility artifacts. To improve distal vessel delineation, assessment was made of the effects of varying flip angles and of the implementation of a cardiac cycle–dependent phase-gradient reordering technique (cardiac compensation). Axial two-dimensional phase-contrast images were obtained in nine volunteers (TR/TE = 40/13.5, 128 × 256 matrix, 28 $cm^2$ FOV, 2 NEX, flow compensation, 5-mm section thickness). For each of three flip angles (40°, 60°, and 80°), three sets of eight axial sections each were obtained with and without cardiac compensation, the former being based on either the initial heart rate or on a continuously monitored heart rate. Signal intensity (SI) was determined in each renal artery and in surrounding stationary tissues. Vessel-to-stationary tissue SI ratios were calculated for each sequence. Changing the flip angle from 40° to 60° increased SI ratios by as much as 50% ($P < .05$) for acquisitions with cardiac compensation; for those without cardiac compensation, SI ratios remained unchanged. Increasing the flip angle from 60° to 80° did not alter SI ratios for any sequence. Implementation of cardiac compensation significantly increased SI ratios at flip angles of 40° and 60° ($P < .05$). No statistically significant difference in SI ratios was noted for the two different forms of cardiac compensation. Implementation of cardiac cycle–dependent phase-gradient reordering at flip angles of 60° and 80° significantly improved image quality, allowing consistent visualization of the renal arteries at a segmental level.

025 • 10:57 AM

### Coronary Artery Visualization in Volunteers with MR Imaging

M Doyle, M Scheidegger, GM Pohost
*University of Alabama at Birmingham*

The recently introduced outflow refreshment (O/R) imaging strategy has been used successfully to image the proximal coronary arteries of volunteers. The O/R strategy produces cross-sectional images in which flowing blood is displayed as a bright signal and other tissues are represented at lower intensities. Outflow refreshment is a multiple thin-section imaging strategy that has good sensitivity to slow flow. Vessels predominantly orthogonal to the imaging planes are highlighted with bright signals. Unlike the majority of MR imaging strategies, O/R can be triggered to the electrocardiograph without extending acquisition time. When combined with the short-gradient-echo (TE = 3.4 msec) FAcE imaging sequence and self-refocusing pulses the O/R strategy presents decreased flow artifacts. Multiple-section cardiac images are acquired in approximately 8 minutes with a body coil. All results were obtained with a Philips S15 Gyroscan system, with 10-mT/m gradients with a minimum rise time of 1.5 msec. Outflow refreshment was used to image a number of sections encompassing the heart base (section thickness 3 to 5 mm). In transverse views the right proximal main coronary artery was seen in the atrial-ventricular groove. In a sagittal orientation the O/R images displayed the left proximal circumflex coronary artery. Approximately the first 3 cm of the left and right coronary arteries were visualized. Cross-sectional views of the proximal coronary artery branches can be seen at multiple levels with the O/R strategy combined with the short-gradient-echo FAcE imaging sequence.

026 • 11:09 AM

### Imaging Protocols That Minimize Breathing and Peristalsis Motion Artifacts in Two-dimensional Phase-Contrast MR Angiography of the Chest and Abdomen

CL Dumoulin, FL Steinberg*, EK Yucel†
*General Electric Research and Development Center, Schenectady, NY; *Cedars-Sinai Hospital, Los Angeles, and †Massachusetts General Hospital, Boston*

Several protocols for two-dimensional phase-contrast MR angiography were evaluated. The nature of motion artifacts arising from peristalsis and breathing was found to vary greatly with the choices of imaging geometry, data acquisition strategy, and postprocessing procedures. The first data acquisition strategy used a time-resolved (ie, prospectively cardiac-gated) data acquisition in which pairs of complex data were acquired from adjacent heartbeats in the cardiac cycle. The second strategy also used a time-resolved data scheme, but acquired pairs of complex data in adjacent TR periods within the same cardiac cycle. While this strategy results in data with half the temporal resolution of the first approach, it proved to be substantially better at suppressing artifacts due to motion of nominally stationary tissue. This appears to be particularly true for random motions associated with peristalsis. The role of imaging geometry was also evaluated. Greatest success was achieved in the pelvis and aortic arch when a coronal (or oblique coronal) projection was acquired with a thick axial slab excitation. Decoupling the excitation and image formation geometries permitted the selective excitation of spins in the region of interest, and specifically prevented the establishment of transverse spin magnetization in moving tissue, such as the myocardium, outside the region of interest. Postprocessing also played a role in improving image quality. Standard deviation calculations of pixel intensity as a function of the cardiac cycle permitted

the pulsatile signals coming from arteries to be selectively highlighted in the presence of steady venous flow and time-invariant background signals. Two-dimensional phase-contrast protocols using the data excitation, acquisition, and postprocessing strategies outlined above were evaluated in healthy volunteers and in a limited patient population. The protocols used minimal TEs and TRs (6 msec and 22 msec, respectively) and a flip angle of 20°. One to three flow-sensitive directions were used as necessary. Examination times were approximately 2 minutes for each flow-sensitive direction. The aortic arch studies made use of oblique image formation to place the arch in the image plane, thereby optimizing the presentation of the vessel takeoffs. Studies in the pelvis used a standard coronal projection. Breathing compensation, even for aortic arch angiography, did not appear to be necessary.

027 • 11:21 AM

### Cardiac Cycle–Specific Data Acquisition in MR Angiography

K Selby, D Saloner, CM Anderson
*Departments of Radiology, Veterans Administration Medical Center and University of California at San Francisco*

Pulsatility can greatly compromise MR angiographic image quality, in particular for the lower extremities, producing turbulent signal loss and phase-encoding ghosts. To address these problems, prospective cardiac gating (as opposed to triggering) has been implemented in MR angiographic studies. Cardiac triggering, in which RF pulses are triggered by an electrocardiographic (ECG) signal, has been used to image pulsatile flow, but it gives reduced contrast between stationary and flowing material. This is because the longitudinal magnetization of stationary material recovers during the time the imager is waiting for the next trigger pulse. Cardiac gating provides a means of overcoming this limitation. In gated mode, TR is constant and a steady-state magnetization is therefore maintained. Pulsatility artifacts are reduced by halting both data acquisition and incrementation of the phase-encoding gradients during the most accelerative portions of the cardiac cycle. Two-dimensional MR angiograms of the popliteal arteries were acquired with cardiac gating. Each ECG pulse initiated a digital signal that halted data acquisition and gradient incrementation for a controlled time interval immediately following each QRS pulse. Phantom studies were also performed, in which a solenoid valve was used to generate pulsatile flow. Two-dimensional gated images were acquired, with data acquisition halted during the times when the valve was open. In both human and phantom studies, gated and ungated images were compared. Gated images showed marked reductions in ghosting and flow artifacts, and a good contrast-to-noise ratio was preserved between flowing and stationary material.

028 • 11:33 AM

### High-Speed Black Blood Imaging of Vessel Stenosis in the Presence of Pulsatile Flow

D Chien, RR Edelman
*Beth Israel Hospital and Harvard Medical School, Boston*

Current MR angiographic techniques suffer from their inability to accurately depict a vessel at a stenosis. The spin dephasing associated with abrupt changes in flow pattern causes significant loss in flow signal, which often exaggerates the degree of stenosis. To overcome this problem, a TurboFLASH method was recently developed that makes flowing spins appear dark while stationary tissues have high signal intensity. With use of a set of prepulses (a nonselective 180° pulse followed immediately by a selective 180° pulse), the flow signal can be nulled by choosing the appropriate time delay between the prepulses and data readout, so that data are acquired when the blood has zero magnetization. The objective of this study was to evaluate the ability of high-speed black blood imaging to correctly identify the degree of stenosis in the presence of pulsatile flow. Stenosis models have been constructed with flexible tubings and images acquired with TurboFLASH black blood imaging (TR/TE = 10 msec/6 msec, FLI = 10°–50°, section thickness = 5 mm, FOV = 23 cm, segmented data acquisition). The ability to obtain good nulling of flow signal over a range of flow velocities (5–200 cm/second) was examined. In addition, the effect of pulsation was studied and images acquired with and without gating were compared. The results demonstrate that TurboFLASH black blood imaging can achieve excellent nulling of flow signal over a wide range of velocities. High flow/stationary contrast and good vessel definition are achieved at the stenosis even in the presence of pulsation. Moreover, a high-resolution, gated image can be acquired in 8–16 seconds.

029 • 11:45 AM

### Background Suppression for 2D Time-of-Flight MR Angiography with Overlapping Presaturation in the Direction of Flow

PM Margosian
*Picker International, Highland Heights, Ohio*

A simple method has been devised for increasing blood contrast in 2D sequential MR angiographic techniques by using thin sections and a presaturation zone that just overlaps each section. The use of thin, axial 2D sections acquired sequentially with a parallel presaturation zone to remove unwanted blood vessels has proved to be a powerful MR angiographic technique for imaging the carotids, thorax, and abdomen. Very thin sections (1.5–2 mm) allow the blood to move completely through in typical TRs (20–30 msec). For example, if flow speed is 20 cm/sec and TR is 25 msec, then blood has moved 5 mm between measurements. If a presaturation zone is placed just downstream from the section and overlaps it by, for example, 2 mm, then blood flowing in one direction is darkened (as is the static material), while blood flowing in the other direction is not. With proper adjustment, contrast enhancement of two times or more can be achieved for vessels with flow velocities $\geq 10$ cm/sec by using section thicknesses $\leq 2$ mm. The idea is to use the presaturation zone to remove unwanted vessels and to reduce the intensity of static material in the imaged section without diminishing the intensity of blood with preferred flow direction, all in a single high-speed acquisition. Several examples from the neck, abdomen, and other parts of the body will be shown.

030 • 11:57 AM

### Two-dimensional Time-of-Flight Angiography at 0.2 T: Sequence and Parameter Choice

U Boettcher, R Hausmann
*Siemens Medical Engineering Group, Erlangen, Germany*

The purpose of this study was to determine optimal parameters for a sequential 2D FLASH angiographic sequences for a 0.2-T field strength. Sequence optimization was performed for the regions of the carotid and popliteal bifurcations. In these regions the vessels are approximately perpendicular to transaxial sections, leading to maximal inflow enhancement and no in-plane flow. Signal from venous blood was suppressed by saturation pulses. All studies were performed in healthy volunteers with a Siemens Magnetom operating at 0.2 T. Three different FLASH sequences were evaluated to find optimal parameters for MR angiography at low field strength: (*a*) TE =

10 msec, bandwidth = 195 Hz/pixel, echo at 33% of the acquisition time; (*b*) TE = 10 msec, bandwidth = 78 Hz/pixel, echo at 25% of the acquisition time; and (*c*) TE = 17 msec, bandwidth = 30 Hz/pixel, echo at 25% of the acquisition time. With the sequences applied to 5-mm sections the optimal flip angles for maximum blood signal were between 70° and 90° for all sequences in this anatomic situation. Because S/N is the key at low field strength the sequence with the highest bandwidth was not investigated further. A comparison of the remaining methods with approximately the same measuring time of 15 min for 40 sections (3-mm section thickness, 33% overlap, 192 × 256 matrix, 250-mm FOV) showed similar results. S/N was approximately the same, and fat suppression with TE = 17 msec for opposed fat and water signal was only slightly better. No influence due to different TEs was observable in the healthy volunteers. The carotid bifurcations were imaged without signal loss. In patients with poststenotic turbulence the sequence with the shorter TE of 10 msec would minimize signal loss due to turbulence. The MIPs of the sequence with TE = 10 msec were slightly smoother. In conclusion, the 2D FLASH sequence with a TE of 10 msec, a bandwidth of 78 Hz/pixel, and large flip angles (70°–90°) is recommended for angiography of the carotid bifurcations and the peripheral vessels in the knee region, because of the short TE and the good S/N of this sequence. At the high flip angles necessary to produce adequate S/N at 0.2 T, in-plane saturation effects in the intracranial vessels produced poor results.

**031 • 12:09 PM**

### Techniques for MR Angiography at Low Field Strength

P Pavone, P Di Renzi, M Gallucci, C Catalano, G Albertini, R Passariello

*Department of Radiology, University of L'Aquila, Italy*

The purpose of this study was to evaluate the most effective technique of obtaining diagnostically relevant images with MR angiography at low field strength. The study used a 0.2-T permanent system (Hitachi Medical) and 2D time-of-flight technique. Comparison was made between axial and coronal images of intracranial vessels. The latter, although slightly influenced by saturation of the signal, provided a better detailed overview of all the brain vascular structures including the circle of Willis. Improvement was also achieved by using contrast agents. At the level of the carotid arteries, axial sections with 2.5-mm thickness made possible a better evaluation. Carotid stenoses were clearly depicted. Coronal images, although allowing an extensive evaluation of the carotid arteries, showed the presence of significant saturation that impaired the evaluation of the carotid bifurcation, resulting in overestimation of lesion. Areas of lack of signal intensity were also seen in normal arteries. Axial, coronal, and sagittal images of the aortic arch, pulmonary arteries, and abdominal and peripheral vessels were acquired. In all cases a relative lack of signal intensity was observed when in-plane flow was present. Section thickness had to be increased to 5 mm in order to obtain a stronger signal. For all images obtained, evaluation with animation display proved to be superior to the evaluation of the single MIP. In conclusion, with use of appropriate technique, optimal imaging of the vascular bed can be achieved with the 2D time-of-flight method at low field strength.

## Monday Morning • Regent Parlor
## Papers 032–039

## CONTRAST AGENTS: EXPERIMENTAL

MODERATORS: TJ Brady, MD • PA Rinck, MD

**032 • 10:45 AM**

### Dy-DTPA-BMA and Gd-DTPA-BMA—enhanced MR Imaging of Acute Cerebral Ischemia

J Kucharczyk, H Asgari, J Mintorovitch, V Vexler, M Tsuura, M Moseley, A Watson

*Neuroradiology Section, University of California at San Francisco, and Salutar Inc, Sunnyvale, Calif*

This study compared the diagnostic efficacy of two nonionic T2*-shortening contrast agents, Dy-DTPA-BMA and Gd-DTPA-BMA (Salutar Inc and Sanofi Winthrop Pharmaceuticals), as perfusion-sensitive agents in acutely ischemic brain. Following unilateral occlusion of the middle cerebral artery (MCA) in experimental cats, the magnetic susceptibility (T2*) effect was evaluated in pre- and postcontrast images. Dy-DTPA-BMA consistently enabled better visualization of perfusion deficits than did the same (0.15–1.0 mmol/kg) doses of Gd-DTPA-BMA on both T2-weighted spin-echo and gradient-recalled echo-planar images. Dy-DTPA-BMA injection advanced the time of detection of ischemic regions in 63% of 52 studies, and lesion conspicuity was improved in 80% of cases. In ischemic lesions less than 5 hours old, washout (restoration of precontrast signal intensity) of contrast was completed within 45 min after injection. However, a delayed hyperintensity was observed on T2-weighted images after Gd-DTPA-BMA injections, which could potentially complicate the interpretation of studies utilizing multiple injections of Gd-DTPA-BMA. Magnetic susceptibility contrast enhancement significantly improves the MR visualization of acute cerebral ischemia. Dy-DTPA-BMA delineates regions of perfusion deficiency better than does Gd-DTPA-BMA.

**033 • 10:57 AM**

### Perfusion/Diffusion MR Imaging of Brain Following Subarachnoid Hemorrhage

M Tsuura, J Mintorovitch, J Kucharczyk, S Rocklage, A Watson

*Neuroradiology Section, University of California at San Francisco, and Salutar Inc, Sunnyvale, Calif*

Subarachnoid hemorrhage (SAH) resulting from rupture of an intracranial aneurysm can lead to decreased cerebral blood flow, raised intracranial pressure with hydrocephalus, and the development of prolonged cerebral arterial vasospasm. Considerable evidence points to cerebral ischemia resulting from reduced cerebral perfusion as the major cause of delayed neurologic deterioration following SAH. The purpose of this study was to evaluate the utility of combined perfusion/diffusion MR imaging in a rat model of experimental SAH. SAH was produced in male Sprague-Dawley rats. Diffusion-weighted and T2-weighted images with and without Dy-DTPA-BMA (0.5 mmol/kg, intravenous) were acquired on days 0, 1, 2, and 3 after SAH. All images were obtained with a General Electric 2-T CSI with self-shielded gradient coils. Increased signal intensity was observed in the right middle cerebral artery (MCA) vascular territory on diffusion-weighted images within 1 hour after SAH, whereas corresponding T2-weighted precontrast images were negative. Twenty-four hours after SAH, no signal intensity changes were visible on T2-weighted precontrast images. Following injection of Dy-DTPA-BMA, however, perfusion deficits were seen within the MCA vascular territory. The delayed onset perfusion deficit observed in this model of SAH parallels observations made in human clinical studies and likely re-

flects ischemic damage due to delayed vasospasm or microcirculatory disturbances caused by increased intracranial pressure. These results indicate that SAH-induced ischemia can be detected with diffusion-weighted imaging and that the underlying perfusion deficit can be characterized with magnetic susceptibility contrast-enhanced MR imaging.

034 • 11:09 AM

### Quantification of Flow: Deconvolution Analysis of First-Pass Gd-DTPA Kinetics

JC Böck, B Sander, J Haustein, W Schörner, R Felix
*Strahlenklinik und Poliklinik, Universitätsklinikum Rudolf Virchow, Berlin*

Deconvolution is a numerical tool used to analyze the kinetics of a contrast agent bolus measured at the input and output of an organ. The result is the organ transport function for the contrast agent bolus. On the basis of the transport function for Gd-DTPA, an attempt was made to quantify flow in a water-perfused organ model used to simulate blood flow in the brain. The model consisted of a pulsatile artificial heart feeding an organ model (water-perfused capillary system bathed in water). A 1.5-T imager and fast T2*-weighted gradient-echo sequence (TurboFLASH) were used. After bolus injection of 5 mmol Gd-DTPA, 30 2D images were acquired at 1-second intervals in the same section position. Regions of interest were defined over the input and output of the organ model. Measured signal intensity kinetics were linearized by logarithmic transformation. A numerical deconvolution algorithm in the time domain was used to compute the organ transport function from the input and output kinetics. From the transport function, the mean transit time of the contrast medium through the organ model was calculated. Flow per unit of water volume contained in the capillaries was obtained from the mean transit time. Since the capillary water volume of the organ model was known, computed flow could be correlated with flow obtained with an independent reference method. The results demonstrated a good correlation ($r > .93$) between the MR estimate of flow and flow obtained with the independent reference method. This study demonstrates the quantification of flow by numerical deconvolution of first-pass Gd-DTPA kinetics in a perfused organ model. Limitations of this approach for the quantification of cerebral blood flow (sensitivity to changes in local blood volume) will be discussed.

035 • 11:21 AM

### Hemodynamic Tolerance after Bolus Injection of MR Contrast Agents: Gd-DTPA versus Gd-DTPA-BMA

M Saeed, A Mühler, RC Brasch, CB Higgins
*Department of Radiology, University of California, San Francisco*

Fast MR techniques have been used to monitor the initial distribution of MR contrast media in the assessment of cerebral and myocardial perfusion. Currently, this functional imaging requires fast injection of MR contrast agents. The hemodynamic effect of rapid administration of ionic Gd-DTPA (Berlex) and nonionic Gd-DTPA-BMA (gadodiamide [Omniscan]) were compared. Three doses (0.1, 0.3, and 0.5 mmol/kg) of Gd-DTPA and Gd-DTPA-BMA were injected centrally (superior vena cava) to determine their effects on the cardiovascular system in a rat model ($n = 6$). Heart rate, left ventricular (LV) pressures, LV rate pressure product, LV ejection time, $dP/dt$, peripheral (arterial) and central (right ventricular) pressures were monitored for 15 min after the injection of each dose. Osmolality of each dilution of both contrast agents was determined by freezing point lowering. Gd-DTPA produced significant changes in the measured hemodynamic parameters at all doses and in a dose-dependent fashion. At the highest dose used (0.5 mmol), Gd-DTPA produced significant ($P < .05$) reduction in LV end-systolic pressure (75% ± 11% of baseline), $dP/dt$ (57% ± 17%), rate pressure product (66% ± 15%), and mean arterial pressure (68% ± 18%). These lower levels all returned to the baseline level within 3–5 min. Excellent correlation between ionic strength and cardiovascular depression was observed after the administration of Gd-DTPA ($r = .99$). On the other hand, nonionic Gd-DTPA-BMA (0.1, 0.3, and 0.5 mmol/kg) had no significant effect on any measured hemodynamic parameter. In conclusion, ionic Gd-DTPA causes significant hemodynamic alterations after bolus injection, but no effects are induced by the nonionic media. Gd-DTPA-BMA may be recommended when bolus injections or high doses are needed, as well as for high-risk patients.

036 • 11:33 AM

### Dual Use of Gd-DTPA-BMA for T1 and T2 Effects in Myocardium

M Saeed, MF Wendland, CB Higgins
*Department of Radiology, University of California, San Francisco*

The low toxicity of Gd-DTPA-BMA permits the use of substantially high doses of this agent, which may provide a longer imaging window. Moreover, the versatility of dose range may permit the single contrast agent to cause differential enhancement based on T1 or T2 imaging. The purpose of this study was to determine the optimum dose of Gd-DTPA-BMA (Omniscan; Sanofi Winthrop and Salutar/Nycomed) for myocardial enhancement based on T1 and T2 shortening. Forty rats were divided into five groups of eight rats each. Rats in groups 1 to 3 received 0.1, 0.3, and 0.5 mmol/kg Gd-DTPA-BMA, respectively. T1-weighted images were acquired before and for 30 min after injection (TE = 15 msec, TR = 300 msec). Rats in groups 4 and 5 received 0.3 and 0.5 mmol/kg Gd-DTPA-BMA, respectively, and T2-weighted images were acquired before and for 30 min after injection (TE = 60 msec, TR = 1.5 seconds). All animals were sacrificed and Gd concentration was determined in myocardium. On T1-weighted MR images, positive correlation was observed between Gd myocardial content and the injected doses. Enhancement of myocardial signal increased as the dose increased from 0.1 to 0.3 mmol/kg (165% ± 10% and 210% ± 12% of baseline, respectively). The 0.5-mmol/kg dose provided no further enhancement (220% ± 15% of baseline). On T2-weighted MR images, the administration of 0.3 mmol/kg Gd-DTPA-BMA produced a slight decrease in signal intensity (at 5 min) followed by complete recovery at 30 min. Greater decrease in signal intensity (32% ± 7% of baseline value) was observed after the injection of 0.5 mmol/kg, and this decrease persisted for 30 min. In conclusion, the net effect of Gd-DTPA-BMA on myocardial signal intensity is dose- and pulse sequence–dependent. In the heart, the dual effect of Gd-DTPA-BMA on T1 and T2 shortening can be exploited for documenting ischemic myocardium.

037 • 11:45 AM

### Gadolinium Phosphonates Used as MR Imaging Agents: Physiologic Effects

IK Adzamli, MP Gilmore, JA Leppo
*Departments of Radiology and Nuclear Medicine, University of Massachusetts Medical Center, Worcester*

Gd-DTPA-HPDP, a diphosphonate-modified Gd-DTPA, is being investigated as a potential MR agent for infarct delineation. Gd-DTPA-HPDP bears a calcium-binding free diphosphonate (diP) that may potentiate systemic hypocalcemia in compromised animals. In this study the so-

| Dose (μmol/kg) | Control | First Pass | Recovery | Ca/P |
|---|---|---|---|---|
| | | Free Diphosphonates | | |
| 50 | 91 ± 06 | 30 ± 01* | 87 ± 05* | 1.10 |
| 100 | 82 ± 05 | 10 ± 01* | 79 ± 08 | 1.00 |
| | | Gd EDTMP | | |
| 100 | 97 ± 12 | 47 ± 03† | 90 ± 11* | 0.36 |

* $P < 0.05$.
† $P < 0.001$, compared to control.

dium salt was toxic (100 μmol/kg) in rats bearing focal myocardial infarction (MI) (but not in normal rats or in rats with diffuse MI). Accordingly, the hemodynamic functional responses to Gd-DTPA-HPDP, HEDP (another free diP), and Gd-EDTMP (bound tetraphosphonate) in an isovolumetric isolated perfused rabbit heart model were investigated. The first-pass and recovery levels of developed pressure (peak systolic pressure − end diastolic pressure [PSP − EDP]) are shown in the Table. The effect of Gd-DTPA-HPDP was identical to that of HEDP. Recovery of developed pressure was achieved either by flushing with Krebs solution or by titrating the medium with $CaCl_2$ (calcium required is in column 5). The mean PSP − EDP (±SEM in mm Hg) is shown in columns 2–4 ($n$ = 3–7). The free diP produced a 66% loss in PSP − EDP at the half dose (rats recovered from this dose of Gd-DTPA-HPDP), compared with a 90% pressure loss at full dose. Gd-EDTMP produced only a 50% drop in pressure at full dose. Premixing the above compounds with the determined amounts of calcium resulted in no changes in PSP − EDP. Therefore, phosphonate-modified paramagnetic agents can be used for MR imaging when administered with calcium, and relevant doses can be estimated with this in vitro model.

038 • 11:57 AM

### MR Imaging Enhancement by Different Molecular Weight Polylysine-(Gd-DTPA)

VS Vexler, O Clement, Y Berthezene, A Mühler, R Kuwatsuru, ME Moseley, RC Brasch
*Contrast Media Laboratory, Department of Radiology, University of California, San Francisco*

Macromolecular paramagnetic contrast media (MMCM) have not yet been clinically tested, but several formulations have been studied in animals to provide a marker of tissue perfusion, relative tissue plasma volume, and capillary leak. The hypothesis underlying this study is that the time course of MR signal tissue enhancement produced by MMCM depends on the molecular weight of the contrast agent. T1-weighted coronal SE (200/6) MR images of liver and kidneys were acquired before and up to 30 min after intravenous administration of polylysine-$(Gd\text{-}DTPA)_{40}$ (25, 50, or 100 kd; 0.025 mmol Gd/kg), albumin-$(Gd\text{-}DTPA)_{35}$ (92 kd; 0.03 mmol Gd/kg), or Gd-DTPA (592 d; 0.1 mmol Gd/kg) in normal rats. The liver was examined as a control tissue in which there was no suspected accumulation or excretion of the contrast medium, and in which the enhancement should normally reflect plasma levels of contrast agent. Results showed a uniform liver signal intensity for all time points for 100-kd polylysine-(Gd-DTPA) and for albumin-(Gd-DTPA). For Gd-DTPA and for the low-molecular-weight polylysine-(Gd-DTPA), signal intensity declined very rapidly at 25 and 50 kd. Comparison of kidney enhancement produced by Gd-DTPA and by different MMCM shows that glomerular filtration contributes to a rapidly declining plasma concentration for the low-molecular-weight polylysine-(Gd-DTPA). It is suggested that owing to slow renal excretion, the high-molecular-weight polylysine-(Gd-DTPA) (100 kd), like albumin-(Gd-DTPA), produces the most consistent tissue enhancement and is suitable as a prototype MMCM.

039 • 12:09 PM

### Manganese-based Paramagnetic Liposomes: Comparative Approaches

EC Unger, TA Fritz, DK Shen, GL Wu*, TE New*, B Kulik*
*Department of Radiology/MRI, University of Arizona, and *ImaR$_x$ Pharmaceutical Corp, Tucson*

This study was conducted to develop more effective liposomal-based blood pool contrast agents. New bifunctional acylated complexes of manganese, iron, and gadolinium were developed and incorporated into liposomes of varying size and membrane composition. Liposomes entrapping manganese chloride were also developed and tested for relaxivity, stability (serum and storage), toxicity, and imaging in a rat liver tumor model. The manganese-based nanosomes had the highest relaxivity, with R1 and R2 values of about 30 $mmol/L^{-1} \cdot sec^{-1}$ for the acylated complex nanosomes and even higher for the nanosomes entrapping $MnCl_2$. Liposomes entrapping dilute concentrations of manganese (eg, below 50 mmol/L $MnCl_2$) had much higher relaxivity per millimole of manganese than did liposomes entrapping higher concentrations of manganese. Imaging showed enhanced liver tumor detection at doses under 1 μmol/kg of the liposomes with acylated complexes of manganese, and at about 2.5 μmole per kg manganese for the nanosomes entrapping manganese; appreciable blood pool enhancement was also observed paralleling the blood pool phase on biodistribution. Very high relaxivity blood pool agents have been developed. Work is under way to take one of these agents into clinical trials.

## Monday Afternoon • Beekman Parlor
## Papers 040–047

### RARE

MODERATORS: DB Plewes, PhD • HE Simon, PhD

040 • 3:45 PM

### Ultrashort-TE Conventional and Fast Spin-Echo Imaging

S Vinitski, DG Mitchell, VM Rao, HV Ortega, FB Mohamed, S Einstein*
*Department of Radiology, Thomas Jefferson University, Philadelphia, and *General Electric Medical Systems Group, Milwaukee*

A number of biologic tissues, such as liver and atherosclerotic plaque, are characterized by their short T2. Pulmonary and temporal lobe imaging is complicated by the presence of large air/tissue interfaces. Therefore, in proton-density and/or T1-weighted Fourier imaging of these organs, TE must be reduced to the minimum. Shortening of TE also reduces motion and some flow artifacts. In fast spin-echo imaging (1), particularly that with long echo trains, reducing the spacing between consecutive echoes should reduce image blurring, as well as suppress susceptibility and motion artifacts. This study concentrated on conventional (SE) and fast (FSE) spin-echo imaging. The conventional spin-echo technique has been redesigned to reduce the minimum TE up to 4.8 msec. This was achieved by keeping all magnetic gradients (except readout) at a maximum (10 mT/m) and using only ramp waveforms. The truncated sinc RF pulse with variable bandwidth and asymmetric echo sampling was also used. A 1.5-T GE Signa imager was used to test the technique in imaging of the upper abdomen. The technique was com-

pared with conventional spin-echo imaging (TR/TE = 400/11 msec, section thickness = 7 mm, FOV = 32 cm, TE = 5.2 msec). The same methodology was applied to FSE imaging (with symmetric echo sampling) and also tested in imaging of the head and upper abdomen. Interecho spacing was shortened to 6 msec. A 1.5-T GE Signa imager was used. Short TE spin-echo imaging significantly improved the contrast-to-noise ratio (C/N) between liver and spleen (7.4 ± 2.1 vs 4.1 ± 1.35, $n = 8$, $P < .01$). It also significantly reduced the intensity of ghost artifacts (34%, $P < .01$), increased the number of available imaging planes by 30%, and enhanced edge detection. The system noise remained the same. In imaging of the temporal bone of the internal auditory canal (IAC), the seventh and eight cranial nerves as well as the inner ear structures (cochlea, vestibule, and semicircular canal) were much better visualized. Additionally, the proposed technique dramatically improved susceptibility-induced artifacts. In FSE imaging of the upper abdomen, the ghost intensities were reduced by 50% to 100% and the images became much crisper and cleaner. In brain imaging, white/gray matter delineation was also substantially improved. No distortions due to eddy current effects were evident with either the SE or FSE technique. In conclusion, the presented methodology substantially improved tissue contrast and reduced motion artifacts in both T1-weighted SE and FSE imaging of the upper abdomen. It also provided detailed delineation of white/gray matter and temporal bone structure, and thus merits further evaluation.

1. Melki PS, Mulkern PV, Panych LP, Jolesz F. JMRI 1991; 1: 319.

041 • 3:57 PM

## Triple-Contrast (Proton Density, T1, T2) RARE Sequence

K Oshio, FA Jolesz

*Department of Radiology, Brigham and Women's Hospital, Boston*

A multisection pulse sequence that gives proton density (PD)–, T1-, and T2-weighted images simultaneously has been developed. The sequence is based on RARE and can acquire PD-, T1-, and T2-weighted images in about 2 minutes. Two different TRs (typically 2,000 and 300 msec) are used alternately. The T1-weighted data are sampled after the shorter TR, and the data set for the PD- and T2-weighted images are acquired after the longer TR in the same way as with the dual-contrast RARE sequence. During the longer TR period, other sections can be excited to perform multisection examination. There are several advantages to acquiring PD-, T1-, and T2-weighted images simultaneously. First, the image set to calculate the physical parameters (PD, T1, and T2) can be obtained without any spatial misregistration. Second, unambiguous information about the physical parameters of the lesion can be obtained in a short time. Third, in abdominal examinations, a multisection sequence guarantees that the section positions of the three images are exactly the same. Also, by adding a fat-saturation pulse before the PD and T2 portions, sections with and without fat suppression can be obtained simultaneously. The triple-contrast RARE sequence was implemented with a 1.5-T GE Signa. Images were obtained with phantoms and volunteers, and pure parameter images (PD, T1, and T2) were obtained without any spatial misregistration problems.

042 • 4:09 PM

## Magnetization Transfer Studies with Multisection RARE Sequences

RV Mulkern, PS Melki*, HS Lilly†

**Radiology Departments, Children's Hospital and Brigham and Women's Hospital, Boston; †GE Medical Systems, Milwaukee*

Classically, magnetization transfer (MT) effects are accessed by applying off-resonance irradiation to a sample and observing the on-resonance signal. As Dixon has pointed out, routine clinical multisection spin-echo imaging experiments automatically invoke MT effects, since "resting" sections are subject to the off-resonance irradiation being used to examine other sections. With the multisection RARE sequences currently in use, there are approximately four times as many 180° pulses per TR as there are in conventional multisection spin-echo experiments. This leads to more off-resonance irradiation and, subsequently, to more MT effects. To qualitatively study MT effects with RARE, the brains of four adult volunteers were imaged with a 16-echo, 12-shot RARE sequence (TR = 4 seconds, and pseudo-echo time = 64 msec) (1.5-T Signa imager, GE Medical Systems). Separate acquisitions, each requiring 52 seconds, were used to obtain 1, 3, 5, 7, 9, 11, and 13 sections, excited in spatially sequential order, with a 5-mm section thickness and a 2.5-mm gap (3.2-msec sync RF pulses). Signal intensities from white matter, gray matter, and cerebrospinal fluid (CSF) were measured from the section common to all acquisitions. Identical experiments were performed with a water phantom. The ratio of signal intensity from an $N$-section acquisition to that of the single-section acquisition $R$ was found to decrease monotonically with $N$ for white and gray matter reaching values of around 0.6 at $N = 13$. To the contrary, $R$ never dropped below 0.9 for CSF or water, substances in which MT effects are unanticipated, and the 10% drop in $R$ is most probably related to RF bleed-through effects. There is a striking, if somewhat predictable, resemblance of the brain tissue $R$ vs $N$ plots to plots of $M_{sat}/M_{unsat}$ vs off-resonance power level ($H_1^2$) obtained with conventional MT experiments. The results suggest that $R$ vs $N$ data, acquired so conveniently with RARE, may provide MT-specific tissue parameters. However, a theoretical analysis of the differences between a "clean" MT experiment, in which only one off-resonance irradiation frequency is applied for a specified time interval, and the considerably more complicated off-resonance patterns occuring during multisection RARE is required if MT parameters are to be extracted from RARE studies.

043 • 4:21 PM

## Why Is Fat Bright on Fast Spin-Echo Images?

PA Hardy

*Division of Radiology, Cleveland Clinic Foundation, Cleveland*

A striking feature of fast spin-echo (FSE) images is that the fat is brighter than on conventional spin-echo (CSE) images. One hypothesis is that the enhanced transverse relaxation due to J-coupling of the protons in the long-chain fatty acids can be effectively reduced through the formation of multiple spin echoes as in a CPMG or FSE sequence. A simple experiment was conducted to test this hypothesis. Vials of doped water and peanut oil were imaged with CSE and FSE sequences on a GE Signa imager (TR = 2,000 msec, TE = 20, 40, 60, 80, and 100 msec). FSE images were obtained with an echo spacing of 20 msec and an echo train length of 16. Different effective TEs were achieved by shifting the echo at which the central $k_y = 0$ line was collected. The Figure shows the variation of image intensity with changes in TE for the CSE and FSE sequences. For water the image intensity is the same

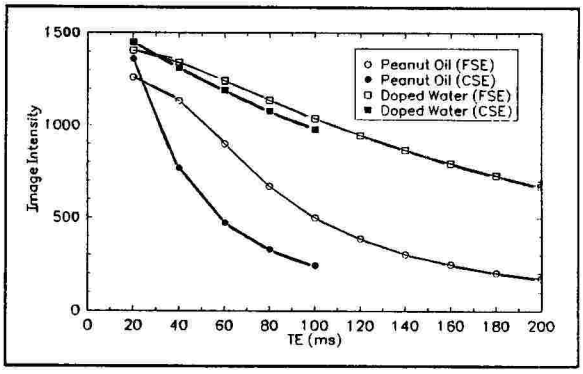


for both CSE and FSE sequences. For oil the image intensity after the first TE value is higher for the FSE images. Repeated refocusing of the transverse magnetization of the oil prevents it from decaying as fast as in a CSE sequence.

044 • 4:33 PM

### Effect of T2 Filtering in Hybrid RARE Imaging on Multiple Sclerosis Plaque Detection

PM Ruggieri, JA Tkach, C VanDyke, D Goodkin, RA Rudick, JS Ross, TJ Masaryk, MT Modic
*Cleveland Clinic Foundation, Cleveland*

While hybrid RARE T2 imaging has the potential to improve patient throughput in MR imaging, the technique introduces additional variables that can affect overall lesion sensitivity. The purpose of this study was to compare the standard T2WSE sequence of the head with several variations of a hybrid RARE T2 sequence to test the effect of different degrees of T2 filtering on lesion detection, using multiple sclerosis (MS) plaques as a clinical model. Twenty-five patients were examined, including five referred for persistent headaches and 20 with known MS. All patients were examined with a 1.5-T GE Signa. The routine axial T2WSE images (2,500/30, 80; 192 × 256 matrix; 5-mm section thickness; 2-mm gap; 1 NEX) were compared with variations of a hybrid RARE sequence: (*a*) 2,000/18, 90; 1 NEX; echo train length (ETL) = 8 but a $256^2$ matrix and 5-mm sections without intersection gap; (*b*) identical echo train with second echo $K_{min}$ centered at 144 msec; and (*c*) reducing the ETL to 4 while increasing $E_{space}$ to 36 msec, and keeping $TE_{eff}$ constant at 144 msec. MS plaques were compared by two neuroradiologists on the basis of presence/absence, size, clarity, and contrast in the different sequences. Normal structures were comparable in appearance on the hybrid RARE images and the traditional T2WSE images. Small objects were more clearly defined when the late-echo image was centered at a shorter $TE_{eff}$ and with a shorter ETL (with longer $E_{space}$) at the same $TE_{eff}$. The total number of plaques identified were identical on the routine and hybrid RARE sequences. Hybrid RARE images provided superior spatial resolution without intersection gap and did not reduce the total number of plaques detected. When maneuvers were used to increase T2 filtering, MS plaques were less well defined. T2 filtering has only a subtle effect on conspicuity of MS lesions, and its apparent clinical impact is negligible with available variations in ETL, $E_{space}$, and $TE_{eff}$.

045 • 4:45 PM

### Hybrid RARE T2-weighted Spin-Echo Imaging in Degenerative Disk Disease

JS Ross, MT Modic, TJ Masaryk, PM Ruggieri, JA Tkach
*Cleveland Clinic Foundation, Cleveland*

The purpose of this study was to evaluate variations in acquisition parameters of a hybrid RARE T2-weighted (T2-RARE) sequence to determine their effect on signal-to-noise ratio, contrast, and resolution, with degenerative disk disease of the lumbar spine as a model. Traditional schemes for spine imaging use T1WSE sequences with conventional T2WSE and/or low-flip-angle gradient-echo studies. Conventional T2WSE sequences are relatively signal-to-noise poor, require refocusing, and have relatively long acquisition times. Low-flip-angle gradient-echo sequences are also relatively signal-to-noise poor, are sensitive to susceptibility artifacts, and do not provide true T2-weighted contrast, especially within the intervertebral disk. The hypothesis was that T2-RARE with multiple $k_y$ lines per excitation and greater practical TR and NEX flexibility would provide improved images in terms of signal-to-noise, contrast, and motion compensation in a shorter acquisition time. The study group of 35 subjects consisted of 10 healthy volunteers and 25 patients suspected to have degenerative disease. The following T2-RARE combinations were obtained on a 1.5-T Magnetom 63SP system. The center of k space was collected at a 90-msec TE. TRs of 2,000, 3,000 and 4,000 msec; 1 and 2 acquisitions; and 2, 4, and 8 $k_y$ lines per excitation were obtained. Conventional T2WSE images (2,000/90/1/192×256) were obtained as the basis of comparison. Compared to traditional T2-weighted spin-echo sequences, (*a*) the number of $k_y$ lines per excitation had no visible effects on the signal-to-noise ratio. (*b*) Increases in the number of excitations from 1 to 2 and TR from 2,000 to 4,000 progressively increased the signal-to-noise on images that could still be acquired in significantly shorter examination times (2–4 minutes). The use of shorter TRs and rectangular field of view allowed acquisitions in less than 2 minutes. (*c*) The T2-RARE sequence demonstrated improved refocusing of the cerebrospinal fluid, which improved image quality with decreased ghosting and enhanced edge detection. Extradural defects were seen as well if not better. (*d*) Soft-tissue contrast and signal intensity within degenerative disks were comparable between the RARE and conventional T2 sequences. (*e*) The theoretical confounding effect of T2 filtering did not appear to be a problem. Hybrid RARE T2-weighted sequences produce a dramatic improvement in image quality, with a preservation of T2-weighted contrast in a markedly reduced examination time. It is proposed that hybrid RARE T2WSE sequences replace conventional T2WSE or gradient-echo images in routine lumbar imaging.

046 • 4:57 PM

### Evaluation of Fast Spin-Echo Sequences for MR Imaging of Pelvic Diseases

RC Haldemann, GP Krestin, S Duewell, B Marincek, GK von Schulthess, M Elmandjra
*Department of Radiology, University Hospital Zurich, Switzerland, and GE-CGR Medical Systems, Buc, France*

The fast spin-echo (FSE) technique is an MR pulse sequence consisting of multiple echoes, each echo being individually phase encoded, which leads to substantially decreased acquisition times in MR imaging. The usually time-consuming T2-weighted images are mandatory for accurate diagnosis of pelvic diseases. To evaluate the quality and usefulness of the new sequence, 30 female patients with various gynecologic diseases were examined with FSE and conventional spin-echo imaging. All patients underwent both techniques in the transverse plane with similar TRs. For FSE images an echo train of 8 echoes was used, with an effective TE of 17 and 85 msec, respectively. Acquisition times were 17 min for the SE sequence (2 NEX) and 5 min for the FSE sequence (2 NEX). The signal intensity of fat, muscle, urine, bone marrow, pathologic tissues, an external probe, and noise was determined in

regions of interest of the same size on each image. Signal-to-noise and contrast-to-noise on FSE images were 30%–50% and 30%–70% higher, respectively, than on SE images. The use of the FSE sequence increased diagnostic confidence in 20% of cases. Therefore, it is concluded that the FSE technique is faster and qualitatively superior to conventional T2-weighted imaging, and its routine use is recommended for pelvic MR imaging.

047 • 5:09 PM

### Quantitative Comparison of Conventional and Fast Spin-Echo Images

S Duewell, B Marincek, GP Krestin, R Haldemann, B Haubold-Reuter, M Saadi-Elmandjra*

*Department of Medical Radiology, University Hospital Zurich, Switzerland, and *General Electric-CGR, Buc, France*

Fast spin-echo (SE) sequences reduce the acquisition time of conventional SE sequences by a factor of 2–16. These sequences consist of a multiple echo train, each echo being individually phase encoded. Echo time is that corresponding to the smallest phase-encoding value to demonstrate that fast SE sequences can replace conventional SE sequences. Conventional and fast SE sequences were quantitatively compared in this study. Fifty patients were examined with conventional and fast SE sequences. Each examination included at least a proton-weighted imaging sequence (TR > 2,000 msec and TE < 20 msec) and a T2-weighted sequence (TR > 2,000 msec and TE > 80 msec). Echo time, field of view, number of signals averaged, and resolution were identical for conventional and fast SE sequences. Eight echoes corresponding to 8 phase-encoding steps were acquired for each 90° pulse. Regions of interest were placed in all patients over the following tissues: bladder (urine), fat, bone marrow, muscle, and liver. In all examined tissues, equal signal-to-noise ratios were found with proton-weighted conventional and fast SE sequences. With T2 weighting, significantly higher signal-to-noise ratios were measured with fast SE sequences in bladder, fat, and bone marrow ($P < .02$). Consequently, the bladder/muscle, fat/muscle, and bone marrow/muscle ratios were found to be higher for fast SE sequences. The higher signal-to-noise ratio for bladder, fat, and bone marrow may be explained by the contribution of high signal from early echoes used for the second and following phase-encoding steps. These findings do not affect the image reading. In no case was pathology overlooked or misinterpreted with fast SE sequences compared with conventional SE imaging.

# Monday Afternoon
# Sutton Parlor North
# Papers 048–055

## FLOW QUANTIFICATION

MODERATORS: RL Ehman, MD • FW Wehrli, PhD

048 • 3:45 PM

### Flow Quantification in Human Coronary Arteries

RR Edelman, WJ Manning

*Departments of Radiology and Cardiology, Beth Israel Hospital, Boston*

MR angiography of coronary arteries has been a long-sought goal. Of equal importance is the noninvasive measurement of coronary artery blood flow, which hitherto has been possible in only a limited sense with transesophageal echocardiography. A modification of a breath-hold segmented TurboFLASH sequence (1) has been developed that permits flow quantification in human coronary arteries and bypass grafts. Healthy subjects were imaged with a 1.5-T Siemens Magnetom system. Cine breath-hold electrocardiograph-gated images were obtained with a segmented TurboFLASH sequence (16 segments, 6 or 8 phase-encoding steps per segment, 25° flip angle, TE = 8 msec, 20 × 15-cm field of view, section thickness = 3 mm). Approximately 8–12 phases of the cardiac cycle were imaged in each breath hold. Temporal resolution was 109 msec for a 128 × 256 matrix and 82 msec for a 96 × 256 matrix. Two sets of cine images were acquired in two separate breath holds. The first set used first-order flow compensation. The second set was partially dephased so that aliasing occurred at either 1 m/sec or 50 cm/sec. Phase images were generated by pairwise manipulation of the rephased and dephased cine images. Flow velocity measurements were validated in a flow phantom over a velocity range of 0–75 cm/sec and tested in healthy volunteers and patients with patent bypass grafts at angiography. The phantom study showed excellent correlation between MR and volumetric flow measurements ($r = .95$). Flow measurements in vivo were in a range consistent with previous reports using intracoronary Doppler probes. It is concluded that noninvasive flow measurement of human coronary arteries is now feasible.

1. Edelman RR, Manning WJ, Burstein D, Paulin S. Breath-hold MR angiography of human coronary arteries. Radiology 1991; 181:641–643.

049 • 3:57 PM

### Quantitative MR Blood Flow Measurements in the Pulmonary Arteries: First Clinical Applications in Preoperative Planning for Central Lung Tumors

AH Gamroth, LR Schad, CM Wacker, W Semmler, U Gehling, E Müller*, G van Kaick

*German Cancer Research Center, Heidelberg, and *Siemens, Erlangen, Germany*

The goal of this study was to establish a noninvasive method based on MR flow measurements for preoperative treatment planning in patients with lung tumors. Estimation of pulmonary blood flow is required in case of pneumonectomy or (bi)lobectomy and routinely performed with right heart catheterization, Doppler US, and perfusion scintigraphy. MR velocity measurements were obtained with the RACE technique (real-time acquisition and evaluation of blood flow in one-dimensional space projection) with an MR unit (1.5-T Siemens Magnetom). The flow in each vessel was calculated by multiplying the mean blood flow velocity (measured with RACE) by the vessel area (determined on a flow-compensated gradient-echo image obtained at the same position). In eight patients with central carcinoma, flow measurements were obtained in a plane perpendicular to the direction of flow through the main, right, and left pulmonary arteries (MPA, RPA, and LPA); the flow in the ascending aorta was also determined. Localization of flow measurements was proximal to any branch artery and acquired within 10 seconds during breath hold. The sum of RPA and LPA flow was compared with the flow in the MPA and the ascending aorta. These results were correlated with right heart catheterization and Doppler US performed within 48 hours. RACE measurements correlated well with the results of right heart catheterization and Doppler US. The advantages of the RACE technique are its capacity to measure flow in the LPA and RPA separately in predefined locations, and the good access it affords to poststenotic regions. This technique allows flow measurements during breath hold, and the short data acquisition time precludes misregistrations due to arrhythmias. RACE is an alternative method of obtaining preoperative information about

pulmonary blood flow in case of parenchymal resection. The clinical results and an estimation of the accuracy of the MR blood flow measurements are discussed in detail.

050 • 4:09 PM

### Quantitative Measurement of Velocity at Multiple Positions with Comb Excitation and Fourier Velocity Encoding for the Calculation of Wave Speed and Local Vessel Wall Distensibility

CL Dumoulin, DJ Doorly*, CG Caro*
*General Electric Research and Development Center and *Imperial College, Schenectady, NY*

An MR imaging technique that simultaneously acquires Fourier velocity-encoded data from multiple stations was developed and tested. The technique employs a comb excitation RF pulse that excites an arbitrary number of sections. As the Fourier velocity phase-encoding gradient pulse is advanced, the phase of each section in the comb is advanced by a unique amount. This causes the signals from the spins in a particular section to appear at a position in the phase-encoding direction that is the sum of the spin velocity and an offset arising from the phase increment given to that excitation section. Fourier velocity encoding was used with the comb excitation to obtain accurate velocity-measurements for each section. Two Fourier velocity-encoding methods were investigated. Both acquire three dimensions of data. The first method resolves data in a single spatial dimension, a velocity dimension, and a temporal dimension. This has proved useful for the evaluation of dynamic blood flow in the body. In these procedures, the temporal resolution of the measurement was increased by interleaving multiple acquisitions. The second method resolves data in two spatial dimensions and one velocity dimension and has proved useful in evaluating steady flow profiles. Spin velocity information is acquired simultaneously for all sections when comb excitation is used. This permits the calculation of pressure wave velocities arising from pulsatile flow. In the absence of pulse wave reflections, two stations separated by a sufficient distance are enough to calculate the wave speed. Data acquired simultaneously at three or more stations permit a more sophisticated analysis that is also capable of detecting reflected waves. Once wave velocities are known, they can be used to determine vessel wall distensibility $D$, using the relationship $D = 1/(\rho C)^{1/2}$, where $\rho$ is the density of the vessel wall and $C$ is the wave speed. Distensibility is an important physiologic parameter as a determinant of ventricular afterload, a predictor of coronary atherosclerosis that may be causally related to the development of atherosclerosis. Studies were performed in healthy volunteers with a 1.5-T imaging system. Typical RF waveforms used for in vivo data acquisition excited five sections, each 5 mm thick and spaced as little as 5 mm apart. Local wave speeds were measured for the aorta and the common carotid, vertebral, and femoral arteries. Wave speed measurements were also made in phantoms and verified with distensibility measurements made by direct observation of diameter changes in response to changes in static pressure.

051 • 4:21 PM

### Interstudy Reproducibility of Velocity-encoded Cine MR Measurements of Aortic Regurgitation

M-C Dulce, G Mostbeck, GR Caputo, M O'Sullivan, CB Higgins
*Department of Radiology, University of California, San Francisco*

Assessment of the response to therapy of patients with aortic regurgitation (AR) requires a technique for measuring AR that is accurate and has good reproducibility between studies. Accordingly, this study assessed the accuracy and interstudy reproducibility of velocity-encoded cine MR (VEC-MR) for quantifying regurgitation volume (RV) and fraction (RF). Twenty-seven VEC-MR studies were performed with a 1.5-T imager in 15 AR patients. In six of these patients a second and third study were conducted within 14 days for the assessment of interstudy reproducibility. Aortic flow was measured with VEC-MR using oblique imaging planes (perpendicular to the direction of flow) at a level 1 cm below the innominate artery. For the volumetric measurements, a biphasic spin-echo sequence [BPSE] or cine MR imaging was used. RV was measured on the aortic flow curve by quantifying ante- and retrograde flow over the cardiac cycle and was compared with RV measurements by a volumetric method (BSPE or cine MR) of right (RSV) and left (LSV) ventricular stroke volume (RV = LSV − RSV). RF was also calculated (RF = RV/LSV). All calculations were performed by two independent observers. Linear regression $r$ and standard error of estimate (SEE) were used for statistic analysis. Results of the study were as follows: (*a*) RV and RF by VEC-MR correlated well with RV and RF by volumetric MR measurements (RV: $r$ = .986, SEE = 3.2 mL; RF: $r$ = .991, SEE = 4.4%). (*b*) Interobserver variability for VEC-MR RV and RF measurements was excellent (RV: $r$ = .995, SEE = 3.2 mL; RF: $r$ = .991, SEE = 3.3%). (*c*) Interstudy variability for VEC-MR RV and RF showed a high reproducibility (RV: $r$ = .980, SEE = 8.4 mL; RF: $r$ = .990, SEE = 3.1%). In conclusion, VEC-MR measurements of RV and RF are accurate and highly reproducible between studies, indicating effectiveness of this noninvasive technique for follow-up and drug monitoring studies.

052 • 4:33 PM

### Diagnosis of Aortic Valve Insufficiency with MR Rheography

G Engels, E Müller*, K Reynen, N Wilke*, K Bachmann
*Medical Clinic II, University of Erlangen, Germany, and *Siemens Medical Engineering Group, Erlangen*

Grading of aortic valve insufficiency is routinely performed with Doppler US or heart catheterization. In addition, new MR rheographic techniques for quantitative blood flow evaluation such as phase mapping and phase contrast (two-dimensional space-resolved techniques with time-averaged measurement of blood flow), as well as RACE (real-time acquisition and evaluation of blood flow in one-dimensional space projection), are now available for the diagnosis of valvular heart disease. The purpose of this study was to evaluate the fraction of regurgitated to ejected blood volume in different cases of aortic valve insufficiency to formulate a grading of this valvular heart disease with MR rheography in comparison with grading with Doppler US or heart catheterization. The MR techniques were used in a plane perpendicular to the blood flow through the ascending aorta at a defined distance from the aortic valve. Ten patients were examined, seven of whom had aortic valve insufficiencies of various degrees. Fraction of regurgitated blood volume was evaluated with MR for each patient and compared with the grading of aortic valve insufficiency done with Doppler US or heart catheterization. The results of the different MR methods show good concordance in the evaluation of regurgitation volumes resulting from various aortic valve insufficiencies. In comparison with the routinely used procedures of Doppler US and heart catheterization, MR rheography produces a similar differentiation of low- and high-grade aortic valve insufficiencies. In conclusion, MR rheographic techniques allow the quantitative evaluation of regurgitated blood flow volume in the case of aortic valve insufficiency. Diagnoses of aortic valve insufficiency

with Doppler US or heart catheterization are at present only semiquantitative; therefore, the development of a new standard of reference in the diagnosis of valvular insufficiencies with MR rheography seems possible.

053 • 4:45 PM

### Real-Time Line-Scan Color Phase-Velocity Mapping of Flow

RK Butts, NJ Hangiandreou, SJ Riederer
*MR Laboratory, Mayo Clinic and Foundation, Rochester, Minn*

The ability to interactively assess blood flow characteristics in real time with Doppler ultrasound (US) has led to a broad range of clinical applications for this modality. Certain limitations of US imaging have led to the investigation of the feasibility of providing a real-time interactive flow-imaging capability with MR imaging. MR imaging techniques such as cine phase contrast, phase-difference gradient echo, and echo-planar imaging provide flow information but with temporal resolutions on the order of several minutes, 1 Hz, and 10 Hz, respectively. The purpose of this study was to integrate a line-scan acquisition technique with a high-speed reconstruction system to allow real-time acquisition and display of velocity maps at 25 Hz. The real-time line-scan technique uses an 11-msec duration, 2D spatially selective RF pulse to excite a 2-cm full-width half-maximum Gaussian column through the vessels of interest. Repetitions of 20 msec are alternately flow compensated and flow encoded along an arbitrary direction of interest. A readout gradient encodes position along the column at an echo time of 7 msec. The high-speed reconstruction system performs a 1DFT, magnitude and phase computations, phase subtraction, and display of successive lines of data that are immediately scrolled up the screen as subsequent lines are acquired. Preliminary in vivo studies clearly demonstrate pulsatile flow in large vessels with 25-Hz temporal resolution. Immediate applications of this technique include the rapid assessment of flow characteristics in large vessels such as the aorta, portal vein, and pulmonary arteries.

054 • 4:57 PM

### Quantitative Cerebrospinal Fluid Velocity Imaging: Comparison of Normals and Patients with Shunt-Responsive Normal Pressure Hydrocephalus

WG Bradley, DJ Atkinson*, WR Nitz*, MN Nissenbaum, S Song, BE Widoff, K Yan, SM Brown
*Long Beach Memorial Medical Center, Calif, and *Siemens Medical Systems, Iselin, NJ*

Previous studies have demonstrated an increased aqueductal cerebrospinal fluid (CSF) flow void in patients with shunt-responsive normal pressure hydrocephalus (NPH). The purpose of this study was to quantitate the aqueductal CSF stroke volume and assess its efficacy as a predictor of shunt response in patients with clinical NPH. Five elderly volunteers and 10 patients with clinical NPH were evaluated with a high-resolution quantitative phase-contrast CSF velocity imaging technique reported previously (FISP 100/16/15, with retrospective cardiac gating into 18 bins, 512 × 512 over 16-cm FOV, 4-mm section perpendicular to aqueduct). Aqueductal CSF stroke volumes and peak systolic velocities were determined. The average peak systolic velocity for the normal volunteers was 55 mm/sec while that for five shunt-responsive NPH patients was 112 mm/sec. The average CSF stroke volume for the normal volunteers was 11 $mm^3$ while that for the patients with shunt-responsive NPH was 32 $mm^3$. Following shunt revision in one symptomatic 73-year-old patient with NPH and atrophy, stroke volume decreased from 9 $mm^3$ to 5 $mm^3$ and symptoms cleared. In conclusion, demonstration of hyperdynamic CSF flow with quantitative CSF velocity imaging is a useful indicator of a favorable response to ventriculoperitoneal shunting for NPH.

055 • 5:09 PM

### Quantification of Blood Flow in Internal Mammary Arteries with Phase-Contrast Imaging

R Negro-Vilar, JF Debatin, HD Sostman, J Strong, CE Spritzer
*Department of Radiology, Duke University Medical Center, Durham, NC*

Noninvasive quantification of blood flow in internal mammary (IMA) coronary bypass grafts with phase-contrast MR imaging could have significant implications for pre- and postoperative patient management. While graft patency has been assessed with conventional spin-echo and gradient-recalled-echo imaging, quantifying blood flow with phase-contrast imaging may enable identification of subtotal stenosis. To validate the technique, assessment was made of the consistency and reliability of MR blood flow quantification in IMAs in healthy volunteers. Ten healthy male volunteers were imaged on four separate occasions. Axial cine phase-contrast images were obtained at the level of the pulmonary artery bifurcation. The imaging parameters were as follows: TR/TE = 32/7.9, 45° flip angle, 5-mm section thickness, 128 × 256 matrix, 28 $cm^2$ FOV, 2 NEX. An anteriorly placed surface coil was used for signal reception. Velocity was encoded from superior to inferior with the velocity-encoding value of 120 cm/sec. Between 15 and 20 phases were reconstructed per RR interval. Based on the measured velocity and luminal area, blood flow was quantified in the IMAs and ascending aorta. IMA flow relative to the ascending aorta was calculated for each acquisition. All 40 examinations were technically adequate, with both IMAs well visualized in all cases. Mean blood flow in the IMAs was similar from side to side, measuring 177 mL/min on the right (3.9% of ascending aortic blood flow) and 164 mL/min on the left (3.6% of ascending aortic flow volume). Among different volunteers, there was considerable variability, with standard deviations of 41 mL on the right and 30 mL on the left. In individual volunteers, however, IMA flow over time, relative to the ascending aorta, was consistent, with standard deviations ranging from 0.1% to 0.6% of the measured blood volume in the ascending aorta. It is believed that this method holds considerable potential in the evaluation of IMA grafts.

## Monday Afternoon
## Sutton Parlor Center
## Papers 056–062

### MRS OF CEREBRAL METABOLISM

MODERATORS: TR Brown, PhD • RK Gupta, PhD

056 • 3:45 PM

### Concurrent Changes in High-Energy Phosphorus Compounds and in Cerebral Blood Flow in Hydrocephalic Rabbits

F Tranquart, M Berson, S Akoka, F Seguin, S Bodard, A Le Pape, L Pourcelot
*INSERM Unit 316-37044 Tours, France*

Intracranial edema and enlargement of the ventricles are important mechanisms in the development of increased intracranial pressure, which by decreasing cerebral perfusion pressure may result in metabolic disturbances in the setting of hydrocephalus. The purpose of this study was to evaluate the relationship between cerebral blood flow

(CBF) and brain metabolism in an animal model of chronic hydrocephalus. The chronic hydrocephalus was induced in eight rabbits by an intracisternal injection of kaolin. The changes in CBF were evaluated with transcranial Doppler US recordings of the basilar artery velocities every week for 4 weeks after kaolin injection. P-31 MR spectroscopy was used to study the metabolic response of the rabbit brain. Each week, a two-turn, double-tuned, (P-31, H-1) home-built surface coil (diameter = 3 cm) was positioned in the same way with a head frame in the upper part of the rabbit's head. One week after kaolin injection, in the acute stage of hydrocephalus, the diastolic flow was reduced by 30% compared with the control value. At the same time, pH decreased from 7.1 (control value) to 7 and Pi/PCr increased from 0.24 (control value) to 0.33. Four weeks after hydrocephalus induction (chronic stage of hydrocephalus), the CBF and high-energy phosphorus compound levels had not changed. Because the observed changes were insignificant, measurement of high-energy phosphorus compounds appears to be inadequate for the follow-up of hydrocephalus. Transcranial Doppler US has proved to be a more precise technique for the evaluation of brain disturbances due to increased intracranial pressure.

057 • 3:57 PM

### Human Lithium Psychopharmacology with in Vivo Quantitative MR Spectroscopy

RG González, AR Guimaraes, P Renshaw, G Sachs, M Garwood, GJ Moore, JF Rosenbaum

*MGH-NMR Center, Department of Radiology, Massachusetts General Hospital, Charlestown, and Psychopharmacology Unit, Massachusetts General Hospital, Boston*

The quantitative lithium-7 MR spectroscopic method used in this study overcomes inherent problems in quantitative MR spectroscopy in the following ways: (*a*) Low signal-to-noise ratios due to low nucleus sensitivity and metabolite concentrations are overcome by sampling a large volume (approximately 1,000 mL) of brain tissue. (*b*) Uncertain T1 effects are minimized by a long TR (25 seconds), and T2 effects are eliminated by collecting the FID immediately after excitation. (*c*) RF transmission is made homogeneous with the use of adiabatic 90° and 180° pulses. (*d*) Errors in the calculation of sampled volumes are minimized by using computerized morphometric analysis software developed in house. (*e*) RF reception inhomogeneities are corrected with a mathematical model based on empirically derived data. Error analysis revealed a precision of better than 5% and an accuracy of about 7%. Ten subjects with bipolar illness were studied. Daily oral dosage of lithium carbonate was 900 mg/day to 1,800 mg/day. Serum levels ranged from 0.54 mmol/L to 0.99 mmol/L, and brain [Li] varied from 0.39 mmol/L to 0.87 mmol/L. A high correlation was found between daily dose and serum [Li] ($R^2$ = .807), but not between daily dose and brain [Li] ($R^2$ = .314). This effect was further demonstrated by a substantial variation in serum-to-brain [Li] ratios of 0.50 to 0.966. These findings indicate that the common guide to lithium dosage, serum [Li], does not necessarily reflect the [Li] in the target organ, the brain.

058 • 4:09 PM

### Quantitative High-Resolution Proton MR Spectroscopy of Alzheimer Disease and Parkinson Disease with N-Acetyl Aspartate as a Neuronal Marker

AR Guimaraes, RM Nitsch, JH Growdon, RG González

*MGH-NMR Center, Department of Radiology, Massachusetts General Hospital, Charlestown, and Department of Neurology, Massachusetts General Hospital, Boston*

N-acetyl aspartate (NAA) is a putative neuronal marker based on spectroscopic, biochemical, and ultrastructural evidence. The aim of this research was to quantify neurodegeneration by using high-resolution MR spectroscopy measurements of NAA from in vitro brain samples. The samples were extracted with chloroform/methanol and the aqueous extracts were analyzed with a one-pulse experiment with a quadrature phase-cycling scheme. A 15-second repetition rate with a total of 120 averages ensured adequate signal/noise and full longitudinal relaxation for proper quantification. Absolute concentrations were calculated using a $CDCl_3/CHCl_3$ external standard in a coaxial insert and calibration standards of 2.5, 5, and 10 mM N-acetyl cysteine, a compound with a methyl resonance at the same chemical shift of the NAA methyl moiety. Brain samples from Alzheimer disease (AD) and Parksinon disease (PD) were compared. Patients were matched according to age and time postmortem; all samples were taken from the frontal cortex. The mean NAA for AD was 7.11 ± .35 mmol/kg wet weight compared with 9.49 ± .56 mmol/kg for PD. The results were found to be statistically significant ($P < .05$). In this preliminary investigation of two common neurodegenerative diseases, a statistically significant discrepancy between NAA concentrations was found. These results suggest that the neuronal marker NAA is decreased in AD brain. It is proposed that measurement of NAA may serve as an antemortem marker for neurodegeneration with use of in vivo proton MR spectroscopy.

059 • 4:21 PM

### Cerebral Lactate and Blood Flow in Patients with Acute Stroke

O Henriksen, P Gideon, B Sperling, TS Olsen, HS Jørgensen, NA Lassen

*Danish Research Center of Magnetic Resonance, Hvidovre University Hospital, Copenhagen*

The relationship between cerebral lactate production and blood flow was studied during the course of cerebral infarction following acute stroke. Eight patients were examined within the first 6 to 50 hours (mean, 30 hours) after the clinical attack and reexamined after 1 and 3 weeks. Lactate content in the brain was estimated by means of proton MR spectroscopy with a STEAM sequence (TE = 272 msec). For quantification of lactate content, unsaturated water signal corrected for T2 decay was used as internal standard. Relative regional cerebral perfusion (rCBF) was estimated with an isotope (Tc-99m-HMPAO) technique and a SPECT gamma camera. Average lactate signal expressed relative to the water signal ranged between $0.04 \times 10^{-4}$ and $1.1 \times 10^{-4}$ (mean, $0.7 \times 10^{-4}$) at the first examination. Thereafter the lactate content decreased toward normal, undetectable levels over the next 3 weeks. The lactate content was higher in the central than in the peripheral part of the infarcted lesion. The rCBF showed severe hypoperfusion in the acute phase. Reperfusion with increasing hyperemia was seen in all cases. There was an inverse correlation between lactate content and rCBF in the infarcted area. The results indicate that in the acute phase the amount of lactate reflects the severity of ischemia. In the subacute phase with hyperemia, how-

ever, the lactate does not reflect hypoxic neuronal tissue with anaerobic glycolysis. Finally, lactate is not primarily responsible for the vasodilatation underlying the reperfusion hyperemia.

060 • 4:33 PM

### Localized H-1 MR Spectroscopy in the Pediatric Brain: A Valuable Tool for the Evaluation of Metabolic Disorders?

W Heindel, H Kugel, B Roth, J Bunke, K Lackner
*Department of Radiology and Children's Hospital, University of Cologne, and Philips Medical Systems, Hamburg, Germany*

This study was designed to evaluate normal and abnormal brain development as well as specific aspects of cerebral metabolic disorders in infants. Children with various metabolic diseases were examined with a 1.5-T MR system (Gyroscan S15, Philips). Following conventional MR imaging, localized spectra were obtained with a 90°-180°-180° spin-echo sequence with different echo times (34 msec, 136 msec, and 272 msec). Repetition time was 2 seconds. The regions of interest were determined from the MR images and usually comprised the basal ganglia or parietooccipital white brain matter. The resonances of choline-containing compounds (Cho), creatine (Cr), and N-acetyl aspartate (NAA) typically showed as the strongest signals on spectra of healthy brain obtained with these parameters. To evaluate the spectral changes caused by metabolic diseases, spectra of healthy children of similar age were used for comparison, since the signal intensity ratios of the observable compounds in children differ significantly from typical ratios in adult brain. The NAA/Cho ratio in particular is far smaller in newborns than in adults and varies with age. For example, this ratio was 0.7 in a 4-week-old child, while it reached 2.45 in a 26-year-old adult (TE = 136 msec). The most striking spectral findings were observed in two children with nonketotic hyperglycinemia. In one patient (age, 10 days at the first measurement) the proton spectrum exhibited a signal at 3.55 ppm of the same intensity as the creatine signal that could be unambiguously assigned to glycine. Subsequent measurements over the next 5 weeks showed a decrease of signal to 30% of the initial value. In a second patient (age, 7 weeks) spectra from the basal ganglia as well as from cerebral white matter showed that the signal intensity ratio of glycine to creatine was 0.5 and did not differ in either region. A study of a child with suspected neurodegenerative disease (age, 20 months) showed a significantly increased ratio of NAA/Cho as compared with that for other children of the same age, indicating Canavan disease. Extremely elevated lactate concentrations were observed in all regions of the brain in a child showing symptoms of Leigh syndrome. Spectra from a 9-year-old child with maple syrup disease exhibited small but noticeable signals, tentatively assigned to valine, leucine, and isoleucine, respectively, while in the case of confirmed citrullinemia, no citrulline signal could be detected because of the method's low sensitivity to amino acids exhibiting a complex spin-spin coupling. Proton MR spectroscopy can provide specific information on some metabolic diseases, even if conventional MR imaging shows only uncharacteristic morphologic changes such as cerebral atrophy or demyelination. The noninvasive nature of MR spectroscopy is particularly advantageous for the examination of children, allowing diagnosis of special diseases as well as therapeutic control.

061 • 4:45 PM

### Clinical Proton MR Spectroscopy of the Pediatric Brain

AA Tzika, DB Vigneron, WS Ball, RS Dunn, DR Kirks
*Department of Radiology, Children's Hospital Medical Center, Cincinnati, and University of California, San Francisco*

Recently modified single-voxel proton MR spectroscopy pulse sequences were assessed in the differential diagnosis of neurodegenerative diseases and intracranial masses in 30 children. Quality proton MR spectra (acquisition time, 4 min) were obtained in vivo with short-echo (TR/TE = 2,000/18 msec), stimulated-echo (STEAM), and long-echo (TR/TE = 2,000/270 msec) spin-echo (PRESS) sequences incorporating optimally shaped pulses. All patients were examined with MR spectroscopy in conjunction with MR imaging with a 1.5-T (GE Medical Systems) whole-body MR imaging system. Short-echo STEAM spectra revealed the presence of short T2 metabolite resonances in addition to the prominent resonances from N-acetyl aspartate (NAA), choline, and creatine; the lactate resonance, when present, was well resolved in the PRESS spectra. Neurodegenerative diseases caused changes ranging from mild to dramatic in the glutamate/glutamine, inositol, NAA, and creatine resonances. Based on MR spectral characteristics, cerebrospinal fluid cysts could be distinguished from tumors, and a single case of a dermoid was differentiated from the spectra of neural tumors. Glycolytic metabolism identified by the presence of lactate was coincident with the histologic finding of necrosis in solid tumors. The results demonstrate that proton MR spectroscopy can complement MR imaging in a clinical pediatric environment.

062 • 4:57 PM

### Implementation and use of Chemical Shift Imaging in Hemorrhagic and Ischemic Cerebral Lesions in the Neonate

MA Rutherford*, DJ Bryant, GA Coutts, IJ Cox, J Sargentoni, LMS Dubowitz*, IR Young
*NMR Unit and *Department of Paediatrics, Royal Postgraduate Medical School, Hammersmith Hospital, London*

With use of large-volume (27–64 $cm^3$) single-voxel spectroscopy it has been shown that proton MR spectroscopy may be useful in the assessment of infants with hypoxic-ischemic encephalopathy (HIE). Babies with a very low N-acetyl aspartate/choline ratio (NAA/Cho) in the neonatal period subsequently had a poor outcome. This work has now been extended to improve spatial resolution. A 16 × 16 matrix of voxels, each of nominal volume (4.5 $cm^3$), was obtained. Data were acquired with 3D chemical shift imaging (TR = 1.5 sec, TE = 130–270 msec). The large water signal was suppressed with a binomial pulse and the signal from superficial fat was reduced by incorporating an inversion pulse. In control neonates, there was no variation in the NAA/Cr plus phosphocreatine (NAA/Cr) ratio between the thalami and basal ganglia and the surrounding brain. In a term infant with a middle cerebral artery infarct, NAA/Cho values were markedly decreased in the infarcted area. There was also a peak in the lactate/fat region. Twelve weeks later the NAA/Cho and NAA/Cr ratios in the surrounding brain were equal to those on the normal side. In a 3-week-old infant with bilateral thalamic and basal ganglia hematoma, the NAA/Cho and NAA/Cr ratios showed no obvious reductions. More precise localization with chemical shift imaging makes it possible to provide more detailed information on NAA/Cr and NAA/Cho ratios and to isolate effects due to focal lesions. This may provide better diagnosis of focal lesions and better prognostic information.

# Monday Afternoon
# Sutton Parlor South
# Papers 063–070

## MRA: BRAIN AND NECK

MODERATORS: SW Atlas, MD • AW Litt, MD

063 • 3:45 PM

### Sequential Two-dimensional MR Angiography with Traveling Ascending Presaturation Pulses: Applications in the Head and Neck

AN Hasso, DB Hinshaw Jr, B Holshouser, J Akamine, W Mansfield, D Atkinson

*Sections of Neuroradiology and MRI, Loma Linda University Medical Center, Loma Linda, Calif*

Two-dimensional Fourier transform (2DFT) MR angiographic techniques are less sensitive to saturation effects and better able to depict small vessels than are 3D time-of-flight techniques. These 2DFT sequences are ideally suited for examination of the cervicocranial circulation. The addition of traveling descending presaturation pulses during imaging of the arterial structures eliminates the inflow signal from venous blood. The utilization of traveling ascending presaturation pulses has been found to eliminate the arterial flow signal and optimally depicts the venous anatomy. A series of examinations was performed in five healthy volunteers and 15 patients with FLASH sequences and a 2DFT protocol on the Siemens Magnetom 1.5-T SP system. A 160–230-mm rectangular field of view, a matrix of 192 × 256, and 3-mm section thickness with 40% overlap were used. Traveling ascending presaturation pulses, each 12 mm wide, were added in all cases. Fifty-five partitions were obtained from each sequence. Two slabs were adequate for demonstrating the anatomy from the skull base to the thoracic inlet. This protocol allowed good demonstration of the venous anatomy in the series of volunteers. In the patient population, venous anomalies such as partial or complete thrombosis in association with thrombophlebitis, arteriovenous fistulas, and vascular tumors were clearly depicted. An unexpected finding was the demonstration of retrograde flow in one or the other of the vertebral arteries due to the presence of a subclavian steal syndrome caused by severe occlusive disease proximal to the origin of the vertebral arteries. The expanded application of 2DFT MR angiographic techniques requires the development of specific protocols allowing the depiction of the venous structures. The recent introduction of a protocol including a series of traveling ascending presaturation pulses has made this possible. An additional benefit is the ability to depict retrograde flow in one or the other of the vertebral arteries.

064 • 3:57 PM

### Novice versus Experienced Readers in MR Angiography of 58 Carotid Arteries

RE Lee, CM Anderson, D Saloner

*Departments of Radiology, VA Medical Center and University of California, San Francisco*

Although MR angiographic images appear quite similar to x-ray angiographic images on first inspection, the MR images represent a record of dynamic vascular flow, not actual anatomic detail. Consequently, MR angiographic images are subject to unique flow-related "artifacts." It is important to understand that, as with all "new" modalities, there is a learning curve involved with the accurate interpretation of MR angiographic images. The present study was performed to evaluate potential differences in image interpretation between readers experienced in MR angiography and readers new to this speciality. Thirty-eight patients were imaged with 3D time-of-flight MR angiographics techniques. In the pilot study, MR angiographic images of 13 internal carotid arteries in a total of 12 patients were retrospectively reviewed in a double-blind fashion by three individuals experienced in interpretation of conventional angiograms but having only minimal exposure to MR angiography (novice). The same images were reviewed by three individuals, each of whom had at least two years of experience with MR angiography (experienced). The degree of vascular stenosis occurring in each vessel was estimated and categorized. In the expanded study, a total of 58 internal carotid arteries were reviewed by using a methodology identical to that used in the pilot study except that a single experienced reader was selected as representative of the experienced panel. The experienced reader had a .941 correlation when compared with angiography (exact match: 41 = 71%; +1 grade: 11 = 19%; and −1 grade: 6 = 10%). Novice panel had a .804 correlation (exact match: 23 = 40%; +1 grade 19 = 32%; +2 grades: 4 = 1%; −1 grade: 9 = 16%; and −2 grades: 3 = 5%). Experienced readers matched x-ray angiographic findings exactly in over 70% of cases studied and came within one grade 100% of the time. Novice readers matched or came within one grade in only 88% of the cases. There appears to be a tendency for the new reader to overestimate the degree of stenosis. This tendency may in large part account for the lower correlations between the novice readers and conventional angiographic findings. The results suggest that the MR angiography novice, even if experienced in the interpretation of conventional angiograms, may tend to overcall pathology. An understanding of MR angiographic artifacts, as evidenced by the experienced MR angiographers in this study, may result in a substantial increase in diagnostic accuracy. It is important to note, however, that it seems unlikely that physiologically significant lesions will be missed even by readers in the process of gaining these new interpretation skills.

065 • 4:09 PM

### Analysis of Aneurysms and Arteriovenous Malformations Missed on Routine MR Images That Are Detected with MR Angiography

WG Bradley, SM Brown, BE Widoff, K Yan, S Song, MN Nissenbaum

*Long Beach Memorial Medical Center, Long Beach, Calif*

The routine parenchymal MR studies (SE 3,000/22 and 90, flow compensation on both echoes, 192 × 256 matrix over 22-cm FOV, 5-mm section, 1.2-mm gap, 1 NEX; Siemens 63SP) of two patients with 6-mm internal carotid artery aneurysms and of one patient with a small left main coronary artery arteriovenous malformation (AVM) were normal, while 3D time-of-flight MR angiography (FISP TR/TE/flip angle = 40/7/15°, $256^2$ over 22-cm FOV, 64 partitions, 4.8-cm axial slab) correctly showed the lesions (as corroborated by subsequent catheter angiography). The purpose of this study was to determine factors potentially responsible for the missed diagnosis on the routine study. Cardiac-gated images were acquired in the brain of a healthy volunteer, gating to every third r wave for a TR of 2,966 msec. The same pair of echoes (TE = 22 and 90 with flow compensation) was used as in the routine study. Images acquired during diastole demonstrated isointense arteries on the 22-msec flow compensation first echo while those acquired during systole were hypointense. The combination of diastolic pseudogating and even-echo rephasing due to flow compensation makes small aneurysms and AVMs isointense on routine MR studies. If small vascular abnormalities are suspected clinically, MR angiography is indicated in addition to the routine parenchymal examination.

066 • 4:21 PM

### MR Venography and MR Imaging of Dural Sinus Disease: Comparison with Angiography and CT

B Ostertun, L Solymosi
*Department of Neuroradiology, University of Bonn, Germany*

At present, CT and x-ray angiography are the standard imaging procedures for imaging venous sinuses. In this study, the potential of MR angiography and MR imaging as noninvasive methods in diagnosis and follow-up is evaluated in comparison with CT and x-ray angiography. Twenty 2D time-of-flight MR angiographic examinations were performed in 14 patients showing suspicious clinical symptoms at CT or MR imaging, such as headache, seizures, atypical hemorrhage, or dural-based tumors. Diagnosis was verified with x-ray angiography and CT in most cases; sensitivity and specificity of all available imaging techniques were compared. Two-dimensional inflow MR angiography depicted the dural sinuses with an image quality that was diagnostically comparable to that of conventional angiography when both transverse and coronal imaging was performed. Thromboses and stenoses found at conventional angiography, CT, or MR imaging were verified with MR angiography in all cases. Follow-up treatment with full heparinization demonstrated improvement as well as progression of thrombosis, which was not necessarily accompanied by a parallel development of clinical symptoms. Appositional thrombi were identified only with MR angiography. In two pregnant women, MR angiography could rule out thrombosis, thus obviating x-ray exposure; both patients proved to have eclampsia. Primary MR angiographic sections and MR imaging demonstrated associated cerebral hemorrhage. In conclusion, diagnosis and follow-up of venous sinus thrombosis and tumor-related obstruction is reliably achieved by combining MR angiography and imaging. Simultaneous MR imaging demonstrates accompanying congestive hemorrhage and differential diagnostic pathology. Thus, MR can, where available, replace repeated CT and x-ray angiography in this indication.

067 • 4:33 PM

### Characterization of Atherosclerotic Plaque with a 1.5-T Imaging System

GE Gold, JM Pauly, GH Glover, JC Moretto, A Macovski, RJ Herfkens
*Departments of Radiology, Electrical Engineering, and Pathology, Stanford University, Stanford, Calif*

The purpose of this study was to show that conventional MR imaging systems can help characterize the components of atherosclerotic plaque. Fresh human aorta with atheromata was suspended in agar heated to body temperature. The specimen was imaged with three-point Dixon, spoiled GRASS, and a short T2 spectroscopic and imaging sequence. It was then examined histologically to obtain correlation between the images and plaque characteristics. The results show that individual plaque components can be identified and correlated with their histologic appearance. The three-point Dixon technique shows superior S/N, depicting intermediate and long T2 components such as cholesterol, muscle, and fibrous tissue. The $B_0$ and T2′ images obtained with this technique also show calcified regions of the atheromata. The spoiled GRASS technique with a TE of 6 msec also depicts intermediate and long T2 plaque components. The short T2 sequence suppresses long T2 components with a variable saturation pulse, allowing identification of very short T2 (TE ~ 150 μsec) plaque components such as calcified tissue. This sequence also obtains chemical spectra from any point in the sample, giving information about the chemical composition of the plaque. The combination of these imaging sequences allows identification of plaque components such as hemorrhage, calcification, cholesterol, and fibrous tissue. The images and spectra correlate well with the histology from the regions in question. These techniques can be applied to in vivo plaque characterization, allowing diagnosis of disease and assessment of therapeutic effectiveness.

068 • 4:45 PM

### Increased Sensitivity of Black Blood MR Angiography: A Role for Optimized Sequences?

MA Nissenbaum, P Margossian, SJ Song, SM Brown, BE Widoff, K Yan, JL Amster, WG Bradley
*Long Beach Memorial Medical Center and Long Beach MRI, Long Beach, Calif*

The purpose of this study was to compare the sensitivity and accuracy of an optimized black blood MR angiographic sequence to conventional time-of-flight MR angiography in the morphologic evaluation of cerebral aneurysms, visualization of small vessels, and grading of vascular stenoses. Ten healthy volunteers and several phantoms were imaged with routine 3D time-of-flight MR angiography ("bright blood," FISP 40/7/15, Siemens 63SP) with a new 3D black blood sequence (FE 50/15/15, Picker Vista HPQ). The sequence included judicious placement of presaturation pulses of optimized flip angle and postprocessing with minimum-intensity projections and, later in the study, seed-planting/ray-tracing algorithms. The latex phantoms included aneurysms as well as stenoses. In the phantom studies, small aneurysms were better seen with black blood techniques. Large aneurysms were not fully visualized on the raw data of either sequence but were seen on the black blood angiographic projections secondary to the inclusion of phantom wall in MR angiography. Perivascular dephasing of cerebrospinal fluid relative to pulsatility occasionally caused focal overestimation of luminal diameters. Three-dimensional time-of-flight overestimated stenoses and had diminished sensitivity for detection of small aneurysms. Small vessels were better seen with black blood techniques. In conclusion, the inclusion of causes of intravoxel dephasing in black blood MR angiography increases the sensitivity of detection for small aneurysms and small vessels. Underestimation of phantom stenoses secondary to inclusion of wall may occasionally be a problem. Black blood MR angiography is a useful adjunct to time-of-flight MR angiography in the assessment of peripheral occlusions and the detection of small aneurysms.

069 • 4:57 PM

### Evaluation of Venous Thrombosis in 17 Cases of Cerebral Meningioma with Spin-Echo Sequences and Phase-Contrast MR Angiography at 0.5 T

F Gelbert, B George, JP Guichard, G Lot, D Reizine, K Mourier, E Assouline, JJ Merland
*Department of Neuroradiology, Lariboisiere Hospital, Paris*

Seventeen patients with meningiomas adjacent to venous sinuses were examined at 0.5 T (MRMAX GE system) with T1- (TR = 600, TE = 24) and T2-weighted (TR = 2,000, TE = 60/120) imaging. Gadolinium was administered in 15 patients. Phase-contrast MR angiography was performed in the sagittal plane with a 2D gradient-echo sequence (TR = 160, TE = 25, 20° flip angle). Angiography was performed in all but two patients. In two cases, there was no extension to the sinus wall; in three cases, the sinus wall was thickened; in two cases, there was a tumoral mass inside the lumen of the sinus without occlusion; and in 10 cases, a complete occlusion was demonstrated. In all

cases, phase-contrast MR angiography showed a venous pattern grossly similar to that on the lateral angiogram. Spin-echo sequences with gadolinium allowed better characterization of thrombosis, while spin-echo sequences without gadolinium appeared less valuable and often overestimated thrombosis. The problem of meningiomatous extension toward the sinus wall in the case of insertion close to a venous sinus is a very important preoperative feature. MR phase-contrast angiography is a valuable method for venous flow imaging that can be proposed as an alternative to angiography. Routine spin-echo sequences with gadolinium give important complementary information about wall invasion and lead to better surgical planning and prognosis.

070 • 5:09 PM

### High-Resolution MR Angiography with Gadopentetate Dimeglumine: Preliminary Results in the Intracranial Circulation

W Lin, EM Haacke, AS Smith, ME Clampitt
*Department of Biomedical Engineering, Case Western Reserve University, and Department of Radiology, University Hospitals of Cleveland, Cleveland*

The use of gadopentetate dimeglumine (Gd-DTPA) has become commonplace for enhancing tumors and different diseases. The use of Gd-DTPA to enhance blood vessels for 3D MR angiography, however, has not yet been intensively studied. This is because both arteries and veins will be enhanced and cause confusion on the maximum-intensity projection (MIP) images. The role of Gd-DTPA for 3D time-of-flight (TOF) MR angiography was studied in 21 patients. The difficulty associated with the enhancement of both arteries and veins is overcome by using a 3D adaptive-based vessel tracking algorithm. A 3D MR angiographic sequence with an echo time of 8 msec was used to acquire 64 sections prior to and immediately after the injection of Gd-DTPA. It was found that the T1 of blood was reduced approximately by a factor of 2 immediately after injection of Gd-DTPA and that it slowly returned to three-fourths of its original value after 30 minutes. Since the T1 of blood was reduced, the contrast between background tissue and vessels was improved in all cases. Moreover, the lumen definition and visualization of small vessels on MIP images were superior after the injection of Gd-DTPA. In two cases, there was a suspected occlusion of the middle cerebral artery because there were almost no peripheral vessels seen on one side of the brain. After the injection of Gd-DTPA, however, more peripheral vessels were seen, indicating a stenosis rather than an occlusion. In two other cases, the definition of aneurysms was significantly improved after injection of Gd-DTPA. In summary, the use of Gd-DTPA in conjunction with 3D vessel tracking allows 3D time-of-flight MR angiography to enhance slow flow as well as contrast between background and vessels.

## Monday Afternoon • Regent Parlor
## Papers 071–079

## CONTRAST AGENTS: HEPATOBILIARY AND GI

MODERATORS: DG Mitchell, MD • DD Stark, MD

071 • 3:45 PM

### MR Imaging of the Liver: Value and Diagnostic Statement of Mn-DPDP

T Vogl, B Schnell, B Hamm, B Eibl-Eibesfeldt, J Lissner
*Department of Radiology, University of Munich, Germany*

The purpose of this open-label, prospective, multicenter study was to evaluate the tolerance and diagnostic value of the new hepatobiliary contrast agent Mn-DPDP. Twenty patients with suspected liver tumors (eight patients with liver metastases, two with hepatocellular carcinomas, two with bile duct carcinomas, two with lymphomas, one with focal nodular hyperplasia, two with cirrhotic nodules, and two with cysts) were examined. All studies were performed with a 1.5-T Magnetom with a body coil and an abdominal belt for reducing motion artifacts. Images were obtained before and after application of 5 or 10 μmol/kg Mn-DPDP. Routinely T1- and T2-weighted SE sequences and two GE sequences (breath-hold FLASH, T1-weighted, and TurboFLASH) were applied. Mn-DPDP significantly increased the signal/noise ratios of liver parenchyma in all T1-weighted sequences, due to the specific liver enhancement. Because of the significantly higher contrast/noise ratios of liver to lesion, all focal liver lesions could be localized and significantly better differentiated after Mn-DPDP application. Within the group of metastases, 25%–120% more delineated lesions could be differentiated after application of Mn-DPDP. In five patients the liver lesions showed a significant enhancement with Mn-DPDP (cirrhotic nodules, $n = 2$; hepatocellular carcinoma, $n = 2$; focal nodular hyperplasia, $n = 1$). These results show the intravenous hepatobiliary contrast agent Mn-DPDP to be a safe, specific drug for MR imaging. Mn-DPDP improves the diagnostic results of liver MR imaging by allowing greater accuracy in the judgment of tumor size and in tumor detection.

072 • 3:57 PM

### Hepatobiliary MR Imaging: First Human Experience with Gd-BOPTA

T Vogl, W Pegios, G Piranova, J Balzer, J Lissner
*Department of Radiology, University of Munich, Germany*

MR imaging examinations to investigate the efficacy of the new hepatobiliary contrast medium Gd-BOPTA were conducted for the first time, as part of a phase I study in eight healthy male volunteers. The examinations were performed by using a 1.5-T supraconducting imager with four different sequence techniques (spin-echo T1, T2, gradient-echo breath hold, TurboFLASH). The safety, efficiency, and extent of enhancement were analyzed following single ascending-dose intravenous administrations of Gd-BOPTA (0.005, 0.05, 0.1, and 0.2 mmol/kg of body weight). Enhancement improved considerably in the liver, biliary system, kidney, and spleen. Increased enhancement of the liver parenchyma was observed after Gd-BOPTA administration, particularly at doses of 0.05 and 0.1 mmol/kg, with both the GE sequence (enhancement ratio, 149%) and the SE T1-weighted sequences (enhancement ratio, 77%). At the 0.2-mmol/kg dose, enhancement of liver parenchyma appeared to be slightly delayed in both sequences. A longer-lasting contrast medium accumulation in the liver was observed, particularly at 0.1 and

0.2 mmol/kg, especially with the GE sequence. A late contrast medium accumulation after 60 min was typical for the gallbladder at doses greater than 0.05 mmol/kg. In conclusion, the newly developed hepatobiliary contrast medium Gd-BOPTA, with low acute and neural toxicity, is a promising new contrast agent for obtaining prolonged enhancement of the liver with a high rate of biliary excretion.

073 • 4:09 PM

### Value of Mn-DPDP–enhanced MR Imaging of Liver Tumors in 141 Patients: Results of Phase II Trials in Germany

EJ Rummeny, C Ehrenheim, B Gehl, B Hamm, M Laniado, A Steudel, TJ Vogl

*Departments of Radiology, Universities of Münster, Hannover, Aachen, Berlin, Tübingen, Bonn, and Munich, Germany*

Evaluation was made of the diagnostic utility and efficacy of Mn-DPDP, a paramagnetic hepatobiliary MR contrast agent for the detection of hepatic tumors. One hundred forty-one patients with hepatic tumors were studied in multicenter phase II trials. MR imaging was performed at 1.0 or 1.5 T. T1-weighted (T1W) images were obtained with gradient-echo, spin-echo (SE), and inversion-recovery pulse sequences before and after injection of Mn-DPDP. T2-weighted (T2W) images were obtained before injection of Mn-DPDP. Mn-DPDP was injected at a dose of 5 μmol/kg or 10 μmol/kg in 70 patients each. Quantitative and qualitative image analysis was performed in all patients. Tumor/liver contrast-to-noise ratios increased after injection of 5 μmol/kg and 10 μmol/kg Mn-DPDP on T1W images and were significantly greater ($P < .01$) than on unenhanced T1W and T2W SE images. Because of better tumor delineation, the number of small lesions ($\leq 1$ cm in diameter) detected was significantly higher ($P \leq .01$) after injection of Mn-DPDP than on unenhanced MR images. No major side effects were reported after injection of Mn-DPDP. Mn-DPDP is a well-tolerated new contrast agent for enhanced detection of liver tumors. These results now justify further prospective Mn-DPDP–enhanced MR imaging trials in patients with hepatic tumors.

074 • 4:21 PM

### Value of Delayed Mn-DPDP–enhanced MR Imaging in the Detection and Differential Diagnosis of Hepatic Tumors

E Rummeny, W Wiesmann, S Menker, K Lodemann, PE Peters

*Department of Clinical Radiology, Westfalian Wilhelms-University, Münster, Germany*

The purpose of this study was to evaluate the use of Mn-DPDP in the differential diagnosis of liver tumors and to monitor the clearance of this contrast agent from nontumorous liver tissue. Twenty patients with proved hepatic tumors (12 with metastases, five with hepatomas [HCC], two with focal nodular hyperplasia [FNH], one with hepatic adenoma [HA]) were studied at 1.5 T. All patients were imaged 0.5 to 1 hour (early images) and 21 to 25 hours (late images) after intravenous injection (PI) of 0.005 or 0.01 mmol/kg of Mn-DPDP with T1-weighted (T1W) gradient-echo images and conventional spin-echo (SE) pulse sequences. Eleven patients were reimaged 40 to 80 hours PI. On T1W images obtained 20 to 30 min after injection of Mn-DPDP, no uptake was found in metastases, but FNH and HA showed diffuse intratumoral uptake of Mn-DPDP. On late T1W images obtained 6 to 30 hours PI, metastases and HCC showed a hyperintense rim. Focal nodular hyperplasia and HA showed intratumoral enhancement and appeared markedly hyperintense to surrounding liver in all cases. Liver/muscle signal-intensity ratio (SIR) increased by 115% on early postcontrast MR images and was still at 15%–42% on MR images obtained up to 30 hours PI, as compared with unenhanced images. On images obtained 40 or more hours PI, the SIR of nontumorous liver tissue with that of unenhanced images in all cases. Mn-DPDP is a promising new contrast agent for differential diagnosis of hepatic tumors. Because of its slow clearance from nontumorous liver tissue, Mn-DPDP provides a broad "imaging window."

075 • 4:33 PM

### Ferric Iron Phytate as a Gastrointestinal MR Contrast Agent

EC Unger, TA Fritz, D Palestrant*, P Granstrom

*Department of Radiology/MRI, University of Arizona, and *ImaR$_x$ Pharmaceutical Corp, Tucson*

This study was performed to develop an effective, safe, and inexpensive gastrointestinal MR contrast agent. A variety of foodstuffs were tested with ferric iron to determine their effect on the relaxivity of ferric iron. After the best compounds were identified, a gastrointestinal MR contrast agent was formulated with osmotic and viscosity agents and was tested in volunteers. Of the materials tested, phytate (inositol hexaphosphate) had the greatest effect, doubling the relaxivity of the ferric iron. MR studies were performed in 10 volunteers after they ingested 900 mL of contrast medium; 200 mg/L of ferric iron gave best contrast in both phantoms and volunteers. There were no significant side effects and no change in serum iron. Blinded analyses of the images demonstrated marked improvements in bowel marking on T1-weighted images. A safe and practical gastrointestinal MR contrast agent has been developed for T1-weighted imaging.

076 • 4:45 PM

### Oral Magnetic Particles for Opacification of the Bowel

M Laniado, EF Grönewäller, KP Aicher, AF Kopp, CD Claussen

*Department of Diagnostic Radiology, Eberhard-Karls-Universität, Tübingen, Germany*

Different oral contrast agents are currently undergoing clinical trials. Oral magnetic particles (OMP) represent a negative contrast medium because of their superparamagnetic properties. In a phase III clinical trial the safety and efficacy of OMP were evaluated in 35 patients with abdominal masses. MR imaging was performed with a 1.5-T unit (Siemens, Erlangen, Germany) with T1-, proton-density, and T2-weighted spin-echo sequences before and after patients' ingestion of 800 mL of OMP. OMP was given in four portions of 200 mL each, with 40-min intervals between portions. T1-weighted images were obtained before and after intravenous injection of 20 mg of N-butyl-scopolamine in 24 of 35 patients. There were no gastrointestinal side effects in 34 of 35 patients. One patient vomited immediately after ingesting 100 mL of OMP. Thirty patients ingested the recommended volume of 800 mL. The taste of OMP was described as "acceptable" in 28 of 35 cases. OMP did not cause susceptibility artifacts on spin-echo images. Homogenous distribution of OMP in the duodenum, jejunum, and ileum was obtained in 70%, 89%, and 90% of cases, respectively. Because of residual fecal material and an ingestion time of only 2 hours, distribution was insufficient in the colon. OMP improved the delineation of the pancreas in seven of 17 cases. Intravenous injection of N-butyl-scopolamine improved the quality of OMP-enhanced T1-weighted images in 17 of 24 cases. Application of OMP increased diagnostic confidence in 45% of studies as compared with plain images. It is concluded that OMP is a safe oral contrast agent that provides reliable marking of the small bowel. The use of hypotonic

agents is recommended for OMP studies if spin-echo sequences are used.

077 • 4:57 PM

### OMR: A Positive Bowel Contrast Agent for Abdominal and Pelvic MR Imaging—Safety and Imaging Characteristics

RM Patten, AA Moss, T Fenton, S Elliott
*University of Washington School of Medicine, Kirkland*

To determine the safety and imaging characteristics of varied doses of OMR—a carbonated solution of ferric iron—as a bowel contrast agent, MR imaging was performed at 1.5 T in 29 volunteers. T1- and T2-weighted spin-echo images of the upper abdomen and pelvis were obtained before and after oral administration of the contrast agent at doses of 100–400 mg of iron in 300–600 mL. In three subjects, gradient-echo imaging was also performed. Two readers scored the images for intraluminal signal intensity, degree and percentage of bowel opacification, and artifact generation. Laboratory parameters and vital signs were monitored, and subjective reaction to OMR was assessed for each volunteer. All dose levels of OMR provided marking of the bowel by increasing intraluminal signal intensity; however, the degree and percentage of small bowel opacification appeared more prominent at dose levels ≥ 200 mg iron/600 mL. Semisolid or watery bowel movements were noted in 31% of subjects but no clinically significant laboratory abnormalities were seen. OMR improved delineation of the head of the pancreas on T1-weighted sequences in 72% of cases but was less useful in defining the body and tail of the pancreas. Bright signal in the moving bowel caused significant artifacts on T2-weighted imaging sequences. OMR is a safe and effective bowel contrast agent for MR imaging. Because artifacts from hyperintense moving bowel may degrade the images, OMR may be most useful on short TR/TE or fast-imaging pulse sequences or when combined with antiperistaltic agents.

078 • 5:09 PM

### Oral Magnetic Particles: Results from Clinical Trials in 500 Patients

I Haugen, T Bach-Gansmo, A Børseth, TF Jacobsen, B Lundby, M Svaland
*Clinical Research and Development, Nycomed AS, Oslo, Norway*

The purpose of this study was to document the efficacy and tolerance of a negative oral contrast agent, oral magnetic particles (OMP), in approximately 500 patients with abdominal and pelvic pathologies. OMP consists of crystalline magnetic iron oxides supported on a carrier matrix and suspended in a viscous solution. The contrast agent reduces the signal intensity from the contrast-filled bowel. Approximately 500 adult male and female patients were included in a clinical trial program (phase II and III) in Europe. An MR examination after ingestion of OMP was compared with a nonenhanced MR examination. OMP concentration and ingested volume were in most cases 0.5 g/L and 800 mL, respectively. During the phase II trials, various concentrations, volumes, and viscosities were evaluated. Spin-echo and fast and ultrafast gradient-echo sequences were applied at different field strengths from 0.02 to 1.5 T. The contrast medium was well tolerated with no serious adverse effects and good acceptability. OMP showed good contrast effect and complete or sufficient distribution throughout the small intestine. OMP gave good signal void with all applied sequences. The diagnostic information from abdominal MR imaging was improved by OMP in 50% of cases, and in more than 60%–70% of upper abdominal cases. The results from this clinical trial program imply that OMP may be a useful oral contrast agent for MR imaging.

079 • 5:21 PM

### Three Years' Experience with Oral Magnetic Particles

PA Rinck*, G Myhr*, O Smevik*, A Borseth†
**MR Center, University of Trondheim, and †Nycomed AS, Oslo, Norway*

Over a period of 36 months, four clinical trials were performed in 130 patients with oral magnetic particles (OMP) as an oral magnetic resonance contrast agent. OMP is a superparamagnetic contrast agent acting as a bulk susceptibility/T2 agent. It leads to signal voids in the gastrointestinal tract on all types of images (T1-, T2-, and intermediately weighted). The goal of the trials was to evaluate the ability of the particles to enhance the gastrointestinal tract in patients with abdominal and pelvic diseases. Fifty percent of the patients underwent pre- and postcontrast examinations. In approximately 80% of these cases, the contrast agent improved the delineation of the gastrointestinal tract, in 63% it facilitated the diagnosis, and in 66% it provided increased confidence in the MR examination. The contrast-enhanced examinations disclosed additional findings in 7% of the patients. Artifacts caused by peristalsis, movement of the diaphragm, and flow in the aorta were less pronounced after contrast than before contrast. Additional artifacts were not observed on conventional spin-echo images, but blurring artifacts destroyed the diagnostic value of subsecond images. Best fast imaging sequences were rapid gradient-echo sequences with extremely short echo times.

## Tuesday Morning • Beekman Parlor
## Papers 101–108

## RAPID IMAGING: CLINICAL APPLICATIONS

MODERATORS: CE Spritzer, MD • DA Vallet, PhD

101 • 10:30 AM

### Urologic and Vascular Complications of Renal Transplants: Evaluation with Enhanced MR Imaging in an Animal Model

PL Choyke, JA Frank, V Hampshire, P Gazetta, MJ Dietz, S Inscoe, J Black

Urologic complications of renal transplants such as urinomas, lymphoceles, hematomas, and obstruction, and vascular complications such as renal infarcts are frequent causes of transplant dysfunction. While other techniques are available, MR imaging combines depiction of multiplanar anatomy with functional analysis when performed with dynamic-enhanced rapid imaging. Dynamic- and static-enhanced renal MR imaging were performed in a porcine model to demonstrate the feasibility of using MR imaging in this manner. Eighteen MR images were obtained in eight minipigs between 1 and 75 days after renal transplantation. Each pig underwent a left or bilateral nephrectomy, with transplantation of an immunologically matched kidney into the left renal fossa. After being sedated the animals were imaged with fat-suppressed T1-weighted images in the axial plane. Dynamic spoiled gradient-recalled (SPGR) (TR = 18 msec, TE = 5 msec, 60° flip angle) imaging was performed in the coronal plane after bolus administration of Gd-DTPA. Postcontrast fat-suppressed T1-weighted images were also obtained. Seven of the eight pigs had urologic or vascular complications, including intrarenal hematoma (two), urinoma with leak of

Gd-DTPA (one), perinephric collections (five), and global (one) or focal (two) infarct with rim enhancement. All were readily identified on the postcontrast fat-suppressed T1-weighted image. Dynamic MR imaging revealed delayed function in seven pigs due to chronic rejection. Static- and dynamic-enhanced MR imaging demonstrates common urologic and vascular insults to the transplanted kidney. This technique combines anatomic detail and functional analysis in the diagnosis of renal transplant dysfunction.

102 • 10:42 AM

### Dynamic Gadolinium-enhanced, Ultrafast Gradient-Echo Imaging of Renal Tumors

TM Weber, CE Spritzer
*Department of Radiology, Duke University Medical Center, Durham, NC*

Good demarcation of renal tumors with gadolinium enhancement is achieved only during the early phase of a dynamic examination. The purpose of this prospective study was to evaluate the efficacy of ultrafast dynamic gadolinium-enhanced imaging for preoperative staging evaluation of renal tumors. To date, nine patients have been evaluated with this technique. Surgical pathology correlation was obtained in all cases. A 1.5-T (GE Signa) system was used to produce multiplanar ultrafast gradient-refocused-echo images following bolus intravenous administration of Gd-DTPA. Typical imaging parameters were as follows: coronal plane, TR = 12 msec, TE = 2.5 msec, 30° flip angle, 10-mm-thick contiguous sections, 256 × 128 matrix, and 1 excitation. At surgery, eight patients had renal cell carcinoma, correctly staged by dynamic enhanced MR imaging. Two of the nine patients had only one kidney and underwent salvage partial nephrectomy. Multifocal renal cell carcinoma, not detectable with CT, was detected with MR imaging in one of these two salvage cases. MR imaging enabled diagnosis of one bilateral renal cell carcinoma not detected with CT. Renal vein and/or inferior vena cava invasion was correctly diagnosed in two of two patients, one of which was not detected with CT. One patient had a small, 2-cm multilocular nephroma at surgery. This MR imaging technique appears to be an accurate method for evaluating renal tumors and staging renal cell carcinoma.

103 • 10:54 AM

### The Role of Spin-Echo and Gradient-Echo Plain and Contrast-enhanced MR Imaging versus CT for Diagnosis and Staging of Renal Cell Carcinoma

GP Krestin, B Marincek, W Gross-Fengels
*Department of Radiology, University Hospital Zürich, Switzerland, and Department of Radiology, University of Cologne, Cologne, Germany*

The use of different MR imaging techniques for diagnosis and preoperative staging of renal cell carcinoma was evaluated in 79 patients with 88 tumors. Gradient-echo (GRE) and spin-echo (SE) images obtained before and after intravenous administration of gadolinium-DTPA were compared with the results of CT and histologic staging. There were no marked differences among various MR techniques: Contrast-enhanced images were superior for evaluation of intrarenal tumor extent, while extrarenal spread and vascular involvement could be evaluated accurately on plain images. GRE MR imaging performed during suspended respiration provided qualitatively superior images but no additional information. Combination of all MR modalities yielded the best results: The T stage was predicted correctly with MR imaging in 84.0% and with CT in 78.4% of cases, while the N stage was accurately assessed in 79.5% and 81.8% of cases, respectively. MR imaging had some advantages in diagnosing perirenal tumor spread and in excluding infiltration beyond Gerota's fascia, but these advantages were not statistically significant. Thus, MR imaging can be considered a viable alternative to CT for staging large renal cell carcinomas, especially in patients with contraindications for iodinated contrast agents.

104 • 11:06 AM

### Dynamic TurboFLASH and Gadolinium in the Evaluation of the Rheumatoid Cervical Spine

MB Rominger, A Roca, WK Bernreuter, T El Gammal, FA Hester, GG Alarcon
*University of Alabama at Birmingham*

Recent advances in ultrafast imaging have enabled the acquisition of diagnostic images of the cervical spine during active motion. Intravenous injection of gadopentetate dimeglumine has proved to be useful in the evaluation of rheumatoid arthritis in other body areas because of pannus enhancement and hence better evaluation of disease. Fifteen patients with rheumatoid arthritis and a positive clinical examination for involvement of the atlantooccipital joint were imaged with a Magnetom 1.5-T imager (Siemens) with the following imaging protocol: sagittal T1-, proton density–, and T2-weighted spin-echo (SE) images of the entire cervical-spine; axial 2D FISP of the atlantooccipital region, followed by sagittal dynamic (extension-neutral-flexion) T1-weighted TurboFLASH (TE = 3, TR = 7, TI = 800, flip angle = 9°) imaging before and after gadopentetate injection; and sagittal T1-weighted SE imaging after contrast. Flexion and extension plain radiographs were obtained for comparison. Three of 15 patients had signs of cord compression in neutral position; 4/15 patients had little movement of the cervical spine due to fixation by the disease. Three of 9 patients (where the cervical spine was not fixed and without cord compression in neutral) showed signs of cord compression, and 1/9 showed an important narrowing after dynamic TurboFLASH. Five of 15 patients had signs of cord compression below C2, while in 12/15 cases, gadopentetate dimeglumine added information to the examination. Enhanced TurboFLASH was superior because of its increased contrast among bone, pannus, and cerebrospinal fluid. The data suggest that gadopentetate dimeglumine and TurboFLASH are valuable in cervical spine evaluation, although TurboFLASH cannot replace a complete study because of its lack of detail.

105 • 11:18 AM

### Ultrafast MR Imaging of the Pelvis: Fast Spin-Echo and Dynamic Gadolinium-enhanced Fast Gradient-Echo Techniques

TM Weber, CE Spritzer
*Department of Radiology, Duke University Medical Center, Durham, NC*

This prospective study was designed to evaluate the efficacy of ultrafast MR techniques for imaging the pelvis. Fast spin-echo (FSE) imaging was used to evaluate the pelvis in 12 patients (gynecologic tumors, $n = 9$; avascular necrosis, $n = 1$; rectal carcinoma, $n = 1$; and myositis, $n = 1$). Six of the nine patients with gynecologic tumors were also evaluated with non–breath-hold dynamic gadolinium-enhanced fast gradient-refocused-echo imaging. A 1.5-T (GE Signa) system was used with a large flexicoil in 11 cases. The body coil was used in the remaining case due to patient size. Typical imaging parameters for FSE were as follows: TR = 3,000 msec, TE = 85–105 msec, 5-mm section thickness with 2.5-mm intersection gap, 256 × 256 matrix, and 1 excitation. Typical imaging parameters for dynamic MPHWARPSP were as follows: TR = 12 msec, TE = 2.5 msec, 30° flip angle, 8-mm-thick contiguous sections, 256 × 128 matrix, and 1 excitation

following intravenous bolus administration of Gd-DTPA. Compared with standard spin-echo techniques, FSE offers improved spatial resolution, equal contrast, and equal or superior diagnostic information in less time. The dynamic gadolinium-enhanced fast gradient-refocused-echo technique appears to offer additional tissue demarcation during the early phase of dynamic examination.

106 • 11:30 AM

### Evaluation of Patients with Obstructive Sleep Apnea: Determination of Occlusion and Narrowing of the Pharyngeal Airway with Ultrafast Spoiled Grass MR Imaging

FG Shellock, CJ Schatz, P Julien, JM Silverman, TKF Foo, F Steinberg, ML Hopp, P Westbrook
*Cedars-Sinai Medical Center, Los Angeles*

Structural abnormalities of the pharyngeal airway are often present in patients with obstructive sleep apnea (OSA). These abnormalities can be detected in awake OSA patients during tidal breathing but require the use of rapid imaging techniques because the changes in airway dimensions are usually transient. Fifteen patients with clinically proved (ie, with overnight sleep studies) OSA underwent ultrafast spoiled GRASS MR imaging of their pharyngeal airways to determine the presence of occlusions and/or narrowings during tidal breathing. Twelve sequential images were obtained at one midsagittal plane section and at eight different axial plane sections through the pharyngeal airway. Images were obtained at the rate of one image per second. Each of the patients had occlusions and/or narrowings of the pharyngeal airway identified with the ultrafast spoiled GRASS MR examination. The site(s) of the occlusions and/or site(s) and extent of the narrowings varied among the patients. Nine of the patients had nonfixed occlusions present in one or more pharyngeal airway sites. Six patients had one or more abnormal narrowings of the cross-sectional areas of their pharyngeal airways. This study demonstrates that ultrafast spoiled GRASS MR imaging may be used to evaluate OSA patients during tidal breathing and is useful for assessing the presence of pharyngeal airway occlusions and/or narrowings.

107 • 11:42 AM

### Ultrafast MR Imaging of the Joints during Active Motion

FG Shellock, JH Mink, A Deutsch, R Kerr, TKF Foo
*Cedars-Sinai Medical Center, Los Angeles*

Many types of joint abnormalities may not be depicted on static MR imaging views because the pathology is related to a particular position within the range of motion of the joint. Recently an ultrafast MR imaging technique was developed that allows imaging of the joints during active motion. Therefore, ultrafast spoiled GRASS MR imaging (ie, short TEs, short TRs, small flip angles, partial echoes) was used to assess the anatomic and functional aspects of various joints during active motion. Patellofemoral joints, shoulders, wrists, cervical spines, and ankles were evaluated with appropriately adjusted fields of view (10–32 cm) and section thicknesses (3–7 mm) to optimize the imaging of these joints. Sophisticated positioning devices were not needed for these studies. The patient actively moved the joint through a given range of motion. Images were obtained at the rate of approximately one per second, which provided sufficient temporal resolution for assessment of the joint during controlled movement. Image quality was adequate for delineation of the anatomic structures of interest. Examination of the joints during active motion often provided additional useful information related to the anatomic and functional aspects of the joints studied. Furthermore, because of the reduced acquisition times required for this procedure, imaging the joints during active movement was easily accomplished along with the routine MR examination.

108 • 11:54 AM

### Cine MR Imaging of the Shoulder

JF Norfray, B Genez, RJ Friedman, BJ Schuette
*Health Images Inc, Effingham, Ill*

The hypothesis underlying this study was that normal and abnormal motion of the shoulder can be assessed with cine MR imaging of the shoulder. To study this newly developed imaging technique, an original shoulder rotating device was designed that allows internal and external rotation of the glenohumeral joint in 20° increments while maintaining the shoulder in the same axial or coronal plane at all times. Images were obtained for 8–16 positions with use of the gradient-echo technique and a dedicated shoulder surface coil and displayed on a dynamic oscillating cine. Acquisition of the gradient-echo images took 10–15 minutes. Images were then displayed in a closed-loop cine format for kinematic evaluation of the glenoid labrum, capsule and capsular ligaments, biceps tendon, rotator cuff, humeral head, and glenoid fossa. Fifty patients were studied, including healthy individuals and patients with instabilities, impingement, and limited range of motion (ROM). All cine MR images of the shoulder were compared with routine MR images and correlated with intraoperative findings where appropriate. Cine MR imaging provides excellent visualization of the anterior glenoid labrum (AGL) and clearly demonstrates its role in stabilizing the glenohumeral joint anteriorly in conjunction with the capsular ligaments. In addition, the cine method was the only technique able to demonstrate the AGL limiting ROM by showing that the AGL became entrapped at the extremes of motion. In summary, cine MR imaging provides better visualization of the soft-tissue structures about the glenohumeral joint than does conventional static MR imaging, dynamically demonstrating normal function and pathologic anatomy.

## Tuesday Morning • Sutton Parlor North
## Papers 109–116

### BRAIN

MODERATORS: MN Brant-Zawadzki, MD
GM Bydder, MD

109 • 10:30 AM

### Histologic Correlations of ρ, T1, T2, and Apparent Diffusion Coefficient of Water in Focal Cerebral Ischemia

JA Helpern, MO Dereski, RA Knight, RJ Ordidge, ZX Qing, LC Rodolosi, M Chopp, KMA Welch
*Henry Ford Health Sciences Center, Detroit, and Parke Davis Pharmaceutical Research, Ann Arbor, Mich*

Histologic grading of ischemic damage ($n$ = 3 to 5, depending on time point studied) and MR imaging assessment ($n$ = 5) of H-1 density (ρ), T1, T2, and the apparent diffusion coefficient of water ($ADC_w$) were performed from 2 hours to 1 week in a rat model of focal cerebral ischemia. Three areas of the ischemic territory were assessed based on (*a*) neuronal damage, (*b*) appearance of hypertrophic astrocytic nuclei, and (*c*) sponginess of the neuropil. Histologic assessment of area *a* demonstrated a progression to severe damage (corresponding with the appearance of eosinophilic neurons) and complete necrosis with eventual cavitation. Ischemic cell damage in area *c* was relatively mild and histologic assessment returned to

normal (ie, reversible damage) by 1 week. The histologic response of area *b* was intermediate to that of areas *a* and *c*. Within 8 hours poststroke, all three areas demonstrated a significant decline in the $ADC_w$ ($P < .01$). In areas *a* and *b*, but not area *c*, T1 and T2 were also significantly elevated ($P < .01$). The $ADC_w$ for area *a* (irreversible damage) remained depressed until there was a dramatic increase in the appearance of eosinophilic neurons, at which time the $ADC_w$ began to increase toward more normal values. The increase in the $ADC_w$ at this time point may be indicative of the loss of cell membrane structure and integrity. Of the three areas studied, area *a* was the only area that also demonstrated a statistically significant increase in $\rho$ ($P < .01$). Additionally, changes in $\rho$ did not follow changes in T2 for $ADC_w$. Thus, the $ADC_w$ was the only parameter capable of acutely (ie, <24 hours) identifying all three areas of brain that demonstrated some degree of ischemic cell damage. Additionally, a significant increase in $\rho$ was associated only with irreversible damage. Quantitation of MR imaging parameters may enable the assessment of all stroke-affected brain regions and may also permit distinction between reversible and irreversible ischemic damage.

110 • 10:42 AM

### Imaging of Anisotropically Restricted Diffusion in Cerebrovascular Disease

JV Hajnal*, IR Young*, A Oatridge, GM Bydder
**Picker International and NMR Unit, Royal Postgraduate Medical School, Hammersmith Hospital, London*

Pulsed-gradient spin-echo sequences were implemented in all three axes both with and without the use of a small gradient set on a 0.15-T prototype imaging system. With echo times of 80–200 msec, *b* values of up to 2,000 sec/mm$^2$ were used in patients with infarction, hemorrhage, and arteriovenous malformations. Patients' ages ranged from 38 weeks of gestation to 76 years. All infarctions were subacute or chronic and showed evidence of increased diffusion in one or more planes, resulting in a reduction in signal intensity. Hemorrhage was more variable. All subacute hematomas showed regions of restricted diffusion that were largely isotropic. The contrast between hemorrhage and surrounding brain was increased with diffusion weighting. A cystic hygroma was distinguished from a subdural hematoma. Late sequelae of hemorrhages included cysts as well as areas of change in the thalamus that were identified only with diffusion weighting. Infarction increases the apparent diffusion coefficient, while subacute hematoma decreases it. Arteriovenous malformations and cysts display an increase in the apparent diffusion coefficient. Changes in disease may be apparent only on diffusion-weighted sequences.

111 • 10:54 AM

### The Blood-Brain Barrier and Regional Cerebral Blood Flow in Cerebral Infarcts

JC Böck, B Sander, J Haustein, W Schörner, R Felix
*Strahlenklinik und Poliklinik, Universitätsklinikum Rudolf Virchow, Berlin*

Contrast enhancement on CCT or MR images in patients with cerebral infarcts results primarily from a disruption of the blood-brain barrier (BBB) and subsequent extravasation of contrast material into the interstitial space. This contrast enhancement in subacute infarcts has been termed "hyperperfusion" or "luxury perfusion," although a correlation between the degree of BBB disruption and regional cerebral blood flow (rCBF) has never been demonstrated. The aim of this prospective study was to establish the relationship between circumscribed disruptions of the BBB and pathologic changes in rCBF in the same location. Thirty-two patients with cerebral ischemic disease were studied. BBB disruption was expressed as the percent increase of signal intensity on T1-weighted images after intravenous gadolinium-DTPA injection (0.1 mmol/kg body weight). Regional cerebral blood flow was expressed as the percent signal intensity decrease on T2*-weighted images immediately after Gd-DTPA bolus injection (1.5 T, gradient echo, TR = 25 msec, TE = 20 msec, acquisition time = 2.5 seconds, 30 sequential images). The correlation between the degree of circumscribed BBB disruption and rCBF was not significant (coefficients of correlation: $r = .4$, $P > .5$). The results show that BBB disruption in cerebral infarcts does not necessarily imply high regional blood flow to the damaged brain tissue. This observation is important because high blood flow appears to be correlated with a better prognosis. By contrast, BBB disruption indicates structural changes and may be associated with a poor prognosis.

112 • 11:06 AM

### Quasi-Simultaneous MR Assessment of Blood-Brain Barrier Disruption and Blood Flow in Brain Tumors

JC Böck, B Sander, J Haustein, W Schörner, R Felix
*Strahlenklinik und Poliklinik, Universitätsklinikum Rudolf Virchow, Berlin*

The degree of blood-brain barrier (BBB) disruption assessed with contrast-enhanced CCT or MR imaging has been shown to correlate with intraaxial brain tumor malignancy. Likewise, the evaluation of tumor blood flow (TBF) with radionuclide methods is advocated for improved brain tumor grading. This complementary information can now be obtained in a single MR examination. Twenty-eight patients with brain tumors were studied. Blood-brain barrier disruption was expressed as the percent increase of signal intensity on T1-weighted images after intravenous Gd-DTPA injection (0.1 mmol/kg body weight). Regional cerebral blood flow was expressed as the percent signal intensity decrease on T2*-weighted images immediately after Gd-DTPA bolus injection (1.5 T, gradient-echo, TR = 25 msec, TE = 20 msec, flip angle = 10°, acquisition time = 2.5 seconds, 30 sequential images). Typical findings include intact BBB and low TBF in low-grade intraaxial tumors; disrupted BBB and heterogeneous TBF in high-grade intraaxial tumors; disrupted BBB and high TBF in extraaxial tumors; and disrupted BBB and low TBF in malignant tumors with a partially necrotic tumor center. This study demonstrates quasi-simultaneous assessment of the blood-brain barrier and tumor blood flow. The results support the notion that additional uncorrelated information is obtained from the assessment of regional cerebral blood flow.

113 • 11:18 AM

### Functional MR Imaging and PET Studies of Primary Human Brain Tumors

HJ Aronen, JW Belliveau, DN Kennedy*, BR Buchbinder, IE Goldberg, A Fischman, M Gruber, J Glas, TJ Brady, F Hochberg, BR Rosen
*MGH-NMR Center, Department of Radiology and *Department of Neurology, Massachusetts General Hospital and Harvard Medical School, Boston*

This study directly compared MR imaging and PET functional measurements of brain tumor activity. Eighteen patients with primary brain tumors were studied with conventional and functional MR imaging methods and the results were compared with those obtained with PET studies of tumor metabolism and blood volume. MR cerebral blood volume (CBV) maps were calculated from first-pass cerebral transit of an intravenous bolus injection of 0.1 mmol/kg $Gd(DTPA)^{2-}$ (ie, Magnevist). MR and PET functional images were translated into a common coordi-

nate system, allowing for direct voxel-by-voxel comparison of MR CBV maps and PET FDG metabolism maps. Finally, all the MR imaging and PET studies were analyzed visually by two independent reviewers. In 16 of 18 cases, good or excellent correlation was obtained. The results demonstrate a close correlation between tumor blood volume and glucose uptake at the microscopic level. Changes in tumor CBV and FDG uptake were correlated with both tumor grade and response to therapy. The results indicate that MR cerebral blood volume mapping offers a new dimension in the characterization of primary brain tumors based on the function of normal and pathologic tissue.

114 • 11:30 AM

### Computer-generated Three-dimensional Reconstructions of Brain Tumors with MR Imaging

R Kikinis, DC Boxer, MR Moore, M Matsumae, PE Steig, PM Black, H Cline, W Lorensen, FA Jolesz

*Departments of Radiology and Neurosurgery, Brigham and Women's Hospital and Harvard Medical School, Boston, and General Electric CRD*

Surgical planning and a thorough understanding of complex anatomic relationships require considerable intuitive transformation of 2D MR data into 3D models. A method of interactively manipulating and viewing MR imaging data has been developed that allows improved understanding of complex anatomy and reveals relationships not readily observable with use of conventional computer-generated 3D reconstructions. MR images (data sets) were obtained preoperatively in patients having an arteriovenous malformation and a 12th nerve tumor with a GE Signa 1.5-T imager using double-echo long TR multisection spin-echo data and 3DFT MR angiograms. Multiple-step image processing was performed on a computer research workstation after data acquisition. First, a filter was applied to reduce noise. Brain, skull, arteries, veins, skin, and tumor were then extracted with a supervised automated segmentation algorithm combined with manual outlining. Finally, 3D surface maps were created with the dividing cubes algorithm and were visualized in an environment that allowed interactive manipulation of the data. By changing viewing angles and cropping selected regions or objects, the physician improved understanding of the anatomic situation. Relationships of tumor to critical structures were revealed with feeding and draining vessels made readily discernible. Modeling of head positioning and the application of various surgical approach trajectories with progressive image cropping were used for surgical planning. Three-dimensional renderings revealed anatomic relationships not easily observed in data interpreted with conventional methods. Interactive manipulation of computer-generated 3D renderings is a powerful tool for the radiologist, surgeon, and clinician. It facilitates the communication of complex anatomy, provides information critical for understanding relationships between anatomic structures, and allows the noninvasive evaluation of surgical approaches.

115 • 11:42 AM

### Cerebral MR Imaging of Very Low Birth Weight Infants at 1 Year of Age

G Nilsen, PA Rinck, O Smevik, J Skranes, T Vik, AM Brubakk

*MR-Center, Medical Section, and Department of Pediatrics, University of Trondheim, Norway*

Cerebral MR imaging was performed in 27 (67.5%) of 40 surviving infants with birth weight < 1500 g at 1 year of corrected age. T1-weighted images of 20/27 infants showed deviating myelin deposition when compared with what has been reported in healthy infants born at term. Areas most affected were central occipital white matter (19 infants) and the centrum semiovale (7 infants). Both correspond to watershed areas known to be at risk for leukomalacia in preterm infants. T2-weighted images showed delayed myelin maturation in the same areas as described for T1. In addition, delayed maturation was seen in the central occipital white matter of two infants and in the centrum semiovale of one infant. Patchy abnormalities involving the white matter were seen in seven infants, while one infant had multiple porencephalic cysts. Mild cerebral atrophy, mainly of the cortex, was found in 10 infants. Irregular shape of the lateral ventricles, especially the posterior horns, was present in 12 infants, 11 of whom also had deviating myelin deposition. Only two infants had MR imaging studies without any aberration. Serial MR imaging studies are needed to determine whether the high percentage of deviating myelination represents delayed development or brain damage in preterm infants.

116 • 11:54 AM

### Role of T2-weighted GRE in the Evaluation of Intracranial Hemorrhage in Infants

LS Kannegieter, CI Mann, RB Dietrich

*Department of Radiological Sciences, University of California, Irvine*

MR imaging with low-flip-angle gradient-recalled-echo (GRE) T2-weighted images has demonstrated its sensitivity in the evaluation of intracranial hemorrhage in adults. Intracranial hemorrhage was evaluated in a pediatric population with a mean age of 47 days (range, 1–240 days). T1- and T2-weighted images were compared with various multiplanar gradient-echo (MPGR) sequences obtained with a 1.5-T imager. The study consisted of nine patients, five male and four female. Image parameters used were as follows: T1W, SE = 500–800/20; T2W, SE = 2,200–3,000/180–200; and GRE, 450/30/10%–20°. A total of 30 hemorrhagic foci of varying ages were identified and subdivided on the basis of the age of each lesion ( < 24 hours, 1–3 days, 3–7 days, and 7–14 days). GRE images were graded on a relative sensitivity scale by two "blinded" radiologists familiar with interpreting MR images as being either contributory or noncontributory to the diagnosis of any lesion(s). Twenty-one hemorrhagic foci were identified on both T1 and T2 spin-echo images and on GRE images. GRE sequences provided a greater confidence level in the detection of 14/30 lesions (46.7%) than did either T1- or T2-weighted views alone. One case (one hemorrhage) was demonstrated only on the GRE image, while in two cases (eight hemorrhages) the lesions were not identified on the GRE images. Low-angle GRE sequences may further define or offer additional diagnostic information in the evaluation of pediatric intracranial hemorrhage but should be used in conjunction with standard spin-echo sequences.

# Tuesday Morning
# Sutton Parlor Center
# Papers 117–123

## MULTINUCLEAR MRS

MODERATORS: RG Gonzalez, PhD
RE Lenkinski, PhD

117 • 10:30 AM

### Topographic and Quantitative Correlation of Proton Spectroscopic Imaging and FDG-PET in Human Brain Tumors

W Heindel, K Herholz, PR Luyten, H Kugel, J Bunke, W-D Heiss, K Lackner

*Departments of Radiology and Neurology, University of Cologne, Cologne, Germany, and Philips Medical Systems, Best, the Netherlands*

Recent technical advances in H-1 MR spectroscopic imaging (SI) allow metabolite maps to be obtained with a spatial resolution comparable with that of positron emission tomography (PET). This study was designed to compare the results of spectroscopic images with corresponding PET images of 2-(F-18)-2-deoxyglucose (FDG) in human brain tumors. A total of 28 patients with histologically classified gliomas were studied with both modalities. MR examinations were performed with a whole-body MR system (Gyroscan S15, Philips) at 1.5 T. "Conventional" MR imaging preceded spectroscopy to define a representative section of 2 resp. 2.5-cm thickness comprising the tumor. Spectroscopic images with an in-plane resolution of 7.0 mm were obtained by combining volume selection with gradient phase encoding. PET scans of approximately 11-mm section thickness were obtained with a 4-ring/7-section PET system (Scanditronix, PC 384). After injection of FDG, glucose uptake was measured with an in-plane resolution of 7.8 mm. Reconstructed PET sections were aligned with the measured SI sections with use of three-dimensional image processing, with morphologic features of PET and MR images as orientational landmarks. Lactate concentration was compared quantitatively with the calculated metabolic rate of glucose (MRGlu). The tumors showed a good qualitative relation between tumor MRGlu and lactate concentration. In benign gliomas (grades I and II) PET typically demonstrated an FDG uptake similar to that of white brain matter. H-1 SI showed increased choline, decreased NAA, and usually no lactate. Malignant gliomas were characterized by a heterogeneous PET image with high FDG uptake in active proliferating regions. Correspondingly, the proton metabolite maps showed increased choline in solid tumor regions compared with contralateral normal brain tissue, while lactate was detected in cystic or necrotic regions. All 10 tumors with abnormal lactate levels exhibited an abnormally high MRGlu exceeding the range of normal white matter. The Kendall rank correlation between lactate concentration and MRGlu index was highly significant ($t_B = 0.72$, $P < .001$). On the other hand, an analysis of local MRGlu and lactate levels revealed that a direct topographic correspondence is not the rule. An evaluation after matching of both functional methods confirmed that foci of elevated FDG did not exactly correspond to foci of increased lactate. For example, in two glioblastomas high lactate was found in the hypometabolic center, where all other metabolites were severely diminished and MRGlu was low, while less lactate was present in a surrounding rim of tissue with increased MRGlu. The spatial resolution of both methods allowed the depiction of heterogeneities within the tumors. This study demonstrates a close qualitative relation between glucose uptake and lactate deposition in human gliomas. The spatial distribution of glucose metabolism, however, does not directly correspond topographically to the distribution of lactate in the tumor. The combination of both methods may prove to be a valuable tool for identifying the most metabolically active parts of brain tumors.

118 • 10:42 AM

### Proton MR Spectroscopy of White Matter Lesions and Brain Tumors: A Comparison

A Jassoy, T Vogl, T Yousry, C Becker, A Dadashi, T Pfluger, R Sauter, J Lissner

*Radiologische Klinik Innenstadt, Munich, Germany*

The purpose of this study was to assess the value of H-1 MR spectroscopy in the differential diagnosis of white matter lesions (WMLs) and brain tumors. Water-suppressed, localized proton MR spectroscopy (localized SE sequence: TR = 1500 msec, TE = 270, 135, or 40 msec; STEAM sequence: TR = 1,500 msec, TE = 20 msec, voxel size = 5–16 mL) with a 1.5-T whole-body imager was used to examine five patients with WMLs, nine with gliomas, nine with meningiomas, and five with brain metastasis. All tumor spectra and all spectra from WMLs were markedly different from spectra of normal brain tissue. In all cases the concentration of NAA was reduced. Almost all spectra of brain tumor showed a reduction in concentration of phosphocreatine (PCr), whereas lesions of chronic multiple sclerosis and one case of progressive multifocal leukoencephalopathy showed a normal concentration of PCr. Spectra of acute symptomatic multiple sclerosis (MS) lesions and spectra of high grade glioma showed a marked reduction in NAA and PCr concentrations, with elevated concentrations of lactate and FFA, while the choline concentration was in the normal range. In contrast to spectra of gliomas, which showed normal or elevated concentrations of inositol, spectra of acute MS lesions showed very little or no inositol. All spectra of brain metastasis showed quite specific features with marked reduction of NAA, PCr, and choline, no detectable inositol, and characteristically elevated concentrations of saturated FFA and cholesterol. Spectra of meningioma did not demonstrate a characteristic pattern, so that imaging proved to have a clear advantage over spectroscopy. In conclusion, localized proton MR spectroscopy may be a useful tool for differential diagnosis of WMLs and brain tumors.

119 • 10:54 AM

### H-1 Spectroscopic Imaging in Gliomas

F Lazeyras, HC Charles, C Schold, R Fredericks, RE Coleman

*Department of Radiology, Duke University Medical Center, Durham, NC*

H-1 MR spectroscopy allows the mapping of the concentration of certain chemical compounds (lipids, lactate, NAA, PCr/Cr, choline). Two-dimensional chemical shift imaging (CSI) was used in connection with the STEAM localization scheme to characterize the chemical content of gliomas versus that of normal tissue. The study was performed on a 1.5-T Signa system. The STEAM volume was selected to maximize the brain tissue observed and to suppress subcutaneous fat (nominally 80 × 100 mm). Field homogeneity was optimized with an automatic shimming procedure. Acquisition parameters were as follows: section thickness, 15 mm; FOV, 200 mm; 16 × 16 phase-encoding steps yielding a 1.2-cm in-plane resolution; TR = 1.5 sec, TE = 20, 135, or 270 msec; total acquisition time = 25 min. NAA concentration was less and choline concentration was greater in all tumors than in normal brain. As in normal brain, no elevation of the free fatty resonances was observed in low-grade tumors, while these resonances were markedly elevated (> 10-fold) in high-grades tumors. In addition, the PCr/Cr peak was slightly reduced in anaplastic tumors. Lactate was not de-

tected because of the presence of fat resonance, even at long echo time. In conclusion, NAA/choline is a sensitive marker for brain tumors. Elevated free fatty resonances may be a marker for high-grade lesions. Lactate concentration could not be assessed in this study.

120 • 11:06 AM

### Brain Metastasis versus Glioma: Value of H-1 Spectroscopy for Metabolic Imaging

T Vogl, A Jassoy, C Becker, A Dadashi, C Hamburger, J Lissner

*Department of Radiology, University of Munich, Germany*

The purpose of this study was to analyze the correlation among proton spectroscopy, histology, and MR imaging, and to evaluate the vascularization and metabolic state of metastases and gliomas. Ten patients with histologically proved brain metastases ($n$ = 4) and gliomas ($n$ = 7) underwent comparative examinations with MR imaging and H-1 spectroscopy. In vivo H-1 spectroscopy was performed at 1.5 T with a spin-echo sequence (TR = 1,500 msec, TE = 1,315 and 40 msec, voxel size = 8 mL). The spectra of patients with metastases showed a greatly reduced NAA concentration. The PCr/cho ratio was reduced in three cases and normal in one. Inositol was missing in three spectra and very low in one case. Remarkably high, sharp peaks were observed at 1.25 and 0.9 ppm (saturated fatty acids and cholesterols, respectively). On the other hand, the spectra of four patients with gliomas showed elevated ino/cho ratios whereas fat compounds were enhanced. Of the seven spectra of patients with gliomas, four showed a normal PCr/cho ratio and three a ratio slightly less than normal. In conclusion, H-1 spectroscopy yielding biochemical specificity in vivo may be useful in obtaining critical informations for the differential diagnosis of brain metastasis and gliomas in ambiguous cases.

121 • 11:18 AM

### Short-Echo-Time Chemical Shift Imaging of Human Brain

T Ng, M Xue, A Majors, MT Modic

*Cleveland Clinic Foundation, Cleveland*

Displays of chemical shift imaging (CSI) are presently generated only with long echo times (ie, TE = 135 or 270 msec) and include only the prominent resonances of choline, creatine/phosphocreatine, and NAA observable in normal brain. Low-level resonances of glutamate/glutamine, inositol, taurine, and GABA, believed to be clinically relevant, are lost in the noise due to T2 weighting. The acquisition in a clinical setting of multiple-voxel (2 mL each) proton spectra containing the low-level resonances described above is herein reported. Multiple-voxel (16 × 16 matrix) proton spectroscopy was performed with a double-echo pulse sequence on a Siemens 1.5-T system with a gradient head coil. Achievable echo time for 2D CSI is 40 msec. For a voxel size of 1 × 1 × 2 cm (2 mL or equivalent) acquisition time is 26 min (TR = 1.5 sec and NS = 4). Total patient time in the magnet, however, including acquisition of localized images and shimming, is approximately 1 hour. High-quality, multiple-voxel spectra containing resonances of glutamate/glutamine, GABA, inositol, and taurine, in addition to the prominent resonances of choline, creatine/phosphocreatine, and NAA, were detected. Three axial CSIs through the pons, lateral ventricles, and parietal lobe above the ventricles were performed in volunteers. MR imaging displays of these resonances provided the spatial distribution of each metabolite. In conclusion, the quality of the short TE CSI spectra is equal to or better than that of spectra obtained with single-voxel STEAM. Regional differences in various parts of the brain were directly compared, and the three main axial CSI images can be used as a proton metabolite atlas for study of normal or diseased brain. Acquisition time is comparable with that for the single-voxel approach.

122 • 11:30 AM

### Three-dimensional H-1 Chemical Shift Imaging of Human Brain

J Hu, TR Brown

*Fox Chase Cancer Center, Philadelphia*

There has been considerable progress in performing localized proton spectroscopy in the human brain with a STEAM sequence to excite a slab and 2D chemical shift imaging techniques to achieve further localization. The extension of these studies to include three dimensions is herein reported. One of the primary difficulties was shimming the main field well enough over a large volume so that water-suppression techniques could be applied. To achieve this, an automatic shimming procedure was used that routinely obtained a linewidth of less than 15 Hz from the whole head. A modified STEAM sequence with an extra CHESS pulse added in the TM period was used to provide additional water suppression. The results suggest that 3D brain data can be successfully acquired with this procedure.

123 • 11:42 AM

### Application of Proton Chemical Shift Imaging Techniques for the Evaluation of Regional Differences in the Human Brain in Vivo

M Schneider, H Kolem, K Wicklow, R Sauter

*Siemens AG, Medical Engineering Group, Erlangen, Germany*

The chemical shift imaging (CSI) technique provides spatial mapping of cerebral metabolites. Since multiple spectra from adjacent locations can be acquired simultaneously without increasing acquisition time, CSI techniques are ideal for the examination of regional differences in the normal brain. Studies were performed in volunteers with a whole-body MR system (Siemens Magnetom) operating at 1.5 T. The standard circularly polarized head coil was used. Two-dimensional Hybrid-CSI sequences have been implemented on the system. The Hybrid-CSI sequences are based on STEAM, SE single-voxel sequences for preselection of a large volume of interest (typical size, 70 × 70 × 15 mm). The selected volume of interest corresponds to a section in coronal orientation including occipital white matter and cerebellum. Two-dimensional in-plane resolution was achieved with use of two phase-encoding gradients (matrix size, 16 × 16 and 32 × 32, respectively). The resulting voxel sizes ranged from 1–4 mL. Water suppression was achieved with use of 3 G RF pulses and subsequent gradient pulses. CSI data sets were acquired with echo times of 20 and 135 msec. Regional differences in the resonances of N-acetyl aspartate, creatine and phosphocreatine, choline, and inositol between the occipital area and cerebellum could be observed with both echo times. These results are in agreement with previous single-voxel studies. With the currently applied integral shim technique, however, not all spectra of the CSI data set show the same high degree of spectral resolution, making a quantitative evaluation of regional differences difficult. This is especially true for the strongly coupled resonances detectable at short echo times (eg, glutamate), where regional differences could not be evaluated unambiguously.

## MRA: Heart, Kidneys, and Peripheral Vessels

MODERATORS: DE Bohning, PhD • SW Young, MD

124 • 10:30 AM

### ECG-gated Two-dimensional–Inflow MR Angiography for Noninvasive Diagnosis of Complex Congenital Heart Disease in Newborns and Infants

M Steinborn, KC Seelos, A von Smekal, J Gieseke, DA Redel, M Reiser

*Departments of Radiology and Pediatric Cardiology, University of Bonn, Germany*

Interventional cardiac catheterization in small children with complex congenital heart disease bears a relatively high risk. It is useful, therefore, to develop noninvasive MR angiographic techniques to assess complex cardiovascular anatomy. Fourteen patients with various surgical shunts, pulmonary arterial and venous anomalies, and patent ductus arteriosus were studied with an electrocardiograph-gated 2D-inflow MR angiographic technique with 3D animation on a 0.5-T Philips Gyroscan T5 system. Special attention was paid to the visualization of the pulmonary arteries. In all cases the MR angiographic findings were correlated with findings from echocardiography, cardiac catheterization, and selectively angulated 2D spin-echo and gradient-echo MR imaging. With a section thickness of 3 mm and minimal overlap, cardiac-gated MR angiography was able to depict vascular anatomy and pathology reliably in all cases, acquiring enough data for a complete workup of thoracic vasculature in 8 to 11 min. It did not provide any further information compared with selectively angulated MR planes when the latter were placed appropriately. Limitations due to poor resolution were found in vascular structures less than 2 mm in diameter. First experience with cardiac MR angiography in newborns and infants shows that it is a useful adjunct for obtaining a quick, noninvasive understanding of complex vascular anatomy. It does not obviate invasive hemodynamic preoperative workup, but might be indicated in conjunction with standard MR imaging sequences for postoperative follow-up studies.

125 • 10:42 AM

### First-Pass Contrast-enhanced MR Imaging of the Heart

N Wilke*†, G Engels*, A Koronaeos*, C Simm†, K Bachmann*, F Wolf†, H Feistel†, RJ Bache, K Ugurbil

**Medical Department of Cardiology and †Department of Nuclear Medicine, University of Erlangen, ‡Siemens Medical Engineering Group, Erlangen, Germany; and University of Minnesota, Minneapolis*

With ultrafast MR imaging, it is feasible to monitor a gadolinium (Gd-DTPA) bolus through the vascular bed of the myocardium as well as the central areas of the circulatory system. Similar to indicator dilution techniques, Gd-DTPA served as an indicator and MR imaging as the detector. Signal intensity time curves (STC) were sampled across the myocardium and information on myocardial perfusion was obtained by calculating the mean transit time (MTT). The left-to-right shunt was assessed from STC sampled in the central circulatory areas. A Turbo-FLASH sequence (TR, 5.9 msec; TE, 3.0 msec; TI, 80 msec; matrix, 90 × 128) was installed on a 1.5-T Magnetom (Siemens AG). Electrocardiograph-triggered images (one image per heartbeat) were taken in either the double-oblique short axis or the four-chamber view with an 18-cm Helmholtz coil. With a high-speed injector a low-dose Gd-DTPA (Schering, AG) bolus was injected centrally into the right atrium to simulate "real" first-pass conditions. MR myocardial perfusion imaging was performed in patients with severe coronary artery disease proved by angiography, scintigraphy (MIBI-Spect), and a positive dipyridamole stress test ($n$ = 18), and in dogs with partial left anterior descending coronary artery occlusions ($n$ = 5). MR first-pass technique was performed in patients with left-to-right shunts proved by angiography and a dye-dilution technique ($n$ = 12). The inverse MTT calculated from the myocardial STC compared with absolute measured myocardial blood flow with microspheres in the dogs proved to be a reliable perfusion parameter ($r$ = .84). Hypoperfused myocardium can be exactly demonstrated by the MR first-pass technique compared with scintigraphic findings. Identification, differentiation, and quantification of intracardiac left-to-right shunts can be achieved with the MR first-pass technique, with excellent correlation with the dye-dilution technique ($r$ = .9).

126 • 10:54 AM

### Subtraction of White Blood Cine Images from Black Blood Cine Images to Improve Blood/Myocardial Contrast

MS NessAiver

*Picker International, Highland Heights, Ohio*

Field-echo cine imaging shows bright blood relative to myocardium. Contrast is usually good at end diastole but degrades by end systole due to saturation of slow-moving blood at the apex. Two-sided presaturation has been shown to allow the collection of cine images with blood that is dark relative to the myocardium, both at end diastole and at end systole. The result is improved absolute contrast but usually a loss in contrast-to-noise ratio. This research demonstrates a method that more than doubles overall contrast while still providing a gain in contrast-to-noise ratio. Images were acquired with Picker International 1.0- and 1.5-T HPQ systems. High-temporal-resolution (20 msec) black-blood cine images were obtained with a bimodal RF pulse of 50°. Bright-blood images were obtained by using the same sequence with a presaturation pulse of 0°. Imaging time was 2 to 4 min per acquisition, for a total imaging time of 4 to 8 min. Similarly, black- and white-blood cine images with 50-msec temporal resolution were acquired by using phase-encode grouping (PEG), with a total imaging time of 1 to 2 min. White-blood images were subtracted from the corresponding black-blood images. Signal intensities were measured in the septum and in the ventricular cavity near the base and at the apex of the heart. Overall contrast improved by two to three times at the base and apex; contrast-to-noise ratio improved by 15%–25% at the base and by 0%–10% at the apex.

127 • 11:06 AM

### MR Angiography of the Diabetic Foot

AN Awad, EC Unger, J Schilling*, A Darkazanli, M Pitt, P Lund, P Capp

*Departments of Radiology/MRI and *Vascular Surgery, University of Arizona, Tucson*

To assess the role of MR angiography in the diabetic patient, a randomly selected series of 12 patients with diabetes mellitus and nonhealing foot ulcers in whom there was clinical suspicion of osteomyelitis were studied with MR imaging and MR angiography. For comparison, MR angiography was also performed in six healthy volunteers. All imaging was performed with a 1.5-T GE Signa. Initially, both 2D and 3D phase-contrast and time-of-flight (TOF) MR angiography were performed in the first two

volunteers. The best image quality was obtained with 2D TOF, and this technique was used in both patients and volunteers (TR = 45 msec, TE = 9 msec, 20° flip angle, 1.5-mm section thickness, 128 locations, total acquisition time = 13 min). MR angiography was performed pre- and postcontrast (intravenous injection of 0.1 mm/kg Gd-DTPA). Osteomyelitis was shown as a region of abnormal bone marrow with decreased signal intensity on T1 images and with increased signal intensity on STIR images. In all patients, MR angiographic studies demonstrated flow in the plantar and dorsal arches. In several patients, multiple stenoses could be seen in a pattern suggesting diffuse atherosclerosis. In most patients the arterial circulation appeared relatively intact, despite nonhealing ulcers or osteomyelitis. Gadolinium-enhanced MR angiography demonstrated localized hyperemia to the infected soft tissues and marrow in 11 of 12 patients (92%). Correlation with bone biopsy or surgical pathology was obtained in five patients and confirmed the MR imaging and angiographic findings. It is concluded that high-quality MR angiographic images of the foot and ankle can be obtained in diabetic patients. This technique holds promise for better evaluation, localization, and definition of the infectious process of the diabetic foot, as well as for improved visualization of ankle and foot vasculature.

128 • 11:18 AM

## MR Angiography of the Renal Arteries

GK Lammert, MG Zelch, JJ Dillinger, PA Hardy, JA Tkach, JS Lewin, PM Ruggieri, MT Modic, D Goldfarb
*Division of Radiology, Cleveland Clinic Foundation, Cleveland*

A reliable MR angiographic technique for the detection of renal arterial stenosis would obviate the need for certain patients to undergo arteriography, an invasive procedure. MR angiography of renal arteries is complicated, however, by respiratory motion and the presence of adipose tissue. This study attempted to develop a reliable time-of-flight (TOF) MR angiographic technique for visualizing the entire renal artery. A series of healthy volunteers and a small number of patients with renal arterial stenosis were examined with sequential 2D and 3D sequences. Various TEs, TRs, $\alpha$ values, and k-space sampling strategies were used. In addition, the position of saturation bands and the use of respiratory gating was varied. The technique providing the most consistently high-quality images was a 3D FISP sequence (TR = 35 msec, TE = 5.9 msec, $\alpha$ = 20°; velocity compensation in readout and section-select directions). Minimizing TE was found to be of greater value than having opposed-phase fat and water. Rectangular FOV and a matrix of 256 × 160 × 64 were used to obtain approximately 1-mm$^3$ voxels. The reduction in imaging time achieved with a rectangular FOV made respiratory gating of the central 20% of k space clinically practical. Minimum blood saturation occurred when the imaging volume was oriented axially and contained the renal artery branch in the top third of the volume. Venous flow was effectively eliminated by using two saturation slabs positioned in a V shape to saturate both kidneys and the superior vena cava. Sampling k space in different orders did not appear to enhance the images. MIP projections of the 3D FISP images typically showed nearly the entire extent of the renal arteries.

129 • 3:57 PM

## Multiple-Volume Time-of-Flight MR Angiography of the Aortic Arch

JS Lewin*, R Hausmann†, AS Smith†, TJ Masaryk*
**Department of Radiology, Cleveland Clinic Foundation, Cleveland; †Siemens Medical Systems; and ‡University Hospitals of Cleveland*

Theory would predict that 3D time-of-flight (TOF) methods would not be applicable to the aortic arch and great vessels due to artifact from the effects of respiratory and cardiac motion on phase encoding in two axes. The purpose of this study was to test the hypothesis that a 3D technique can visualize the aortic arch and its primary branches with high spatial resolution and a short examination time, and that multiple thin-volume acquisition can minimize the effects of progressive spin saturation and increase vessel visualization. Six volunteers and six patients (two with suspected vasculitis, two with suspected great vessel aneurysms, one with a congenital variant, and one with surgical reimplantation of the carotid) were imaged with a new 3D FISP method with sequential overlapped volume acquisitions (20° flip angle, TR = 24 msec, TE = 6 msec, 1.2-mm isotropic resolution, velocity compensation, cephalad presaturation pulse). Either two 64-partition, 75-mm-thick or five 32-partition, 37-mm-thick volumes were acquired, with 30% overlap. Examinations were performed on a standard 1.5-T system. Total examination time varied from 8 to 13 minutes. Maximum-intensity projection postprocessing was subsequently performed. Conventional contrast arteriography was performed in four of the six patients. The brachiocephalic, bilateral common carotid, and subclavian arteries and their origins were well visualized in all volunteers and two younger patients with the 75-mm volume method. Two older patients demonstrated signal loss in the subclavian and distal common carotid arteries with this method. The use of multiple thin (37-mm) volumes significantly reduced signal loss from progressive spin saturation, allowing good vascular visualization in all subjects, but required an increase of approximately 30% in examination time. Diagnostic studies were obtained in stenotic lesions from atherosclerosis ($n$ = 2) and vasculitis ($n$ = 1), common or internal carotid artery occlusion ($n$ = 2), subclavian aneurysm ($n$ = 1), marked atherosclerotic tortuosity ($n$ = 1), normal arch variants ($n$ = 2), and a postoperative carotid-subclavian anastomosis ($n$ = 1), demonstrating excellent correlation with intraarterial digital subtraction angiographic (DSA) images. Several patients demonstrated more than one finding. While the subclavian aneurysm in one patient was visualized, suboptimal evaluation of its distal extent was noted due to spin saturation, despite the use of thin overlapping volumes. Artifact from physiologic motion was not noticeable in any study. In conclusion, (*a*) the use of multiple thin overlapping volumes allows improved visualization of the aortic arch and great vessels as compared with a thick-volume technique; (*b*) the multiple 3D TOF method allows diagnosis of stenosis, occlusion, anatomic variants, and anastomotic patency with excellent correlation with intraarterial DSA and without noticeable motion artifact; and (*c*) while the results were reproducible in the volunteers and most patients, the suboptimal evaluation of the distal extent of a subclavian artery aneurysm in one patient suggests that significantly slowed flow from decreased cardiac output, critical stenosis, or within a large aneurysm may reduce vessel visualization due to the persistent effects of spin saturation. Clinical application in patient evaluation is ongoing.

130 • 11:42 AM

### MR Angiographic Evaluation of Peripheral Vascular Disease with Poor Visualization at Conventional Angiography

JM Haltom, SE Harms, KA Glastad, DP Flamig, CM Talkington

*Department of Radiology, Baylor University Medical Center, Dallas*

Conventional angiography can be insensitive to slow flow in the lower extremities of patients with vascular occlusive disease. This study investigated the use of MR angiography in identifying flow in the lower extremities of patients with severe claudication in whom little or no flow had been identified with conventional angiography. MR angiography was performed on a 1.5-T GE Signa imager with 4.6 software. Two-dimensional TOF and 3D rotating delivery of excitation off-resonance (RODEO) acquisitions were performed. Two-dimensional TOF provided 64 sections with a 128 × 256 matrix. Spatial presaturation was used inferiorly with 2D TOF to reduce the intensity of venous flow. RODEO, a fat-suppressed T1-weighted steady state sequence, yielded a 128 × 256 × 256 matrix with an imaging time of about 4 min. MIP renderings were obtained with the GE independent console. In a series of 15 patients, MR angiography demonstrated flow in lower-extremity vessels, the conventional angiographic visualization of which was limited. Two-dimensional TOF was most sensitive to slow flow but RODEO provided the best overall anatomic detail when flow velocities were sufficient to allow visualization of vessels. Retrograde flow was not visualized with 2D TOF due to the use of inferior presaturation. These results were verified either intraoperatively or with Doppler sonography. In three patients no flow could be documented with any method. In patients with peripheral vascular disease, selected MR angiographic techniques can be helpful in selecting those who may benefit from limb salvage procedures, thereby reducing morbidity associated with amputation.

131 • 11:54 AM

### Two-dimensional-Inflow and Phase-Contrast MR Angiography in Peripheral Vascular Occlusive Disease

B Krug*, H Kugel*, J Bunke[§], P van Dijk[§], M Dietlein*, D Hannibal*, A Altenburg*, R Schmidt†, L Wallroth-Marmor†

**Department of Radiology, †Department of Surgery, and ‡Department of Medical Documentation and Statistics, University of Cologne, Germany, and §Philips Medical Systems*

The purpose of this study was to evaluate the effectiveness of 2D-inflow and phase-contrast MR angiography in diagnosing peripheral vascular occlusive disease. Fifty-seven patients with arteriosclerosis of the aortoiliac and femoropopliteal arteries proved by intravenous ($n$ = 28) or intrarterial digital subtraction angiography (DSA) ($n$ = 29) were examined with a 1.5-T MR imager (Gyroscan S15, Philips). Two-dimensional-inflow ($n$ = 54) (multiple single-section technique, TE = 13 to 15 msec, $\alpha$ = 60°; FOV, 30 to 40 cm; section thickness, 2 to 3 mm; matrix, 256 × 256; first-order flow compensation, venous presaturation) and phase-contrast MR angiography ($n$ = 29) (rapid sequential excitation [RSE] MR angiography, TE = 12–13 msec, $\alpha$ = 60°, one coronal section of 10- to 15-cm thickness, electrocardiograph gating) were used. RSE MR angiography was achieved by adjusting flow sensitivity and trigger delay to values determined by prior MR velocity measurements. The spectrum of pathology included stenoses less than 50% ($n$ = 38), stenoses less than 90% ($n$ = 36), stenoses less than 99% ($n$ = 18), and occlusions ($n$ = 42). The MR angiographic and DSA examinations were evaluated by four "blinded" radiologists with a topographic questionnaire that included signs of image quality and a differential diagnosis. Statistical analysis was done with kappa statistics, the McNemar test, and contingency tables. Even in smaller arteries (profunda femoral arteries, trifurcation), 2D-inflow MR angiography proved to be equal to intravenous DSA with respect to image quality and the level of diagnostic information contained in the examinations. Intraarterial DSA was diagnostically superior to both 2D-inflow MR angiography and intravenous DSA. Because of poor spatial resolution as well as susceptibility and flow sensitivity–induced artifacts, the image quality of phase-contrast MR angiography is insufficient to allow its clinical use. Phase-contrast MR angiography representing blood flow rather than morphology allowed a more efficient evaluation of poststenotic flow disturbances in isolated cases, which might be of prognostic value. In conclusion, 2D-inflow MR angiography is a useful, noninvasive method for evaluating peripheral arteriosclerotic disease.



## Tuesday Morning • Regent Parlor
## Papers 132–139

### PERFUSION, DIFFUSION, AND FUNCTIONAL IMAGING

MODERATORS: MS Cohen, PhD • JR MacFall, PhD

132 • 10:30 AM

### Measurements of the Concentration of Oxygen in Vivo in Tissues under Physiologically Pertinent Conditions and Concentrations

HM Swartz, RB Clarkson, KC Chang, JF Glockner, KJ Liu, SW Norby, AI Smirnov, T Walczak, M Wu

*University of Illinois, Urbana*

One of the principal goals of in vivo MR techniques is to measure [$O_2$], especially to determine the presence of significant hypoxia. Although various MR techniques have been used for this purpose, to date they have not provided the desired information with the necessary sensitivity and accuracy. The "other" MR technique, electron paramagnetic resonance (EPR or, equivalently, electron spin resonance) offers great promise of meeting this need. Three interrelated factors have led to the successful development of this approach: (*a*) the sensitivity of the EPR spectra of many paramagnetic materials to [$O_2$]; (*b*) the discovery of paramagnetic materials that have the required sensitivity to concentrations of oxygen in the pertinent ranges (0.1 to 40 μmol/L [$O_2$]) and also have high stability in tissues and a lack of toxicity; and (*c*) the development of instrumental approaches that have permitted the use of EPR in live animals with sufficient sensitivity and safety. The studies have been carried out at 1.1 GHz, with a low-field magnet (400 G) and a microwave bridge. High-quality spectra have been obtained in vivo from skeletal muscle, heart, kidney, and brain of living rats and/or mice with either a loop gap resonator as a surface probe or a probe coupled with a resonator. The latter approach has made it possible to obtain well-resolved spectra from deep within tissues (75 mm) and from organs in situ. Recently these techniques have been extended to include the capacity to obtain undegraded data on [$O_2$] simultaneously from two or more sites with a magnetic field gradient. There appear to be no obstacles to the immediate application of these techniques in experimental studies and no discernible long-term obstacles to their routine use in patients.

133 • 10:42 AM

## Functional Echo-Planar MR Imaging at 1 T

M Stehling, M Fang, R Ladebeck, F Schmitt

*Siemens Medical Systems and Department of Neurosurgery, University Hospital, Erlangen, Germany*

Functional MR imaging (1) of the central nervous system has become feasible with echo-planar imaging (EPI). Most applications have been shown at high field strength ($\geq 1.5$ T). Despite the fact that the EPI prototype MR imager operates at medium field strength (1.0 T), it has been possible to measure cerebral blood flow, perfusion, and diffusion in patients and volunteers. Different appoaches have been used. Perfusion can be measured in Gd-DTPA time course studies by observing susceptibility-related signal drop. Mapping of blood-brain barrier (BBB) permeability is possible by evaluating signal increase after initial bolus passage in areas where the BBB is compromised. With multisection sequences, 3D maps can be obtained. The use of deoxyhemoglobin, rather than Gd-DTPA, as a natural contrast agent has recently been investigated. Long TE (> 180 msec) EPI sequences can be used for detection of hemoglobin saturation and related cerebral signal intensity changes. Principal component analysis is used regularly for evaluation of these dynamic studies. The feasibility of imaging (at 1.0 T) brain function, as in the optical cortex during optical stimulation, is currently being investigated. The potential and limitations of EPI and of the specific problems that have been encountered will be discussed.

1. Stehling MK, et al. Echo-planar imaging: magnetic resonance imaging in a fraction of a second. Science, October 1991.

134 • 10:54 AM

## Functional MR Imaging of Primary Visual and Motor Cortex

KK Kwong, JW Belliveau, CE Stern, DA Chesler, IE Goldberg, BP Poncelet, DN Kennedy, RM Weisskoff, MS Cohen, R Turner*, H-M Cheng, TJ Brady, BR Rosen

*MGH-NMR Center, Charlestown, Mass, and *NIH Laboratory of Cardiac Energetics, NHLBI, Bethesda, Md*

High-speed, noninvasive MR imaging methods sensitive to changes in cerebral blood flow, blood volume, and oxygenation have been used to generate functional MR imaging maps of human visual and motor cortex activation. These MR imaging techniques provide high spatial and temporal resolution information and can be used to correlate behavioral and physiologic changes with underlying anatomy. Seven healthy subjects underwent dynamic MR imaging with a modified echo-planar imaging technique (1.5 T, GE Signa, modified by Advanced NMR Systems). Changes in blood oxygenation were detected with a gradient-echo (GE) imaging sequence sensitive to variations in T2* (TR = 3,000 msec, TE = 40 msec). Changes in tissue perfusion were evaluated with a spin-echo inversion recovery (IR), T1-sensitive pulse sequence (TI = 1,100 msec, TR = 3,500 msec, TE = 42 msec). Typically a series of between 80 and 128 images were acquired continuously with the same imaging pulse sequence (either GE or IR). Figure 1 shows signal intensity changes as a function of time for a region of interest within primary visual cortex during darkness and during 7.8-Hz photic stimulation. Figure 2 displays signal intensity changes within primary motor cortex during repetitive hand movements and during resting state.

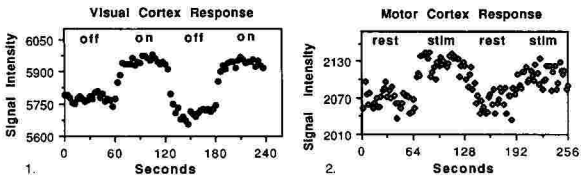


135 • 11:06 AM

## Echo-Planar Imaging of Cerebral Capillary Percent Deoxyhemoglobin Change on Task Activation

PA Bandettini, EC Wong, RS Tikofsky, RS Hinks*, JS Hyde

*Department of Radiology, Medical College of Wisconsin, Milwaukee, and *GE Medical Systems, Milwaukee*

It is well known that cerebral metabolism and blood flow are enhanced during the activation of regions of the cerebral cortex involved in the performance of specific tasks. It has also been demonstrated that induced local increase of cerebral blood flow exceeds concomitant local increase in tissue metabolic rate, causing a significant decrease in the oxygen extraction fraction (1), and thus a decrease in %deoxyhemoglobin (Hb). The paramagnetic character of deoxy-Hb has been extensively studied in vitro (2) and in larger vessels (3,4). The hypothesis is that capillary deoxy-Hb causes a bulk susceptibility differential between each capillary and the surrounding tissue, setting up microscopically inhomogeneous static fields that cause a net intravoxel dephasing of spins. On cerebral tissue activation, the local decrease in %deoxy-Hb causes a decrease in the susceptibility differential between capillary and tissue, thus decreasing intravoxel dephasing and allowing increased signal in a gradient-recalled sequence. The observed change in signal corresponds closely with the change in signal predicted by a simulation correlating normalized voxel signal intensity with known physiologic parameters of capillary size, density, geometry, and oxygen extraction fraction; and the empirical relationship between bulk susceptibility, %deoxy-Hb, and field strength for various capillary orientations and blood hematocrits. The recently introduced imaging protocol, which observed activation of the visual cortex during photic stimulation (5,6), involved collecting a series of axial gradient-recalled echo-planar images. That method has been expanded on by the imaging of task activation centers in all three planes. With use of a local head xyz gradient coil of original design fitted to a GE Signa 1.5-T magnet, sets of 128 coronal, axial, and sagittal gradient-recalled echo-planar images of the brain (TE = 50 msec, TR or image spacing of 2,000 msec) were obtained in seven subjects. At image number 64, the subjects were instructed to begin the task of touching their thumb to each finger in a sequential manner. In each instance, an immediate (< 2,000 msec) increase of 3% to 9% in signal was observed in the cortical areas corresponding to the task. Also, in sets taken in which the subjects stopped the task at image number 64, an immediate decrease of 3% to 9% in the signal in the same cortical areas was observed. Echo-planar imaging of dynamic capillary %deoxy-Hb contrast is a powerful new tool for the flexible, noninvasive, and high-resolution assessment of regional cerebral activation.

1. Fox PA, Raichle ME. Proc Natl Acad Sci USA 1986; 83: 1140–1144. 2. Thulborn KR. Biochim Biophys Acta 1982; 714:265–270. 3. Ogawa S, Lee TM, Nayak AS, Glynn P. Magn Reson Med 1990; 14:68–78. 4. Wright GA, Hu BS, Macovski A. JMRI 1991; 1:275–283. 5. Brady TJ. SMRM Book of abstracts 1991; 1:2. 6. Hoppel BE, Weisskoff RM, Thulborn KR, Moore J, Rosen BR. SMRM Book of abstracts 1991; 1:308.

136 • 11:18 AM

## Signal Changes in Dynamic Contrast Studies: Theory and Experiment In Vivo

RM Weisskoff, BJ Hoppel, BR Rosen
*MGH-NMR Center, Department of Radiology, Massachusetts General Hospital, Charlestown, Mass*

Recent MR imaging experiments have exploited high-susceptibility contrast material—exogenous agents, such as lanthanide chelates, and endogenous iron in the body, such as deoxygenated hemoglobin—to produce "functional" MR images. Herein is presented a theoretical framework to explain and quantify the spatial dephasing component of signal loss by modeling the vascular bed as a collection of randomly oriented cylinders. In this model, signal loss can be expressed exactly as a function of tissue blood volume, contrast agent susceptibility, and imaging parameters. These predictions were tested in vivo on an intact rabbit model at 1.5 T with an echo-planar, offset spin-echo sequence, which naturally separates the intervoxel dephasing effects from diffusion-related T2 changes by displacing the spin echo and the center of k space by $\tau$ msec. This sequence was implemented on a GE 1.5-T imager modified for single-shot imaging by Advanced NMR Systems. In these studies, 8 to 12 injections of a long-lived superparamagnetic contrast agent (AMI-227; Advanced Magnetics, Cambridge, Mass; total dose, 3 mg Fe/kg body mass) were administered, producing eight cardiac-gated images with different $\tau$ offset values ($\tau = -30$ to $+40$ msec) 1 minute after each injection. Total imaging time after each injection (depending on heart rate) was approximately 25 seconds. The agent concentration within the blood was quantified by measuring the susceptibility of arterial blood drawn before and after the injections. By plotting signal change versus agent concentration at each $\tau$ value, a dose response curve was produced for each animal. The slopes of these curves at increasing $\tau$ offset agrees with the vascular model prediction for a blood volume of 3%–4%. Measurements taken in the same animals under hypercapnia and anoxia (before and after injection of additional exogenous contrast materials) are also interpreted with this theoretical framework.

137 • 11:30 AM

## Acute Human Cerebral Infarctions Evaluated with Diffusion-weighted MR Imaging

S Warach, D Chien, W Li, M Ronthal, RR Edelman
*Department of Neurology and Radiology, Harvard Medical School and Beth Israel Hospital, Boston*

The work of Moseley and others with animal models of cerebral ischemia has suggested that there is a decrease in diffusion in acute infarction and that this decrease is evident before changes on T2-weighted images. These hypotheses were investigated in human stroke. Twenty-one patients were studied one to four times as early as 105 minutes after stroke onset. A turboSTEAM technique was used on a 1.5-T whole-body imaging system (Siemens) (TR = 12 msec, TM = 800 msec, $\alpha = 11°$, gradient duration = 4 msec, matrix = 128 × 128, FOV = 280, minimum of four acquisitions). Images were acquired with no diffusion-sensitizing gradients and then with strongly diffusion sensitizing gradients. The technique was validated with phantoms of water, acetone, and dimethyl sulfoxide, which yielded diffusion coefficients similar to published values. A *b* value of 294.1 sec/mm$^2$ was calculated. Patients also underwent standard T1- and T2-weighted spin-echo imaging. The mean (standard deviation) apparent diffusion coefficient (ADC) for control regions (usually contralateral cortex) in the 21 patients was $2.44 \times 10^{-3}$ ($0.95 \times 10^{-3}$) mm$^2$/sec. Statistically significant changes in the ADC of infarcts relative to control regions were found over time. ADC was decreased to a mean (standard error of mean) of 60% (3.8%) of control in infarcts less than 48 hours old and decreased to a mean of 78% (9.5%) of control in infarcts 5–12 days old, while ADC was increased to 137% (15.3%) of control in chronic infarcts (more than 7 months old). These abnormalities were also evident at qualitative inspection of the images, allowing for easy differentiation of acute/subacute infarcts from chronic infarcts. In the earliest case the lesion was apparent only on diffusion images, spin-echo images being judged as normal by three "blinded" independent observers. The greatest decreases in ADC (as low as 15% of control) were observed in cases of sufficient brain swelling to cause a mass effect, consistent with the hypothesis that reduced ADC in ischemic infarction is related to cytotoxic edema. Diffusion-weighted imaging of human cerebral infarctions can demonstrate the size and location of lesions as early as is clinically practicable and should be useful in the early evaluation of strokes and the design of trials for early therapeutic interventions.

138 • 11:42 AM

## Effectiveness of Relaxivity Contrast Perfusion Technique for Detection of Acute Cerebral Ischemia: Contrast Agent Dose Dependence

VM Runge, GS Thomas, JE Kirsch, CE Woolfolk, UY Ryo
*Magnetic Resonance Imaging and Spectroscopy Center, University of Kentucky, Lexington*

Doses of 0.25, 0.5, and 1.0 mmol/kg of intravenous gadoteridol were compared for detection of decreased first-pass brain enhancement, due to surgically induced unilateral cerebral ischemia in the middle cerebral artery (MCA), on turboFLASH MR images during bolus contrast agent injection in cats. Baseline MR images were obtained at 1.5 T, followed by occlusion of the MCA. At 8 min following ligation, sequential turboFLASH images were acquired during intravenous bolus contrast injection. Cerebral perfusion was quantitated with Tc-99m macroaggregates of albumin. Five animals with confirmed MCA ischemia were studied at a dose of 0.25 mmol/kg, five at 0.5 mmol/kg, and four at 1.0 mmol/kg. Postprocessing included the calculation of subtracted images from the turboFLASH data set with a precontrast image as baseline. At a dose of 0.5 mmol/kg, perfusion defects (appearing as decreased enhancement of gray matter on first pass of the contrast agent) were noted in all five animals on both raw and subtracted images. At a dose of 0.25 mmol/kg, decreased first-pass enhancement was noted on two turboFLASH studies (raw images), with the other three cases normal even on inspection of subtracted images. At a dose of 1.0 mmol/kg, only two of four cases demonstrated decreased first-pass enhancement of gray matter, and then only on subtracted images. Percent enhancement of normal gray matter was maximum (61%) at a dose of 0.5 mmol/kg. With the relaxivity contrast perfusion technique, enhancement of brain tissue is strictly dependent on changes in intravascular (capillary bed) signal intensity, limiting its sensitivity. Doses both below and above 0.5 mmol/kg demonstrated poorer sensitivity, the former presumably because of smaller T1 effects and the latter potentially because of competing T2 effects.

139 • 11:54 AM

## Relation between Gd-DTPA Concentration and Signal Intensity on T2*-weighted Images of the Brain after Intravenous Bolus Injection

JC Böck, B Sander, J Haustein, W Schörner, R Felix
*Strahlenklinik und Poliklinik, Universitätsklinikum Rudolf Virchow, Berlin*

Fast T2*-weighted images acquired during the first pass of a paramagnetic contrast agent through the brain can be used to obtain information on cerebral blood flow and vol-

ume. Quantification of cerebral blood flow relies on a signal that is linearly related to concentration. This study examined the relation between the intravascular Gd-DTPA concentration in the brain and the signal intensity decrease on T2*-weighted images. In 10 patients without evidence of cerebral pathology, T2*-weighted images were acquired during and after injection of Gd-DTPA (1.5 T, gradient-echo sequence, TR = 25 msec, TE = 20 msec, flip angle = 10°, acquisition time = 2.5 seconds, 30 sequential images). The following Gd-DTPA doses contained in 20 mL were injected manually (~5 sec): 0.0, 0.00625, 0.0125, 0.025, 0.05, and 0.1 mmol/kg body weight. Signal intensity (SI) was measured on an image before injection ($SI_0$) and on the image with the maximal signal intensity reduction ($SI_M$). From these data relative concentration ($C_R$) was calculated as $C_R = -1n\ SI_M/SI_0$. Linear coefficients of correlation between the injected dose and $C_R$ ranged from $r = .95$ to $r = .99$. As expected, the slopes of the regression lines differed considerably among subjects. It is concluded that logarithmic transformation of relative signal intensity changes on T2*-weighted images yields a parameter that is linearly related to the intravascular concentration of Gd-DTPA. The degree of contrast dilution in the blood contained between the injection site and the brain appears to vary greatly among individuals. Consequently, absolute Gd-DTPA concentrations in cerebral blood vessels and microvasculature cannot be determined on the basis of signal intensity measurements alone.

## Tuesday Afternoon • Beekman Parlor
## Papers 140–147

### RAPID IMAGING: Interventional and 3D

MODERATORS: R Kikinis, MD • RB Lufkin, MD

140 • 3:45 PM

#### Monitoring of Interstitial Laser Ablation Therapy and Cryotherapy with T1-weighted RARE MR Imaging

R Matsumoto, K Oshio, FA Jolesz
*Department of Radiology, Brigham and Women's Hospital, and Harvard Medical School, Boston*

A real-time monitoring device is necessary to assess ongoing thermal effect on tissue during both interstitial laser ablation therapy and cryotherapy. Taking a single-section image every 30 sec with T1-weighted RARE made it possible to visualize reversible and irreversible MR intensity changes during the procedures ex vivo and in vivo. This provided sufficient temporal and temperature resolution for the purpose. Imaging parameters used were as follows: four-echo excitation, effective TE = 18 msec, TR = 300 msec, 5-mm section thickness, 20-cm FOV, 256 × 192 matrix, and 1 NEX. Imaging time was 16 sec per image. Ex vivo and in vivo imaging during laser irradiation of animal liver showed reversible intensity change that can be explained by T1 increase due to temperature change. On images acquired during hypothermia, a sudden drop in MR intensity was observed around 0°C, as was the intensity change attributable to T1 increase, and this enabled visualization of the process and extent of freezing and thawing. Temperature sensitivity of this sequence was evaluated in the pig liver ex vivo. Calculated T1 showed an approximately linear relationship with temperature, by 5 msec (1%–2%)/°C in the range of 7.8°–63.3°C, and the T1 uncertainty corresponded to a temperature resolution of 4.5°–6.4°C.

141 • 3:57 PM

#### Real-Time Monitoring of Laser-induced Interstitial Thermotherapy in Cerebral Gliomas with MR Imaging

T Kahn*, F Ulrich†, M Bettag†, R Schober†, R Seitz§, S Hessel‖, M Deimling#, WJ Bock‡, U Mödder*
*Departments of *Diagnostic Radiology, †Neurosurgery, ‡Neuropathology, and §Neurology, Heinrich-Heine University, Düsseldorf, ‖MBB-Medical Technology, Munich, and #Siemens Medical Engineering Group, Erlangen, Germany*

Laser-induced interstitial thermotherapy is a new therapeutic approach in cerebral gliomas with poor accessibility. The purpose of this study was to evaluate the ability of MR imaging to monitor thermotherapy in real time. A 68-year-old woman with an anaplastic astrocytoma (WHO III) in the right parietal operculum was treated with MR imaging–guided laser therapy. After stereotactic CT-guided biopsy was performed, a special light guide with a directed circumferential beam characteristic was introduced with a laser applicator to the tumor center. The nonmetallic design of the fiber tip requires no cooling and allows the transmission of 3–10 W of power via the 1,060-m Nd: YAG laser. The position of the tip of the light guide was controlled with multiplanar reconstructions of a T1-weighted 3D TurboFLASH sequence. For laser intervention, continuous waves at a power intensity of 4 W were applied over a period of 10 min. To monitor the therapy, a 2D FLASH sequence (TR = 70 msec, TE = 6 msec, 40° flip angle, 3-mm section thickness, five sections) with an acquisition time of 15 seconds was applied repeatedly during the course of the intervention. After 2 min a high-signal-intensity spot approximately 1 mm in diameter appeared adjacent to the tip of the fiber. During the course of the laser therapy, the diameter of the bright area increased to 5 mm. After the therapy a T2-weighted spin-echo sequence showed a low-signal-intensity area in the center of the tumor, corresponding to the bright spot on the T1-weighted images. Follow-up studies were performed 7, 14, and 27 days after therapy. For each examination pre- and post-Gd–DTPA 3D TurboFLASH sequences were combined with an axial T2-weighted spin-echo sequence. The diameter of the central high-intensity region on the T1-weighted images increased to 12 mm after 14 days. After administration of Gd-DTPA a local disruption of the peripheral enhancing rim was noted in the neighborhood of the central lesion. Previous thermotherapeutic animal experiments in normal rat brain and F-98 glial transplantation tumor showed a central zone of coagulation necrosis surrounded by a sharply demarcated rim of edema. The signal intensities of the MR studies correlated with the histologic findings. The preliminary results of this study show that MR imaging has great promise in monitoring interstitial laser therapy.

142 • 4:09 PM

#### Use of MPRAGE MR Imaging for 3D Brain Display

M Brant-Zawadzki*, G Gillan*, D Atkinson†
*Department of Radiology, Hoag Hospital, Newport Beach, Calif, and †Siemens Medical Systems, Iselin, NJ*

The purpose of this study was to evaluate 3D MPRAGE acquisitions for volume and surface rendering of brain MR imaging. Six patients referred for MR evaluation of brain focal lesions were imaged with a Siemens Magnetom 63 SP (TR/TE/α = 10/4/12, 200 × 256 matrix, 250-mm FOV). Sagittal slabs of 160 mm were used with either 64 or 128 partitions for an acquisition time of 3:11 or 6:22. Pixel size was 1.25 × 1 mm. Section thickness was either 2.5 or 1.25 mm. Images were obtained both pre- and post-gadolinium. Resultant 3D data sets were processed on a

commercially available 3D workstation (ISG Technologies, Toronto). Correlative surgical observation was performed in four cases. All data sets were successfully volume and surface rendered with no significant problems. The MPRAGE sequence clearly depicted gray/white matter, edema, surface gyri, and deep sulci, as well as major cortical veins. Brain pathology was clearly depicted in all cases. The noncontrast images proved superior to gadolinium-enhanced images for brain surface rendering and ventricles and sulci. Postcontrast images proved superior for reconstruction of tumors and cortical veins. The 64-partition, 2.5-mm-section data set proved sufficient for all postprocessing. Three-dimensional rendition allowed easy overlay of lesion, brain, vessels, and scalp features. The location of the central sulcus was easily traced mediolaterally and projected onto the cortical surface. In conclusion, high-quality 3D MR data sets for surface and volume rendering of brain structures may be obtained in just over 3 min with MPRAGE. Anisotropic 3D data sets are acceptable for 3D postprocessing, provided voxel sizes are kept relatively small.

143 • 4:21 PM

### MR Imaging of the Postoperative Lumbar Spine: Value of Gadolinium-enhanced Multiplanar Reconstruction with T1-weighted 3D-acquired Data Sets Yielding 1-mm Isotropic Resolution

MA Nissenbaum, N Palmer, BE Widoff, SJ Song, SM Brown, K Yan, JL Amster, WG Bradley
*Long Beach Memorial Medical Center, Long Beach MRI, Long Beach, Calif*

The purpose of this study was to assess the utility of RF-spoiled, T1-weighted 3D sequences yielding 1-mm isotropic data sets with multiplanar reformatting in the evaluation of the postoperative lumbar spine. Lumbar 3D acquisitions were made with a 1.5-T Picker HPQ MR imager with RF-spoiled fast sequences (20–55/7–9/20–30, 128 partitions, 12 min/1 NEX) and gadolinium enhancement. The data sets were viewed in orthogonal and novel sagittal and coronal double and triple oblique projections tailored to better differentiate scar-encased disk from rootlet, and to better visualize nerve root displacement, angulation, and intracanalicular encasement with scar. The sensitivity, specificity, and confidence of diagnosis were compared with those of conventional spin-echo sequences in 15 previously operated patients, studied prospectively in a blinded fashion by three experienced radiologists. Contrast-to-noise ratio measurements were made for wrapped disk and scar. Sagittal and coronal triple oblique projections along nerve roots and through neural foramina allowed confident diagnosis of scar-related complications in all cases. Nerve root angulation and differentiation of nerve root encasement from "wrapped" disk was diagnosed with significantly more sensitivity and confidence on the enhanced 3D studies. Clinical utility was judged superior to spin echo in a majority of patients. In conclusion, reformatted gadolinium-enhanced RF-spoiled fast imaging of the lumbar spine, yielding 1-mm isotropic resolution, provided increased sensitivity, specificity, and diagnostic confidence in the evaluation of pathology in the operated lumbar spine.

144 • 4:33 PM

### Lumbar Myelography with Three-dimensional MR Imaging

RJ Zisch, W Artmann, *HP Hollenbach
*General Hospital, Wels, Austria, and *Siemens, Erlangen, Germany*

As in many other fields, MR imaging has changed diagnostic strategy in patients with herniated disk disease. Invasive methods such as x-ray myelography are being used less frequently. Thus far, MR imaging diagnosis of herniated disk disease has been limited to purely tomographic techniques. The technical innovation of 3D sequences, with the possibility of 3D reconstruction, opens up new applications for MR imaging in many fields. An attempt was made to duplicate x-ray myelography by using a special, heavily T2-weighted, 3D gradient-echo sequence with very high contrast between cerebrospinal fluid (CSF) and surrounding tissue. Three-dimensional reconstructions of the thecal sac were performed with a special postprocessing routine, creating myelogram-equivalent images. The high signal values from CSF in the 3D data set were projected onto a new 2D plane, suppressing the surrounding tissue. Images were calculated in multiple projections in 360° and the projections displayed in a cine loop, so that the thecal sac appeared to rotate in space. The method was tested for usefulness in 30 patients with proven disk disease. Except for purely intraforaminal and lateral disk herniations, all herniated disks could be visualized with MR myelography because of their indentation in the contour of the thecal sac. By showing the effect of pathology on the thecal sac in a three-dimensional way, MR myelography might become a helpful noninvasive method of diagnosing spinal disease, thereby replacing x-ray myelography.

145 • 4:45 PM

### Three-dimensional MR Imaging of Different Phases of Mouth Opening Movement

TJ Vogl, J Assal, D Eberhard, P Weigl, J Lissner
*Department of Radiology, University of Munich, Germany*

The purpose of this study was to show the changes in facial surfaces and intraarticular structures during masticatory muscle function. Fifteen asymptomatic volunteers were examined at incremental degrees of mouth opening on a 1.5-T Magnetom with a hydraulic calibrated bite opener. Three-dimensional MR imaging was performed with MPRAGE, a fast TurboFLASH 3D sequence (TR = 10 msec, TE = 4 msec, flip angle = 15°, 128 sections, section thickness = 1.4 mm). Total examination time for each subject was about 1 hour. With the application of a cine program, adequately windowed 3D images were selected and arranged sequentially to create a movie of temporomandibular joint (TMJ) motion. This study demonstrates the advantages of 3D imaging with surface reconstruction and high spatial resolution within the topographic correlation of TMJ surroundings in the window technique. The rotation and translation phases of lower jaw opening movements can be clearly identified. Changes in smooth tissue, the function of superficial parts of the masseter, temporal, and pterygoid muscles, and condylar movement during the phases of mouth opening (0.5, 1.0, 2.0, and 3.0 cm) are demonstrated, limited, however, by insufficient visualization of the articular disk and time of examination. In conclusion, 3D MR imaging has proved to be well suited for visualization of the complexity of 3D coordinated TMJ movements for clinical consideration.

146 • 4:57 PM

### Analysis of Gd-DTPA Enhancement in T1-weighted 3D MP-RAGE Sequences

JP Mugler III, JR Brookeman
*Departments of Radiology and Biomedical Engineering, University of Virginia, Charlottesville*

T1-weighted 3D MP-RAGE sequences with inversion-recovery magnetization preparation yield high-resolution 3D data sets with imaging times of 5 min or less and represent a potentially valuable method of screening the brain for focal lesions. Initial clinical experience has shown,

however, that for some lesions MP-RAGE images demonstrate poor Gd-DTPA contrast enhancement compared with standard 2D short TR/TE spin-echo (SE) images. Superficial comparison of the sequences does not yield an explanation for this discrepancy. Therefore, theoretical models have been used to analyze the relative enhancement characteristics of the SE and 3D MP-RAGE sequences. Signal difference-to-noise (SD/N) and contrast-to-noise (C/N) ratios were calculated for three lesion T1/T2 combinations with respect to two normal tissues (gray and white matter). Lesion proton densities equal to those of the respective normal tissue and cerebrospinal fluid were considered. Gd-DTPA concentration ([Gd]) was varied from 0 to 10 mmol/L, assuming that the enhanced lesion relaxation rates varied linearly with the concentration. SD/N values for SE rose rapidly with increasing [Gd], peaked at a [Gd] of 1–1.5 mmol/L, and then decreased more slowly, whereas SD/N values for 3D MP-RAGE increased more slowly to a relatively constant level at high [Gd]. The SD/N values for SE exceeded those for 3D MP-RAGE for [Gd] up to 2–5 mmol/L. The range of [Gd] over which SE exceeded 3D MP-RAGE and the relative increase of SE both increased with increasing (unenhanced) lesion T1 and proton density. C/N values were calculated by normalizing the SD/N values by the average signal level of the normal tissue and lesion. Except for [Gd] below 0.5 mmol/L, the C/N values for 3D MP-RAGE exceeded those for SE. The theoretical results were used to redesign the 3D MP-RAGE sequence to provide improved enhancement characteristics at low [Gd]. Experimental evaluations of this modified sequence are currently being performed.

147 • 5:09 PM

### Contrast-enhanced High-Resolution Phase-Contrast Vascular MR Imaging: Initial Clinical Experience

MA Bernstein, PA Turski, RK Tu, D Crosby, D Weber
*Department of Radiology, University of Wisconsin, Milwaukee, and GE Medical Systems.*

High-resolution 2D phase-contrast MR angiograms of the intracranial vasculature were obtained without and with intravenous contrast enhancement (Gd[HP-DO3A], Bristol Meyers Squibb, Institute for Medical Research; and gadopentetate dimeglumine, Berlex Imaging) with a 256 × 256 (FOV = 18) or 512 × 256 (FOV = 22) matrix (TE = 8.7 msec, TR = 30 msec, flip angle = 30°, section thickness = 10–60 mm, VENC = 40–80 cm/sec). Receive and transmit attenuation values were maintained within a 10% range for the pre- and postcontrast images. In selected patients, phase images were generated to determine the direction of blood flow. To increase intravascular signal intensity (by decreasing saturation of in-plane flow), intravenous contrast material was administered. Eleven patients with occlusive vascular disease (arterial and venous), AVMs, and aneurysms were studied. After administration of intravenous contrast material, there was an increase of approximately 60% in intravascular signal intensity in small arteries and venous structures on the MR angiograms obtained with a velocity encoding of 80 cm/sec. The 512 × 256 postcontrast images provided the best delineation of small vessels. Because of the virtually total elimination of background signal on the phase-contrast images, there was no degradation of the vascular anatomy by enhanced soft tissues. In conclusion, flow aliasing can be avoided and directional flow information (phase images) preserved on phase-contrast MR angiograms with use of a relatively high velocity encoding. High-VENC phase-contrast MR angiograms can be made more sensitive to slow flow by using intravenous contrast material.

## Tuesday Afternoon
## Sutton Parlor North
## Papers 148–155

## MUSCLES/JOINTS

MODERATORS: R Kier, MD • JB Kneeland, MD

148 • 3:45 PM

### MR Imaging in Muscle Diseases: Experience after 374 Examinations

WA Kaiser, BCG Schalke*, MF Reiser
*Radiologische Universitätsklinik, Bonn, and *Neurologische Universitätsklinik, Würzburg, Germany*

Since March 1984, 374 patients with various muscle diseases including progressive muscular dystrophies ($n$ = 80), myotonic dystrophy ($n$ = 20), neural muscular atrophy ($n$ = 20), myosities ($n$ = 46), sarcoidosis ($n$ = 9), metabolic or histologic defects ($n$ = 44), spinal muscular atrophy ($n$ = 13), tumors ($n$ = 18), trauma ($n$ = 18), and stenosis or occlusion of vessels ($n$ = 32) have been examined with superconductive magnets with field strengths varying between 0.35 and 1.5 T (Siemens Magnetom, Philips Gyroscan). According to morphologic criteria (symmetric, asymmetric, homogeneous, focal pathologic changes) different MR imaging patterns of muscle changes in the upper limb could be described, and which patterns yield at least a diagnostic estimation of the disease and in some cases even a characteristic "fingerprint." Pattern I may demonstrate acute myositis, neural muscular atrophy, alcoholic myopathy, diabetic myopathy, cortisone myopathy, ischemia/vessel stenosis or occlusion, mitochondrial myopathy, or uremic myopathy; pattern II, chronic Duchenne muscular dystrophy, chronic myositis, or status after bilateral poliomyelitis; pattern III, limb girdle dystrophy, chronic myositis, centronuclear myopathy, or familiar hypokalemic paralysis; and pattern IV, status after unilateral poliomyelitis, trauma, tumor, or hematoma. Furthermore, MR imaging is extremely useful in the planning of a biopsy, which must be performed in a moderately affected muscle. The efficacy and duration of therapy can also be determined with MR imaging. In summary, MR imaging is of great value in the development of a diagnostic strategy (eg, diagnosis and differential diagnosis) for muscle diseases, the planning of muscle biopsy and operation, and the control and monitoring of therapy.

149 • 3:57 PM

### MR Imaging of Anomalies of the Pediatric Foot

AM Hubbard, RS Davidson, JS Meyer, S Mahboubi
*The Children's Hospital of Philadelphia*

MR Imaging of the foot was performed in 20 children between the ages of 2 months and 6 years. Fifteen patients evaluated had clubfoot deformities; the majority of these had undergone previous surgery and had a residual deformity of the foot. Five patients were evaluated for possible skew foot deformity. All patients were imaged with a standard T1-weighted spin-echo sequence and most underwent a 3D FISP volume acquisition. In children with previous clubfoot deformity repairs, MR imaging was especially helpful in delineating the navicular bone, which was often delayed in ossification. In children with residual clubfoot deformity, the majority were found to have not only an abnormal position but also abnormal shape of the navicular bone, which probably contributed to the persistent deformity of the foot. In cases of suspected skew foot, MR imaging was able to show relationships among the hind-, mid- and forefoot structures. MR imaging was helpful in planning further corrective surgery of the foot. Furthermore, it was able to provide valuable anatomic information regarding the bones of the midfoot, particularly those that had

not yet ossified, owing to the patient's age or underlying abnormality.

150 • 4:09 PM

### MR Imaging of Leg Edema

G Nilsen, PA Rinck, R Haaverstad, HO Myhre, OD Sæther
*MR-Center, Medical Section, and Department of Surgery, University of Trondheim, Norway*

MR imaging was used in the diagnosis of various conditions giving rise to leg edema, with special attention given to leg edema following femorodistal vascular reconstruction for obliterating atherosclerosis ($n = 14$), deep venous thrombosis ($n = 6$), chronic lymphedema ($n = 6$), and closed muscular compartment syndrome ($n = 2$). Leg volume increase was measured according to the formula for a truncated cone. Interstitial fluid hydrostatic pressure ($P_{if}$) was recorded with the wick-in-needle technique. T1- and T2-weighted spin-echo series with 10-mm transverse sections were obtained with MR imaging. Following vascular reconstructions, leg volume increased 26% on the operated side. In the operated leg, no gradient in $P_{if}$ was found between the posterior muscular compartment and the subcutaneous tissue. There was, however, a statistically significant higher $P_{if}$ in the subcutaneous tissue compared with that in the anterior muscular compartments ($P < .05$). In the operated group, MR imaging revealed edema around the entire circumference of the leg, restricted to the subcutaneous tissue. In contrast, edema of the leg muscles, particularly in the posterior compartments, was typical in patients with deep venous thrombosis. The chronic lymphedema group showed circumferential subcutaneous edema alone or in combination with a fibrotic honeycomb pattern. Edema of the affected muscular compartment was easily observed in patients having closed compartment syndrome. In conclusion, the use of MR imaging is promising in the investigation of conditions giving rise to leg edema. It is likely that the formation of postreconstructive edema takes place in the subcutaneous tissue. Although the location and appearance of the edema fluid is similar to that observed in lymphedema, the findings do not discriminate among the various mechanisms responsible for leg edema following vascular reconstruction.

151 • 4:21 PM

### Osteomyelitis Diagnosis/Staging: Comparison of MR Imaging, CT, and In-111 White Blood Cell and Tc-99 Scanning

PT Weatherall*, GE Maale†, CS Sherry†
**Department of Radiology, University of Texas Southwestern Medical Center, and Departments of †Orthopedics and ‡Radiology, Presbyterian Hospital, Dallas*

Preoperative diagnostic imaging examinations of 100 patients with subsequently proved chronic osteomyelitis were retrospectively analyzed to determine the value of each imaging technique in comparison with plain radiographic examinations. All 100 patients underwent radiographic examinations prior to surgery. Sixty-seven of the patients were known to be infected preoperatively. Other examinations included Tc-99 bone scan ($n = 94$), In-111 white blood cell scan ($n = 85$), CT ($n = 90$), and MR imaging ($n = 58$). Eighty-three patients had stage 3 chronic osteomyelitis (Cierny classification) or greater. A score relative to the radiographic examination was given ($-1$ = misleading, 0 = no benefit, +1 = additional information gained, +2 = obvious value, +3 = critical information). A +3 score was reserved for detection of unsuspected additional foci of involvement or extension, which would not have been discovered at surgery or when one examination was correctly positive and other examinations were falsely negative. The most valuable examination was also determined. A deficiency in the study (besides possible bias) was the lack of evaluation of false-positive results. MR imaging was most valuable for diagnosis in 79% and for therapy in 77% of cases. In the same categories, the other studies were rated as follows: Tc-99, 20%/14%; In-111, 24%/15%; and CT, 17%/32%, with totals greater than 100% resulting because not all studies were performed in each patient. Twenty-nine percent of the MR imaging studies were given a +3 rating for surgical planning value, whereas the other adjunctive imaging studies did not frequently provide additional critical information (CT, 7%; In-111, 2%; and Tc-99, 2%). Orthopedic hardware (33 patients) caused difficulty in interpretation for all four methods, but affected Tc-99 and In-111 studies less. Seven of 27 CT and three of 13 MR imaging examinations were inadequate because of artifact. MR imaging was the most valuable adjunctive preoperative study for successful surgical eradication of chronic osteomyelitis, primarily because of its ability to demonstrate the full extent of bone and soft-tissue compartment involvement.

152 • 4:33 PM

### MR Imaging in Human Lymphedema: Comparison with Lymphangioscintigraphy

EC Unger, TC Case*, CL Witte*, MH Witte*, W Williams
*Department of Radiology/MRI and *Department of Surgery, University of Arizona, Tucson*

MR imaging was performed in 32 patients (24 female and eight male; mean age, 41 years) with peripheral lymphedema (19 primary and 13 secondary) and the findings compared with those of isotope lymphography (lymphangioscintigraphy) (LAS). MR imaging characteristically showed diffuse dermal and subcutaneous edema, a nonedematous, occasionally hypertrophied skeletal muscle compartment, variability in regional lymph node size and appearance depending on the underlying clinical disorder, serpiginous "channels" or "lakes" consistent with dermal collateral lymphangiectasis and sequestered lymph, and increased subcutaneous fat. In contrast, LAS showed dermal diffusion ("backflow"), crossover with retrograde tracer backflow (reflux), delayed tracer transport, and, depending on the cause of lymphedema (ie, primary or secondary), discrete or poorly defined lymph trunks (tracer "bands") and delayed or nonvisualized regional lymph nodes. MR imaging in conjunction with LAS provides accurate baseline anatomy and staging of lymphatic disorders from which further objective data can be adduced after therapy for lymphedema. In contradistinction to LAS, MR has the capacity to visualize lymph trunks, nodes, and soft tissues proximal to sites of lymphatic obstruction. Whereas paramagnetic or superparamagnetic agents (eg, iron oxide) may further intensify lymphatic truncal-nodal MR images, use of LAS and MR imaging has all but rendered conventional oil-contrast lymphography obsolete in the diagnosis and follow-up of lymphologic disorders.

153 • 4:45 PM

### MR Evaluation of Ulnar Collateral Ligament Injury in Baseball Pitchers

SA Mirowitz, S London
*Jewish Hospital, Washington University School of Medicine, St Louis*

The ulnar collateral ligament (UCL) is an important structure that acts to stabilize the medial aspect of the elbow. Trauma to this ligament may occur as a result of repetitive throwing injuries, particularly in baseball pitchers. Diagnosis of UCL injury has been based on clinical findings of valgus instability and medial joint pain. There have been no previous imaging studies that have allowed direct evaluation of this structure. Eleven baseball pitchers (seven

professional, four amateur) with clinical evidence of UCL injury were evaluated with MR imaging. Surgical correlation was available in four patients, in whom UCL reconstruction was performed. MR findings in the presence of UCL injury included laxity, irregularity, poor definition, and increased signal intensity on T2-weighted images within and adjacent to the UCL. Optimization of technical factors such as use of appropriate surface coil, section thickness, and imaging planes is critical for evaluation of the UCL due to its small size. The results indicate that MR imaging is useful in documenting the presence and severity of injury to the UCL and in distinguishing this entity from other causes of elbow pain.

154 • 4:57 PM

### Can MR Imaging Replace Radiography in Diagnosing Sacroiliac Joint Disease?

KF Neufang, A Hoffmann, P Huttmann, SJ Albig, A Barth, K Lackner

*Institute of Diagnostic Radiology and Medical Clinic II, University of Cologne Medical School, Cologne, Germany*

The purpose of this study was to determine if MR imaging of the sacroiliac joints (SIJ) (*a*) exhibits specific findings of spondylarthritis (SPA), (*b*) is equivalent or superior to radiography in confirming or excluding the clinical diagnosis of SPA, (*c*) can differentiate between SPA and noninflammatory SIJ disease, and (*d*) can replace x-ray tomography in younger patients. A prospective study was made in 31 patients (16 women and 15 men, aged 21–61 years). Clinical diagnoses based on the proposals of the European Spondylarthropathy Study Group (ESSG) served as the standard of reference. Eighteen patients had SPA (eight ankylosing, seven reactive, one psoriatic, two undifferentiated) and 13 had noninflammatory SIJ disease (eight degenerative, three fibromyalgia, one undifferentiated connective tissue disease). X-ray examinations were performed with film tomography (Barsony's view); MR imaging was performed with a 1.5-T Philips Gyroscan (T1WI: SE = 500/25; T2WI: SE = 2,000/20, 80; T2*WI: FFE = 28/20/14°: axial multi-section sequences, no contrast media). Radiographs and MR images were analyzed in blinded fashion. SPA appeared on MR images as paraarticular bone marrow edema and widening of or increased signal intensity (T2WI) within the SIJ space (stage I); bone erosions and paraarticular fatty bone marrow infiltration (stage II); or ankylosis (stage III). MR imaging stage I findings were present in 7 of 15 radiologically normal SIJs in patients with a clinical diagnosis of SPA. All SIJs of patients with noninflammatory SIJ disease were free of bone marrow edema, SIJ effusion, or ankylosis. Five of 10 SIJs in patients with noninflammatory SIJ disease (subarticular bone sclerosis) appeared normal at MR imaging. Focal fatty bone marrow infiltration and thickening of the subarticular bone were seen in 6 of 16 SIJs of patients with noninflammatory SIJ disease. SPA was demonstrated (excluded) radiographically in 8 of 18 (12 of 13) cases, and with MR imaging in 14 of 18 (13 of 13) cases, suspected clinically to have (not to have) SPA. In conclusion, (*a*) MR imaging can identity and stage SPA and (*b*) it tends to be superior to x-ray tomography, demonstrating paraarticular bone marrow edema in moderate or early stages of SPA, when radiographs are still negative; (*c*) degenerative SIJ disease is better demonstrated with radiography than with MR imaging; and (*d*) in younger patients, suspected of having SIJ disease Barsony's view should be followed by MR imaging, which is expected to replace x-ray tomography, at least in this age group.

155 • 5:09 PM

### MR Imaging of the Temporomandibular Joint: Correlation with Pathologic Findings

H Mizuno*, H Mizuno*, T Watabe*, A Heshiki*, S Takaku†, T Sano†, M Yoshida†

*Departments of *Radiology and †Oral Surgery, Saitama Medical School, Saitama, Japan*

The fast imaging with steady precession sequence (FISP) was performed in 90 subjects, including 15 asymptomatic volunteers, to evaluate the temporomandibular joint (TMJ). Ten patients underwent menisectomy, and MR findings were correlated with pathologic findings. All subjects were studied with a superconducting MR unit at 1.5 T. A 2-mm sagittal plane was obtained with a 2D or 3D FISP acquisition technique (TR/TE = 30/12 msec, flip angle = 40°). Cine MR imaging with 2D FISP was also performed in some volunteers and patients to analyze the functional anatomy. Three-dimensional FISP images of the TMJ made it possible to evaluate disk components and intensities, fluid collection in the joint cavity, condylar shape, and adjacent vessels. Seventy-five patients showed not only abnormal meniscal displacement and deformity and condylar deformity but also degenerative disks with edema, adhesion, or perforation associated with osteoarthritis, fracture, and avascular necrosis. In the patients who underwent menisectomy, MR imaging well demonstrated degenerative disks and abundant fluid collection in the joint cavities. These MR findings correlated well with macroscopic and microscopic findings. In conclusion, 2D or 3D FISP images showed normal and pathologic anatomy of the TMJ in good detail. Severe disk degenerative changes were especially well demonstrated as bright or dark areas on FISP images and correlated well with pathologic findings.

## Tuesday Afternoon
## Sutton Parlor Center
## Papers 156–163

## CARDIAC IMAGING

MODERATORS: L Eastwood, PhD • CB Higgins, MD

156 • 3:45 PM

### High-Resolution MR Angiography of Human Coronary Arteries with Fat Suppression and a Breath-Hold Segmented TurboFLASH Sequence

RR Edelman, WJ Manning

*Departments of Radiology and Cardiology, Beth Israel Hospital, Boston*

The feasibility of MR angiography of human coronary arteries has been demonstrated recently with use of a segmented TurboFLASH pulse sequence (1). Since the epicardial coronary arteries are embedded in fat, it was hypothesized that flow contrast could be improved with use of fat suppression. Healthy subjects were imaged with a 1.5-T Siemens Magnetom system. They were positioned prone over a planar surface coil with interposition of an egg-crate mattress for greater comfort. Breath-hold electrocardiograph-gated images were obtained with a segmented TurboFLASH sequence (16 segments, eight phase-encoding steps per segment, incremental flip angle, 20 × 15-cm field of view, 3-mm section thickness). Fat suppression was accomplished by applying a 16-msec-duration Gaussian pulse before each segment (flip angle = 140°). Sequential axial images were obtained from the aortic root to the base of the heart, in addition to ob-

lique images oriented along the coronary arteries. Projection angiograms were created by using a maximum-intensity projection algorithm after limited editing of the images. Fat suppression resulted in an approximately threefold improvement in flow contrast/noise. Small distal or branch vessels measuring ≤2 mm in diameter, such as diagonal branches of the left anterior descending coronary artery and obtuse marginal branches of the left circumflex artery, were visible. The improvement in flow contrast simplified the creation of projection angiograms. It is concluded that the combination of fat suppression with segmented TurboFLASH permits high-resolution imaging of human coronary arteries, including distal or branch vessels.

1. Edelman RR, Manning WJ, Burstein D, Paulin S. Breath-hold MR angiography of human coronary arteries. Radiology 1991; 181:641–643.

157 • 3:57 PM

## Fast Spiral Coronary Artery Imaging

CH Meyer, BS Hu*, DG Nishimura, A Macovski
*Magnetic Resonance Systems Research Laboratory, Stanford University, and *Division of Cardiovascular Medicine, Stanford University Hospital, Stanford, Calif*

A flow-independent method for reliably imaging coronary arteries within a breath hold with interleaved spiral k-space imaging has been developed. Cardiac motion is frozen by gating, readout occurring when the heart is relatively quiescent, with a relatively short readout window (17.5 msec). Respiratory motion is frozen by obtaining the image during a single breath hold (20 heartbeats or less). Because the coronary arteries lie along the surface of the heart, it is possible to avoid the interference of blood in the chambers by carefully positioning the axial and graphically prescribed oblique sections so that the chamber blood does not obscure the vessels of interest. Fat is suppressed with use of a spectral-spatial excitation pulse; because most of the coronary tree lies in a bed of fat, this provides excellent definition of the vessel wall. For relatively thin sections (under 1.5 cm), muscle suppression is usually not necessary; for thicker sections, muscle can be suppressed by using pulsed magnetization transfer contrast, late echoes, or limited inflow enhancement. Resolution is 1.1 × 1.1 mm, which is sufficient to image the main coronary arteries, the primary branches, and some of the secondary branches. To date, six healthy volunteers and two patients with known coronary artery disease have been successfully imaged. Images of the left anterior descending, circumflex, first and second diagonal, posterior descending, and right coronary arteries have been obtained. The patient studies show good correlation with prior x-ray angiograms; more experience will determine if lesions can be reliably visualized with this technique.

158 • 4:09 PM

## Three-dimensional Cardiac Function Analysis with Tagged MR Imaging

H Azhari, JL Weiss, WJ Rogers, EP Shapiro
*Division of Cardiology, Johns Hopkins University, Baltimore*

Accurate noninvasive assessment of left ventricular function is essential for both early detection of diseases and for evaluation of applied therapeutic procedures. The recent advent of MR imaging tagging enables one to mark noninvasively the myocardium and to study its deformations throughout the cardiac cycle. This technique has been combined with 3D computer reconstructions of the left ventricle to study cardiac function in canine heart models with acute ischemia. Five anesthetized, closed-chest dogs with a ligated left anterior descending (LAD) coronary artery were studied with a Resonex 0.38-T iron core resistive imager. The dogs were atrially paced and imaged with the spin-echo technique (TE = 30 msec, TR = twice the cardiac cycle). Four electrocardiogram-gated short-axis images with "star-shaped" tags and four matching tagged long-axis images were acquired at end diastole and end systole and combined to yield 3D reconstructions of 24 myocardial cuboids at each state. A comparison of function was made between the center of the ischemic zone and the remote normal zone by using percent wall thickening (%T) and circumferential ($E_x$) and longitudinal ($E_y$) endocardial strains (shortening) as a measure for myocardial function and maps of perfusion obtained with postmortem analysis. The results show a clear discrimination between the two zones for the three parameters studied ($P < .01$) (Table). Nevertheless, an evaluation of the quality of discrimination with the $t$ statistic demonstrates that %T is the superior discriminatory index. In conclusion, 3D tagged MR imaging function analysis can serve as a reliable, noninvasive method for locating ischemic regions in the heart, particularly when wall thickening is used.

| | Ischemic | Remote Normal | $t$ |
|---|---|---|---|
| %T | −5.7 ± 6.4 | 19.3 ± 6.9 | 21.7 |
| $E_x$ | −0.03 ± 0.05 | 0.13 ± 0.06 | 9.0 |
| $E_y$ | −0.04 ± 0.06 | 0.09 ± 0.06 | 7.4 |

159 • 4:21 PM

## Assessment of Midwall Left Ventricular Contractility in Hypertrophic Cardiomyopathy with MR Tagging

RD White, JA Tkach, N Obuchowski, HM Lever, NB Ratliff
*Departments of Diagnostic Radiology, Cardiology, and Pathology, Cleveland Clinic Foundation, Cleveland*

The pathophysiology of hypertrophic cardiomyopathy (HC) is poorly understood, with myocardial contractility in the left ventricle (LV) variably perceived as being hyper- or hypodynamic. This is due at least in part to the inability to noninvasively detect, localize, and quantitate the characteristic histologic changes (ie, myofiber disarray and fibrosis) in vivo in humans and relate them to systolic function. In this study, an 11-phase myocardial grid-tagging technique for dynamic short-axis LV imaging was used on a conventional MR imaging system (1.5-T Siemens Magnetom SP) to assess myocardial systolic mechanics in the septal (S) and lateral (L) midwalls of the LV, both in cases of HC prior to S myectomy ($n = 4$) and in a normal (N) group ($n = 4$). For this purpose, manual measurements of decreasing equatorial distance (D) between tagging intersection points in the LV midwalls between end diastole (ED) and end systole (ES) were used in modified equations to determine mean velocity (V) of circumferential fiber (cf) shortening $\{[(EDD - ESD) \div (\pi \times midS - midL\ diameter)] \div [ET \div \sqrt{R\text{-}R}]\}$ and max Vcf shortening $\{[max\ decrease\ D\ per\ 2\ intervals \div (\pi \times midS - midL\ diameter)] \div [duration\ 2\ intervals \div \sqrt{R\text{-}R}]\}$, each corrected (c) for both cardiac cycle length and ED dimension. Time to greatest decrease in D was used for ejection time (ET) of the LV. These parameters are ejection-phase contractile indices (circ/sec), independent of preload and heart rate but dependent on afterload and indicative of basal inotropic state. For both parameters, combined S and L values in the HC group (mean Vcfc, 0.78–5.34; max Vcfc, 1.30–8.21) were significantly less ($P < .05$) than those in the N group (4.64–10.73 and 6.75–13.98, respectively). Considering contractility of

specific LV midwalls, assessment based on mean Vcfc provided clear discrimination between the S-wall function of HC cases (range = 0.78–2.25, mean = 1.34) and N individuals (range = 4.64–7.48, mean = 5.77), but did not reveal clear-cut differential function for the L wall (HC: range = 2.16–5.34, mean = 3.13; N: range = 4.89–10.73, mean = 6.74). Similar but less pronounced distinction between systolic function for the S wall (HC: range = 1.30–4.42, mean = 2.66; N: range = 6.75–10.40, mean = 8.71) and the L wall (HC: range = 3.41–8.21, mean = 5.31; N: range = 7.23–13.98, mean = 9.75) was made based on max Vcfc. Further, the same two HC patients had the most depressed mean and max Vcfc values for the S midwall, as well as two of the three worst grades of myofibril disarray and the two worst grades of fibrosis at pathologic evaluation of the myectomy samples. The results of this preliminary work indicate that MR imaging myocardial tagging can be used to detect, localize, and quantitate the impairment in LV midwall contractility due to HC with proved abnormal histology, and that the tissue changes characteristic of HC may not be as uniformly distributed as they are often described.

160 • 4:33 PM

### Use of Breath-Hold Cine Acquisitions to Improve 3D Representations of the Heart

D Atkinson*, Yu-Ming Kuo†, M Brant-Zawadzki†, G Gillan†
*Siemens Medical Systems, Iselin, NJ, †Department of Radiology, Hoag Memorial Hospital, Newport Beach, Calif, and †Department of Radiology, Long Beach Memorial Hospital, Long Beach, Calif*

At present, 3D cine representations of heart wall motion are limited by long data acquisition times and associated respiratory motion. Blurred edges, ghosting artifacts, and misregistration of 2D sections compromise reconstruction of 3D models. Recently, a new technique has been developed to acquire a high-resolution 2D cine data set within one breath hold (1). With this technique, cineangiographic 3D models were reconstructed showing true dimensions along multiple axes. These breath-hold results were compared with those of standard non–breath-hold acquisitions. With a combination of an ultrafast FISP sequence and k-space segmentation, a 20-phase cine study can be computed within one breath hold. The FISP sequence used a TR/TE/$\alpha$ of 6/4/15° and an acquisition of eight lines per R wave, for a data acquisition window of 50 msec per phase. Successive sections 5 mm thick and with 1-mm overlap were acquired at end expiration. Multiphase acquisitions were correlated and reconstructed to produce a cineangiographic 3D model of the heart on a commercially available workstation (ISG Technologies, Toronto). Breath-hold acquisitions produce improved 3D models compared with standard acquisition methods. In addition, this method demonstrated a significant reduction in acquisition time and is amenable for use with presaturation pulses to mark intrachamber flow patterns.

1. Atkinson DJ, Edelman RR. Cineangiography of the heart in a single breath hold with a segmented Turbo-FLASH sequence. Radiology 1991; 181:357–360.

161 • 4:45 PM

### Optimization of Semi-Quantitative Evaluation of Left Ventricular Function with Algorithm Derived from Quantitative Short-Axis Determination

G Beyl, A von Smekal, KC Seelos, M Reiser, HJ Biersack
*Department of Nuclear Medicine and Radiology, University of Bonn, Germany*

Truly quantitative approaches to the calculation of left ventricular functional parameters still require timely data acquisition and processing. A mathematically optimized approach with a specifically selected, limited number of short-axis sections of the left ventricle could reduce examination and processing time without substantial changes in the evaluation of left ventricular function compared with truly quantitative short-axis left ventricular function values. Ten healthy volunteers and 10 patients with myocardial infarction and myocardial aneurysm were studied with a quantitative short-axis, multisection, multiphase fast-field-echo sequence on a 0.5-T Philips Gyroscan system. Left ventricular ejection fraction, mass, and wall thickening were calculated. From these data, a mathematical model was developed to calculate the same parameters from four multiphase short-axis sections. Values for ejection fraction and mass varied ±3% between the semiquantitative and quantitative approaches in healthy volunteers. In deformed left ventricular anatomy, however, the deviation between the two approaches was as much as 12% (mean, 7%). In cases of normally shaped or modestly deformed left ventricular dimensions, the semiquantitative approach proved to be efficient in determining left ventricular functional parameters. In grossly deformed left ventricular anatomy this semiquantitative method is limited by the use of a small, predetermined number (four) of sections. Major remodeling changes still require a truly quantitative approach for precise determination of left ventricular functional parameters.

162 • 4:57 PM

### Evaluation of Ventricular Septal Defects in Congenital Heart Disease with Septum-angulated Cine MR Imaging and Color Doppler Echocardiography

KC Seelos, A von Smekal, P Kaas, DA Redel, M Reiser
*Departments of Radiology and Pediatric Cardiology, University of Bonn, Germany*

A new approach to imaging ventricular septal defects (VSD) was evaluated with a single-section, multiphase gradient-echo sequence with its angulation following the course of the ventricular septum. Depending on the degree of curvature of the septum, blood flow through defects was visualized almost perpendicular to the plane with phase-related changes in signal. Sixteen patients with various types of ventricular septal defects (membranous VSDs, muscular VSDs, and atrioventricular (AV) canal type VSDs were studied. Five of these patients were also examined after surgical closure of the VSD. Ten patients without VSD were examined to assess the appearance of a normal ventricular septum with special consideration of pitfalls due to partial-volume averaging. The number, size, and shape of defects were determined and compared with findings from color Doppler echocardiography in all cases. Defects ranged from 0.6 to 4.5 cm in diameter. Flow-related signal changes during the cardiac cycle were analyzed by correlating MR findings with shunt hemodynamics (bidirectional and turbulent flow). Septum-angulated cine MR imaging was sensitive in the detection of muscular and AV canal type VSDs and provided superior functional and morphologic information. Limitations of this technique were evident in the depiction of small membranous VSDs. Although quantitative information is still lacking, septum angulation appears to be a means of successfully optimizing MR imaging in cases of congenital heart disease.

163 • 5:09 PM

### Characterization of the First Passage of Dy-DTPA-BMA with Echo-Planar MR Imaging: Detection of Myocardial Ischemia

MF Wendland, M Saeed, T Masui, CB Higgins
*Department of Radiology, University of California, San Francisco*

Administration of Dy-DTPA-BMA (Salutar, Nycomed, and Sterling-Winthrop) may provide a new method of assessing relative perfusion by monitoring the first pass of this agent in normal and ischemic hearts. Echo-planar MR imaging was combined with use of magnetic susceptibility–enhanced contrast media to determine dose dependence of signal loss and the potential to detect ischemic regions during the first pass of Dy-DTPA-BMA. Two groups of animals were designated: Group 1 ($n = 6$) consisted of normal rats and group 2 ($n = 6$) of rats that had been subjected to left coronary artery occlusion. Electrocardiogram-gated echo-planar images (TE = 9.9 msec, TR = 2.0 seconds, 64 × 64-mm matrix, acquisition time = 33 msec) were acquired in sets of 16 images. In normal rats, myocardial signal intensity decreased after the administration of Dy-DTPA-BMA in a dose-dependent fashion. Abrupt decrease in left ventricular (LV) blood signal upon introduction of Dy-DTPA-BMA was followed by an initial rapid recovery approximately 10 seconds in duration. Signal from myocardium exhibited a slow recovery phase extending over a 20-second period after introduction of the agent. The maximum signal reduction in myocardium was delayed by 2 seconds relative to that of LV blood. Similar findings were obtained in rats subjected to regional ischemia except that the signal intensity of the ischemic region did not change after injection of Dy-DTPA-BMA. This provided clear demarcation of the ischemic zone during the peak effect of the bolus. Plots of $\Delta R2^*$, calculated from the maximal signal decrease in myocardium, versus injected doses were well correlated, suggesting that $T2^*$ shortening caused by the contrast agent is monoexponential. In conclusion, echo-planar MR imaging can be used to monitor the dynamic differential influence of magnetic susceptibility contrast media on normal and ischemic myocardium.

## Tuesday Afternoon
## Sutton Parlor South
## Papers 164–172

## MRA AND PERFUSION TECHNIQUES

MODERATORS: WT Dixon • O Nalcioglu, PhD

164 • 3:45 PM

### MR Imaging Detection of Model Pulmonary Emboli in Dogs

JR MacFall*, JJ Wu*, HD Sostman*, LW Hedlund*, TKF Foo†
**Duke University Medical Center, Durham, NC, and †GE Medical Systems*

Ultrafast 2D or 3D gradient-echo (GRE) pulse sequences (TR = 7 to 14 msec, TE = 2.7 to 4 msec) can produce high-quality MR pulmonary angiograms and are candidate sequences for the detection of pulmonary embolism (PE). Conventional GRE sequences (TR ≈ 50 msec, TE ≈ 13 msec) have been successfully used to detect thrombus in systemic veins. The purpose of this study was to determine whether experimentally created PE can be detected with the ultrafast sequences. Clots were created from venous dog blood mixed with thrombin and epsilon amino caproic acid to match the T1 and T2 of thrombi observed in vivo. Barium-impregnated threads were included in the clot for x-ray confirmation of their location. The clots were injected into the jugular vein of anesthetized mongrel dogs and allowed to lodge in segmental pulmonary arteries. Imaging was performed with conventional radiography, digital subtraction angiography, and experimental 2D and 3D ultrafast ("white-blood") MR pulmonary angiography (1.5-T, Signa, GE Medical Systems). Preliminary results show that dark areas corresponding to the known location of the clots can be seen on the individual cross-sectional images from the MR angiographic studies. Visualization of the clots in the maximum-intensity pixel projections is hampered by motion artifacts, interfering vessels, and residual intensity of stagnant blood. Three-dimensional volume display helps to remove some of the ambiguities resulting from vessel overlap and minor motion artifacts.

165 • 5:21 PM

### Gd-DTPA Perfusion in Cardiac MR Imaging: First Results with a TurboFast Imaging Technique

KC Seelos, A von Smekal, J Gieseke, J van Vaals, M Reiser
*Department of Radiology, University of Bonn, Germany, and Philips Medical Systems*

The purpose of this study was (*a*) to investigate the potential of a TurboFast imaging technique for dynamic perfusion studies in patients with ischemic heart disease and intra- or paracardiac masses, and (*b*) to optimize a sequence in terms of time and spatial resolution. Fifteen patients with ischemic heart disease, six patients with intra- or paracardiac masses, and nine healthy volunteers were studied with a single-section TurboFast imaging sequence on a 0.5-T Philips Gyroscan T5 system. After bolus administration of Gd-DTPA, first-pass perfusion of the contrast agent was documented in perfused normal myocardium, ischemic myocardium, mass, and reference tissues with time-intensity curves. Perfusion profiles were obtained that were consistent with the underlying pathology confirmed with other studies and/or clinical findings, and with physiologic understanding of normal tissues. Statistical significance among the various pathologic entities was not established and single-section acquisition was considered a preliminary limitation for complex evaluation. The results demonstrate that TurboFast imaging can provide adequate time and spatial resolution in cardiac MR perfusion imaging. The technique appears to be promising for use in noninvasive screening of ischemic heart disease and might aid in the differential diagnosis of intra- or paracardiac masses.

166 • 4:09 PM

### Improved Time-of-Flight MR Angiography of the Brain with Magnetization Transfer Contrast

RR Edelman, SS Ahn, D Chien, A Goldman, W Li, M Mantello, J Kramer, J Kleefield
*Department of Radiology, Beth Israel Hospital, Boston*

It was hypothesized that the creation of magnetization transfer contrast (MTC) with off-resonance RF pulses could be used to improve flow contrast and enhance the depiction of small vessels on projection angiograms of the brain (1). Sagittal 2D (39/8/30°) and axial 3D flow-compensated gradient-echo images (38/6/20°) were obtained with a 1.5-T Siemens Magnetom system, with and without application of off-resonance RF pulses. In healthy volunteers, 2D and 3D sequences were tested over a range of voltages (0–70 V) for the off-resonance pulses. Flow contrast/noise was quantified. Two-dimensional sequences with and without MTC were also tested in a phantom con-

sisting of 6% agar and tubes of blood. Phantom studies demonstrated no substantial signal loss due to off-resonance pulses for blood and a 19% loss for agar. Flow contrast improved for 2D and 3D sequences as the voltage of the MTC pulse was increased. Projection angiograms acquired with off-resonance pulses showed a marked improvement in conspicuity of small arteries (55 of 80 arteries), with only a slight improvement in visualization of small veins. It is concluded that the application of off-resonance pulses markedly improves the quality of projection angiograms of the intracranial arteries, with a lesser improvement for intracranial veins.

1. Balaban RS, Chesnick S, Hedges K, Samaha F, Heineman FW. Magnetization transfer contrast in MR imaging of the heart. Radiology 1991; 180:671–675.

167 • 4:21 PM

### Variable-Tip-Angle Slab Selection for Improved Three-dimensional MR Angiography

G Laub, DE Purdy

*Siemens Medical Systems, Iselin, NJ*

Three-dimensional gradient-echo pulse sequences can provide excellent angiographic images of the vessels in relatively thin slabs of tissue. As blood traverses the slab, its signal is weakened by saturation, setting a practical limit on slab thickness. A small RF pulse tip angle helps to prevent this saturation, but reduces MR signal and contrast. Ideally, a more balanced signal distribution could be obtained by using small tip angles for the unsaturated blood entering the slab, and increasingly larger tip angles for the partially saturated blood as it courses through the slab. If the flow is roughly perpendicular to the selected slab, this change in tip angle can be achieved by constructing an RF pulse that only weakly excites the spins on one side of the slab (where the blood enters), but increases the tip angle toward the other side of the slab. For example, a transverse cranial slab might have a 15° tip angle in the region of the circle of Willis, but an increasing tip angle superior to this position. The appropriate excitation profile (Fig 1) may be obtained with a specially shaped RF pulse or with a Gaussian pulse truncated by a saturation band (Fig 2). Experiments with the pulse illustrated in Figure 2 show increased conspicuity of the branches of the posterior cerebral and middle cerebral arteries.

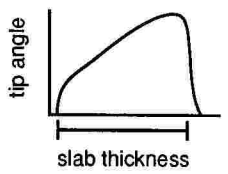


1.

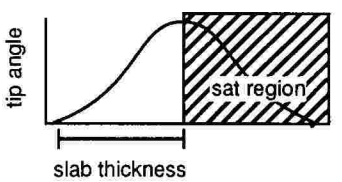


2.

168 • 4:33 PM

### Temperature MR Imaging: Comparison of T1 and Diffusion-based Approaches

D Le Bihan*, J Mattiello†, RL Levin†

**Diagnostic Radiology Department, †National Research Council, and ‡Biomedical Engineering and Instructional Program, National Institutes of Health, Bethesda, Md*

MR imaging has been proposed as a noninvasive technique for mapping temperature, based on either T1 or diffusion measurements. The purpose of this study was to evaluate and compare both approaches. Experiments were conducted on a 4.7-T system equipped with high-performance shielded gradient coils with gel phantoms. Heating was induced within the magnet bore. Temperature in the phantom was monitored with optic fiber probes. Measurements were made between 23°C and 37°C. Diffusion coefficients were determined in selected regions of interest on images obtained with use of 6 different *b* values. T1 measurements were made in the whole sample with an inversion-recovery sequence and 11 different inversion time intervals. The accuracy of the diffusion coefficient at each temperature was 1%, and the activation energy was 0.180 ± 0.001 eV. The accuracy of T1 was 1.5%, and the activation energy was 0.082 ± 0.003 eV. These activation energy values were then used to predict temperatures in the same phantoms. The predicted temperatures were found to be within 0.2°C and 0.5°C, respectively, of the probe measurements made based on diffusion and T1. The intrinsic sensitivity to temperature was found to be more than two times larger for diffusion than for T1 (2.4%/°C vs 1.0%/°C, respectively). Furthermore, T1 measurements were less accurate because of sensitivity to $B_1$ inhomogeneities and variations in coil tuning/loading at high temperatures. Diffusion-based temperature measurements thus appear more accurate and reliable, despite potential sensitivity to eddy currents and motion artifacts.

169 • 4:45 PM

### Fundamental Problems in Assessing Diffusion and Perfusion MR Images

D Le Bihan, P Douek, M Argyropoulou, R Goldberg, R Turner, N Patronas, M Fulham, G Di Chiro

*Diagnostic Radiology Department, BEIP, NHLBI, and NINDS, National Institutes of Health, Bethesda, Md*

The purpose of this study was to address some problems that arise in the assessment of clinical diffusion and perfusion MR images and to propose solutions. The study was performed in a series of patients with brain tumors. Diffusion and perfusion studies were performed on a 1.5-T whole-body MR imager equipped for echo-planar imaging. Perfusion data were obtained with both the IVIM imaging approach and Gd-DTPA dynamic imaging. All images were processed on a Sun workstation with home-designed dedicated image processing software. Both calculated images and regions of interest were used. Data were compared with those obtained from conventional MR and 2-fluorodeoxy-glucose positron emission tomographic images and from surgical biopsy when available. To be considered valid, diffusion/perfusion images must pass several tests: (*a*) Patient immobility relative to images of a given data set must be checked, and can be assessed by displaying the images in cine-loop mode; (*b*) degree of cerebrospinal fluid contamination of IVIM data might be determined in regions of interest by assessing the value of the pseudo-diffusion diffusion coefficient and the flowing fraction with the IVIM model; and (*c*) integrity of the blood-brain barrier may be recognized from the late segment of the Gd-DTPA dynamic time course study. Only after all these requirements are satisfied will useful information regarding tissue characterization and function—information that is not present on more conventional images—be found on both diffusion and perfusion images.

170 • 4:57 PM

### Measurement of Microvascular Flow in Rabbit Kidney with Perfluoroctyl Bromide (PFOB)

B Özdemirel*, AG Wile†, A Berkmen, O Nalcioglu*

*Department of Radiological Sciences, *Division of Physics and Engineering, and †Department of Surgery, University of California, Irvine*

A composite pulse sequence for measuring microvascular flow by using perfluoroctyl bromide (PFOB) as an intravascular contrast agent has been developed with a 1.5-T GE Signa system. The pulse sequence incorporates the spin-echo Fourier imaging method with chemical shift artifact correction, electrocardiograph gating, motion arti-

fact suppression, and interleaved flow and diffusion-sensitive acquisition techniques. The use of PFOB as a contrast agent serves three purposes. First, the measurement of capillary volume becomes possible. Second, the sensitivity of the measurements to diffusion in surrounding stationary tissue is eliminated. Finally, some useful information about the capillary geometry can be obtained. In addition, the use of PFOB also facilitates the effective suppression of bulk motion artifacts caused by flow-sensitizing gradients in in vivo studies. Interleaved acquisition of the images with the necessary chemical shift correction methods is compulsory because of the dynamic nature of the biologic tissues. The first image of an interleaved set is acquired with only the imaging gradients. This image gives the microvascular volume and provides the reference intensity level for all calculations. Two different gradient waveforms are introduced in the other interleaved data acquisitions (Figure). The two sets of bipolar pulses (waveform *a*) are velocity compensated and induce an attenuation in image intensity due to molecular diffusion and third- or higher-order flow effects. Images acquired with waveform *b* are sensitive primarily to constant velocity flow. The velocity-compensated images provide the necessary information about the diffusion and temporal random behavior of the microvascular flow. The nonlinear effect due to restricted diffusion inside the droplets of PFOB emulsion is taken into account in these calculations. Before the data are analyzed, the results of the calculations are used to correct for the effects of these processes on the constant velocity flow sensitive images. The experiments were performed on the ex situ kidneys of New Zealand rabbits. A perfusant containing 30% PFOB by volume was circulated through the kidneys with a roller pump. The interleaved imaging experiment was repeated at three different flow rates. Experimental results confirmed the pulse sequence.

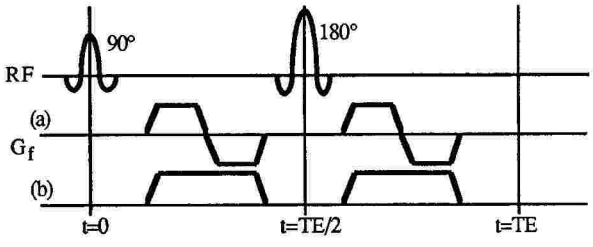


171 • 5:09 PM

### Renal Parenchymal Transit Time Index Measured with Echo-Planar MR Imaging and Contrast Agent

JA Cannillo, J Rogowska, GL Wolf
*Center for Imaging and Pharmaceutical Research, Massachusetts General Hospital, Charlestown, Mass*

Indicator-dilution techniques have been used to determine mean transit times of dye through kidney. With MR imaging and contrast agents that reflect physiology, it is now possible to collect localized time-activity curves. This study examined the transit times and signal intensity relationships that exist when both fast imaging techniques and MR contrast agents (MRCAs) are used, and in altered physiologic states. Radiolabeled microspheres are used as a standard to quantify normal tissue blood flow. Three groups of animals—(*a*) normal, (*b*) overhydrated via isotonic saline loading, and (*c*) dehydrated via hemorrhage—had MRCA administered by left ventricular bolus and systemically distributed in amounts proportional to tissue blood flow. Contrast agent pharmacokinetics were followed through changes in intensity within regions of interest. The regions were imaged serially for 3 min postinjection. Sixty 3-second images of the same location were collected by using an inversion-recovery pulse sequence in echo-planar mode (TR = 3,000 msec, TE = 26 msec, TI = 100 msec). Time-intensity data showed a characteristic curve when regions of interest were taken from the kidney cortex and medulla. These curves were interpreted to show renal hemodynamic phases during the in vivo course of the MRCAs that are consistent with corresponding microsphere tissue perfusion data and expected physiology. The typical cortical curve showed common prominent peaks that occurred temporally relative to hydration states: A "vascular" phase, representing the arrival of the MRCA, occurred between 0 and 6 sec; a second, "tubule" phase, initiated when the MRCA reached the loop of Henle, occurred 15–23 sec postcontrast; and a third, "ductal" peak occured at 60–90 sec. Depending on relative hydration states, the transit times of the contrast agent change and the occurrences of these phases are shifted in time. Thus, a time index can be derived when these peaks occur and inferences can be made about relative physiologic conditions.

172

**PAPER WITHDRAWN**

## Tuesday Afternoon
## Regent Parlor
## Papers 173–180

## CONTRAST AGENTS: Chest, Breast, and Bone

MODERATORS: VM Runge, MD • D Thickman, MD

173 • 3:45 PM

### Detection of Thoracic Abnormalities with Nonionic MR Contrast Media

N Kanth, M-C Dulce, M O'Sullivan, G Gamsu, CB Higgins
*Department of Radiology, University of California, San Francisco*

Gadodiamide (Gd-DTPA-BMA) is a new nonionic contrast medium that has been shown in animal studies to have a greater safety index than does Gd-DPTA. In humans with thoracic abnormalities, use of this contrast medium has not been previously reported. The purposes of this study were (*a*) to test the effect of gadodiamide injection (Omniscan; Sanofi Winthrop) on contrast between normal tissue (muscle, fat, lung) and lesion in patients with thoracic abnormalities, and (*b*) to assess the contrast-to-noise (C/N) and signal-to-noise (S/N) ratios between normal tissue and lesion with different MR sequences. Fifteen patients with thoracic abnormalities were evaluated in transaxial planes with a 1.5-T imager. Precontrast T1-weighted, proton-weighted, and T2-weighted images were obtained. At 5, 30, and 45 min after intravenous injection (p.i.) of 0.2 mmol/kg Gd-DTPA-BMA, T1-weighted imaging was repeated, and at 10 min p.i., T1-weighted imaging with fat saturation (SAT) was repeated. Signal intensities [SI] of the lesion, muscle, fat, lung tissue, and noise were measured. Gd-DTPA-BMA improved the S/N (SI lesion/SI

| | T1 (precontrast) Mean ± SD | T1 (30 min p.i.) Mean ± SD | T2 (precontrast) Mean ± SD | P (precontrast) Mean ± SD | T1 SAT (10 min p.i.) Mean ± SD |
|---|---|---|---|---|---|
| C/N (muscle) | 3.8 ± 3.7 | 14.4 ± 8.8 | 12.2 ± 7.6 | 8.9 ± 7.4 | 17.8 ± 14.3 |
| C/N (fat) | −28.6 ± 11.8 | −16.4 ± 8.5 | −6.8 ± 5.3 | −19.6 ± 9.8 | 12.0 ± 15.8 |
| C/N (lung) | 14.2 ± 6.2 | 26.2 ± 13.4 | 16.1 ± 8.2 | 21.1 ± 9.8 | 33.4 ± 18.2 |
| S/N | 15.8 ± 6.4 | 28.4 ± 13.7 | 17.3 ± 8.1 | 22.6 ± 9.9 | 36.7 ± 18.7 |

C/N (muscle) = SI lesion − SI muscle/noise; C/N (fat) = SI lesion − SI fat/noise; C/N (lung) = SI lesion − lung tissue; P = proton density–weighted.

noise) by approximately 90% at 5–45 min postinjection ($P < .01$) (Table). In conclusion, gadodiamide significantly improved C/N and S/N between normal and abnormal thoracic tissue, and T1-weighted images with fat saturation at 10 min p.i. showed the highest S/N and C/N.

**174 • 3:57 PM**

### Contrast-enhanced MR Imaging of the Chest

RC Bittner, J Gurok, W Schörner, HG Hieckel*, W Auffermann, JC Böck, R Loddenkemper†, R Felix

*Department of Radiology, UKRV, Freie Universität Berlin, *Chest Hospital Heckeshorn, Berlin, and †Klinikum Buch, Berlin*

To date, contrast material has been considered unnecessary for MR chest examinations. Apart from high spatial resolution of plain T1-weighted images, this is due to the excellent lesion contrast of T2-weighted images. The diagnostic value of contrast-enhanced MR imaging in chest pathologies was studied. One hundred fifty-eight examinations were performed in 129 patients with various benign and malignant thoracic diseases with 0.5-T and 1.5-T whole-body MR systems. In all patients, electrocardiograph-gated T1- and T2-weighted spin-echo images were obtained. After intravenous injection of Gd-DTPA, the T1-weighted sequence was repeated. Section thickness was 4–8 mm in transverse and coronal (sagittal) planes. Plain T1- and T2-weighted images were compared with Gd-DTPA–enhanced T1-weighted images. Inferior results after Gd-DTPA enhancement were noted in 12 examinations. No significant diagnostic gain postcontrast was noted in 66 examinations. In 80 examinations, Gd-DTPA–enhanced images provided additional diagnostic information compared with unenhanced images. Differential diagnosis became more precise after contrast enhancement (eg, malignant lymphoma vs thymoma) in 16 cases; Gd-DTPA provided superior assessment of the spread of disease to neighboring structures (eg, chest wall and vascular invasion) in 47 patients; and lesion detection (eg, pleural disease) was improved in 17 cases. Gd-DTPA–enhanced T1-weighted images combine excellent spatial resolution with high lesion contrast, comparable with that of the T2-weighted sequences. In most MR examinations of the chest, contrast-enhanced T1-weighted images may replace the blurry and time-consuming T2-weighted images.

**175 • 4:09 PM**

### MR Mammography: Experience after 650 Examinations

WA Kaiser, MF Reiser

*Radiologische Universitätsklinik, Bonn, Germany*

The purpose of this study was to find an optimal MR mammographic (MRM) technique and to evaluate the use of MRM in the detection of breast cancer. Different techniques were used to conduct more than 650 MRM examinations, beginning in March 1984 (spin-echo, gradient-echo, fat-water, 2D, 3D, dynamic). Dynamic imaging was performed in 470 cases following injection of 0.1 mmol/kg Gd-DTPA. In 283 cases the MRM result was compared with histopathologic findings. The remaining cases were controlled by mammography and clinical follow-up of up to 6 years. In all of the 81 carcinomas that were investigated with dynamic techniques, a uniform enhancement of signal intensity of more than 90% was observed within 1 min after injection of Gd-DTPA, whereas in all but 10 benign lesions a slower and more progressive enhancement was observed (sensitivity, 98.8%; specificity, 99.7%; positive predictive value, 89.0%; negative predictive value, 99.7%; accuracy, 97.6%). MR mammography performed with gradient-echo sequences and contrast medium injection is a new and reliable method of detecting tumor angiogenesis in breast carcinomas. This method is especially useful in mammographically or clinically difficult cases.

**176 • 4:21 PM**

### Is Gd-DTPA–enhanced MR Imaging the Most Sensitive Method for the Detection of Multicentric Breast Carcinomas?

H Oellinger, S Heins, B Sander, U Flesch, H Witt, R Felix

*Radiation and Polyclinic, University Hospital Rudolf Virchow, Free University of Berlin*

MR imaging of the breast is becoming more and more established in clinics. In general, MR imaging gives a more morphologically detailed view than does mammography. Startling differences were found in multicentric carcinomas (MCC): in this study five of six MCC were detected with MR imaging but only one with mammography. Forty-six patients were examined with a 1.5-T Magnetom (Siemens, Erlangen, Germany). Seventeen were excluded from the study for various reasons (one male, two interrupted examinations, three technical problems, three no surgery, eight plastic surgeries); 29 patients with suspected carcinoma were included. Gd-DTPA (Magnevist; Schering, Berlin) was used as a contrast agent (0.2 mmol/kg body weight). T2-weighted SE (TR = 2,500 msec, TE = 90 msec), proton-weighted (TR = 2,500 msec, TE = 15 msec), and T1-weighted 3D FLASH (TR = 22 msec, TE = 6 msec, flip angle = 40°) sequences were used. The T1-weighted 3D FLASH sequence was repeated twice postcontrast to include prolonged enhancing lesions. Findings were compared with mammographic and histologic findings. The sensitivities of both methods were determined for selected lesions (Table). If future studies confirm these results, MR imaging would be indicated preoperatively for women with single suspect lesions detected with mammography.

| | MR Imaging | Mammography |
|---|---|---|
| Fibroadenoma | 0.59 | 0.82 |
| Dysplasia | 0.74 | 0.55 |
| Carcinoma | 0.96 | 1 |
| MCC | 0.85 | 0.18 |

177 • 4:33 PM

## Pharmacokinetic Mapping with Dynamic Gd-DTPA–enhanced MR Imaging in Cervical Carcinoma

M Müller-Schimpfle, T Hess, H Junkermann*, G Brix, W Semmler, G van Kaick

*Department of Oncological Diagnostics and Therapy, German Cancer Research Center, and *Department of Gynecological Radiology/Radiotherapy at the University, Heidelberg, Germany*

The purpose of this ongoing study was to assess the role of dynamic Gd-DTPA–enhanced MR imaging in (*a*) tumor demarcation before therapy and (*b*) follow-up during and after combined chemo- and radiation therapy. Cases of histologically proved inoperable cervical carcinoma ($n = 8$) or recurrent tumor after operation ($n = 2$) were included in this study. MR examinations were performed prior to ($n = 10$) and 1, 3, and 6 months after ($n = 6$) the beginning of therapy with a 1.5-T Magnetom SP. T1- and T2-weighted images were acquired in sagittal and transverse orientations (SE = 500/15, SE = 2,400/22, 120, and SE = 2,800/15,90). Dynamic MR examinations with 64 rapid T1-weighted SE images were performed during and after infusion of 0.1 mmol/kg Gd-DTPA over 4 min. Pharmacokinetic parameters (amplitude [A] of contrast enhancement, tissue distribution time) were calculated according to the signal-time curve and displayed as parameter images. Before therapy, the tumors showed a high signal intensity on T2-weighted images in all cases. Evaluation of pharmacokinetic data of the tumor regions revealed a lower amplitude of enhancement but a shorter tissue distribution time when compared with the mean values of myometrium ($A_{TU} = 2.7 \pm 0.5$ vs $A_{MY} = 3.9 \pm 1.6$, mean relative values). The wide range of values, however, impaired accurate differentiation. During therapy, the signal intensity on T2-weighted images decreased (6/6). The amplitude decreased in 4 of 6 cases, while a prolongation of the distribution time was observed in 5 of 6 cases. In conclusion, pharmacokinetic parameters do not seem to differentiate reliably between cervical carcinoma and myometrium, but might provide additional information for monitoring therapy response.

178 • 4:45 PM

## Gd-DTPA in MR Imaging of Scintigraphically Cold Nodules of the Thyroid

WD Stern, W Vogl, G Weisser, W Kaiser, G Köveker*, M Laniado

*Departments of Radiology and *Surgery, Eberhard-Karls-Universität Tübingen, Germany*

The purpose of this study was to evaluate the potential of MR imaging with Gd-DTPA in differentiating benign from malignant lesions. Eighteen patients with scintigraphically cold lesions of the thyroid were studied with a 1.5-T MR imaging unit (Siemens, Erlangen, Germany) with a Helmholtz-type surface coil. T1-weighted (SE = 600/15) and T2-weighted (SE = 2,500/22, 90) axial images were obtained and Gd-DTPA (Schering, Berlin) was intravenously injected as a bolus (0.1 mmol/kg). Seventeen single-section gradient-echo images (GE = 25/10/30°) were acquired over 2.5 min in a representative section showing the nodule at its greatest extent. Next, contrast-enhanced T1-weighted SE images (section thickness = 4 mm with a 1-mm intersection gap) were obtained. In all cases, diagnosis was confirmed with surgery. Surgery revealed 2 carcinomas, 11 regressive nodules, and 5 adenomas. Gd-DTPA improved the delineation of nodules in the thyroid. Carcinomas were seen as hyperintense areas on T2-weighted images, with inhomogeneous contrast enhancement and ill-defined margins. Both carcinomas were diagnosed correctly with MR imaging. In multinodular goiters with regressive changes, a pattern of inhomogeneous signal intensity with hyperintense foci and inhomogeneous enhancement was observed. In three of these cases, malignancy was suspected on the basis of MR imaging. In all remaining cases, MR imaging diagnosis was correct. Adenomas appeared as well-defined nodules showing rim enhancement at dynamic imaging. Contrast-enhanced T1-weighted SE images showed heterogeneous enhancement due to degenerative changes. MR imaging findings corresponded with pathologic findings. Preliminary results indicate that Gd-DTPA–enhanced MR imaging aids in the differential diagnosis of benign and malignant focal lesions of the thyroid gland.

179 • 4:57 PM

## MR Arthrography with Contrast Enhancement: Evaluation of Articular Cartilage in the Knee

SM Brown*, MA Nissenbaum*, DJ Atkinson†, SJ Song*, BE Widoff*, K Yan*, PR Kurzweil*, D Jackson*, WG Bradley*

**Long Beach Memorial Medical Center, Long Beach, Calif, and †Siemens Medical Systems, Iselin, NJ*

Multiple attempts have been made to visualize hyalin (articular) cartilage abnormalities with MR imaging. When compared with arthroscopy, these attempts have been largely unsuccessful. An intraarticular injection of Gd-DTPA was used in an attempt to improve visualization of hyaline cartilage defects of the patella, femoral condyles, and tibial plateau with T1-weighted gradient-echo sequences. Thirty patients with knee pain underwent routine MR imaging (T2-weighted sagittal and coronal images) of the knee as well as MR arthrography with contrast enhancement (MR ACE). The latter was performed after intraarticular injection of 40 mL of a 2-mM solution of Gd-DTPA in normal saline while the patient lay supine on the MR imaging table. T1-weighted spin-echo and gradient-echo sequences were obtained in the first five patients, after which only gradient-echo sequences (MP RAGE technique; TR = 13 msec, TE = 6 msec, TI = 1,000 msec, 12° flip angle, effective section thickness of 1.25 mm, 160 × 256 matrix) were used. MR imaging findings were correlated with arthroscopic findings by using the standard 4-level grading system. MR ACE with T1-weighted gradient-echo sequences proved to be of much greater value than T1-weighted spin-echo sequences in the first five cases. Grade 2–4 hyaline cartilage defects were well demonstrated with the gradient-echo sequences. Abnormalities described at MR ACE correlated well with arthroscopic findings, with the exception of the mildest fibrillation (grade I). The procedure was well tolerated by all 35 patients. In conclusion, MR ACE accurately demonstrated all but the mildest (grade I) cartilage defects of the knee. It is recommended whenever serious evaluation of the hyaline cartilage is necessary.

180 • 5:09 PM

## Enhanced MR Imaging of the Temporomandibular Joint: Is It Worthwhile?

MA Mikhael

*McGaw Medical Center of Northwestern University, Evanston, Ill*

The purpose of this study was to evaluate the benefits of Gd-DTPA–enhanced MR imaging of the temporomandibular joint (TMJ) relative to those of nonenhanced studies, an evaluation made necessary by the high cost of contrast material added to the cost of MR imaging. One hundred twelve patients with suspected TMJ problems were studied with MR imaging. Of the 47 patients with TMJ abnormalities, the last 27 were studied before and after Gd-DTPA injection. Abnormalities included anterior condylar

subluxation ($n$ = 7), anteromedial disk displacement without reduction ($n$ = 18), anteromedial displacement with reduction ($n$ = 20), fractured mandible ($n$ = 2), nonunion, pseudoarthrosis, and anteromedial displacement ($n$ = 1), and destroyed frozen joint with adhesions ($n$ = 2). In this series, MR imaging was found to have a specificity of 100% in the diagnosis of abnormal derangements of the temporomandibular joint and 64% for perforation of the disk, as correlated with surgical and/or videoarthrographic findings. Enhanced MR images showed clear delineation of the capsule and ligaments better than did the nonenhanced MR images, but did not increase the capacity to diagnose the perforated disks. In conclusion, it is believed that gadolinium enhancement should be used for better delineation if the fibrous capsule and ligamentous attachments are to be radiologically evaluated. If the study is being done mainly to determine the position and pathologic abnormalities of the interarticular meniscus and bone structures, MR imaging without contrast enhancement is diagnostic.

# Tuesday Afternoon • Nassau Suite
# Papers 181–189

## ARTIFACTS AND SAFETY

MODERATORS: RR Price, PhD • SR Thomas, PhD

181 • 3:45 PM

### Optimizing MR Image Quality and Acquisition Speed

P Sprawls, SK Sheppard
*Department of Radiology, Emory University School of Medicine, Atlanta*

Optimum MR image quality and general system performance depend on the user's ability to select appropriate imaging methods and parameter values. This is a complex procedure because one parameter often affects several quality characteristics of the image in addition to acquisition speed. A graphic model has been developed that can be used to evaluate the different imaging methods and the effect of changing parameter values. Two desirable image attributes—good detail and a high signal-to-noise ratio (S/N)—plus imaging speed are represented as specific foci or goals on a unique two-dimensional display of multidimensional parameter space. Each protocol parameter is represented by quantitative scales connecting the imaging goals. A specific imaging protocol is represented by a single operating point within the parameter space. The effect that changing imaging methods and parameter values has on the various image characteristics and imaging speed is easily visualized and quantitatively evaluated. Special emphasis is given to the various fast-imaging methods with respect to their image quality characteristics and optimum clinical applications.

182 • 3:57 PM

### Motion Artifact Reduction with Gerchberg-Saxton Algorithm in Multisection Spin-Echo Imaging

J Wilbrink, LH Zang
*Hitachi Instruments Inc, San Jose, Calif*

The Gerchberg-Saxton algorithm was applied to an image already partially corrected for motion. This algorithm provided significantly improved image quality compared with what had already been accomplished with the initial motion correction scheme. The Gerchberg-Saxton algorithm can be used for the correction of motion artifacts as long as the motion is purely translational and within the imaging plane. The algorithm replaces the phases of the measured data with the phases in the fast Fourier transform of the image with the outlying ghosts removed. Since the phase changes should be a linear function of the readout and phase-encode positions of the sample, it is possible to do a line fit through the expected phase changes. Problems occur when the signal-to-noise ratio is too small (ie, for higher-order phase encodings). Also, when the motion is too great, it is harder to separate the ghosts from the image and the line fit becomes problematic because of phase wrapping. Different line fit methods were used in an attempt to solve the wrapping problem. This experiment made use of an 8-section SE sequence in which the phase-encode direction alternated between x and y. For both directions, different phase-encoding offsets were used so that relatively low-order phase encodings were spread out during acquisition. Images of a moving knee (motion in both x and y directions with an amplitude of up to 40 mm and a velocity of up to 5 mm/sec) were acquired with a 0.5-T Hitachi MRH-500. First, the image was motion compensated, with an error in the position estimates of a few millimeters. (This research is reported elsewhere.) Next, the Gerchberg-Saxton algorithm was applied. After 5 to 10 iterations of the algorithm, image quality improved tremendously and did not visibly improve thereafter. The algorithm provided an improved position estimate with subpixel ( < 1 mm) accuracy in both x and y directions for all times. In conclusion, the application of the Gerchberg-Saxton algorithm provided greatly improved image quality. The algorithm currently takes about 40 seconds per iteration step with a SUN SparcStation 1 and in most cases can be run automatically without any user intervention.

183 • 4:09 PM

### Wavelet Encoding in the Section-Select Dimension

LP Panych, PD Jakab
*Department of Radiology, Brigham and Women's Hospital, and Harvard Medical School, Boston*

A 2D Fourier transform multisection imaging procedure is implemented in which wavelet encoding is used in the section-select direction (z). With respect to data collection, the procedure is identical to a standard multisection approach except that the RF pulse is designed to give section profiles that are wavelet functions. In x and y, reconstruction is by Fourier transformation. The reconstructed sections are then inverse wavelet transformed in the z direction. The required section profiles for wavelet encoding have been obtained with a small-bore (30-cm) 1.9-T animal imaging system. Wavelet encoding has the advantage of providing finer resolution in the section-select direction without taxing the gradient amplifiers. In addition, interpolation in this direction is inherently better because the wavelet section profiles are smoother than the standard box-shaped profiles and, in the case of the wavelet function being examined, are based on cubic splines.

184 • 4:21 PM

### MR Movies from Motion Ghosts

QS Xiang, RM Henkelman
*Department of Medical Biophysics, University of Toronto, Canada*

It has been previously shown that a ghosted image can be decomposed into a ghost mask superimposed over an ideal ghost-free image. With temporal interleaved data acquisitions, a set of images can be obtained that have a defined relationship among the ghosts so that both the ghost mask and the ghost-free image can be determined independently (1). This study demonstrates that the ghost mask carries useful dynamic information. Therefore, ghosts should not simply be discarded but properly pro-

cessed and used. The ghost-free image represents the time-averaged spin density distribution during the entire course of imaging. Similarly, the ghosts indicate the strength and phase of harmonics of various orders contained in the motion. When the ghost-free image and the ghosts of different orders are spatially aligned and summed with proper temporal phase weighting, a time-dependent dynamic image can be generated with the following equation:

$$\rho(x,y;t) = I_0(x,y) + \Sigma\, G_n \exp(i2\pi P_0 t/T_0),$$

where $\rho(x,y;t)$ is the time-varying spin density, $I_0(x,y)$ the ideal ghost-free image, $G_n$ the ghost of order $n$ which is the complex pixel value in the ghost mask at position $(x, y + nP_0)$, $T_0$ the known total imaging time, and $P_0$ the total number of motion periods during the imaging, equal to the ghost spacing measured in pixels from the ghost mask. Experimental data from both phantoms and human subjects will be presented. This method provides a way of obtaining a "movie" of the moving object from motion-induced ghosts.

1. Xiang QS, Henkelman RM. 10th SMRM 1991; 196.

185 • 4:33 PM

## Suppression of Motion Artifacts due to Diffusion or Microvascular Flow-sensitizing Gradients

B Özdemirel, O Nalcioglu
*Department of Radiological Sciences, Division of Physics and Engineering, University of California, Irvine*

Gradient waveforms designed for the acquisition of images sensitive to molecular diffusion or microscopic random directional flow velocities on the order of millimeters per second can induce severe artifacts resulting from any bulk motion. Quantitative measurements on the diffusion or flow-sensitive images require the acquisition of a reference image without the sensitizing gradient pulses. Correction of motion artifacts is possible using the phase information in the reference image raw data, regardless of the range of phase fluctuations. Two major sources of bulk motion are tissue pulsation and respiratory motion in localized in vivo imaging studies. Electrocardiograph gating, which is also essential for the accuracy of flow measurements, can eliminate artifacts resulting from tissue pulsation. Gating with respect to a secondary source of motion is not practicable in many cases because significant changes in TR cause unwanted variations in image intensity depending on T1. If motion is simultaneous in the entire FOV—in other words, if the raw data magnitude information is not affected by motion—there is a constant phase error along each data acquisition line. Dispersion of phase information causes signal intensity loss in addition to ghost artifacts along the phase-encoding direction when the averaging of multiple data acquisitions is necessary. In this case, the original image intensity can be recovered only if the phase errors in each data acquisition line are corrected prior to averaging. Raw data collected for the reference image also provide reference phase information. The reference image is acquired only with the imaging gradients that are much smaller than the diffusion or flow-encoding gradient pulses, and presumably the image is free from motion artifacts. Phase errors are calculated for each data acquisition line from phase comparisons with the corresponding data acquisition of the reference image raw data. Correction of phase errors is achieved by multiplying with complex reverse-phase terms. The developed algorithm was tested in a moving phantom designed to induce motion artifacts on flow-sensitive images. The algorithm also gave encouraging results in the in vivo F-19 imaging experiments in rabbit kidneys. This motion artifact suppression algorithm can be effectively applied to any kind of periodic or random motion, provided the motion range is small compared with voxel size and phase errors due to normally applied imaging gradients are insignificant. Interleaved acquisition of the reference, diffusion-sensitive, and flow-sensitive images enhances the accuracy of phase calculations and comparisons.

186 • 4:45 PM

## Extraction of Noise Spikes in MR Imaging

MJ Sanz, EM Haacke
*University Hospitals of Cleveland and Case Western Reserve University, Cleveland*

Many new sequences require driving of the gradient coils to their limits and stressing the system in such a way as to generate noise spikes in the raw data. This leads to banding and sometimes severe loss of image integrity. A method to eliminate these noise spikes has been formulated. A phantom imaged along with the subject or a control region in the subject is used to locate the noise spikes. Starting with complex or magnitude images, one can remove these spikes from the raw data and recover the missing information with interpolation. A new image is created by manually removing all nonphantom, nonnoise signals from the image. The resulting truncated image consists only of a rectangular box (the phantom) of uniform intensity, plus whatever noise is in the image. Two-dimensional fast Fourier transform of the truncated image yields a product of two sinc functions. An envelope that fits over the theoretically expected signal is passed over the raw data of the truncated image to filter out any noise spikes. Once the noise spikes are located, they can be removed from the original raw data. After the noise spikes are removed, a bilinear interpolation is performed to regenerate the missing information. The method described works extremely well, producing a clean image with virtually no noise present, even when a very large number of spikes exist.

187 • 4:57 PM

## Subjective Perceptions of Temperature Changes and Comfort Associated with Clinical MR Imaging

FG Shellock, T Meeks, S Myers
*Cedars-Sinai Medical Center and UCLA School of Medicine, Los Angeles, Calif*

Increases in tissue temperature are known to occur during clinical MR imaging performed at high specific absorption rates (SARs). Patients' perception of these temperature changes and their relative comfort have not previously been investigated. Therefore, 20 patients were studied with MR imaging of the lumbar spine at whole-body–averaged SARs ranging from 0.3 to 1.0 W/kg (mean, 0.5 W/kg) for a time period ranging from 32 to 93 min (mean, 64 min). Room and magnet bore ambient conditions were constant (temperature, 21°C ± 1; RH, 45% ± 5%; and air flow, 0.1 L/min). Body and skin temperatures measured at multiple sites were recorded immediately before and after imaging. A 7-point scale (1 = cold, 7 = hot) was used to determine patients' subjective perception of temperature change, and a 4-point scale (1 = comfortable, 4 = very uncomfortable) was used to determine the patients' comfort level associated with the imaging procedure. Seventy percent (14/20) of the patients felt an increase in temperature during imaging, and three of these patients felt uncomfortable as a result of this perceived temperature increase. All 14 of these patients had statistically significant increases in body and skin temperature. Since patient discomfort is important because it may produce movement and related body motion artifacts, techniques that reduce discomfort resulting from perceived temperature changes should be imple-

mented. These include reducing the ambient temperature and/or increasing air flow in the environment to make the imaging procedure more comfortable.

188 • 5:09 PM

### SAR in High-Duty-Cycle Adiabatic Pulsing Schemes for MR Imaging at 4 T

ER Ritenour, M Lau, BE Hammer, M Garwood, H Merkle
*Department of Radiology, University of Minnesota, Minneapolis*

Specific absorption rates (SARs) were calculated for various configurations of surface coils used to transmit adiabatic pulses in fast imaging (high duty cycle) sequences. Adiabatic pulses were transmitted with surface coils with a 4-T Siemens/Sisco whole-body system. Power deposition was calculated from the current density induced in tissue. SAR was calculated for Helmholtz, concentric circular, and single-loop coil geometries. Measurements of temperature in phantoms containing saline solution were made with fiberoptic probes. Computer simulations of power density demonstrated an approximate dependence of SAR on the third power of the coil radius and the square of the magnetic field strength at the center of the coil. For a duty factor of 30%, peak local SAR values were 1.5–15 W/kg for coil radii of 2.5–5 cm at 1 cm from the coil. Maximum temperature rise in a homogeneous phantom (total imaging time, 156 sec) was 6°C. Both calculated and measured power deposition and the associated temperature rise resulting from the transmission of adiabatic pulses with surface coils at 4 T can result in values exceeding current FDA guidelines in extreme cases. However, adjustments in imaging protocol, including the use of spacers between the coil and sample, can keep SAR at acceptable levels.

189 • 5:21 PM

### Test of MR Imaging Capacity to Suppress Plasma Melatonin Concentrations in Normal Humans

JS Schiffman*, HM Lasch*, MD Rollag†, T Tasciyan†, A Flanders†, GC Brainard*, DL Burk†
**Departments of Neurology and †Radiology, Jefferson Medical College, Philadelphia, and ‡Department of Anatomy, USUHS, Bethesda, Md*

Melatonin suppression is a sensitive and standard assay of the ability of visible electromagnetic radiation (light) to affect the neuroendocrine axis. Melatonin synthesized in the pineal gland is controlled by the suprachiasmatic nucleus on a circadian basis and is modulated by environmental light cues. Exposure of the eyes to bright light at night, when melatonin synthesis is highest, will suppress plasma melatonin concentrations. Animal studies have indicated that a static, inverted magnetic field or the 1.5-T field of a standard MR imager will also affect pineal physiology via the retinohypothalamic pathway. In this study, MR imaging of the brain was evaluated for its ability to modulate melatonin synthesis in eight healthy adult male volunteers. The study was undertaken to detect a possible direct biologic interaction of clinical MR imaging in humans. Eight subjects were exposed to three conditions, each on separate nights between 1:00 AM and 2:00 AM when melatonin is expected to be high: (*a*) a 1-hour series of routine pulsing sequences that produced T1- and T2-weighted images of the brain in axial, sagittal, and coronal planes on a GE 1.5-T Signa imager operating at 63.9 MHz; (*b*) 1 hour in a mock MR imaging unit listening to a recording of the imaging; and (*c*) 1 hour in a similar mock unit listening to the recording and illuminated with 3,500 lux of broadband white, fluorescent light. Subjects were kept in a dim environment (10 lux) and a 0.6-gauss field for at least 4 hours prior to each experimental procedure. Two samples of peripheral venous blood were drawn, one before and one after each condition, and were analyzed for melatonin content with radioimmunoassay. Data were analyzed with a 3 × 2 repeated-measures analysis of variance model. Significant interaction between groups was observed with $F(2,6) = 7.96$ and $P = .021$. The change in melatonin concentrations (final concentration as a percentage of initial concentration) for each 1-hour procedure was calculated for all individuals. Subjects exposed to dark displayed a typical increase (mean ± SEM = 125.3 ± 6.5) over time. Subjects exposed to light displayed a characteristic suppression of melatonin content (72.2 ± 9.3). Those exposed to the experimental imaging conditions displayed an increase in melatonin content (132.9 ± 15.0) comparable with that of the dark control. Post hoc analysis with a Student-Newman Keuls test showed a significant difference ($P < .005$) between magnet and light values, but no significant difference between magnet and dark values. Thus, MR imaging did not suppress plasma melatonin concentrations in the subjects. This result is at variance with that of animal studies and suggests one of several possibilities: (*a*) there is a "window" effect or a specific threshhold effect in human subjects for magnetic modulation of the retinohypothalamic pathway to the pineal; (*b*) humans have compensatory mechanisms that mask MR imaging stimulation of the pineal; or (*c*) MR imaging does not act on the neural pathway in humans as it does in animals.

## Wednesday Morning
## Sutton Parlor North
## Papers 201–208

## KNEE/SHOULDER

MODERATORS: JJ Busch, MD • FG Shellock, PhD

201 • 10:30 AM

### Improved MR Imaging Detection of Recurrent Meniscal Tears in the Postoperative Knee with Intraarticular Contrast Material

GR Applegate, BD Flannigan, BS Tolin, JM Fox, W Del Pizzo
*Southern California Orthopaedic Institute, Van Nuys, Calif*

Routine MR imaging lacks sensitivity in the detection of recurrent meniscal tears in the postoperative meniscus. The goal of this investigation was to improve MR sensitivity with use of intraarticular contrast material. The MR evaluation of 67 prospective patients who had recently undergone knee surgery included T1-weighted images acquired after injection of intraarticular contrast material. Forty milliliters of gadopenetetate dimeglumine/saline solution (1:100) was used. Nineteen patients underwent arthroscopy following MR imaging and comprised the study population. Two independent reviewers evaluated the pre- and postcontrast studies separately. A third reviewer reviewed the videotapes of the arthroscopies. The follow-up arthroscopies were performed 1.5 to 33 weeks (average, 7.9 weeks) following the MR studies. In the detection of recurrent meniscal tears, the precontrast studies had a sensitivity of 65.5% and a specificity of 78%, compared with 85% and 100%, respectively, for the postcontrast studies. Positive predictive values for the pre- and postcontrast studies were 80% and 100%, respectively. Accuracy for the postcontrast studies was 91%, compared with 68% for the precontrast studies. On routine MR images the postoperative meniscus frequently appears amorphous, with areas of increased signal that may represent recurrent tears, healed or healing tears, or me-

niscal degeneration. The use of intraarticular contrast material improved definition of the meniscal remnant and detection of recurrent tears. These preliminary data suggest that MR imaging with intraarticular contrast material may be useful in the detection of recurrent meniscal tears.

202 • 10:42 AM

### MR Imaging Evaluation of Menisci: Comparison of Spin-Echo and Gradient-Echo Imaging Techniques

JA Markisz, A Serra, RB Rafal, PA Kosovsky, WM Williams, RA Schneider, JP Whalen

*Department of Radiology, Cornell University Medical Center, New York, NY*

Gradient-echo (GRE) imaging of the knee has been proposed as a rapid and sensitive method of detecting meniscal tears. This study was undertaken to compare the results of GRE and spin-echo (SE) studies. Consecutive 3-mm sagittal T1-weighted SE images were compared with comparable 2D GRE images in two groups of patients: (*a*) 27 asymptomatic volunteers between the ages of 20 and 30, with no history of knee surgery or knee pain, and (*b*) 15 patients complaining of knee pain, who subsequently underwent arthroscopic surgery. The images were evaluated independently for meniscal pathology by four radiologists using a numerical rating system. A meniscus was considered to be torn if abnormal signal within it extended to an articular surface. Of 54 asymptomatic menisci, 6 were thought to demonstrate abnormalities consistent with tears on both the SE and GRE images. The remaining 48 menisci were considered normal on all SE images. Eighteen of these menisci demonstrated significant abnormalities consistent with tears on the GRE images. Twenty-five of the 30 menisci imaged for knee pain were thought torn on SE images. Twenty-two of these tears were confirmed with arthroscopy. All 25 "abnormal" menisci on SE images and one of the five menisci without SE abnormality had GRE images suggestive of significant tears. Abnormalities were thought to be more prominent on the GRE images, although the high rate of false-positive studies in asymptomatic patients makes this technique of questionable clinical utility.

203 • 10:54 AM

### MR Imaging Detection of Articular Cartilage Pathology

EM White, PC Kezdi, HJ Sweeney, WG Robb, GG Ghahremani

*Departments of Radiology and Orthopedic Surgery, Evanston Hospital, McGaw Medical Center of Northwestern University, Evanston, Ill*

MR imaging has become widely used in the evaluation of joint pathology, particularly in detecting meniscal and ligamentous abnormalities. This study was undertaken to determine the accuracy of MR imaging in identifying the presence and grading the severity of articular cartilage lesions in the knee joint. MR examinations performed in 87 patients who subsequently underwent knee arthroscopy were reviewed. All studies were performed with a 1.5-T superconducting magnet with T1- and T2-weighted SE pulse sequences. Articular cartilage abnormalities were graded into one of four groups by using criteria correlative with an established arthroscopic classification system. Lesions varied from minimal deformity of the cartilaginous surface (grade 1) to marked loss of the articular cartilage and exposure of the underlying bone cortex (grade 4). During review of MR studies, the observers were blinded to arthroscopic findings. Results of MR and arthroscopic examinations in the detection and grading of articular cartilage abnormalities were subsequently compared. In detection of articular cartilage pathology, MR imaging had a sensitivity of 98% and a specificity of 78%. The overall accuracy in identifying articular cartilage abnormalities was 94%. In grading specific lesions, MR imaging correlated with arthroscopic findings in 14% of grade 1 lesions, 86% of grade 2 lesions, 84% of grade 3 lesions, and 100% of grade 4 lesions. In conclusion, MR imaging is a valuable noninvasive technique for examining the articular cartilage of the knee joint, particularly in detecting grade 2–4 lesions. Since articular cartilage defects may cause or significantly contribute to symptoms, the appearance of the cartilaginous surface should be carefully examined in all MR studies.

204 • 11:06 AM

### "Functional" Patella Alta Determined with Axial-Plane Imaging of the Patellofemoral Joint: Association with Abnormal Patellar Alignment and Tracking

FG Shellock, S Kim, J Mink, A Deutsch, J Fox

*Cedars-Sinai Medical Center, Los Angeles*

"Patella alta" refers to an abnormal superior position of the patella in relation to the femoral trochlear groove and may be partially responsible for abnormal patellar alignment and tracking. The purpose of this study was to develop a new criterion for determining patella alta by using axial plane MR imaging of the patellofemoral joint, which shows the exact position of the patella relative to the femoral trochlear groove. This criterion of altered patellar height was used during assessment of patients with suspected patellar alignment/tracking abnormalities. Ninety-six symptomatic joints with suspected patellofemoral abnormalities were studied with kinematic MR imaging. "Functional" patella alta was designated if the inferior pole of the patella was positioned above the superior aspect of the femoral trochlear groove as viewed on serial axial-plane, T1-weighted images of the extended knee. Forty-four (46%) joints had patella alta. Of these, 3 (7%) had normal alignment, 23 (52%) had lateral subluxation, 14 (32%) had medial subluxation, 2 (5%) had patellar tilt, and 2 (5%) had lateral to medial subluxation. There was a statistically significant ($P < .05$) higher percentage of joints with lateral subluxation observed for the joints with patella alta compared with the joints with normal patellar height. Overall, patellar malalignment was observed in a high percentage (93%) of joints with patella alta. The determination of patella alta with use of the above criterion should alert the radiologist to the presence of patellar malalignment/maltracking, particularly lateral subluxation.

205 • 11:18 AM

### Assessing Patellar Tracking with Motion-triggered MR Imaging: First Clinical Results

C Muhle, J Brossmann, C Schröder, UH Melchert, L Besch, C Büll

*Department of Radiology, Christian-Albrechts-University Kiel, Germany*

Motion-triggered MR imaging (MTMRI) cine studies were made to assess the patellofemoral joint during active knee movement in 37 patients with known recurrent patellar dislocation or suspected patellar malalignment. Twenty-six symptomatic patients (group 1) with suspected patellar malalignment were examined. Ten patients (group 2) were examined after patellar realignment surgery. In one patient, MTMRI was performed both pre- and postoperatively. Knee arthroscopy was performed in six patients from group 1. The examined knees were positioned in a nonferromagnetic positioning device and were extended and flexed actively about 50 times/min. Patella-skin shifting was perceived by a pneumatic pressure transducer. Cyclic pressure alterations were converted into a trigger

signal and used for gating as in electrocardiograph-triggered MR imaging. Eight time frames were generated with the gradient-echo technique during extension of the knee. MTMRI demonstrated normal patellar alignment in 13 patients of group 1, a lateral subluxation in 10 patients, a medial subluxation in 2 patients, and an excessive lateral pressure syndrome in 1 patient. Of the group 2 patients, one had no patellofemoral abnormalities, six had a medial subluxation of the patella, two had lateral subluxation, and one had an excessive lateral pressure syndrome. The patient examined both before and after a lateral retinaculum release operation had a lateral subluxation preoperatively and a medial subluxation postoperatively. The clinical usefulness of motion-triggered MR imaging in diagnosing patellar tracking abnormalities under active knee motion before and after patellar realignment surgery is demonstrated. In all (6 of 6) patients examined before patellar realignment surgery, the MTMRI diagnosis was confirmed with knee arthroscopy.

206 • 11:30 AM

### Bone Bruises and Chondral Lesions in Anterior Cruciate Ligament Tears: A Prospective Study

JP Schils, KP Spindler, DW Piraino, BJ Richmond, GH Belhobek, JT Andrish, JA Bergfeld

*Departments of Radiology and Orthopaedic Surgery, Cleveland Clinic Foundation*

The purpose of this study was to prospectively utilize MR imaging, as tested by arthroscopy, to evaluate articular cartilage injury and bone bruise (BB) in acute anterior cruciate ligament (ACL) tears; the hypothesis is that anterior subluxation and impaction of the posterior tibia on the anterior femur results in articular cartilage injury and BB. Fifty-four patients (mean age, 24 years) with a clinical diagnosis of acute ACL tear were prospectively entered into a study that included preoperative MR imaging for assessment of the cartilage and subchondral bone and a detailed arthroscopic evaluation of the articular cartilage. The diagnosis of BB was determined with MR imaging, and the presence or absence of chondral lesion was assessed with arthroscopy. BB of the distal femur and proximal tibia was present in 80% of patients, with 68% in the lateral femoral condyle (LFC), and 53% in the lateral tibia plateau (LTP). Simultaneous involvement of the LFC and LTP occurred in 65% ($P = .02$). Arthroscopy showed abnormal cartilage of the LFC in 15 patients (28%). In eight patients, these documented cartilage lesions were not present on MR images. In six other patients with MR evidence of osteochondral fracture of the LFC, no visible cartilage injury was present at arthroscopy. Two MR findings in association with a BB of the LFC demonstrated a significant relationship with injury to the cartilage at arthroscopy: abnormal cartilage signal and thin and impacted subchondral plate. While the association of BB and ACL tear has been described before, this prospective study demonstrated a significant association of BB in the lateral compartment, which supports the hypothesis that the mechanism of injury involves anterior subluxation and impaction. This study further demonstrated that MR imaging has a promising role in the evaluation of associated cartilage injury with ACL tears. MR imaging and arthroscopy may be complementary, as discordance between the two methods still exists due to the limitations of each modality.

207 • 11:42 AM

### Improved Shoulder Imaging with Standard Surface Coils

WS Kubal, AEH Bampton, G Leong, BA Wirth, RA Blinder, D Simmons

*Department of Radiology, Medical College of Virginia, and HH McGuire VAMC, Richmond, Va*

Quadrature surface coils significantly improve signal-to-noise ratio in multiple clinical applications. Unfortunately the high cost of these devices precludes many centers from taking full advantage of their improved imaging characteristics. Herein is presented an inexpensive method of arranging standard surface coils to produce a quadrature-receiving array that provides substantial improvement in signal-to-noise ratio. Imaging was performed with a GE Signa 1.5-T unit. Phantoms and patients were imaged with use of two perpendicularly mounted standard product surface coils. The coils were positioned posterior and lateral to the shoulder joint. The output cables from the coils were joined by a standard "T" connector to the receiver input port at the magnet bore. To achieve quadrature coil configuration, one of the cables was lengthened by one-quarter wavelength at 63.8 MHz to provide a 90° phase shift between the signals from the two coils. No software modifications were required. Phantom imaging showed approximately a 40% increase in signal-to-noise ratio. Shoulder imaging demonstrated similar improvement in signal-to-noise ratio as well as improved signal homogeneity across the clinically relevant field of view. This increase in signal-to-noise ratio can allow improvement in in-plane resolution or a reduction in the number of excitations needed. An inexpensive quadrature receiver array made with standard surface coils has been demonstrated. This device is easy to use and provides excellent images for clinical shoulder imaging.

208 • 11:54 AM

### Rotator Cuff Tears: Simplified MR Imaging Diagnosis with Surgical Correlation

JD Reeder, ML Dvorkin, GW Pushkin

*Whitesquare Imaging and Franklin Square Hospital, Baltimore*

Previous studies have used changes in tendon morphology and signal, obscuration of subacromial fat, and the presence of subacromial fluid to diagnose rotator cuff tears. The hypothesis for this study was that a full-thickness hyperintense tendon defect on T2-weighted oblique coronal images represents the most important criterion for a diagnosis of supraspinatus tendon discontinuity. A review of 67 oblique coronal T1- and T2-weighted MR images was performed in 65 patients who underwent surgery and in two patients evaluated with arthrography. The study included 24 rotator cuff tears and 43 cases in which no full-thickness tear was present (including the two arthrographic cases). The following diagnostic criteria were evaluated (with resultant sensitivity and specificity): definite full-thickness tendon defects (83%, 100%), definite and probable full-thickness tendon defects (96%, 95%), full-thickness defects and probable defects accompanied by subacromial fluid (92%, 98%), and full-thickness tendon defects and probable full-thickness and partial defects with subacromial fluid (96%, 88%). The results suggest that the presence or absence of subacromial fluid does not affect accuracy. Identification of a definite or probable full-thickness tendon defect alone provides excellent diagnostic sensitivity and specificity. The greater diagnostic significance of this single criterion compared with other studies may represent a function of 4-mm contiguous (gapless) section acquisition. Giving particular attention to the most anterior distal portion of the su-

praspinatus tendon (a high-risk site for tear) also enhances diagnostic accuracy.

# Wednesday Morning
# Sutton Parlor Center
# Papers 209–216

## SPINE/HEAD AND NECK

MODERATORS: JS Ross, MD • KR Maravilla, MD

209 • 10:30 AM

### MR Imaging of Cervical Disk Disease: Value of Gd-DTPA

P Schubeus, B Sander, W Schörner, N Hosten, R Felix
*Department of Radiology, UKRV, Free University, Berlin*

The purpose of this study was to assess the value of Gd-DTPA administration in MR imaging of cervical disk herniations. Thirty-four patients with 40 disk herniations were examined with a 1.5-T whole-body imager. Plain T1-weighted (TR = 500 msec, TE = 5.8 msec, flip angle = 70°) and low-flip-angle images (TR = 800 msec, TE = 5.8 msec, flip angle = 10°) were obtained with a 2D FLASH sequence. After administration of 0.1 mmol Gd-DTPA the T1-weighted sequence was repeated. Section thickness was 2 mm. Contrast between disk herniations and cerebrospinal fluid was sufficient without contrast enhancement in all cases. Contrast between the herniated material and the intraforaminal structures was classified as sufficient in 13 of 40 cases on the plain images and in all cases after contrast enhancement. Delineation of 30 of 40 disk herniations was sufficient on the plain images, whereas all images showed sufficient delineation after administration of Gd-DTPA. The diagnostic value of the image was found to be improved after contrast agent administration in 3 of 12 lateral and 7 of 8 intraforaminal disk herniations, whereas the definition of posterior and posterolateral herniations was already sufficient on the plain images. In conclusion, Gd-DTPA administration is recommended in cases of lateral or intraforaminal disk herniations that are not clearly defined on plain images.

210 • 10:42 AM

### Three-dimensional High-Resolution MR Myelography

DJ Schnapf, EM Haacke, P Wielopolski, G Laub, A Bogdan, D Wilson
*York Imaging Center, Case Western Reserve School of Medicine, Cleveland; Siemens Medical Systems, Iselin, NJ; and Georgetown University School of Medicine, Washington, DC*

The purpose of this study was to develop and evaluate 3D MR high-resolution myelographic (3D HRM) protocols and to determine their role in clinical imaging. Eight hundred forty-three patients were imaged with 1.0-T and 1.5-T Siemens SP imagers. Three-dimensional HRM studies were performed with either a True FISP or RARE ROAST pulse sequence. Data were processed with a maximum-intensity projection algorithm. Continuous 1-mm multiplanar reconstructions were also obtained. The intradural pathologies evaluated included postoperative arachnoiditis ($n$ = 18), intradural tumor ($n$ = 14), spinal cord arterioventricular malformation ($n$ = 2), diastematomyelia ($n$ = 2), and syrinx ($n$ = 4). The majority of cases involved extradural pathology such as herniation and stenosis, but also included a wide variety of other lesions such as synovial cyst. The sequences were frequently helpful in clarifying asymmetric disk bulge/herniation by depicting direct compression of nerve roots, thereby reducing the number of equivocal cases and increasing accuracy. The ability to visualize individual nerve roots was especially helpful in diagnosing arachnoiditis. An extremely important use for this procedure is the evaluation of spinal stenosis, in which there is frequently a generalized prominence of soft tissue. The 3D anatomic display can clarify the levels of significant stenosis. 3D HRM is brief, reproducible, and easy to interpret, and is complementary to conventional MR examinations of the spine. The procedure is particularly useful in the evaluation of arachnoiditis and stenosis. Its short imaging time of 4 min allows 3D HRM to be a useful adjunct in the evaluation of spinal disease.

211 • 10:54 AM

### MR Imaging Appearance of Os Odontoideum in Skeletal Dysplasia

JL Sherman*, SE Kopits†
**MRI of Colorado, Colorado Springs; University of Colorado, Denver; and †International Center for Skeletal Dysplasia, Towson, Md*

Os odontoideum is the most common odontoid anomaly and represents either a failure in development and fusion of the primary or secondary ossification center of the odontoid or the sequelae of trauma to the odontoid in early childhood (1–3). It is most often recognized as an isolated abnormality. The purpose of this study was to determine the occurrence of os odontoideum in patients with skeletal dysplasia and to compare the MR imaging appearance of isolated os odontoideum with that of os odontoideum in patients with skeletal dysplasia. Flexion/extension sagittal MR imaging was performed in 80 patients with skeletal dysplasia. Five different skeletal dysplasia syndromes, including mucopolysaccharidosis, spondylometaphyseal dysplasia, metatropic dysplasia, pseudoachondroplasia, and Conradi disease, were identified in eight patients with os odontoideum. There were signs of myelopathy in five cases and of C1-2 instability in all cases. In addition, there were marked differences in the shape of the odontoid process and arch of C1, depending on the underlying disease process. The defect in the odontoid process, however, was similar in location. It is concluded that patients with skeletal dysplasia are more likely to develop os odontoideum than are healthy individuals and are therefore subject to increased risk of subluxation, with acute or chronic myelopathy.

1. Fielding JW, Mensinger RN, Hawkins RJ. Os odontoideum. J Bone Joint Surg 1980; 62A:376–383. 2. Hensinger RN, Fielding JW, Hawkins RJ. Congenital anomalies of the odontoid process. Orthop Clin North Am 1978; 9:901–912. 3. Michaels L, Prevost MJ, Crang DF. Pathological changes in a case of os odontoideum (separate odontoid process). J Bone Joint Surg 1969; 50A:965–972.

212 • 11:06 AM

### Clinical Evaluation of the GEMS Technique in the Spine

JL Sherman, PM Pattany, DH Jarvis
*MRI of Colorado/Tesla Imaging Corp, Colorado Springs*

The gradient-echo, multi-spin-echo GEMS sequence is designed with the first echo as a TE16 gradient echo, and at TE/2 (45 msec) a 180° RF pulse is applied to form a spin echo at TE (90 msec). This technique eliminates the need to apply an extra 180° RF pulse, and the second echo is compensated up to the third order (pulsatility) of motion. With a TR of 2,000 msec, the excitation RF pulse applied for the gradient echo is 150°. This makes it possible to obtain high T2 contrast at the second echo. The den-

sity-weighted gradient-echo technique is recognized as useful in showing cortical bone margins, ligaments, cartilage, gas, and water. The standard SE 2,000/20–90 multiecho technique was compared with the GEMS 2,000/GE16-SE90 technique. All images were acquired with identical section thickness, signal averages, and field of view. Ten volunteers and 20 patients were studied with both techniques with 0.5-T and 1.5-T Picker MR imagers. The images were evaluated for the presence of pathologic abnormalities, artifacts, anatomic detail, and tissue contrast. It was found that the GEMS technique more clearly depicted the margins of intervertebral disks. Spinal nerve roots were more easily identified. Gas in degenerative disks was easily recognized on the gradient-echo images but poorly depicted on the density-weighted spin-echo images.

213 • 11:18 AM

### Sagittal Spin-Echo versus Gradient-Echo Imaging of the Lumbar Spine: A Prospective Study

TW Twiford, Jr, JW Yeakley, LA Kramer
*University of Texas Health Science Center at Houston*

While MR imaging with axial T1-weighted (T1W) and proton-density–weighted (PDW) sequences combined with sagittal T1W and T2-weighted (T2W) sequences has been prospectively shown to be equivalent to CT and myelography in the evaluation of lumbar canal stenosis and herniated disk disease, the sensitivity and specificity of modifications to this protocol remain largely unproved. This study was performed to test the hypothesis that gradient T2*W sagittal sequences can replace T2W and PDW spin-echo (SE) sagittal sequences without compromising diagnostic sensitivity. To prove this hypothesis, 50 consecutive patients were prospectively imaged with—in addition to the standard lumbar protocol of T1W axial—gradient T2*W axial and sagittal SE (T2W and PDW) sequences, and an additional T2*W gradient sequence. The results of the examinations with PD/T2W SE and T2*W sagittal sequences were separated, numbered, randomized, and independently reevaluated by three trained radiologists for evidence of disease. For each pulse sequence a form was completed, grading the severity of intranuclear disease, desiccation, ligamentous hypertrophy, spinal stenosis, herniation, foraminal stenosis, and osteophyte formation at all intervertebral interspaces. The evaluations of both pulse sequences were statistically compared for each patient to determine sensitivity of gradient T2*W sagittal sequences compared with that of PD/T2W SE sagittal sequences in detecting disease. The results of this study indicate that T2*W gradient sagittal sequences are as sensitive in the detection of lumbar disk herniation as are PD/T2W SE sequences; however, T2*W gradient pulse sequences, show significant limitation in the detection of canal stenosis and intranuclear disease compared with SE sequences.

214 • 11:30 AM

### Comparison Study of MR Imaging, Myelography, and CT-Myelography in the Diagnosis of Disk Herniation and Spinal Stenosis

KL Gupta, AM Righi
*Department of Radiology, Tulane University Medical Center, New Orleans*

MR imaging, myelography, and CT-myelography were compared in the diagnosis of herniated nucleus pulposus (HNP) and spinal stenosis. The sensitivity and specificity of these techniques were analyzed alone and in various combinations. A retrospective evaluation of 57 patients (119 levels with 59 surgical explorations) was used. All patients underwent all three tests, and each set of results was read blindly by two neuroradiologists without knowledge of the clinical presentation. Surgical operative notes were reviewed for confirmation and comparison of the results. Forty-seven patients (70 levels) were evaluated for HNP. MR imaging demonstrated a sensitivity of 71.4%; myelography, 59.3%; CT-myelography, 77.8%; myelography with CT-myelography, 76.4%; CT-myelography with MR imaging, 74%; MR imaging with myelography, 72%; and all techniques combined, 68%. Specificity was 73% for MR imaging, 89.2% for myelography, 73% for CT-myelography, 82% for myelography with CT-myelography, 74% for CT-myelography with MR imaging, 82% for myelography with MR imaging, and 79% for all techniques combined. Twenty-eight patients (47 levels) were evaluated for spinal stenosis. Sensitivity was 87% for MR imaging and CT, 82% for myelography, 81% for myelography with CT-myelography, 87% for MR imaging with CT-myelography, 85% for MR imaging with myelography, and 85% for all combined. Specificity was 75% for MR imaging, 87% for myelography, 75% for CT-myelography, 81% for myelography with CT-myelography, 75% for MR imaging with CT-myelography, 81% for MR imaging with myelography, and 79% for all combined. MR imaging, CT, and myelography remain complementary in the evaluation of HNP and spinal stenosis.

215 • 11:42 AM

### Tumors of the Larynx and Hypopharynx: Prospective Correlative Study with MR Imaging, Endoscopy, and Pathology

T Vogl, W Steger, G Grevers, J Lissner
*Department of Radiology, University of Munich, Germany*

The purpose of this study was to create a distinct scheme for the different examination techniques for laryngeal and hypopharyngeal tumors, and to improve the specificity of the MR imaging findings by elucidating certain ways of tumor infiltration and the different tumor appearances with various pulse sequences and after Gd-DTPA application, and to correlate the result with endoscopic and pathologic findings. Fifty-five patients with laryngeal and hypopharyngeal carcinomas and various benign laryngeal lesions were examined with a 1.5-T Magnetom. T1- and T2-weighted sequences in different section orientations and in combination with Gd-DTPA were used routinely. The carcinomas were classified according to the TNM system and the results correlated with the primary endoscopic classification and with the final pathologic findings. MR imaging allowed an exact diagnosis in 87% of all laryngeal and hypopharyngeal tumor patients; only carcinomas staged T1 were either overestimated or overlooked in most cases. In cases of lymph node involvement, sensitivity reached 82%, and in 85% the classification of either a metastatic or inflammatory infected lymph node or a primary lymphoma was correct. Endoscopic examination provided excellent information about the morphologic structure of the tumors and depicted 96% of all T1-classified tumors, but demonstrated a lower specificity in higher-classification carcinomas than did MR imaging. By combining these two methods, an overall accuracy of 98% could be achieved. MR imaging yielded the best results with long and short sequences; however, the value of plain and contrast-enhanced T1-weighted sequences was greater than that of T2-weighted sequences. In conclusion, current diagnostic strategy for the diagnosis of laryngeal tumors consists of a primary endoscopic examination in combination with MR imaging with Gd-DTPA. An exact classification of laryngeal carcinomas or an exact description of location and extent of benign laryngeal lesions is usually achieved with this strategy.

216 • 11:54 AM

### Carcinomas of the Floor of the Mouth: Staging with US and MR Imaging

R Bruening, D Hueltenschmidt*, M Naegele, M Reiser
*Departments of Radiology and *Oral Surgery, University of Bonn, Germany*

In this study the diagnostic values of percutaneous ultrasound and MR imaging for staging infiltration into the diaphragma oris were compared. The results were compared with the intraoperative situs. Ultrasound was performed with 7.5-MHz equipment. MR images (1.5 T, Gyroscan; Philips), both plain and enhanced with Gd-DTPA (0.1 mmol/kg), were obtained in the transverse and coronal planes. The images were interpreted independently by three radiologists. Twenty-one patients were included in the study. Ultrasound provided sufficient delineation of infiltration of the genioglossus and the mylohyoid muscle. With respect to tumor spread crossing the midline, US could not achieve high predictive value. MR imaging without Gd-DTPA led to overestimation of tumor size in some cases. After injection of Gd-DTPA, staging correlated well with intraoperative findings. MR imaging was superior to US especially in the detection of tumor spread across the midline. In conclusion, MR imaging is superior to US in preoperative staging, and there is good correlation with operative findings.

## Wednesday Morning
## Sutton Parlor South
## Papers 217–224

## ABDOMEN

MODERATORS: PL Davis, MD • PY Poon, MD

217 • 10:30 AM

### Differential Diagnosis and Follow-up of Pediatric Renal Masses in MR Imaging and MR Angiography

T Pfluger, T Vogl, A Jassoy, M Kellner, A Muntau, J Lissner
*Radiologische Klinik Innenstadt der Universität München, Germany*

Differentiation between Wilm tumors and other abdominal masses is necessary in establishing indication for preoperative chemotherapy according to the SIOP 9 protocol. To optimize therapy planning, exact staging and follow-up examinations are indispensable. The value of MR imaging and MR angiography in this context is discussed. In a prospective study, 38 MR examinations were performed in 25 patients. All examinations were performed with intravenous application of Gd-DTPA. In 10 cases, Gd-DTPA was administered postoperatively, and in 12 cases MR angiography was performed. Histologic findings revealed unilateral nephroblastoma in eight cases, bilateral nephroblastoma in four cases, nephroblastomatosis in four cases, neuroblastoma in five cases, focal dysplastic lesions associated with Drash syndrome in one case, and, in one case each, a pheochromocytoma, a rhabdomyosarcoma, and a hepatoblastoma. Both the tumor capsule and the perirenal fat tissue were clearly delineated in all cases. In the five cases involving nephroblastomatosis or Drash syndrome, MR was more sensitive in detecting small lesions than was CT or sonography. In 80% of all cases, there was no abnormality of the abdominal vasculature. In 20% of cases, compression of the inferior vena cava with development of collaterals was found. At follow-up examination a reduction in tumor mass was detected in 90% of cases, and in 10% a progression was evident. In two cases, hemorrhage was observed during chemotherapy. In two other cases, venous MR angiography made it possible to visualize resumption of vena cava flow in response to chemotherapy. It has been shown that MR imaging and MR angiography are superior to the other imaging modalities in locating small lesions and evaluating extent of tumor spread for the determination of biopsy sites and the planning of operative strategy. This series demonstrated that MR angiography and MR imaging with intravenous and oral application of Gd-DTPA are the modalities of choice for appropriate therapy planning and follow-up examinations.

218 • 10:42 AM

### Gd-DTPA–enhanced MR Imaging in the Evaluation of Extracranial Masses in Children

RB Dietrich, AK Goyal, MT Schrader, K Yan, WG Bradley, Jr
*Department of Radiological Sciences, University of California, Irvine*

Although there are now early studies defining the role of Gd-DTPA–enhanced images in the evaluation of extracranial pathology in adults, their use in evaluating pediatric mass lesions has yet to be determined. Twenty-five MR imaging studies obtained in 19 children with suspected mass lesions were retrospectively reviewed. The ages of the patients (10 female, 9 male) ranged from 1 day to 16 years (mean, 6.3 years). Eleven studies were performed at initial presentation and 14 following treatment with surgery and/or chemotherapy. Multiplanar T1W and T2W images were obtained initially in all cases with a 1.5-T imager. Additional T1W images were also obtained following Gd-DTPA administration. All images were reviewed by three authors, and post-Gd-DTPA images were compared with both pre-Gd-DTPA T1W and T2W images. Following administration of Gd-DTPA, (*a*) 21 of 21 lesions enhanced, although this was minimal in three lesions; (*b*) the full extent of tumor was better appreciated in 12 of 21 lesions; and (*c*) there was increased confidence in diagnosis in 4 of 25 cases. In no case did administration of Gd-DTPA change the suspected diagnosis or treatment; in one case, however, post-Gd-DTPA findings confused the diagnosis. Gd-DTPA–enhanced images may provide additional useful information in selected cases and may clarify specific issues, such as exact extent of involvement of adjacent organs and relationship of tumors to the kidney in renal/perirenal lesions.

219 • 10:54 AM

### Adrenal Cortical Adenomas: Diagnosis with Chemical Shift MR Imaging

DG Mitchell, M Cruvella, TE Matteucci
*Department of Radiology, Jefferson Medical College of Thomas Jefferson University, Philadelphia*

MR spectroscopic/histologic correlation has revealed that lipid signals are common in adrenal cortical adenomas but absent in malignant lesions (1). It was hypothesized that chemical shift imaging might allow identification of lipid in cortical adenomas, distinguishing them from malignant lesions. More than 80% of upper abdominal MR imaging examinations conducted over the past 3 years included chemical-shift–sensitive sequences. These consisted of fat suppression and/or a T1-weighted sequence with the phases of fat and water signal opposed (OP). Initially, spin-echo OP images were obtained by offsetting the timing of the 180° refocusing pulse relative to the gradient-refocused echo. More recently, a multisection spoiled gradient-echo sequence (TR = 80–140 msec, flip angle = 90°) with TE = 2.3 msec has been used, which approximates an OP image. These images were compared with conventional in-phase (IP) images to document presence of tissue lipid. T2-weighted images (SE = 2,500/100)

were also obtained. Cases involving adrenal masses were selected retrospectively from dictated reports. Fat was considered present if the signal intensity of the adrenal relative to liver or muscle was less on OP than on IP images. Determination of lesion benignancy or malignancy was based on presence or absence of growth, or a lack of malignancy diagnosed after 1 year. Of 16 adrenal masses, nine contained evidence of fat at MR imaging. All nine of these masses were benign. In seven lesions, MR imaging did not depict fat; six of these lesions were malignant. All lesions had higher signal intensity than did liver on T2-weighted images. It is known that fat is present in adrenal cortical adenomas and myelolipomas but absent in malignant lesions. This retrospective study indicates that simple comparison of IP with OP or fat-suppressed images allows the diagnosis of cortical adenoma in many cases, potentially obviating biopsy and aggressive follow-up. A larger prospective study is now needed.

1. Leroy-Willig A, Roucayrol JC, Luton JP, et al. In vitro adrenal cortex lesions characterization by NMR spectroscopy. Magn Reson Imaging 1987; 5:339–344.

220 • 11:06 AM

## MR Imaging of Gastrinomas

IM Feuerstein, R Gupta, J Norton, R Jensen, M Cannon, J O'Niell, JL Doppman

*National Institutes of Health, Bethesda, Md*

The hypothesis of this research was that MR imaging can be clinically useful in the detection of gastrinomas (gastrin-secreting islet cell tumors). A secondary educational purpose was to demonstrate the imaging appearance of gastrinomas with different pulse sequences. Comparison was made with CT in all instances. Nineteen patients were prospectively evaluated with MR imaging and CT. All patients underwent exploratory laparotomy. The images were retrospectively reviewed by a blinded reader who was unaware of the results of surgery or of the other studies. MR imaging was performed at 0.5 T with T1-weighted, T2-weighted spin-echo, and STIR sequences. Surgery identified 23 lesions in the 19 patients. MR imaging helped identify gastrinomas in 13 patients (68%). Thirteen of 23 tumors (57%) were detected, with sizes ranging from 0.8 to 5.5 cm. Fifteen lesions (65%) were pancreatic, five (22%) duodenal, two (9%) in porta hepatis, and one (4%) in the greater omentum. Sensitivity of pancreatic, duodenal, and porta/omental lesions was 67%, 0%, and 100%, respectively. STIR sequences were the most sensitive and showed the highest lesion conspicuity. T1-weighted sequences were intermediate in sensitivity, and T2-weighted sequences were by far the least sensitive. It is believed that MR imaging, particularly with the STIR sequence, is useful in detecting extraduodenal gastrinomas. To date, no imaging modality can satisfactorily detect small duodenal gastrinomas.

221 • 11:18 AM

## MR Imaging of Malignant Tumors of the Pancreas

RF Thoeni, NK Do, P Shyn

*University of California, San Francisco*

T1- and T2-weighted spin-echo sequences without fat saturation (T1- and T2-SE) were prospectively compared with T1 and T2 SE with fat saturation (T1- and T2-SE fatsat) and with gradient-echo sequences before and after injection of gadopentetate dimeglumine to assess their respective values in diagnosing malignant tumors of the pancreas. Sixteen patients with clinically suspected pancreatic malignancy were examined with a 1.5-T GE Signa imager with SE sequences (TR = 550–600, TE = 12–20; TR = 2,000–250, TE = 30/80–100) with and without fat saturation. GRE (GRASS or spoiled GRASS, TR = 50–100, TE = 13–15, flip angle = 40°–70°) and T1-SE images were obtained before and after injection of gadolinium. Of the 16 patients with suspected pancreatic tumors, 10 had an adenocarcinoma, two had metastatic disease, and four had a normal pancreas. Proof was obtained with surgery in two patients, with biopsy in 11, and with at least two follow-up CT studies over a period of 1½ years in four patients. The tumors measured from 2 to 10 cm in diameter. All 12 proved that adenocarcinomas were correctly identified with MR imaging; however, one patient without pancreatic tumor was misdiagnosed as having a small lesion. The remaining three normal pancreas glands were correctly assessed. T1-SE fatsat best showed the lesions (11/12), and in only one case did GRE with gadolinium alone enable diagnosis of the lesion (a small tumor). T2-SE fatsat was superior to T2-SE in 15 cases. On the basis of contrast difference between tumor and normal parenchyma, the tumor was identified on GRE images without gadolinium in only two instances. In conclusion, MR imaging with T1-SE fatsat is a promising technique for the detection of pancreatic tumors (sensitivity, 91.6%), and GRE with gadolinium is needed only if initial results are equivocal. MR imaging may prove to be an important diagnostic tool, particularly if oral contrast material becomes available.

222 • 11:30 AM

## Use of Nutritional Supplement Formula as a Gastrointestinal Contrast Agent for MR Imaging

SA Mirowitz, N Susman

*Jewish Hospital, Washington University School of Medicine, St Louis*

A method for enhancing the gastrointestinal tract on abdominal MR images is desirable in order to allow differentiation of stomach and/or bowel from normal or pathologic tissues. The practicability of using nutritional supplement formula as a gastrointestinal contrast agent was investigated. Nutritional supplement formula (350–800 mL, Ensure Plus; Ross Laboratories) was administered orally to 12 patients undergoing abdominal MR imaging. Bowel enhancement was evaluated in these patients with conventional T1- and T2-weighted pulse sequences with a 1.5-T imager, and the properties of this material were studied in a phantom model. Excellent enhancement of the stomach was achieved on all T1- and T2-weighted images. This allowed improved delineation of the pancreatic tail and gastric wall. Enhancement of the small bowel and colon was not as intense or consistent. The mechanism of contrast enhancement with this agent is related to the paramagnetic trace elements, oil emulsion, and corn syrup that it contains. This material has been used extensively for many years and has an established record for safety and patient tolerance. Nutritional supplement formula represents a simple, inexpensive, readily available, and effective means of enhancing the upper gastrointestinal tract on MR images.

223 • 11:42 AM

## Contrast Enhancement of the Gastrointestinal Tract on MR Images with Intravenous Gd-DTPA

SA Mirowitz

*Jewish Hospital, Washington University School of Medicine, St Louis*

The purpose of this study was to evaluate whether use of intravenous gadopentetate dimeglumine would result in contrast enhancement of the normal gastrointestinal tract. Gadopentetate dimeglumine was intravenously administered in 17 consecutive patients without known gastrointestinal diseases who were undergoing abdominal

MR imaging. T1-weighted and fat-suppressed T1-weighted (TR = 400–600, TE = 11–15) images were acquired with a 1.5-T imager before and after slow intravenous administration of 0.1 mmol/kg gadopentetate dimeglumine. The stomach, small bowel, and colon were analyzed for the presence and relative intensity of contrast enhancement. Diffuse enhancement of the gastrointestinal tract wall was observed in all patients following contrast material administration. Enhancement appeared diffuse throughout collapsed segments of the gastrointestinal tract and was most conspicuous on fat-suppressed T1-weighted images. Such enhancement was usually most apparent in the small bowel and least apparent in the stomach. This study demonstrates that enhancement of the normal gastrointestinal tract occurs routinely when intravenous gadopentetate dimeglumine is administered. Furthermore, it suggests the potential usefulness of intravenous as opposed to orally administered contrast agents in providing enhancement of the gastrointestinal tract on MR images.

224 • 11:54 AM

### Dynamic Enhanced MR Imaging of the Kidneys and Adrenal Glands with TurboFLASH

D Schnapf, G Laub, A Bogdan, D Wilson
*York Imaging Center, Siemens Medical Systems, Iselin, NJ, and Georgetown University School of Medicine, Washington, DC*

The purpose of this study was to establish protocols and evaluate the efficacy of dynamic enhanced MR imaging of the kidneys and adrenal glands with TurboFLASH. Thirty-seven patients were imaged with 1.0-T and 1.5-T Siemens SP imagers. Following a bolus injection of gadolinium, TurboFLASH images were obtained at the rate of one image per second (TE = 3 msec, TR = 6 msec). Total imaging time was less than 1 min. The examination successfully detected 2 of 2 adrenal tumors that were not well evaluated with CT or ultrasound. Six benign cysts and six renal tumors were studied. Dynamic images were helpful in evaluating neoplastic spread to the liver, vena cava, and lungs. Although the results are preliminary, the ability of dynamic TurboFLASH imaging to assess a variety of renal and adrenal pathologies is encouraging. Physiologic information may be useful in further assessing the presence of renal vascular hypertension. The examination is performed rapidly and is not degraded by motion. Dynamic TurboFLASH imaging can be a useful adjunct to routine MR imaging in selected cases.

## Wednesday Morning
## Regent Parlor
## Papers 225–232

## IMAGE PROCESSING

MODERATORS: LP Clarke, PhD • JL Duerk, PhD

225 • 10:30 AM

### Applications of Three-dimensional MR Imaging in Neurosurgery and Neuroscience

TM Peters, AC Evans, DL Collins, CJ Henri, TS Marrett
*Montreal Neurological Institute, McGill University, Montreal*

Stereotactic neurosurgery is becoming a popular means of approaching deep-seated lesions in the brain, and 3D MR imaging techniques are being used for image guidance to the target point. In addition, neuroscience investigators increasingly rely on the correlation of physiologic information from positron emission tomography (PET) with anatomy obtained from MR imaging. For neurosurgical procedures, 3D MR images obtained under stereotactic conditions are correlated with vascular information obtained either from stereoscopic digital subtraction angiography or from MR angiography. The resulting 3D data sets are presented to the user as stereoscopic volume-rendered images that can be manipulated both as part of the surgical planning exercise and during surgery itself. Such techniques allow stereotactic surgery to be performed for deep brain lesions with a minimum of invasion of critical structures or vessels. For the study of functional pathways in the brain, image volumes obtained from PET are registered with the corresponding 3D MR volumes with an algorithm that determines the optimum fit between homologous points from each volume. Image volumes are also transformed into a standard coordinate space that allows patient studies from a given population to be compared objectively. For quantitative analysis of correlated data, a computerized 3D brain atlas has been constructed from the manual segmentation of 63 2-mm MR sections. This atlas contains 120 anatomic and functional structures and may be customized to fit individual patients, allowing measurements of regional anatomy or physiology on either a serial basis for individual patients, or across a patient population.

226 • 4:09 PM

### Multiple-Thin-Slab Time-of-Flight MR Angiography: Postprocessing with Vessel Tracking Algorithms

W Lin†, TJ Masaryk*, JA Tkach*, EM Haacke†
**The Cleveland Clinic Foundation and †University Hospitals of Cleveland*

Three-dimensional time-of-flight (TOF) MR angiography is clinically advantageous in part because of short acquisition times. Nevertheless, drawbacks include spin saturation and available maximum-intensity postprocessing algorithms that limit vascular contrast to a relatively confined region of interest. The purpose of this study was to combine and compare conventional 3D TOF acquisition parameters with a multiple-thin-slab technique used in conjunction with a vessel tracking algorithm. Fifteen subjects (10 healthy volunteers and 5 patients with suspected vascular disease) formed the study group. All studies were performed with a 1.5-T Magnetom 63 SP system. Single-slab and dual-slab 3D TOF acquisitions were performed through the circle of Willis and intracranial circulation (40/7/1/192–256). Each volume acquisition consisted of 64 sections, each 1 mm thick. The dual-slab acquisition used 25%–50% overlap between the two volumes. The data sets were subsequently postprocessed with both the standard maximum-intensity projection algorithm and a vessel tracking/connectivity algorithm. The vessel tracking algorithm was modified from the method of Pelc, implementing an adaptive rather than constant threshold. Seed points were manually selected, with signal threshold established on the basis of two standard deviations above local (perivascular) stationary tissue mean signal intensity. A 3 × 3 × 3 kernel centered at the seed point was then used to check the 26 surrounding points. If a neighbor pixel had a signal intensity higher than the threshold, this point was classified as vascular and the coordinates of the point stored in a buffer file. Once all 26 neighbor pixels were checked, a set of coordinates from the buffer was retrieved as a new seed point. Multiple iterations of this process were performed until all pixels in the 3D volume had been checked. Compared with conventional single-volume or dual-volume 3D TOF studies postprocessed with the maximum-intensity projection algorithm alone, the two-slab technique postprocessed with the vessel connectivity algorithm demonstrated significantly improved vascular contrast over the conventional TOF studies.

While there was some exaggeration of artifact secondary to flow void at the carotid siphons, small artery detail was significantly improved. In conclusion, the combination of increased contrast through the use of dual thin-slab acquisitions with improved flow-related enhancement, as well as reduced background signal intensity through the use of the vessel tracking algorithm, significantly improves the quality of 3DFT TOF MR angiography. By slightly shortening the TR and using a rectangular field of view, it is possible to acquire both of the thin slabs in a time frame comparable with that of conventional single-volume 3DFT studies.

227 • 10:54 AM

## Brain Volume Measurement with Scatter Plot Analysis in HIV Infection

M Paley*, I Wilkinson*, K Chong†, M Hall-Craggs†
*Department of Physics and Bioengineering, University College of London, and †Department of Radiology, Middlesex Hospital, London

Scatter plot analysis has recently been used by several groups for rapid segmentation of tissues. A two-dimensional histogram of pixel intensities from a dual-echo image is formed on which tissues cluster into defined regions. By counting the number of pixels in the cluster and comparing that figure with the total number of pixels in the section, a measure of brain volume can be obtained from the known section volume. This method is being used in the measurement of brain tissue volumes in a cohort of approximately 100 asymptomatic HIV seropositive and seronegative volunteers and patients suffering from AIDS or AIDS-related complex. The cohort are being followed at 6-month intervals. A 30-section contiguous dual-echo TE 20/90 sequence covering the entire brain and cerebellum has been used (TR, 3,500 msec; section thickness, 5 mm) with a Siemens 1.5-T Magnetom SP imager. Data sets are transferred to a Sun Sparcstation 2 for offline analysis. A number of algorithms have been investigated for fully automatic segmentation, including dual thresholding, contouring, and statistical sampling. The effects of sequence parameter choice and machine stability have been studied. Measurements of ventricular and total cerebrospinal fluid (CSF), as well as of gray matter, white matter, lesion, and total brain volume, have been performed in 25 cohort patients to date, representing the first time point in the follow-up sequence. Twelve ward patients have also been examined and show marked increase in ventricular and total CSF volumes compared with the cohort, as well as large reductions in white matter volume due to progressive multifocal leukoencephalopathy, toxoplasmosis, or other causes.

228 • 11:06 AM

## Multidimensional Tissue Characterization of Primary Brain Tumors with MR Imaging

DN Kennedy, HJ Aronen, JW Belliveau, I Goldberg, RC McKinstry, AJ Fischman, N Alpert, R Lindgood, M Gruber, F Hochberg, BR Rosen
*Departments of Neurology and Radiology, MGH-NMR Center, Massachusetts General Hospital, Charlestown, Mass*

MR imaging is an intrinsically multidimensional technique. Images reflecting T1, T2, and proton density are conventionally produced. Recent developments in functional imaging with high-speed MR imaging permit the extension of this dimensionality to include diffusion (D) and cerebral blood volume (CBV). Furthermore, image data from other imaging modalities, after registration, also extend the dimensionality of characterizable tissue parameters (ie, MR spectroscopy, SPECT, positron emission tomography [PET]). Seven patients with primary brain tumors were studied prior to treatment with a protocol that included T1- (pre- and postcontrast agent), T2-, and proton-density–weighted MR images, construction of D and CBV maps, and a PET FDG study. Each image data set was registered and a voxel-by-voxel and regional evaluation of each parameter performed. Thus, each voxel or region had a characteristic "fingerprint" in these seven parametric dimensions. Regional analysis was performed for normal gray and white matter, cerebrospinal fluid, and tumor. An example is provided in the Table for one of the tumor regions evaluated in this study. Since many of the lesions were heterogeneous, cluster analysis could be performed on the region within the lesion to define domains of tumor tissue displaying differing characteristics. Finally, correlation and covariance analysis was performed among the various image characteristics observed in each region. The possibility of synergistically combining information to reflect various tissue parameters may increase tissue specificity in the evaluation of primary human gliomas.

| T1Pre | T1Post | PD | T2 | D | rCBV | FDG |
|---|---|---|---|---|---|---|
| − | − | + | + | + | +0− | +0− |

+ = image intensity higher than normal
0 = image intensity normal
− = image intensity lower than normal

229 • 11:18 AM

## Quantitative MR Imaging of Excitotoxic Lesions in Rats

AR Guimaraes, D Borsook, CA Miller, MR Prakash, DN Kennedy, S Hyman, RG González
*MGH-NMR Center and Center for Imaging and Pharmaceutical Research, Department of Radiology and Molecular Neurobiology Laboratory, Neuroscience Center, Massachusetts General Hospital, Charlestown, Mass*

Kainate (KA), a rigid analog of glutamate, is a potent excitotoxin that produces well-characterized lesions in the rat brain. It has been shown that MR imaging provides valuable information regarding lesion characterization and accurate quantitative measures of lesion volume and ventricular and total brain volume, previously unattainable with noninvasive means. Unilateral lesions of the right corpus striatum were made in male Sprague-Dawley rats (250 g) with 0.2 and 4 μg of KA. Weekly images of the brain were acquired at 4.7 T for 5 weeks following injection. Control and 0.2-μg doses caused no abnormal changes on T2-weighted MR images. Lesion and ventricular volumes were accurately determined with morphometric analysis software developed at the laboratory. One week postinjection, the lesion volume was 136.03 μL, and decreased by 10% to 120 μL over the next 4 weeks. This was attributed to a decrease in the edema induced by the lesion. Measurement of ventricular volumes showed an increase of approximately 400% in absolute ipsilateral ventricular volume from week 1 to week 4, indicative of a high degree of focal atrophy induced by the lesion. Yet the contralateral ventricle showed a less dramatic increase in absolute volume (~200%) over the same time period. This supports the claim of generalized atrophic conditions in the contralateral hemisphere induced by the neurotoxin. In conclusion, a noninvasive, quantitative MR imag-

ing method for determining the structural extent of brain damage has been developed. The method provides an accurate measurement of lesion volume and atrophic change induced by excitotoxin administration.

230 • 11:30 AM

### Three-dimensional Heart Wall Motion Reconstructed with SPAMM

AA Young, C-N Chang, L Axel
*Department of Radiology, University of Pennsylvania, Philadelphia*

Herein is presented a method for reconstructing the 3D motion and deformation of the left ventricle (LV) with MR image tagging. Five short-axis and five long-axis (LA) images were acquired at five phases of the cardiac cycle between end-diastole and end-systole. Spatial modulation of magnetization (SPAMM) was used to produce two orthogonal sets of tagging planes. Inner and outer contours of the LV were determined manually, and the intersections of tagging planes were tracked with the aid of a SPAMM image analysis package. The 3D motion was reconstructed with the aid of a deformable model of the LV, consisting of an ensemble of 16 finite elements. The undeformed configuration of the model was defined by fitting surfaces to the initial contours of the LV. The reconstructed 3D motions of the intersections were used to fit the deformation from the initial state to each of the four deformed states. The method was tested on simulated data from an incompressible cylinder and applied to data acquired from seven healthy volunteers. A number of kinematic parameters were extracted at various points. Displacement increased uniformly from apex to base (4.7 mm ± 2.9 near the anterior apex to 15.7 mm ± 1.5 near the posterior base). Rotation about the LA increased from base to apex (−2.3° ± 2.1° near the lateral base to 24.2° ± 11.9° near the lateral apex). The direction of greatest shortening was aligned approximately with the subepicardial fibers in all midventricular regions, while the direction of greatest lengthening was approximately radial. The main limitation of the method is the present sparseness of data. This situation will improve with increasing image resolution, decreasing stripe spacing, longer persistence of the tags, and shorter image acquisition times.

231 • 11:42 AM

### Wavelet Analysis for MR Image Segmentation

D Kruchten*, J Chang*, A Kadik*, T Vullo†, PT Cahill*†
**Polytechnic University, Brooklyn, and †New York Hospital, New York, NY*

Area and volume determinations from radiologic images are of interest in the evaluation of neurologic diseases, such as hydrocephalus, multiple sclerosis, and schizophrenia. In this study, the use of wavelet analysis to segment the cerebral ventricles was evaluated and compared with two other independent manual methods. MR images often contain strong fluctuations in signal intensity caused in part by nonuniformities in RF coils, eddy currents, and motion artifacts. An optimal image segmentation (IS) method should be fast, independent of signal intensity, operator independent, and insensitive to noise and motion artifacts. Eight-echo (TR/TE = 2,150/33) MR images were acquired at 0.6 T with a section thickness of 7.5 mm and were analyzed for a number of individual studies. Images of the ventricular areas were obtained with a region of interest on a CRT terminal, as well as a graphic tablet, by three observers. Wavelet analysis of each image was achieved by (*a*) using an antisymmetric seven-coefficient analyzing wavelet to compute the nonorthogonal dyadic wavelet transform as defined by Mallat, and (*b*) linking the local extrema of the wavelet transform across scales as well as between nearest neighbor extrema within scales. Computer processing time with a Sun Sparc workstation was approximately 1 min per image. Analysis of the resulting borders of the ventricles showed that, on average, only 1% to 2% of the edge pixels were not identified. Left and right ventricular cross-sectional areas derived from wavelet analysis agreed to better than 4.5% with those derived from the manual methods, which had an operator variability of 5.2%. In conclusion, the results of this study show that, when applied to MR images, wavelet analysis potentially meets the above criteria for an efficient IS algorithm.

232 • 10:42 AM

### Clinical Evaluation of a Three-dimensional Surgical Planning Technique for Brain Tumors

JL Sherman*, DJ Sceats†, PM Pattany*, DH Jarvis*, N Palmer†
**MRI of Colorado, †Colorado Springs Neurological Associates, and ‡Picker International, Highland Heights, Ohio*

The short TE 3DFT RF-spoiled fast sequence is a robust technique that produces high-resolution, heavily T1-weighted images resistant to motion and magnetic susceptibility artifact. The image data can be very quickly and practically manipulated, reprocessed, and displayed. Cerebral surface anatomy, 3D brain models, vascular models, computer-generated surgical "cutaways," and standard 2D images can be generated from one data set acquired in 8–12 min. The routine usefulness of the 3D image data in the clinical practice of neurosurgeons was evaluated. Twenty patients with brain tumors were studied. All patients were studied with the RF-spoiled 3D fast technique in addition to the standard spin-echo techniques. The 3D image data were manipulated on the ViStar (Ardent Titan III) medical imaging supercomputer. The 3D image manipulation facilitated understanding of the exact anatomic relations of brain tumors to adjacent normal structures. Cortical lesions could be localized to specific gyri with the surface mapping technique. External landmarks could be precisely correlated with tumor location by overlaying 2D multiplanar and 3D surface-rendered images. Surface-rendered images with progressive removal of surface features in simulated surgical postures were helpful in determining the appropriate surgical approach. Determination of the relation of brain tumors to the major cerebral arteries and dural venous sinuses was helpful and obviated the need for conventional angiography. The 3D manipulations were most useful in cases involving small tumors, in which the goal was to minimize surgical exposure of the brain. Interactive manipulation of the 3D image data by the radiologist and neurosurgeon together was more useful than when performed separately.

## Wednesday Morning
## Murray Hill Suite
## Papers 233–240

# RELAXOMETRY AND EXPERIMENTAL CONTRAST AGENTS

MODERATORS: PA Hardy, PhD • RL Nunnally, PhD

233 • 10:30 AM

### Comparison of Quantitative MR Imaging and Xeromammographic Textural Analysis for Characterizing Features Related to Breast Cancer Risk

CS Poon, MJ Bronskill, M Ilzuka, J Byng, MJ Yaffe, NF Boyd, PY Poon

*Sunnybrook Health Science Centre, Ontario Cancer Institute, St. Michael's Hospital, and University of Toronto, Toronto*

Mammographic dysplasia is one of the most important risk factors for breast cancer. Quantitative characterization of the features associated with mammographic dysplasia may lead to a more objective and reliable estimation of the risk, with significant implications for screening and the management of high-risk populations. In this study, quantitative MR imaging techniques were compared with textural analysis of xeromammograms with respect to the characterization of features associated with mammographic dysplasia. The study included 10 patients with Wolfe pattern DY and 7 with pattern N1. Mammograms of the DY breasts were ranked in order of decreasing density by two experienced radiologists. The MR imaging studies included measurement of relative water content of the whole breast, and T1- and T2-weighted imaging of a single 10-mm coronal section midway between the chest wall and nipple. T2 pixel histograms for DY breasts indicated two peaks corresponding to fat and fibroglandular tissue, and the fourth moment about the fat peak was calculated. For xeromammographic textural analysis, the mean, standard deviation, skewness, kurtosis, and fractal dimension were calculated over the breast portion of the digitized images. Relative water content, T1, and T2 moment were significantly different for DY and N1 breasts ($P < .0001$). Relative water content for all DY breasts was >40%, while that for all N1 breasts was <40%. Relative water content and T1 also correlated well with the ranking of mammograms in order of decreasing dysplasia. Only standard deviation from xeromammographic textural analysis showed a significant difference between DY and N1 breasts ($P < .015$), but with considerable overlap. No definite correlation between the results from textural analysis and rank of dysplasia was observed. In general, quantitative MR imaging is superior to xeromammographic textural analysis in objectively distinguishing DY from N1 breast parenchymal patterns.

234 • 10:42 AM

### Fast T1 Measurements with TurboFLASH

U Stöber, E Rummeny, C Eissing, P Vassallo, W Müller-Warmuth, PE Peters

*Department of Radiology and Physical Chemistry, University of Muenster, Germany*

Signal behavior for TurboFLASH (TF) imaging with a 180° preparation pulse is strongly T1-weighted because of the inversion-recovery (IR) mechanism. The accuracy of T1 measurements with application of this sequence in stationary and flowing phantoms and in volunteers and patients was evaluated. T1 measurements were tested for accuracy with phantoms of various $MnCl_2$ concentrations (T1 = 270–3,300 msec). For clinical evaluation, 10 healthy volunteers and 24 patients with known focal liver disease were examined with the same protocol. All measurements were performed with a 1.5-T imaging system (Magnetom, Siemens). Ten single-section-mode TF sequences with 128 selective 8° pulses were used for data acquisition (TR = 7 msec, TE = 4 msec) of a 128 × 128 image matrix. Time delay between inversion pulse and readout pulse varied from 0 to 4,000 msec. Mean signal intensities were obtained from regions of interest and fitted to the absolute value of an IR curve with a nonlinear least-squares fit. Signal intensities from phantoms correlated well with the fitted function for monoexponential relaxation. T1 as estimated with TF measurements showed a regular underestimation compared with spectroscopic T1 values of the stationary and slow-flowing phantoms. With application of a linear calibration factor, accuracy could be improved to 4%. For phantoms with flow rates comparable with blood flow rates, no calibration factor was needed. In vivo measurements in volunteers and patients showed that T1 values obtained with TF imaging are comparable with those provided by time-consuming spin-echo techniques. Therefore, TF imaging can be used for fast T1 evaluation in a clinical setting.

235 • 10:54 AM

### Mask Technique for Robust Volume of Interest Localization

SJ Graham, MJ Bronskill

*Sunnybrook Health Science Centre, University of Toronto, Toronto*

Determination of multiple T2 relaxation components in vivo may provide additional tissue-specific information beyond current MR imaging capabilities. Signal-to-noise ratio and number of echoes sampled with conventional imaging protocols are insufficient, however, for detailed multicomponent T2 relaxation analysis. Therefore a robust "mask" localization technique has been developed that, when implemented prior to a CPMG or CPFH sequence of hard pulses, provides accurate multicomponent T2 estimates within a small volume of interest (VOI). The mask technique has been implemented initially in a single dimension. One acquisition uses a cosine-sinc pulse and gradient spoiling to saturate magnetization outside the VOI. A second acquisition incorporates an additional sinc pulse to saturate the intended VOI, thereby producing a mask of the residual longitudinal magnetization outside the VOI. Subtraction of these acquisitions produces a signal from the VOI only. Theoretical calculations indicate that the mask technique is significantly more sensitive in measuring multicomponent T2 relaxation than is current MR imaging. The performance of the mask technique has been assessed with a GE 1.5-T clinical MR imager, and VOI widths of less than 1 cm are easily obtained with as little as 1% signal contamination from outside the VOI. Measurements indicate low sensitivity to fat/water chemical shift and inhomogeneous $B_0$ and $B_1$ fields. Accurate localized bicomponent T2 estimates have also been demonstrated. These results indicate a robust localization technique that could improve the diagnostic capability of MR relaxation time measurements.

236 • 11:06 AM

### In Vitro MR Study of Collagen in Human Aortic Wall

P Vinée, B Meurer, A Constantinesco

*Department of Radiology, Uni-Klinik, Freiburg, Germany, and CRM-EAHP and CHU Hautepierre, Strasbourg, France*

The H-1 wide-line line shape of human aortic walls ($n = 12$) was analyzed in native state and after histologically controlled lysis of either collagen (formic acid) or

elastin (trypsin) to identify the line-shape components. H-1 MR in vitro measurements were performed at 60 MHz. Ninety-degree pulses of 4-μsec duration were repeated every 7 T1s for quantitative measurements. The signal was digitized at two sampling rates: 5 MHz for the faster and 50 kHz for the slower decaying component. This allowed simultaneous recording of water and soluble, mobile spins. T1 was measured with inversion recovery. The recorded free induction decay (FID) signals were fitted with an exponential for the slow decay and a gaussian for the beginning of the signal (fast-decaying component). The gaussian time constant $T_{2F}$ of the fast-decaying component provided a measure of the line-shape second moment $M_2$ (Van Vleck), which is simply related to the mean pair distances of hydrogen atoms $i$ and $j$ in the investigated sample. Knowledge of the crystal positions of collagen made possible a reliable estimation of theoretical $M_2$, which could then be calculated. Histologic examination after selective lysis and FID curves clearly permits attribution of the fast component to tissue collagen. Mean measured $M_2$ of collagen is 3.68 $G^2$, and calculated theoretical $M_2$ is 10.2 $G^2$. A rotational reduction of this theoretical value to make it agree with the measured one, taking into account that the motion is fast compared with inverse linewidth, is easily achieved with the equation, $M_{2exper} = M_{2theor} \times (3\cos^2\Phi - 1)/2$. Calculation gives $\Phi = 42°$, which agrees well with the former C-13 and deuterium MR observations. This result complements the description of collagen in tissue, previously formulated only with multinuclear MR studies in tendons in tediously labeled specimens.

237 • 11:18 AM

## MR Microscopy of Ozone-Injured Lung

L Hedlund, GA Johnson, JD Crapo, LY Chang, G Cofer
*Duke University Medical Center, Durham, NC*

The lungs of ozone-exposed rats were imaged to determine if MR microscopy could be used to detect this type of inhalational injury. Fisher 344 rats were exposed to 1 ppm ozone 12 hours a day for 7 days. At 1 to 9 days after exposure, the rats were anesthetized with halothane and imaged in vivo with a 2-T CSI system (GE). Three single 2-mm-thick sections were obtained with a CPMG sequence with 8 echoes (8–64 msec) and a bird-cage coil 6 cm in diameter. Imaging was cardiac gated and breathing was image synchronous. TR was about 2 sec and in-plane resolution was 150 μm. T2 images were calculated pixel by pixel with a least-squares method. Regions of interest were then sampled from areas on the axial images free of major vessels or airways. Lung injury was found to be subtle in most rats, with relatively little difference between means and control. Analysis of frequency histograms of T2 values, however, consistently showed shifts to the longer T2s in the injured lung (Figure). In one example, there were significant shifts of T2 to longer values, and spin-echo images from the injured animal clearly showed areas of high signal in both lungs. Although preliminary, these observations suggest that frequency histogram analysis of pulmonary T2s may be useful in detecting and characterizing inhalational injury due to ozone in the rat.

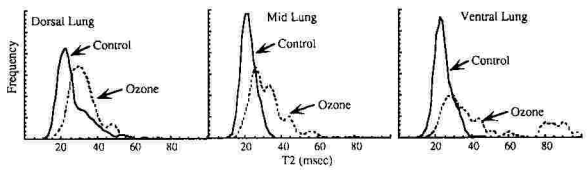


238 • 11:30 AM

## Alternative Approach to Measuring T2* in Trabecular Bone

JC Ford, FW Wehrli
*Department of Radiology, Hospital of the University of Pennsylvania, Philadelphia*

During the past two years a method for assessing trabecular density on the basis of a measurement of MR line broadening has been developed and evaluated in healthy volunteers and patients with osteoporosis. The method is based on fitting the region-of-interest signal measured as a function of echo time to an interferogram that requires a multiparameter curve fit. In this study a simplified data collection and analysis protocol was developed that greatly reduces the number of data samples and fitting parameters. Instead of being taken every millisecond (to satisfy the Nyquist criterion), samples were simply taken at the time points where fat and water (the marrow constituents) are in phase—in practice, 4–5 TE values (Figure)—and the data fit to a single exponential decay. This is possible as long as the modulation frequency Δf (fat/water chemical shift difference) is subject-invariant. The fat/water phase difference ($\Delta\phi_0$) at TE = 0 must also be subject-invariant to obtain images at in-phase TE values, ensuring an optimum signal-to-noise ratio (SNR). An analysis of 16 subjects yielded $\Delta f = 215$ Hz ± 9 and $\Delta\phi_0 = 27° \pm 11°$. Analysis of simulated data (fat/water ratio = 0.375, T2* = 22 msec, chemical shift difference = 215 Hz, 57% gaussian noise) yielded T2* values of 22.8 ± 2.0 and 21.7 ± 1.8 msec for the abbreviated and complete protocol, respectively. While of course the true T2* cannot be ascertained in vivo for validation purposes, a comparison of the data in three subjects showed considerably lower standard deviation among the five lumbar vertebral bodies for the new abbreviated protocol (Table). Application of the abbreviated protocol in 16 healthy female subjects resulted in an age-related T2* increase of 0.08 msec/year, in good agreement with the full protocol, which yielded an increase of 0.09 msec/year. Finally, this new approach should be superior to suppression of one of the spectral components, since it provides the full SNR.

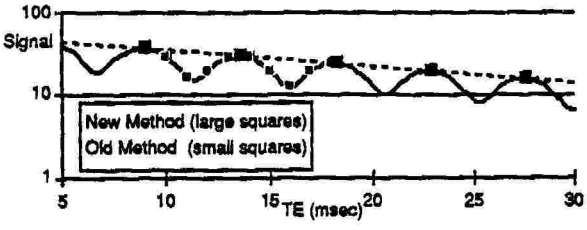


| Subject | Abbreviated Protocol | Full Protocol |
|---|---|---|
| 1 | 15.5 ± 1.4 | 17.3 ± 6.3 |
| 2 | 14.3 ± 0.8 | 19.7 ± 3.5 |
| 3 | 14.6 ± 1.1 | 19.4 ± 4.4 |

239 • 11:42 AM

## Gastric, Pancreatic, and Renal Enhancement with the MR Imaging Contrast Agent Mn-DPDP

MK Sidhu, HH Muller, DL Rubin, SW Young
*Department of Radiology, Stanford University School of Medicine, Stanford, Calif*

The purpose of this study was to evaluate extrahepatic enhancement caused by Mn-DPDP. Twenty-four patients were divided equally into four dose groups (3, 5, 8, and 10 μmol/kg Mn-DPDP via intravenous infusion) and imaged

pre- and postcontrast. Abdominal imaging was performed with a 1.5-T imager. Regions of interest were measured in normal gastric mucosa, pancreas, renal cortex, and renal medulla on precontrast and 5-min postcontrast T1-weighted images. Enhancement was defined as percent change in signal intensity, standardized to background, from pre- to postcontrast. Mean postcontrast enhancement for the four indicated doses respectively was as follows: gastric mucosa: 8%, 43%, 43%, and 66%; pancreas: 50%, 31%, 63%, and 58%; renal cortex: 38%, 50%, 61%, and 60%; and renal medulla: 8%, 23%, 32%, and 32%. Enhancement was statistically significant ($P < .05$) for all organs at doses of 8 and 10 μmol/kg, for stomach and pancreas only at 5 μmol/kg, and for no organs at 3 μmol/kg. In conclusion, Mn-DPDP causes statistically significant enhancement of the gastric mucosa, pancreas, and kidneys at doses of 8 and 10 μmol/kg. In addition to its use in hepatic imaging, this agent may prove useful in the detection of gastric, pancreatic, and renal pathology.

240 • 11:54 AM

### Mn-DPDP—enhanced MR Imaging of Pancreatitis

Y Baba, BP Kreft, MM Lerch, A Tanimoto, AK Saluja, ML Steer, DD Stark

*Departments of Radiology and Surgery, Massachusetts General Hospital, and Beth Israel Hospital, Harvard Medical School, Boston*

The diagnostic potential of the cell-specific contrast agent Mn-DPDP in pancreatic disease was studied with ex vivo relaxometry in an experimental model of acute pancreatitis. The pancreatitis was induced in rats with intravenous infusion of caerulein (5 μg/kg/h), a model that parallels the histologic and serologic features of acute pancreatitis in humans. Tissue relaxation times of controls and of animals with pancreatitis were measured at 10 MHz before and 1 hour after administration of Mn-DPDP (20 μmol/kg) and correlated with histology, water content, and serum amylase levels. T1 and T2 values in animals with pancreatitis were 84% and 109% higher, respectively, than in the controls, and showed excellent correlation ($r = .9$; $P < .01$) with tissue water content. Serum amylase levels in pancreatitis rose by 88%. Light microscopy and electron microscopy revealed changes characteristic of early pancreatitis. Mn-DPDP decreased the T1 (31%) and T2 (9%) values of normal pancreas significantly ($P < .01$). In animals with pancreatitis, no significant enhancement was detected, indicating reduced Mn-DPDP uptake. Reduced enhancement with Mn-DPDP in pancreatitis might provide the basis for new pancreatic imaging methods.

## Wednesday Afternoon
## Sutton Parlor North
## Papers 241–248

## RAPID IMAGING

MODERATORS: D Flamig, MD • J Listerud, PhD, MD

241 • 2:45 PM

### Two-Echo IR-RARE Imaging with Alternating Echo Times

JN Rydberg, SJ Riederer

*MR Laboratory, Mayo Clinic and Foundation, Rochester, Minn*

Fast spin-echo or RARE imaging has shown promise for reducing acquisition time for T2-weighted images. The use of such techniques for T1-weighted imaging, however, can cause reduction in small-object contrast. The objective of this work was to incorporate two echoes into an inversion-recovery (IR) acquisition for the purpose of improving T1-weighted imaging. TR/TI values were maintained at 2,000/700 msec, with the first and second echoes acquired at 18 and 36 msec, respectively. Traditional RARE view order echo assignments change TE slowly with view number, causing an intrinsic low-pass or high-pass filter effect depending on the desired effective TE. For this work the two echoes were assigned in an alternating fashion to view number. The net filter can be expressed as a uniform (desired) response plus a high-frequency modulation that causes ghosts at ±FOV/2. With extended FOV, these ghosts can be discarded. Results indicate that 192 × 256 two-echo IR-RARE (effective TE ≈ 27 msec) has a 30% better contrast-to-noise ratio (C/N) for corpus callosum to thalamus and a 50% better C/N for cerebellar gray-to-white matter when compared with 192 × 256 two-excitation partial-saturation spin echo (TR/TE = 500/11 msec). Image data acquisition times and section counts were comparable (IR-RARE, 3:35 with 11 sections; spin echo, 3:14 with 12 sections). It is concluded that RARE techniques with alternating echo assignments show promise for improved T1-weighted imaging with present imaging times.

242 • 2:57 PM

### Optimization of T2-weighted Turbo Spin Echo in Breath-Hold Imaging

JJ van Vaals, GH van Yperen

*Philips Medical Systems, Best, the Netherlands*

A fast T2-weighted imaging method called Turbo Spin Echo (TSE) has recently been developed on the basis of the MEMS (1) and RARE (2) methods. TSE was optimized to allow T2 imaging within a short breath-hold period. With the TSE method a number of profiles (called the Turbo Factor) are acquired per excitation. To perform T2-weighted imaging (TR ≈ 2 seconds) in a single breath hold, a large Turbo Factor is required to limit the imaging time per section. In the implementation of TSE any value for the Turbo Factor can be used, with an echo spacing as short as 12 msec. This in combination with reduced matrix, half-scan, and selectable profile ordering allows for optimum matching of the examination parameters to the required TE within the shortest imaging time. Clinical examples will be shown of abdominal studies in which 10–16 sections were acquired in 20–30 seconds. Typically, a 200 × 256 matrix size is acquired with half-scan. The Turbo Factor, usually 30–35, and the profile order are adapted to match an effective echo time of typically 80–150 msec. This allows imaging of a single section in 4–5 times TR. Obviously, the multiple-section technique was used to measure as many as five sections in that same period. Thus far, T2-weighted imaging in the abdomen has always been hampered by motion artifacts. With the described protocol, which allows large Turbo Factors, short echo spacing, half-scan, and optimized profile order, it is now possible to obtain high-quality TSE images with strong T2 contrast within a breath-hold period of 10 seconds or less.

1. Mehlkopf AF, van der Meulen P, Smidt J. Magn Reson Med 1984; 1:295–297. 2. Hennig J, Nauerth A, Friedburg H. Magn Reson Med 1986; 3:823–833.

243 • 3:09 PM

### Rapid and Restricted One-dimensional Spectroscopic Imaging Performed with a RARE—Inner Volume Imaging Combination

K Oshio, RV Mulkern*

*Radiology Departments, Brigham and Women's Hospital and *The Children's Hospital, Boston*

Rapid acquisition with relaxation enhancement (RARE) sequences were recently used to quickly generate one-di-

mensional chemical shift images (1D CSIs) of selected sections by reading out phase-encoded echoes in the absence of a frequency-encoding gradient. A 128 × 256 (spatial × spectral) matrix with a 16-Hz/pixel spectral resolution was generated in only 64 sec with a 2-sec TR. Of course the resulting spectra come from columns spanning the entire section, leading to heterogeneous tissue contributions to the spectra. This problem can be solved by applying a second phase-encode gradient orthogonal to the first to generate 2D CSIs, the disadvantage being prolonged imaging times. Alternatively, one can maintain the high speed of the 1D CSI acquisition while restricting the lengths of the interrogated columns by making the 180° refocusing pulses selective to a plane orthogonal to the plane excited by the initial 90° excitation pulse. Such an inner-volume imaging spectroscopic RARE sequence was implemented with a 1.5-T Signa imager (GE Medical Systems, Milwaukee), and 128 spectra were generated from 5 × 5 × 1-mm voxels in only 64 sec. The technique is conveniently applied to rapidly acquire spectra from voxels within bone marrow. The spectra are of suitable quality for fat/water peak area quantification and form the basis for quantitative bone marrow cellularity measurements. This rapid method provides a marked increase in spatial coverage and resolution compared with that offered by the single-voxel spectroscopic approaches that have already proved so useful in measuring bone marrow cellularity in patients with hematologic disorders.

244 • 3:21 PM

## STIR-like Images Obtained with Snapshot GRASS with Centric Phase-Encoding Ordering

NG Campeau, AE Holsinger-Bampton, SJ Riederer
*Magnetic Resonance Research Lab, Mayo Clinic, Rochester, Minn*

Short TI inversion recovery (STIR) is a sequence that provides increased signal from increases in both T1 and T2, which characterize most pathology. Unfortunately, STIR sequences are time-consuming, often requiring 10 min or more. The purpose of this work was to determine whether STIR-like images could be obtained with magnetization-prepared gradient-echo techniques. The sequence under consideration used a 180° contrast preparation pulse followed by a short TR gradient-echo readout sequence with centric ordering of phase-encoding views. Sequence parameters were studied to optimize STIR-like contrast in the abdomen (nulled fat and bright lesions against a gray liver signal). The mechanisms producing this contrast were studied with a computer model that numerically solved the Bloch equations repeatedly. A short TI of 50 to 150 msec provides images with STIR-like contrast. Fat can be effectively suppressed with a TI of 50 msec. An entire section may be imaged within a single breath hold, in less than 9 seconds (256 phase encodes, 2 excitations). The desired increased signal from tissues with increased T1 and T2 is reversed by the readout, and it is important to acquire the low-frequency portions of k space prior to this reversal. Results were verified with phantoms, and in healthy subjects by using the liver-spleen contrast difference as a model for liver pathology. Excellent breath-hold images of the liver, free of motion artifact, were obtained with a phased-array multicoil that provided an increased signal-to-noise ratio.

245 • 3:33 PM

## Partial-Angle Inversion-Recovery Imaging: Spin-Echo and Snapshot Implementation

S Vinitski, DG Mitchell, TA Tasciyan, HV Ortega, FB Mohamed, S Albert*
*Thomas Jefferson University Hospital and Jefferson Medical College, Philadelphia, and *Beth Israel Medical Center, New York, NY*

It has been shown that the use of short TI spin-echo inversion-recovery (IR) imaging can increase combined T1 and T2 contrast. Unfortunately the TI interval needed to suppress the fat signal is usually too short (100–150 msec) to be used in the interleave mode. This results in a significant loss in the number of imaging planes compared with the spin-echo technique with identical TR and TE. Furthermore, use of the TurboFLASH technique with the preparatory RF pulse applied a few hundred milliseconds before the start of data acquisition, coupled with k-space segmentation (1), also limits the number of available imaging planes during breath hold. The effects of varying the inversion RF pulse flip angle on image contrast and imaging time in both IR spin-echo and TurboFLASH imaging (theoretically) were investigated in phantoms and healthy volunteers. Signal intensity in an IR pulse sequence as a function of excitation and inversion flip angles was calculated from the solution to the Bloch equations (2) and was used to determine the contrast behavior of a lesion/liver model. Imaging experiments were performed with a 1.5-T Signa GE imager. Theoretical and experimental results were consistent with one another. Reducing or increasing the inversion pulse from 180° resulted in the shorter TI needed to null the signal from the tissue of interest, some decrease in contrast-to-noise ratio (C/N), and substantial increase in the number of imaging planes per given TR in spin-echo or within breath hold in TurboFLASH imaging. Since MR imaging of large organs such as liver is characterized by a high signal-to-noise ratio and C/N, as well as the need to increase the number of imaging planes, this technique was applied to MR imaging of the upper abdomen. In conventional TurboFLASH imaging of the upper abdomen, a TI of 500 msec and four segments were used to null the spleen signal. By changing the TI from 500 to 250 msec and the inversion RF pulse from 180° to 115°, however, it was possible to increase the number of imaging sections during breath hold by as much as 50%, while the liver/spleen C/N was decreased by only 25%. Furthermore, to improve the useful duty cycle, the remaining dead time during the TI interval was used to introduce a selective-excitation fat suppression scheme. In short TI IR imaging (TR/TE = 1,500/60 msec) it was possible to maintain fat signal suppression by changing the inversion RF pulse from 180° to 115° and TI from 130 msec to 65 msec. Although spleen/liver C/N dropped by 37%, this allowed the number of imaging planes to be increased from 8 to 12. In conclusion, the use of partial-inversion RF pulses in IR imaging can reduce imaging time and/or increase the number of imaging planes, but at some expense to C/N.

1. Edelman RR, Hahn PF, Buxton R, et al. Radiology 1987; 161:125–131. 2. Vinitski S, Griffey RH. JMRI 1991; 1:451–456.

246 • 3:45 PM

## A New Selective Prepulse For Fat-suppressed TurboFLASH

Jintong Mao, W Dean Bidgood, Jr
*Department of Radiology, University of Florida, Gainesville*

TurboFLASH can acquire a high-resolution (eg, 128 × 256) image in less than 1 second. In this technique, all the phase-encoding lines are acquired after a single 180° prepulse that is used to control image contrast. The 180° pre-

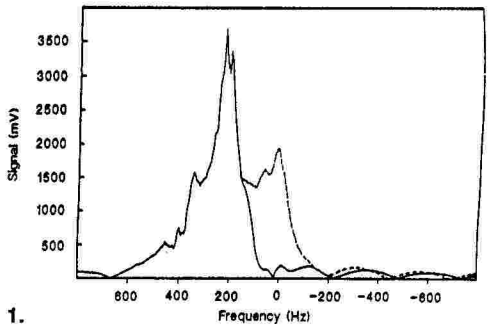


1.

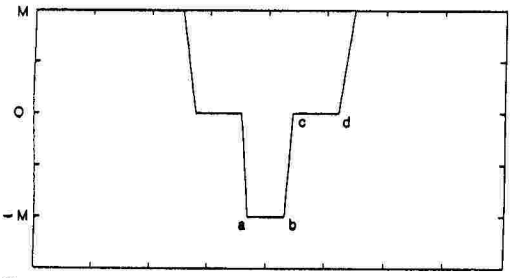


2.

pulse can be replaced by a selective presaturation pulse that is used to saturate the fat signal. The goal of this study was to introduce a single selective pulse that would excite the water signal to 180° and the fat signal to 90° simultaneously. The image contrast can be controlled by the timing of the 180° component, with the fat component suppressed by a dephasing gradient, so that a fat-suppressed TurboFLASH image is obtained. A spectrum of the abdomen of a volunteer is shown in Figure 1. The water (solid line) and fat (dashed line) peaks are inhomogeneously broadened due to susceptibility effects. An ideal response profile is shown in Figure 2. The above goal can be reached if the broadened water peak is matched to the a-b section and the broadened fat peak to the c-d section of the ideal profile simultaneously. The ideal profile cannot be realized but can be approximated by an optimized profile. An initial trial pulse for optimization is obtained by applying a Fourier tranform to the ideal profile. The conjugate gradient method is used to optimize the pulse. The optimized selective pulse that excites the water signal to 180° and the fat signal to 90° simultaneously has been obtained, and the investigation of application of this pulse to the TurboFLASH sequence is under way.

247 • 3:57 PM

## Single-Breath-Hold Quantitative Flow Imaging with Phase-Encode Grouping

MS NessAiver
*Picker International, Highland Heights, Ohio*

Phase-encode grouping (PEG) has been shown to allow the acquisition of up to 16 frame cines during a single breath hold. It has been demonstrated that accurate estimates of blood flow in the heart and major vessels at eight points in the cardiac cycle can also be obtained in a single breath hold by interleaving the reference and sensitized data acquisitions. A phase-encode group typically requires on the order of 50 msec to acquire some portion of k space for a given image. Because blood velocities in the heart and major vessels can change significantly during that time, interleaving the reference and sensitized acquisitions between groups would result in a large error. A technique was implemented whereby the corresponding reference and sensitized views were interleaved within a group so that the temporal displacement of corresponding views was less than 13 msec. Hence, a single reference/sensitized group required 100 msec, allowing 6 to 8 frames to be acquired in volunteers and patients with heart rates between 60 and 85 beats per min. Additional points in the cardiac cycle could be measured by repeating the imaging with varying delays after the R-wave trigger. Flow velocities measured in a single breath hold correlated well with measurements obtained with more traditional flow imaging methods, taken at the same point in time in the cardiac cycle as were the central phase-encode views of the PEG method. Examples will be shown in the heart and major vessels of healthy volunteers and patients with valve abnormalities.

248 • 4:09 PM

## Contrast-prepared Rapid Imaging: Improved Efficiency and Image Quality

AEH Bampton*, SJ Riederer†
**Department of Radiology, McGuire VAMC, Richmond, Va, and †MR Laboratory, Mayo Clinic, Rochester, Minn*

Signal-to-noise ratio (SNR), contrast, resolution, imaging times, and efficiency are important issues in rapid abdominal imaging. Used with centric view order, averaging, and a phased-array coil, magnetization-prepared rapid gradient-echo imaging provides abdominal images with 256 × 256 resolution and higher T1-weighted contrast and SNR than that of spin-echo images, without motion artifact. The averaging technique requires one shot per data set and a pause between shots for recovery, so a two-average image is acquired in approximately 8 seconds. With the pause between shots for interleaving, two images can be acquired in 12 seconds. The phase-offset multiplanar (POMP) technique can be used to double imaging efficiency while maintaining image quality. POMP was used to acquire two sections with two averages. Because the required 512 phase encodings are too many to follow a single preparation phase, they were divided such that each half of k space was acquired in one shot. The centric approach was maintained by incrementing the phase encodings from lowest to highest spatial frequency for each shot. A reasonably uniform inversion across both sections was obtained by increasing the inversion slab thickness significantly. Lastly, part of the RF phase modulation was performed by the receiver rather than the transmitter to prevent phase errors in the transient magnetization. The magnetization-prepared rapid POMP images are similar in quality to normally averaged images. The SNR is slightly different, perhaps caused by phase errors and the inversion slab profile. The SNR difference is reduced somewhat by using a nonselective inversion. When POMP and interleaving are combined, four images can be acquired in 12 seconds. In this way, high-quality images of the entire liver can be obtained in three 12-second breath holds.

## Wednesday Afternoon
## Sutton Parlor Center
## Papers 249–256

### BRAIN/ORBIT

MODERATORS: BD Pressman, MD
WTC Yuh, MD, MSEE

249 • 2:45 PM

**Active Disease Burden in Multiple Sclerosis Measured by Volume or Number of GD-DTPA–enhancing Lesions at MR Imaging**

L Stone, ME Smith, M Armstrong, R Martin, D McFarlin, H McFarland, JA Frank

*Neuroimmunology Branch, National Institutes of Health, Bethesda, Md, and Georgetown University Medical Center, Washington, DC*

Lesions detected with Gd-DTPA–enhanced MR imaging appear and disappear without concurrent changes in expanded disability status scores (EDSS) or clinically measurable exacerbations in patients with early relapsing remitting multiple sclerosis MS (RRMS). This study examined blood-brain barrier disruption observed on serial Gd-DTPA–enhanced MR images as a measure of disease activity in MS patients by determination of lesion volume and number. Ten patients with early RRMS were imaged monthly for up to 28 months at 1.5 T with T2-weighted and pre- and post-Gd-DTPA infusion (0.1 mmol/kg) T1-weighted (SE 600/20) spin-echo images with 5-mm contiguous sections. Gd-DTPA–enhancing lesions were counted. Total enhancing lesion volumes were calculated with Analyze software (Mayo Foundation). Monthly neurologic examinations were used to determine EDSS scores. A total of 228 Gd-DTPA MR images were obtained. Of the 562 total lesions, 518 (92%) were considered new, as the lesions rarely persisted over 2 months. Although 23 exacerbations occurred, EDSS scores returned to baseline by the end of the study (2.63 ± 1.69 vs 2.68 ± 1.72). A cyclical increase and decrease in volume and number of enhancing lesions was observed in some patients. The factors affecting the exacerbations and remissions of disease in RRMS patients are not understood, but these studies allow insight into the natural history of disease processes with or without clinical exacerbations. Additionally, the measurement of lesion number and volume may provide a quantitative tool for determining efficacy of therapeutic interventions in drug trials.

250 • 2:57 PM

**Clinical Use of Magnetization Transfer Inversion-Recovery Sequences**

CJ Baudouin, JV Hajnal*, A Oatridge, IR Young*, GM Bydder

*NMR Unit, Royal Postgraduate Medical School, Hammersmith Hospital, and *Picker International, London*

The application of off-resonance RF pulses results in a reduction of both available longitudinal magnetization and observed T1 in tissues that undergo magnetization transfer (MT). Most imaging sequences used to date have primarily exploited the reduction in available magnetization. In this study, the use of MT sequences that are also sensitive to the reduction in T1 was investigated. Imaging was performed at 0.15 T. Values for the reduction in available magnetization and T1 were obtained in normal tissues in volunteers by using spin-echo sequences with variable-duration off-resonance RF pulses. Twenty patients (19 adults, 1 neonate) with intracranial lesions (12 neoplastic, 5 infarcts, 3 other) were imaged with inversion-recovery and mildly T2-weighted spin-echo sequences with and without a saturating pulse. The TI of the inversion-recovery sequence was varied from 100 to 500 msec. Shorter TI inversion-recovery sequences with additional RF (TI = 100 or 180 msec) pulses showed markedly improved lesion conspicuity in tumors and infarction. In four patients the addition of saturating pulses to medium TI (TI = 500 msec) inversion-recovery sequences resulted in increased lesion contrast in visualization of subacute hemorrhage. In conclusion, lesion conspicuity can be markedly improved with use of off-resonance pulses. Inversion-recovery MT sequences can produce very high contrast in a variety of brain lesions.

251 • 3:09 PM

**Embolization of Arteriovenous Malformations: MR Imaging, MR Angiography, and MR Flow Studies**

JC Böck, HP Molsen, B Sander, J Haustein, W Schörner, R Felix

*Strahlenklinik und Poliklinik, Universitätsklinikum Rudolf Virchow, Berlin*

Interventional embolization alone or followed by surgery or irradiation is an accepted treatment for intracranial arteriovenous malformations (AVMs). Frequently, multiple embolizations have to be performed until complete occlusion or significant reduction of the vascular bed of the malformation is obtained. The possibility of recanalization and recruitment mandates multiple, possibly noninvasive, follow-up studies such as MR imaging (MRI) and MR angiography (MRA). MR blood flow studies (MRF) have not yet been used in the evaluation of the perfused vascular bed of AVMs. The aim of this study was to demonstrate the usefulness of MRI, MRA, and MRF in postembolization follow-up studies. Seven patients with AVM were studied before and repeatedly after embolization. Proton-density-, T2-, and T1-weighted images were obtained, followed by time-of-flight MRA. During and after intravenous injection of 0.1 mmol/kg Gd-DTPA, fast T2*-weighted images (MRF) were acquired, followed by post-contrast T1-weighted imaging. MRI, MRA, and MRF were complementary in their demonstration of the effect of embolization, which ranged from near complete to negligible. MRI demonstrated the reduction of the nidus size, MRA demonstrated reduction of flow effects in feeding and draining vessels as well as in the nidus, and MRF very sensitively depicted the decrease of the perfused microvascular bed. It is concluded that the combination of MRI, MRA, and MRF is a useful noninvasive diagnostic tool for follow-up studies after embolization of AVMs.

252 • 3:21 PM

**Intracranial Aneurysms: Evaluation with MR Angiography**

DJ Schnapf, EM Haacke, W Lin, G Laub, A Bogdan, D Wilson

*York Imaging Center, York, Pa; Case Western Reserve University, Cleveland; Georgetown University School of Medicine, Washington, DC; and Siemens Medical Systems*

The purpose of this study was to evaluate the efficacy and role of MR angiography (MRA) in the detection of intracranial aneurysms. Over 2,000 MRA studies of the head were performed with 1.0-T and 1.5-T Siemens SP imagers. A high-resolution 3D time-of-flight velocity-compensated asymmetric short-echo (7–8 msec) sequence was used with a 512 matrix and submillimeter voxel resolution. When rigid MRA aneurysm protocols were used, the detection rate for intracranial aneurysms was approximately 2.7% of the random population. When other techniques such as tumor MRA protocols were used, however, the rate of detection fell by more than 50% to 1.2% of the pop-

ulation imaged. Of the 37 aneurysms found in the series, 83% were 5 mm or less. Six patients were studied with aneurysm clips, and susceptibility artifacts were not found to be a problem in the detection of additional aneurysms. This prospective study indicates that protocols can be established to detect small intracranial aneurysms at levels consistent with published autopsy statistics. In the future, the traditional four-vessel conventional cerebral angiogram may become a highly specialized single-vessel examination.

253 • 3:33 PM

### MR Interferographic Examination of Brain Motion

J Hennig, K Wahkloo, FD Jüngling
*Radiology Clinic, University of Freiburg, Germany*

MR interferography with the GINSEST sequence allows the quantitative measurement of motion and has long been used in ECG-dependent heart wall motion studies. Since the experiment intrinsically allows arbitrary sensitization to motion, the sequence can also be used to examine the much slower effects produced by ECG-dependent brain motion. Brain motion is clearly demonstrated with bipolar sensitizing gradients of amplitude 10 mT/m and a duration of 35–60 msec. The experiment was performed in a multisection mode; typically, five images were acquired at different times during the ECG cycle. The most pronounced effects measured in a study of 22 healthy volunteers were downward motion of the brain stem on the arrival of the systolic pulse wave (100–150 msec after the R wave) and an elastic deformation of the cerebellum with concomitant downward motion. The corpus callosum demonstrated considerably more pulsatility than did the surrounding structures. The different structures of the central brain displayed remarkably independent motion patterns. Cerebrospinal fluid (CSF) motion was displayed by the experiment, as was brain motion. The time course of brain motion showed a very abrupt velocity peak corresponding to the arrival of the pulse wave, with little or no motion before or after; CSF motion appeared to be driven by brain motion but was present during the whole ECG cycle, with flow reversal during diastole in most parts of the CSF-filled spaces. Lateral motion was much weaker than craniocaudad motion and was observed primarily in the central brain and temporal lobes. Signal intensity variations attributable to anisotropic restricted diffusion as observed by Bydder were demonstrated on the interferographic images, a side effect of the strong motion sensitization necessary for the observance of lateral motion. Therefore, MR interferography is a versatile tool for measuring and separating IVIM and IVCM within a single experiment.

254 • 3:45 PM

### Role of Fat Suppression and Gd-DTPA in the MR Imaging Diagnosis of Malignant Tumors of the Eye

CF Gonzalez, P DePotter, A Flanders
*Department of Radiology, Thomas Jefferson University Hospital, Philadelphia*

The purpose of this study was to assess the ability of MR imaging with Gd-DPTA enhancement and fat suppression to identify malignant ocular tumors and differentiate them from retinal detachments and benign lesions. Sixty patients with pathologically proved intraocular tumors were studied with fat-suppressed, Gd-DPTA–enhanced T1- and T2-weighted spin-echo images. All studies were performed with a GE (Signa) 1.5-T unit. The patients were also studied with CT, high-resolution US, and color Doppler studies, and the results were correlated with those from MR imaging. MR imaging was useful in differentiating choroid melanoma from benign lesions such as choroidal hemangioma and subretinal effusions. It was not as useful as CT or US, however, in differentiating retinoblastoma from other closely related diseases such as Coat disease and toxocariasis. Differentiation between choroidal melanoma and intraocular metastatic lesions was best accomplished with Gd-DPTA–enhanced, fat-suppressed MR imaging, although this differentiation was not always possible. In conclusion, Gd-DPTA–enhanced studies in combination with fat-suppression techniques are useful in diagnosing malignant ocular lesions.

255 • 3:57 PM

### Enhanced MR Imaging, US, and Surgical Correlation of Orbital Tumors

KL Gupta, AM Righi, BG Haik
*Department of Radiology, Tulane University Medical Center, New Orleans*

Enhanced MR imaging was compared with US with respect to the imaging of orbital tumors. Ninety-seven orbital mass lesions were examined with MR imaging and US. Forty-two lesions had surgical correlation. Contrast-enhanced MR imaging demonstrated better soft-tissue contrast within the whole orbit, which facilitated specific diagnoses of hemorrhage, masses, and soft-tissue infiltration. Use of contrast material and additional gradient-echo pulse sequences facilitated and enhanced this evaluation. US was more sensitive for small lesions of 2 mm or less. One melanoma, two retinoblastomas, and accompanying subretinal fluid collections were detected only with US. Intracranial involvement and deeper portions of the retrobulbar area, however, were better evaluated with MR imaging. In conclusion, MR imaging and US are complementary in the evaluation of orbital tumors.

256 • 4:09 PM

### MR Imaging of the Head in Wegener Granulomatosis

H Koltze, C Muhle, R Asmus, RP Spielmann, G Dunker, B Nölle, A Beigel, WL Gross
*Department of Radiology of the Christian-Albrechts-University Kiel, Germany*

The purpose of this study was to evaluate diagnostic MR imaging criteria in Wegener granulomatosis of the head. Twenty-five patients with biopsy-proved Wegener granulomatosis were imaged with a Philips Gyroscan 1.5-T magnet. Axial T2-weighted (TR, 3,000 msec; TE, 20 msec; section thickness, 5–7 mm) and coronal T1-weighted images (TR, 400–650 msec; TE, 15–20 msec; section thickness, 5–7 mm) were acquired. Twelve patients were reexamined after intravenous injection of Gd-DTPA (0.1 mmol/kg) with T1-weighted sequences. Nine patients underwent additional CT. All 25 patients demonstrated abnormalities of the orbit, nasopharynx, oral cavity, paranasal sinuses, or cerebral tissues at MR imaging. Thickening of the linings of the nasal cavity, paranasal sinuses, ear, and mastoid cells was noted in 23 patients. Four patients had granulomas of the orbit, and six had granulomas of the paranasal sinuses. Increased signal intensity of the granulomas was noted after intravenous injection of Gd-DTPA in two of four patients. Bone erosion or destruction that was well seen at CT in three patients could not be identified with MR imaging. Macro- or microinfarction of the brain parenchyma was noted in eight patients. Wegener granulomas are characterized by loss of signal intensity on T1- and T2-weighted images. MR imaging is more sensitive in identifying and distinguishing granulomas from inflamed or thickened mucosa and tumor than is CT. Two of four granulomas showed partial signal enhancement after intravenous injection of Gd-DTPA. Eight of 25 patients had macro- or microinfarction of brain tissue. MR imaging

could not identify bone erosion or destruction with certainty and had to be supplemented with an additional CT examination.

## Wednesday Afternoon
## Sutton Parlor South
## Papers 257–264

## CHEST/PELVIS

MODERATORS: MJ Fulmer, MD • DH Sostman, MD

257 • 2:45 PM

### MR Imaging in the Evaluation of Carcinoma of the Cervix after Radiation Therapy

Z Campos, H Hricak, KG Bis
*Department of Radiology, University of California, San Francisco*

The purpose of this study was to assess the ability of MR imaging to differentiate between normal postirradiated cervix, residual or recurrent cervical cancer, and radiation tissue injuries with both unenhanced and contrast-enhanced imaging. Forty-two patients were divided into two groups: Group 1 ($n$ = 21) underwent MR imaging before and after radiation therapy (XRT); group 2 ($n$ = 21) underwent MR imaging only after XRT (6–8 months). Imaging was performed with a 1.5-T GE unit (unenhanced T1- and T2-weighted images and gadopentate dimeglumine–enhanced [0.1 mmol/kg] [CE] T1-weighted images). MR imaging findings were correlated with radiation dose, time after radiation, and histology ($n$ = 25) or clinical follow-up ($n$ = 17). Analysis of post-XRT images revealed similar accuracy in both groups and comparison with pretreatment images did not improve image interpretation. Complete tumor response was present in 21 patients, all of whom showed reconstitution of the cervical zonal anatomy on T2-weighted images. CE T1-weighted images showed diffuse cervical enhancement and failed to demonstrate reconstitution of the normal anatomy. Sixteen patients had bulky, residual, or recurrent disease; in general, MR imaging showed morphologic findings of tumor mass that demonstrated high signal intensity on T2-weighted images and heterogeneous enhancement with demonstration of necrosis on CE T1-weighted images. Five patients demonstrated an increased width and high signal intensity of the endocervical canal, with cervical stroma being normal or showing localized high signal intensity on T2-weighted images. Recurrent tumor could not be differentiated from radiation changes. Biopsy showed residual tumor in two patients and granulation tissue in three. In conclusion, unenhanced MR imaging demonstrated reconstitution of cervical zonal anatomy in patients with no recurrent disease and was helpful in detecting tumor recurrence when the tumor mass was greater than 2 cm in diameter. Contrast-enhanced images did not improve accuracy in evaluation. MR imaging was not able to differentiate between radiation changes and recurrent tumor; in this subgroup of patients, biopsy remains essential.

258 • 2:57 PM

### Seminal Vesicle Hemmorhage Simulating Tumor Invasion at Endorectal MR Imaging

SA Mirowitz
*Jewish Hospital, Washington University School of Medicine, St Louis*

The status of the seminal vesicles is of major importance in patients with prostatic carcinoma, as tumor involvement indicates a poorer prognosis and alters therapeutic options. The diagnosis of seminal vesicle invasion is based on observation of relative decreased signal intensity foci on T2-weighted MR images. Similar findings have been observed in the absence of tumor invasion in eight patients who underwent previous prostatic needle biopsy. Areas of abnormally decreased signal intensity were observed in the seminal vesicles of all patients at T2-weighted endorectal MR imaging. In 7 of 8 patients, foci of abnormally increased signal intensity were present on T1-weighted images. These foci were of variable location and extent, and usually did not follow the expected pattern of spread from the primary tumor site. Radical prostatectomy was performed in all patients and showed the seminal vesicles to be normal. Signal patterns observed on MR images appear to represent hemorrhagic breakdown products including intra- and extracellular methemoglobin and deoxyhemoglobin. Such hemorrhage may be related to prostatic needle biopsy performed prior to MR imaging, which has been shown to result in trauma to the seminal vesicles, or to retrograde transport of blood from the site of prostatic biopsy via the ejaculatory ducts. Awareness of this phenomenon will assist in accurate interpretation of MR examinations for staging of prostate cancer.

259 • 3:09 PM

### Endorectal Coil MR Imaging of the Prostate: Pitfalls in Determining the Extent of Intraprostatic Adenocarcinoma

ML Schiebler, MD Schnall, E Outwater, RS Owen, HY Kressel, H Pollack
*Department of Radiology, Hospital of the University of Pennsylvania, Philadelphia*

The authors studied the pitfalls commonly encountered when trying to determine the site and amount of tumor with endorectal MR imaging studies after comparison with histopathology, and categorized these pitfalls into two major groups: avoidable and unavoidable. Thirty-five endorectal coil MR imaging examinations performed in patients who had undergone radical retropubic prostatectomy for adenocarcinoma were blindly reviewed. Errors in determining tumor location were categorized in each case by position in the gland and by histopathology based on whole mounts of the resected prostate, with special attention to the specific area in question. There were six unavoidable and two avoidable errors in 35 examinations. Three of the unavoidable errors involved intraprostatic disease less than 5 mm in size; two involved mucoid carcinoma that was not recognized at all because of its high signal intensity on the T2-weighted images, and one involved densely glandular benign prostatic hypertrophy in the peripheral zone, which was of low signal intensity on the T2-weighted images. There were two avoidable errors regarding tumoral involvement of the periapical portion of the gland, which were recognized in retrospect. Careful comparison of the T1-weighted images with the T2-weighted images also helped distinguish postbiopsy hemorrhage from tumor in 10 other cases. There were three cases of initially suspected tumoral involvement at the proximal portion of the seminal vesicles on the axial images that were correctly determined to be nodules of benign prostatic hypertrophy on the sagittal images. Many common errors in the interpretation of the extent of intraprostatic adenocarcinoma on endorectal MR images can be avoided by giving careful attention to the pitfalls described in this report.

260 • 3:21 PM

### Prostate Cancer Staging with Endorectal MR Imaging: Comparison of Conventional and Fat-suppressed T2-weighted Pulse Sequences

SA Mirowitz, JJ Brown, JP Heiken
*Jewish Hospital, Washington University School of Medicine, St Louis*

The use of fat suppression has been noted to improve tissue contrast and artifact control when body coil imaging of the pelvis is performed. The objective of this study was to evaluate whether use of fat suppression confers similar advantages when endorectal surface coil MR examinations are performed for the evaluation of patients with prostate cancer. Fifty consecutive patients were imaged with conventional T1-weighted (TR, 600; TE, 20) and conventional and fat-suppressed proton-density–/T2-weighted (TR, 2,500; TE, 35/80) sequences. Thirteen of 50 patients subsequently underwent radical prostatectomy and constituted the study group for which conventional and fat-suppressed images were directly compared by three reviewers. Criteria assessed included the relative ability of each sequence to demonstrate zonal distinction, periprostatic venous plexus, fibromuscular stroma, capsule definition, seminal vesicle architecture, tumor conspicuity, capsular penetration and/or seminal vesicle tumor invasion, artifact control, and overall image quality. No significant improvement in depiction of anatomic or pathologic features was demonstrated for fat-suppressed images, although this method resulted in fewer artifacts. It is concluded that use of fat saturation does not result in significant improvement over conventional T2-weighted images in endorectal MR imaging of the prostate.

261 • 3:33 PM

### Bull's-Eye Sign: Useful for Distinction between Bone Metastases and Hematopoietic Islands at MR Imaging

ME Schweitzer, C Levine, DG Mitchell, C Piccoli, L Gomella
*Department of Radiology, Jefferson Medical College of Thomas Jefferson University, Philadelphia*

Islands of hematopoietic marrow can complicate the interpretation of MR images, as, for example, in patients with prostate cancer. Pelvic MR images of 79 patients with biopsy-proved prostate cancer and no evidence of metastatic disease at either bone imaging or clinical follow-up were reviewed. Axial images (TR, 500–600; TE, 20) were obtained with a 1.5-T unit and were each studied by two examiners. Patterns of hematopoietic (low-signal) marrow were mapped on the basis of location, symmetry, margins, and relative amount. Seventy of 79 (88.6%) patients had a total of 297 islands of hematopoietic marrow. Of these islands, 75.6% were symmetric. In 291 of 297 (98%) of these low-signal areas a focal central area of high intensity was noted, presumably representing a central area of yellow marrow. This central area of high signal was not noted in any patient with metastates and, given the histopathology of bone metastases, central high signal is not expected to occur. The bull's-eye sign is a helpful indicator of islands of hematopoietic marrow that might otherwise be confused with metastatic deposits.

262 • 3:45 PM

### MR Imaging of Breast Implants

C Janus, D Drake, R Morgan
*University of Virginia Medical Center, Charlottesville*

Approximately 150,000 American women undergo augmentation mammoplasty annually, and 2 million women in the United States currently have breast implants. Complication rates associated with the procedure have been estimated as high as 30% to 50%. Symptoms and signs of a ruptured implant are often vague, and there may not be a history of trauma. Mammography and ultrasound are of limited diagnostic accuracy. This study was undertaken to evaluate the potential role of MR imaging in evaluating breast implants for rupture or leakage. Eight women ranging in age from 28 to 53 years who had undergone bilateral breast implantation were studied. Both breasts were evaluated in each patient with a 1.0-T MR imager (Siemens) with a breast coil. Each examination consisted of T1-weighted images in the axial and sagittal planes and a T2-weighted imaging sequence in the sagittal plane. Findings were positive for damage to the implant in seven cases (six patients) and were suspicious in one patient. Damage to the implant was manifested by asymmetry or irregularity in contour of the implant associated with extrusion of fluid content. There was excellent correlation between surgical and MR imaging findings. Advantages of MR imaging include excellent tissue contrast, multiplanar imaging, and elimination of the need for breast compression. Large-scale studies are needed to help define the role of MR imaging in diagnosing complications due to breast implants.

263 • 3:57 PM

### Minianeurysm: Convincing Sign of Localized Right Ventricular Dysplasia Demonstrated with Cine MR Imaging

P Germain, B Kastler, G Roul, A Constantinesco, A Gangi, P Zimmerman, JL Dietemann, A Sacrez
*University Hospital, Strasbourg, France*

Diagnosis of localized right ventricular dysplasia (RVD) is a difficult and clinically important challenge. This is related to the paucity of relevant information obtained with conventional imaging diagnostic methods, particularly the insufficiency of right ventricular x-ray angiography and limited visualization of the right ventricle with 2D echography. Fifteen patients without global enlargement of the right ventricle were referred for suspicion of localized RVD. The imaging protocol included one axial electrocardiograph-gated spin-echo sequence and two or three cine MR sequences (axial [right midventricular] and sagittal [encompassing the pulmonary infundibulum]). Wall motion was assessed by two trained operators using landmarks positioned along the right ventricular boundary. Contrary to previously reported results with spin-echo MR imaging (wall thinning, fatty infiltration), anatomic features appeared nonspecific in this series. Nevertheless, cine MR clearly depicted small segmental dyskinetic areas of the right ventricular wall, or "minianeurysms." This convincing abnormal pattern was located twice anteriorly (at the base and midportion of the pulmonary infundibulum) and once inferiorly (at the posterior portion of the right ventricular floor). In conclusion, minianeurysm pattern on cine MR images could be a relevant, convincing indicator for the diagnosis of localized right ventricular dysplasia.

264 • 4:09 PM

### Heart Involvement in Lymphomas: Is MR Imaging Competitive with Two-dimensional Echocardiography?

JD Tesoro-Tess, S Biasi, L Balzarini, E Ceglia, R Petrillo, Y Reyner, P Piotti, R Musumeci
*Istituto Nazionale Tumori, Milan, Italy*

MR imaging demonstrated good capability for detecting lymphomatous involvement of the chest at disease presentation and seems to have greater possibilities in comparison with CT for both multiplanar and multiecho imaging. At present, 2D echocardiography is the simplest and least expensive method for imaging the heart and is considered the preferred tool for identifying both pericardial and

myocardial involvement. In this study, MR imaging and echocardiographic examinations performed in a group of 36 consecutive previously untreated patients with mediastinal lymphomas (22 with Hodgkin disease and 14 with Non-Hodgkin lymphoma) at disease presentation were described and compared. MR imaging was performed with a 1.5-T superconductive magnet. Transverse and coronal electrocardiograph-gated, mainly T1-weighted images (TR = RR, TE = 17, section thickness = 8 mm) were acquired. US examinations were performed according to standard planes (long and short axis combined with apical four-chamber view) with both 3.5- and 5.0-MHz probes. In 23 of 36 (63.8%) patients adenopathies extended beyond the cardiac contours in contiguity with the pericardium. Both US and MR imaging correctly identified a pericardial effusion (15 of 17 [88.2%] for MR imaging vs 14 of 17 [82.3%] for US). However, the panoramic view offered by MR imaging permitted better definition of the relationship of adenopathies to parietal pericardium as well as to myocardium or extrapericardial diffusion.

# Wednesday Afternoon
# Regent Parlor
# Papers 265–272

## PULSE SEQUENCES

MODERATORS: L Axel, MD • BK Rutt, PhD

265 • 2:45 PM

### Variable Refocusing Flip Angle with Hybrid RARE Imaging

JA Tkach*, GH Glover†, J Dillinger*, PA Ruggieri*, A Shimakawa†

*Cleveland Clinic Foundation, Cleveland; †Stanford University School of Medicine, Stanford, Calif; and †GE Medical Systems, Milwaukee

Hybrid RARE (HR) sequences use 180° refocusing pulses (β). The acquisition TR, effective TE (TEF), number of $k_y$ lines per excitation (KYE), interecho spacing, and tissue relaxation parameters determine the signal behavior and severity of the concomitant data filtering. To date, the acquisition parameters have been manipulated to obtain T1, T2, and spin-density (ρ) HR images. More complex and potentially interesting types of signal and contrast behavior can be obtained by varying the flip angle of β. Alterations in β can also be used to acquire T1, T2, and ρ HR images with improved section profiles and reduced SAR at no expense to imaging time or coverage and with minimal loss in signal-to-noise (S/N) and contrast-to-noise (C/N) ratios. Standard and variable β phantom and human head HR images were acquired with a 1.5-T GE Signa with a circularly polarized transmit/receive head coil. Conventional T1, T2, and ρ images were acquired as controls. The images were evaluated and compared with respect to S/N, C/N, edge definition, and artifacts. β schedules in which the modified flip angle either remained constant across or changed between pulses within a given echo train were tested. Analogous theoretical measures were calculated from the Bloch equations for the analogous set of tissue and acquisition parameters. HR signal versus echo was plotted as a function of phase-encoding step as dictated by the total number of in-plane phase-encoding lines collected (KYE, TEF). The full width at half maximum of the corresponding PSF was used as a theoretical measure of edge definition. There was good agreement between the theoretical and experimentally derived results in all cases. It was always possible to reduce the flip angle of β to 120° and 165° for T1 and ρ/T2 HR acquisitions, respectively, before the loss in S/N and desired C/N became perceptible. More dramatic and/or complex variations in the β schedule produced HR images with strikingly different signal behaviors compared with those collected with the standard flip angle of 180° (eg, predominantly ρ-weighted image with TEF = 90 msec, β = 45°).

266 • 2:57 PM

### Recursive Method for Generating Object-guided Two-dimensional–Selective RF Pulses

RC Grimm, RL Ehman, JF Greenleaf

*Mayo Clinic and Foundation, Rochester, Minn*

Previous work has shown that it is possible to use acquired-echo waveforms as subsequent RF excitation pulses. This "recursive" process offers interesting possibilities for tailoring the pattern of excitation along a 1D projection. The objective of this study was to extend recursive methodology to 2D imaging and, specifically, to develop a technique for generating custom 2D-selective RF pulses with patterns of excitation determined by the distribution of spins in the imaged object. In the RF definition phase of this technique, a single-shot gradient-echo sequence with a TE of 3.5 msec interrogates the object with a 7-cycle spiral readout trajectory in k space, lasting 16 msec and starting at the origin. The sampling rate is constant, but the azimuthal rate of the spiral is decreased linearly over time to sample the covered portion of k plane uniformly. In the application phase of this technique, the time-domain echo data obtained in the definition phase are simply copied to the RF excitation waveform table of the imager. The same spiral gradient pattern played during the definition phase is used while this pulse is applied. Phantom studies have demonstrated that the recursive 2D excitation technique provides a spatial pattern of excitation matching the distribution of spins interrogated during the definition phase, with a resolution consistent with the k-space trajectory of the recursive RF pulse. In vivo studies are in progress. The results have encouraged the evaluation of potential applications of the 2D recursive technique, such as "image-guided" 2D spatial saturation pulses for surface coil imaging and high-resolution "inner-volume" imaging with targeted 2D excitation.

267 • 3:09 PM

### Single-Shot Localization of a True Three-dimensional Volume of Conformable Shape

S Singh, E Zerhouni

*Department of Radiology, The Johns Hopkins University School of Medicine, Baltimore*

Many applications of spatial localization techniques require the isolation of a true 3D volume. Furthermore, it would be advantageous if the shape of the volume of interest (VOI) could be made to conform to in vivo targets for maximizing the signal-to-noise ratio in the VOI data while minimizing extraneous contamination. In this work, the previously developed projection presaturation (PP) technique was extended to localize a true 3D volume of conformable shape in all dimensions. In a 2D version of PP, a series of selective radio-frequency (RF) pulses is applied in the presence of a stepwise rotating gradient to suppress the magnetization of the region outside the region(s) of interest (ROIs), the spins of which remain unaffected during localization. In general, the ROI is a cylindric polyhedron (CP) of convex surfaces with its axis parallel to the axis of gradient rotation. The above approach has now been extended to the case of 3D localization by isolating an appropriate number of 2D CPs of appropriately chosen orientations that intersect one another. The volume of intersection, the only volume element in which magnetization is left untouched, at least in principle, during localization, then defines a true 3D VOI (of conformable shape). Each set of saturation RF pulses designed to isolate indi-

vidual 2D CPs saturates the outer region only partially. Consequently, the overall saturation of the volume outside the VOI is at the same level as in 2D localization and is achieved in almost the same localization time. In vivo target shape determines the shape of the VOI being conformed. This in turn determines the shape of the cross section of the 2D CPs, the cross sections being the projection of the VOI onto the planes orthogonal to the axis of the individual CPs. In the case of a VOI of spherical symmetry, for example, the intersecting CPs will be the right circular cylinders of identical (circular) cross sections. In general, the CP cross sections will have different shapes and sizes. This 3D localization technique has been implemented with a 1.5-T GE Signa system in a phantom (23-cm-diameter spherical gel phantom) as well as in vivo in humans, and VOIs of various shapes, including spherical VOIs, have been localized. Spherical VOI localization is currently being applied to MR angiography and localized spectroscopy.

268 • 3:21 PM

### Suppression of Moving Spins with DEFT Pulses

L Axel, L Dougherty, ML Schiebler
*Department of Radiology, Hospital of the University of Pennsylvania, Philadelphia*

Suppression of signal from moving blood relative to that of the surrounding wall of the left ventricle is important for quantitative cardiac imaging. Selective out-of-plane saturation may be ineffective due to the intermittent nature of blood flow. An alternative method of suppressing the magnetization of moving spins has been implemented with a modified DEFT pulse that incorporates pulsed magnetic field gradients and is applied prior to conventional spin-echo imaging. The basic DEFT pulse idea of driving transverse magnetization back along the static field has been modified with the addition of a pair of magnetic field gradient pulses between the RF pulses ($90^\circ_x$, $180^\circ_y$, $-90^\circ_x$). There is no net effect on stationary spins, but moving spins will be left with a net phase shift. This phase shift depends on the velocity, strength, duration, and separation of the gradient pulses. The result of this preparatory DEFT pulse sequence is the suppression of the final longitudinal magnetization of moving spins. This effect is offset, however, by the T2 decay of stationary spins during the pulse sequence, resulting in a loss of transverse magnetization. This encourages use of maximum-strength gradient pulses and sequences of short duration. A sequence can be repeated prior to imaging to enhance the relative suppressive effect. This sequence was implemented in conjunction with conventional cardiac-gated spin-echo imaging with gradient moment nulling with a commercial 1.5-T imaging system (GE Signa). There was moderate suppression of blood signal relative to the myocardium (on the order of 30%), although the myocardial signal was also decreased. The modified DEFT sequence may be useful in suppressing moving spins adjacent to an organ of interest. Its usefulness is limited, however, when adjacent stationary tissues also have a short T2.

269 • 3:33 PM

### Analysis and Reduction of Motion Artifacts on the Second Echo of a Multiecho Sequence

PM Pattany, JL Sherman, K Wong, DH Jarvis
*MRI of Colorado/Tesla Imaging Corporation, Colorado Springs*

Motion artifact suppression technique (MAST) has greatly reduced the artifacts generated by physiologic motion in MR imaging (1). In multiecho sequences, however, artifacting seems to be more prominent on the second echo than on the equivalent single-echo spin-echo sequence. The MAST technique compensates for motion in the frequency-encode and section-select directions. In the phase-encode direction of a multiecho sequence, however, a standard phase-encode gradient is applied for spatial encoding, and two additional gradient lobes of constant amplitude are applied around the second 180° RF pulse to remove any transverse magnetization it has generated. Therefore, any motion that occurs in the phase-encode direction would have extra random phase shift, proportional to the amplitude of the motion. This in turn leads to artifacting on subsequent second-echo images. In this study, the two lobes of constant amplitude were replaced with motion-compensated gradient waveform lobes, which compensated up to the third order (pulsatility) of motion in the phase-encode direction on the second echo, but also removed any transverse magnetization generated by the 180° RF pulse. Studies were performed in several volunteers and patients with 0.5-T and 1.5-T Picker MR imaging systems, with and without MAST in the phase-encode direction. Images acquired with MAST in the phase-encode, frequency-encode, and section-select directions showed marked reduction of artifacts.

1. Pattany PM, Phillips JJ, et al. J Comput Assist Tomogr 1987; 2:369–377.

270 • 3:45 PM

### Contrast Optimization for Submillimeter Imaging of the Inner Ear

P Schmalbrock, MA Brogan, DW Chakeres, VA Hacker, K Ying, BD Clymer
*Departments of Radiology and Electrical Engineering, Ohio State University, Columbus*

The goal of this study was to optimize the contrast-to-noise ratio (C/N) among fluids, nerves, and bone structures in MR imaging of the temporal bone region and to compare the results with computer simulations. Submillimeter-resolution images of the inner ear were acquired with a 3DFT method that uses short, truncated RF pulses, optimized gradient lobes, and fractional echoes. Echo time was limited to a minimum of 7 msec by the phase-encode gradient. C/N was measured at a TR of 25–50 msec and flip angle of 15°–90° with various spoiler and/or rephaser gradients. The small size of the observed anatomic structures leads to significant overlap of high- and low-intensity structures within a single voxel. Thus, quantitative evaluation of signal intensity for a given tissue necessitates regional histogram analysis and integration of information from several sections. Initial analysis of the data indicates that optimal contrast between nerves and cerebrospinal fluid in the internal auditory canal is obtained with a TR of 25 msec, flip angles of 50°–60°, and gradient rephasing leading to steady state.

271 • 3:57 PM

### Improving the Contrast in Gradient-Echo Images with Pulsed Magnetization Transfer

RA Jones, PA Rinck, TE Southon
*MR-Center, University of Trondheim, Norway*

Magnetization transfer contrast (MTC) can improve image contrast by reducing the signal obtained from tissues in

which there is a significant restricted proton pool (Hr). The standard method of saturating Hr and thereby inducing MTC is to apply a long, low-power pulse several kilohertz off resonance. This sequence, however, requires use of a relatively long TR (> 400 msec) if maximum MTC is to be obtained. In addition, MTC obtained from this type of sequence is reduced when multiple sections are used. A pulsed magnetization transfer contrast (PMTC) sequence has been developed that consists of a standard gradient-echo (GRE) sequence with one or more binomial (1313) pulses included in the recovery delay. The binomial pulse has a low amplitude (20 T) and typically has an effective pulse length of 1.2 msec. The pulse has no effect on the free proton signal, since the frequency bandpass about resonance covers the range of chemical shifts and field inhomogeneities encountered in clinical systems (up to 1.5 T). Hr is saturated across the full frequency spectrum, since the behavior of Hr magnetization during the pulse is dominated by its rapid T2 relaxation. If the binomial pulses are relatively closely spaced, the saturation of Hr is maintained and strong MTC is developed, leading to a significant improvement in contrast compared with the conventional GRE sequence. The PMTC sequence offers more effective use of the applied RF power than does the current method of inducing MTC, can be used with multiple sections, and is easier to implement because the binomial pulse is applied on resonance.

272 • 4:09 PM

### Two-dimensional Gradient-Echo versus Three-dimensional RF Spoiled FAST: Perceptual Differences in Cervical Neural Foraminal Morphology

BE Widoff, SJ Song, MA Nissenbaum, SM Brown, K Yan, N Palmer, WG Bradley

*Long Beach MRI Center, Long Beach, Calif*

MR imaging of the cervical spine has proved suboptimal for evaluation of the neural foramina due to the partial-volume averaging of pedicles in standard 3–5-mm sections. A new MR technique was evaluated in an attempt to improve neural foraminal assessment. MR imaging of the cervical spine was performed in 25 patients. A conventional T2*-weighted, 2D gradient-echo technique (TR, 700; TE, 18; FA, 30°; FOV, 25 cm; 3-mm sections; NSA, 4) was compared with a new 3D RF-spoiled FAST technique (TR, 22–24; TE, 7; FA, 20°; FOV, 25 cm; NSA, 1; 128 partitions) with 1-mm isotropic spatial resolution, suitable for multiplanar reformatting on a Picker ViStar workstation. Conventional 3-mm axial images were compared with RF-spoiled FAST 1-mm and summed 3-mm axial images and with oblique reformations. The effect of the degree of obliquity on the appearance of the neural foramina was assessed. The neural foramina appeared larger on the 1-mm and summed 3-mm axial RF-spoiled FAST images due to improved tissue contrast on these T1-weighted images compared with the conventional 3-mm T2-weighted images. Although partial-volume averaging artifact is eliminated on the 1-mm partitions, these images did not show subtle uncovertebral osteophytes that were seen on the oblique reformations. The variation in obliquity at different levels within the cervical spine did not significantly affect assessment of the neural foramina. In conclusion, the 1-mm isotropic RF-spoiled FAST technique with oblique reformations improves MR assessment of the cervical neural foramina.

## Wednesday Afternoon
## Murray Hill Suite
## Papers 273–280

## CONTRAST AGENTS: HEPATOBILIARY AND GI

MODERATORS: ME Bernardino, MD
GD Fullerton, PhD

273 • 2:45 PM

### Contrast-enhanced MR Imaging in the Evaluation of Hepatocyte Function

MK Sidhu*, HH Muller*, J Aggeler*†, AL Jones†, SW Young*

**Department of Radiology, Stanford University School of Medicine, Stanford, Calif, and †Veterans Administration Medical Center, Liver Center, University of California, San Francisco*

The purpose of this study was to determine if hepatotoxicity can be detected with the hepatocyte-specific agent Mn-DPDP. Acute hepatotoxicity was induced in rats with intraperitoneal injection of 3 g/kg ethanol or normal saline 2 hours prior to imaging. Chronic hepatotoxicity was induced by allowing rats to ingest an ethanol-containing liquid diet for 1–4 weeks. T1- and T2-weighted imaging (1.5 T) was performed before and after intravenous administration of 50 μmol/kg Mn-DPDP. After the imaging, livers were excised and examined with electron microscopy (EM). In acute cases, enhancement with Mn-DPDP was significantly lower in ethanol-treated animals on T1-weighted images (ethanol, 66.5% ± 9%, control, 83.6% ± 10%, $P < .02$). T2 contrast effect was also lower in ethanol-treated animals, but not significantly so. There was a significant difference in signal intensity on precontrast T2-weighted images ($P < .01$) but not on the corresponding T1-weighted images. EM revealed severe ethanol-induced hepatocyte damage. In chronic cases, enhancement on T1-weighted images was lower in the 1–3-week ethanol groups and significantly so in the 2-week group (ethanol, 92.1% ± 4%, control, 99.5% ± 4%, $P < .05$). T2 contrast effect was lower in ethanol-treated animals at all time points, although not significantly so. There was no significant difference in precontrast intensity on either T1- or T2-weighted images. EM demonstrated progressive ethanol hepatotoxicity from 1 to 4 weeks. In conclusion, Mn-DPDP–enhanced T1-weighted MR imaging can distinguish between normal and ethanol-damaged livers in cases in which unenhanced MR imaging cannot.

274 • 2:57 PM

### Detection of Liver Cancer in the Presence of Hepatitis: Cell-Specific MR Contrast Agents

A Tanimoto*, BP Kreft*, Y Baba*, L Zhao*, JP Finn†, DD Stark*

*Department of Radiology, *Massachusetts General and †New England Deaconess Hospitals, Harvard Medical School, Boston*

Primary liver cancer is often associated with inflammatory changes in the liver. It was expected that hepatocyte-targeted contrast media would show reduced uptake and decreased efficacy in detecting tumor in the presence of hepatitis. To evaluate this hypothesis the enhancement of a hepatocyte-specific paramagnetic contrast agent (Mn-DPDP) and of a superparamagnetic iron oxide coated with arabinogalactan (SPIO-AG) were studied in an experimental tumor model in the presence of hepatitis. Carcinosarcoma was implanted into the livers of 40 rats 6–8 days prior to study, and hepatitis was induced by oral administration of a 1:1 mixture of carbon tetrachloride (0.4 ml/

kg) 24 hours prior to study. Liver and tumor relaxation times for controls and for animals with hepatitis were measured with ex vivo relaxometry (0.94 T) before and after contrast agent administration. In vivo MR imaging (SE 310/15, SE 2,000/45 and 90) was performed at 1.0 T. In the absence of contrast agent, relaxometry showed decreased T1 and T2 contrast between inflamed liver (hepatitis) and tumor tissue. Contrast-to-noise ratio (CNR) in animals with hepatitis was not different from that in controls on the unenhanced T1-weighted (SE 310/15) images, but decreased significantly ($P < .05$) on the T2-weighted images. After administration of Mn-DPDP (SE 310/15) or SPIO-AG (SE 2,000/45), CNR in animals with hepatitis and controls was similar. The results indicate that enhanced tumor detection with hepatocyte-specific contrast agents is not affected by associated inflammatory liver disease.

275 • 3:09 PM

### Gd-BOPTA—enhanced Detection of Liver Tumors

BP Kreft*, A Tanimoto†, Y Baba†, L Zhao†, J Chen†, JP Finn†, L Zhao†, DD Stark†

*Department of Radiology, University of Bonn, Germany, and †Harvard Medical School, Boston*

To evaluate the influence of tumor histology on the diagnostic efficacy of the hepatocyte-specific contrast agent Gd-BOPTA, different tumor models were studied histologically with ex vivo relaxometry and in vivo MR imaging. Adenocarcinoma, carcinosarcoma, rhabdomyosarcoma, or hepatoma was implanted into the livers of 128 rats. Relaxation times of liver and tumor were measured at 0.94 T prior to and over a period of 2 hours following administration of Gd-BOPTA (75 μmol/kg). Dynamic MR imaging (SE 310/15) was performed at 1.0 T, and signal-to-noise ratio (SNR) and contrast-to-noise ratio (CNR) were evaluated over 2 hours. Quantitative data were correlated with histologic findings. Gd-BOPTA maximally decreased liver T1 in all four models by 55% to 72% within the first 30 min. Peak liver enhancement in animals with adenocarcinoma and rhabdomyosarcoma occurred 5–10 min after contrast agent administration, and in animals with infiltrating tumors (carcinosarcoma and hepatoma) after 20–30 min. Substantial nonspecific tumor enhancement occurred only in the early phase after contrast agent administration (5–10 min), except in cases of highly vascularized carcinosarcoma (5–20 min). Gd-BOPTA maximally increased liver SNR on the T1-weighted images (SE 310/15) 5–30 min after contrast agent administration, with earlier peak enhancement in animals with noninfiltrating tumors. Tumor-liver CNR in all models increased by 97% to 247% 20–30 min after contrast agent administration. It is concluded that Gd-BOPTA–enhanced MR imaging improves tumor detection independently of tumor histology. Delayed imaging reduces nonspecific tumor enhancement, maximizing liver-tumor contrast.

276 • 3:21 PM

### Radiation Injury to the Liver: Cell-specific MR Imaging with Superparamagnetic Iron Oxide and Gd-Ethoxybenzyl(EOB)-DTPA

O Clément, A Mühler, V Vexler, Y Berthezène, R Kuwatsuru, RC Brasch

*Contrast Media Laboratory, University of California, San Francisco*

The hypothesis of this study was that a hepatocellular-specific MR contrast agent (Gd-EOB-DTPA) and superparamagnetic iron oxide (SPIO), an RES-specific contrast agent, enable assessment of liver-cell and phagocytic functions separately in the same animal in a model of hepatic irradiation injury. Rats received a single irradiation dose (15 to 70 Gy) to the right liver, with a lead shield over the left liver. Three days after irradiation, T1-(TR 200, TE 6) and proton density–weighted (TR 700, TE 25) SE images were acquired with a 2-T imager before and after injections of 0.1 mmol/kg Gd-EOB-DTPA and 10 μmol Fe/kg AMI-25. Biliary excretion of Gd-EOB-DTPA was measured in whole-liver-irradiated and control rats. The liver signal was homogeneous on precontrast images and following administration of Gd-EOB-DTPA. Following AMI-25 and for irradiation doses > 50 Gy, a statistical difference was found between the irradiated and the shielded parts of the liver with a precise demarcation between irradiated and nonirradiated zones. This indicated a decreased uptake of SPIO in the injured part of the liver. Although a mild hepatocellular injury was confirmed with electron microscopy, biliary excretion of Gd-EOB-DTPA was the same in irradiated (79%) and control rats (74%). Increased radiosensitivity of the Kupffer cells compared with hepatocytes was demonstrated with contrast-enhanced MR imaging. SPIO may be used for quantitation of hepatic injury, while Gd-EOB-DTPA may be potentially useful in detecting focal lesions in underlying liver disease.

277 • 3:33 PM

### Liver MR Imaging: Intravenous Contrast Agent Dose Dependence of Focal Lesion Detection

VM Runge, JE Kirsch, GS Thomas, CE Woolfolk

*Magnetic Resonance Imaging and Spectroscopy Center, University of Kentucky, Lexington*

The effect of different contrast doses (0.1 [$n = 7$], 0.25 [$n = 6$], and 0.5 [$n = 9$] mmol/kg intravenous gadoteridol [Squibb Diagnostics]) on detection of focal liver lesions was investigated in 22 rabbits. Dynamic (10-second-duration) breath-hold MR images were acquired at 30-second intervals, beginning immediately precontrast and continuing to 10 min postcontrast, and compared with conventional (enhanced and nonenhanced) non-breath-hold T1- and T2-weighted techniques. A liver abscess model with nonenhancing (central necrosis) and enhancing (rim) components was studied, permitting statistical comparison with anatomic correlation. Prominent enhancement of lesion rim was consistently observed postcontrast at 0.5 mmol/kg. Lesion rim enhancement was less prominent and at times incomplete at 0.25 mmol/kg, and poorly (or not at all) visualized at 0.1 mmol/kg. Enhancement of liver parenchyma was proportional to administered dose, near maximum within 50 seconds after administration of 0.5 mmol/kg. Lesion detectability as assessed with statistical measurements (SD/N) and blinded readers was superior on breath-hold postcontrast T1-weighted images at a dose of 0.5 mmol/kg, compared with doses of 0.1 and 0.25 mmol/kg and conventional non-breath-hold studies.

278 • 3:45 PM

### Optimizing Tumor-Liver Contrast Following Administration of Gd-Ethoxybenzyl(EOB)-DTPA: Comparison with Gd-DTPA

A Mühler, O Clément, V Vexler, Y Berthezène, R Kuwatsuru, RC Brasch

*Contrast Media Laboratory, University of California, San Francisco*

The hypothesis of this study was that a new hepatocellular MR contrast agent, Gd-EOB-DTPA (70% biliary excretion), can substantially improve lesion-to-liver contrast and expand the "imaging window" compared with strictly extracellular Gd-DTPA. A mammary adenocarcinoma was implanted into rat livers. MR imaging was performed at 2 T with a T1-weighted SE sequence (TR 200, TE 6) before and after administration of 0.1 mmol/kg Gd-DTPA or Gd-EOB-DTPA (positive liver enhancement). Additionally, Gd-EOB-DTPA was used as a negative liver enhancer by ap-

plying a STIR sequence (TR 1,000, TI 65, TE 6). Enhancement levels were measured between 1 min and 1 hour postcontrast with calculation of contrast-to-noise ratios (C/Ns). Before contrast agent administration, liver tumors were observed as hypointense lesions on SE images (C/N = −6.5) and as hyperintense lesions on STIR images (C/N = +7.2). Following administration of Gd-DTPA, contrast between tumor and liver never exceeded preinjection values. Following injection of Gd-EOB-DTPA, persistent positive liver enhancement of more than 200% (spin echo) following injection of Gd-EOB-DTPA resulted in an increase of C/N values to −31.1. With the STIR sequence, Gd-EOB-DTPA produced signal void from liver parenchyma and substantially improved C/N of tumors (+38.0). Gd-DTPA has limited utility for the detection of liver masses due to its rapid equilibration with the extracellular fluid space. Gd-EOB-DTPA dramatically increases contrast between tumor and liver over a period of at least 1 hour. Because of strong T1 relaxation enhancement within the hepatocyte, Gd-EOB-DTPA may be used effectively as a positive or negative liver enhancer depending on the sequence used.

279 • 3:57 PM

### Copolymeric MR Contrast Agents

DK Shen, EC Unger, GL Wu*, TA Fritz, B Kulik*, TE New*
*Department of Radiology/MRI, University of Arizona, Tucson, and *ImaR$_x$ Pharmaceutical Corp, Tucson*

To date, protein or polysaccharides have been used to synthesize blood pool MR polymeric contrast agents. In this study a different approach has been taken. Block copolymeric MR contrast agents have been synthesized in which the polymers are comprised of repeating subunits of one or more linker polymers and one or more complexes of manganese, gadolinium, or other paramagnetic ions. The authors have tested several of these copolymeric MR contrast agents for toxicity, biodistribution, clearance, stability, and MR imaging. These copolymeric MR contrast agents may be either linear or branched. Most work to date has been with the linear copolymer poly-EDTA-EOEA-DP-Mn. The authors have synthesized and tested two different molecular weights, 40,000 and 100,000, for this copolymer. Poly-Mn-EDTA-EOEA-DP-Mn has a relaxivity three times higher than that of simple monomeric complexes of the respective paramagnetic ion (eg, Mn-EDTA). Clearance for this copolymer is via both renal and hepatobiliary routes. LD50 is comparable with that of Gd-DTPA, and MR images show blood pool and renal enhancement. The agent also improves detection of hepatic tumors in rats. MR angiographic images show vascular enhancement greater than that for Gd-DTPA. Paramagnetic copolymers hold promise as blood pool contrast agents. Work is under way to develop the best candidate agent for clinical trials.

280 • 4:09 PM

### Clay/Paramagnetic Hybrid: A Biphasic Oral Contrast Agent over a Wide Range of Dilutions

JF Mammone, DG Mitchell, M Feroze, SE Vinitski
*Department of Radiology, Jefferson Medical College of Thomas Jefferson University Hospital, Philadelphia*

MR imaging of the abdomen has been limited by lack of a suitable oral contrast agent. Another limitation may be dilutional effects of the small bowel. Clay-based agents such as Kaopectate have exhibited promising relaxation properties but have been limited by palatability and patient tolerance. In an effort to reduce the amount of clay required, ferrous sulfate has been added to diluted suspensions and its effects evaluated in vitro. In vitro imaging studies were performed with distilled water and Kaopectate in ratios ranging from 1:1 to 2:1, with the addition of up to 10 mM/L ferric sulfate. T1 and T2 were measured with a 1.5 T MR imaging unit. Additional studies were performed on 1:1 and 2:1 water:Kaopectate samples containing 10 mM/L $Fe^{2+}$ that were subsequently diluted in 10% increments to simulate the effect of gastrointestinal secretions on the contrast agent. The addition of 10 mM/L of $Fe^{2+}$ effectively lowered T1 and T2 of water/Kaopectate mixtures, with the effect being greater at higher dilutions. For example, T1 decreased by 55% and 86% in a 1:1 mixture and 20:1 mixture, respectively. The clay/$Fe^{2+}$ mixture maintained positive T1 contrast up to a 10-fold dilution on simulation of the effect of gastrointestinal secretions. Negative T2 contrast was improved by the added $Fe^{2+}$ over all concentrations and was maintained at a 5-fold dilution level. In conclusion, the addition of $Fe^{2+}$ can safely and effectively improve the relaxation properties of clay-based oral contrast agents and provide flexibility in contrast characteristics. This may permit use of a reduced quantity of clay agent and improve patient tolerance for in vivo applications.

# Notes

# Notes

# Notes

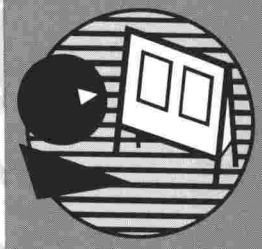

SMRI

## SCIENTIFIC POSTERS

The Scientific Poster Exhibits offer SMRI attendees an opportunity to examine and discuss scientific material in a more intimate atmosphere. Discussion periods, moderated by individual Scientific Poster presenters, are scheduled daily throughout the Meeting. A schedule of the discussion times follow:

| | |
|---|---|
| Section: | **Neuro, Head & Neck, Spine, Pediatrics** |
| Day, Date: | **Sunday, April 26** |
| Time: | **12:15 pm - 1:15 pm** |
| Section: | **Body, Musculoskeletal** |
| Day, Date: | **Monday, April 27** |
| Time: | **12:15 pm - 1:30 pm** |
| Section: | **Imaging Techniques** |
| Day, Date: | **Tuesday, April 28** |
| Time: | **12:15 pm - 1:30 pm** |
| Section: | **Spectroscopy, Instrumentation, Image Processing, & Miscellaneous** |
| Day, Date: | **Wednesday, April 29** |
| Time: | **12:15 pm - 1:00 pm** |

Please note that the Poster Exhibit hours have been extended this year to accommodate your busy schedule. The **exhibit hours**, (8:00 am - 8:00 pm Sunday-Tuesday; 8:00 am - 1:00 pm Wednesday), will open prior to and remain open following the balance of the scientific programming.

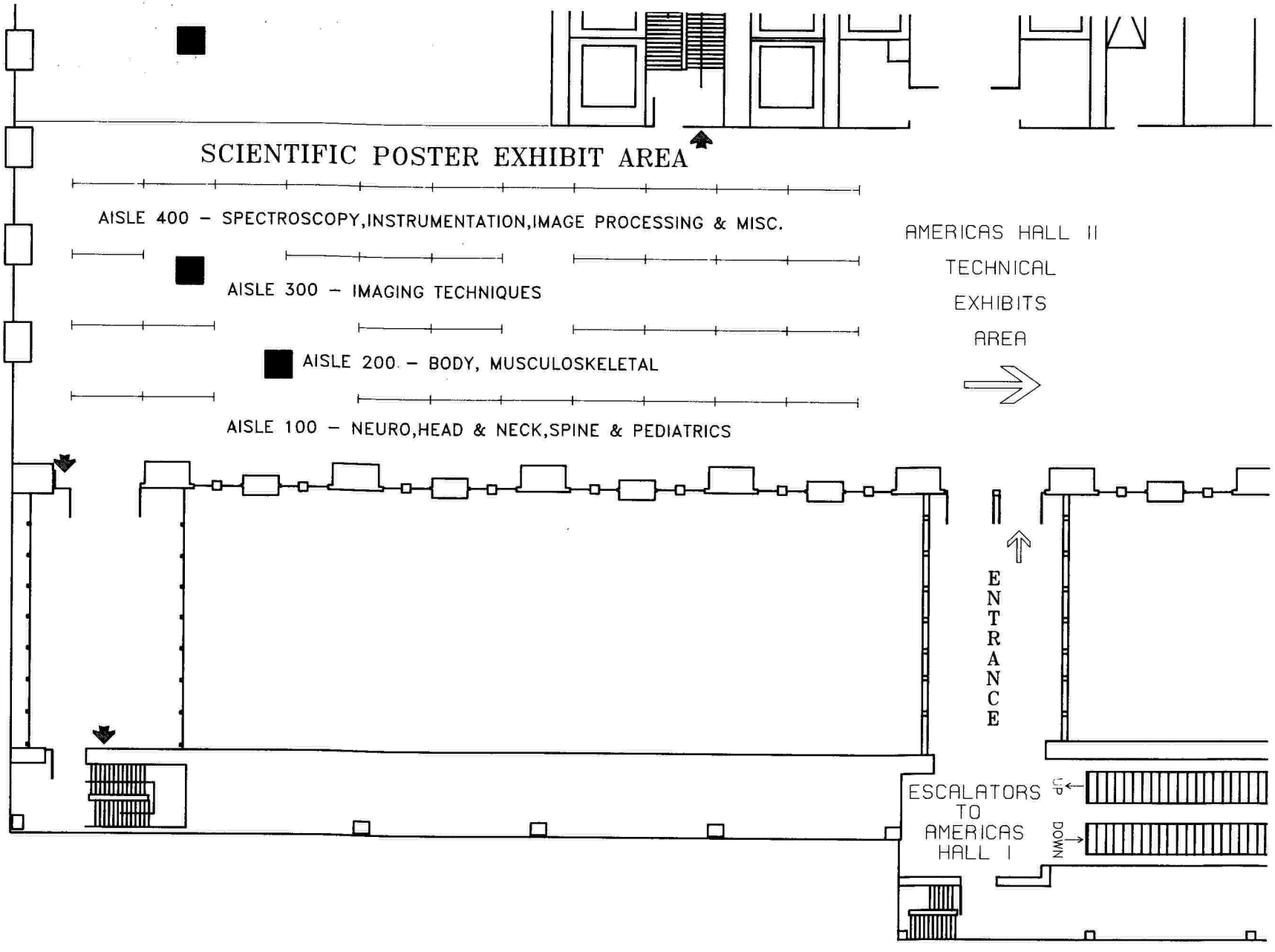
SCIENTIFIC POSTER EXHIBIT AREA
AISLE 400 – SPECTROSCOPY,INSTRUMENTATION,IMAGE PROCESSING & MISC.
AISLE 300 – IMAGING TECHNIQUES
AISLE 200 – BODY, MUSCULOSKELETAL
AISLE 100 – NEURO,HEAD & NECK,SPINE & PEDIATRICS
AMERICAS HALL II
TECHNICAL
EXHIBITS
AREA
ENTRANCE
ESCALATORS
TO
AMERICAS
HALL I
UP
DOWN

# SMRI '92 Tenth Annual Meeting
# Poster Abstracts

## Sunday, April 26, 12:15 PM–1:15 PM
## Neuro, Head and Neck, Spine, Pediatrics

Posters P100–P124

P100

### Phase-Contrast MR Angiography at 0.5 T in Spinal Vascular Malformations

F Gelbert, JP Guichard, D Reizine, KL Mourier, Y Rolland, PY Gobin, B George, JJ Merland

*Department of Neuroradiology, Lariboisiere Hospital, Paris*

Ten patients with a proved vascular malformation of the spinal cord underwent phase-contrast MR angiography performed with a 0.5-T unit (MR MAX system, GE, Milwaukee) in sagittal orientation with 2D gradient sequences (TR = 160, TE = 25, with a flip angle of 20°). Section thickness was 20 mm. Image matrix was 160 × 160. The number of excitations was 10 in eight patients and four in two patients, with an acquisition time of 15 to 5 minutes. Routine SE sequences (TR = 500, TE = 24; TR = 2,000, TE = 60/120) were also performed. All patients underwent selective angiography. Four patients underwent MR angiography and x-ray angiography before and after treatment (surgical or endovascular). MR angiography showed an abnormal vascular pattern within the spinal canal in all cases, comparable with selective angiographic images. The arteries were not differentiated from the veins. The nidus was identified in all cases of intramedullary vascular malformations. MR angiography provided a better characterization of the length and course of abnormal vessels than did spin-echo sequences. In the postoperative cases it also better showed the remaining abnormal vessels detected with angiography. The authors were able to image all types of vascular malformations, but in the case of perimedullary fistulas and dural arteriovenous fistulas, the range of velocity had to be reduced to the slow flow in these malformations. Phase-contrast MR angiography may be regarded as a future reliable alternative to x-ray angiography.

P101

### Serial-enhanced MR Studies in Multiple Sclerosis of the Spinal Cord: Value in Diagnosis and Evaluation of Treatment

MA Mikhael

*McGaw Medical Center of Northwestern University, Evanston, Ill*

The purpose of this study was to detect active multiple sclerosis disease that necessitates treatment and to determine the correlation between the efficiency of treatment and the regression of the disease. Thirty-two cases of suspected multiple sclerosis of spinal cord were studied with MR before and after gadolinium injection. Serial studies for positive cases were performed every 2 weeks. For confirmation of the clinical diagnosis of multiple sclerosis, a T2-weighted image (TR = 2,000 msec, TE = 70 msec) of the spinal cord is needed. For differentiation of old plaques from active acute disease that requires aggressive medical treatment, it was important to perform gadolinium-enhanced MR (TR = 600 msec, TE = 20 msec). Active acute plaques showed enhancement after 20 mL of Gd-DTPA was injected intravenously. Serial enhanced MR images showed the active plaque to gradually lose its clear delineated margins and high-intensity signal after the 4th week and to completely lose enhancement after 6–8 weeks. The segment of spinal cord that shows enhancement is usually swollen. The swelling lags behind loss of enhancement of the plaque. From this series, enhancement of the active plaques further stresses the fact that the blood-brain barrier is disturbed in lesions of active multiple sclerosis. For confirmation of the clinical diagnosis of multiple sclerosis, a T2-weighted image of the spinal cord is needed to visualize the plaques. Gadolinium is useful as a marker for new and clinically active lesions and should be used to determine the efficiency of medical treatment. In this series symptomatology and enhancement showed clear correlation with the clinical findings. The disappearance of enhancement lags slightly behind clinical improvement. The efficiency of treatment with steroids and/or plasmapheresis was estimated and correlated with the MR findings and the degree and duration of enhancement in active plaques.

P102

### Prospective Comparison of Low and Standard Doses for Intravenous Contrast Enhancement with Gadoteridol on Brain MR Images

MA Brack, VM Runge, RA Garneau, C Lee, V Burke

*Magnetic Resonance Imaging and Spectroscopy Center, University of Kentucky, Lexington*

Lesion enhancement and diagnostic utility were assessed prospectively in 18 patients with confirmed intracranial pathology using gadoteridol (Gd HP-DO3A, Squibb Diagnostics) at doses of 0.05 and 0.1 mmol/kg. The patient population consisted of adults aged 24–81 years (mean age, 54 years; 11 men and seven women) with intracranial pathology established with previous imaging studies. MR imaging was performed at 1.5 T, with precontrast T1- and T2-weighted examinations performed first. Immediate postcontrast images were obtained following injection of 0.05 mmol/kg intravenously, supplemented by delayed imaging 10 and 20 minutes postcontrast, to establish the time course of enhancement. An additional dose of 0.05 mmol/kg was administered intravenously 30 minutes following the initial contrast injection, for a total dose of 0.1 mmol/kg, followed by immediate acquisition of the final postcontrast image set. Diagnoses included metastases ($n$ = 6), glioblastoma multiforme ($n$ = 5), pituitary macroadenoma ($n$ = 3), meningioma ($n$ = 2), grade II astrocytoma ($n$ = 1), arteriovenous malformation ($n$ = 1), cerebral infarction ($n$ = 1), mesial temporal sclerosis ($n$ = 1), and chronic ischemic changes ($n$ = 1). Fourteen cases demonstrated at least one enhancing lesion, with improved (subjectively) contrast enhancement and border

definition at 0.1 mmol/kg in all cases. In six cases (33%), clinically significant additional diagnostic information was obtained following administration of 0.1 mmol/kg, compared with 0.05 mmol/kg, including two cases with identification of additional lesions. In two other cases, the detection of one additional metastasis at 0.1 mmol/kg was not considered clinically significant. Region of interest analysis and multireader case review are in progress.

P103

## Carotid Artery Blood Flow Measurements with MR Velocity Mapping

HG Bogren*, MH Buonocore*, W-Z Gu†
*Department of Radiology, *University of California Davis Medical Center, Sacramento, and †Shanghai Railway Hospital*

Ante- and retrograde flow was measured in the ascending aorta and in the right and left common, internal, and external carotid arteries of 12 normal subjects. Five subjects were right-handed, five left-handed, and two ambidextrous. The common carotid flows were 400–500 mL/min, the internals were 200–300 mL/min, and the externals were 100–300 mL/min. All right-handed subjects had higher flow in the left internal carotid artery than in the right. All left-handed subjects had higher flows in the right carotid than in the left. Of the two ambidextrous subjects, one had equal flow on both sides and one had more flow in the left internal carotid. The sum of internal and external carotid artery flows equaled the common carotid artery flow within 5%–10%, but there were exceptions in three of 11 measurements, in which larger discrepancies were found. Retrograde flow and very little antegrade flow occurs in all extremity arteries such as the subclavian arteries in diastole, but not in the internal carotid arteries, which have a large antegrade flow all through systole and diastole. The diastolic flow in the internal carotids appears to be generated via retrograde flow in the subclavian arteries and in the aortic arch. Retrograde flow in the aortic arch supplies the coronaries, but surplus retrograde flow turns into antegrade flow during diastole and appears to supply the internal carotid arteries. Subjects with large retrograde flow in the ascending aorta have larger diastolic forward flow in the internal carotid arteries than those with small retrograde flow in the aorta.

P104

## Fractal Analysis and Segmentation of MR Images in Multiple Sclerosis

J Chang*, A Kadik*, D Kruchten*, PT Cahill†
*Polytechnic University, Brooklyn, NY, and †The New York (NY) Hospital*

MR images of chronic multiple sclerosis (MS), which are characterized by a large number of various-sized lesions and periventricular effusions, are difficult to quantify. Fractal analyses were used to evaluate MR images of MS patients followed serially over time. MR images (15 sections; TR/TE = 2,100/33, 66, 99; section thickness = 7.5 mm) were acquired at 0.6 T. First, the MR signals arising from the scalp and bone marrow in the skull were removed by an edging algorithm. These images were also segmented with a cross algorithm (CA) into seven regions consisting of cerebrospinal fluid, white and gray matter, MS plaques/periventricular effusions, and their overlapping areas. The CA was validated on phantoms of known geometry consisting of 11 tubes filled with sequential dilutions of propylene glycol in water. The resulting (segmented and nonsegmented) images were divided into 6 × 6 regions, and the local fractal dimensions of these areas was determined with a "covering blanket" method. The fractal images were then converted into histograms, and the first, second, and third moments determined for those fractal values that were within 90% of the maximum. The MS images were also analyzed independently with an accepted global analysis method (GAM). In serial MR studies of the same patient, the kurtosis and skewness of the fractal images changed by over 100% and correlated with previous GAM results. The fractal algorithm, which required 2 minutes of computer time for each MR image, was also validated with use of Takagi surfaces of known dimensions (2.0–3.0). Histograms of fractal images, with a finite number of parameters, potentially can provide a means of characterizing changes observed with serial MR studies either locally or globally in MS.

P105

## Use of Turbo Spin Echo for Diagnosis of Rheumatoid Arthritis of the Cervical Spine

MAJF van der Laar*, AR Rozeboom*, JA den Boert†, JJ van Vaals†
*Medisch Spectrum Twente Hospital, Enschede, The Netherlands, and †Philips Medical Systems, Best, The Netherlands*

The workup of patients with cervical spine problems due to rheumatoid arthritis (RA) is laborious. Moreover, some of the procedures involved are uncomfortable and not without risk. Although with MR imaging it is possible to acquire all information needed, with standard imaging techniques such an examination would be too coarse to be adequate or too long to be acceptable, given the limited cooperation that can be expected from the RA patient, especially when he or she has to flex the neck. The authors' hypothesis was that the turbo spin-echo (TSE) technique should offer the increased versatility needed to allow MR imaging to be used as a substitute diagnostic procedure. TSE is derived from the MEMS (1) or RARE (2) method. Typically, 10 to 20 echoes follow each excitation pulse, each one with a different $k_y$ value. The effective TE can be selected by choice of the echo number for which $k_y = 0$. TSE is especially suitable for T2-weighted imaging, for which case a gain in time of a factor 10, compared with standard SE imaging, is easily reached with very little compromise of signal-to-noise ratio. The protocol for cervical spine involvement in RA (total examination time of 35 minutes) now is (*a*) neutral position: sagittal T1-weighted SE, sagittal T2-weighted TSE, and transverse T2-weighted TSE; and (*b*) maximum flexion: sagittal T2-weighted TSE and transverse T2-weighted TSE. In the sagittal sections the approach of the dens to the cerebellar tonsils is observed, as is the erosion of the dens. Transverse sections are taken through the plane of the ring of the atlas. They show the freedom of play of the dens to C-1 as well as the relations of the bone structures to the ligament, synovium, liquor, and myelum. All RA patients with suspected involvement of the cervical spine undergo imaging with this MR system, using the new TSE-based protocol. The statistical outcome of blinded readings of this alternative versus the original diagnostic approach will be presented.

1. Mehlkopf T, et al. Magn Reson Med 1984; 1:295–297.
2. Hennig J, et al. Magn Reson Med 1986; 3:823–833.

P106

## Complex Congenital Anomalies: Evaluation with MR Imaging

KE Macaulay, CH Hoffman, RB Dietrich
*Department of Radiological Sciences, University of California, Irvine*

Infants born with complex congenital anomalies present an immediate and difficult problem. Detailed information, frequently obtained with multiple modalities, is needed to define the full extent and severity of the abnormalities. Such information, together with clinical and laboratory

data, is essential before decisions can be made with regard to sex assignment, prognosis, and surgical planning. The ability of MR imaging to clearly demonstrate abnormal anatomy in multiple planes, together with its ability to show an overall view of the body, makes it a potentially advantageous aid in the evaluation of infants with complex congenital anomalies. In this exhibit the authors demonstrate the ability and limitations of MR imaging in the evaluation of six children with complex congenital anomalies. Diagnoses include conjoined twins ($n$ = 2), OEIS syndrome ($n$ = 2), split notocord with dorsal enteric fistula, and lissencephaly with ambiguous genitalia.

P107

### Quasi-simultaneous MR Assessment of Blood-Brain Barrier Disruption and Blood Flow in Brain Tumors

JC Böck, B Sander, J Haustein, W Schörner, R Felix
*Strahlenklinik und Poliklinik, Universitätsklinikum Rudolf Virchow, Berlin*

The degree of blood-brain barrier (BBB) disruption assessed with contrast-enhanced CCT or MR imaging has been shown to correlate with intraaxial brain tumor malignancy. Likewise, the evaluation of tumor blood flow (TBF) with radionuclide methods is advocated for improved brain tumor grading. This complementary information can now be obtained in a single MR examination. The authors studied 28 patients with brain tumors. BBB disruption was expressed as the percentage of increase of signal intensity on T1-weighted images after intravenous Gd-DTPA injection (0.1 mmol/kg of body weight). Regional cerebral blood flow was assessed as the percentage of signal intensity decrease on T2*-weighted images immediately after Gd-DTPA bolus injection (1.5 T, GRE, TR = 25 msec, TE = 20 msec, flip angle = 10°, image acquisition time = 2.5 seconds, 30 sequential images). Typical findings include intact BBB and low TBF in low-grade intraaxial tumors, disrupted BBB and heterogeneous TBF in high-grade intraaxial tumors, disrupted BBB and high TBF in extraaxial tumors, and disrupted BBB and low TBF in malignant tumors with a partially necrotic tumor center. This study demonstrates quasi-simultaneous assessment of the BBB and TBF. The results support the concept that additional uncorrelated information is obtained from the assessment of regional cerebral blood flow.

P108

### MR Findings Following Transplant Therapy for Parkinson Disease

RA Rauch, R Rand, C Markham, D Becker, R Lufkin
*The University of Texas Health Science Center at San Antonio, and UCLA Medical Center*

Parkinson disease is a degenerative disease of the nervous system of unknown etiology. The region of the brain that appears to be most affected is the dopaminergic system. Until recently, the only method of therapy for patients with Parkinson disease involved systemic manipulation of neurotransmitters and their chemical precursors. This frequently resulted in side effects when the medications affected regions of the brain beyond the intended target. Surgical transplantation of dopamine-producing neuronal tissue into the corpus striatum offers the possibility of local delivery of neurotransmitter while limiting the systemic side effects. While transplantation therapy for Parkinson disease is still in its infancy and its ultimate success remains uncertain, the authors present their findings of MR imaging in patients who have undergone this surgery. The authors reviewed the MR images of four patients before and after autologous adrenal medulla transplantation to the nondominant hemisphere's caudate head. One patient underwent imaging following gadolinium administration. All postoperative images showed a defect in the anterior corpus callosum from the stereotactic surgery to place the tissue within the caudate head. The caudate head on the side of the surgery showed increased volume following surgery. One of the four patients showed evidence of hemorrhage into the caudate head, but no other defects were seen within the caudate. No abnormal enhancement was seen after gadolinium administration. All patients showed slight to moderate improvement in motor skills bilaterally following surgery. No changes were identified in the opposite caudate or in the substantia nigra.

P109

### MR Imaging and Neuropsychological Evaluation of Schizophrenics

K Weingarten, P Wilner, G Kanwal, M Long, T Vullo, L Kantor, PT Cahill
*The New York (NY) Hospital–Cornell Medical Center*

Previous reports have shown anatomic differences in the brains of schizophrenics (SCs), such as enlarged ventricles, decreased gray matter in the temporal lobes, and a smaller corpus callosum compared with controls. The purpose of this study was to evaluate quantitative MR imaging and neuropsychological (NP) test results in SCs vs age- and sex-matched controls. Thirteen SCs and 11 age- and sex-matched volunteers have been evaluated with extensive NP tests. T1- (TR/TE = 950/35) and T2- (TR/TE = 2,300/35, 70, 105) weighted 5.0-mm MR images were acquired at 0.6 T, and image processing algorithms were used to obtain first and second order statistical information. Although all MR imaging studies were read as normal by a neuroradiologist, the prefrontal and left temporal lobes of the SCs were quantitatively measured to be smaller than those of the controls. MR imaging data from the prefrontal lobe demonstrated that the linear density and kurtosis of the distribution was smaller for the SCs than for controls ($P$ = .06). In SCs, the left temporal lobe had lower T1 values, lower third-order moments and skewness, and smaller local texture values than controls. No differences were measured in the right temporal lobe or in T2 values for the prefrontal or temporal lobes. Controls performed significantly better in NP tests than SCs for indices of short-term memory (prefrontal cortex, $P$ = .01) and of recall of verbal stimuli (left temporal lobe, $P$ = .02). MR data (third moments) of the left temporal lobe correlated with corresponding NP test results ($P$ = .03). To the author's knowledge, this is the first study to identify and correlate anatomic abnormalities, as demonstrated with MR imaging, with known NP impairments in SCs. This provides the potential basis for the investigation of the as yet unknown pathologic determinants in schizophrenia.

P110

### Sensitivity and Specificity of Echo-Planar Imaging for Detection of Neuropathology

MS Yoon, LA Johnson, AA Mosher, RJ Carbonneau, K Nadeau, MS Cohen, RM Weisskoff, KR Thulborn
*Massachusetts General Hospital NMR Center, Charlestown*

The sensitivity and specificity for detection of lesions in the brain have been determined for echo-planar SE imaging (EPI), with conventional SE imaging used as the gold standard, for T1-weighted (with and without gadolinium), T2-weighted, and proton-density–weighted contrast images. Conventional images of corresponding contrast, obtained with a GE Signa 1.5-T imager, have been used as the gold standard for the EPI images. EPI images were obtained with the Signa retrofitted implementation from Ad-

vanced NMR. T1-weighted EPI images were obtained with partial saturation. The T2-weighted EPI images were obtained at low resolution (256 × 128) and at high resolution (512 × 128). Proton-density contrast was obtained in short TE, finite TR (3 sec), single-shot (256 × 128) EPI images. The set of conventional images required 15 minutes of acquisition time, whereas the set of EPI images required only 14.4 seconds (low-resolution T2-weighted images) or 20.4 seconds (high-resolution T2-weighted images). All sets of conventional and EPI images were randomized with respect to case and contrast type to minimize bias due to prior knowledge of previous image sets of the same case. Readings were performed independently by two radiologists certified by the American Board of Radiology. Twenty-eight patients with ages ranging from 6 to 74 years, referred with known diagnoses or nonspecific complaints of seizures or headaches, were studied. The sensitivity and specificity for detection of intraaxial lesions were calculated for each image type. The sensitivities of EPI images were 0.74 for T1-weighted without gadolinium, 0.95 for T1-weighted with gadolinium, 0.81 for T2-weighted (256 × 128), 0.84 for T2-weighted (512 × 128), and 0.74 for proton-density–weighted images. Specificities were all above 0.96.

P111

### High-Dose Gadolinium-enhanced MR Study in the Evaluation of Central Nervous System Metastases

WTC Yuh, JD Engelken, MG Muhonen, NA Mayr, ET Tali, H Nguyen, F Gao, DJ Fisher
*The University of Iowa Hospitals and Clinics, Iowa City*

The authors studied the efficacy of higher doses of gadolinium in the MR evaluation of central nervous system metastases. Twenty-three patients with a clinical suspicion of central nervous system metastases were prospectively studied with gadoteridol (ProHance, Squibb Diagnostics), a nonionic, low-osmolality contrast agent. Each patient received an initial injection of 0.1 mmol/kg gadoteridol, followed 30 minutes later by an additional dose of 0.2 mmol/kg. No clinically significant effects were noted. No significant difference in lesion contrast was noted between the MR images obtained immediately after the initial injection of gadoteridol and those obtained after 10 and 20 minutes. After the additional dose of gadoteridol, however, there was significant improvement in visualization (70 of 71 lesions) and detection of lesions (42 new lesions in 18 of 23 patients). The initial-dose (0.1 mmol/kg) examinations identified 22 areas that were possible metastatic lesions. The high-dose (0.3 mmol/kg) examinations showed 19 of these areas to contain definite lesions and one to contain a possible lesion, and allowed the other two possible lesions to be excluded. Two patients had no detectable lesions. The additional information gained with high-dose examinations contributed to a potential modification in the treatment of nine of 23 patients.

P112

### Cystic Acoustic Neurinomas

ET Tali, WTC Yuh, H Nguyen, F Gao, TM Koci, JR Jinkins
*The University of Iowa Hospitals and Clinics, Iowa City*

Cystic acoustic neurinoma is an uncommon entity. The authors retrospectively reviewed MR examinations and clinical charts of seven patients who had pathologically proven acoustic neurinomas with MR evidence of cyst formation. Both intramural and extramural cysts were demonstrated in six of seven patients, whereas the seventh originally had only intramural cysts, but an extramural cyst was found at the 23-month follow-up study. The intramural cyst showed peripheral enhancement and higher signal intensity than cerebrospinal fluid on both T1- and T2-weighted images. Previous reports that multiple small intramural cysts may coalesce to form a larger cyst were corroborated in one case at a follow-up study. In contrast to the intracranial arachnoid cysts, the extramural/arachnoid cysts had higher signal intensity than cerebrospinal fluid on both T1- and T2-weighted images. They tend to cause indentation of the surrounding brain tissue, with the epicenter located between the tumor and brain on the opposite side of the internal auditory canal. This finding suggests a different fluid content and mechanism from that of the typical intracranial cyst for the formation of extramural/arachnoid cysts caused by the elevation and deformation of the leptomeninges by the tumor.

P113

### Morphometric MR Imaging Study of Basal Ganglia and Limbic System in Schizophrenia

CC Castro, GP Spoto, TL Jernigan, JR Hesselink
*Magnetic Resonance Institute, University of California, San Diego*

The purpose of this study was to establish possible morphologic differences in basal ganglia and limbic system structures between normal and schizophrenic patients. Axial and coronal double-echo MR images (TR = 3,000 msec, TE = 30/80 msec) of 33 schizophrenics and 21 matched controls were acquired with a 1.5-T GE Signa unit. Images were analyzed with a computer-based image processing system. Regions of interest were drawn around the temporal lobe, hippocampal formation, cortex of the parahippocampal gyrus, putamen, and globus pallidus. The total volume of each structure was calculated and expressed as a percentage of the supratentorial cranial volume. Compared with controls, schizophrenics were found to have significantly smaller temporal lobes ($P < .04$ at right, and $P < .02$ at left) and a larger left putamen ($P < .04$). A tendency to have larger right putamen ($P < .08$) and smaller right hippocampal formation ($P < .08$) was also noted in schizophrenics, with values slightly above significance. The cortex of the parahippocampal gyrus and the globus pallidus were not significantly different between groups. An MR imaging morphometric study of basal ganglia and limbic system structures in schizophrenic patients showed the presence of smaller temporal lobes and larger left putamen than those in controls.

P114

### MR Imaging Findings of Central Pontine Myelinolysis in Liver Transplant Patients

WTC Yuh, MP D'Alessandro, MN Hart, RJ Corry
*The University of Iowa Hospitals and Clinics, Iowa City*

In a recent autopsy review of liver transplant patients who underwent a neuropathologic examination, 13% were found retrospectively to have central pontine myelinolysis (CPM) that could not be diagnosed prospectively or retrospectively with head CT. The authors studied brain MR images of liver transplant patients who presented with central nervous system (CNS) symptoms to assess the findings and incidence of CPM as well as to follow its progression and how MR appearance correlates with neurologic course. The authors retrospectively reviewed the brain MR studies of five (of a total of 20) liver transplant patients who presented with CNS symptoms. A total of 22 MR examinations were performed, with sequential examinations for each patient. All five patients had abnormal MR findings, and the diagnoses included CPM (three patients), global cerebral anoxia due to cardiac arrest (one patient), and infarction (one patient). All three patients

with CPM had normal electrolyte and liver function study results during the course of their CNS symptoms. All three patients with CPM showed correlation of pontine T2 signal changes with clinical symptoms during the acute and recovery phases. Two of the patients with CPM recovered completely neurologically but still showed residual pontine T2 signal changes. The fourth patient with brain death and the fifth patient with left middle cerebral artery infarct had no pontine lesions. CPM is not uncommon in liver transplant patients with CNS symptoms. Severity of clinical symptoms appears to correlate with pontine findings on T2-weighted images. T1-weighted images are of no help in the diagnosis of CPM. CPM frequently reverses, and the patient's neurologic recovery is also demonstrated by diminished pontine signal abnormality on T2-weighted images.

P115

## Malignant External Otitis: MR Imaging and CT Appearance

R Bruening, F Gorgulla, M Naegele, M Reiser
*Departments of Radiology and Head and Neck Surgery, Bonn, Germany*

The object of this study was to evaluate the potential role of diagnostic imaging in staging and therapy/control of necrotizing external otitis. The extent to the deep skull base region and to the subtemporal space was mapped. MR imaging and CT were performed in 19 patients with suspected otitis. MR imaging was performed with a 1.5-T superconducting unit (Gyroscan, Philips). Gd-DTPA was injected for better delineation. CT was performed with a high-resolution technique. High-resolution CT was superior in depicting destruction of the temporal bone, especially in small lesions. MR imaging and CT both demonstrated opacification of the middle ear and the mastoid. Both imaging modalities displayed the mass effect. MR imaging enabled more exact staging of the tissue changes in the external meatus and along the eustachian tube, as well as the extension into the subtemporal space. In acute inflammation, MR imaging showed high contrast enhancement. MR imaging is a highly sensitive tool for the staging of malignant external otitis. MR imaging is the imaging modality of choice for depicting the extent into the deep skull base region.

P116

## Quantitative Characterization of Maxillary Sinusitis with MR Imaging

EW Sod*, KD Juhlin*, NM Szeverenyi†, RJ Phipps*, JD Allison†, DA Leopold§, CT Stafford†
**Norwich Eaton Pharmaceuticals, Norwich, NY; †State University of New York Health Science Center, Syracuse; ‡Medical College of Georgia, Augusta; and §Johns Hopkins, Baltimore, MD*

The utility of MR imaging for monitoring and quantifying the course of acute maxillary sinusitis was assessed. Multiecho-sequence coronal images through the maxillary sinus cavity were collected over time. Three or four echoes were collected for each 5-mm coronal section, with adjacent sections being interleaved to eliminate crosstalk. The volumes of the sinus contents (mucus and mucosa) and air space were measured using Cavalieri's principle for contiguous T2-weighted images. Assuming a single exponential decay, T2 values were calculated for each voxel in the sinus cavity with a least-squares regression on the logarithm of the multiecho intensity data. Frequency plots of these data suggested two overlapping distributions of T2 values. To characterize and understand the distribution of the T2 values, the data were modeled as a mixture of two distributions. The model consists of a distributional form (normal or long normal) for each component and a mixture parameter that indicates the proportion of the distribution attributable to each component. This results in a five-parameter model whose values summarize and characterize the state of the sinus at a particular visit. Combining the parameters with the volume measurements allows temporal examination of the sinusitis episode.

P117

## MR Imaging in the Evaluation of Head and Neck Tumors in Children

H Tonami*, H Yokota*, T Nakagawa*, T Okimura*, I Yamamoto*, T Kajimoto†, K Yamashita‡
*Departments of *Radiology, †Pediatric Surgery, and ‡Otolaryngology, Kanazawa Medical University, Ishikawa, Japan*

Twenty-six children with various head and neck tumors were examined with MR imaging, and the results were compared with those of other imaging modalities. Head and neck tumors included two rhabdomyosarcomas, two lymphoepitheliomas, one metastatic neuroblastoma, two neurofibromas, one pseudolymphoma, one pleomorphic adenoma, two infantile fibromatoses, seven hemangiomas, five lymphangiomas, and three cysts. The diagnosis was pathologically established in all cases. The children included 13 boys and 13 girls ranging in age from 14 days to 15 years. Twelve children underwent repeated follow-up studies for the evaluation of residual or recurrent lesions. All MR studies were performed with a 0.5-T unit. Sections were obtained with SE pulse sequences and both T1- and T2-weighted images were available in each case. Gd-DTPA–enhanced T1-weighted images were added in six cases. In all cases, MR imaging was superior in the detection and localization of tumors because of its multiplanar capability, lack of bone artifacts, and excellent soft-tissue contrast. CT, however, was necessary for the evaluation of associated bone lesions. Although MR imaging does not provide histologic specificity, these results indicate that MR imaging is a modality of choice in the detection, localization, and management of head and neck tumors in children.

P118

## Contrast-enhanced MR Imaging, US, and Ophthalmoscopic Evaluation of Choroidal Melanoma

KL Gupta, AM Righi, BG Haik
*Department of Radiology, Tulane University Medical Center, New Orleans*

Contrast-enhanced MR imaging and US were compared in imaging of choroidal melanoma. Forty-two choroidal melanomas greater than 2 mm in diameter were examined with MR imaging, US, and ophthalmoscopy. Twenty-eight patients underwent contrast-enhanced MR imaging. Tumor size correlated well between MR imaging and US (coefficient of correlation = 0.83 for precontrast imaging and US, and 0.92 for postcontrast imaging and US). All the tumors were detected with US. US provided diagnostic imaging and additional evaluation of the globe. Contrast MR imaging provided a specific signal pattern for the lesion and superb retrobulbar visualization. Enhanced MR imaging and US are complementary in evaluating uveal melanoma.

P119

## MR Imaging of the Mandible

D Yankelevitz, T Vullo, C Henschke, JP Whalen, PT Cahill
*New York (NY) Hospital–Cornell Medical Center*

The mandible may be one of the more sensitive bones to the age-related problem of osteoporosis. The changes seen in the mandible due to osteoporosis are unique in that the

trabecular bone in the alveolar ridge is much more sensitive than the remainder of the bone. These changes are manifested clinically by periodontal disease, fracture, and tooth loss. Current radiologic evaluation of the mandible generally consists of dental radiographs (bite wing and panoramic views) on which gross dimensions including the height of the alveolar ridge can be measured. In this study, high-resolution MR imaging was used for the evaluation of the mandible in man and dogs. A double-saddle RF coil was custom fabricated to fit the human chin and tuned for 0.6 T. Axial and oblique sagittal MR images (TR/TE = 500/35, resolution = 0.65 × 0.65 × 4 mm) were acquired in normal volunteers who did not have dental work that causes MR artifacts. In dogs, high-resolution mandible images (TR/TE = 750/33, resolution = 0.115 × 0.115 × 0.75 mm) were acquired in vitro at 2.0 T in all three standard anatomic planes. In MR images of the mandible, the mental foramen could be clearly distinguished from the alveolar ridge, the height of the alveolar ridge was easily measured, and the pulp chambers were identified within the dentine of the teeth. On high-resolution in vitro canine MR images, bone trabeculae were clearly delineated from the bone marrow, which, in normal mandible, is primarily fatty nonhematopoietic tissue. In summary, MR imaging appears to be useful in evaluating the alveolar ridge for changes that may make prediction of periodontal disease possible.

P120

## MR Imaging, Myelography, and CT Myelography: Comparison Study in the Diagnosis of Disk Herniation and Spinal Stenosis

KL Gupta, AM Righi
*Department of Radiology, Tulane University Medical Center, New Orleans*

MR imaging, myelography, and CT myelography were compared in the diagnosis of herniated nucleus pulposus (HNP) and spinal stenosis. The sensitivity and specificity of these parameters were analyzed alone and in various combinations. A retrospective evaluation of 57 patients for a total of 119 levels with 59 surgical explorations was employed. All patients underwent all three tests, and each set was read blindly by two neuroradiologists without knowledge of the clinical presentation. Surgical operative notes were reviewed for confirmation and comparison of the results. Forty-seven patients for a total of 70 levels were evaluated for HNP. MR imaging demonstrated a sensitivity of 71.4%, myelography of 59.3%, CT myelography of 77.8%, myelography with CT myelography of 76.4%, CT myelography with MR imaging of 74%, MR imaging with myelography of 72%, and all combined of 68%. The specificity was 73% for MR imaging, 89.2% for myelography, 73% for CT myelography, 82% for myelography with CT myelography, 74% for CT myelography with MR imaging, 82% for myelography with MR imaging, and 79% for all tests combined. For spinal stenosis, 28 patients for a total of 47 levels were evaluated. The sensitivity was 87% for MR imaging and CT, 82% for myelography, 81% for myelography plus CT myelography, 87% for MR imaging with CT myelography, 85% for MR imaging with myelography, and 85% for all together. The specificity was 75% for MR imaging, 87% for myelography, 75% for CT myelography, 81% for myelography with CT myelography, 75% for MR imaging with CT myelography, 81% for MR imaging with myelography, and 79% for all. MR imaging, CT, and myelography remain complementary in evaluation of HNP and spinal stenosis.

P121

## Focal Muscle Lesions in Mitochondrial Myopathy: MR Imaging Evaluation

JL Fleckenstein, RG Haller, MS Girson, RM Peshock
*University of Texas Southwestern Medical Center, Dallas*

Focal atrophy and fatty replacement of individual muscles with sparing of the sartorius and gracilis muscles characterize many myopathies, including muscular dystrophy. To determine whether this pattern also occurs in mitochondrial disorders, the authors investigated six patients with mitochondrial myopathy associated with progressive external ophthalmoplegia. MR imaging was performed at 0.35 T with T1-weighted, T2-weighted, and STIR sequences of the upper and lower extremities. The characteristic finding in these patients was a fine, diffuse, fatty infiltration of thigh muscles (ie, "marbling") evident on T1- and T2-weighted images. STIR images revealed little evidence of associated edemalike processes (eg, inflammation and necrosis). Five of six patients showed particularly prominent fatty infiltration of the sartorius and gracilis muscles, while selective involvement of other limbs was not seen. These results suggest that selective vulnerability of the extraocular muscles in mitochondrial disorders is shared by the sartorius and gracilis muscles. Selective sparing or involvement of the sartorius and gracilis muscles may have implications for diagnosis and pathophysiology in myopathies.

P122

## Sacral Stress Fractures: MR Characterization

ME Schenk, JP Schils, DW Piraino, BJ Richmond, GH Belhobek, MT Modic
*Department of Radiology, Cleveland (Ohio) Clinic Foundation*

The purpose of this study was to evaluate and characterize the MR findings in sacral fractures. Patients with osteopenia, metabolic bone disease, total hip replacements, and a history of radiation therapy are at risk of developing stress fractures in the sacrum as well as other areas. Sacral stress fractures are of note in that they often present clinically as radiculopathy or cauda equina symptoms mimicking lumbar canal stenosis or disk or metastatic disease. The MR findings are often overlooked or misinterpreted as more malignant disease. The study group consisted of 11 patients in whom a combination of clinical evaluation and multiple imaging modalities (MR, radionuclide study, plain radiograph, and CT) were diagnostic of stress fracture of the sacrum. Ten of these 11 patients demonstrated a longitudinal decrease in signal intensity on T1-weighted SE images within the sacral alae paralleling the sacroiliac joints and lateral to the sacral foraminae. This was bilateral in eight patients and unilateral in two and best appreciated on axial images. Eight patients had an additional horizontal area of decreased signal intensity traversing the S1/S2 syndesmosis. This was appreciated on both axial (five of 11) and sagittal (eight of 11) images. More variable findings include angulation between S1 and S2 or spondylolisthesis of S1. A greater awareness of sacral stress fractures and familiarity with their MR appearance will aid in early recognition and subsequent appropriate treatment. A vertically oriented alae component in combination with a transverse sacral body component is characteristic of a sacral stress fracture. Noncharacteristic signal intensity changes would require additional imaging to distinguish fractures from other lesions such as those of metastatic disease.

P123
### MR Imaging of Fetal Abnormalities
WTC Yuh, ET Tali, F Gao, H Nguyen, D Fisher
*The University of Iowa Hospitals and Clinics, Iowa City*

The authors studied the pregnancies of 28 women with abnormal findings at fetal US. Fetal movement is a known drawback in prenatal MR imaging. The authors achieved transient fetal paralysis (30–60 minutes) with pancuronium bromide. This poster demonstrates the MR findings in confirmed cases of hydrocephalus, alobar holoprosencephaly, iniencephaly, diastematomyelia, hemimegaencephaly, hydranencephaly, partial agenesis of corpus callosum, Dandy-Walker syndrome, quadrigeminal plate cistern cyst, intracranial lipoma, hypoplastic extremities, pentalogy of Cantrell, diaphragmatic hernias (with and without herniated liver), polycystic kidneys, fetal ascites, and extrapulmonary sequestration. MR imaging appears to be a useful adjunct to US in selected cases.

P124
### Enhanced MR Imaging of Cervical Spines after Cervical Fusion
KL Gupta, AM Righi
*Department of Radiology, Tulane University Medical Center, New Orleans*

Enhanced MR imaging was used in patients who had undergone anterior cervical fusion in order to establish criteria for evaluation of the postoperative cervical spine. A retrospective study of 35 patients after cervical fusion involved enhanced MR images evaluated by two neuroradiologists without knowledge of clinical presentation. Plain radiographs and charts were then reviewed for clinical and surgical correlation. The signal characteristics of the vertebral bodies and intervening disks were recorded both before and after gadolinium injection. A normal evolution of signal characteristics was seen in both the vertebral bodies and disks. Distinction between normal and abnormal changes was helpful in the workup of fusion instability. Enhanced MR imaging will be of paramount importance in the workup of fusion instability because of its noninvasive nature. This study lays the foundations for the distinction of normal evolutionary changes in the postoperative cervical spine.

## Monday, April 27, 12:15 PM–1:30 PM
## Body, Musculoskeletal

Posters P200–P233

P200
### MR Tomography and MR Angiography in Subdiaphragmatic Radiation Therapy Planning
M Müller-Schimpfle*, A Köster†, B Betsch*, G Brix*, B Kimmig†, G Layer*, W Semmler*, G van Kaick*
**Department of Oncological Diagnostics and Therapy, Germany Cancer Research Center, and †Department of Radiology/Radiotherapy at the University, Heidelberg, Germany*

The aim of this study was to assess the anatomic variability of the splenic pedicle and to individualize field shaping in subdiaphragmatic radiation therapy with noninvasive visualization of abdominal organ and blood vessel anatomy. Within a 14-second breath-holding period, strongly T1-weighted coronal images displaying the kidneys and the spleen were acquired with a rapid-acquisition SE technique (TR msec/TE msec = 150/10). Additionally, coronal MR angiography acquisition was performed by using a sequential GRE sequence (FLASH 2D 30/10,30° flip angle) with a breath-holding technique. For 3D reconstruction of the MR angiogram, a maximum-intensity-projection algorithm was used. A selected MR tomogram and MR angiogram were superimposed by a computer program and projected onto the simulation film. This method was employed in 36 patients with malignant lymphoma. Anatomic variations of the splenic pedicle were typed according to their location in projection onto the left kidney. The resulting superimposed images allowed good demarcation of kidneys, spleen, liver, and lumbar vertebrae, as well as abdominal vascular anatomy. The splenic pedicle crossed the left kidney above the upper pole in one-fourth of all cases, whereas in another fourth, the kidney was crossed in projection onto the middle third of the renal parenchyma. The individual irradiation field was exactly defined and thereby led to reduction of the irradiated kidney parenchyma of up to 50%. This technique is capable of displaying the variable subdiaphragmatic anatomy and of achieving a noninvasive, optimized treatment plan for lymphatic irradiation.

P201
### Sequential MR Imaging Study of Atheroma in Thoracic Aortas of Hypercholesterolemic Rabbits
L Macartney, W Kerns, F Tobin, R Kapadia, R Mestetsky, S Sarkar
*SmithKline Beecham Pharmaceuticals, King of Prussia, Pa*

The purpose of this study was to evaluate the utility of MR imaging for the detection of atheroma in the thoracic aortas of hypercholesterolemic rabbits in vivo. The authors also evaluated the feasibility of MR imaging for the sequential monitoring of atheroma progression. Hypercholesterolemia was induced in 12 New Zealand white rabbits by administering a high-fat diet for 16 weeks. Individual rabbits were anesthetized with an intramuscular injection of a mixture of ketamine/acetylpromazine/xylazine, and MR images were collected with a 1.5-T GE clinical system using a flow-compensated, cardiac-gated, SE imaging sequence. Transverse sections (5 mm thick) of the thoracic aorta were imaged. Atheroma was identified as a high-signal-intensity region within the lumen of aorta. Four rabbits were killed immediately after this baseline imaging, and the MR images were compared with results of standard morphologic techniques. The excellent correlation between the MR and necropsy results, shown in the Table, suggests that aortic atheroma (> 1 mm in thickness) can be visualized with MR imaging at 1.5 T. The remaining eight rabbits were maintained for subsequent evaluation 12 and 24 weeks later. The authors have been able to localize and sequentially evaluate aortic atheroma in individual rabbits. The results of this sequential study to visualize and quantitate the progression of atheroma will be discussed.

| Rabbit | MR Imaging of Thoracic Aorta | Macroscopic Thoracic Aorta |
|---|---|---|
| 1 | + | + |
| 2 | – | +* |
| 3 | + | + |
| 4 | + | + |

*Thin, diffuse atheroma < 1 mm thick.

P202

## A New Approach to the Study of Myocardial Strain: Optical Flow in Cine MR Images

HJ Vesselle, SC Amartur
*Department of Radiology, University Hospitals of Cleveland, Case Western Reserve University, Cleveland*

The noninvasive estimation of myocardial strain is drawing considerable attention, as strain reflects the amount and direction of cardiac deformation, which change under ischemic conditions. Strain measurements have recently been reported with tagging and phase-contrast mapping. Here, the authors propose an alternative that does not rely on any special pulse sequence strategy. The authors have previously reported the use of optical flows computed from a set of cine MR images to characterize the intricate motion of the heart. The method uses image brightness variations between consecutive frames to compute in-plane displacements $[U = (u_1, u_2)^T]$ of moving image features. For each instant sampled in the cardiac cycle, a dense displacement field (pixel level) is obtained throughout the myocardial wall, allowing resolution of intramural displacement gradients. From such displacement fields that contain both the rigid and nonrigid components of cardiac motion, cardiac deformation is evaluated by computing the displacement gradient tensor $\mathbf{G}$ for each pixel, given by $\mathbf{G} = (\nabla u_1, \nabla u_2)^T$. The Green strain tensor $\mathbf{E}$ was derived as $\mathbf{E} = (\mathbf{F}^T\mathbf{F} - \mathbf{I})/2$, with $\mathbf{F}$ defined as $\mathbf{F} = \mathbf{I} + \mathbf{G}$, where $\mathbf{I}$ is the identity tensor. The spatial differentiation operations were regularized with the Beaudet operators. This method was applied to sets of short-axis cine MR images obtained in a normal volunteer with retrospective cardiac gating and a 30-msec interframe spacing. Results demonstrate the method's ability to depict transmural gradients in myocardial strain as well as intramural and regional differences in strain throughout the entire cardiac cycle, with high spatial and temporal resolution.

P203

## MR Imaging Evaluation of the Effect of Enalapril on Aortic Stenosis–induced Left Ventricular Hypertrophy

T Cui*, RS Mezrich*, P Scholz*, A Rakhit†, F Douglas†
**Robert Wood Johnson Medical School, New Brunswick, NJ, and †Ciba-Geigy Pharmaceuticals, Summit, NJ*

The current study was designed to apply MR imaging techniques in determining the effect of enalapril on regression of left ventricular hypertrophy (LVH) caused by aortic stenosis. Aortic stenosis was surgically induced in 8-week-old dogs for the development of LVH. The enalapril treatment was started 1 month later and continued for 6 months. The study groups included hypertrophy untreated ($n = 6$) and treated ($n = 14$) and controls with ACEI ($n = 5$) and without ACEI ($n = 9$). Images were acquired with a 0.6-T system with a gated, multiplanar sequence (TE = 30 msec, TR = 90% of R-R interval). Six sections were imaged from base to apex. Images at end diastole and end systole were determined at R-wave and the down slope of T-wave. Left ventricular mass and percentages of shortening of endocardium and epicardium were calculated from MR images. The ratios of left ventricular mass to body weight were 6.2 ± 0.6 in treated and 6.2 ± 0.4 in untreated hypertrophic subjects compared with 4.5 ± 0.1 in both controls ($P < .001$). The mean circumferential percentages of shortening of endocardium and epicardium were uniform in controls, whereas these values were progressively decreased from equator to apex in hypertrophic and treated subjects ($P < .05$). However, endocardial shortening was significantly increased only at the equator in treated dogs (37% ± 8%) compared with hypertrophics (24% ± 4%) and controls (26% ± 2%) ($P < .03$). Differences in the wall thickness between hypertrophic and treated dogs at all levels were insignificant. The authors conclude that enalapril did not result in regression of LVH induced by aortic stenosis as studied with MR imaging.

P204

## Optimizing Tumor-Liver Contrast Following Administration of Gd-EOB-DTPA with Comparison to Gd-DTPA

A Mühler, O Clément, V Vexler, Y Berthezène, R Kuwatsuru, RC Brasch
*Contrast Media Laboratory, University of California, San Francisco*

A new hepatocellular MR contrast agent, Gd–ethoxygenzyl (EOB)–DTPA (70% biliary excretion) can substantially improve the lesion-to-liver contrast, and can expand the "imaging window," compared with strictly extracellular Gd-DTPA. A mammary adenocarcinoma was implanted into rat livers. MR imaging was performed at 2 T with T1-weighted SE (TR/TE = 200/6) before and after 0.1 mmol/kg Gd-DTPA or Gd-EOB-DTPA (positive liver enhancement). Additionally, Gd-EOB-DTPA was used as a negative liver enhancer by applying a STIR sequence (TR/TE/TI = 1,000/65/6). The enhancement levels were measured between 1 minute and 1 hour after contrast agent administration with calculation of contrast-to-noise ratios (C/Ns). Before contrast agent administration liver tumors were observed as hypointense lesions on SE images (C/N = −6.5) and as hyperintense lesions on STIR images (C/N = +7.2). Following Gd-DTPA administration contrast between tumor and liver never exceeded preinjection values. Following injection of Gd-EOB-DTPA, persistent positive liver enhancement of more than 200% (SE) following injection of Gd-EOB-DTPA resulted in increase of C/N values to −31.1. With the STIR sequence, Gd-EOB-DTPA produced a signal void in liver parenchyma and improved C/N of tumors substantially (+38.0). Gd-DTPA has limited utility for detection of liver masses due to its rapid equilibration with the extracellular fluid space. Gd-EOB-DTPA dramatically increases contrast between tumor and liver over at least 1 hour. Owing to strong T1 relaxation enhancement within the hepatocyte, Gd-EOB-DTPA may be used effectively as a positive or negative liver enhancer depending on the sequence used.

P205

## 19-F T2 Measurement of PFOB in Vivo with Intercellular $Po_2$

Q Guo, DJ Schumacher, RB Buxton, RF Mattrey
*Department of Radiology, University of California, San Diego, Medical Center*

Emulsified perflubron (PFOB) accumulates in the reticuloendothelial cells of liver, spleen, and bone marrow and in macrophages. It is well known that the 19-F spin-lattice relaxation rate 1/T1 of PFOB is linearly related to $Po_2$. The authors have shown in vitro that the transverse relaxation time rate 1/T2 of PFOB is also affected by $Po_2$ but is three times more sensitive than 1/T1. In this study, T2 changes were evaluated and compared with T1 changes as affected by alteration of intercellular $Po_2$ in an abscess model. Abscesses were created in two rabbits with *Escherichia coli* inoculation in the calf. Two days later, 10 g/kg PFOB emulsion was infused intravenously. Ten days after infusion, when blood PFOB levels were significant, the rabbits were imaged with a 5-cm-diameter cylinder coil tuned to the 19-F resonance in a 1.5-T whole-body imager. After anesthesia the T1 and T2 of 19-F in the abscess were measured with a preimaging spectroscopic technique without the application of any gradient fields. These measure-

ments were done while the rabbits were breathing room air (20% oxygen) and pure oxygen and then following sacrifice (total ischemia). The apparent T2 and T1 of 19-F were calculated from a nonlinear least-squares fit to the partial-saturation signal intensity data acquired with TEs of 25, 100, 200, and 400 msec, and TRs of 1, 2, 4, 8, 14, and 16 seconds. Both T2 and T1 of 19-F in the abscess were changed significantly when the $FIo_2$ was increased from 20% to 100%. For room air, pure oxygen, and after sacrifice, the T1 values in one rabbit were 5.4, 4.0, and 9.0 seconds and the T2 values were 0.50, 0.39, and 0.91 seconds, respectively. These values in the second rabbit were 5.8, 4.6, and 7.1, and 0.57, 0.49, and 0.67 seconds, respectively. These results acquired in vivo show that the slope of the relaxation time rate (1/T) versus $Po_2$ for the transverse relaxation is greater than the longitudinal relaxation.

P206

## MR Signal Characteristics of Barium-Attapulgite Oral Contrast Formulations

GS Foster

*Department of Diagnostic Radiology, Rush-Presbyterian-St Luke's Medical Center, Chicago*

An ideal negative gastrointestinal MR contrast agent should yield a null signal, or a signal significantly less than that of free water with a variety of clinically useful imaging pulse sequences. Barium has been reported to be an effective negative contrast agent in the upper gastrointestinal tract, but has not shown consistent signal suppression in the distal small bowel, due to dilutional effects. Clay compounds such as attapulgite have been shown to have superior relaxation properties compared with barium. The use of clay compounds may be limited by untoward pharmacologic effects. Mixtures of barium and attapulgite might provide satisfactory nulling of intraluminal signal and could be administered in volumes appropriate for oral contrast administration. A phantom was constructed containing prototype oral contrast preparations, as well as reference samples containing either water or corn oil. The following formulations were used: (*a*) barium (40% wt/wt) [B] (E-Z-Paque; E-Z-Em, Westbury, NY); (*b*) attapulgite (40 mg/mL) [A] (Advanced Formula Kaopectate; Upjohn, Kalamazoo, Mich); (*c*) barium-attapulgite 3:1 solution; (*d*) barium-attapulgite 10:1 solution; (*e*) barium-attapulgite 100:1 solution; and (*f*) barium-attapulgite 10:1 solution suspended in a 25% corn oil emulsion. The phantom was evaluated with a 1.5-T clinical imager (GE Signa), with GRE, SE, and IR pulse sequences. The signal intensity of each sample was evaluated relative to the reference samples. T1 and T2 were calculated. Attapulgite (40 mg/mL) demonstrated the lowest signal intensity at all pulse sequences evaluated. Signal suppression by attapulgite was 77%–100% on SE, IR, and GRASS sequences relative to the water reference. Signal suppression relative to water on SPGR sequences was related to TE. Barium-attapulgite 3:1 solution demonstrated less signal than barium and water at all sequences. Other tested solutions demonstrated less signal than water on IR and T2-weighted sequences but not on SPGR or T1-weighted sequences. Attapulgite has signal characteristics that appear to make it an ideal "negative" oral contrast agent. However, at the tested concentration, the maximum recommended daily dose of attapulgite is 210 mL. This volume is unlikely to be sufficient to adequately displace small bowel contents. As this product is marketed as an antidiarrheal agent, it is possible that higher doses could have adverse effects on patients. Barium-attapulgite solutions offer improved signal characteristics compared with barium alone and compare favorably with the attapulgite preparation. With a barium-attapulgite 3:1 solution, a total contrast volume of 840 mL could be administered. Further clinical studies are necessary to determine the effect of administration of this contrast agent dose on intraluminal signal and possible dilutional effects in vivo.

P207

## Utility of Gadolinium Chelates in Liver MR Imaging: Dose Evaluation with Dynamic Imaging

MV Johnson, VM Runge, RA Garneau, MA Brack, JE Kirsch

*Magnetic Resonance Imaging and Spectroscopy Center, University of Kentucky, Lexington*

Conventional spin-echo and breath-hold images were compared prior to and following bolus contrast agent administration (0.1–0.3 mmol/kg gadoteridol intravenously) to assess lesion detectability and diagnostic utility in liver MR imaging. Precontrast T1- and T2-weighted spin-echo images were first obtained. Immediately prior to and at 30-second intervals following bolus contrast agent injection, breath-hold (10 seconds), multisection spin-echo images were acquired. Then, at 5 and 15 minutes postcontrast, paired non–breath-hold and breath-hold T1-weighted images were obtained. Image analysis was performed with region-of-interest measurement, with $SD/N = SI_{lesion} - SI_{liver}$/noise. Dynamic contrast-enhanced CT was performed for correlation. Dynamic postcontrast fast MR imaging provided additional information for all patients with space-occupying liver lesions (four of six), irrespective of dose, over all preconstrast images. The nature of this information included improved lesion border definition, distinction of benign cysts from neoplasia, improved lesion visualization and characterization, and detection of additional lesions. By SD/N measurement, neoplastic tissue was best distinguished from normal liver on immediate (0–2 minutes) postcontrast breath-hold images versus all other imaging techniques, regardless of dose. The SD/N on breath-hold dynamic contrast-enhanced images was superior to that of the next best imaging technique by 43%–78%. At 0.3 mmol/kg, lesion discrimination was also markedly improved on non–breath-hold T1-weighted images, a result not obtained at 0.1 mmol/kg. Preliminary results in this ongoing clinical trial indicate improved lesion detectability with an intravenous gadolinium chelate, gadoteridol, on dynamic postcontrast breath-hold liver images, with greater utility for high dose (0.3 mmol/kg).

P208

## MR Imaging of Spinal Arachnoid Cysts

R Silbergleit, EM Spickler, SR Aravapalli

*Henry Ford Hospital, Detroit*

The purpose of this study was to evaluate the usefulness of MR imaging in preoperative evaluation of spinal arachnoid cysts. Spinal MR studies of six patients with surgically proven spinal arachnoid cysts were reviewed retrospectively. Comparison was made with results of other imaging studies, including plain radiography, CT, myelography, and postmyelography CT. In all six patients, MR helped define the nature and extent of the lesion. In one case, MR demonstrated the extent of the lesion to be greater than suspected at myelography. MR was particularly useful in diagnosing those cases in which the arachnoid cyst did not communicate freely with the subarachnoid space. Myelography and postmyelography CT in these cases showed a nonspecific intradural extramedullary mass. MR clearly demonstrated the cystic nature of the lesion. CT better demonstrated the degree of cord compression in one case in which the axial MR images were suboptimal. MR imaging is effective and useful in diagnosing and determining the extent of spinal arachnoid cysts.

P209

## MR Imaging of Gastrointestinal Tract: Proposal of Cost-Free, Noninvasive Contrast Medium

L Balzarini*, S Aime†, L Barbero†, E Ceglia*, M Fasano†, R Petrillo*, Y Reyner*, JD Tesoro-Tess*, R Musumeci*

*Istituto Nazionale Tumori, Milano, Italy, and †University of Turin (Italy)*

After the occasional observation in a nourished baby of good-contrast delineation of the upper gastrointestinal tract, the authors tried a series of different commercial fresh and lyophilized milks in both experimental and clinical tests. The laboratory evaluations were made with a 0.5-T magnet, while imaging was performed with a 1.5-T magnet. After selection of the most effective lyophilized product, prepared in conformity with commercial instructions, a group of patients with gastric and rectal cancer were examined. The most intense positive contrast effect, due to shortening of T1, was obtained with Nidina 1 (Nestle). This result is related to the concentration of the paramagnetic ions (manganese and iron) bound in the macromolecules of milk, such as casein. The best imaging sequence was a spin-echo T1-weighted sequence. After the patient's ingestion of milk, good delineation of the stomach with sufficient distribution in duodenum and in the very proximal bowel was achieved, as well as good depiction of the rectum and rectosigmoid junction after enema. The practical value of this paramagnetic complex depends on its being noninvasive, economic, and tolerable; thus, the authors suggest the use of Nidina 1 in patients with gastric and rectosigmoid cancer in order to increase the diagnostic efficacy of MR imaging.

P210

## MR Flow Measurements in Pulmonary Arteries versus Lung Perfusion Scintigraphy in Patients with Central Bronchogenic Carcinoma

AH Gamroth*, LR Schad*, CM Wacker*, W Semmle*, U Gehling*, E Müller†, JH Clorius*, G van Kaick*

*German Cancer Research Center, Heidelberg, and †Siemens, Erlangen, Germany*

Parenchymal resection in patients with lung cancer requires a separate evaluation of the blood supply in both lungs. Routinely, this is done by means of lung perfusion scintigraphy (Tc-99m). The purpose of this study was to determine whether MR global flow measurements of main, right, and left pulmonary arteries (MPA, RPA, and LPA) are a suitable tool for this clinical investigation. MR blood velocity measurements were performed with the RACE technique (real-time acquisition and evaluation of blood flow in 1D space projection) with an MR unit (Magnetom, 1.5 T, Siemens). The RACE measurements were obtained in 10 seconds with breath holding in a plane perpendicular to the flow of the pulmonary arteries. The flow was calculated in each vessel by multiplication of mean blood flow velocity (measured with RACE) by the vessel area (determined on a flow-compensated GRE image at the same position). Eight patients, aged 48 to 66 years, with central bronchogenic carcinoma were examined. MR findings were correlated with those of perfusion scintigraphy. Quantitative evaluation of blood flow was possible in RPA and LPA in all cases. Measurements in MPA were difficult in patients with elongated ascending aortas with use of RACE. The ratio of MR blood flow measurements of RPA and LPA correlates well with the results of perfusion scintigraphy (RPA to LPA). The advantages of RACE are the possibility of real-time blood flow measurements and the determination of absolute flow values in pre- and poststenotic regions. Disadvantages can appear in complex anatomic situations by superimposition of neighboring blood vessels. These preliminary results show that MR blood flow quantification in the pulmonary arteries can be used as an alternative method for global estimation of blood flow (RPA to LPA) in patients with central bronchogenic tumors. The clinical results and an estimation of the accuracy of MR blood flow measurements are discussed in detail.

P211

## Evaluation of Multilevel Flow Pattern in True and False Lumina of the Thoracic Aorta in Patients with Aortic Dissection after Surgical Intervention

A von Smekal*, KC Seelos*, J Gieseke†, M Reiser*, HJ Biersack*

*Department of Nuclear Medicine and Radiology, University of Bonn (Germany), and †Philips Medical Systems, Bonn*

By determination and evaluation of multilevel blood flow patterns in the true and false lumina of the thoracic aorta in patients with thoracic aortic dissection who have undergone surgical treatment, it should be possible to evaluate the effect of the surgical intervention. Especially in cases of leakage at the site of anastomosis of the graft, the hemodynamic significance of a persisting dissection should be quantitated to monitor further development of the ongoing dissection. Aortic flow with profiles at different levels of the ascending and descending aorta and the arch were obtained by using a cardiac-gated cine velocity-sensitive FLAG sequence with a 1.5-T Philips Gyroscan. Depending on the patient's heart rate, approximately 16 equally spaced intervals during the cardiac cycle were studied. After data processing, multiple regions of interest corresponding to the different lumina of the aorta and/or arterial branches were defined throughout the intervals, and flow profiles were derived. The ratios of the flow volume velocity in the different lumina of the dissected aorta were calculated. The hemodynamic effect of the surgical treatment on the different lumina of the dissected aorta could be demonstrated. Pathologic structures and flow patterns were identified. The ratios derived from the aortic lumina at different levels provide the physician with helpful information regarding surgical success and allow monitoring of short-term as well as long-term changes in the hemodynamics of the different aortic lumina to determine the need for further therapeutic intervention.

P212

## Gradient-Echo MR Imaging of Portal Vein Thrombosis: Technique and Results

C Martinoli, G Cittadini Jr, C Pastorino, CE Neumaier, M Bertolotto, I Rosemberg, GA Rollandi, G Grozio, G Garlaschi

*Institute of Radiology "R," University of Genoa (Italy)*

The MR appearance of thrombosis of the portal vein and its branches with GRE sequences is described. The study consisted of two parts. In the first part, five healthy volunteers were examined to select the optimal section plane for each portal vessel to be studied. Given the "time-of-flight" effect of GRE sequences, an imaging plane axial to the direction of flow is needed to obtain maximal signal enhancement of flowing blood. This procedure was performed first to increase signal differences between flowing blood and thrombus and to ameliorate the sensitivity in assessing slow venous flows. In the second part of the study, 13 patients with thrombosis of the portal system diagnosed with Doppler sonography, CT, and digital subtraction angiography were examined with GRE technique. GRE MR imaging helped confirm the presence and define the extent of vessel thrombosis with high diagnostic accuracy. Namely, GRE MR imaging depicted all eight thromboses of the main portal vein and of the right lobe intrahe-

patic branches; all seven thromboses of the left lobe intrahepatic branches and of the left portal vein; all nine thromboses of the right portal vein; all five thromboses of the superior mesenteric vein, and six of seven thromboses of the splenic vein. In addition, it proved an accurate means of detecting portosystemic collateral vessels (periportal, perigastric, and umbilical). It is concluded that GRE sequences with appropriate technique can be effectively performed as a complement to conventional SE MR imaging to obtain further details on portal vessels. In diagnostic imaging, these sequences may be helpful for confirming Doppler findings and for overcoming Doppler limitations in obese patients and patients with abundant intestinal gas.

P213

### Do Rapid Spin-Echo Imaging Technique Parameters Matter?

A Ling*†, NA Avila*†, AJ Dwyer†, JA Frank†
*Georgetown University, Washington, DC, and †National Institutes of Health, Bethesda, Md*

To evaluate the sensitivity of a rapid spin-echo imaging technique (PRISE) to variations in sequence parameters (TR and flip angle), the upper abdomens of 11 patients were studied at 0.5 T with TRs of 167, 233, and 300 msec, and flip angles of 90°, 125°, and 145° during suspended respiration at multiple interleaved levels. Conventional T1-weighted upper abdomen images (TR = 300 msec, angle = 90°) were also obtained. Signal intensity and variability of visible intraabdominal organs, intraabdominal fat, and skeletal muscle were measured with standard region-of-interest technique. Liver-to-lesion contrast-to-noise ratio (C/N) measurements were calculated for the five of 11 patients who had liver metastases. Organ signal-to-noise ratio (S/N) declined as data collection time decreased. Changes in TR and flip angle did not affect S/N; no optimum TR or flip angle regimen was identified. While a small C/N decrease for the shortest TR at all flip angles was observed, these differences were insignificant. In all instances, S/N and C/N of conventional T1-weighted images exceeded those of PRISE images. Among the parameter ranges investigated, none optimized objective measures of PRISE image quality; this pulse sequence is not sensitive to variations in technique. Although markedly decreased imaging times permit multiple images to be obtained during a single suspended breath, anticipated motion artifact improvement was overwhelmed by decreases in S/N and C/N.

P214

### Benign Focal Liver Lesions: Classification with Dynamic Contrast-enhanced MR Imaging with Turboflash Sequences

W Judmaier*, M Lener*, K Wicke†, G Judmaier†
*Department of Magnetic Resonance and Spectroscopy, †Department of Internal Medicine, †Division of Radiology, and †Division of Gastroenterology, University of Innsbruck (Austria)*

Because of the high sensitivity of ultrasound (US), focal liver lesions are frequently detected in patients lacking hepatic symptoms. The specificity of US, however, does not allow for a satisfactory classification of these incidental findings. The authors investigated 36 patients with dynamic Gd-DTPA TurboFLASH imaging to establish criteria for the differentiation of benign focal liver lesions. The specificity of MR imaging should allow omitting further investigations in these patients with contrast-CT scintigraphy and biopsies. The examinations were carried out with a 1.5-T Magnetom (Siemens) using T1- and T2-weighted SE imaging. In addition, a dynamic contrast-enhanced series was obtained by injecting a bolus of 0.1 mmol/kg Gd-DTPA and acquiring a selected section at an interval of 4 seconds over a duration of 3 minutes. A constant and typical enhancement pattern was observed in liver hemangioma ($n$ = 22) and focal nodular hypoplasia ($n$ = 10). Two liver cell adenomas showed a clearly different enhancement pattern; however, this result was not statistically significant. The MR classification of the liver lesions was consistent with the final classification achieved combining sonographic, CT, and clinical results. MR imaging, however, failed to depict two focal nodular hypoplasias and two additional hemangiomas.

P215

### The Effect of Different Sampling of K Space on Fast Spin-Echo Images of the Knee

DW Piraino, BJ Richmond, JP Schils, PA Hardy, JA Tkach, PB Weber
*Department of Radiology, Cleveland Clinic Foundation*

A conventional T2-weighted spin-echo (CSE) examination of the knee requires a long TR to achieve T2 weighting and a sufficient number of sections. The consequence is a long imaging time (8 minutes). In fast SE (FSE) imaging, it is possible to image the entire knee with 22 sections in 2 minutes. The different methods of acquiring an FSE image remain to be evaluated as to their efficacy in musculoskeletal imaging. The authors hypothesized that altering the ordering of k-space sampling within a given echo train length (ETL) would have a noticeable effect on the appearance of FSE knee images. The authors imaged the knee of a healthy volunteer with CSE and FSE sequences on a 1.5-T imager. Both images were acquired with a 2,500-msec TR, 256 × 192 × 1 matrix, and 22 3-mm sections. The FSE images were made with ETL-8, and different ordering of k-space acquisition was achieved by varying TE from 18 to 144 msec while keeping the echo spacing constant at 18 msec. In comparing the images, there was no change in the type or appearance of artifacts. On the FSE images, as TE increased, the perceived T2 weighting increased, but to achieve comparable T2 weighting at TE = 90 msec with CSE, it was necessary to increase TE to 144 msec. With TE = 144 msec, the appearance of edges, such as tendons with fat and muscle, was improved, presumably as a result of collecting the high-frequency data at higher signal strength. The shortened acquisition time of the FSE technique made imaging with a 4,000-msec TR and 256 × 256 × 2 matrix clinically feasible, as imaging time was reduced to 4 minutes 17 seconds.

P216

### Fast Abdominal Imaging with Gd-DTPA: Comparison of Five Techniques

KC Li, W Whitney, C McDonnell
*Department of Radiology, Stanford (Calif) University School of Medicine*

The objective of this study was to find the best available pulse sequence for providing the highest contrast-to-noise ratio per unit time for the following situations: no breath holding, up to 10 seconds of breath holding, and up to 20 seconds of breath holding. Five fast imaging pulse sequences were tested: MPSPGR, MPGRASS, WARP, IR-WARP, and DEQ-WARP. A contrast phantom consisting of 10 test tubes with Gd-DTPA saline solutions at different concentrations (0.02–10 mmol/L) (T1 = 140–3,000 msec) was prepared. The phantom was taped to the anterior abdominal walls of patients undergoing dynamic Gd-DTPA–enhanced MPSPGR breath-hold abdominal imaging to determine the range of T1s normally encountered. The different sequences were then optimized by using healthy volunteers and the contrast phantom for providing the best liver-spleen contrast-to-noise ratio (L/S) and

contrast-to-noise ratio for the contrast phantom (CP) with T1s between 230 and 1,400 msec. The contrast-to-noise ratios divided by time per section were then calculated to compare the sequences. For no breath holding, IR-WARP with bandwidth (BW) of 32 kHz, TI of 1,000 msec, and flip angle (FA) of 30° provided the best contrast-to-noise per unit time for L/S, and TI of 600 msec and FA of 90° was best for the CP. For up to 10 seconds of breath holding, MPSPGR with four sections, BW of 32 kHz, and FA of 50°–60° was best for L/S and CP. For up to 20 seconds of breath holding, MPSPGR with 12 sections, BW of 32 kHz, and FA of 50°–60° was best for L/S and FA of 80° was best for CP (imaging time = 20.5 seconds). With continued development of various fast imaging sequences, it is important to objectively select the most appropriate available sequence and parameters for specific clinical requirements before starting clinical research protocols. The authors have presented a way of achieving this goal.

P217

### MR Imaging in Patients with Inferior Vena Cava Filters

AT Watanabe, AS Gomes, GP Teitelbaum, JOF Roehm, A van Breda

*Department of Radiological Sciences, University of California, Los Angeles*

The MR appearance and safety of six types of inferior vena cava filters in 21 patients were evaluated. MR images of 21 patients with the following types of intravascular filters were obtained: the Greenfield filter (one patient), the Mobin-Uddin umbrella filter (two patients), the Bird's Nest filter (11 patients), the Simon Nitinol filter (four patients), and the LGM filter (two patients). There were 14 men and seven women with an age range of 24–78 years. The filters had been placed 1 day to several years prior to the MR studies. MR imaging of the head, spine, abdomen, and pelvis was performed with 1.5-T superconducting MR units. The filters create varying degrees of MR image artifact and distortion. The Bird's Nest filter creates the greatest artifact. The ferromagnetism, torque, and composition of the various filters are presented for correlation. Diagnostic MR images of the brain, spine, and pelvis may be obtained in the presence of inferior vena cava filters. No documented complication or filter displacement was encountered as a result of the MR studies. In many cases, MR imaging was useful in evaluating filter position, in visualizing intraluminal thrombi, in determining caval patency, and in assessing the presence of retroperitoneal collateral veins. The applications and pitfalls of GRE imaging are also presented. MR imaging of patients with intravascular filters appears to be safe. Certain filters severely limit the diagnostic usefulness of abdominal MR images. In many instances, MR imaging may be useful in evaluating vascular anatomy and in visualizing trapped thromboemboli.

P218

### MR Imaging of Hemorrhagic Adrenal Lesions in Infants

MT Schrader, RB Dietrich

*Department of Radiological Sciences, University of California, Irvine*

Although adrenal hemorrhage is the most common adrenal mass seen in the neonatal period, early differentiation of this entity from both benign and malignant lesions that cause enlargement of the gland is important. This exhibit reviews the entity and describes the spectrum of MR imaging findings that may be seen. Emphasis is placed on the key imaging characteristics found with different ages of hemorrhage and in differentiation from other adrenal lesions. The MR images from 10 studies of eight infants with nine hemorrhagic adrenal lesions were retrospectively reviewed and correlated with results of other imaging studies and clinical history. T1-weighted coronal images (SE 500–600/28–30) were obtained in all cases. In addition, axial T2-weighted images (SE 1,500–3,000/56–90) were obtained in seven cases and additional T1-weighted images in four. One patient underwent imaging following Gd-DTPA administration. Newborns with adrenal hemorrhage imaged between 1 and 6 days following birth ($n = 4$) demonstrated medium signal intensity (SI) on both T1-weighted and T2-weighted images. Those imaged between 7 and 20 days ($n = 2$) demonstrated high SI peripherally and medium SI centrally on T1-weighted images. Lesions in subjects older than 20 days had signal characteristics of proteinaceous fluid (medium SI on T1-weighted images and high SI on T2-weighted images). In two cases, fluid-fluid levels were identified and thin rim enhancement was seen in one case following Gd-DTPA administration. Two studies of a child with hemorrhagic neuroblastoma showed homogeneous high SI on both T1- and T2-weighted images, an appearance not seen in the cases of isolated adrenal hemorrhage. High SI rims and fluid-fluid levels may be findings specific for adrenal hemorrhage.

P219

### Statistical Analysis of Essential Knee Structure Quantitation: MR Imaging Study

PK Paul*, L Hanie*, A Rakhit*, AW Dunton*, FL Douglas*, A Parikh†, RS Mezrich†

**Ciba-Geigy Pharmaceuticals, Summit, NJ, and †University of Medicine and Dentistry of New Jersey, New Brunswick*

This report presents an MR imaging quantitation data base of essential knee structures such as articular cartilage, fibrocartilage, and joint space in normal subjects. Such a data base currently does not exist and would be a valuable reference to evaluate similar structures in various arthritic disorders. MR images of 91 subjects (38% male and 62% female), radiologically diagnosed as normal, were digitized with a viewbox and video camera. Images were analyzed with a MacII workstation. Three variables, thickness, volume, and width, were measured for those structures and evaluated for age, sex, height, and weight. Mean femoral, tibial, and patellar cartilage thickness measures were 1.8, 1.1, and 2.1 mm, respectively. Corresponding measurements with respect to volume were 9.3, 2.6, and 2 $cm^3$. Mean medial and lateral meniscal volumes were 3.4 and 2.9 $cm^3$, respectively, whereas the width of medial tibiofemoral, lateral tibiofemoral, and patellofemoral joint spaces (intermarrow) were 6.7, 7.0, and 18.4 mm, respectively. A quantitative data base on normal knee was obtained and analyzed against demographic variables. Of all variables, sex showed the best relationship, followed by height and weight. Age relationship was negligible. Volume measurements appeared to provide a more predictable relationship with these variables compared with those for thickness, for example, femoral cartilage versus height ($P < .01$ [volume] and $P < .02$ [thickness]).

P220

### MR Imaging Characteristics of Patella Dislocation Injuries

M Kirsch*, H Friedman†, SW Fitzgerald*, LF Rogers*

**Northwestern Memorial Hospital, Chicago, and †Northeast Illinois MRI, Prairie View*

The purpose of this study was to review the spin-echo and gradient-echo (GRE) characteristics of patella dislocation. The MR characteristics in 20 patients with clinically suspected or surgically proven patella dislocation were retrospectively reviewed. Examinations were performed with

0.2-T permanent and 0.5- and 1.5-T superconducting MR imagers. Proton-density, T1- and T2-weighted, and GRE 2D and 3D sequences were performed. Sagittal, axial, and coronal planes were imaged. There was a characteristic pattern of injury observed with disruption of the medial patella retinaculum, impaction injury on the lateral femoral condyle as well as the medial articular surface or medial aspect of the patella, joint effusion, and lateral tilt of the patella. Loose intraarticular osteochondral fragments were also identified, as was lipohemarthrosis. Axial sequences best demonstrated the retinacular disruption and were felt to be best for diagnosis of the injury. T1-weighted and 3D GRE images were the most useful in determining the location and extent of bone injury, while T2* 2D GRE images best demonstrated articular cartilage trauma. In conclusion, MR imaging was useful in diagnosis or confirmation of patella dislocation, and a characteristic constellation of MR findings was seen with this injury.

P221

### Exercised-enhanced MR Imaging Demonstrates Variations in Skeletal Muscle Recruitment During Standard Treadmill Exercise with the Bruce Protocol

J Kuo, JD Bondy, J Fleckenstein, J Payne, RM Peshock
*University of Texas Southwestern Medical Center, Dallas*

The Bruce treadmill protocol is used widely in the determination of exercise capacity and cardiovascular fitness. However, the pattern and degree of muscle utilization during treadmill exercise are not clear. MR imaging immediately after exercise can be used to determine the exact muscles used during exercise due to changes in muscle water content that alter the MR signal intensity of the muscle. Six healthy volunteers underwent maximal exercise testing with the standard Bruce protocol followed by immediate imaging of the lower extremities at 0.35 T with an SE 1,000/30,60 pulse sequence. All subjects completed stage 4 or 5 of the protocol, achieving greater than 85% of the maximum predicted heart rate without symptoms other than leg fatigue. Analysis of the images showed marked variation in the distribution of muscles used at peak exercise. The gluteus muscles showed increased signal intensity in all six subjects. Sartorius and gracilis muscles also showed increased signal intensity in all subjects, but the degree of increase was variable in spite of similar exercise levels. Vastus intermedius and biceps femoris did not increase in signal intensity even with maximal exercise. With maximal bicycle exercise, patterns of recruitment were more homogenous. Thus, exercise-enhanced MR imaging demonstrates that similar levels of exercise with a well-defined treadmill exercise protocol result in varying patterns of muscle recruitment. These variations must be taken into account in the interpretation of studies done using treadmill exercise and suggest that exercise-enhanced MR imaging should be a standard tool in the evaluation of skeletal muscle exercise.

P222

### Critical Mediator of MR Imaging Enhancement of Exercised Muscle

J Fleckenstein, B Archer, R Haller, M Girson, R Parkey, RM Peshock
*University of Texas Southwestern Medical Center, Dallas*

To evaluate the relative importance of perfusion and glycogenolysis in exercise-enhanced MR imaging of muscle, an ischemic clamp model of handgrip exercise was employed. In protocol 1 (P1), T1 and T2 times of muscle were studied in 10 healthy subjects. In protocol 2 (P2), a fast, short-$\tau$ IR sequence was employed (1,500/30/95, 1.1 minute) in two patients with impaired glycogenolysis due to myophosphorylase deficiency (MPD, McArdle disease) and in three controls. In P1 and P2, MR imaging of the proximal forearm was performed prior to exercise, during vascular occlusion (VO) following exercise (VO1), during VO following 1 minute of reperfusion (VO2), and after discontinuing VO. In P1, T1 and T2 increased in the absence of perfusion during VO1, additional increases occurred during VO2, and reinstitution of continuous flow was associated with a fall in successive T2 measurements. In P2, signal intensity of exercised muscle increased in controls during VO1 and VO2, but in MPD the effect was negligible during both VO1 and VO2. Given that postexertional hyperemia is normal or exaggerated in MPD, these data indicate that exertional hyperemia is neither required nor sufficient for signal enhancement to be observed, but glycogenolysis is necessary whether or not perfusion occurs.

P223

### Assessment of Mass Lesions of the Foot and Ankle with MR Imaging

R Kier
*Department of Radiology, Yale University School of Medicine, New Haven, Conn*

The role of MR imaging for delineation and characterization of mass lesions of the foot and ankle was assessed. Twenty-one patients were referred for MR imaging of mass lesions in the foot and ankle detected initially with either palpation (15 patients) or radiographs (six patients). Images were obtained with a 1.5-T system using a combination of T1- and T2-weighted spin-echo pulse sequences. Masses detected on MR images were analyzed for size, location, signal intensity, and involvement of adjacent structures. The location and signal behavior of masses was used to attempt lesion characterization. In all cases, MR imaging accurately depicted the location of tumors and involvement of adjacent structures. In three cases, MR imaging excluded a discrete mass, showing evidence of plantar fasciitis. In the remaining 18 patients, the combination of signal features and tumor location suggested a specific diagnosis in 11 patients (61%): plantar fibromatosis (one bilateral and one unilateral), ganglion ($n$ = 2), lipoma, Morton neuroma, neurilemmoma, hemangioma, aneurysmal bone cyst, osteoid osteoma, and giant-cell tumor. In four other cases, correlation with radiographs suggested likely diagnoses: Ewing sarcoma ($n$ = 2), chondroma, and metastasis. MR imaging precisely defines the local extent of tumors of the foot and ankle, and often suggests specific diagnoses.

P224

### MR Imaging of Glenoid Labral Tears Related to the Long Head of the Biceps Tendon

AM Smith*, TR McCauley*, P Jokl†
*Departments of *Radiology and †Orthopedic Surgery, Yale University School of Medicine, New Haven, Conn*

Isolated superior labral tears related to the biceps tendon have been recently described. They are difficult to diagnose clinically, so diagnosis is often delayed. The purpose of this retrospective study is to describe the MR appearance of tears of the superior labrum. Retrospective review of the shoulder arthroscopy reports for patients who underwent MR imaging with a 1.5-T unit and subsequent arthroscopy by a single surgeon identified six patients with tears of the superior labrum (average age, 36 years; range, 17–65 years). Imaging included coronal oblique proton density–weighted and T2-weighted spin-echo images and axial gradient-echo images in all patients. In four patients, coronal oblique gradient-echo images were also obtained. Images were reviewed by a single radiologist. The superior labrum had increased signal on proton den-

sity–weighted and gradient-echo sequences in all patients. In two patients the tear of the superior labrum could not be identified. In one patient a fluid-filled cleft could be seen in the labrum. In two patients linear increased signal with all imaging sequences could be seen extending from the articular surface to the substance of the labrum. One of these patients also had deformity of the labrum. In one patient there was marked deformity of the labrum with inferior displacement from its normal site of attachment. Radiologists interpreting MR images of the shoulder should be aware of the MR findings of superior labral tears, as these tears can be a significant cause of patient disability and are difficult to diagnose clinically.

P225

### Contrast Optimization in Three-dimensional Ultrafast Abdominal MR Imaging

M Hasegawa, M Amanuma, H Mizuno, H Mizuno, T Watabe, A Heshiki

*Department of Radiology, Saitama (Japan) Medical School*

The purpose of this study was to evaluate the TI value that can optimize T1-weighted contrast of tissue interfaces in any arbitrary area of the abdomen when a 3D MPRAGE (magnetization-prepared rapid GRE) sequence is used as a routine ultrafast MR imaging method. From June to September 1991, the authors performed 3D MPRAGE sequences as well as conventional SE sequences in 34 patients with various lesions in the abdomen using a 1.5-T superconducting unit (Magnetom, Siemens). The imaging parameters were a 40–50-cm FOV; a 130 × 256 matrix; a 3D partition of 128; TR/TE = 10/4 msec; and flip angle = 10°. The TI value was varied from 50 to 200 msec in these patients to measure the region of interest–based contrast ratio of lesion to surrounding tissue. The data were compared with those from T1-weighted SE images as well as with the detectable size and number of the lesions. The results indicated that the MPRAGE images with TI of 150 msec were optimal for contrast delineation of tissue interfaces in any arbitrary area of the abdomen and provided lesion detectability comparable with that of T1-weighted SE images, although the average contrast ratio of lesion to surrounding tissue on the former was slightly lower than on the latter: 0.59 ± 0.3 and 0.73 ± 0.2, respectively. In conclusion, a 3D MPRAGE sequence with an optimized TI value can be used as a routine imaging method for lesion detection in any area of the abdomen.

P226

### Evaluation of Bone Marrow Disorders with the STIR Sequence

H Mizuno*, H Mizuno*, A Heshiki*, S Kusumoto†, I Jinnai†, K Hirashima†

**Departments of Radiology and †First Internal Medicine, Saitama (Japan) Medical School*

The purpose of this study was to evaluate bone marrow in hematologic disorders with the STIR sequence. Eighty patients entered the study: 18 cases of myelodysplastic syndrome (MDS), 18 of chronic myelocytic leukemia, 11 of multiple myeloma, nine of aplastic anemia, eight of acute myelocytic leukemia, three of chronic lymphocytic leukemia, three of myelofibrosis, and others. A sagittal plane in lumbar spine was imaged with a 1.5-T superconducting MR unit using a surface coil. Pulse sequences of STIR (TR = 2,000 msec, TI = 160 msec, TE = 20 or 100 msec) were applied in addition to T1-weighted sequences (TR = 500 msec, TE = 15 msec). Bone marrow in MDS indicated heterogeneous or homogeneous hypointensities on T1-weighted images and STIR with long TE images compared with heterogeneous hyperintensities on STIR with short TE images, while T1-hyperintense and STIR-hypointense bone marrow was demonstrated in aplastic anemia. In other hematologic disorders, multiple myeloma was divided into two groups: nodular and diffuse types. These lesions were recognized as high-intensity areas on STIR images, and moderately decreased intensities were noted in the irradiation areas with decreasing serum M-protein. Myelofibrosis showed hyperintense bone marrow on STIR images, microscopically proved abundant fibroblastic cells, and interstitial water components. On the other hand, acute and chronic myelocytic leukemia showed high intensity on STIR images with short TE and various intensity on STIR images with long TE. In conclusion, STIR images with double echo demonstrated well the infiltrative changes of bone marrow. In particular, STIR with short TE showed cellularity, and STIR with long TE showed interstitial components.

P227

### MR and CT Imaging Appearance of Asymptomatic Paravaginal Cysts

AL Moulopoulos, DG Varma, C Charnsangavej

*Department of Diagnostic Radiology, University of Texas M. D. Anderson Cancer Center, Houston*

The authors retrospectively reviewed the MR and CT appearance of paravaginal cysts incidentally noted on pelvic imaging studies in 13 patients undergoing staging for primary malignancies (two cervical carcinomas, one parasacral desmoid, and 10 extrapelvic neoplasms). Patient ages ranged from 24 to 68 years (mean, 50.1 years). Patients did not complain of any cyst-related symptoms. Surgical proof was obtained in a Bartholin gland cyst, and follow-up studies over a period of time ranging from 1.5 to 8 months were available in seven (54%) patients. The sizes of the cysts ranged from 4 mm to 3 cm. In four (31%) cases (one CT and three MR studies) the cysts were hemorrhagic. On MR images, nonhemorrhagic cysts were visualized as sharply demarcated, homogeneous, low-signal-intensity lesions with T1-weighted sequences and were hyperintense on T2-weighted images. T1-weighted sequences with gadopentetate dimeglumine performed in one case did not reveal any enhancement. Hemorrhagic cysts exhibited varying stages of hemorrhage at MR imaging, with evidence of temporal change and, in one case, resolution of the cyst after 8 months. On CT scans, nonhemorrhagic cysts were visualized as well-defined, low-attenuation foci, and one hemorrhagic cyst was noted as a well-defined area of high attenuation. MR and CT examination may reveal incidental paravaginal cysts (Bartholin, mucous, mesonephric, or inclusion), some of which may be hemorrhagic. Their appearance must be recognized, especially in patients undergoing staging for malignancies of the genital tract, to avoid confusion with other lesions.

P228

### MR Imaging Detection of Pelvic Fistulas

E Outwater, ML Schiebler, MD Schnall, HY Kressel

*Department of Radiology, Hospital of the University of Pennsylvania, Philadelphia*

The presence of a pelvic fistula, such as enterovesical, rectovaginal, vesicovaginal, and enterocutaneous, often can be definitively diagnosed on the basis of clinical signs. Contrast-enhanced radiographic studies, including CT, however, have had mixed success in demonstrating the course of these fistulas. The authors undertook a retrospective study to determine whether MR imaging can depict fistulous tracts and to elucidate the characteristics of these tracts on MR images. Twelve patients with proven fistulas were identified with a computerized search of clinical MR records. Six patients had colovesical fistula, two patients had vesicovaginal fistulas, two patients had rectovaginal fistulas, two patients had enterocutaneous

fistulas, and one patient had a urethrocutaneous fistula (one patient had both a rectovaginal and vesicovaginal fistula). MR imaging studies had been performed with a variety of techniques; ten patients were imaged with the body coil using T2-weighted images in at least two planes, with TR/TE = 2,500/20–40/80; two patients were imaged with a four-coil phased array system and T2-weighted fast spin-echo pulse sequences. On T2-weighted MR images, fistulas were demonstrated in 10 of 12 patients. These appeared as fluid-filled tracts that completely connected the lumens of the bowel, bladder, urethra, or vagina to one another or to the skin. Focal discontinuity of the muscularis of these organs was seen at the entry point of the fistula. Actual demonstration of the fistula tract, as opposed to findings suggesting that a fistula was present, was achieved in four of seven cystographic contrast studies, two of six barium enema studies, none of two intravenous urographic studies, and none of six CT scans. MR imaging can demonstrate the course of many pelvic fistulas because of intrinsic soft-tissue/fluid contrast on T2-weighted studies and multiplanar imaging capability.

P229

## MR Imaging in the Evaluation of Female Infertility

BJ Wagner, TE Farley, RT Scott Jr, PJ Woodward
*Department of Radiology, Wilford Hall USAF Medical Center, Lackland Air Force Base, Tex*

Infertility is a disorder affecting approximately 3.5 million couples in the United States. Hysterosalpingography has long been the mainstay of the radiographic evaluation of patients. Many patients, however, must undergo laparoscopy as part of their evaluation in order to demonstrate external morphology. The purpose of this display is to demonstrate the utility of MR imaging in illustrating a variety of congenital and acquired entities encountered in these patients, including mullerian duct anomalies, submucosal leiomyoma, hydrosalpinx, and endometriosis. Correlative sonograms, hysterosalpingograms, and images from fiberoptic hysteroscopy will be shown.

P230

## Interstudy Variability of Left Ventricular Mass Measurement: Comparison between M-Mode Echography and MR Imaging

P Germain, B Kastler, G Roul, JL Dietemann, JM Mossard, P Bareiss, A Sacrez
*University Hospital, Strasbourg Hautepierre, France*

Monitoring of left ventricular mass (LVM) is important in the assessment of antihypertensive drug effects. At present, this is mainly achieved with M-mode echography but with a rather high variability (10%–15%). This prospective work was designed to compare the interstudy variability of M-mode echography with that of MR imaging, in order to define whether MR imaging could be a better tool for LVM follow-up. After giving informed consent, 20 echogenic patients without evidence of coronary artery disease were entered into the study. Two separate MR and two separate M-echographic examinations were performed within 4 days by operators unaware of the other investigation results. M-echography was done according to Devereux's method, with the Penn-Cube formula (four signals averaged). The MR protocol included multisection (eight to 12) true short-axis SE imaging (10 mm thick with 1–3-mm gap) encompassing the entire LV. Planimetry was manually traced with standardized window settings. Interstudy correlations were as follows: $r = .89$ and SEE = 22.7 for echography, and $r = .96$ and SEE = 11.2 for MR imaging. Mean interstudy variability indexes were 11% ± 6.4% and 6.7% ± 3.8%, respectively ($P < .0021$). The threshold value corresponding to the 95th percentile of the variability was 21.5% with echography and 13.5% with MR imaging. Consequently, with MR imaging, the LVM change *detectability gain* compared with echography is 5% for $n = 4$, 3% for $n = 8$, and below 2% for $n \geq 20$ ($n$ = number of patients involved in a follow-up study). For study protocols designed to measure LVM change, MR imaging provides significant benefit, compared with echography, if the number of patients is limited (on the order of 10 patients) or if the interval for LVM monitoring is too short to allow detectable modifications with standard echography.

P231

## MR Imaging during Arterial Portography with MnDPDP: Visceral Organ Enhancement and Other Preliminary Considerations

RC Nelson, JL Chezmar, GH Thompson, JB Webber, MH Garrison, HB Spencer, DL Dillehay
*Department of Radiology, Emory University School of Medicine, Atlanta*

The purpose of this study was to assess the potential for performing hepatic MR imaging during arterial portography with MnDPDP in anticipation of using this technique for focal lesion detection. Seven pigs underwent superior mesenteric arterial catheterization and injection of 10 μmol/kg MnDPDP, followed by MR imaging at 1.5 T (SE 140/10/4) preinjection, and at 15 minutes and 30 minutes postinjection. Serial liver function tests were performed over 7 days. At an interval of not less than 1 week, the same dose of MnDPDP was administered intravenously, followed by MR imaging with an identical sequence and imaging times. Enhancement of the liver, spleen, pancreas, and renal cortex was determined for both intraarterial (IA) and intravenous (IV) MnDPDP. The results are listed in the Table. There was no significant alteration in liver function within 1 week of IA administration. Preliminary data suggest that MR imaging during arterial portography with 10 μmol/kg MnDPDP does not adversely affect liver function in pigs. Hepatic enhancement at either 15 or 30 minutes following IA injection was not significantly different from that following IV injection. There was, however, less enhancement of the renal cortex, pancreas, and spleen following IA injection at both 15 and 30 minutes. Comparatively less enhancement of nonhepatic organs may also imply less enhancement of hepatic tumors, higher lesion-to-liver contrast, and perhaps superior lesion sensitivity with this imaging technique.

| | Mean Enhancement (%) | | | |
|---|---|---|---|---|
| | Liver | Spleen | Pancreas | Renal Cortex |
| IA | | | | |
| 15 min | 86 ± 14 | 14 ± 10 | 27 ± 9 | 45 ± 15 |
| 30 min | 90 ± 18 | 15 ± 11 | 30 ± 15 | 51 ± 15 |
| IV | | | | |
| 15 min | 81 ± 4 | 17 ± 4 | 34 ± 6 | 51 ± 7 |
| 30 min | 96 ± 8 | 23 ± 7 | 35 ± 10 | 62 ± 16 |

P232

## Effects of Opposed-Phase and Fat-Saturation Techniques on Negative Contrast Agents

GS Foster
*Department of Diagnostic Radiology, Rush-Presbyterian-St Luke's Medical Center, Chicago*

Dephasing of spins may occur in opposed-phase images due to local field inhomogeneities, resulting in artifacts and local signal loss. Frequency-selective techniques may cause signal loss due to saturation effects. Since signal from the lumen of the gastrointestinal tract may mimic pathology, reduction in intraluminal signal would facili-

tate the interpretation of images. It is possible that opposed-phase or chemical shift presaturation techniques may enhance the intraluminal signal loss induced by "negative" gastrointestinal contrast agents. Reference samples of water and corn oil were placed in a phantom containing sample oral contrast solutions. The following solutions were tested: (*a*) barium (40% w/w [B] E-Z-Paque; E-Z-Em, Westbury, NY); (*b*) attapulgite (40 mg/mL [A] Advanced Formula Kaopectate; Upjohn, Kalamazoo, Mich); (*c*) barium-attapulgite (B:A) 3:1 solution; (*d*) B:A 10:1 solution; (*e*) B:A 3:1 solution suspended in a 33% corn oil emulsion; and (*f*) B:A 10:1 solution suspended in a 33% corn oil emulsion. With a 1.5-T clinical imager (GE Signa), SE and SPGR images were acquired without and with the use of fat-selective presaturation pulses. SPGR sequences with varying TE and the Dixon opposed-phase technique were used to evaluate the effects of dephasing. Fat saturation sequences resulted in reduction of signal from the corn oil reference but did not significantly alter the signal of oral contrast agents. Signal intensity of oral contrast solutions on SPGR images as a function of TE was not significantly affected by the relative phase of fat and water protons and was predominantly related to T2*. On the opposed-phase images obtained with the Dixon technique, there was enhancement of signal loss in B:A–corn oil emulsions. This effect was not seen in samples not containing oil. B:A–corn oil emulsions on opposed-phase images showed signal-canceling properties similar to that of attapulgite and were superior to that observed with barium on in-phase images. The reduction in signal observed on opposed-phase images in solutions containing corn oil has implications for the development of "negative" oral contrast agents. B:A–corn oil emulsions demonstrate signal characteristics similar to that of B:A mixtures on T2-weighted images. The lower concentrations of attapulgite present in the corn oil emulsions would minimize any possible adverse pharmacologic effect of attapulgite by enabling a lower administrated dose of attapulgite. B:A–corn oil emulsions would also make suitable negative oral contrast agents for T1-weighted images if the opposed-phase technique is used. Further studies are necessary to evaluate the effects of these agents in vivo.

## Tuesday, April 28, 12:15 PM–1:30 PM
## Imaging Techniques

Posters P300–P343

P300

### The Effects of Tortuous Capillary Flow in MR Imaging

KR Minard

*Department of Physics, Rice University, Houston*

A statistical model of tortuous capillary flow was developed and investigated both theoretically and experimentally. In the model, tortuous capillary flow is treated as a stochastic transport process in which flowing nuclei experience random displacements about the average direction of intracapillary flow. These random displacements are attributed to the velocity fluctuations that result from capillary tortuosity. A simple picture of the intravoxel environment is developed by considering an arbitrary distribution of tortuous capillaries in which statistical correlations between the effects of average intracapillary flow and capillary tortuosity are assumed to be negligible. By treating the fluctuating nuclear velocity that results from capillary tortuosity as an Ornstein-Uhlenbeck process, a powerful new expression for the form of the received MR spin echo is derived. By using this expression, an experimental technique is developed that utilizes both velocity-compensated and noncompensated diffusion-matched spin-echo imaging sequences to measure important transport parameters. These include the coefficients of the mechanical dispersion tensor and the statistical moments of the average capillary flow distribution. This technique is tested in a variety of flow phantoms, and experimental results are shown to correlate extremely well with the developed theory. Experimental results confirm that it is possible to measure transport parameters that are very sensitive to the structure of the capillary network and suggest that MR images that base contrast on their measured values might be useful for the early detection of abnormal tissue before blood flow is seriously impaired.

P301

### Minimization of Flow-induced Signal Loss in MR Angiography

SN Urchuk, DB Plewes

*Department of Medical Biophysics and Sunnybrook Health Science Centre, University of Toronto*

Signal loss and ghosting associated with rapid and/or disturbed flow remains a significant limitation of bright-blood MR angiography. Strategies for minimizing these artifacts include gradient moment nulling, compact gradients, and short TEs. To improve the performance of these techniques, the authors have undertaken an optimization of the gradient waveforms used in conventional angiographic sequences. The approach to this problem is based on a Fourier analysis of the phase variance induced by velocity fluctuations, which develops the following expression for the phase variance given by the integral over all frequencies: the power spectrum of the motion $D(f)$ times the frequency spectrum of the effective field gradient $S(f)$. By use of a model of $D(f)$, the phase variance was minimized subject to gradient-power and spatial-encoding constraints. Theoretical predictions were compared with experimental measurements of signal loss. The results indicate that gradient moment nulling above first order is an ineffective means to reduce the signal loss in regions of disturbed flow, as the magnitude of $S(f)$ is increased by the extra time required to null additional gradient moments. Performance can be improved by shortening gradient durations, which decreases the magnitude of $S(f)$ and shifts its peak value to higher frequencies. This is an effective strategy, as $D(f)$ will decrease with increasing frequency. Thus, specification of the gradient power required to minimize signal loss is possible, given some knowledge of $D(f)$.

P302

### Contrast Enhancement of Time-of-Flight MR Angiography of Large Vessels by Use of Gating and K-Space Segmentation

PM Margosian

*Picker International, Highland Heights, Ohio*

An approximation routinely made in time-of-flight MR angiography is to ignore the pulsatile nature of blood flow during the heart cycle, simply use first-order motion compensation and short TEs, and hope for the best. For large blood vessels with highly pulsatile flow, such as the carotids, and femorals, this approach often causes difficulties that are most commonly manifested as ghosting artifacts or as signal dropout. Simple cardiac gating is one solution to this problem, but leads to prohibitively long acquisition times. A practical compromise is to break up the heart cycle into two or three segments, use gating with k-space segmentation, and make what is in effect a two- or three-frame "cine." The goal is to make one image during fast flow and another of the same position during slow flow, at a cost of only double or triple the acquisition time.

When this is done, the contrast of the "fast" image is greater than that of the ungated image, the contrast of which in turn is greater than that of the "slow" image. Artifacts are also reduced. For larger vessels with dramatic flow speed variations during the heart cycle, one can subtract the slow image from the fast image at each section position to achieve considerable background suppression. Examples are shown for carotids, femorals, and other large vessels.

P303

### Automatic "Unsharp Transform" Phase Correction of Flow-encoded Acquisitions: Applications to Flow Quantification and Synthetic Phase-Contrast MR Angiography

PM Margosian, H Liu
*Picker International, Highland Heights, Ohio*

A 2D automatic phase correction method has been developed that facilitates reliable flow quantification imaging of blood vessels and development of phase-contrast MR angiographic images from the same data, despite difficulties such as susceptibility effects and eddy current–induced distortions. Acquire two raw data sets (*R1, R2*), one of which is motion compensated (first order), while the other is motion sensitized to produce a known phase shift for a specified flow velocity. Ideally, flow velocity is measured by the phase difference of the complex images (*I1* and *I2*) made from the data. In practice, low-frequency phase errors are caused by misalignment of *R1* and *R2*. Calculate (*I1*) (*I2**). Its phase measures flow and low-frequency errors. Form *I1'* from the magnitude of *I1* and *I2'* from the magnitude of *I2* and the calculated phase difference. Back transform *I2'*, zero all but the central 20 × 20, apply the 2D Hamming filter, and forward transform to form *I2'b*, which has mostly the low-frequency phase errors. The corrected phase of (*I2'*) (*I2'b**) measures flow; most errors are removed. Form *I2''* from magnitude of *I2* and corrected phase. The magnitude of *I1* − *I2''* is then a phase-contrast image; its imaginary part is a directional flow-sensitive image. Examples for various blood vessel sizes are shown.

P304

### Simultaneous Fat and Tissue Suppression for Contrast-prepared MR Angiography

D Brown Richardson*, SJ Riederer†
**Duke University Medical Center, Durham, NC, and †MR Laboratory, Mayo Clinic, Rochester, Minn*

Contrast-prepared MR angiography with the centric phase-encoding order provides increased blood/tissue contrast relative to standard time-of-flight MR angiography, with a twofold decrease in imaging time. However, when the preparation phase is set to null signal from the predominant static tissue, the fat, with its short T1, is almost fully recovered at the start of the acquisition, so that the fat signal competes with the vascular inflow signal in the maximum intensity projection. Spectral saturation suppresses the fat signal but increases the TR too much for use with contrast-prepared imaging. In the method proposed here, the necessary fat suppression is achieved in the preparation phase; the acquisition sequence is not altered. The magnetization levels of both fat and the primary surrounding tissue are nulled simultaneously by using two section-selective inversion pulses in the preparation phase and adjusting the inversion times appropriately. Fresh blood flows into the imaging section during the second inversion time. During image acquisition, the fat signal rapidly approaches a relatively high steady state, again because of its short T1. The resulting high-pass k-space filter causes edge enhancement and comparatively bright outlines in otherwise well-suppressed regions of fat. However, since the steady-state fat signal intensity is much lower than the vascular inflow signal, the two signals do not compete in the projection images. When venous saturation is used, chemical shift properties can be employed (SLIP) to reduce the steady-state fat signal, thereby decreasing the edge enhancement effect. With this technique, high-quality MR angiograms, with high vascular signal intensity and adequate suppression of fat and other static tissues, can be acquired in half the time of traditional time-of-flight methods.

P305

### Comparison of 3D Magnitude and Phase-Contrast MR Angiography for Lower Extremity Studies

S Rajan, B Lo, S Lossef, R Patt
*Department of Radiology, Georgetown University Hospital, Washington, DC*

This study involves the comparison of MR angiographic images derived from phase- and magnitude-contrast (PC and MC) techniques for lower extremity vessels. Studies were performed in phantoms, normal volunteers, and patients with vascular disease. A 3D rephase-dephase FISP pulse sequence (TR/TE = 37/18 msec) was used for MC, and for PC a 3D FLASH (TR/TE = 37/22 msec) pulse sequence was used. In both cases flow sensitivity along one direction (z) was probed. Coronal 3D slabs, 40 to 5 mm thick, were imaged with 32 phase-encode steps. The MC data were processed by subtraction of rephase and dephase images followed by maximum-intensity projections (MIPs). The PC data were processed by subtraction of the raw data (from each 3D partition) followed by 2DFT and MIP of the resulting images. The imaging was done with a 1.5-T imager and a dedicated transmit-receive RF coil with a 30-cm field of view. A constant-velocity flow phantom was used for studying velocity dependence of image contrast. Both straight and angled flow sections were incorporated to study the direction dependence. The popliteal and trifurcation regions of normal volunteers and patients with atherosclerotic vascular disease were imaged. The images were evaluated for overall quality and small vessel conspicuity. Phantom studies showed that the PC pulse sequence was more sensitive to slow flow, whereas the MC pulse sequence yielded better background suppression. In normal volunteers, the MC method gave significantly better images than the PC technique. In patients with vessel disease, the two methods proved to be comparable. These results indicate that while the PC method yields better slow flow signal, the MC method is more suitable for pulsatile flow. Further reductions in TEs (using shielded gradients) are expected to improve the PC method. However, shorter TEs have been shown to not result in improvement with the MC pulse sequence.

P306

### High-Resolution MR Angiography

GP Stomp, JJ van Vaals, HH Tuithof, JP Groen, L Hofland
*Philips Medical Systems, Best, The Netherlands*

The application of MR angiography in clinical practice requires artifact-free, high-resolution images in order to compete with invasive x-ray angiography. To enable this, the authors developed a dedicated gradient coil with a bore size that allows imaging of heads, extremities, and small infants. High-resolution MR angiography with acceptable imaging times and short TEs to reduce turbulence artifacts, requires strong gradient fields with short switching times. This is most easily realized in a dedicated "small"-bore gradient coil. The authors designed an insert-shielded gradient coil with an inner diameter of 40 cm that can be used in a 1.5-T whole-body system. For MR

angiography a gradient strength of 20 mT/m switchable in 400 μsec in all three orthogonal directions was used. In this setup, high-resolution MR angiography images of internal carotid vessels and hands were made with a send-receive RF head coil or dedicated surface coils. A TE of 2.3 msec can be achieved for a 256 × 256 matrix size. For a 512 × 512 matrix size, flow-compensated gradient-echo imaging was realized with a TE of 4.3 msec. Typically, a 512 × 512 × 64 3D data set was acquired and interpolated to 1024 × 1024 × 128 before calculating the MIPs. The authors will present comparative studies between "low"- and high-resolution MR angiography. The dedicated insert coil allows high-resolution MR angiography with short TEs, thereby reducing turbulence artifacts, improving visualization of small vessels, and enhancing the sharpness of the angiograms.

P307

### A Triggered MR Angiography Strategy to Improve Stenosis Detection

M Scheidegger, M Doyle, GM Pohost
*Cardiovascular Disease Department, University of Alabama at Birmingham*

Bright blood MR angiographic techniques suffer signal loss in stenotic regions due to either high-velocity jets or disturbed flow patterns. Incorporating triggering into the recently introduced outflow refreshment angiographic strategy allowed accurate detection of a severe stenosis in a phantom with pulsatile flow. Incorporating triggering did not extend the imaging time. Outflow refreshment is a multiple-section acquisition strategy that rapidly advances the section selection in the direction of flow. Each section partially overlaps the previous one, resulting in partial static tissue signal suppression. Flow refreshment results in a bright blood signal; thus, angiograms are formed by maximum intensity projection (MIP) processing. A pulsatile flow pump was used to generate physiologic flow conditions in a 1.9-cm-diameter pipe with a sinusoidal stenosis (75% area reduction). On one side of the pipe an agar gel was placed to simulate static tissue. Triggered and nontriggered angiograms were generated. All results were acquired with a Philips S15 Gyroscan using the short-gradient-echo FAcE sequence (TE = 3.4 msec) in conjunction with the outflow refreshment imaging strategy. Triggering the acquisition resulted in the stenosis being clearly visualized on the MIP angiogram, whereas the untriggered study resulted in signal reduction, leading to approximately a 2-cm segment loss in the MIP angiogram. Measurements performed on the source (ie, tomographic) images and MIP angiograms confirmed that the triggered study accurately depicted the stenosis. Triggering is easily incorporated into the outflow refreshment angiographic strategy and allows accurate visualization of a severe stenosis with pulsatile flow.

P308

### Comparison of Selection Pulses for MR Angiography

M Scheidegger, M Doyle, GM Pohost
*Cardiovascular Disease Department, University of Alabama at Birmingham*

Two pulses suitable for thin-section MR angiography were compared with the standard sinc pulse. Angiography was performed with the outflow refreshment imaging strategy, which rapidly excites a number of thin sections and requires a large flip angle. The imaging sequence used was the short TE gradient-echo FAcE sequence. The "standard" pulse was taken as an asymmetrically truncated sinc pulse (duration, 5 msec). A 270° Gaussian (duration, 3.5 msec; truncation level, 2.5%) and a delayed refocusing pulse (duration, 7 msec; delay, zero) were compared. All results were obtained with a Philips S15 Gyroscan 1-m bore system, with 10 mT/m gradients (nonshielded) with a minimum rise time of 1.5 msec. When tested in a static agar gel phantom, the delayed refocusing pulse displayed excellent section profiles, while the Gaussian pulse had considerably less sharp edges. For pulsatile flow phantoms and volunteers' necks, the sinc pulse and the delayed refocusing pulse both exhibited considerable flow artifacts. The Gaussian 270° pulse possessed the shortest duration-bandwidth product and exhibited virtually no flow artifacts. For thin-section (1–3 mm) excitations the Gaussian 270° pulse resulted in the shortest TE (3 msec) and yielded the best images. The excellent angiograms generated had low artifact and high spatial resolution (1 × 1 × 1 mm) and were virtually free of signal voids.

P309

### Geometric Distortions and Signal Fluctuations in MR Angiography

D Saloner, R van Tyen, C Anderson, J Tsuruda
*Department of Radiology, Veterans Affairs Medical Center, San Francisco, and University of California, San Francisco*

MR angiography studies of tortuous vessels in healthy subjects are often marked by high variability in signal intensity, with regions of signal dropout and/or regions of high signal strength. In addition, the morphology of the vessels has been noted to vary significantly with specifics of the pulse sequence. The authors have investigated the origins of these artifacts and implemented techniques to correct for them. Signal dropout as noted in conventional MR angiographic studies (TE = 7.5 msec) of the carotid siphon was significantly reduced with a sequence having a TE of 5 msec. This improvement is to be expected in tortuous vessels in which the rapid changes in direction of flow generate high-order motion terms that are not corrected by standard velocity-compensated sequences. Additional signal variability results from misregistration effects due to TPF, the temporal delay between phase-encoding and frequency-encoding intervals. This effect can result in focal areas of high signal intensity or "phase pileup" and can indeed generate significant distortions in vascular geometry. The extent of the geometric distortions was studied in phantom studies, healthy volunteers, and a number of patients who had conventional x-ray angiograms for other reasons. The strongest determinant of the appearance of the vascular geometry was the orientation of the frequency-encoding axis. Minimizing TPF provided further improvement in vascular geometry definition. The short TE sequences applied with frequency encoding along the head-foot axis provided the best correlation between x-ray and MR studies.

P310

### Numeric Simulations of Magnetization Evolution along Nonlinear Flow Trajectories

R van Tyen*, D Saloner*, LD Jou†, S Berger†
**Department of Radiology, Veterans Affairs Medical Center and University of California, San Francisco, and †Department of Mechanical Engineering, University of California, Berkeley*

MR angiographic studies aimed at evaluating vessels for the presence of aneurysms, vessel patency, or the degree and extent of vascular stenosis are now routinely performed. The way in which signal is distributed in these images is not always intuitively obvious: "streamlines" of high intensity often appear along the medial wall of the internal carotid artery; signal diminution is seen in the carotid bulb of healthy volunteers and in the siphon of the internal carotid artery; and dark lines appear down the

center of normal vessels. The appearance of such intensity variations depends on the particular sequence used. In addition, the signal variability reflects the complex flow patterns known to occur in curving and branching vessels with pulsatile flow. To understand some of these features, the authors have performed a two-step numeric simulation of the evolution of magnetization in a flowing fluid. In the first step, a hydrodynamic simulation providing particle velocities and trajectories for flow through a geometrically realistic model of the carotid bifurcation was performed. In the second step, the magnetization vector of each particle moving along the precalculated trajectory and experiencing the applied RF pulses and magnetic field gradients appropriate for the specific imaging sequence under evaluation was calculated. The RF pulses, magnetic field gradients, and timing parameters used in standard pulse sequences on commercial imagers were taken as input for this step. The contribution of intravoxel phase dispersion to the dropout of signal seen in the carotid bulb of healthy volunteers was evaluated. For flow velocities appropriate to flow rates in the bulb, only small deviations from phase compensation were seen. In regions of flow separation, the recirculating flow moves sufficiently slowly that phase dispersion is not appreciable. Signal variations were predicted because of the signal "pileup" resulting from misregistration between the phase-encoding and readout intervals. Significant variations in phase compensation are predicted in situations in which the flow velocities are not only time varying but the net displacement is large and the particles experience large changes in magnetic field strengths.

P311

### Effects of TE on Signal Intensity of Mixed Water/Fat

KJ Jung*, SK Hilal*, ZH Cho†

*Department of Radiology, Columbia University, New York, and †Department of Radiological Sciences, University of California, Irvine*

In Dixon's water/fat imaging method the gradient-echo time is shifted by $\tau$ ($\delta\omega_0\tau = \pm n\pi$), in which $\delta$ represents chemical shift and $\omega_0$ the Larmor frequency, from either the RF TE in spin-echo imaging or the center of an RF pulse in gradient-echo imaging. If there are both water and fat in a voxel as in bone marrow, the signal of a voxel becomes $f(x,y) = \rho_W(x,y) + \exp(-i\delta\omega_0\tau)\,\rho_F(x - \delta\omega_0/\gamma G_x, y)$ in 2D axial Fourier imaging, where $\rho_W$ and $\rho_F$ are water and fat densities of a voxel, respectively, and $G_x$ is the readout gradient. When $\delta\omega_0\tau = \pm(2n + 1)\pi$, the signal intensity of a voxel with mixed water/fat is reduced due to the destructive phase interference between the water and fat signals. As an extreme case, the voxel signal can be void if $\rho_W(x,y) = \rho_F(x - \delta\omega_0/\gamma G_x, y)$ and $\delta\omega_0\tau = \pm(2n + 1)\pi$. Two spin-echo images of a rabbit's knee at $\delta\omega_0\tau = 0$ and $\pi$ were obtained with a 3-T magnet. An amplitude difference image was then made by subtracting the image obtained at $\delta\omega_0\tau = \pi$ from the image obtained at $\delta\omega_0\tau = 0$. In the difference image, bone marrow and interstitial fat appear bright, as shown in the Figure. Even lump fat can experience the phase interference when it is overlapped with the adjacent water tissue by the position shift of $\delta\omega_0/\gamma G_x$ in the readout direction. Therefore, the direction of the readout gradient also affects the region of the signal reduction when $\delta\omega_0\tau \neq 0$. This signal reduction of mixed water/fat will result in the incorrect phase map and consequently incorrect water/fat images in Dixon's water/fat imaging method. This phenomenon also suggests that the signal intensity of mixed water/fat can be controlled by adjusting the TE in multiples of $\tau = \pi/\delta\omega_0$, especially in gradient-echo imaging.

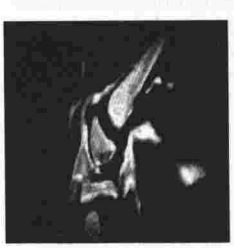

P312

### Measurement of Noise Texture for an MR Imager

SM Mohapatra, JR Prince, DA Wilson

*MR Center of Oklahoma, University of Oklahoma Health Sciences Center, Oklahoma City*

Noise texture and contrast resolution are the two primary physical parameters affecting image quality. Recently published data on noise texture for MR imagers are contradictory. One publication suggests white noise and another demonstrates textured noise. To resolve this controversy the authors have evaluated noise texture in their MR imager using the noise power spectrum (NPS), the Selwyn granularity index (SGI), and integrated spectra analysis (ISA). Data from both air and phantom images have been analyzed. A Philips Gyroscan S15 system was used for all measurements. Images of air and a uniform section of a Philips head coil phantom were obtained with a spin-echo sequence: TR = 1300 msec, TE = 50 msec, FOV = 256 mm, with matrix sizes ranging from 64 to 256 with a single transaxial section of 5-mm thickness. The influence of pre- and postimaging filters was investigated. The NPS was calculated from the autocorrelation function (ACF). Computer simulations were also performed for both uncorrelated and correlated Gaussian random noise for comparison. The ACF for air was found to be a delta function that results in white noise for the NPS. These results are confirmed with the SGI and the ISA. For the phantom, however, the ACF is nominally equal to a triangular function with positive correlation. The resulting NPS is given by a $\text{sinc}^2$ function with structured noise at low frequencies. The SGI and ISA are compatible with this observation. Application of different pre- and postimaging filters does not change the overall results. It is concluded that noise is white in data derived from air but textured in data derived from phantoms on the authors' system. For their system, information obtained from the unloaded coil and without phantoms is not applicable to the interpretation of the effect of noise texture on image quality in MR imaging.

P313

### MR Imaging Observation of Tendon Signal Dependence on Orientation Angle

JW Robinson, JW Roby, IL Cameron, GD Fullerton

*Research Imaging Center, Cellular and Structural Biology, Radiological Sciences, The University of Texas Health Science Center at San Antonio*

It is known that the MR signal from human tendon depends on the orientation with respect to $B_o$ (long axis of the magnet). During a T1-weighted imaging experiment, bovine tendon aligned with $B_o$ experiences an eightfold decrease in signal strength compared with the signal strength at 55° to $B_o$. During a gradient-echo imaging experiment, bovine tendon aligned with $B_o$ experiences a fourfold decrease in signal strength compared with the signal strength at 55° to $B_o$. These effects are clearly demonstrated in controlled imaging configurations. The researcher or physician must be aware of this changing contrast due to orientation (and dependence on selected pulse sequence) when performing studies in the knee or other anatomy containing collagen-rich tissues.

P314

### An Automatic Flow-Quantitation Processing Method and Application

H Liu

*Picker International, Highland Heights, Ohio*

A new method of flow processing is presented that is fully automated yet robust in the presence of unwanted phase

complications caused by various nonidealities such as $B_0$ field inhomogeneity and susceptibility effects. For phase-sensitive quantitative flow imaging, two sets of raw data are obtained in the experiment. One is a reference data set ($Z_1$) and another is a velocity-sensitized data set ($Z_2$). In this flow-processing method, $Z_1$ is convolved with the transposed complex conjugate of $Z_2$ to produce a new raw data set. An echo center offset correction is done on this much "cleaner" raw data set. To correct the echo center offset in the read direction, a line at the central phase-encoding step is used. The data are then Fourier transformed and zero padded, then inverse Fourier transformed back to the time domain. The true echo center is determined by a combination of searching for the maximum-intensity point and finding the gravitational center. The center in the phase-encoding direction is determined similarly. To remove background noise in the final flow map, a threshold value is obtained by statistically analyzing the high-spatial-frequency portion of the new raw data. This flow-processing technique has been applied to both cardiac flow and cerebrospinal fluid flow cases. Flow images of these two extreme cases will be shown.

P315

## Curved Flow Artifacts in MR Imaging

LR Frank, RB Buxton

*MR Institute, Department of Radiology, University of California, San Diego*

The movement of spins during the period between the phase-encoding or section-selection procedures and the echo center is known to cause displacements of these spins in the resulting image if the flow is oblique to the read direction. For the particular case of straight flow, a vessel is either bodily shifted or has a magnitude distribution that is distorted in the oblique direction. It has been shown that it is possible to remove this artifact by nulling the first moment of the phase-encoding gradient with respect to the echo center. However, vasculature generally possesses some degree of curvature. Furthermore, flow patterns are generally such that spins follow a curved path *within* vessels. It is common in the MR imaging literature to discuss orders of motion higher than velocity as being due to unsteady flow. However, higher orders also exist due to the path followed by a spin in steady flow (ie, along time-independent streamlines). For instance, constant velocity in a circular path has an infinite number of moments. The authors have extended the study of misregistration of obliquely flowing spins to include general curved spin paths and have demonstrated these effects in phantoms for the specific case of flow in a helical tube. Further, the existence of curved flow artifacts in clinical situations was verified, as was the efficacy of utilizing oblique flow compensation to reduce these effects. It is shown that oblique flow compensation, although only a first-order approximation to the displacement artifact problem, significantly reduces distortions caused by curved flow for moderate values of velocity $v$ and TE, although it can introduce distortions of its own that become increasingly severe as $v$TE/$R$ increases (where $R$ is the radius of curvature). Standard flow compensation was shown to be susceptible to the effects of flow curvature, with uncompensated higher moments contributing to signal loss.

P316

## A Rapid Method of Estimating T1 of Cardiac Tissue

PA Hardy, RD White, JA Tkach

*Division of Radiology, Cleveland Clinic Foundation*

Numerous myocardiac pathologies may be characterized by estimating the tissue T1. The long acquisition time of conventional IR imaging is, however, prohibitive. Using TurboFISP, the authors have developed a technique of making a series of triggered images with different TIs from which an accurate estimate of cardiac T1 can be obtained. The TurboFISP sequence employs both segmented and reordered k-space acquisition. The magnetization is inverted and recovers for a minimum time TI. The next electrocardiographic trigger commences the collection of eight phase-encode lines via short gradient echoes (TE = 1 msec). The acquisition of k space is reordered to have $k_y = 0$ obtained with the first echo. Each of the eight $\alpha$ pulses are chosen to ensure maximum signal sampled. T1 is found by fitting region of interest values to the equation $S(TI) = A + B \exp(-TI/T1)$. The Figure shows the comparison of T1 estimates made with the segmented acquisition method and estimates made from spin-echo images. The data fall close to the line of identity, indicating reasonable agreement between the two methods. With this technique the authors are imaging patients with different myocardial diseases in order to develop a data base for myocardial tissue characterization.

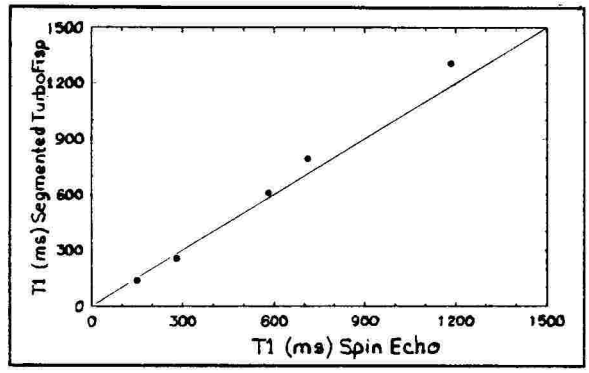


P317

## Analysis of Transmural Left Ventricular Deformation with Tissue Tagging

WJ Rogers, GA MacGowan, D Burkhoff, H Azhari, EP Shapiro

*The Johns Hopkins University School of Medicine, Baltimore*

Myocardial tissue tagging is a noninvasive means of quantifying regional myocardial wall deformation. Tags arranged in a radial or grid pattern have been used to measure various strain components within volume elements of the left ventricular wall (LVW), and current analysis strategies have measured continuous deformation across the wall and have assumed that tags remain as straight lines throughout the cardiac cycle. Because of the complex fiber orientation across the ventricular wall, a means of measuring the complex deformation patterns as one moves across the wall is required. Using a high-resolution internal RF coil, the present study details a means of measuring the pattern and magnitude of regional transmural deformations in an isolated, blood-perfused, isovolumic canine heart. Four tags were arranged in a radial position in each LV short-axis image. Images were acquired at end diastole, midsystole, end systole, and middiastole with tags applied during late diastole 50 msec prior to the first image. The transmural tag shape was defined by fitting an Akima function to multiple operator-selected points along each tag. The tag shown in the Figure is from a basal level near the RV insertion, with the top left of each graph representing where the tag meets the epicardium and the lower right representing the tag-endocardium intersection. Tag shape was determined by a stepwise fit to increasing-order polynomial regression. The degree of curvilinearity was quantified by the ratio of actual tag length

to the chord length between epicardial and endocardial points and varied from 1.10 at 70 msec to less than 1.01 at 260 msec. These values were determined for each of the four time points for four LV short-axis levels. End systole (70 msec) and middiastole (140 msec) were best fit with third-order curves, while end diastole (260 msec) and midsystole were found to be second-order forms. The authors conclude that tags do not maintain linearity throughout the cardiac cycle, and the patterns of deformation seen in midsystole are not the same as in middiastole (at the same pressure), suggesting mechanical hysteresis.

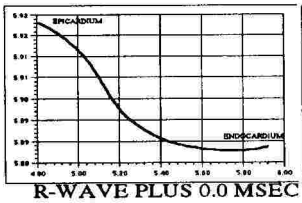

R-WAVE PLUS 0.0 MSEC

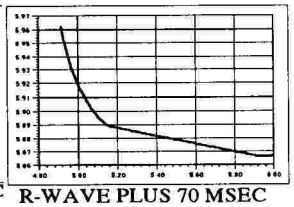
R-WAVE PLUS 70 MSEC

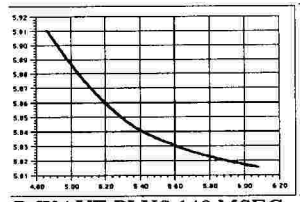
R-WAVE PLUS 140 MSEC

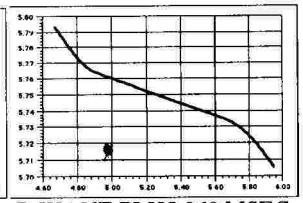
R-WAVE PLUS 260 MSEC

P318

## Cardiac Function Analysis with Phase-Encode-Grouping—acquired Images

MS NessAiver

*Picker International, Highland Heights, Ohio*

Left ventricular volumes can be obtained by measuring the area and length of the ventricle in an image containing its long axis and assuming that the ventricle is an ellipsoid of revolution. Stroke volume is estimated by making this measurement at end diastole (ED) and end systole (ES). Unfortunately, it is difficult to ensure that an image sequence contains the true long axis at both ED and ES owing to the irregular motion of the heart. One solution is to acquire multiple cines at slightly different position and orientation and with the largest area times length at both ED and ES. This is rarely done due to the long time required for each acquisition. An alternative method is to acquire multiple contiguous short-axis cines, also providing right ventricular measurements, but this also requires a lengthy acquisition time and an even longer time for analysis. The purpose of this research is to show that accurate measurements of both ventricles can be obtained using cine images obtained with phase-encode grouping. Phase-encode grouping has been shown to allow the acquisition of up to 16-frame cines during a single breath hold. For left ventricular measurements, four approximate long-axis studies at slightly different positions and orientations were performed in 2 minutes. Ten short-axis studies requiring 5–6 minutes were used for left and right ventricular measurements. Stroke volumes were calculated with a ViSTAR workstation and compared with results obtained by integrating blood flow in the aorta and pulmonary arteries.

P319

## Improving Cardiac Imaging in the Presence of Flow and Motion for Motion Studies

S Singh, E Zerhouni

*Department of Radiology, The Johns Hopkins University School of Medicine, Baltimore*

In recent years, RF tagging techniques for noninvasive assessment of myocardial motion, which is understood to be a sensitive indicator of a diseased heart, have been introduced. The techniques are capable of producing a high density of tags, so that it should be possible to track even small regions in the myocardium in order to obtain more detailed motion description; however, the flow and motion artifacts, which appear in the phase-encoding direction in standard cardiac images, largely degrade the image quality, thus making any quantitative assessment of motion difficult and less accurate. The authors report the application of the projection presaturation (PP) technique to improve cardiac image quality by suppressing the motion and flow artifacts propagating from the outer region into the region of interest (ROI) in a single shot. The PP sequence, which uses a series of selective RF pulses in the presence of a rotating gradient (RG) to suppress the magnetization outside the contoured ROI(s), was implemented with a 1.5-T GE Signa system by using phantoms and volunteers. In the PP sequence, 6–12 gradient steps chosen at equal angular intervals over 0–$\pi$ rotation of the RG were used. In addition to the RG spoiler (amplitude, 1 G/cm), an additional spoiler (amplitude, 1 G/cm) applied during the interpulse interval along the axis of gradient rotation was used to effectively increase the resultant spoiler gradient amplitude (to 1.4 G/cm), thus dephasing the existing transverse magnetization after PP RF excitation at each step in a short time ( $<2$ msec). For oblique section imaging, the resultant gradient amplitude was kept at 1 G/cm at most. To minimize the (unwanted) delay between the last PP RF and the start of the imaging sequence, the last spoiler segments in the PP sequence were eliminated. Frequency-offset sinc pulses with a tip angle of 60°–75° were used at 12–6 gradient steps, respectively, to isolate well-defined cylindrical ROIs (of circular as well as elliptical cross section), enclosing or within the human heart. Additional positionable saturation bands were placed in the third dimension, immediately after 2D localization, to saturate the blood entering from this direction into the ROI. Images of localized ROIs, first in the phantom and then in the human heart, have been obtained with adequate suppression of motion/flow artifacts, thus improving cardiac image quality for accurate motion studies of the tagged heart.

P320

## Cardiac-Gated, Dual-Phase, Multisection Fast Imaging for Rapid Determination of Left Ventricular Ejection Fraction

A von Smekal*, KC Seelos*, J van Vaals†, J Gieseke†, M Reiser*, HJ Biersack*

**Department of Nuclear Medicine and Radiology, University of Bonn, and †Philips Medical Systems, Bonn, Germany*

A quick and reliable method to quantitatively determine left ventricular ejection fraction could greatly expand the use of MR imaging in cardiology. An electrocardiograph-gated, multisection, dual-phase, fast-imaging sequence on a T5 Philips Gyroscan was used to acquire functional images of end systole and end diastole in the left ventricle. In a short-axis plane, contiguous multiple sections were acquired. The end-diastolic and end-systolic delay times were determined relative to the length of the RR interval. The acquisition time for both phases and 10 contiguous short-axis sections, from apex to base, depends on the pa-

tient's heart rate but is approximately 9 minutes. With this fast-imaging sequence, quantitative measurements of left ventricular ejection fraction were performed in 20 patients with various cardiac diseases. The results were compared with a multisection, multiphase, fast field echo sequence and showed a high correlation between the two methods and the two observers ($P < .01$). This new approach accelerates data acquisition for quantitative evaluation of left ventricular ejection fraction and therefore expands the usefulness of MR imaging in the diagnosis and therapy monitoring of cardiovascular diseases.

P321

## Comparison Between Restrospective and ECG-Gated Flow Phase Mapping

L Søndergaard*, F Ståhlberg*, C Thomsen*, L Malmgren*, E Mueller†, O Henriksen*
*Danish Research Centre of Magnetic Resonance, Hvidovre, Denmark, and †Siemens Medical Engineering Group, Erlangen, Germany

Restrospective gating offers several advantages over classic electrocardiographic (ECG) gating in, for example, cardiovascular imaging, but it may also involve signal manipulation such as zero filling, filtering, and interpolation. This work compared the performance of the two gating techniques in quantification of pulsatile flow. The authors used two phase mapping sequences that were completely identical except for the different gating strategy; both gave 32 frames covering the entire flow cycle. In vitro, the comparison was carried out on flow with a steady pulsation rate of 1.1 Hz from a peristaltic pump. As a reference, volume flow was measured with a stopwatch and measuring glass. In vivo, the abdominal aorta flow in a healthy volunteer was measured (heart rate, 55 bpm or 1.1 Hz). As a reference, a one-dimensional, real-time MR flow measurement method (RACE) was used. The results of the in vitro–measured dynamic velocity ranges were 111 cm/sec and 79 cm/sec for ECG and retrospective gating, respectively. The corresponding volume flow (0.37 L/min and 0.36 L/min) agreed well with the external reference measurement (0.35 L/min). In vivo, larger differences were found between the two sets of measurements (Figure). From the RACE measurement, the length of the systolic flow peak was determined to be 24% of the R-R interval, whereas with ECG and retrospective gating the corresponding values were 22% and 37%, respectively. In conclusion, the results indicate that low-pass filtering of the MR phase information is made when retrospective gating is used. Such filtering may especially affect peak flow measurements and can become a source of error when flow pulses of short duration are studied.

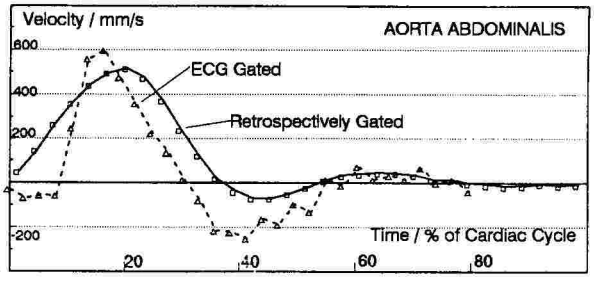


P322

## Time Course of MR Signal Loss Due to Turbulent Flow

JH Gao, DO Kuethe, LJ Neuringer
*Francis Bitter National Magnet Laboratory, Massachusetts Institute of Technology, Cambridge*

The authors have measured the decay of the MR signal due to turbulent flow as a function of time $\tau$ of the bipolar gradient. The data were developed with a gradient-echo sequence applied to water flow in a 1.25 ± 0.05-cm-diameter Plexiglas pipe with Reynolds numbers (Re) in the range 3,500–13,000. A 1.06-G/cm bipolar gradient was applied perpendicular to the flow direction for times varying between 0 and 3 msec. A 0.06-G/cm section-selective gradient was used to ensure that the excited flowing nuclear spins did not exit the RF coil before echo formation; the read gradient was 0.08 G/cm. The signal loss from these additional gradients was less than 4% of the bipolar gradient and was ignored in the calculations. Various theories predict the signal decay to vary as $\exp(-\kappa\tau^n)$, where $\kappa$ is a constant with $n$ in the range between 3 and 5 (1–4). The experimentally determined value $n = 2.74 \pm 0.12$, in the range $3{,}500 < Re < 13{,}000$, differs from these theories. The result that the signal decay was slower than predicted is provocative, since conceivable departures from ideality would probably lead to faster signal loss.

1. De Gennes PG. Phys Lett 1969; A29:20. 2. Fukuda K, Hirai A. J Phys Soc Japan 1979; 47:1999. 3. Kuethe DO. Phys Rev 1989; 40:4542. 4. Gao JH, Gore JC. Med Phy 1991; Vol 18.

P323

## Rapid MR Measurement of Pulsatile Velocity Waveforms

NJ Hangiandreou, JP Felmlee, RL Ehman, SJ Riederer
*MR Research Laboratory, Mayo Clinic and Foundation, Rochester, Minn*

The purpose of this work was to measure blood velocity with MR rapidly enough (20–30 Hz) to construct and view an estimate of the velocity waveform in real time. Phase encoding is not performed, hence every measurement constitutes a projection. The complex signal from static structures (which would obscure the vessel signal) is first measured by placing a saturation band on one side of the image plane to remove the blood signal in the vessel of interest. This static signal is stored in memory. In subsequent repetitions without saturation, the stored static signal is subtracted in a complex manner from the projection data. This subtraction results in the complex signal originating in the vessel of interest only. The acquisition is toggled between flow compensation and flow sensitization, and the phase difference between successive repetitions is used to measure velocity. These measurements are separated in time by the interval 2 × TR, or approximately 40 msec, resulting in a velocity waveform sampled at about 25 Hz. This method was tested in a phantom consisting of both flowing and static materials, and produced waveform measurements very similar to those obtained in a free tube. The carotid arteries of normal volunteers were also examined. The measured waveforms were qualitatively very similar to clinical carotid waveform tracings (obtained, for example, with Doppler US). This technique provides a simple means of measuring pulsatile velocity waveforms. With improvements in implementation, it should prove clinically useful for assessing temporal flow patterns in many vessels of the body.

P324

## Experimental Study of the Effects of "Fractional" Gating on Flow Measurements

MH Buonocore, L Gao, HG Bogren
*Department of Radiology, University of California Davis Medical Center, Sacramento*

Flow measurement by gated velocity-encoded phase imaging is subject to errors from many sources, but predominantly from beat-to-beat inconsistencies in the flow. Nongated flow studies have the most extreme form of beat-to-beat variation, since there is no separation of systolic and

diastolic flow data. In nongated imaging the phase-encode step is updated typically at a rate eight- to 16-fold higher than in gated studies, so nongated studies can be done more quickly or more sections can be obtained. The purpose of this study was to compare the net flow error from gated, nongated, and so-called "fractionally gated" velocity-encoded scans. Asynchronously gated velocity-encoded phase imaging with the VINNIE sequence (GE Medical Systems, Milwaukee) was carried out in 10 subjects. With TR = 33, TE = 9, and flip = 30°, the unencoded and encoded waveforms were alternately played out for an effective temporal resolution of 66 msec. The actual raw data were collected by updating the phase-encode step once at each electrocardiographic trigger. When there was no cardiac gating, the phase-encode step was updated every 2 × TR. The ungated data were generated from the larger raw data set by first computing the times at which each phase-encode step would have occurred and linearly interpolating the raw data to that point in time. This procedure was also carried out for two and four phase-encode updates per R-R interval. These scans are referred to as ½ and ¼ gated. Results show that the estimate of the *mean* flow is independent of the gating fraction. For any gating fraction, the data show that the flow measurement obtained is an unbiased estimate of the average flow over the R-R interval. However, the standard error of these estimates increases substantially with gating fraction. For fully gated flow measurements of the ascending aorta, a standard error of the estimate for the net flow is 6%, while for nongated flow measurements it is about 20%. There is a significant loss of measurement accuracy when gating is not full. This study allows the physician to make an informed trade-off between flow measurement accuracy and imaging time or number of sections.

P325

### Low-Flow Detectability Limits and Velocity Sensitivity in MR Imaging: Extrinsic and Intrinsic Parameter Dependence

D Saloner*, B Nordell†, F Stahlberg†, and C Thomsen†
**Department of Radiology, Veterans Affairs Medical Center and University of California, San Francisco, and †Scandinavian Flow Group, Lund, Sweden*

The authors have investigated the dependence of low-flow detectability limits and velocity sensitivity on a number of intrinsic and extrinsic parameters, including image pixel size, TR, the degree of flow sensitivity built into the pulse sequence, and the T1 of the material. MR imaging techniques provide the capability to quantitate flow velocities not only in the arteriovenous system, but also in substantially slower flow situations. Studies of cerebrospinal fluid motion require the ability to detect extremely low flow states, as in the determination of hydrocephalus shunt patency, and they require the ability to quantitate accurately flow velocities, as in the measurement of cerebrospinal fluid production in the brain. Studies were conducted in flow phantoms capable of a range of steady flow conditions. Images were acquired with a sequence providing interleaved images with varying flow sensitivity. Image subtraction of the phase images on a pixel-by-pixel basis provided a map of flow velocities. The images were evaluated to determine the proportionality of signal intensity to measured flow volume. The standard deviation of the signal in the stationary background material provided a measure of the signal threshold below which flowing spins could not be distinguished from stationary material. The lower limit of flow detectability was found to decrease with increasing voxel size, increasing TR, shorter T1, and higher encoding sensitivity. The flow sensitivity was found to increase with decreasing voxel size and with higher encoding sensitivity. Flow sensitivity was unaffected by changes in TR or by different values of T1. The noted dependencies can be explained from an understanding of the response of the longitudinal magnetization to a train of RF pulses and from the influence that has on issues of signal-to-noise ratio.

P326

### Susceptibility Contrast with a Bolus Saline Injection

MS Albert, J-H Lee, W Huang, CS Springer
*Department of Chemistry, State University of New York, Stony Brook*

Perfusion imaging following the bolus administration of a solution containing a nondiamagnetic agent has proven to be powerful and consequently has developed rapidly. There are several drawbacks to this procedure, however. These include the use of a significantly hyperosmolar injection solution, a significant injection (volume) rate, and a significant "dead" time between injections. The authors have developed an alternative approach that may avoid these problems. Over approximately 5 minutes, the authors administered 0.41 mmol Fe/kg of AQUAMAG (Advanced Magnetics; a concentrated preparation of the superparamagnetic colloidal iron oxide/dextran, AMI-25, suspension) to an anesthetized female Swiss-Webster mouse (weight, 29 g) positioned in the imaging coil of a 9.4-T MSL-400 (Bruker) instrument. This set up a difference in magnetic susceptibility between the blood vessel lumens, in which these 100–200-nm-diameter particles have a half-life of 40 minutes, and the extravascular spaces. The difference was estimated to be 1.5 ppm for possibly a half hour after the end of the infusion. The authors then carried out four serial bolus injections via the left external jugular vein. Each comprised 120 μL of physiologic saline (0.9%) delivered in a period ranging from 10 to 3.6 seconds. A phase-refocused, steady-state, free precession type of fast imaging sequence, similar to FADE and double-echo SSFP, was employed, with signal detection on only the second echo to provide maximal T2 weighting. Imaging parameters included 128 × 128 pixels, a 25 × 25 mm FOV, a TE of 3 msec, and a TR of 27 msec. Each image was obtained in 3.5 seconds. Series of 32 images were collected in succession to create 2-minute "movies" with a delay of 200 msec between images. Signal from an axial brain section of 2-mm thickness was collected from a region within the dorsal aspect of the brain supplied by the middle cerebral artery. The superior sagittal sinus and transverse sinus were clearly visible on the images from this section. Plots of the time courses of the total intensity of the image section for the four bolus injec-

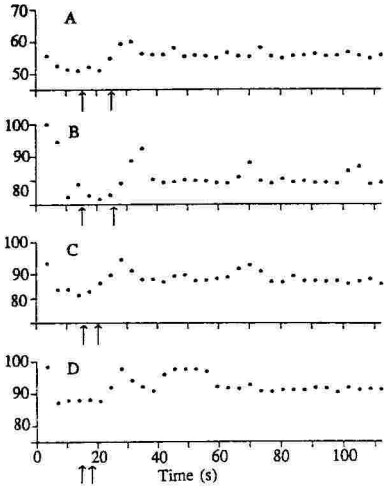

tions are shown in the Figure. The first image or two of a kinetic sequence are often anomalously bright until the steady state is attained. The injection periods are delimited by arrows. The experiments were 5 to 10 minutes apart and are shown in chronologic order (*A* to *D*). Each one shows a transient brightening as the bolus of saline temporarily washes the iron oxide out of the brain vasculature and eliminates the susceptibility difference. As expected, this is the opposite of the case following traditional contrast agent bolus injection. It is encouraging to see measurable effects with such small animals and such small injections. The first pass appears to be quite repeatable. Unexpectedly, there were indications of subsequent passes at intervals of 15 seconds in three of the four experiments and 40 seconds in three of the four experiments. These are as yet unexplained because the pass interval for a discrete bolus in such small animals, with such rapid hemodynamics, is estimated to be about the same as the injection and imaging intervals, respectively.

P327

## Antisymmetric Pulsed Gradients Cure Cross-Term Errors in Diffusion Measurements

X Hong, WT Dixon
*Emory University School of Medicine, Philips Magnetic Resonance Research Center, Atlanta*

Diffusion coefficients *D* are measured by comparing signal to the square of pulsed gradient strength. Besides pulsed diffusion sensitizing gradients, susceptibility-induced gradients and imaging gradients may be present. If all are temporally symmetric (Fig 1), cross terms in the square of the total gradient affect the calculation of *D*. Antisymmetric gradients cancel these cross terms but at the cost of diffusion sensitivity. Stejskal and Tanner, Lowe, Neeman, and van As et al suggest other methods. In 6-cm-FOV images using the conventional method with TE = 55 msec, $D_{app}$ of water changes from 1.6 to 2.2 ($\times 10^{-5}$ cm$^2$/sec) when the sensitizing gradient direction is reversed. Antisymmetric gradients give the geometric mean of the other readings, 1.9 ($\times 10^{-5}$ cm$^2$/sec) (Fig 2, in which the bottom line represents diffusion gradients read parallel, the top line represents diffusion gradients read antiparallel, and the middle line represents antisymmetric gradient pulses [correlation coefficients, 1.000]). In an apple, background gradients or restricted diffusion (appears not to be the problem here) reduce the measured *D* to less than half the value measured in its juice, depending on the gradient duration (Fig 3, in which ASGP indicates antisymmetric gradient pulse, and 6-, 10-, and 14-msec bars represent symmetric gradients, conventional methods). Antisymmetric gradients give good agreement. Measuring *D* by more than one method allows background gradient and compartment size to be calculated.

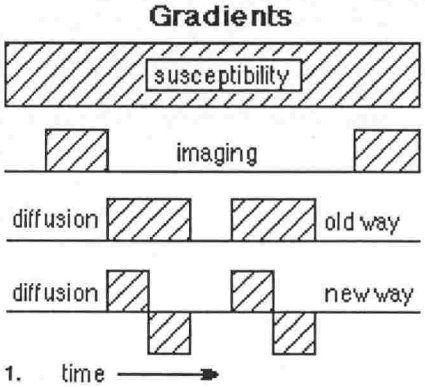


1.

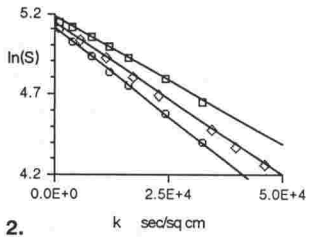


2.

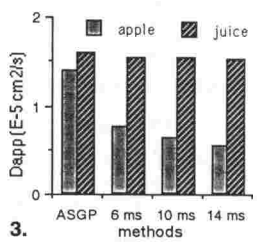


3.

P328

## Localized Continuous-Saturation Perfusion Measurements in Rats at 2.0 T

EG Walsh, SC Moore, K Minematsu, L Li
*Department of Biomedical Engineering, Worcester (Mass) Polytechnic Institute*

Detre et al have recently demonstrated a cerebral perfusion imaging method based on the continuous saturation (or adiabatic inversion) of the arterial blood supply at 4.7 T. Because the image pixel signal-to-noise ratio for this technique is significantly worse at 2.0 T, the authors combined this technique with a localized PRESS readout to benefit from recording a perfusion "signal" averaged over a larger volume. The sequence was implemented with a GE 2.0-T CSI imaging spectrometer (2T-45 series) with 20-G/cm shielded gradients. All experiments involved readout of 125-mm$^3$ volume elements from both left and right hemispheres of Sprague-Dawley rats using a PRESS readout with TE = 20 msec, and a 32-msec acquisition window. Signals were first acquired at three different TR values to permit calculation of T1, which is necessary for the flow estimation. For the perfusion measurement, axial saturation pulses were delivered to the neck at intervals of 50 msec continuously during the TR interval (> 1.5 seconds). To obtain control measurements with no arterial blood saturation, an axial section was selected outside the head an equal and opposite distance from the readout voxel. For hypercapnia experiments, baseline data were first acquired with animals breathing air and 1.25% isoflurane. This was followed by measurements after 10 minutes on a 5% carbon dioxide mixture. The mean increase in perfusion was determined with this method to be 143% ± 95% ($n$ = 5). Selective arterial occlusion affecting primarily the right hemisphere showed a mean change in blood flow for the occluded hemisphere of −81% ± 19% ($n$ = 3), with a corresponding change of −19% ± 22% for the control (left) hemisphere. After reperfusion, blood flow was observed to increase in all animals, but the measured change in flow was highly variable. This could be attributed to varying degrees of occlusion and/or the duration of occlusion. Echo-planar imaging following bolus injection of superparamagnetic particles indicated only a partial restoration of flow to the previously occluded region. Repeated measurements indicated a short-term (< 1 minute) variability of approximately 10% of the measured perfusion value. The expected uncertainties resulting from MR noise were approximately 3%–4%, indicating that biologic motion is probably the dominant source of measurement uncertainty. These results indicate potential for application of the continuous wash-in method on lower-field-strength systems.

P329

## SPOR: A Robust Fast Spin-Echo Sequence

WA Kudrle, PA Narayana
*University of Texas Medical School at Houston*

In 1990, Bogden and Joseph showed that the fast spin-echo sequence RASEE has potential advantages over FATE and is useful for time course studies. However, RA-

SEE is optimized only for TRs below 100 msec and therefore requires either a large buffer or fast transfer rates to a host computer for large data sets. Also, the flip angle and TR in RASEE must be matched to produce a given T1 weighting, and the contrasts are similar to those of gradient-echo rather than standard spin-echo images. To make the sequence more robust and produce contrast seen on spin-echo images, the authors added a saturation recovery (SR) pulse and spoiler gradients at the end of RASEE, and named it SPOR (*spo*iled *R*ASEE). This combination includes a variable TR to allow for data transfer times. Also, the SR pulse can create different T1 weightings regardless of the TR used and, coupled with the spoiler gradients, induces a more effective spoiling of steady-state transverse magnetization and produces a contrast value similar to those of standard spin-echo images. The authors have produced T1-, T2-, density-, and diffusion-weighted images of phantoms and in vivo rat tails with SPOR. The signal-to-noise ratio for SPOR images with TR = 300 msec is approximately half that of standard T2-, density-, and diffusion-weighted spin-echo images with TR = 2,000 msec. Our studies indicate that SPOR can be used to significantly shorten the imaging time and yet retain the advantages of conventional spin-echo techniques. The imaging time could be further reduced by incorporating half-Fourier techniques.

P330

### Suppression of Long T2 Components for Short T2 Imaging

J Pauly, S Conolly, A Macovski
*Magnetic Resonance Systems Research Laboratory, Stanford, Calif*

The authors have been developing pulse sequences for imaging very short T2 components. Images of T2s less than 1 msec can be made on their 1.5-T GE Signa system. One problem is the complete absence of any T2 contrast. Ideally, images that show only the short T2 components would be produced. One approach is to subtract two images acquired at different TEs. This incurs a significant signal-to-noise ratio (S/N) penalty. A better approach uses the fact that short T2 components are difficult to excite. An excitation pulse rotates the equilibrium magnetization away from the $+z$ axis, while relaxation effectively rotates it back. If the relaxation rate is substantially greater than the excitation rate the magnetization is left unperturbed. If the relaxation rate is substantially less than the excitation rate the magnetization can be rotated into the transverse plane, where it can be suppressed by a dephasing gradient. This leaves the short T2 components still aligned with the $+z$ axis, which can then be imaged with a short T2 pulse sequence. This has several advantages over the subtraction method. There is almost no loss in S/N with the long T2 suppression pulse. Only one image is acquired, which reduces imaging time. After describing the basic ideas, the authors will give an analytical expression for the T2 selectivity of a rectangular long T2 suppression pulse. The selectivity and sensitivity will be compared with that of the subtraction method. Images will be presented demonstrating that short T2 selective images are practical on commercial imaging machines.

P331

### Experimental Verification of an Analytic Solution to Bloch Equations

D Kwiat, JP Felmlee, SJ Riederer
*Magnetic Resonance Research Laboratory, Department of Diagnostic Radiology, Mayo Clinic, Rochester, Minn*

An exact solution to the Bloch equations allows analysis of the effects of the RF and the gradient waveforms on the section profile. This is important for the design of improved RF pulses. A closed-form solution to the Bloch equations (with relaxation effects assumed negligible) in the presence of time-dependent RF and gradient magnetic fields was derived recently in the form of a $3 \times 3$ matrix. This matrix propagator operates on an initial magnetization vector, and propagates it in time under almost arbitrary RF and gradient fields. This allows simulation of the section profiles that are obtained from specified section-selective gradients and RF pulses. In this work the accuracy of the predicted results was determined by comparing them with those determined independently in known analytic solutions to selective RF pulses and experimentally measured section profiles. For the case of a constant RF in the presence of a section-selective gradient, the solution resulted in the exact form as derived by Mansfield. A sinc-modulated section-selective RF pulse was used in a simulation for a wide range of nutation angles, to predict the section profile of a 2-cm-thick section according to the magnitude of the transverse magnetization along the section. The results were compared with an experimentally measured section profile, and were in excellent agreement within ±5% error. The propagator solution to the Bloch equations appears to have high accuracy, as determined by its ability both to reproduce known analytic results and to accurately predict experimental results.

P332

### A Shinnar–Le Roux Algorithm for Design of 2D and 3D Spatially Selective RF Pulses

MH Buonocore
*Department of Radiology, University of California Davis Medical Center, Sacramento*

The 1D Shinnar–Le Roux (SLR) algorithm for RF pulse design is based on a hard pulse approximation of the pulse in the presence of a constant field gradient. Each instantaneous RF excitation acts at a single spatial frequency of the spin phase that is linearly related to the temporal location of the excitation from the start of the pulse. Although the spatial frequency components are interdependent, the sequence of RF excitations can be deduced by computing backward from higher to lower spatial frequencies, with each computational step "peeling off" the highest-frequency response to leave the lower-frequency responses. The 1D SLR algorithm is as follows: (*a*) Describe the desired spatial spin response with the second component of the SU(2) spinor defined by $|\beta(k)| \leq 1$; (*b*) determine the amplitude of a compatible first component of the spinor, denoted $\alpha(k)$, using the spinor normalization condition; (*c*) determine the minimum phase (which is required from the physics) of $\alpha(k)$ by a 1D Hilbert transform; and (*d*) from the $\beta(k)$ and the compatible $\alpha(k)$, apply the backward computation to determine the sequence of RF excitations. For a 2D and 3D spatially selective RF pulse, time-varying field gradients in two or three directions are played out. Immediate extension of the SLR algorithm to higher dimensions is difficult because (*a*) the extension of the 1D Hilbert transform is not generally known, and (*b*) the spin response to any given 2D or 3D RF pulse may not be minimum phase. The higher-dimensional SLR algorithm follows essentially the same steps. The extension of the Hilbert transform of the compatible $\alpha(k_x,k_y)$ or $\alpha(k_x,k_y,k_z)$ can be found using Wiener-Doob or other spectral factorization technique. Cartesian k-space trajectories of the time-varying gradients must be used to generate the minimum phase response. The algorithm will be applied to the generation of small-flip-angle 2D and 3D spatially selective pulses with near linear phase, for use in pulse sequences for measurement of regional blood flow. This algorithm has wide application, but whether it is better than Pauly's k-space algorithm has not been determined.

P333

## Image Contrast Changes Due to Jeener-Broekaert—Type Prepulse

L Kasuboski, RP Gullapalli
*Picker International, Highland Heights, Ohio*

The purpose of this investigation was to determine the contribution of the dipolar interaction to the contrast changes observed during magnetization-transfer contrast experiments. The Jeener-Broekaert sequence was used as a spin preparation to transfer Zeeman order into dipolar order. The resultant system was then imaged with a conventional field echo sequence. Both the time for the system to achieve dipolar equilibrium and the time the system was left in the dipolar state were varied to characterize the effects observed. Initial investigations have focused on joints in which tissues exist in a variety of motional regimes. Tissues such as ligaments and cartilage appeared to have increased signal intensity on these dipolar-weighted images. The intensity of fat and fluid seemed invariant to the preparation. Muscle appeared to lose signal intensity. In addition, the contrast between muscle and bone decreased as the time the sample was left in the dipolar state increased. The contrast changes observed with this sample preparation method are consistent with those observed with "conventional" magnetization-transfer techniques, with the advantage of decreased RF requirements.

P334

## Suppression of T1 Contrast for Short TR Imaging

S Conolly, C Meyer, A Macovski
*Magnetic Resonance Systems Research Laboratory, Stanford, Calif*

It is well known that short TR sequences show strong T1 contrast. It is also well known that this T1 contrast effectively cancels T2 contrast. Hence, a late echo from a short TR sequence shows very little contrast. To avoid T1 contrast, typical T2-weighted images use a long TR (1–3 seconds). The authors have developed pulse sequences that suppress T1 contrast for short TR imaging. The pulse sequence consists of an $\alpha$ pulse followed by two spin-echo pulses. The second echo may be T2 weighted. In addition to generating the second spin echo, the second $\pi$ pulse also restores the longitudinal magnetization. In the limit of zero TE, this sequence behaves like a small-tip, short TR sequence. By reducing the flip angle of the $\alpha$ pulse below the Ernst angle, one can control the T1 contrast arbitrarily. Of course, this T1 contrast suppression comes at the cost of reduced signal-to-noise ratio efficiency. The relation between the signal-to-noise ratio efficiency and the variation in T1 contrast is roughly inverse linear. The authors have obtained standard 2D Fourier transform images with a 1.5-T GE Signa, showing good T2 contrast on second-echo images (TR = 330 msec, TE = 25/75 msec). For these images, the $\alpha$ pulse angle was set to limit the T1 contrast to 5% over the range of T1 found in the brain. This technique has also been used in conjunction with a fast imaging sequence that reads k space in a spiral fashion. T2-weighted images of the abdomen have been obtained with this fast imaging pulse sequence.

P335

## Accuracy in Magnetization and Image Signal Intensity Simulations

AEH Bampton*, SJ Riederer†
**Department of Radiology, McGuire Veterans Affairs Medical Center, Richmond, Va, and †Magnetic Resonance Laboratory, Mayo Clinic, Rochester, Minn*

Simulation models are particularly useful in understanding the magnetization and image signal intensity behavior of MR pulse sequences involving transient magnetization. They also may be used for prediction, if reasonably accurate. The time evolution of magnetization in standard and magnetization-prepared FLASH and GRASS sequences was simulated with the common rotation matrix model. The effects of field inhomogeneity, nonideal section profile, and residual transverse magnetization were included. An experimental measure of magnetization behavior was obtained by applying the pulse sequences without phase encoding to a uniform phantom and transforming the data in the readout direction only. The root mean square (RMS) error was less than 3%, including oscillations and experimental noise. Modeling image signal intensity is a two-part process. First, the raw data are formed from the theoretical Fourier transform of the chosen 1D object (truncated by the k-space acquisition matrix) and multiplied by the k-space filter due to transient magnetization of the imaging sequence, as simulated above. In the image reconstruction process, a Fermi filter is applied to the raw data, the inverse Fourier transform computed, and the magnitude "image" formed. If the object simulates multiple materials, the raw data are generated separately for each material and the data for all materials are summed before the reconstruction. Simulated 1D "images" were compared with a line through experimentally acquired images of a gel phantom containing cylindric "lesions" of a second gel. The RMS error between simulated and experimental images was less than 5%, including areas of edge enhancement, blurring, and ghosting. The simulations presented here result in highly accurate predictions of magnetization and image signal intensity behavior.

P336

## CPMG Effects on Lipids at 1.5 T

GA Wright*, JM Pauly*, GH Glover†, A Macovski*
**Department of Electrical Engineering, Stanford (Calif) University, and †Department of Radiology, Stanford University Hospital*

In RARE, a method to rapidly generate T2-weighted images with multiple-echo acquisition, signal from lipids is enhanced compared with standard spin-echo imaging. Several hypotheses for this effect have been proposed, including stimulated echo generation by imperfect refocusing pulses and CPMG effects associated with chemical exchange and/or scalar coupling. The authors' aim was to examine these potential sources. The basic sequence used is a hard 90° pulse followed by a train of hard refocusing pulses, each separated by an interval $\tau_{180}$. After this train, a single section-selective refocusing pulse is included, followed by a 2DFT data acquisition at TE. Keeping TE constant at 160 msec but changing $\tau_{180}$ from 160 to 8 msec, the lipid signal increases by at least a factor of two, while other tissues such as gray matter are relatively unaffected. This is true whether one centers the RF frequency on water or fat. This method eliminates progressive errors due to imperfect section profiles. Furthermore, the refocusing train minimizes effects of $B_0$ and $B_1$ errors. Thus, enhancement is not likely due to refocusing error in this case. Conditions in which CPMG effects on scalar coupling are relevant are realized in the lipid molecule; chemical exchange effects are unlikely due to the stability of the various proton sites. Some proton groups in the lipid molecule with observable coupling are separated by a chemical shift at 1.5 T comparable with the range of $1/\tau_{180}$ under consideration. In this situation, decreasing $\tau_{180}$ decreases the phase difference developed between the coupled species and hence reduces scalar coupling effects. This, combined with differential T2 characteristics of the various proton groups in the lipid, may explain much of the lipid signal enhancement described above.

P337

## The Effects of External Field Gradients on the Echo-Planar Measurement of T2 in Flowing Systems

MS Yoon, VH Scholz, RM Weisskoff, KR Thulborn
*Massachusetts General Hospital NMR Center, Charlestown*

The measurement of T2 of blood in vivo, as used to determine the venous oxygen content with MR imaging, has errors associated with flow through external field gradients. The size of this error in T2 is estimated for two echo-planar pulse sequences for flow in static field gradients over the physiologic flow velocity range (0 to 15 cm/sec). The echo-planar images were obtained with a GE Signa 1.5-T imager retrofitted with resonant gradient technology by Advanced NMR. Pulse sequence A used a nonselective 90° and section-selective 180° pulse train. Pulse sequence B used nonselective 90° and 180° pulses followed by a section-selective 180° pulse. Both sequences were moment nulled in the z direction and at the center of k space in the phase-encoding direction. The phantom was a 1-L plastic bottle filled with 1% agar solution with four linear tubes positioned at the center of the agar (*a*), at the agar-plastic interface (*b*), at the plastic-air interface (*c*), and at 2.5 radii from the center of the bottle surrounded by air (*d*), all aligned in the z direction. This geometry results in static field gradients over each tube because of the magnetic susceptibility differences among the solution, agar, and air. The solution of water doped with AMI 227 (Advanced Magnetics) gave a T2 comparable with that of venous blood (100 msec). The errors in T2 at flow velocities of 15 cm/sec relative and 0 cm/sec were calculated for the four tubes for pulse sequences A and B as (*a*) 21%, (*b*) 26%, (*c*) 50%, and (*d*) 54%, and (*a*) 4%, (*b*) 6%, (*c*) 17%, and (*d*) 35%, respectively. Pulse sequence B produces T2 values with acceptable error for flow velocities less than 15 cm/sec for geometries and field gradients modeled by this phantom.

P338

## Multidimensional Global Optimization Methods Applied to Magnetization-prepared, Variable-Flip-Angle Gradient-Echo Imaging

FH Epstein*, JP Mugler III*†
*Departments of *Biomedical Engineering and †Radiology, University of Virginia, Charlottesville*

Owing to the transient signal response in single-shot and multishot magnetization-prepared, ultrashort TR, gradient-echo pulse sequences (eg, TurboFLASH, Snapshot GRASS, 3D MP-RAGE), optimization of the data acquisition segment of these sequences should not be restricted to only the traditional parameters of TR, TE, and flip angle. Instead, varying the flip angle and/or TR as a function of the phase-encoding step should be recognized as a potentially powerful means to determine the signal response and consequently signal-to-noise and contrast-to-noise ratios. Furthermore, it may be desirable to specify the required signal response and subsequently compute the necessary sequence parameters rather than to simply implement best-guess parameters and note minor improvements in image quality. Consideration of these parameters then requires the use of multidimensional global optimization algorithms applied to computer simulations of the signal response. The authors have applied the simulated annealing algorithm and the downhill simplex method to the optimization of these types of sequences with variable flip angle. The optimization algorithms and pulse sequence simulations were run on a SUN SPARCstation computer equipped with a SKY station vector processor. With these techniques, variable flip angle vectors have been derived that result in prescribed signal responses for 3D MP-RAGE imaging of tissues in the brain while retaining high signal-to-noise and contrast-to-noise ratios. Similarly, the authors derived optimal variable flip angle vectors for TurboFISP imaging of a doped water phantom and used these values to experimentally verify the simulation/optimization results on a 1.5-T whole-body imager (Magnetom 63SP, Siemens Medical Systems) by measuring the signal response from the phantom. Optimal variable flip angle sequences are currently being evaluated in healthy volunteers. By making use of nontraditional parameters such as variable flip angle, the overall image quality for this class of pulse sequences can be improved. The authors have demonstrated that by employing computer simulations coupled with multidimensional global optimization methods, optimal values for these parameters can be derived.

P339

## A Half-Fourier Gradient-Echo Technique for Dynamic MR Imaging

WH Perman
*Mallinckrodt Institute of Radiology, Washington University School of Medicine, St Louis*

Important information about local neuronal functional and cerebrovascular status can be provided by the measurement of regional cerebral blood flow, regional cerebral blood volume, and regional cerebral mean tissue transit time. Determination of these hemodynamic parameters with MR imaging and intravascular paramagnetic contrast agents requires rapid sequential measurements of contrast agent concentration in arterial blood and brain tissue. Recently, the author and colleagues developed the SDFLASH pulse sequence that simultaneously obtains sequential images from the brain and the internal carotid arteries in the neck with 1-second temporal resolution at a spatial resolution of 6.2 × 3.1 mm on a standard MR imager. The purpose of this work was to implement asymmetric field of view (smaller field of view in phase-encoding direction) and gradient-echo, half-Fourier techniques to allow the choice of either decreasing imaging time while maintaining spatial resolution or increasing spatial resolution at the same imaging time. Although half-Fourier techniques have been successfully applied to RF spin-echo imaging, they have not worked with gradient-echo imaging because asymmetries in the static magnetic field produce significant phase errors in the data that severely degrade image quality. The author and colleagues have developed a technique that allows the use of half-Fourier gradient-echo data collection for dynamic MR imaging that achieves a spatial resolution of 2.3 × 1.5 mm at 1-second temporal resolution, or 4.5 × 3.1 mm at 0.5-second temporal resolution. The author will present the technique and illustrate its uses with both phantom and in vivo images.

P340

## Post–Gd-DTPA Lesion Conspicuity with 180° Prepared RF-Spoiled Gradient-Echo Imaging

SD Rand, U Schmiedl, KR Maravilla
*Department of Radiology, University of Washington, Seattle*

The RF-spoiled, gradient-recalled-echo (SPGR) sequence affords excellent anatomic detail with rapid sequential section or volumetric (3D) data acquisition modes. However, post–Gd-DTPA lesion conspicuity with SPGR is considerably less than that obtained with the conventional T1-weighted spin-echo (SE) technique. The authors' hypothesis is that central nervous system lesion enhancement with SPGR could be considerably improved through the introduction of a 180° magnetization preparation pulse with an appropriate inversion time (WARPSPGR).

Mathematical predictions of in vitro signal strengths of Gd-DTPA–doped water samples, defined by region of interest (ROI) cursors, were verified experimentally for the WARPSPGR (TI/TR/TE/number of excitations/flip angle) and SE (TR/TE/number of excitations/flip angle) sequences operating in sequential section mode. Post–Gd-DTPA lesion signal strength and relative lesion contrast, defined as (lesion ROI − background ROI)/background ROI, were compared in eight patients with WARPSPGR (1,200/11/5/4/15°) and SE (600/12/1/90°). Image contrast (gray scale) is introduced into T1-weighted SE and SPGR images through the TR parameter. However, image contrast enters WARPSPGR images through TI, as TR, TE, and flip angle are reduced to sample the spin density (with a minimum of saturation) that has been "prepared." As expected, the post–Gd-DTPA lesion signal strength obtained with SE, which ranged from 422 to 903 (arbitrary units) among eight patients, exceeded that measured with WARPSPGR, which varied from 106 to 196. However, relative lesion contrast obtained with WARPSPGR, which ranged from 0.38 to 1.9, was similar to that measured with SE, which varied from 0.42 to 2.3. A minor blurring of edges within phantom WARPSPGR images was observed in the phase-encode direction. This blurring may be improved with variable-flip-angle excitations that accentuate the high spatial frequencies (high-order phase encodings), or with segmentation of phase encodings. Edge blurring of rim-enhancing lesions on clinical WARPSPGR images was attributed primarily to the diffusion of Gd-DTPA over an average of 26 minutes that separated the SE and WARPSPGR images in the protocol. In conclusion, the WARPSPGR sequence yielded similar post–Gd-DTPA lesion-to-background image contrast compared with SE, but at considerably shorter acquisition times.

P341

## Highly Accurate T1 and T2 Estimates in Less than 3 Minutes

AEH Bampton*, SJ Riederer†
*Department of Radiology, McGuire Veterans Affairs Medical Center, Richmond, Va, and †MR Laboratory, Mayo Clinic, Rochester, Minn

Accurate T1 and T2 image-based measurement techniques (using inversion-recovery and spin-echo sequences) require extremely long imaging times (21–85 minutes) due to the 5–10-second TR, but rely on just two or four data points for the exponential fit. Reducing the TR invites corruption from stimulated-echo and steady-state effects, while increasing the number of data points increases imaging time proportionally. The measurement technique presented here uses a 10-second TR and 16 data points, but requires only 2 minutes 40 seconds of imaging time, because it is based on projection rather than image data. The projection measurements are acquired at 10-second intervals. For T1 measurements, an inversion-recovery sequence is used and the inversion time is incremented with repetition. T2 measurements are made with a spin-echo sequence with incrementing of TE. Nonselective inversion pulses are used to eliminate inversion slab profile effects. Thus, the raw data matrix contains spatial information along the readout direction and T1 or T2 data in the other direction. After a Fourier transform is performed in the readout direction, the data points at the center of the material are fit to an exponential curve. Because a projection is used, this technique is limited to materials that are relatively homogeneous in one direction (eg, a row of vials). However, the 16-point estimates are essentially free of unwanted T1/TR and stimulated-echo effects, even for very long T1 and T2 values, and have less than 1% bias and small $\chi^2$ values. This technique provides accurate results and is 16–64 times faster than traditional image-based techniques using the same parameters. Speed can be increased by reducing the TR or number of data points.

P342

## Multiexponential T2 Relaxation in Patients with Phenylketonuria

U Stöber, U Bick, H Möller, W Müller-Warmuth, PE Peters
*Department of Radiology and Physical Chemistry, University of Munster, Germany*

In vivo measurements of multiexponential T2 relaxation in phenylketonuria (PKU) lesions with MR imaging are potentially useful for the evaluation of disease activity. The examinations were performed with a 1.5-T imaging system (Siemens Magnetom). The T2 relaxation was measured by applying a CPMG sequence in single-section mode (32 echoes, TE = 22–512 msec, TR = 2 seconds, matrix = 256 × 128, FOV = 200, section thickness = 7 mm). Phantoms, 10 volunteers, and eight patients were studied. Two patients underwent an additional two examinations following a diet treatment. The mean signal values of the ROIs for all TE were fitted with a nonlinear least-squares algorithm using mono- and multiexponential models. The accuracy of monoexponential T2 in phantoms reached 3%, but the detection of multiexponentiality strongly depends on the differences and values of the T2 components. In normal white matter (WM), the T2 relaxation process was found to be a monoexponential function with a mean T2 of 76 ± 6 msec. In the WM lesions of PKU, the magnetization decay curve is more accurately fitted with a biexponential function, in all cases generally leading to a fast T2f (18–84 msec) and slow T2s (84–480 msec) component. Some of the relaxation curves give evidence for a three-compartment model. The changes in T2 relaxation correlate with the plasma concentration of phenylalanine. In both cases of the repeated T2 measurements in patients under diet treatment, a strongly decreasing long component was found. As in other recent studies, the authors have found that T2 decay in normal WM is monoexponential, but WM lesions show distinct multiexponential patterns. The slow component may represent mainly the influence of interstitial free water. A prolongation of this component may indicate a higher content of edema. The fast component may characterize the myelin-bound water and therefore myelin disorders. In the future, T2 relaxometry may provide the possibility of monitoring of PKU.

P343

## Fast T1 Measurements with TurboFLASH

U Stöber, E Rummeny, C Eissing, P Vassallo, W Müller-Warmuth, PE Peters
*Departments of Radiology and Physical Chemistry, University of Munster, Germany*

For TurboFLASH (TF) imaging with a 180° preparation pulse, the signal behavior is strongly T1 weighted due to the inversion-recovery (IR) mechanism. The authors evaluated the ability and accuracy of T1 measurements by applying this sequence in stationary and flowing phantoms and in volunteers and patients. Accuracy of T1 measurements was tested with phantoms of various manganese chloride concentrations (T1 = 270–3,300 msec). For clinical evaluation, 10 healthy volunteers and 24 patients with known focal liver disease were examined with the same measurement protocol. All measurements were performed with a 1.5-T imaging system (Magnetom, Siemens). The 10 single-section mode TF sequences used 128 selective 8° pulses for data acquisition of a 128 × 128 image matrix (TR = 7 msec, TE = 4 msec), and the delay between inversion pulse and readout pulses varied from 0 to 4,000 msec. The mean signal intensities were obtained from ROIs and fitted to the absolute value of an IR curve

with a nonlinear least-squares fit. Signal intensities from phantoms correlated well with the fitted function for monoexponential relaxation. T1 relaxation times estimated with TF measurements showed a regular underestimation compared with spectroscopic T1 values of the stationary and slowly flowing phantoms. By applying a linear calibration factor the accuracy could be improved to 4%. For phantoms with flow rates comparable with blood flow, no calibration factor was needed. In vivo measurements in volunteers and patients showed that T1 values obtained with TF imaging are comparable with those provided by time-consuming spin-echo techniques. Therefore, TF imaging can be used for fast T1 evaluation in a clinical setting.

## Wednesday, April 29, 12:15 PM–1:00 PM
## Spectroscopy, Instrumentation, Image Processing, and Miscellaneous

P400–P440

P400

### Multimodality Intracerebral Angiography: Registration and Integration of Conventional Angiograms and MR Angiographic Data

R Grzeszczuk*, DN Levin*, Y Cao*, KK Tan*, CA Pelizzari†, S Mojtahedi*

*Departments of *Radiology and †Radiation Oncology, University of Chicago*

Conventional angiograms (XRAs) have higher spatial and temporal resolution than MR angiograms but do not contain as much 3D information as MR angiograms. The authors registered the two studies and then used the integrated data set to create a 3D vascular model with higher spatial and temporal resolution than the model derived from MR angiography alone. A frameless stereotaxic system was used for retrospective registration of multiplanar XRA films and MR angiograms with the subject and with each other. Then, any point on each XRA film could be identified with a projection line through the MR angiographic data. This technique was used to project intravascular points in cerebral MRA images onto each of the multiplanar XRA films. Note that these MR angiographic points include those from small vessels incompletely visualized with fragmented flow signal. In this way, corresponding points were identified along vessels in multiple XRA views. The vessel segments between these points were then back-projected from the XRA films to reconstruct the 3D configuration of the vessel. Thus, the XRA films were used to "interpolate" between vessel points that were not necessarily connected by flow signal in the MR angiographic volume. The method was tested on an MR head phantom containing tubular "vessels" filled with radiographic contrast agent. Studies of patient volunteers are being planned. The results suggest that this multimodality angiographic technique will create images of intracerebral vasculature with the three-dimensionality of MR angiography and the higher spatial and temporal resolution of conventional angiography.

P401

### An Improved Format for Maximum-Intensity Projection: The Traveling MIP

W Lin, EM Haacke, TJ Masaryk

*Department of Biomedical Engineering, Case Western Reserve University, Cleveland; Department of Radiology, University Hospitals of Cleveland; and Department of Radiology, Cleveland Clinic Foundation*

To create a subtraction-like image from a set of time-of-flight MR angiographic images, the maximum-intensity projection (MIP) is used. This method has several disadvantages that make it less reliable: The background noise level is elevated, which reduces vascular contrast, and variation of image intensity from section to section causes some vessels to be lost. A local MIP or targeted MIP can be used to avoid the problem, but it gives only local vascular information rather than an entire view of vascular structure. The purpose of this study was to implement a hybrid, 3D, vessel tracking–based method: the traveling MIP, or TMIP. This method starts with a user input seed point or multiple seed points. A $5 \times 5 \times 3$ or $9 \times 9 \times 3$ kernel centered at the seed point is used to perform the local MIP. The vessel tracking scheme is then followed by using a $3 \times 3 \times 3$ kernel to check the 26 points around the seed point. When a neighbor point has a signal intensity higher than a threshold, the coordinates of this point are stored in a buffer and this point is classified as vessel. The threshold value is selected from a region of background in one of the 3D sections. The mean value and standard deviation (SD) are calculated for the selected region. The threshold is then set as the mean value plus one SD. All the points classified as vessels are used to perform the TMIP. The total data processing time for 64 sections is roughly 1–2 minutes with this program. The results include the MIP images, vessel-tracked images, and TMIP images. In all cases, the results of TMIP show better lumen definition, more small vessels, and an improvement in contrast on the projection images.

P402

### Recognition of Susceptibility-induced Geometric Distortions in MR Imaging: Implications for the Use of Markers in Radiation Therapy Treatment Planning

MA Moerland*, R Bhagwandien*, CJG Bakker†

**Department of Radiotherapy and †NMR Institute, University Hospital Utrecht, the Netherlands*

In radiation therapy treatment planning, geometric accuracy is of major importance. MR imaging distortions may have machine-dependent causes such as static field inhomogeneity and nonlinear gradients, or patient-dependent causes such as chemical shift and susceptibility. Several methods based on phantoms with known geometric characteristics have been proposed to correct for distortions of the first category. This study focuses on susceptibility artifacts. The aim of the study is to investigate the severity of these artifacts with respect to the use of external markers for radiation therapy treatment planning. The method is based on the following relationship between the $x$ coordinate of the object $x_0$ and the image $x$: $x = x_0 + \Delta B/G$, where $\Delta B$ is susceptibility-induced field inhomogeneity and $G$ is the readout gradient strength (machine-dependent errors have been corrected if necessary). A set of two images is acquired with different gradient amplitudes $G_1$ and $G_2$ from which the following relationship between the real coordinate of an object $x_0$ and the image coordinates $x_1$ and $x_2$ can be derived: $x_0 = (G_2x_2 - G_1x_1)/(G_2 - G_1)$. The head of a healthy volunteer surrounded with markers was imaged with a 1.5-T Philips Gyroscan S15 with gradients of less than 3 mT/m. Displacements of the tubes were most severe on images acquired with small readout gradients and close to the head. Errors of up to 8 mm were observed for small- and up to 2 mm for large-gradient images. The outer contour of the head was slightly distorted. The contour of the brain was distorted at tissue-air interfaces, but the ventricles and the sulci of the brain were not distorted. For a typical brain study, image distortions of up to 4 mm are expected. Corrections are necessary for accurate radiation therapy treatment planning, especially for obtaining reliable marker positions.

P403

## Four Years of Manufacturer-Independent MR Imaging Quality Assessment

G Gomiscek, E Moser, H Imhof
*Institute for Medical Physics and MR Institute, University of Vienna*

To ensure the optimal performance of a complex medical diagnostic device for routine clinical application as well as for spectroscopy, manufacturer-independent quality assessment measurements have been performed. The performance of a 1.5-T MR imager has been tested once each year since installation in 1987. As test objects, five phantoms developed by a European Community research project were used. Image parameters (homogeneity, signal-to-noise ratio, ghosting, and geometric distortion) and section parameters (thickness, warp, resolution, and null position) were evaluated. The T1 and T2 of known test substances (doped gels) were also determined. To get reference data, these measurements were also undertaken on an identical system in the manufacturer's application laboratory. The quality assessment measurements in the first year disclosed some initial problems that could be solved by the manufacturer's local service. Nevertheless, the overall performance was comparable with that of the reference imager and turned out to be good in comparison with 15 European installations. In the following years the overall quality of the imager remained acceptable, but some significant deviations were discovered in parameters important for quantitative data analysis as well as image quality. In conclusion, the authors' experience proves that quality assessment should not be left to the manufacturer only, especially if the MR device is not being used only for routine clinical diagnosis.

P404

## One-Chamber Dynamic Cardiac Phantom for MR Imaging

T Cui, NS Negin, RS Mezrich, JA Gronlund-Jacob, NA DeMarco
*Department of Radiology, Robert Wood Johnson Medical School, New Brunswick, NJ*

The cardiac output, ejection fraction, and myocardial mass are important indicators of cardiac status and function. MR imaging provides a noninvasive way to assess these parameters. Development of a dynamic cardiac phantom specifically for MR imaging is desirable to assist both pulse sequence development and quantitative measurements. The phantom the authors developed allows control of stroke volume, rate, ejection fraction, and systolic and diastolic intervals. It consists of a source reservoir, a hydraulic pump, a compliance chamber, a one-way valve controlled by a logic timing circuit, and a calibration reservoir. Fluid is pumped from the source reservoir into the compliance chamber, then emptied via the one-way valve to the calibration reservoir. The compliance chamber is composed of one balloon placed inside another. The space between balloons is filled with K-Y jelly that simulates myocardium, while water flowing through the inner balloon simulates blood. The hydraulic pump operates continuously with a variable flow rate that regulates stroke volume of the phantom. The heart rate and systolic and diastolic periods of the phantom are controlled by a timing circuit through the valve. The timing circuit also synchronizes imaging with the phantom by providing the gating signal. All metallic components of the phantom are placed away from the magnet to avoid interference. The phantom images are reconstructed in cine mode, which provides excellent visualization of cardiac movement. This cardiac phantom can be applied to simulate clinical and pathologic parameters that are studied with MR imaging.

P405

## Superparamagnetic Contrast Agent Visualized with Image Segmentation

G Kühne*, A Blaakman†, J Hornak†, LX Tiefenauer*, RY Andres*
**Paul Scherrer Institute, Villigen, Switzerland, and †RIT, Rochester, NY*

Superparamagnetic particles (SPPs), coated with biospecific labels such as antibodies, are potentially useful contrast agents for MR imaging. The expected concentration of such particles in a target tissue is in the submicromolar range, and the resulting image contrast may be poor, necessitating methods for unequivocal identification. Owing to the almost exclusive T2 relaxivity of SPPs, unusual T1/T2 ratios will be found in the target region, providing a means for identification of contrast agents. Tissue-equivalent phantoms containing increasing amounts of SPPs were imaged together with a human head. T1 and T2 were calculated for each pixel of normal tissue and phantom, respectively, and displayed in a 2D histogram. Pixels derived from brain white matter were characterized by a narrow T2 range (approximately 80 msec) and a wide T1 range (800–1,500 msec). Pixels derived from phantoms containing more than 0.6 μg/mL iron can easily be discriminated from white matter due to the shortened T2. Selection of pixels with this unusual T1/T2 ratio and reassembly into an image exclusively shows the location of the SPP contrast agent. When biospecific superparamagnetic contrast agents become available, it will thus be possible to clearly discriminate their expected low contrast from contrast inherent on any MR image.

P406

## MR Image Segmentation: An Alternative to the Use of MR Contrast Agents

LP Clarke*, RP Velthuizen*, AM Bensaid†, L Hall†, S Phuphanich*, ML Silbiger*
**Department of Radiology, College of Medicine, and †Department of Computer Science and Engineering, University of South Florida, Tampa*

Intensity-based image segmentation techniques are proposed that use multispectral MR image data sets to enhance the contrast between soft tissues. These techniques were applied to pre- and postcontrast studies to quantitatively evaluate the tumor/edema boundary definition in each case. Fifteen patients with brain tumors undergoing radiation or chemotherapy treatment protocols were studied. Pattern recognition techniques were applied to multispectral data (T1-, T2-, and proton density–weighted images) as opposed to the use of image gray scale methods such as seed growing techniques. The methods developed include supervised techniques such as the maximum likelihood, back-propagation artificial neural net, and cascade correlation methods, and unsupervised techniques such as fuzzy c-means and approximated fuzzy c-means. Both the supervised and unsupervised techniques provided enhanced contrast detail at the tumor/edema boundary on the precontrast study, with boundary definition similar to that of the postcontrast study, allowing for factors that may affect the spatial distribution of the contrast material. The algorithms were executed on a highly supported computer platform (Sun Microsystems with VX and MVX accelerator boards) for image processing. Typically user-friendly interactive methods were developed for selection of training regions in feature space and the spatial domain. Preliminary data suggest that these software methods potentially provide cost-effective alternative methods to the use of MR contrast material.

P407

## PINT: Pseudoinversion Null T2 Images to Enhance Contrast

RJ Kurland, WW Woodruff, Jr, GR Funkhouser, A Jones
*Department of Special Imaging/MRI, Geisinger Medical Center, Danville, Pa*

The authors have developed an MR image processing technique that can be used to enhance contrast in a way similar to that achieved with magnitude reconstruction inversion-recovery (MIR) imaging. A synthetic image is constructed from a T2 map through the relation $I(i,j) = K\,|\{1 - 2 \times \exp[-TI/T2(i,j)]\}|$, where $I(i,j)$ is the synthetic image intensity at pixel $i,j$; T2 (i,j) is the spin-spin relaxation time corresponding to pixel $i,j$; TI is a delay time; and $K$ is an adjustable parameter assigned for optimum dynamic range. Note that a null occurs for TI = T2 × ln2. Thus, as indicated in the Figure, contrast between different tissue types can be enhanced by choice of TI($Ti$) to give the appropriate null. A SparcStation1 was used for calculation of the T2 maps and PINT images from images taken from clinical studies. The discrimination between different tissue types was assessed by use of an automated binary segmentation routine. From these segmentation results, the authors conclude that better discrimination was achieved on the PINT images than on conventional T2-weighted images. PINT images of brain and spine lesions will be used to demonstrate enhanced contrast between fluid (cyst/edema) and tumor.

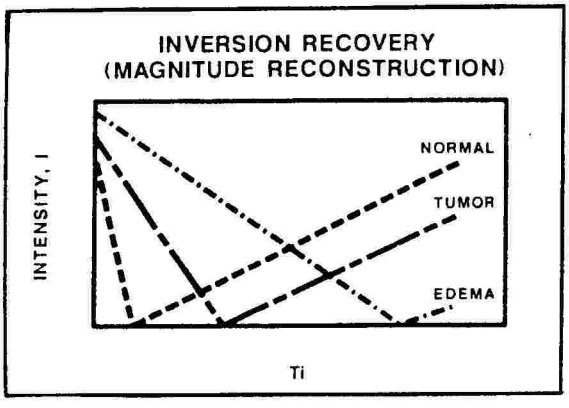


P408

## Autosegmentation of Ventricles in Cardiac Short-Axis Cine Images

A Apicella, M NessAiver, C Wood
*NMR Division, Picker International, Highland Heights, Ohio*

Cardiac MR imaging experiments yield massive amounts of data, often precluding manual processing. The authors describe a novel, fast, and reliable statistical segmentation algorithm for automatically determining left and right ventricular volumes from cardiac cine images. Results are presented from both patient and phantom data. The algorithm first locates that portion of the image containing the ventricles, analyzes the histogram with unsupervised parametric clustering to determine suitable intensity ranges for blood and tissue, and then applies a region-growing algorithm to determine ventricular area. A similar procedure is followed for each of the numerous anatomic and temporal sections obtained in the experiment, with past results used to guide segmentation of the remaining sections. The region of interest containing the heart is located by forming a motion image from the absolute value of the difference of two successive temporal images. The center of mass of the motion image lies near the heart and is taken as the center of the region of interest. The width and height of the region of interest is the square root of the second central moment of the motion image. The histogram of the region of interest is then analyzed to determine the intensity range of tissue and blood. All pixels are classified on the basis of these ranges, and a region-growing algorithm is applied to collect all connected pixels having the same class.

P409

## Tissue Segmentation with 3D Feature Map

S Vinitski, S Seshagiri, AE Flanders, CF Gonzalez, PM Consigny, ML Thakur
*Department of Radiology, Thomas Jefferson University Hospital, Philadelphia*

There are a number of methods aimed at improving tissue characterization in MR imaging: spectroscopy, relaxometry, use of contrast agents, microcirculation imaging, segmentation, and so forth. The purpose of this study was to design software for tissue segmentation based on 3D feature maps and to test this software in biologic tissues. This work is based on the algorithm developed by Cline et al (1). They calculated the probability distribution of each tissue of interest. Two image inputs (eg, proton density and T2 weighted) are required. The signal intensities of each pair of identically located pixels are used as coordinates in a 2D plot. Unfortunately, many tissues (defined probabilistically) have overlapping coordinates. The authors hypothesized that adding a third input image would make the separation of clusters in 3D feature space greater, with resulting improvement in tissue segmentation. A Sun SparcStation2 was used. First, the display routine was created to allow simultaneous display of three 2D segmentation images based on a data set containing three or more imaging series. Second, the algorithm describing probability distribution (1) was modified to accommodate the third dimension. Data sets were obtained from MR spin-echo, gradient, and inversion-recovery imaging. A dedicated data acquisition software program was also created (2). A 1.5-T GE Signa imager was used. Results have shown that three 2D segmentation images show variable degrees of tissue segmentation, and that prior to experiments, it is not possible to know which pair of images will produce the best results. The 3D feature map creation required intensive computations: 2.5 hours using the SparcStation2 with 32 Mbytes of memory and 90 Mbytes of swapping space. However, the segmentation image based on 3D feature maps was always either better than or equal to the best of three 2D segmented images. Images appeared crisper and sharper, and the random color points (ie, statistical noise) were greatly reduced. Further, when the third image was of deliberately low contrast, the resulting 3D segmentation image effectively "filtered out" inferior input. This method was successfully applied to tissue characterization in neurologic imaging, MR imaging of atherosclerotic plaque, and imaging of pulmonary embolism with the use of contrast agents. In conclusion, the proposed technique provides excellent tissue segmentation and, thus, merits further evaluation and development.

1. Cline HE, Lorensen WE, Kikinis R, Jolesz F. J Comput Assist Tomogr 1990; 14:1037. 2. Vinitski S, Mitchell DG, Tasciyan TA, et al. Proc IEEE Biol Eng 1990; 12:82.

P410

## Evaluation of Frequency Filtering for Surface Detection and of Space-Time Analysis for Wall Motion on MR Imaging Heart Sequences

G Marcenaro*, GA Rollandi†, C Martinoli, C Pastorino†, M Tistarelli*, F Beltrame*

**Department of Informatic, Systemistic and Telematique, and †Institute of Radiology, University of Genoa, Italy*

The evaluation of heart wall motility has already been reported by several authors using various imaging techniques (US, nuclear medicine, and MR imaging). In most cases, elaboration of 3D medical data requires too much interactivity between operators and systems. Therefore, simple algorithms have to be exploited in order to deal with a large amount of data in a reasonable time. In this study, the authors have processed raw data (before Fourier transformation) obtained with spin-echo gated sequences in the heart (0.5-T unit, Esaotebiomedica, Genoa, Italy). Heart surfaces were fully demonstrated by direct application to the raw data of "edge detection" (local maximum value of the first spatial derivative or zero crossing points in the second spatial derivative). The data processed in the frequency domain show two advantages: they are void of discretization errors due to the limited support of the derivation mask, and the derivative operations in the frequency domain are much simpler than in the spatial domain, and can be easily implemented with an MR imaging conventional computer and performed automatically, without interaction with the operator. Heart motion was evaluated by computing the velocity field in a sequence of images. Optical flow was computed by using gradient-based techniques. The authors have applied a simple differential technique to sequences of MR images, based on calculation of the first- and second-order derivatives of image brightness.

P411

## Observation of F-19 by Adjustment of the $B_0$ Field

SB Pickup

*Department of Radiology, University of Missouri Hospital, Columbia*

The Siemens Helicon magnet for whole-body imaging was designed to allow routine ramping of the primary field. Clinical imaging is performed at 1.5 T, while spectroscopic and other research applications may be performed with improved signal-to-noise ratio at 2.0 T. Although magnet ramping can be performed in about 15 minutes, the field generally requires approximately 1 hour to stabilize enough for imaging applications. The ability to ramp the primary field is achieved largely through the cryogen recycling system, which collects and recompresses the excess boil-off during ramping as well as during routine operation. Although the passive shims built into the magnet tube are designed for maximum field homogeneity at the two fields for which the system was designed to operate, the active shims have sufficient range to achieve suitable homogeneity at an arbitrary field strength. Thus, the primary field strength becomes a parameter that can be adjusted to suit imaging needs. This capability has been used for the observation of F-19 with an unmodified 1.5-T proton transmitter and receiver electronics at a field strength of 1.59 T. This approach eliminates the need for construction or modification of the RF electronics. Furthermore, all of the proton coils are available for observation of the rare nucleus. The frequency response of a variety of coils (including the whole-body coil) over the F-19 chemical shift range will be presented. Some F-19 spectra and images of phantoms will also be displayed. Potential clinical applications of this technique will be discussed.

P412

## MR Angiography Display Alternatives Using Connectivity

D Saloner*, R van Tyen*, W Hanson†, J Tsuruda*

**Department of Radiology, VA Medical Center, San Francisco, and University of California, San Francisco, and †IBM Research Center, Palo Alto, Calif*

A connected-voxel algorithm for extracting flow signal from 3D angiography data sets has been evaluated and refined. The algorithm has been implemented on an IBM RS6000 workstation permitting rapid user interactivity. The use of graphic objects to display the identified connected objects permits real-time rotation of the data to any desired viewing angle. The standard display technique for MR angiograms, the maximum-intensity projection (MIP), is known to have shortcomings. The lumen size is underestimated, small vessels are lost, and overlapping vessels confound image interpretation. The authors have extended a connected-voxel algorithm (1) that uses thresholding and a search that reduces the full data set into connected objects. The objects can be viewed as graphic objects, permitting rapid orientation to any desired obliquity. Unwanted objects can be identified and selectively removed from the data, avoiding vessel overlap. Once in the desired orientation, the original signal intensity values can be restored and one of a number of alternative display methods can be used to view an image of this reduced data set. These include the MIP and intensity summation methods or surface-rendering techniques. A possible consequence of invoking thresholding is the loss of low intravascular signal and the appearance of interruptions in the vessel. The authors have provided the capability to perform dilation and/or erosion operations to restore voxels lying along the edges of the identified objects, resulting in more vascular continuity and better retention of intravascular signal. The algorithm has been demonstrated to provide superior image display capabilities in clinical studies, including identification of an aneurysm neck, intravascular plaque, and lumen definition.

1. Saloner D, Hanson W, Tsuruda J, et al. JMRI 1991; 1:423–430.

P413

## Low-Cost MR Tomography for Education

G Gomiscek*, E Moser*, AF Fercher*, J Pirs†, B Marin†, V Erzen†, R Blinc†, N Gurker†

*Institutes for *Medical Physics and †Technical Physics, University of Vienna, and †Institute J. Stefan, University of Ljubljana, Yugoslavia*

The rather complex theory of NMR and MR tomography cannot be understood easily without practical experience. However, a clinical MR imager cannot be used to learn the basics of NMR and MR imaging because of its complexity and expense. The authors developed a small MR imager/spectrometer, specially designed for educational purposes. The system consists of a low-resolution MR spectrometer with a permanent magnet (0.2 T, 8 MHz) and a data acquisition unit. A gradient coil is added to generate a linear gradient (20 mT/m) for imaging experiments. The data acquisition unit can be used as a storage oscilloscope or as a communication unit to a personal computer, with which the filtering and image reconstruction is performed. A computer program also demonstrates all basic experiments and explains their main features. With this instrument, all basic features of NMR (FID, SE, CP, and IR) and MR imaging (frequency encoding, FFT, filtering, and image reconstruction) can be demonstrated. The effect of T1 and T2 relaxation in test substances on the amplitude of the MR signal can be measured. Furthermore, the optimization of image contrast in phantoms containing the same test substances can be shown in order to understand the

T1- and T2-weighted images in routine clinical applications. The authors' experience gained in education of more than 2,000 students of medicine and technical sciences with this instrument proves the high acceptance and usefulness of this "simple" MR imager/spectrometer.

P414

## Development of Flexible QD Coil for 0.3-T Vertical-Field MR Imaging

H Yoshino, H Takeuchi
*Research and Development Center, Hitachi Medical Corp, Chiba, Japan*

The authors had already developed the body QD coil, composed of a saddle coil and a solenoidal coil, making use of the rigid bobbin for 0.3-T vertical-field MR imaging. They have now developed a flexible QD coil for the purpose of achieving higher signal-to-noise ratio (S/N) by improving the filling factor, and have evaluated image quality. The flexible QD coil is free to deform so that it is difficult to maintain isolation and reduce the frequency difference between the two coils. The first problem was solved by making certain parts of the flexible QD coil rigid, which restricts the degree of freedom of deformation, so as to orthogonalize the sensitivity direction of the two coils even if they do deform. To solve the second problem, an inductance was connected to one coil in series in order to adjust the variation of inductance to the other coil. The authors applied this flexible QD coil and compared it with the rigid QD coil for imaging normal volunteers to evaluate the S/N of these coils and the change of resonance frequency with deformation. The flexible QD coil has more than 20% higher S/N than the rigid QD coil. The difference in resonance frequency between the saddle and solenoidal coils due to deformation is acceptably small (less than 7 kHz; the range must be less than 30 kHz not to reduce S/N) for practical use. The newly developed flexible QD coil achieves higher S/N stably, even if the coil is deformed, and increases patient throughput.

P415

## Compact Planar MR Imaging Gradient Coil Upgrade for Narrow-Gap Resistive Magnets

Y Shiferaw, RG Pratt, SR Thomas
*Department of Radiology, University of Cincinnati*

The hypothesis of this work is that a low-current, power-efficient, and easily implementable planar gradient coil upgrade can be fabricated for older, narrow-gap, resistive iron-core magnet systems being converted for MR imaging research. In general, an adaptive coil system should possess the following properties: (*a*) coils and coil formers should occupy as small a portion of the imaging volume as possible; (*b*) fields produced by the coil system should exhibit properties similar to those of larger systems, ie, linearity, maximum usable volume, low inductance, and so forth; and (*c*) the effects of the proximity of the pole faces should be incorporated into the design scheme. The coil configuration that was designed and built consisted of sets of planar, concentric circular current loops similar to Anderson coils. These loops (inner loop diameter = 1.2 cm, outer loop diameter = 2.2 cm) produced gradients in the transverse direction, while a Maxwell pair (loop diameter = 4.6 cm) produced gradients in the axial direction. This system was constrained to fit into a 4.1-cm magnet gap between the two pole faces (diameter = 30.5 cm). Computer simulations were used to determine the optimal coil geometry and dimensions. The fields produced by this system were mapped with a gauss meter (Hall probe). The coils were inserted into the magnet and a set of 1D projections of a capillary filled with water were obtained. These projections demonstrated excellent linearity of the gradient fields in the volume of interest. The results show that these gradient coils possess properties superior to those of the existing shim coil system. The maximum gradient magnitude obtainable from the current limited shim coil system was 0.5 G/cm with a usable volume of 1 $cm^3$. The tests performed on the new system show that gradient magnitudes of 1.2 G/cm (with 2 A flowing through the loops) and a usable volume of 1.5 × 1.5 × 2 $cm^3$ are achievable. The current rating for the new coils is 5 A, which will allow a gradient field strength maximum of 3 G/cm.

P416

## An MR Imaging Coil for the Middle Ear

DJ Gilderdale, DJ Bryant, GM Bydder, IR Young
*NMR Unit, RPMS, Hammersmith Hospital, London*

The signal-to-noise ratio (S/N) in the MR image is limited by the percentage of magnetic flux from the receiver coil that intercepts the region of interest, the so-called "filling factor." For a surface coil, the deeper the region of interest is, the more unfavorable is the filling factor. The S/N can be dramatically improved in such cases if a smaller coil is placed adjacent to the region of interest. Such a region of interest is the middle ear. Inserts are manufactured routinely that bring a small sound-carrying tube adjacent to the surface of the tympanic membrane. For use with such an acrylic ear insert, a receiver coil has been manufactured that may be placed within 2 mm of the tympanic membrane, allowing the middle and some outer ear structures to be visualized with higher S/N than that typically achieved with external coils. The ear coil has been used for proton imaging at 1.6 T, being coupled to the receiver preamplifier via a ¼λ transmission line that acts as a current voltage transformer when receiving and forms part of a resonant, pin diode–switched decoupling circuit during $B_1$ excitation. Preliminary results have demonstrated an S/N increase consistent with the size of the coil and its proximity to the middle ear. Patient acceptability appears to be satisfactory.

P417

## Theoretical and Experimental Analysis of Unloaded Bird-Cage Coils

R Pascone, T Vullo, R Zipagan, JP Whalen, PT Cahill
*Manhattan College, Riverdale, NY, and New York Hospital, New York, NY*

Although several theoretical formulations of bird-cage resonator design have been reported, no thorough analysis has been presented that describes the complete inductance characteristics and resonant behavior of such coils. In this study, a full description of unloaded low-pass and high-pass resonators is given and correlated with experimental measurements. A lumped element transmission line approach was used to provide general expressions for input impedance, current patterns, and resonant frequencies in terms of arbitrary end ring and column circuit model impedances $Z_1$ and $Z_2$. From the resonant mode current patterns, the specific inductances (including both self and mutual) for individual segments within $Z_1$ and $Z_2$ as well as the total impedance of the coil were determined with the well-known formulas of Grover. Nine low-pass and three high-pass bird-cage coils having different geometric characteristics and capacitor values were fabricated, and the resonant mode frequencies were measured and compared with theoretical calculations. For the low-pass coils, the overall average differences between observed frequencies and frequencies calculated from self plus mutual inductances were 0.66 (±0.57), 0.90 (±0.74), 1.52 (±1.15), and 1.91 (±1.24) MHz for modes 1, 2, 3, and 4, respectively. For the high-pass coils, the agreement for modes 1, 2, 3, and 4 was 1.19 (±0.56), 2.48 (±0.34), 2.30 (±0.48), and 2.37 (±0.57) MHz, respectively. Overall,

excellent agreement was obtained between calculated and observed mode frequencies in unloaded coils. Analyses concerning coil loading and shielding can now be investigated with this validated theoretical model.

P418

### Time-Multiplexed RF Coils

JR Porter, SM Wright
*Department of Electrical Engineering, Texas A&M University, College Station*

The use of coil arrays and multiple receiver channels has been proposed as a method of increasing signal-to-noise ratio (S/N) per unit time in MR imaging. By using decoupled receiver coils and independent receiver channels, multiple images can be obtained and combined into an image with higher S/N or a larger field of view, depending on the particular application. Unfortunately, a high cost is associated with the additional receiver channels needed. The authors propose an alternative method for acquiring simultaneous images, in which the signals from two receiver coils are multiplexed into a single receiver channel. The method requires slight modifications to the filters, an RF switch, and provision for a switching signal controlled by the data acquisition system. While requiring very little additional hardware, this method effectively allows two coils to be used simultaneously with no decrease in S/N. In principle, the method can be extended to more than two coils. The method was tested by imaging a pair of phantoms, each placed over a 6.5-cm-diameter surface coil. The coils were separated by 21 cm to provide greater than 20-dB decoupling. Images were obtained from each coil with a standard spin-echo sequence. Next, images were obtained simultaneously by using the multiplexing hardware. After separation of the multiplexed echoes, two images were reconstructed, one from each coil. No decrease in S/N was observed due to multiplexing. The proposed method obtains two images in the time required to obtain a single image with a standard system. No loss in S/N occurs in either image due to the multiplexing method. This method offers a low-cost alternative or adjunct to multiple-channel receiver systems.

P419

### Application of Principal-Component Analysis to Dynamic EPI Perfusion Studies

R Ladebeck, M Stehling, M Fang, F Schmitt
*Siemens Medical Systems and Department of Neurosurgery, University Hospital, Erlangen, Germany*

Susceptibility-contrast EPI images of the brain have been obtained with a TR of 1.25 seconds during the passage of a Gd-DTPA bolus (0.2 mmol/kg). The image matrix was 128 × 128 pixels in a field of view of 23 cm, yielding an in-plane resolution of 1.8 × 1.8 mm. One hundred images were measured before, during, and after injection of the bolus. The time course of signal intensity is mainly determined by the amount of signal reduction, the time of maximal signal drop, and the behavior after the bolus passage. To evaluate perfusion measurements, this time dependence must be analyzed. This is typically achieved by calculating cerebral blood vessel maps. The authors have applied principal-component analysis (PC) (1) to facilitate the complete time dependence. With this method up to 10 PCs (basic functions describing the time dependence), together with the individual scores (weighting values), can be calculated for each pixel. The scores can be displayed as synthetic images containing the complete information of the pixel intensity time course (four PCs were usually sufficient). The method can be used to compare series of perfusion measurements by using PCs trained on a selected series to describe the others (eg, series without/with optical stimulation). The authors found that PCs trained on pathologic tissue differed significantly from those trained on healthy tissue. This might give a better depiction of pathologies. The authors have used this method to examine healthy volunteers and patients with cerebral ischemia and brain tumors.

1. Wold S, et al. Chemometrics Intell Lab Syst 1987; 2:37–52.

P420

### Localized STEAM Spectroscopy with Designer Prefocused Pulses

TP Roberts, NJ Shah, TA Carpenter, LD Hall
*Herchel Smith Laboratory for Medicinal Chemistry, Cambridge, England*

In this work the authors describe the application of a recently developed "designer" pulse to the STEAM volume-localized spectroscopy sequence. The pulse is purely amplitude modulated and was designed by numerical optimization with simulated annealing. The authors believe that this pulse has a number of properties rendering it particularly suitable for use in localized spectroscopy experiments. First, the magnetization response to the pulse has a sharply defined band of excitation, leading to better definition of the desired volume and good suppression of out-of-volume signals. Second, the pulse is "prefocused," that is, the excited spins are in phase immediately after application of the pulse and so no refocusing gradient lobe is required. Finally, a reduced "spoiler" gradient is required in the period TM between the second and third section-selective pulses, as the pulse inherently dephases undesired transverse components of magnetization; this allows the interval TM to be kept short. The modified sequence thus requires substantially less switching of the field gradients and so benefits from reduced eddy current distortions. The authors present in vivo spectra of the human brain, obtained with a Picker International HP-2055 equipped with Spectra Vista. The authors show that the spectra can be obtained at shorter TEs than with conventional STEAM due to significant reduction in eddy currents, and demonstrate improved delineation of the region of interest. The increased signal-to-noise ratio resulting from a shorter TE can be used to reduce the voxel size or the number of signals averaged.

P421

### Using $d\phi/dt$ to Evaluate the Effect of Eddy Currents in MR Spectroscopy

WR Riddle, SJ Gibbs, JM Fitzpatrick, MR Willcott
*Department of Radiology and Radiological Sciences, Vanderbilt University, Nashville, Tenn*

The specification of magnetic field homogeneity in MR spectroscopy is typically indicated by the width of a single spectral line. For a free induction decay (FID) of a single-resonance sample obtained without field gradients, the slope of phase ($d\phi/dt$) is constant and equal to the resonance frequency. To measure the effects of eddy currents induced by field gradients, FIDs were measured in water contained in a 100-mL, round-bottomed flask. Pulses of different durations and different strengths were placed in a field gradient before acquisition of each FID. Phase ($\phi$) was calculated with a four-quadrant arctangent, and the slope of the phase (in hertz) was calculated with the following equation:

$$\frac{d\phi_n}{dt} = \frac{\phi_n - \phi_{n+1}}{2\pi\Delta t},$$

in which $\Delta t$ is the dwell time. When field gradients precede the FID, $d\phi/dt$ is no longer a constant. A plot of $d\phi/dt$ over time shows the change in the detected resonance frequency with respect to time. If the RF transmitter is stable, the change in detected resonance frequency is indica-

tive of temporally changing magnetic field strength. The plot of $d\phi/dt$ over time is a tool for evaluating the effects of eddy currents in MR spectroscopy.

P422

### In Vivo Phosphorus-31 MR Spectroscopy of the Calf in Patients with Occlusive Arterial Disease

G Brinkmann, UH Melchert, M Gleim, K Förger
*Department of Diagnostic Radiology and Anesthesiology of the University of Kiel, Germany*

The energy metabolism of the calf muscle was studied in seven patients with occlusive arterial disease and intermittent claudication before and after lumbar sympathectomy with the help of phosphorus-31 MR spectroscopy. Spectra of the calf were obtained before, during, and after 4 minutes of treadmill exercise. The pH value and the relative concentration of phosphocreatine (PCr), as well as the increase of this metabolite during recreation, were calculated from spectra. The results were compared with the clinical status before and after therapy. After sympathetic blockage, there was a high correlation between the increase in painless walking distance and regeneration of PCr in the muscle cells. This study demonstrated that biochemical agreement with the observed clinical status could be achieved with the help of a noninvasive method.

P423

### Experimental Study of Radiation Injury to Rat Brain Assessed with P-31 MR Spectroscopy

M Matoba, H Yokota, M Ohguchi, K Higashi, H Tonami, T Okimura, I Yamamoto
*Department of Radiology, Kanazawa Medical University, Ishikawa, Japan*

Radiation therapy for primary brain tumors and metastases has been actively undertaken, although the development of central nervous system radiation injury has become a serious clinical problem. In the present experimental animal study, changes in the central nervous system occurring after irradiation were investigated with MR imaging, and the influence exerted by irradiation on brain high-energy acid metabolism was assessed with P-31 MR spectroscopy. The heads of rats were subjected to bilateral en bloc irradiation (10 MeV, 40 Gy). The irradiated group underwent MR imaging studies 2 days and 1, 2, 4, and 8 weeks after the irradiation, and was then subjected to magnetic field–type microwave irradiation, and studied with P-31 MR spectroscopy. MR imaging studies revealed no changes up to 8 weeks after irradiation. Transient decreases in intracellular pH determined with P-31 MR spectroscopy were found at 2 and 4 weeks. With regard to the signal intensity ratio with the peak of inorganic phosphate (Pi) as the standard, both phosphomonoester (PME)/Pi and phosphocreatine (PCr)/Pi ratios showed transient decreases after 2 days, with PME/Pi and PCr/Pi ratios again showing decreases after 2 and 4 weeks, respectively. P-31 MR spectroscopy sensitively demonstrated irradiation-induced changes in the central nervous system that were not distinguished by MR imaging, and is thought to be useful in the assessment of radiation injury.

P424

### F-19 MR Studies on the Effect of Hyperglycemia on Intracellular Free $Ca^{2+}$ in the Perfused Rat Kidney

TL Dowd*, RK Gupta*†
*Departments of *Physiology and Biophysics and †Biochemistry, Albert Einstein College of Medicine, Bronx, NY*

Hyperglycemia is a condition observed in both insulin-dependent and non–insulin-dependent diabetes mellitus. Previously, this laboratory has shown that intracellular $Na^+$ concentration was increased in tubules from diabetic rats, and a large increase in intracellular $Na^+$ was also observed during hyperglycemia (25-mmol/L glucose). The authors have investigated the effect of hyperglycemia (25-mmol/L glucose) on the intracellular free $Ca^{2+}$ concentration in the perfused rat kidney. Kidneys were isolated from four Sprague-Dawley rats (200–300 g) and perfused with a modified Krebs-Henseleit solution containing 5-mmol/L glucose and 6.7% albumin and gassed with 95% oxygen and 5% carbon dioxide at 37°C. The kidney was loaded with 20 μmol/L of the acetoxymethylester of the intracellular indicator 5FBAPTA, and F-19 spectra were collected to measure the intracellular free $Ca^{2+}$ concentration (Figure; left, 5-mmol/L loading, and right, 25-mmol/L loading). All spectra were collected at 376 MHz with a GE Omega 400WB spectrometer at 37°C. An initial control intracellular free $Ca^{2+}$ concentration of 383 ± 15 mmol/L was measured at 5-mmol/L glucose, which then increased by 79% to a value of 684 ± 28 mmol/L, 30 minutes after addition of 20-mmol/L glucose. This effect was reversible, as shown by a return of free $Ca^{2+}$ to nearly the baseline value (452 ± 31 mmol/L) 20–30 minutes after dilution of the glucose to 5 mmol/L. Whether this effect of hyperglycemia on intracellular free $Ca^{2+}$ is due to an increase in osmolarity on addition of 20-mmol/L glucose or to its effects on ion transport systems remains to be investigated. These results may lend some insight into the mechanism of kidney enlargement in diabetes.

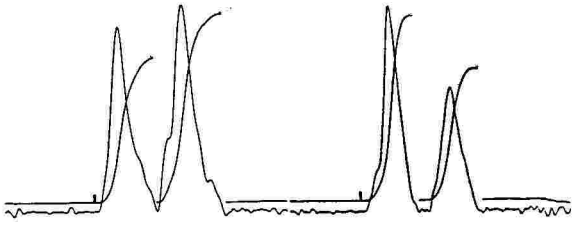

P425

### P-31 MR Studies of the Mechanisms for Appetite Control by the Liver

NE Rawson*, H Blum†, MD Osbakken†, MI Friedman†
**Monell Chemical Senses Center and †Department of Medicine, University of Pennsylvania School of Medicine, Philadelphia*

The fructose analog 2,5-anhydro-D-mannitol (2,5-AM) acts in liver to trigger feeding behavior in rats. In vitro studies indicated that 2,5-AM is phosphorylated to 2,5-AM-1-P and 2,5-AM-1,6-diP, and produces a depletion of adenosine triphosphate in hepatocytes. The hypothesis that in vivo changes in these phosphorylated metabolites are responsible for the initiation of feeding after 2,5-AM is being investigated with P-31 MR spectroscopy. The authors conducted in vivo P-31 MR spectroscopy of liver in rats receiving a jugular infusion of 150 mg per 3 mL of 2,5-AM or an equal volume of isosmotic saline over 1 hour. Spectra were averaged over 7-minute intervals and collected sequentially. At 90 minutes, freeze-clamped liver samples were taken for later analysis with high-resolution P-31 MR spectroscopy and enzymatic techniques. The data shown in the Table are mean ± SE percentages of baseline values. The increase in PME was rapid and represents phosphorylation of 2,5-AM, as shown by high-resolution P-31 MR spectroscopy of liver extracts. These data verify that hepatic phosphorylation of 2,5-AM and ATP depletion occur in vivo after 2,5-AM infusion. The changes in phosphorylated metabolite levels over time parallel the time course of the feeding response with 2,5-AM infusion,

| Metabolite | 2,5-AM ($n$ = 6) | | | Controls ($n$ = 3) | | |
|---|---|---|---|---|---|---|
| | Initial (%) | Final (%) | $P$ | Initial (%) | Final (%) | $P$ |
| PME | 100.0 ± 6.9 | 312.3 ± 37.1 | <.001 | 100.0 ± 2.4 | 79.0 ± 14.3 | NS |
| PDE | 100.0 ± 6.0 | 74.0 ± 8.2 | <.01 | 100.0 ± 3.1 | 102.8 ± 19.9 | NS |
| ATP | 100.0 ± 4.7 | 71.6 ± 5.1 | <.001 | 100.0 ± 2.9 | 92.2 ± 6.7 | NS |
| Pi, other PME | 100.0 ± 5.5 | 18.9 ± 5.6 | <.001 | 100.0 ± 2.4 | 79.0 ± 14.3 | NS |
| Total phosphates | 100.0 ± 3.3 | 123.0 ± 4.3 | <.001 | 100.0 ± 2.3 | 78.3 ± 4.7 | <.01 |

The increase in PME was rapid and represents phosphorylation of 2,5-AM, as shown by high-resolution $P$-31 MR spectroscopy of liver extracts. These data verify that hepatic phosphorylation of 2,5-AM and ATP depletion occur in vivo after 2,5-AM infusion. The changes in phosphorylated metabolite levels over time parallel the time course of the feeding response with 2,5-AM infusion, and therefore may play a role in control of appetite by the liver.

and therefore may play a role in control of appetite by the liver.

P426

## Metabolic and Functional Cardiac Regulation during Hypothermia

H Blum, T Ivanics, D Zhang, MD Osbakken
*Department of Medicine, University of Pennsylvania School of Medicine, Philadelphia*

The authors propose that regulation of work done by the normal heart is not generally limited or regulated by mitochondrial capability. To demonstrate this, the authors exposed hearts to hypothermic conditions and changed the coronary perfusion pressure and flow. Langendorff perfused rat hearts were studied with P-31 MR spectroscopy. The perfusion pressure (PP) was varied from 145 to 20 cm $H_2O$. The temperature of the perfusion buffer was varied from 37°C to 20°C. Heart rate (HR) and left ventricular systolic pressure (LVSP) were continuously recorded through a catheter placed in the left ventricle. The coronary effluent was collected for flow measurement. Hearts were freeze-clamped in liquid nitrogen immediately after the MR experiment. They were weighed and later used for high-pressure liquid chromatography (HPLC) measurement of perchloric acid extracts of phosphate compounds. Creatine plus phosphocreatine (PCr) was determined from HPLC measurements. MR data were quantitated by using previously determined intracellular volume ratios and the HPLC results from control hearts. It was assumed that all adenosine triphosphate (ATP), PCr, and inorganic phosphate (Pi) were fully observable with MR spectroscopy. Adenosine diphosphate (ADP) was calculated from the assumed equilibrium of the creatine kinase reaction. The equilibrium constant for this reaction was corrected for the measured temperature. The change in free energy accompanying hydrolysis of ATP ($\Delta G$) was calculated from $\Delta G = \Delta G_o - RT \ln [(ATP)/(ADP) \times (Pi)]$. Cardiac $VO_2$ was estimated from the product of HR and LVSP and was equated with mechanical function. HR × LVSP changed by almost two orders of magnitude with PP and temperature. It was directly proportional to PP and exponentially dependent on temperature, with an activation energy of 72.7 kJ/mol. The specific coronary flow (mL/min/g) was linearly related to the PP but also exponentially dependent on temperature, with an activation energy of 77.0 kJ/mol. Conversely, ATP, ADP, PCr, and $\Delta G$ were best described as temperature independent with a dependence on PP, which had a broad maximum or minimum in the range 60–120 cm $H_2O$. Myocyte pH increased with PP and decreasing temperature. This study shows that cardiac cellular bioenergetic parameters remain constant over a wide range of PP and temperature. The isolated heart accomplishes this stability by changing mechanical function to match the specific coronary flow. This verifies that mechanical output increases with increasing PP or coronary flow (Gregg phenomenon). Over broad limits, output of the perfused heart is flow limited, with putative mitochondrial regulators unchanging and therefore ruled out as intermediates between production and utilization of energy.

P427

## Alcohol-induced Alterations in Brain Bioenergetics and Free Magnesium

BM Altura, RL Barbour, RK Gupta
*State University of New York Health Science Center, Brooklyn, NY, and Albert Einstein College of Medicine, Bronx, NY*

Several clinical investigations have suggested that excessive alcohol consumption (ALC) predisposes humans to stroke and sudden death. Experimentally, the authors have shown previously in intact rats that ALC produced graded contractile responses and rupture of cerebral microvessels in vivo at a concentration range (10–500 mg/dL) that parallels that needed for its graded effects of euphoria, mental haziness, muscular incoordination, stupor, stroke, and coma in humans. The authors have also demonstrated that magnesium deficiency can cause vasospasm and rupture of cerebral microvessels in vivo. The present studies, with in vivo P-31 MR spectroscopy at 9.4 T and anesthetized rats, were undertaken to determine if administration of acute doses of alcohol, associated with strokelike events and sudden death (ie, blood alcohol concentration = 200–300 mg/dL or 1.5–2.0 g/kg), exerts any influence on brain cellular bioenergetics, intracellular free magnesium ($[Mg^{2+}]_i$) and intracellular pH ($[pH]_i$). Approximately 30 minutes after intraperitoneal administration of alcohol, brain phosphocreatine–adenosine triphosphate ratios (uncorrected for relaxation effects) dropped from 2.4 by approximately 10%, inorganic phosphate (Pi) rose 20%–30%, $[Mg^{2+}]_i$ went from 575 ± 46 to 346 ± 37 μmol/L, while $[pH]_i$ remained unchanged (7.30 ± 0.06 vs 7.22 ± 0.05). Brains of animals that went into respiratory failure, after ALC, exhibited 90% reductions in phosphocreatine, elevation in Pi and $[Mg^{2+}]_i$, and marked intracellular acidosis. These results suggest that heavy or binge-drinking of alcohol ($a$) can result in rapid alterations in brain bioenergetics, $[Mg^{2+}]_i$, and $[pH]_i$, and ($b$) may result in strokelike events and sudden death due to cerebrovasospasm caused by depletion of $[Mg^{2+}]_i$.

P428

## MR Studies of Isolated Myocytes to Model Heart Metabolism

MD Osbakken, T Ivanics, R Mitra, D Zhang
*Departments of Medicine and Biochemistry/Biophysics, University of Pennsylvania, Philadelphia*

To investigate mechanisms of myocardial metabolic regulation removed from extrinsic influences of neurotransmitters, perfusion, and contractile function, an isolated cardiomyocyte model was developed. Myocytes were isolated from adult Sprague-Dawley rats, incorporated in agarose beads, and studied with P-31 and C-13 MR spec-

troscopy. Myocyte viability and function over time, at different temperatures and RF conditions, were documented. Various physiologic interventions were applied to validate the model. Thirty-minute exposure of myocytes to iodoacetate (IA, 50 mmol/L) to inhibit glycolysis produced reversible small decreases in inorganic phosphate (Pi), phosphocreatine (PCr), and adenosine triphosphate (ATP). Thirty-minute exposure to oligomycin (0.05 μg/mL) to inhibit oxidative phosphorylation elicited reversible increases in Pi and decreases in ATP, with minimal change in PCr. Thirty-minute exposure to dinitrophenol (DNP, $2 \times 10^{-4}$ mol/L), to uncouple oxidative phosphorylation, produced reversible increases in Pi and decreases in PCr and ATP. After validation of the model, myocytes were used to evaluate the effects of acetylcholine (ACH) on metabolic function. Superfusion with ACH ($10^{-6}$ and $10^{-5}$ mol/L) produced a biphasic response: $10^{-6}$ mol/L, Pi and ATP increased and PCr decreased; $10^{-5}$ mol/L, Pi and ATP decreased and PCr did not change. P-31 saturation transfer studies to estimate the forward rate constant $K_f$ of creatine kinase (CK) and the flux of PCr to ATP demonstrated that ACH ($10^{-6}$ mol/L) decreased both functions. Administration of increasing doses of ACH ($10^{-9}$–$10^{-6}$ mol/L) to myocytes previously superfused to steady state with $^{13}$C-2 acetate demonstrated a dose-related increase in incorporation of label into glutamate C-2, C-3, and C-4; this suggests that ACH induced an increase in citric acid cycle activity. Administration of ACH to myocytes previously superfused to steady state with $^{13}$C-3 pyruvate demonstrated an increased incorporation of label into glucose; this suggests that ACH may stimulate gluconeogenesis. The authors conclude (*a*) the myocyte model (in conjunction with MR) can be used to study metabolism, and (*b*) ACH may be an important regulator of myocardial metabolism.

P429

### H-1, H-2, O-17, and Cl-35 Nuclear Relaxation Studies of Water in the Amphibian Oocyte

GA Morrill, M Varsney, AB Kostellow, RK Gupta
*Department of Physiology and Biophysics, Albert Einstein College of Medicine, Bronx, NY*

Multinuclear relaxation studies of water in amphibian (*Rana pipiens*) oocytes were designed to examine the state of intracellular water following release of the prophase block by progesterone. The oocytes were superfused with Ringer's solution in a 10-mm-diameter MR tube. The content and relaxation behavior of intracellular water were studied at 4.7 T with a Varian XL-200 and analyzed with multiexponential computer analysis using the Simplex algorithm. Cl-35 MR was used to measure extracellular space as a check on the multiexponential analysis. The H-2 relaxation data (2% $^2H_2O$ added) were uncomplicated by the presence of cross relaxations that modulate the H-1 relaxation behavior of intracellular water. Both O-17 and H-2 relaxations could be adequately fitted to a two-compartment model, representing intra- and extracellular water, while analysis of H-1 relaxation data required the use of more than two exponentials, suggesting the contribution of cross relaxations. T1 of both H-2 and O-17 for intracellular water was found to be an order of magnitude shorter than that for extracellular water. In prophase-arrested oocytes, the H-2 T1 was 0.46 seconds and 0.044 seconds for extra- and intracellular $^2H_2O$, whereas the O-17 T1 was 1.5 and 0.16 msec for extra- and intracellular $H_2O^{17}$, respectively. These data confirm the existence of slow water exchange between the intracellular and extracellular environments in oocytes on the MR time scale. Following stimulation by the meiotic agonist progesterone, the intracellular H-2 T1 decreased by about 9% during the first 10–15 minutes, then increased by about 10%–15% over the next hour, returning to the pretreatment baseline 2 hours after hormonal stimulation. These T1 changes correlate with increasing intracellular pH and plasma membrane conductance, presumably reflecting sequential changes in water environment in the oocyte cytoplasm. H-2 relaxation measurements in vivo following ingestion of $D_2O$ may be a useful probe for tissue physiologic state.

P430

### Qualitative and Quantitative Proton MR Spectroscopy of Synovial Fluid in Arthritic Diseases

MB Rominger*, PA DeMuth†, MJ Jablonsky†, JJ Listinsky*, WK Bemreuter*, NR Krishna†, PJ Kenney*
**Department of Radiology and †NMR Core Facility, University of Alabama at Birmingham*

Fifteen synovial fluid samples (five of rheumatoid arthritis [RA], five of osteoarthritis [OA], and five of crystal disease [CD]) were studied to detect abnormal metabolites and diagnostic differences in lactate and hyaluronate concentration that could be used in future in vitro and in vivo studies. Proton MR spectra were recorded with a Bruker 9.4-T spectrometer (WH 400) at 400 MHz. Measurements were obtained with a Hahn spin echo with water suppression by presaturation (spin-echo time, 0.14 seconds; TR, 3.82 seconds; 400 acquisitions and 8,000 data points). Chemical shift and spectrum integration were referenced to 2-mmol DSS/D20 in an internal capillary tube. No disease-specific peak could be assigned. Lactate concentration was higher in RA (mean ± SD, 8.41 ± 1.99) than in CD (mean ± SD, 3.37 ± 1.38) or OA (mean ± SD, 3.18 ± 0.41). There was no significant difference in the concentration of hyaluronate among the three different diseases. Although preliminary, these data indicate there may be diagnostic utility in lactate concentrations.

P431

### Early Changes in Brain N-Acetyl Aspartate Following Acute Stroke

O Henriksen, P Gideon, B Sperling, P Christiansen, TS Olsen, PA Søborg
*Danish Research Center of Magnetic Resonance, Hvidovre University Hospital, Copenhagen*

Evidence obtained so far indicates that N-acetyl asparatate (NAA) is largely located within neuronal tissue and may thus be used as an indicator of neuronal loss/survival under pathologic conditions. Using the unsaturated water signal corrected for T2 decay as an internal standard, it is possible to quantify the NAA content as measured with H-1 MR spectroscopy. The aim of the study was then to characterize the early time course of the NAA loss in severely ischemic brain tissue following acute stroke. Eight patients were examined between 6 and 50 hours (average, 30 hours) after the clinical incident. The patients were reexamined 1 and 3 weeks after the clinical attack. NAA was measured with H-1 MR spectroscopy using STEAM sequences with TEs of 46, 136, and 272 msec, respectively. The measurements were done twice with a voxel size of 27 mL and a smaller central voxel size of 8 mL to evaluate regional variation between the central and peripheral parts of the infarcted area as visualized with MR imaging. Regional cerebral blood flow was measured with SPECT using Tc-99m–HMPAO. Eight healthy volunteers served as controls. Calculated NAA concentrations ranged between 9 and 13 mmol/L (average, 11 mmol/L) in the healthy subjects. In the patients the NAA content decreased from normal to minimum levels, ranging between 0 and 5 mmol/L between 6 and 24 hours after the clinical attack. The loss of NAA was more pronounced in the central than in the peripheral part of the infarcted area. The results indicate that the NAA content may be preserved during the first 6 hours after the acute stroke, but de-

creases to minimum values within the following 24 hours. Measurement of NAA content may have important clinical implications for therapy planning.

P432

## Response of Cardiac Energetics to Elevated and Low Magnesium in the Perfused Rat Heart

RL Barbour, RK Gupta, TL Dowd, SD Reiner, F Wu, BT Altura, BM Altura

*State University of New York Health Science Center, Brooklyn, and Albert Einstein College of Medicine, Bronx, NY*

Evidence has accumulated to indicate that $Mg^{2+}$ may play a role in the regulation of cardiac hemodynamics. The authors have shown that magnesium deficiency can result in coronary vasospasm. Using P-31 MR spectroscopy, the authors have examined the response of isolated rat hearts to alterations in extracellular $Mg^{2+}$ ($[Mg^{2+}]_o$). Reduction in $[Mg^{2+}]_o$ (from 0.3 to 0.6 mmol/L) resulted in a progressive decline in cardiac performance associated with reduced coronary flow (CF), stroke volume, and cardiac output, leading to cardiac failure. These events were accompanied by a decline in intracellular free $Mg^{2+}$ ($[Mg^{2+}]_i$) (from 0.6 to 0.4 mmol/L) and decreased efficiency in the utilization of oxygen as evidenced by a rightward shift in the plot of CF versus oxygen consumption. In contrast, elevation in $[Mg^{2+}]_o$ (from 2.4 to 4.8 mmol/L) resulted in a rapid elevation in $[Mg^{2+}]_i$ (from 0.6 to 1.2 mmol/L), phosphocreatine (by 22% to 40%), and $pH_i$ (from 7.11 to 7.24), paralleled by a decline in inorganic phosphate. Adenosine triphosphate (ATP) levels were largely unaffected. Elevated $[Mg^{2+}]_o$ was also observed to increase the cytosolic phosphorylation potential from approximately 40 to 110 $mmol/L^{-1}$ and the free energy available from ATP hydrolysis from approximately 56 to 59 kJ/mol. Hemodynamically, elevated $[Mg^{2+}]_o$ increased CF, stroke volume, and cardiac output and reduced the rate-pressure product and shifted the CF versus oxygen consumption plot to the left. These findings suggest that (*a*) $[Mg^{2+}]_o$ can modulate cardiac hemodynamics, oxygen consumption, cellular energy levels, and contractility and myocardial efficiency, and (*b*) $[Mg^{2+}]_o$ may be a regulatory cation in myocardial muscle.

P433

## Phase Rotation: An Efficient Tool for Removal of Spurious Echoes in Short TE Localized Spectroscopy with STEAM or PRESS

J Hennig

*Radioligische Klinik, University of Freiburg, Germany*

Voxel selection for localized spectroscopy by STEAM or PRESS uses a combination of three RF pulses to generate a stimulated or refocused primary echo from the selected region. A severe problem of this selection scheme is that the three pulses used for volume selection intrinsically generate unwanted signals such as the FID from each pulse and a spin echo from each pair of pulses. These unwanted signals are conventionally removed from the acquisition window by introducing spoiler gradients. A disadvantage of this approach is that the required spoiler gradients lead to longer TEs and might even affect the spectrum quality due to eddy current effects. A different approach that totally omits all spoiler gradients introduces a phase-cycling scheme called phase rotation. Single-excitation spectra are acquired into a 2D data set, where the phase of each of the three RF pulses for voxel selection is increased by a constant amount. Two-dimensional Fourier transformation then yields the desired spectrum as one line in the resultant 2D data set, whereas all unwanted signals are displaced in the f1 direction. A practical implementation uses a PRESS experiment with TE of 20 msec on a whole-body system (Bruker S200). A single-excitation spectrum is dominated by unwanted signals, especially lipid from the skull generated by single-pulse FIDs. Phase increments of 22.5°, −22.5°, and 22.5° between successive excitations were used for the localization pulses. The resultant spectrum after 128 scans (8-mL voxel) shows no contamination from unwanted signals, which appear displaced in the f1 direction of the 2D data set. Conventional phase-cycling schemes, which are based on cancellation, should, in principle, also lead to removal of unwanted signals. For in vivo experiments, which are characterized by limited reproducibility from one scan to the next due to patient-dependent factors, it can be demonstrated, however, that phase rotation gives vastly superior results and offers an attractive way to reach short TEs even on systems with only moderate eddy current behavior.

P434

## Reduction of Eddy Current Effects in Volume-Localized STEAM Spectroscopy by Using Bipolar Gradients

HK Lee, O Nalcioglu

*Department of Radiological Sciences, Division of Physics and Engineering, University of California, Irvine*

It is well known that eddy currents are induced in the surrounding magnet and other conducting materials in the presence of a time-varying gradient field. Eddy currents result in the reduction of signal intensity as well as line broadening. Such effects become particularly severe with a complex pulse sequence such as the solvent-suppressed STEAM spectroscopic sequence with a short TE. Shielded gradients and pre-emphasis gradient waveforms may reduce such unwanted eddy currents. However, such techniques may be insufficient for accurate and reliable localized spectroscopic measurements. The method proposed here cancels the eddy currents during volume-localized STEAM spectroscopy by applying balanced bipolar gradient pulses. The basic assumption is that such a magnetic coupling mechanism that generates eddy currents may be expressed as a multiexponentially decaying function and is a time-invariant linear system. Another assumption is that the eddy current– induced secondary fields are usually much less than the volume-localization gradients. The unit step response of such a coupled network may be modeled by a multiexponential decay function as

$$g(t) = \left(\sum_{k=0}^{K} \alpha_k e^{-t/\tau_k}\right) u(t),$$

where $\alpha_k$ and $\tau_k$ are the magnetic coupling and time constants, respectively. Since the eddy current response is assumed to be linear and time invariant, when another gradient pulse is applied with a reversed polarity and a time shift $t_0$, the eddy current response is given by

$$g(t - t_0) = -\eta \left(\sum_{k=0}^{K} \alpha_k e^{-(t-t_0)/\tau_k}\right) u(t - t_0),$$

where $\eta$ is the amplitude adjustment factor. By applying such a balanced bipolar gradient pulse with a new variable $t' = t - t_0$, the accumulated eddy current field may be expressed as

$$g_e(t') = \left(\sum_{k=0}^{K} \alpha_k e^{-t_0/\tau_k} e^{-t'/\tau_k} - \eta \sum_{k=0}^{K} \alpha_k e^{-t'/\tau_k}\right) u(t').$$

If the time shift $t_0$ is sufficiently smaller than each time constant $\tau_k$, then the major eddy current sources may be canceled or minimized. The technique was applied to volume-localized STEAM spectroscopy on a 1.5-T system. The pulse sequence is shown in the Figure. The authors

have observed that the balanced bipolar gradients not only cancel out the eddy current effects but also cause rephasing or dephasing of the magnetizations.

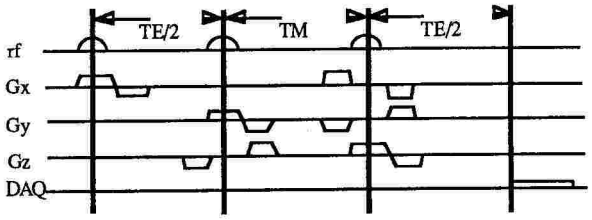


P435

### In Vivo Proton MR Spectroscopy of Exercised Tibialis Anterior Muscle: Effect of Heparin on Lipid Mobilization

PA Narayana, EF Jackson, JM Slopis, IJ Butler
*University of Texas Medical School at Houston*

Lipids are an important energy substrate for muscle, but little is known about lipid mobilization to a working muscle. Using image-guided proton MR spectroscopy, the authors have recently demonstrated a 50% increase in lipids in the stressed tibialis anterior (TA) muscle. They have hypothesized that this increase is a result of blood-borne fatty acid mobilization. The present studies were designed to verify this hypothesis by performing in vivo MR spectroscopy of exercised muscle in humans after increasing the plasma fatty acid concentration by the administration of heparin. All MR studies of exercised TA muscle were performed with a 1.5-T whole-body imager using a 15-cm-diameter bird-cage resonator. A 4.5-$cm^3$ region of interest (ROI) in the TA muscle was localized with the stimulated-echo sequence. Prior to the administration of heparin, control spectra were acquired from the ROI. Thirty minutes following the administration of heparin, no increase in lipids was observed in the resting muscle. However, within 1 minute after selectively stressing the TA muscle by dorsiflexion at 40% maximum voluntary contraction, MR spectroscopic data showed an increase of 100% in the lipid signal. This increase was twice that observed without heparin administration (in the same subjects determined on different days). The plasma free fatty acid concentration is known to double in 30 minutes after the administration of heparin. These observed changes in lipids with and without heparin in stressed TA muscle seem to suggest that fatty acids are mobilized to the TA muscle immediately after the onset of exercise. These studies also indicate an important role for proton MR spectroscopy in noninvasively assessing lipid mobilization to an exercised muscle.

P436

### Integrated 3D Display of Gyral Anatomy and MR Spectra on the Brain Surface

Y Cao*, GJ So*, DN Levin*, CD Gregory†, MJ Dawson†, T Raidy†, PC Lauterbur†, CA Pelizzari‡
*Departments of *Radiology and ‡Radiation Oncology, University of Chicago; †Biomedical MR Laboratory, University of Illinois at Chicago; and †GE Medical Systems, Milwaukee*

The authors seek to display the relationship between MR spectroscopic data and an MR imaging–derived 3D rendition of the same brain. MR spectroscopy–detected biochemical abnormalities could then be localized with respect to specific gyral convolutions (such as those associated with movement, sensation, speech, and hearing) that can only be identified on 3D brain models. Spatially resolved P-31 spectra were obtained from the whole brain by means of a 4DFT CSI sequence, run on a 1.5-T whole-body imager equipped with a dual-tuned P-31/H-1 head coil. Without moving the subject the same coil was used to acquire a volume of proton images. With the aid of a surface-matching algorithm, the H-1 data (and coincident P-31 data) were retrospectively registered with a more highly resolved volume of H-1 brain images, obtained with a standard head coil. The latter set was used to create a 3D model of brain gyral anatomy. The registered P-31 data were processed with MR imaging–derived masks of the brain surface and then displayed on the MR imaging–derived 3D model in two ways: (*a*) Color coding was used to show how any P-31 metabolite was distributed over the surface, and local P-31 spectra were displayed at points on the brain surface chosen with an interactive, roving cursor. These methods were tested in a P-31 phantom with a "lesion" and in human volunteers. The resulting display of the phantom data showed the expected relationship between the P-31 and H-1 attributes of the "lesion." The human experiments suggested that the combined display would make it possible to sharpen the interpretation of MR spectroscopic data by relating them to gyral anatomy, only depicted by MR imaging–derived 3D models.

P437

### Automated Correction of Main Magnetic Field in Human CSI Examinations

J Hu, T Willard, R Srinivasan, J Murphy-Boesch, TR Brown
*Fox Chase Cancer Center, Philadelphia*

The authors have implemented a procedure to automatically shim the main magnetic field by using a 3D CSI sequence to measure the field over the sample and correct it with every shim coil available. Initially the procedure measures values of the fields of each of the 12 shim coils once with an 8 × 8 × 8 CSI matrix. For each iteration the field distribution in the subject is measured on the same CSI grid. A new shim current vector that produces the most homogeneous field is calculated with standard matrix inversion techniques with a least-squares algorithm. This is input to the shim currents and the process repeated. Iteration is required because of unavoidable errors due presumably to the coarse voxel sizes used. The water peak position rather than the fat peak position is used to calculate the field map by always selecting the largest peak in the individual spectrum for analysis. The authors have used this technique in connection with studies of heads and arms with a 1.5-T Siemens Helicon. In the head studies, a 45-Hz linewidth of the water peak of the whole brain can, after two iterations of the procedure, be reduced to 10–15 Hz without high-order distortion. In the arm studies, because the arm is off the magnet center in the $y$ and $x$ directions by 16 and 3 cm, respectively, high-order distortion surrounding the base of the peak can be seen even after extensive manual shimming. The authors' automatic shimming technique can correct this high-order distortion because it takes into account the true field distributions of each shim coil. Comparisons on nonlocalized P-31 spectra of the brain before and after automated shimming show improved quality in the linewidths and signal-to-noise ratios of all resonances for most voxels. One iteration of the automated shim takes approximately 10 minutes.

P438

### Four-Ring Bird-Cage Resonators for Integrated H-1 Imaging and Clinical Spectroscopy

J Murphy-Boesch, R Srinivasan, L Carvajal, TR Brown
*Fox Chase Cancer Center, Philadelphia*

Single- and dual-tuned four-ring bird-cage resonators are particularly well suited for integrated clinical MR imaging and MR spectroscopic examinations of the head. Four-

ring bird-cage resonators consist of one inner bird-cage structure and two outer bird-cage structures that are inductively coupled through the legs of the inner structure. The resonators can be operated in quadrature mode, affording both high sensitivity and low transmitter power. The single-tuned coil has excellent $B_1$ field homogeneity at the proton frequency, making it highly suitable for acquiring H-1 images and for quantitation of H-1 spectra. The dual-tuned resonators exhibit greatly reduced tuning interactions between frequencies, permitting rapid, noniterative tuning in the bore of the magnet. To implement the resonator, circuit models have been developed for tuning of the proton mode by using measurements from a prototype coil. Sensitivity and transmitter efficiencies for the dual-tuned resonators (LP-HP and LP-LP), when compared with single-tuned two-ring bird-cage resonators, were found to be within 5% for the P-31 frequency and within 20% for the proton frequency. Both high-quality H-1 images and proton-decoupled P-31 3D CSI data sets have been obtained from normal volunteers in an integrated examination requiring only a single episode of tuning and no midexamination movement of the subject.

P439

### Peak Variance, T1, and Quantitation of Human Myocardial P-31 Metabolites

C-W Li*, MG Crowley*, JL Evelhoch*, WG Negendank†
*Wayne State University, Detroit, and †Fox Chase Cancer Center, Philadelphia

Confident interpretation of changes in serial myocardial P-31 MR spectroscopy in a clinical study in a patient requires knowledge of serial variances of key parameters. Factors influencing variance include noise; ability to reproduce patient, coil, and voxel positions; and partial-volume averaging with blood or chest wall. Fully relaxed (TR = 21 seconds) and partially saturated (TR = 2.3 seconds) P-31 MR spectra gated to mid-diastole were obtained at 1.5 T by using a semiprone left anterior oblique position, a 12-cm surface coil, ISIS localization to a 3 × 6 × 6-cm slab occupied primarily by the left ventricle and septum, and AHP pulses. T1s were measured on four occasions by progressive saturation with a three-parameter fit. Metabolites were quantitated by replacement of the VOI with a 20-mmol/L inorganic phosphate phantom and a phenylphosphonate reference to correct for coil loading, and were adjusted for partial-volume effects of blood by using MR imaging in three dimensions. Saturation factors (mean ± SD) in four serial studies over 1 month were 2.59 ± 0.26 for phosphocreatine (PCr) and 1.87 ± 0.22 for β-NTP, thus 1.41 for PCr/β-NTP. Mean T1 (± estimated SD) was 5.8 ± 0.1 seconds for PCr and 3.9 ± 0.1 seconds for β-NTP. Myocardial PCr was 6.1 ± 1.4 mmol/kg, and NTP was 3.9 ± 0.9 mmol/kg. In a volunteer studied eight times over 2 months, mean ± SD PCr/NTP was 1.64 ± 0.22 in fully relaxed spectra and 1.16 ± 0.24 in partially saturated spectra. The variances are essentially those expected from noise levels inherent in the experiment, indicating excellent reproducibility of instrument and technical performance. These results provide a basis for estimation of confidence limits required to interpret changes in serial spectra in a cooperative patient in a clinical study.

P440

### In Vivo Assessment of Reversible Rat Pancreatic Ischemia and Acute Pancreatitis with Lactate-edited H-1 MR Spectroscopy at 2.0 T

CH Sotak*†, M Siech†
*Department of Biomedical Engineering, Worcester (Mass) Polytechnic Institute; †Department of Radiology, University of Massachusetts Medical School, Worcester; and ‡Department of Surgery, Medical Academy of Magdeburg, Germany

It is known that acute pancreatitis (AP) is associated with changes in the energy supply of the pancreas and such changes are assumed to be an inducing factor of the disease. The levels of high-energy phosphates have been reported to be reduced in high-field P-31 MR studies of AP in excised rat pancreas; however, the authors have not been able to observe significant changes in the in vivo P-31 MR spectra of rat pancreas following induction of AP with an alternate procedure. Consequently, since ischemia is thought to play a role in this disease, the authors have investigated the use of lactate-edited H-1 MR spectroscopy in an in vivo rat pancreas model to evaluate pancreatic ischemia following cessation and restoration of blood flow and after the induction of AP. Lactate-edited H-1 rat pancreas spectra were obtained with a 2.0-T, 45-cm imaging spectrometer (GE CSI-II) using a 1D, double-quantum coherence transfer technique. To study the effects of reversible ischemia on the pancreas, the celiac trunk and superior mesenteric artery were reversibly occluded with a ligature. The MR protocol for the reversible ischemia experiment consisted of (*a*) acquiring three 5-minute control lactate spectra prior to occlusion; (*b*) occlusion for 30 minutes, during which six lactate spectra were obtained; and (*c*) reperfusion, followed by acquisition of 5-minute lactate spectra for up to 1 hour. For AP studies, an ethanol/enzyme–induced juice edema was used to produce AP in the ensuing 24 hours. In reversible ischemia experiments, the pancreatic lactate signal increased following occlusion, compared with the control level, in 14 of 15 animals. On release of the ligature, only seven of the animals showed decreases in pancreatic lactate to near control levels in the hour following reperfusion. In the remaining animals, the lactate level either remained constant or increased after ligature release, indicating little or no reperfusion. In five of 13 AP animals, varying amounts of lactate were observed in the H-1 spectrum. In the remaining animals, there was either no evidence of lactate or the low signal-to-noise ratio in the lactate methyl region of the spectrum precluded a confident assignment of the metabolite. In conclusion, the authors have demonstrated the feasibility of using in vivo, lactate-edited H-1 MR spectroscopy for studying ischemia in the pancreas and have seen some evidence for ischemia in the in vivo AP rat model. This technique should be valuable in evaluating the progress of AP and the efficacy of various therapeutic interventions.

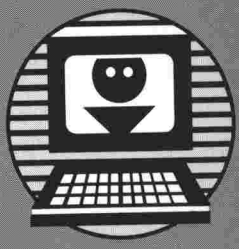

SMRT TECHNOLOGIST PAPERS

SMRI

## SMRT TECHNOLOGIST PAPERS

1992 marks the first Annual Meeting of the Combined Section of Magnetic Resonance Technologists (SMRT), a joint venture between the SMRI and SMRM. The following papers are interleaved with significant and topical plenary symposia and will be 10 minutes in length with 2 minutes following for discussion.

# SMRT Technologist Manufacturer's Workshop

## GE Medical Systems

On Saturday, April 25th, General Electric Medical Systems will present a workshop for users of its MR equipment:

**New Advances in Imaging**

**Fast Spin Echo**
single echo/dual echo
basics/physics
Signa implementation
clinical applications

**Fast Gradient Echo**
Fast SPGR/Fast GRASS
Fast Multi-Planar SPGR
Tissue Prepared Fast GRASS
basics/physics
Signa implementation
clinical applications

**512 Acquisition Matrices**
Signa implementation
clinical applications

All technologists are welcome to discover GE's new advances in MR imaging.

## PHILIPS

Magnetic Resonance Imaging is a technology-intense imaging modality. Modern day healthcare requires the rapid inception and implementation of the latest imaging technology. Philips leads the way in MRI ingenuity and implementation.

The purpose of this presentation, Philips Medical Imaging MRI latest technology, is to provide an overview in the following areas:

**Hardware Features** such as
Two Dedicated Quadratura Pediatric Coils

**Multiple Fast Scan Techniques**
Turbo Field Echo
Turbo Spin Echo

**Angio Techniques**
High Resolution Angio
Gated Inflow
Magnetization Transfer Contrast

**Other Specialized Imaging Features**

**A Review of Philips Latest MRI Features**

## PICKER

On Saturday, April 25th, Picker International will present a workshop for users of Vista MR equipment. The topics covered during the session will include the latest MR techniques, with special emphasis on new angiographic sequences and on the use of Rf-Fast scanning in clinical imaging. The application of fat-suppression techniques will also be reviewed. The program will conclude with a discussion session in which all Vista users will be invited to participate.

## RESONEX

At the manufacturer's workshop session for Resonex MRI system operators, Resonex will be presenting the latest information on new features, and products to be released in the near future.

New coils to be discussed will include E.V. Cervical Spine, Bilateral TMJ, and contoured shoulder.

The HP computer upgrade with the 5.0 and soon to be released 5.1 version software and the improvements in imaging and time efficient operations will be discussed at length.

Technologists are encouraged to bring an example of an outstanding study performed at their facility. These can be cases of subtle pathologies that required a creative approach toward imaging procedures, or that utilized unusual positioning requirements. These will be presented in a round table discussion to be held at the end of the session.

## TOSHIBA

Toshiba America Medical Systems is very excited about its newest image enhancement programs and advanced hardware technologies.

**MRT-35A Imaging System**
V6.0 software package scheduled for general release in June. This latest upgrade package provides advanced capabilities such as 3-D Time of Flight MRA Flexible, Pre-Saturation, Mixed TR/Fast T2 Imaging, Fluoro MRI and many other features. This package provides various image quality improvements in addition to throughput savings of 10 minutes per scan for an additional two patients per day.

**MRT-50A Imaging System**
The MRT-50A is introducing its Super Program which will feature shielded gradient coils for increased power and speed while maintaining lower eddy currents. It will also have significant clinical benefits that will provide high image quality, high spatial resolution, and shorter echo times.

**MRT-150A Imaging System**
The MRT-150A, a 1.5 tesla high-field system, uses innovative magnet technology that provides high-field clinical performance with the siting and economic advantages associated with mid-field systems. It has advanced sequencing techniques allowing for fast sequencing techniques for spin echo and field echo sequences. There is also an MRA workstation for angiography studies. The MRt-150A imaging system will also be available on a mobile unit which will make it a practical high-field imaging system.

# SMRI '92 Tenth Annual Meeting
# Technologist Abstracts

## Saturday • Trianon Ballroom
## Technologist Papers T001–T006

MODERATORS: LB Irilli, RT • R Bell, BSRT

T001 • 9:30 AM

### Study of in Vivo Human Brain Metabolism with H-1 MR Spectroscopy

LM Needham, LS Goldojarb, M Singh, JM Halls, PM Colletti, MR Terk, JR Gober

*American Health Services Corp, Philips Medical Systems, and University of Southern California School of Medicine, Los Angeles*

Brain cells, under normal conditions, derive their energy through oxidative glucose metabolism, but during anaerobic or ischemic conditions metabolism is shifted to produce lactate. The exact metabolic pathway within stimulated regions of the brain is not understood. Therefore, the goal of these experiments was to study the lactate metabolism of the primary stimulated auditory cortex in healthy people with H-1 MR spectroscopy. Image-guided H-1 MR spectroscopy was performed on the primary auditory cortex in healthy volunteers before and during stimulation with a 1-kHz sound. A Philips S15-HP MR unit was used to acquire sagittal and coronal multisection SE H-1 MR images for guiding the localization of the H-1 MR spectroscopy signals. The 90°-180°-180° double SE PRESS sequence was used for spatial localization, and water suppression was accomplished with a water-selective inversion pulse and acquisition at the zero crossover point of the water protons. The Figure shows spectra of the auditory cortex before and during auditory stimulation. Typical brain resonances for creatine/phosphocreatine (Cr), choline (Ch), and *N*-acetyl aspartate (NAA) were observed before stimulation. The spectrum acquired during stimulation showed a lactate resonance. This study shows that increased lactate metabolism occurs in the primary auditory cortex of normal individuals during auditory stimulation.

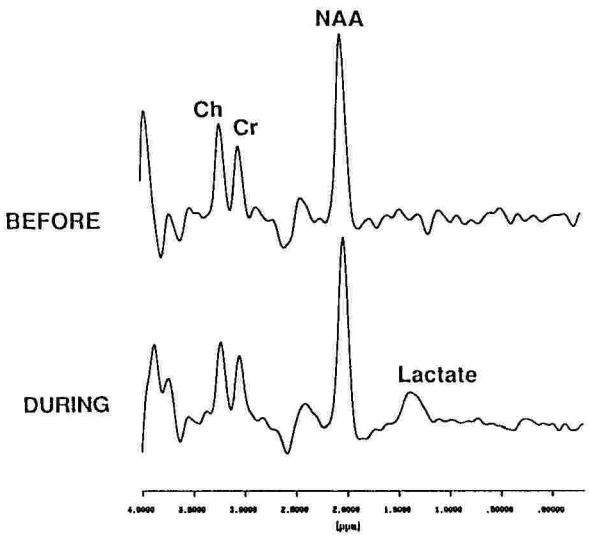


T002 • 9:42 AM

### Study of in Vivo Human Myocardial High-Energy Phosphate Metabolism with P-31 MR Spectroscopy

LS Goldojarb, LM Needham, SL Norris, LJ Haywood, JM Halls, PM Colletti, MR Terk, JR Gober

*American Health Services Corp, Philips Medical Systems, and University of Southern California School of Medicine, Los Angeles*

Assessment of left ventricle (LV) metabolism and function is important in numerous disease states such as hypertrophic and dilated cardiomyopathies, valvular insufficiencies, anemia and ischemic heart disease, and transplant rejection. These conditions can produce left heart failure; however, little is known about the in vivo pathophysiology in the human LV. Therefore, the goal of this study was to study the high-energy phosphate metabolism of the LV in patients, with use of P-31 MR spectroscopy. H-1 image-guided P-31 MR spectroscopy was performed in the LV of healthy volunteers and patients with hypertrophic cardiomyopathy, sickle cell disease (SCD), and valvular insufficiencies. A Philips S15-HP MR unit was used to acquire cardiac-triggered, axial, multisection SE H-1 MR images and ISIS P-31 MR spectrograms. The Figure shows spectra of the LV before and after aortic valve surgery. Typical myocardial resonances for phosphomo-

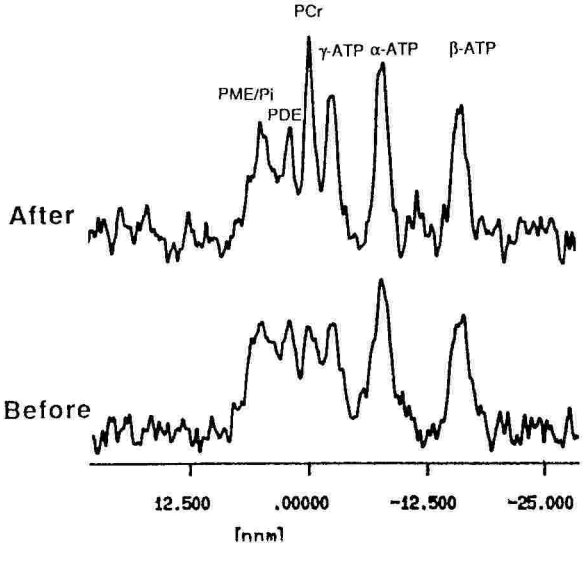

noester/inorganic phosphate (PME/Pi), phosphodiester (PDE), phosphocreatine (PCr), γ-adenosine triphosphate (γ-ATP), α-ATP, and β-ATP were observed. The PCr/β-ATP ratio can be used as a reliable measure of tissue ischemia. The depressed PCr/β-ATP ratio in the 'before' spectrum indicates significant myocardial ischemia. The normal PCr/β-ATP ratio in the 'after' spectrum indicates that aortic valve replacement restored normal metabolism to the LV. This study shows that abnormal phosphate metabolism can be demonstrated with P-31 MR spectroscopy in the resting LV in some patients with heart disease and that normal metabolism can be restored with appropriate treatment.

T003 • 11:42 AM

### Musculoskeletal MR Imaging with the STIR Technique

MC Connor
*Vail Imaging Center, Vail, Colo*

The hypothesis of this paper is that T1- and T2-weighted SE imaging may not be an adequate evaluation of musculoskeletal trauma. STIR imaging will often demonstrate subtle areas of abnormality (ie, fractures, contusions, tears) not visualized with the more conventional pulse sequences. With this presentation, STIR imaging will be compared with standard pulse sequences as well as other imaging modalities. The demonstration and presentation of pathology will be discussed.

T004 • 11:54 AM

### Signal Suppression Techniques at 1.5 T

CK Watson
*Department of Radiology/MRI, Hospital of the University of Pennsylvania, Philadelphia*

In MR imaging, those imaging parameters that are under user control are used to maximize signal intensity and increase the S/N. There are, however, cases in which high signal intensity can obscure pathology and subsequently make the diagnosis of lesions more difficult with MR imaging. In those isolated cases, we select options that allow signal suppression. The purpose of this paper is to discuss signal suppression techniques that include the Dixon technique, chemical shift selective suppression, spatial presaturation (SAT), and STIR. The Dixon technique exploits chemical shift artifact to achieve signal suppression. In anatomic regions in which there are fat and water in the same voxel of tissue, signals from fat and water are averaged during image formation. Since the protons in fat and water have slightly different frequencies, there are times during their rotations that they are completely out of phase. If we sample the signals from fat and water precisely at this time, the signals cancel and the sum is zero; hence, no signal intensity is seen in that area. Therefore, by altering the time that chemical shift is allowed to evolve (in gradient-echo imaging, this time corresponds to the TE such that fat and water are out of phase), signal suppression in anatomic locations in which fat and water interface is seen. Along similar lines, chemical shift selective suppression exploits the difference in frequency between fat and water to achieve signal suppression. This method locates the frequency from water and then adds a 90° RF pulse in the frequency location that corresponds to fat, and in doing so, suppresses the signal from fat. This technique can also be used to suppress the signals from water by placing additional RF pulses in the frequency location of water. SAT suppresses signal in a similar manner. SAT uses 90° RF pulses prior to the imaging sequence, so that those spins receive a second pulse with the imaging volume and become saturated. The result is a suppression of signal in a discrete location on the image that corresponds to the location of the applied SAT pulse. Finally, STIR techniques exploit the differences in the longitudinal (T1) relaxation times of various tissues. In STIR imaging, we begin the sequence with a 180° inverting pulse, wait some time, then apply a 90° RF pulse to acquire the image. The time between the 180° pulse and the 90° pulse is the TI. With selection of a TI such that, for example, fat has recovered sufficiently, the 90° RF pulse would transfer the magnetization from these spins to a position along the z axis, hence resulting in no signal. In general, these techniques have aided in the differentiation of a variety of lesions in MR imaging. In particular, chemical shift selective techniques have proved to be useful in the diagnosis of fatty lesions and/or those located in an anatomic location in which fat is abundant, whereas spatial techniques have helped to decide vascular patency issues.

T005 • 2:15 PM

### MR Imaging of the Wrist: Advances in Technology

JA Strandt
*Department of Radiology, Medical College of Wisconsin, Milwaukee*

Technologic advances in MR imaging allow imaging of small anatomic structures not previously seen radiographically. Because of the high soft-tissue resolution and the noninvasiveness of the procedure, MR imaging has become the method of choice in musculoskeletal imaging. High-resolution images of the wrist can be obtained with several considerations. Coils that are small in size and either commercially available or specially designed are used. Exceptionally fine images are routinely obtained with a 4-inch-diameter solenoid coil. This is a volume coil that serves to both excite the tissue and receive the signal. These coils take advantage of the high S/N inherent in small coils and enable more strenuous imaging parameters to be used. Patient setup and imaging strategies will be discussed. The development of software both for imaging and postprocessing manipulation allows even greater information to be retrieved from MR imaging of the wrist. Special software sequences have been designed to obtain small (6–8-cm) fields of view and very thin (2–3-mm) sections, providing extremely high resolution. Postprocessing has also become beneficial to study the anatomic structures of the wrist. Three-dimensional data sets are acquired and reformatted into multiple planes at the workstation. This presentation will show advanced techniques for producing high-resolution MR images of the wrist, including SE, gradient-echo, and volume acquisitions. Anatomy will be reviewed to identify the osseous, ligamentous, and cartilaginous structures. Cases will be displayed to show pathology on MR images of the wrist.

T006 • 2:27 PM

### Clinical Utility of 3D MR Imaging and Multiplanar Reformatting for Evaluation of the Knee

J Steward, PM Colletti, JR Gober
*Philips Medical Systems and University of Southern California School of Medicine, Los Angeles*

A typical 2D examination of the knee would include a scout image, an angulated sagittal SE image for anterior and posterior cruciate ligaments and menisci, an angulated coronal SE image for bone marrow and cortex, and an axial FFE image for patellar tendon and cartilage. It is not always possible to optimally show both anterior and posterior cruciate ligaments with a single angulated sagittal image; thus, additional images may be required. The purpose of this study was to determine whether a single 3D acquisition with multiplanar reformatting could augment or replace one or all of the above 2D studies. Patients were imaged with a Philips Gyroscan 1.5-T S15-ACS

MR unit with use of a wrap coil. The image matrix was 256 × 256, with isotropic pixels to give a 1-mm spatial resolution. A TR of 40 msec and a TE of 9 msec with one signal average resulted in an acquisition time of about 8 minutes. The 3D data set was then exported via EtherNet to a Philips Gyroview independent workstation for multiplanar reformatting and viewing. The 3D acquisition decreased total patient imaging time by one third, compared with the standard examination. Resolution and S/N were superior for the 3D technique, which improved diagnostic power for ligamentous and soft-tissue injury. Meniscal tears were identified in multiple planes, but the results were otherwise comparable to those of 2D techniques. Linear and curved reformatted images allowed exquisite depiction of ligaments. Data processing and viewing of 3D images on the independent workstation proved to be an important new approach because it alleviates competition for imager time. Three-dimensional MR imaging with multiplanar reformatting was shown to be a new and important method for evaluation of the knee.

## Sunday • Trianon Ballroom
## Technologist Papers T007–T015

MODERATORS: LB Irilli, RT • R Bell, BSRT

T007 • 9:30 AM

### MR Angiography: Clinical Applications

C Towle, M Depies, M Guell, J McGovern
*Institute of Medical Imaging, Milwaukee*

Clinical applications of MR angiography, such as evaluation of blood flow in the brain and use of MR angiography as an adjunct to traditional imaging modalities and as a general screening device for vascular disease will be discussed.

T008 • 9:42 AM

### Principles of Velocity-Encoding Selection in Phase-Contrast MR Angiography

MA Bernstein,* SP Souza†
**GE Medical Systems and †GE Corporate Research & Development, Milwaukee*

Unlike time-of-flight, phase-contrast MR angiography requires the selection of the velocity-encoding parameter (VENC). VENC is the fastest flow velocity that can be imaged without flow-related aliasing. This additional parameter allows the acquisition to be sensitized for either fast or slow flow. The process of selecting the proper VENC for a clinical application is greatly simplified when several basic principles are mastered. Rather than list recommended VENC values for different blood vessels, this presentation reviews those principles. The S/N in phase-contrast angiography is proportional to $v$/VENC, where $v$ is the velocity of the flowing blood. Therefore it is advantageous to reduce VENC as much as possible. For phase-contrast angiography in which quantitative or directional flow information is required, flow-related aliasing is not acceptable, so VENC should be set near or slightly above typical values of $v$ for the vessel of interest. If aliasing occurs, the apparent direction of the flowing blood can be reversed. Aliasing also causes the apparent flow speed to underestimate the true speed. In the more typical situation, in which quantitative or directional flow information is not required, a considerable amount of flow-related aliasing can be tolerated without image degradation. This greatly simplifies the selection of VENC. As illustrated in the Figure, allowing flow-related aliasing in the center of the vessel can improve the apparent vessel diameter, as well as bring vessels with slower flow out of the noise floor. With reference to the Figure, suppose the large vessel has a true maximum flow velocity of 40 cm/sec. (The apparent noise floor is indicated by the shaded region.) The VENC selection of 80 cm/sec displays apparent vessel narrowing (dotted line). At VENC = 40 cm/sec the apparent narrowing is reduced, but the smaller vessel is still obscured. At VENC = 20 cm/sec the smaller vessel is now visible, and vessel narrowing is minimized. The "hole" in the middle of the large vessel arising from flow-related aliasing does not present a serious problem, since the peak vessel S/N is equal in the VENC = 20 and 40 cm/sec cases. Also, if the acquisition is 3D phase contrast followed by an MIP projection, the hole in the middle of the vessel will be undetectable due to the nonlinearity of the projection process.

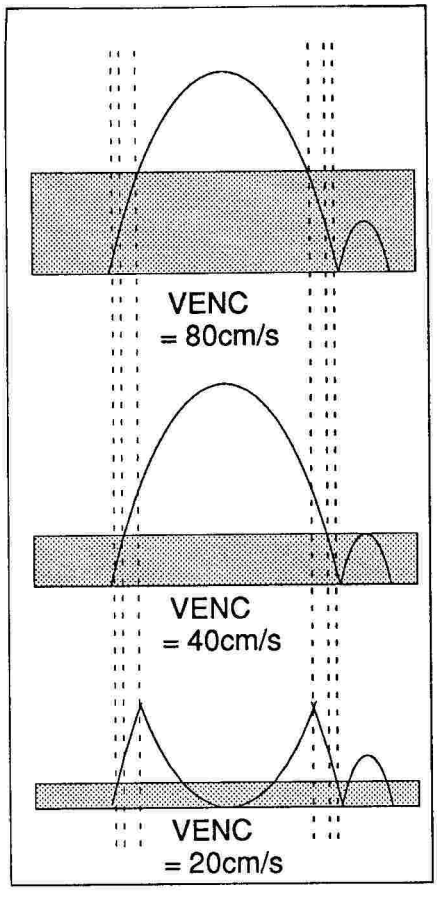


T009 • 11:30 AM

### Postprocessing of Two-dimensional Inflow MR Angiography of the Aorta

B Burrow
*Department of Radiology, Emory University School of Medicine, Atlanta*

MR angiography is noninvasive, requires no contrast material, and offers a reconstructed 3D view of vessels. By using a combination of maximum-intensity projection (MIP), multiplanar reformatting (MPR), and surface rendering techniques, the author has demonstrated excellent images of the aortic arch. The question is, can this information alone reduce or eliminate the need for an invasive cardiac catheterization? Ten patients aged 10–65 years were evaluated for possible aortic aneurysms. Surface renderings were generated of the pulmonary arteries, aorta, and superior vena cava. All images were acquired

on a 1.5-T Philips ACS imager, and images were postprocessed on a Philips Gyroview workstation equipped with 3D MR angiography and MPR options. The acquisition protocol was TR = heart rate, TE = 6 msec, flip angle of 60°, retrospective cardiac gating, trigger delay of 180–240 msec, acquisition window of 300–400 msec, 30 5-mm-thick axial sections, 2-mm overlap, 256 × 204 matrix, 2 NSA, 270 FOV, and imaging time of 15–25 minutes. On the basis of these images alone, without cardiac catheterization, five patients underwent surgery, two patients were treated with conservative medical management, one patient refused surgery, and two patients with a history of patch angioplasty repair were normal. This technique provides excellent visualization of repaired coarctation in aortic disease. Imaging time is about 1 hour; postprocessing time is about 30 minutes. At the author's institution, this is an important tool in the presurgical planning and postoperative assessment of aortic disease.

T010 • 11:42 AM

### Preliminary Results in MR Imaging of the Facial Nerve

JA Strandt

*Department of Radiology, Medical College of Wisconsin, Milwaukee*

The facial nerve is a complex structure within the temporal bone and consists of four distinct areas: the first or anterior genu, the vertical segment, the horizontal segment, and the posterior or second genu. Imaging of the facial nerve is desirable in patients with symptoms of Bell palsy or other pathologic conditions. The natural contrast of the nerve tissue against the low signal intensity of the aerated temporal bone enables the nerve to be easily visualized. Because the facial nerve was often seen incidentally at routine imaging of the temporomandibular joint, a small surface coil was first used for this study. Sections were acquired in a vertical oblique plane to display the entire nerve on one image. Subsequent studies have shown that similar results can be obtained by using the standard head coil and prescribing the vertical oblique plane. This method eliminates repositioning of the patient for surface coil imaging. Sections may also be acquired in the direct sagittal plane and reformatted into an oblique plane at the workstation. Imaging of the facial nerve has been performed on both 1.5-T and 0.5-T GE Signa Systems. Intravenous contrast material is used in some cases. Standard T1-weighted SE sequences are acquired with a 3-mm section thickness, 24–26-cm field of view, and 256 × 256 or 512 × 256 matrix. Images are slightly magnified when filmed for interpretation. Postprocessing by reformatting at a workstation has also improved the final image display. By knowing facial anatomy, utilizing optimum imaging techniques, and taking advantage of postprocessing features, it appears that facial nerve imaging can be quite easily performed at midfield or high field strength, with use of the commercially available head coil.

T011 • 2:15 PM

### MR Imaging versus US in Evaluation of Pregnant Patients

S Karsan, MD Mitchell

*Department of Diagnostic Imaging, College of Allied Health Sciences, Thomas Jefferson University, Philadelphia*

In the past decade, US has become the primary diagnostic tool in the evaluation of obstetric cases. In some instances, it has been necessary to use CT for further evaluation. Whereas US has limitations due to technical factors, and CT requires exposure of the fetus to ionizing radiation, MR imaging avoids these disadvantages. It allows in vivo characterization of fetal tissues and fluids within the amniotic sac. It offers excellent spatial resolution, for evaluation of small features, while its multiple sources of contrast can resolve anatomic and pathologic features not detectable with US. Several studies have indicated the advantages of MR imaging where US is restricted, such as the study of fetal lung development (US has no "acoustic window" for lungs). MR imaging is useful in assessing growth retardation and other abnormalities such as cavum veli interpositi and hydrocephalus. It is ideally suited to complement obstetric US because of its ability to distinguish normal and diseased tissues by more than just morphologic criteria. Fetal assessment in a patient with oligohydramnios makes fetal assessment with US difficult, due to reduced amniotic fluid volume; MR imaging can still provide a quality image. MR imaging can help differentiate between genitourinary abnormalities within the fetus and intrauterine growth retardation, which can be confused on US images. MR imaging gives superb delineation of the cervix during pregnancy, allowing earlier diagnosis of placenta previa, abruptio placentae, or placental aging. While US is almost always chosen to evaluate adnexal masses, it is nonspecific. MR imaging can show the size of these masses and their relationship to the fetus and the birth canal, and can be particularly valuable for observing malignancies during pregnancy. US is likely to remain the imaging modality of choice in routine prenatal screening. It is in instances in which a particular pathology will be distinguished or confirmed only with MR imaging that we can appreciate its full worth. MR imaging can provide crucial information in situations that would previously have required radiation exposure. MR imaging is important now and growing still, but its safety is not certain and its cost is often prohibitive. It will probably be used in pregnancy only in special cases. US will retain its importance in diagnosis of prenatal conditions.

T012 • 2:27 PM

### MR Imaging of an Unusual Pediatric Liver Tumor

TA Duffy, RT*† MD Mitchell, PhD*

**Department of Diagnostic Imaging, College of Allied Health Sciences, Thomas Jefferson University, Philadelphia and †Department of Radiology, Mercer Medical Center, Trenton, NJ*

An 11-month-old boy presented to a community hospital with flulike symptoms and abdominal pain. When antibiotic therapy failed to relieve the symptoms, a US examination of the abdomen was performed. This examination revealed a mass but was equivocal as to the nature of the mass and its specific location in the abdomen. The patient was referred to a tertiary pediatric hospital for further diagnostic evaluation. Results of bone marrow biopsy were negative. A contrast-enhanced CT scan was attempted, but the patient had an allergic reaction to the iodinated contrast material, and the examination was discontinued. MR imaging revealed a large vascular mass in the right lobe of the liver. At biopsy, it was proved to be a hepatoblastoma, an extremely rare and highly vascular form of tumor. The patient underwent an 8-month regimen of chemotherapy, with three anti-neoplastic agents, to shrink the tumor before attempts to surgically remove it. During the course of chemotherapy, frequent MR imaging examinations and hepatic angiography were performed to evaluate progress. The tumor regressed sufficiently to allow its successful surgical removal. The right lobe of the liver, which was removed along with the tumor, has subsequently regenerated cancer free. Follow-up MR imaging and hepatic angiographic examinations continue to be performed. The patient is now 32 months of age, 1 year after surgery. There is no evidence of recurrence of the cancer.

T013 • 4:00 PM

## Evaluation of Adrenal Masses: Role of MR Imaging

KE Withers, RA Burn

*Department of Radiology, Duke University Medical Center, Durham, NC*

The adrenal glands commonly host a number of benign and malignant lesions. Differentiating the two is imperative for patient treatment. It is believed that MR imaging currently meets this diagnostic challenge. Currently, operating with a research-capable software configuration with a 1.5-T MR unit (GE Signa), the authors' adrenal protocol begins with an axial T1-weighted sequence. Thin, 3-mm, interleaved sections display basic adrenal anatomy. Motion artifacts are minimized by employing respiratory compensation, spatial presaturation, and a short TR. Once the lesion is identified, it is further characterized by determining the absolute T2 value, based on a dual-echo (2,500/40,80 msec) T2-weighted sequence. Malignant lesions have shown significantly higher absolute T2 values than nonmalignant lesions. To further enhance the diagnostic certainty, the authors employ a new superfast gradient-recalled-echo technique (WARP-SPGR, TR/TE = 39/3, 30° flip angle, 1 NEX, 256 × 128 matrix) after injection of Gd-DTPA. By acquiring a set of 3–5 images every 30 seconds for as long as 10 minutes, the enhancement characteristics of the lesion are determined over time. Images are acquired in axial or coronal projections. Malignant lesions show greater enhancement with significantly delayed washout. The authors' clinical experience with this protocol supports results of an early 1991 European investigators reported an overall sensitivity of 100% in detecting adrenal masses and a specificity of 91% in differentiating benign adenomas from metastases. The authors are optimistic about the potential of this protocol in their effort to meet the diagnostic challenge posed by adrenal masses.

T-104 • 4:12 PM

## Advanced Education: A Necessity for Success in MR Imaging

MD Mitchell

*Department of Diagnostic Imaging, College of Allied Health Sciences, Thomas Jefferson University, Philadelphia*

The rapid growth of MR imaging is presenting many new career opportunities to diagnostic imaging professionals. The expansion of opportunities in operation of these instruments is obvious. However, the increased complexity of MR imaging instruments and protocols, compared with those of other diagnostic imaging modalities, requires increased responsibility from these persons. Rapid proliferation of MR facilities is leading to expansion of career opportunities in administration and supervision. The need for many more-qualified personnel for operating these instruments is leading to expansion of career opportunities in MR education. Success in all of these careers requires skills beyond those previously demanded of most diagnostic imaging professionals. The Advanced Placement Program developed by this department is presented as a model advanced education program. It is designed for working professionals who hold certification as radiologic technologists. The core curriculum includes study of various imaging modalities and of cross-sectional anatomy. Major options build on this base. A major in administration includes coursework in management and finance, while the education major covers educational methods and psychology. The imaging-specialist major includes in-depth study of diagnostic imaging physics and pathology. All major options culminate in supervised field experiences and the writing of a special project paper. A new MR imaging specialist major option is under development. With credit granted for current professional certification and previous coursework, students graduate with the degree of Bachelor of Science in Diagnostic Imaging. Graduates of this program have found success in a variety of careers, expanding their perspective on their profession and bringing new responsibilities and rewards. This program has great flexibility, which is necessary to accommodate the varying needs and interests of the students. While students progress at their own pace, most can complete the program in two years of evening study. Flexibility and accessibility will be important in meeting the educational needs of a diversified population.

T015 • 4:24 PM

## MR Imaging of Postenucleated Socket Syndrome

M Guell, RT, M DePies, RT

*Institute of Medical Imaging, Milwaukee*

WITHDRAWN

The postenucleated socket syndrome (PESS) refers to a set of changes in the enucleated orbit represented by rotation and displacement of the contents inferiorly and posteriorly. The authors used MR imaging as a tool to prospectively analyze the orbits of patients suffering from PESS, in an effort to better understand the pathophysical features and mechanisms involved. MR imaging findings of 10 patients with PESS were studied. Sagittal and coronal, and axial T1-weighted 3-mm images were acquired on a 1.5-T imager. The MR imaging findings of the enucleated orbit will be presented.

# Notes

# Notes

# Notes

# SMRI

## INDICES AND INFORMATION

- Technical Exhibits Floorplan
- 1992 Annual Meeting Acknowledgements
- Author Index
- SMRT Membership Information
- SMRI Membership Information
- CME Information/Certificate of Attendance

## PLAN YOUR INDIVIDUAL ITINERARY

To help you plan your week at SMRI, the Printed Program index lists all plenary sessions, proffered papers, scientific poster presentations and technologist papers. All papers are categorized by author with the abstract number of each symposia, paper, or exhibit found following the author name. The first ten co-authors are listed individually.

The type of work is indicated by one of five abbreviations preceding the abstract number. An abbreviation key appears on the next page. All numbers listed in the index reference the paper number and not the page number on which the abstract may be found.

Please note that other pertinent information regarding the Technical Exhibits Program, Annual Meeting Acknowledgements, and SMRI and SMRT membership information may also be found in this section.

# THE NEW YORK HILTON & TOWERS

## AMERICAS HALL I

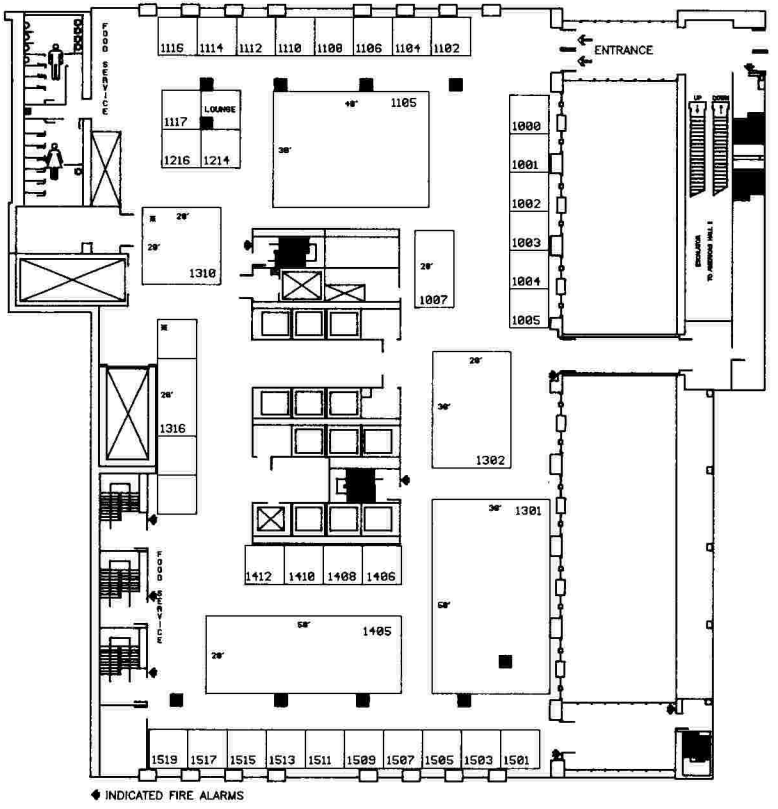


## AMERICAS HALL II

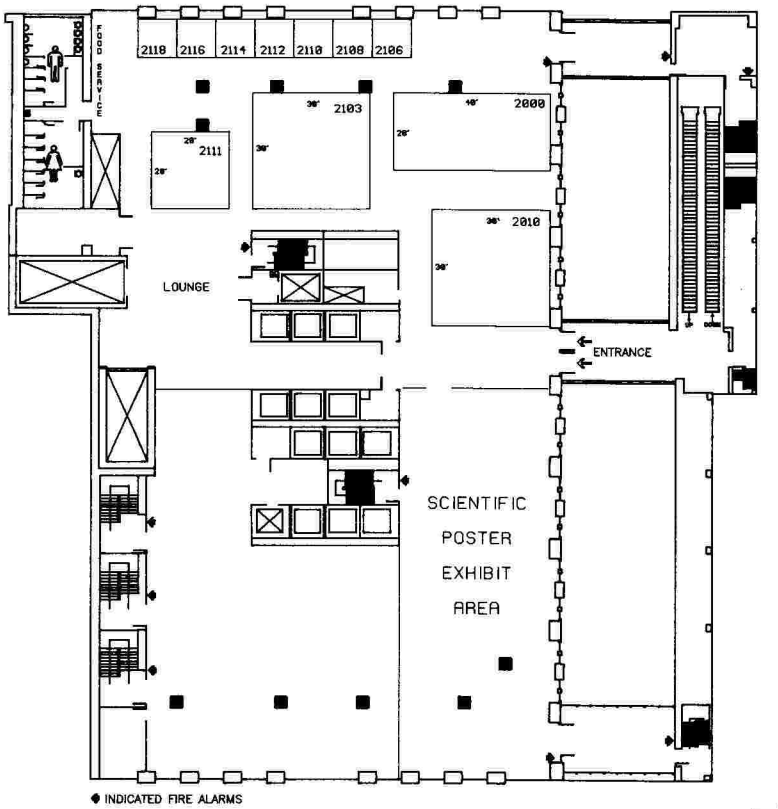


# Society for Magnetic Resonance Imaging

**April 25 – 29,1992**

SCALE
0' 5' 10' 15' 20' 30' 40' 50'

Prepared by
[redacted]
Freeman Decorating Company
NEW YORK

| | |
|---|---|
| Society for Magnetic Resonance Imaging | |
| AMERICAS 1 & 2 | |
| APRIL 25 - 29,1992 | |
| SMRI9201 | |
| #22201103 | 0000 |
| 1/28/92 | 0 |
| 1/29/92 | 0 |
| 0 | 0 |
| 0 | 0 |
| Jim BJ | |

# 1992 Technical Exhibitors

**Alliance Pharmaceutical Corporation**
3040 Science Park Road
San Diego, CA 92121
619/558-4300

**Analogic Corporation**
8 Centennial Drive
Peabody, MA 01960
508/977-3000

**Applied Radiology**
80 Shore Road
Port Washington, NY 11050
516/883-0164

**Berlex Laboratories**
300 Fairfield Road
Wayne, NJ 07470
201/305-5082

**Diagnostic Imaging Magazine**
600 Harrison Street
San Francisco, CA 94107
415/905-2417

**E-Z-EM, Incorporated**
717 Main Street
Westbury, NJ 11590
516/333-8230

**Eastman Kodak Company**
255 East Avenue
Rochester, NY 14650
716/724-5985

**Elscint, Inc.**
245 Pleasant Street
Hackensack, NJ 07601
201/342-2000

**Fuji Medical Systems USA, Incorporated**
333 Ludlow Street
Stamford, CT 06902
203/353-0300

**General Electric Medical Systems**
P.O. Box 414 (W-439)
Milwaukee, WI 53201
414/544-3461

**Hitachi Medical Systems America, Incorporated**
1993 Case Parkway
Twinsburg, OH 44087
216/425-1313

**ISG Technologies, Incorporated**
3030 Orlando Drive
Mississauga, Ontario
Canada
416/672-2100

**Image Data Corporation**
11550 I.H. 10 West
San Antonio, TX 78230
512/641-8340

**Instrumentarium Imaging**
300 West Edgerton Avenue
Milwaukee, WI 53207
414/747-1030

**Kaiser Permanente**
393 Walnut Center, 6th Floor
Pasadena, CA 91188
818/564-3500

**Kurzweil Applied Intelligence, Incorporated**
411 Waverley Oaks Road
Waltham, MA 02154
617/893-5151

**Magnacoustics, Inc.**
200 Granada Street
Atlantic Beach, NY 11509
516/239-0042

**Medical Advances, Incorporated**
10431 West Watertown Plank Road
P.O. Box 26425
Milwaukee, WI 53226
414/258-3808

**Medrad, Incorporated**
271 Kappa Drive
Pittsburgh, PA 15238-2670
412/967-9700

**Mosby Yearbook, Incorporated**
11830 Westline Ind. Drive
St. Louis, MO 63146
800/325-4177

**Nonin Medical, Incorporated**
12900 Highway 55
Plymouth, MN 55441
612/553-9968

**Novus Technologies, Incorporated**
5830 Oberlin Drive, Suite 201
San Diego, CA 92121
619/625-0111

**Nuclear Associates**
100 Voice Road
Carle Place, NY 11514
516/741-1640

**Otsuka Electronics**
2555 Midpoint Drive
Fort Collins, CO 80525
303/484-0428

**Pergamon Press**
395 Saw Mill River Road
Elmsford, NY 10523
914/345-6440

**Philips Medical Systems North America Incorporated**
710 Bridgeport Avenue
Shelton, CT 06484
203/926-7647

**Picker International**
595 Miner Road
Highland Heights, OH 44143
216/473-3721

**Radiology Today/Slack Incorporated**
6900 Grove Road
Thorofare, NJ 08086
609/848-1000

**Raven Press**
1185 Avenue of the Americas
New York, NY 10036
212/930-9500

**Reality Imaging Corporation**
6661 Cochran Road
Solon, OH 44139
216/349-2548

**Resonex**
720 Palomar
Sunnyvale, CA 94086
800/443-8666

**Sanofi Winthrop Pharmaceuticals**
90 Park Avenue
New York, NY 10016
212/907-3221

**Shimadzu Medical Systems**
101 West Walnut Street
Gardena, CA 90248
310/217-8855

**Siemens Medical Systems, Incorporated**
186 Wood Avenue, South
Iselin, NJ 08830
908/321-4500

**Squibb Diagnostics**
P.O. Box 4500
Princeton, NJ 08543
609/243-5203

**Toshiba America Medical Systems, Incorporated**
2441 Michelle Drive
Tustin, CA 92681
714/730-5000

*Published based on information available January 30, 1992*

SMRI

# 1992 Annual Meeting Acknowledgements

**Break/Luncheon Service**
Pre-session coffee service will be provided in the Registration Area, Second Floor Promenade, daily. Saturday's morning and afternoon breaks will be served in the Rendezvous Trianon; luncheon service will be provided in the Sutton Complex, Second Floor, Saturday and in Americas Hall I and II, Technical Exhibits Area, thereafter. Please avail yourself of the services provided.

**Pre-Session Coffee Breaks**
The Society gratefully acknowledges the generous contribution received in support of these events from Eastman Kodak Company.

**Luncheon Service**
The Society gratefully acknowledges the generous contributions received in support of these events from the following:

**Saturday:** Picker International
**Sunday:** Siemens Medical Systems, Inc.
**Monday:** Berlex Imaging
**Tuesday:** Philips Medical Systems North America, Inc.

**Technical Exhibits Reception**
The Society gratefully acknowledges the generous contribution received in support of this event from Toshiba America Medical Systems, Inc.

**Educational Grants**
The Society gratefully acknowledges the generous grants received from General Electric Medical Systems, Sanofi Winthrop Pharmaceuticals, and Squibb Diagnostics in support of educational and scientific programs at the Annual Meeting.

# One Simple MResource

**SMRI,** the critical link between science and the clinical application of medicine, provides yet another important and helpful tool…
**the MResource Guide.**

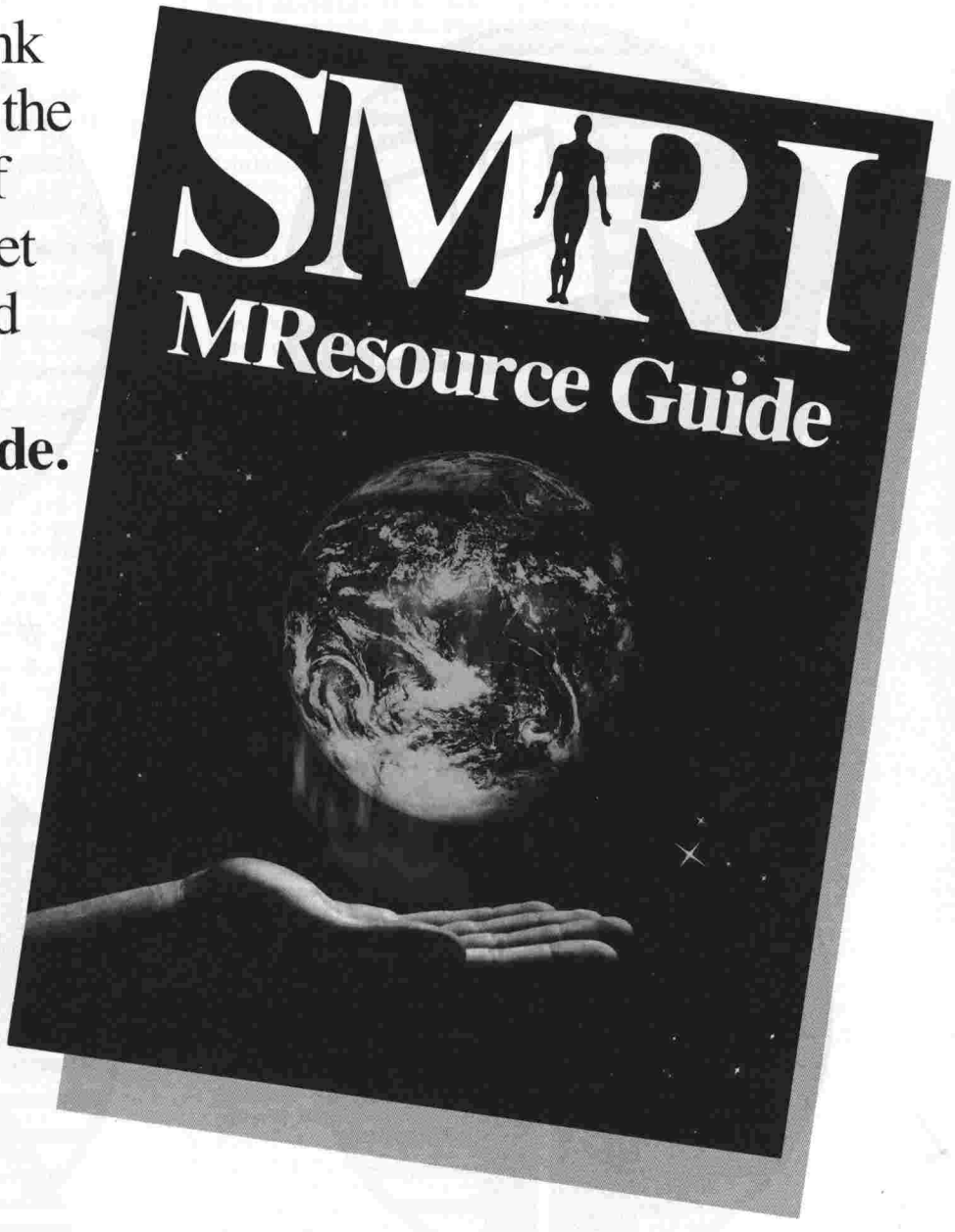


## What to expect

- MR equipment, service and accessory manufacturers listed by product and company name
- A compendium of MR definitions, pulse sequences and acronyms

The inaugural MResource Guide will be published inside the JMRI September/October 1992 issue. Additional copies of the Guide will be available and may be ordered by faxing this Order Form to the **SMRI** Central Office at 312.951.6474. If questions, call 312.751.2590.

***Take control of a critical variable in magnetic resonance…order your MResource Guide today.***

**Number of MResource Guides** ☐

**@ $15.00 each** $ ☐

**Payment enclosed (U.S. funds only)** ☐

**MasterCard/Visa** ☐

**Name** _____

**Address** _____

_____

**City/State/Zip Code** _____

**Country** _____

**Phone** _____

**Name** _____

**Account #/Exp. date** _____

## Key to Abbreviations in Author Index

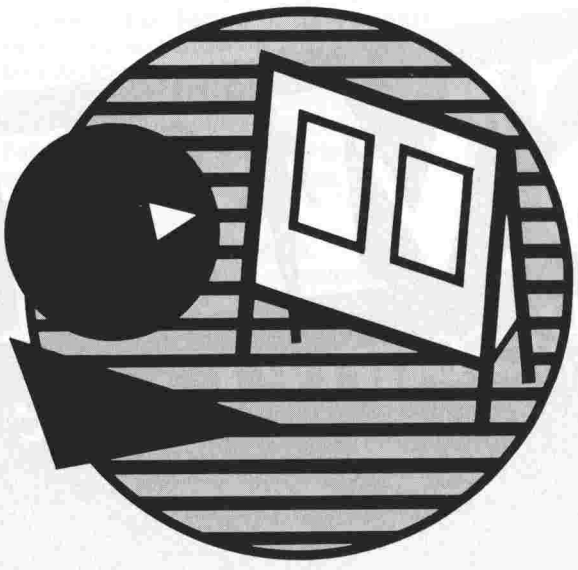

P–scientific poster presentations

#–proffered papers

PS–plenary symposia

T–technologist papers

---

**Key to Abbreviations:**

**PS–plenary symposia**

**#–proffered papers**

**P–scientific poster presentations**

**T–technologist papers**

# Author Index

# E



# F



# G



# H

# I



# J



# K



# L



# M

# N



# O



# P

# Q



# R



# S

# T



# U



# V



# W



# X



# Y



# Z

COMBINED SECTION FOR MAGNETIC RESONANCE TECHNOLOGISTS

# SMRT

## Membership Application

The Society of Magnetic Resonance in Medicine, Inc., and the Society for Magnetic Resonance Imaging, Inc., non-profit professional associations, combined efforts in 1991 and formed the Section for Magnetic Resonance Technologists. SMRT is devoted to advancing the education, training and quality of Magnetic Resonance Technologists, to promoting world-wide communication of information in the field of Magnetic Resonance, and to establishing a forum for dissemination of this information.

Annual Meetings of SMRT

*New York (1992)*
*New York (1993)*

### Membership Benefits

Associate Membership in the Society of Magnetic Resonance in Medicine and the Society for Magnetic Resonance Imaging.

The journals, *Magnetic Resonance in Medicine* (published monthly) and/or the *Journal of Magnetic Resonance Imaging* (published bimonthly) at a special SMRT member's rate. Subscriptions begin with the January issue for applications made January through September 30 and with the January issue of the following year for applications submitted October through December. Subscription to the journal(s) is optional.

SMRT Newsletter (published biannually) will bring you the latest technical and educational news breakthroughs, as well as information on upcoming SMRT events.

SMRT Membership Directory, published annually.

Advance notice and substantially reduced registration fees for the Annual Meeting and SMRT workshops, as well as SMRM and SMRI meetings and workshops.

### Membership Categories and Qualifications (please check one category).

Prior to final acceptance by the SMRT Policy Board, each application is reviewed by the Membership Committee for verification of eligibility.

### ❑ Technologist (Voting) Member:

An individual who (i) shares the stated purposes of the SMRT; (ii) is (A) certified by the American Registry of Radiologic Technologists, (B) a Registered Diagnostic Medical Sonographer, (C) a Certified Nuclear Medicine Technologist, (D) or certified by an equivalent professional certifying organization; and (iii) has practiced as a technologist in the field of magnetic resonance for a minimum of one year. Members have the right to vote and hold office. The applicant must submit a curriculum vitae and verification of the above qualifications. Sponsorship: Endorsement of two or more voting members of the SMRT, of the SMRM, or of the SMRI; OR if the individual (i) shares the stated purposes of the SMRT, (ii) can demonstrate appropriate equivalent professional competence in radiologic practice or in work in support of biochemical, biophysical or biological programs, (iii) and has practiced as a magnetic resonance technologist for a minimum of two years. The applicant must submit a curriculum vitae, as well as a letter of verification from his/her department head or administrator verifying two years' practice in an NMR modality. Sponsorship: Endorsement of two or more voting members of the SMRT, of the SMRM, or of the SMRI.

### ❑ Technologist (Non-Voting) Member:

An individual who shares the stated purposes of the SMRT but does not meet the qualifications for voting membership. The applicant must submit a curriculum vitae. Sponsorship: Endorsement of one or more voting members of the SMRT, of the SMRM, or of the SMRI.

Sponsor #1 Name (please print)

Sponsor #1 Signature

Sponsor #1 Society Affiliation

Sponsor #2 Name (*please print*)

Sponsor #2 Signature

Sponsor #2 Society Affiliation

# CANDIDATE INFORMATION FORM

**I.D.#** FOR OFFICE USE ONLY

Please mail the completed application, sponsorship form(s), membership fee, CV, and if applicable, letter of verification to:

**SMRT**
Combined Section for Magnetic Resonance Technologists

Membership Coordinator
1918 University Avenue
Suite 3C
Berkeley, CA 94704 USA

Telephone: (510) 841-1899
Facsimile: (510) 841-2340

(Please Print Legibly) Date _____

Name _____

Degree _____ Title _____

Addresses **(Check preferred journal mailing address)**

❑ Office _____

_____

Country _____ Telephone _____

Fax _____

❑ Home _____

_____

Country _____ Telephone _____

Fax _____

**ALL APPLICANTS**, please answer the following:

Are you currently working in the field of MRI? _____Yes _____No Date you were registered as an R.T. ___/___/___

Please list the types of scanners used: _____

_____

Other Professional Affiliations: ___AAN ___AAPM ___ACR ___ARRS ___ASNR ___ASRT ___ESMRMB

___RSNA ___SMRM ___SMRI ___SNM ___Other _____

*Dues Payment*

**$70.00** per year for Technologist [ ] Voting [ ] Non-Voting

**$125.00** per year for Technologist [ ] Voting [ ] Non-Voting With Journal, *Magnetic Resonance in Medicine*

**$120.00** per year for Technologist [ ] Voting [ ] Non-Voting With Journal, *Journal of Magnetic Resonance Imaging*

**$175.00** per year for Technologist [ ] Voting [ ] Non-Voting With Both Journals

**Payment Methods:**
**Check:** Must be payable "to" (not "through") a U.S. Bank in U.S. dollars and must be imprinted with the computer encoding and routing information authorized by the American Banking Association. Please make checks payable to **SMRM**.
**Travelers' checks:** Travelers' checks in U.S. dollars for the exact amount, properly countersigned, are acceptable.
**International Money Order:** Must be in U.S. dollars and imprinted with the computer encoding and routing information authorized by the American Banking Association. U.S. dollar International Postal Money Orders imprinted as stated above are acceptable.
**Credit Cards:** Visa MasterCard and EuroCard are accepted. To pay by card, please check: Visa [ ] MasterCard [ ] EuroCard [ ]

Card #: _____ Exp. Date ___/___ Signature: _____

**DO NOT PAY BY WIRE.**

# MEMBERSHIP APPLICATION

SMRI

## Society for Magnetic Resonance Imaging

The organizational goals of this Society are to:

- Provide an equal opportunity to physicians and basic scientists to contribute to the development of MRI.
- Provide an international multidisciplinary forum for the advancement of magnetic resonance imaging.
- Promote the applications of magnetic resonance techniques to medicine and biology, with special emphasis on imaging.
- Prepare and disseminate technical and product information related to research techniques, equipment and clinical applications of magnetic resonance.
- Develop educational and training material and methods for the application of magnetic resonance to medicine and biology.

**All individuals involved in the field of magnetic resonance imaging are invited to join the Society.**

The classifications of membership are defined as follows:

**FULL:** A person who shares the stated purpose of the Society, who is involved in the field of magnetic resonance imaging, and who has completed postgraduate studies or equivalent training in any subject or work of significant merit in the area of magnetic resonance.

**TECHNOLOGIST:** A person who shares the stated purpose of the Society and who has technical or professional background in the area of magnetic resonance imaging or an allied field.

**STUDENT:** A person who shares the stated purpose of the Society and who is engaged in full-time study, graduate or undergraduate.

**CORPORATE:** A corporate entity that has a major interest in the development and application of NMR instrumentation in MRI or MRS formedical or biological purposes. Selection to corporate membership must be confirmed by ⅔ vote of the Board members present at the meeting following application for such membership.

**ASSOCIATE:** A person who shares the stated purpose of the Society, but does not qualify for other categories of membership.

The Full, Associate and Corporate membership rates include a subscription to the bimonthly journal, **Journal of Magnetic Resonance Imaging (JMRI)**. Those applying for Technologist and Student membership categories may obtain a subscription to the journal by remitting an additional $50. In order to be considered for MEMBERSHIP, please provide the information requested on the reverse side. Please note: two sponsors, one of whom must be a **SMRI** member, must be listed on each application.

**PLEASE SEND THESE THREE IMPORTANT ITEMS WITH THIS APPLICATION:**

1. **Completed Candidate Information Form** (see reverse),
2. **Your curriculum vitae; and,**
3. **Appropriate remittance to:**

**Membership Department**
**Society for Magnetic Resonance Imaging**
**213 West Institute Place, Suite 501**
**Chicago, Illinois 60610**

SMRI

SOCIETY FOR MAGNETIC RESONANCE IMAGING

# CANDIDATE INFORMATION FORM

In order to be considered for membership, please provide the information requested on the reverse side. A complete curriculum vitae of your education, employment and publications MUST accompany this application.

**1. Name:** _____
(first)

_____
(middle)

_____
(last)

**Degree:** _____

**2. Address:** _____

_____

_____

**City/State/Zip/Country:** _____

_____

_____

Tel. ( ) _____

Fax ( ) _____

The above address is your ☐ office ☐ home.

The above telephone/fax numbers are your ☐ office ☐ home information.

**Employed By/Affiliated With:**

_____

**Title:** _____

**3. Sponsor I** (mandatory*):

Name: _____

Tel. No.: _____

**Sponsor II** (mandatory*):

Name: _____

Tel. No. _____

*only one sponsor must be a **SMRI** member; second sponsor must be an individual in MR field.

**4. Classification Codes** (Enter code which best describes your professional classification ): _____

**A.** Clinical scientist
(specialty _____)

**B.** Basic scientist
(specialty _____)

**C.** Resident/trainee
(specialty _____)

**D.** Radiology Support Personnel and Hospital Staff:
(a) technologist,
(b) engineer,
(c) radiology business manager,
(d) radiology administrator,
(e) nurse,
(f) hospital administrator,
(g) radiology educator,
(h) hospital purchasing agent.

**E.** Qualified Non-Health Sciences Personnel:
(a) architect,
(b) computer analyst,
(c) investment banker.

**F.** Non-Hospital-Based Medical Care Provider:
(a) purchasing consultant,
(b) equipment consultant,
(c) imaging center entrepreneur.

**5. Professional Affiliations:** _____

(a) AAN
(b) AAPM
(c) ACR
(d) ARRS
(e) ASNR
(f) ASRT
(g) ESMRMB
(h) JMRM
(i) RSNA
(j) SMRM
(k) SMRT
(l) SNM

**6. Please check your area of specialty from the following fields of study:**
☐ **M.D.**: Radiology, Neurology, Cadiology, Other: _____
☐ **Ph.D.**: Physics, Bio-Chemistry, Spectroscopy, Biology, Other: _____
☐ **Other**: _____

_____

**7. Please check your primary workplace from those listed below:**
☐ University Hospital/Medical School
☐ Industry
☐ Private Hospital/Clinic
Number of Beds _____
☐ Government Lab
☐ Other: _____

**8. Please check appropriate Membership Classification:**
☐ Full ($125)
☐ Technologist ($70)
☐ Student ($25)
☐ Associate ($125)

☐ I am applying for Student or Technologist Membership and am enclosing an additional $50.00 for a subscription to the **Journal of Magnetic Resonance Imaging.**

Signature: _____

Date: _____

## Extremely Important

**Remember!**
Your application package MUST include all of the following elements before approval procedures may begin:

**Completed Application**, with two sponsors listed (**SMRI**-member or non-member colleagues required)
**Curriculum Vitae**
**Membership Fee** (for all categories but technologist, please make check payable to **SMRI**; for technologist category applicants, please make check payable to SMRT).

SMRI

SOCIETY FOR MAGNETIC RESONANCE IMAGING


# *Future Meetings*

***1994 • March 5-9 • Dallas, TX***

***1995 • March 25-29 • Washington, D.C.***

**Society for Magnetic Resonance Imaging**
213 West Institute Place
Suite 501
Chicago, IL 60610
312.751.2590

# SMRI

# CERTIFICATE OF ATTENDANCE

This is to certify that _____
was registered for the educational and/or scientific activities at the 10th Annual Meeting of the SMRI, April 25-29, 1992, at the New York Hilton and Towers in New York, NY.

**Society for Magnetic Resonance Imaging**
**Educational and Scientific Program**
**New York, NY**
**April 25-29, 1992**

As an organization accredited for continuing medical education, the American College of Radiology certifies that this continuing medical educational offering meets the criteria for Category 1 credit for up to 33 hours, provided it is completed as designed.

This form is provided to assist registrants in the recording of Category I Credits earned, hour-for-hour, at the 10th Annual Meeting. The SMRI will not record credits earned by individuals. Please keep this record for your own files. Do not send this to the ACR office or to the AMA office.

| Day | Hours Attended/ Credit Earned | Maximum Credit Possible |
|---|---|---|
| Saturday | _____ | 6½ Hours |
| Sunday | _____ | 7 Hours |
| Monday | _____ | 6½ Hours |
| Tuesday | _____ | 6½ Hours |
| Wednesday | _____ | 6½ Hours |

Total Credits Earned: _____

Total Credits Available: 33 Hours

**E. Mark Haacke, Ph.D., *Certifying Official***
Society for Magnetic Resonance Imaging

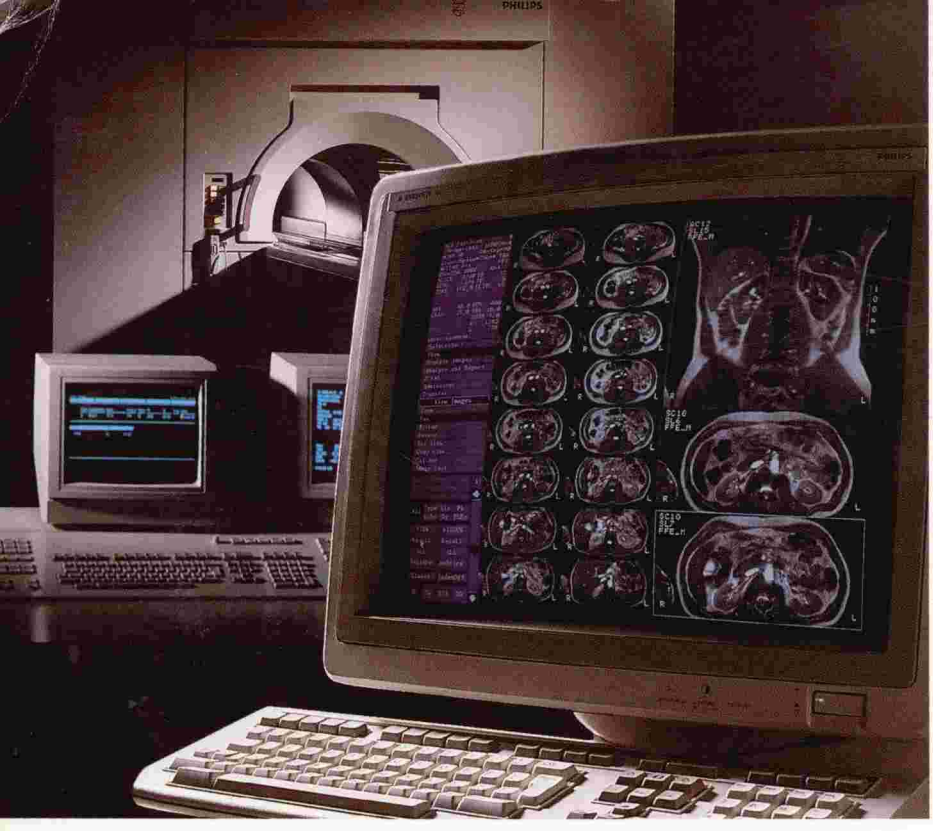

# Finally. Total abdominal screening in less than 2 minutes.

MR

At Philips, the measure of a system is not only how fast it obtains an image. But also how much it improves diagnostic confidence. Expands clinical applications. And enhances throughput and efficiency. By all measures, GYROSCAN S15/ACS is setting the standard in MR today. And in the process, expanding MR's role from advanced problem-solver to screening modality of choice. Evaluate the S15/ACS for yourself. See how it eliminates motion artifacts in abdominal studies. Notice the superior contrast and resolution of its head and joint studies. And pay particular attention to today's most advanced cardio, angio and FAST Scan packages. You'll understand why GYROSCAN S15/ACS is today's most promising platform for future MR developments. For all the details, just call **1-800-999-5883, ext. 26.**

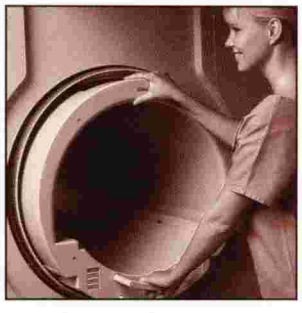

*GYROSCAN S15/ACS will quickly and economically incorporate new applications and advances in technology thanks, in part, to this unique removable body coil.*

FINDING THE ANSWER. MAKING IT WORK.

CT • PACS • DIGITAL • VASCULAR • MR • ULTRASOUND • R/F • RADIOGRAPHY • MAMMOGRAPHY • CARDIOVASCULAR • COMPUTED RADIOGRAPHY • THERAPY • SURGERY • UROLOGY • CT • PACS • DIGITAL • VASCU

**Philips Medical Systems**

PHILIPS

PHILIPS

JMRI • SMRI 1992 PRINTED PROGRAM ■ Volume 2 (P)

PAGES 1–188